Fuel Cell Handbook
(Seventh Edition)

By
EG&G Technical Services, Inc.

Under Contract No. DE-AM26-99FT40575

U.S. Department of Energy
Office of Fossil Energy
National Energy Technology Laboratory
P.O. Box 880
Morgantown, West Virginia 26507-0880

November 2004

DISCLAIMER

TABLE OF CONTENTS

LIST OF FIGURES

LIST OF TABLES AND EXAMPLES

FORWARD

Fuel cells are one of the cleanest and most efficient technologies for generating electricity. Since there is no combustion, there are none of the pollutants commonly produced by boilers and furnaces. For systems designed to consume hydrogen directly, the only products are electricity, water and heat. Fuel cells are an important technology for a potentially wide variety of applications including on-site electric power for households and commercial buildings; supplemental or auxiliary power to support car, truck and aircraft systems; power for personal, mass and commercial transportation; and the modular addition by utilities of new power generation closely tailored to meet growth in power consumption. These applications will be in a large number of industries worldwide.

In this Seventh Edition of the Fuel Cell Handbook, we have discussed the Solid State Energy Conversion Alliance Program (SECA) activities. In addition, individual fuel cell technologies and other supporting materials have been updated. Finally, an updated index assists the reader in locating specific information quickly.

It is an important task that NETL undertakes to provide you with this handbook. We realize it is an important educational and informational tool for a wide audience. We welcome suggestions to improve the handbook.

Mark C. Williams

Strategic Center for Natural Gas
National Energy Technology Laboratory

PREFACE

The last edition of the Fuel Cell Handbook was published in November, 2002. Since that time, the Solid State Energy Conversion Alliance (SECA-www.seca.doe.gov) has funded activities to bring about dramatic reductions in fuel cell costs, and rates as the most important event to report on since the 2000 edition. SECA industry teams' have continued to evaluate and test fuel cell designs, candidate materials, manufacturing methods, and balance-of-plant subsystems. SECA's goal is to cut costs to as low as $400 per kilowatt by the end of this decade, which would make fuel cells competitive for virtually every type of power application. The initiative signifies the Department's objective of developing a modular, all-solid-state fuel cell that could be mass-produced for different uses much the way electronic components are manufactured and sold today.

SECA has six industry teams working on competing designs for the distributed generation and auxiliary power applications. These teams are headed by: FuelCell Energy, Delphi Battelle, General Electric Company, Siemens Westinghouse, Acumentrics, and Cummins Power Generation and SOFCo. The SECA industry teams receive core technology support from leading researchers at small businesses, universities and national laboratories. Over 30 SECA R&D projects are generating new scientific and engineering knowledge, creating technology breakthroughs by addressing technical risks and barriers that currently limit achieving SECA performance and cost goals.

U.S. Department of Energy's (DOE's) SECA program, have considerably advanced the knowledge and development of thin-electrolyte planar SOFC. As a consequence of the performance improvements, SOFC are now considered for a wide range of applications, including stationary power generation, mobile power, auxiliary power for vehicles, and specialty applications. A new generation of intermediate temperature (650-800 ^{o}C) SOFCs is being developed under the U.S. DOE's SECA program. Fuel processing by an autothermal, steam, or partial oxidation reformer that operates between 500-800 °C enables fuel cell operation on gasoline, diesel fuel, and other hydrocarbon fuels.

This Handbook provides a foundation in fuel cells for persons wanting a better understanding of the technology, its benefits, and the systems issues that influence its application. Trends in technology are discussed, including next-generation concepts that promise ultra-high efficiency and low cost, while providing exceptionally clean power plant systems. Section 1 summarizes fuel cell progress since the last edition, and includes existing power plant nameplate data. Section 2 addresses the thermodynamics of fuel cells to provide an understanding of fuel cell operation. Sections 3 through 7 describe the five major fuel cell types and their performance.

Polymer electrolyte, alkaline, phosphoric acid, molten carbonate, and solid oxide fuel cell technology descriptions have been updated from the previous edition. Manufacturers are focusing on reducing fuel cell life cycle costs. In this edition, we have included over 5,000 fuel cell patent abstracts and their claims. In addition, the handbook features a new fuel cell power conditioning section, and overviews on the hydrogen industry and rare earth minerals market.

ACKNOWLEDGEMENTS

The authors of this edition of the Fuel Cell Handbook acknowledge the cooperation of the fuel cell community for their contributions to this Handbook. Many colleagues provided data, information, references, valuable suggestions, and constructive comments that were incorporated into the Handbook. In particular, we would like to acknowledge the contributions J. Thijssen.

The authors wish to thank M. Williams, and H. Quedenfeld of the U.S. Department of Energy, National Energy Technology Laboratory, for their support and encouragement, and for providing the opportunity to enhance the quality of this Handbook.

This work was supported by the U.S. Department of Energy, National Energy Technology Laboratory, under Contract DE-AM21-94MC31166.

1. TECHNOLOGY OVERVIEW

This chapter provides an overview of fuel cell technology. First it discusses the basic workings of fuel cells and basic fuel cell system components. Then, an overview of the main fuel cell types, their characteristics, and their development status is provided. Finally, this chapter reviews potential fuel cell applications.

1.1 Introduction

Fuel cells are electrochemical devices that convert chemical energy in fuels into electrical energy directly, promising power generation with high efficiency and low environmental impact. Because the intermediate steps of producing heat and mechanical work typical of most conventional power generation methods are avoided, fuel cells are not limited by thermodynamic limitations of heat engines such as the Carnot efficiency. In addition, because combustion is avoided, fuel cells produce power with minimal pollutant. However, unlike batteries the reductant and oxidant in fuel cells must be continuously replenished to allow continuous operation. Fuel cells bear significant resemblance to electrolyzers. In fact, some fuel cells operate in reverse as electrolyzers, yielding a reversible fuel cell that can be used for energy storage.

Though fuel cells could, in principle, process a wide variety of fuels and oxidants, of most interest today are those fuel cells that use common fuels (or their derivatives) or hydrogen as a reductant, and ambient air as the oxidant.

Most fuel cell power systems comprise a number of components:

- Unit cells, in which the electrochemical reactions take place
- Stacks, in which individual cells are modularly combined by electrically connecting the cells to form units with the desired output capacity
- Balance of plant which comprises components that provide feedstream conditioning (including a fuel processor if needed), thermal management, and electric power conditioning among other ancillary and interface functions

In the following, an overview of fuel cell technology is given according to each of these categories, followed by a brief review of key potential applications of fuel cells.

1.2 Unit Cells

1.2.1 Basic Structure

Unit cells form the core of a fuel cell. These devices convert the chemical energy contained in a fuel electrochemically into electrical energy. The basic physical structure, or building block, of a fuel cell consists of an electrolyte layer in contact with an anode and a cathode on either side. A schematic representation of a unit cell with the reactant/product gases and the ion conduction flow directions through the cell is shown in Figure 1-1.

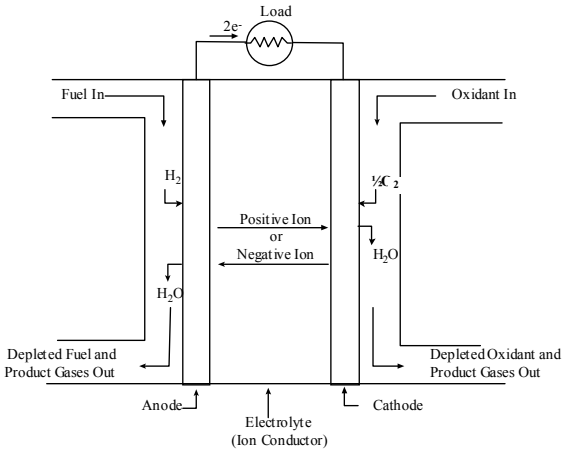

Figure 1-1 Schematic of an Individual Fuel Cell

In a typical fuel cell, fuel is fed continuously to the anode (negative electrode) and an oxidant (often oxygen from air) is fed continuously to the cathode (positive electrode). The electrochemical reactions take place at the electrodes to produce an electric current through the electrolyte, while driving a complementary electric current that performs work on the load. Although a fuel cell is similar to a typical battery in many ways, it differs in several respects. The battery is an energy storage device in which all the energy available is stored within the battery itself (at least the reductant). The battery will cease to produce electrical energy when the chemical reactants are consumed (i.e., discharged). A fuel cell, on the other hand, is an energy conversion device to which fuel and oxidant are supplied continuously. In principle, the fuel cell produces power for as long as fuel is supplied.

Fuel cells are classified according to the choice of electrolyte and fuel, which in turn determine the electrode reactions and the type of ions that carry the current across the electrolyte. Appleby and Foulkes (1) have noted that, in theory, any substance capable of chemical oxidation that can be supplied continuously (as a fluid) can be burned galvanically as fuel at the anode of a fuel cell. Similarly, the oxidant can be any fluid that can be reduced at a sufficient rate. Though the direct use of conventional fuels in fuel cells would be desirable, most fuel cells under development today use gaseous hydrogen, or a synthesis gas rich in hydrogen, as a fuel. Hydrogen has a high reactivity for anode reactions, and can be produced chemically from a wide range of fossil and renewable fuels, as well as via electrolysis. For similar practical reasons, the most common oxidant is gaseous oxygen, which is readily available from air. For space

applications, both hydrogen and oxygen can be stored compactly in cryogenic form, while the reaction product is only water.

1.2.2 Critical Functions of Cell Components

A critical portion of most unit cells is often referred to as the three-phase interface. These mostly microscopic regions, in which the actual electrochemical reactions take place, are found where either electrode meets the electrolyte. For a site or area to be active, it must be exposed to the reactant, be in electrical contact with the electrode, be in ionic contact with the electrolyte, and contain sufficient electro-catalyst for the reaction to proceed at the desired rate. The density of these regions and the nature of these interfaces play a critical role in the electrochemical performance of both liquid and solid electrolyte fuel cells:

- In liquid electrolyte fuel cells, the reactant gases diffuse through a thin electrolyte film that wets portions of the porous electrode and react electrochemically on their respective electrode surface. If the porous electrode contains an excessive amount of electrolyte, the electrode may "flood" and restrict the transport of gaseous species in the electrolyte phase to the reaction sites. The consequence is a reduction in electrochemical performance of the porous electrode. Thus, a delicate balance must be maintained among the electrode, electrolyte, and gaseous phases in the porous electrode structure.
- In solid electrolyte fuel cells, the challenge is to engineer a large number of catalyst sites into the interface that are electrically and ionically connected to the electrode and the electrolyte, respectively, and that is efficiently exposed to the reactant gases. In most successful solid electrolyte fuel cells, a high-performance interface requires the use of an electrode which, in the zone near the catalyst, has mixed conductivity (i.e. it conducts both electrons and ions).

Over the past twenty years, the unit cell performance of at least some of the fuel cell technologies has been dramatically improved. These developments resulted from improvements in the three-phase boundary, reducing the thickness of the electrolyte, and developing improved electrode and electrolyte materials which broaden the temperature range over which the cells can be operated.

In addition to facilitating electrochemical reactions, each of the unit cell components have other critical functions. The electrolyte not only transports dissolved reactants to the electrode, but also conducts ionic charge between the electrodes, and thereby completes the cell electric circuit as illustrated in Figure 1-1. It also provides a physical barrier to prevent the fuel and oxidant gas streams from directly mixing.

The functions of porous electrodes in fuel cells, in addition to providing a surface for electrochemical reactions to take place, are to:

1) conduct electrons away from or into the three-phase interface once they are formed (so an electrode must be made of materials that have good electrical conductance) and provide current collection and connection with either other cells or the load
2) ensure that reactant gases are equally distributed over the cell
3) ensure that reaction products are efficiently led away to the bulk gas phase

As a consequence, the electrodes are typically porous and made of an electrically conductive material. At low temperatures, only a few relatively rare and expensive materials provide sufficient electro-catalytic activity, and so such catalysts are deposited in small quantities at the interface where they are needed. In high-temperature fuel cells, the electro-catalytic activity of the bulk electrode material is often sufficient.

Though a wide range of fuel cell geometries has been considered, most fuel cells under development now are either planar (rectangular or circular) or tubular (either single- or double-ended and cylindrical or flattened).

1.3 Fuel Cell Stacking

For most practical fuel cell applications, unit cells must be combined in a modular fashion into a cell stack to achieve the voltage and power output level required for the application. Generally, the stacking involves connecting multiple unit cells in series via electrically conductive interconnects. Different stacking arrangements have been developed, which are described below.

1.3.1 Planar-Bipolar Stacking

The most common fuel cell stack design is the so-called planar-bipolar arrangement (Figure 1-2 depicts a PAFC). Individual unit cells are electrically connected with interconnects. Because of the configuration of a flat plate cell, the interconnect becomes a separator plate with two functions:

1) to provide an electrical series connection between adjacent cells, specifically for flat plate cells, and
2) to provide a gas barrier that separates the fuel and oxidant of adjacent cells.

In many planar-bipolar designs, the interconnect also includes channels that distribute the gas flow over the cells. The planar-bipolar design is electrically simple and leads to short electronic current paths (which helps to minimize cell resistance).

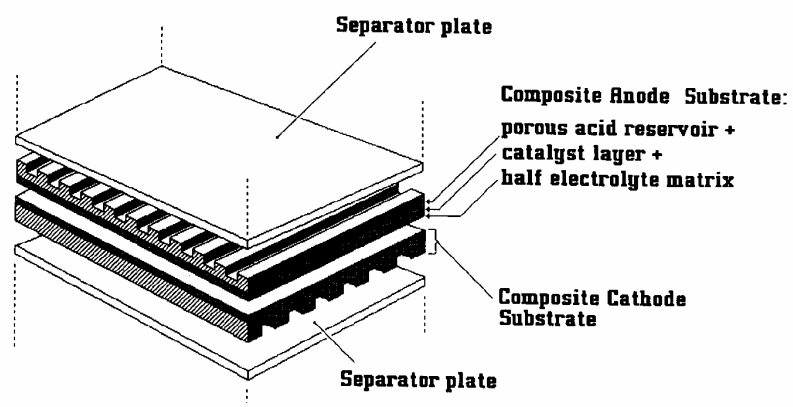

Figure 1-2 Expanded View of a Basic Fuel Cell Unit in a Fuel Cell Stack (1)

Planar-bipolar stacks can be further characterized according to arrangement of the gas flow:

- Cross-flow. Air and fuel flow perpendicular to each other
- Co-flow. Air and fuel flow parallel and in the same direction. In the case of circular cells, this means the gases flow radially outward
- Counter-flow. Air and fuel flow parallel but in opposite directions. Again, in the case of circular cells this means radial flow
- Serpentine flow. Air or fuel follow a zig-zag path
- Spiral flow. Applies to circular cells

The choice of gas-flow arrangement depends on the type of fuel cell, the application, and other considerations. Finally, the manifolding of gas streams to the cells in bipolar stacks can be achieved in various ways:

- Internal: the manifolds run through the unit cells
- Integrated: the manifolds do not penetrate the unit cells but are integrated in the interconnects
- External: the manifold is completely external to the cell, much like a wind-box

1.3.2 Stacks with Tubular Cells

Especially for high-temperature fuel cells, stacks with tubular cells have been developed. Tubular cells have significant advantages in sealing and in the structural integrity of the cells. However, they represent a special geometric challenge to the stack designer when it comes to achieving high power density and short current paths. In one of the earliest tubular designs the current is conducted tangentially around the tube. Interconnects between the tubes are used to form rectangular arrays of tubes. Alternatively, the current can be conducted along the axis of the tube, in which case interconnection is done at the end of the tubes. To minimize the length of electronic conduction paths for individual cells, sequential series connected cells are being developed. The cell arrays can be connected in series or in parallel. For a more detailed description of the different stack types and pictorial descriptions, the reader is referred to Chapter 7 on SOFC (SOFC is the fuel cell type for which the widest range of cell and stack geometries is pursued).

To avoid the packing density limitations associated with cylindrical cells, some tubular stack designs use flattened tubes.

1.4 Fuel Cell Systems

In addition to the stack, practical fuel cell systems require several other sub-systems and components; the so-called balance of plant (BoP). Together with the stack, the BoP forms the fuel cell system. The precise arrangement of the BoP depends heavily on the fuel cell type, the fuel choice, and the application. In addition, specific operating conditions and requirements of individual cell and stack designs determine the characteristics of the BoP. Still, most fuel cell systems contain:

- Fuel preparation. Except when pure fuels (such as pure hydrogen) are used, some fuel preparation is required, usually involving the removal of impurities and thermal conditioning. In addition, many fuel cells that use fuels other than pure hydrogen require some fuel processing, such as reforming, in which the fuel is reacted with some oxidant (usually steam or air) to form a hydrogen-rich anode feed mixture.
- Air supply. In most practical fuel cell systems, this includes air compressors or blowers as well as air filters.
- Thermal management. All fuel cell systems require careful management of the fuel cell stack temperature.
- Water management. Water is needed in some parts of the fuel cell, while overall water is a reaction product. To avoid having to feed water in addition to fuel, and to ensure smooth operation, water management systems are required in most fuel cell systems.
- Electric power conditioning equipment. Since fuel cell stacks provide a variable DC voltage output that is typically not directly usable for the load, electric power conditioning is typically required.

While perhaps not the focus of most development effort, the BoP represents a significant fraction of the weight, volume, and cost of most fuel cell systems.

Figure 1-3 shows a simple rendition of a fuel cell power plant. Beginning with fuel processing, a conventional fuel (natural gas, other gaseous hydrocarbons, methanol, naphtha, or coal) is cleaned, then converted into a gas containing hydrogen. Energy conversion occurs when dc electricity is generated by means of individual fuel cells combined in stacks or bundles. A varying number of cells or stacks can be matched to a particular power application. Finally, power conditioning converts the electric power from dc into regulated dc or ac for consumer use. Section 8.1 describes the processes of a fuel cell power plant system.

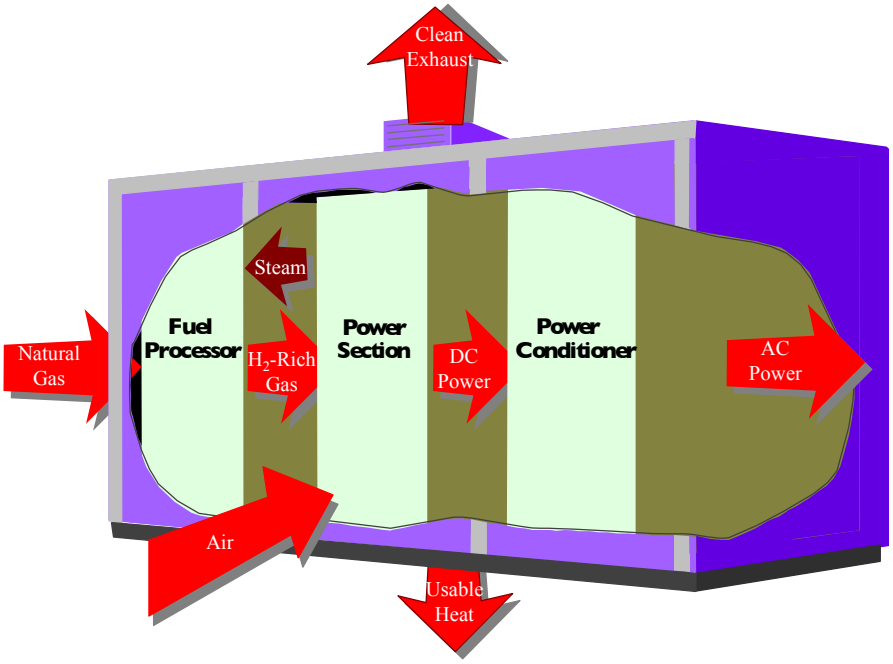

Figure 1-3 Fuel Cell Power Plant Major Processes

1.5 Fuel Cell Types

A variety of fuel cells are in different stages of development. The most common classification of fuel cells is by the type of electrolyte used in the cells and includes 1) polymer electrolyte fuel cell (PEFC), 2) alkaline fuel cell (AFC), 3) phosphoric acid fuel cell (PAFC), 4) molten carbonate fuel cell (MCFC), and 5) solid oxide fuel cell (SOFC). Broadly, the choice of electrolyte dictates the operating temperature range of the fuel cell. The operating temperature and useful life of a fuel cell dictate the physicochemical and thermomechanical properties of materials used in the cell components (i.e., electrodes, electrolyte, interconnect, current collector, etc.). Aqueous electrolytes are limited to temperatures of about 200 °C or lower because of their high vapor pressure and rapid degradation at higher temperatures. The operating temperature also plays an important role in dictating the degree of fuel processing required. In low-temperature fuel cells, all the fuel must be converted to hydrogen prior to entering the fuel cell. In addition, the anode catalyst in low-temperature fuel cells (mainly platinum) is strongly poisoned by CO. In high-temperature fuel cells, CO and even CH_4 can be internally converted to hydrogen or even directly oxidized electrochemically. Table 1-1 provides an overview of the key characteristics of the main fuel cell types.

Table 1-1 Summary of Major Differences of the Fuel Cell Types

	PEFC	AFC	PAFC	MCFC	SOFC
Electrolyte	Hydrated Polymeric Ion Exchange Membranes	Mobilized or Immobilized Potassium Hydroxide in asbestos matrix	Immobilized Liquid Phosphoric Acid in SiC	Immobilized Liquid Molten Carbonate in $LiAlO_2$	Perovskites (Ceramics)
Electrodes	Carbon	Transition metals	Carbon	Nickel and Nickel Oxide	Perovskite and perovskite / metal cermet
Catalyst	Platinum	Platinum	Platinum	Electrode material	Electrode material
Interconnect	Carbon or metal	Metal	Graphite	Stainless steel or Nickel	Nickel, ceramic, or steel
Operating Temperature	40 – 80 °C	65°C – 220 °C	205 °C	650 °C	600-1000 °C
Charge Carrier	H^+	OH^-	H^+	$CO3^=$	$O^=$
External Reformer for hydrocarbon fuels	Yes	Yes	Yes	No, for some fuels	No, for some fuels and cell designs
External shift conversion of CO to hydrogen	Yes, plus purification to remove trace CO	Yes, plus purification to remove CO and CO_2	Yes	No	No
Prime Cell Components	Carbon-based	Carbon-based	Graphite-based	Stainless-based	Ceramic
Product Water Management	Evaporative	Evaporative	Evaporative	Gaseous Product	Gaseous Product
Product Heat Management	Process Gas + Liquid Cooling Medium	Process Gas + Electrolyte Circulation	Process Gas + Liquid cooling medium or steam generation	Internal Reforming + Process Gas	Internal Reforming + Process Gas

In parallel with the classification by electrolyte, some fuel cells are classified by the type of fuel used:

- Direct Alcohol Fuel Cells (DAFC). DAFC (or, more commonly, direct methanol fuel cells or DMFC) use alcohol without reforming. Mostly, this refers to a PEFC-type fuel cell in which methanol or another alcohol is used directly, mainly for portable applications. A more detailed description of the DMFC or DAFC is provided in Chapter 3;

- Direct Carbon Fuel Cells (DCFC). In direct carbon fuel cells, solid carbon (presumably a fuel derived from coal, pet-coke or biomass) is used directly in the anode, without an intermediate gasification step. Concepts with solid oxide, molten carbonate, and alkaline electrolytes are all under development. The thermodynamics of the reactions in a DCFC allow very high efficiency conversion. Therefore, if the technology can be developed into practical systems, it could ultimately have a significant impact on coal-based power generation.

A brief description of various electrolyte cells of interest follows. Detailed descriptions of these fuel cells may be found in References (1) and (2).

1.5.1 Polymer Electrolyte Fuel Cell (PEFC)

The electrolyte in this fuel cell is an ion exchange membrane (fluorinated sulfonic acid polymer or other similar polymer) that is an excellent proton conductor. The only liquid in this fuel cell is water; thus, corrosion problems are minimal. Typically, carbon electrodes with platinum electro-catalyst are used for both anode and cathode, and with either carbon or metal interconnects.

Water management in the membrane is critical for efficient performance; the fuel cell must operate under conditions where the by-product water does not evaporate faster than it is produced because the membrane must be hydrated. Because of the limitation on the operating temperature imposed by the polymer, usually less than 100 °C, but more typically around 60 to 80 °C. , and because of problems with water balance, a H_2-rich gas with minimal or no CO (a poison at low temperature) is used. Higher catalyst loading (Pt in most cases) than that used in PAFCs is required for both the anode and cathode. Extensive fuel processing is required with other fuels, as the anode is easily poisoned by even trace levels of CO, sulfur species, and halogens.

PEFCs are being pursued for a wide variety of applications, especially for prime power for fuel cell vehicles (FCVs). As a consequence of the high interest in FCVs and hydrogen, the investment in PEFC over the past decade easily surpasses all other types of fuel cells combined. Although significant development of PEFC for stationary applications has taken place, many developers now focus on automotive and portable applications.

Advantages: The PEFC has a solid electrolyte which provides excellent resistance to gas crossover. The PEFC's low operating temperature allows rapid start-up and, with the absence of corrosive cell constituents, the use of the exotic materials required in other fuel cell types, both in stack construction and in the BoP is not required. Test results have demonstrated that PEFCs are capable of high current densities of over 2 kW/l and 2 W/cm^2. The PEFC lends itself particularly to situations where pure hydrogen can be used as a fuel.

Disadvantages: The low and narrow operating temperature range makes thermal management difficult, especially at very high current densities, and makes it difficult to use the rejected heat for cogeneration or in bottoming cycles. Water management is another significant challenge in PEFC design, as engineers must balance ensuring sufficient hydration of the electrolyte against flooding the electrolyte. In addition, PEFCs are quite sensitive to poisoning by trace levels of contaminants including CO, sulfur species, and ammonia. To some extent, some of these disadvantages can be counteracted by lowering operating current density and increasing

electrode catalyst loading, but both increase cost of the system. If hydrocarbon fuels are used, the extensive fuel processing required negatively impacts system size, complexity, efficiency (typically in the mid thirties), and system cost. Finally, for hydrogen PEFC the need for a hydrogen infrastructure to be developed poses a barrier to commercialization.

1.5.2 Alkaline Fuel Cell (AFC)

The electrolyte in this fuel cell is concentrated (85 wt percent) KOH in fuel cells operated at high temperature (~250 °C), or less concentrated (35 to 50 wt percent) KOH for lower temperature (<120 °C) operation. The electrolyte is retained in a matrix (usually asbestos), and a wide range of electro-catalysts can be used (e.g., Ni, Ag, metal oxides, spinels, and noble metals). The fuel supply is limited to non-reactive constituents except for hydrogen. CO is a poison, and CO_2 will react with the KOH to form K_2CO_3, thus altering the electrolyte. Even the small amount of CO_2 in air must be considered a potential poison for the alkaline cell. Generally, hydrogen is considered as the preferred fuel for AFC, although some direct carbon fuel cells use (different) alkaline electrolytes.

The AFC was one of the first modern fuel cells to be developed, beginning in 1960. The application at that time was to provide on-board electric power for the Apollo space vehicle. The AFC has enjoyed considerable success in space applications, but its terrestrial application has been challenged by its sensitivity to CO_2. Still, some developers in the U.S. and Europe pursue AFC for mobile and closed-system (reversible fuel cell) applications.

Advantages: Desirable attributes of the AFC include its excellent performance on hydrogen (H_2) and oxygen (O_2) compared to other candidate fuel cells due to its active O_2 electrode kinetics and its flexibility to use a wide range of electro-catalysts.

Disadvantages: The sensitivity of the electrolyte to CO_2 requires the use of highly pure H_2 as a fuel. As a consequence, the use of a reformer would require a highly effective CO and CO_2 removal system. In addition, if ambient air is used as the oxidant, the CO_2 in the air must be removed. While this is technically not challenging, it has a significant impact on the size and cost of the system.

1.5.3 Phosphoric Acid Fuel Cell (PAFC)

Phosphoric acid, concentrated to 100 percent, is used as the electrolyte in this fuel cell, which typically operates at 150 to 220 °C. At lower temperatures, phosphoric acid is a poor ionic conductor, and CO poisoning of the Pt electro-catalyst in the anode becomes severe. The relative stability of concentrated phosphoric acid is high compared to other common acids; consequently the PAFC is capable of operating at the high end of the acid temperature range (100 to 220 °C). In addition, the use of concentrated acid (100 percent) minimizes the water vapor pressure so water management in the cell is not difficult. The matrix most commonly used to retain the acid is silicon carbide (1), and the electro-catalyst in both the anode and cathode is Pt.

PAFCs are mostly developed for stationary applications. Both in the U.S. and Japan, hundreds of PAFC systems were produced, sold, and used in field tests and demonstrations. It is still one of the few fuel cell systems that are available for purchase. Development of PAFC had slowed

down in the past ten years, in favor of PEFCs that were thought to have better cost potential. However, PAFC development continues.

Advantages: PAFCs are much less sensitive to CO than PEFCs and AFCs: PAFCs tolerate about one percent of CO as a diluent. The operating temperature is still low enough to allow the use of common construction materials, at least in the BoP components. The operating temperature also provides considerable design flexibility for thermal management. PAFCs have demonstrated system efficiencies of 37 to 42 percent (based on LHV of natural gas fuel), which is higher than most PEFC systems could achieve (but lower than many of the SOFC and MCFC systems). In addition, the waste heat from PAFC can be readily used in most commercial and industrial cogeneration applications, and would technically allow the use of a bottoming cycle.

Disadvantages: Cathode-side oxygen reduction is slower than in AFC, and requires the use of a Platinum catalyst. Although less complex than for PEFC, PAFCs still require extensive fuel processing, including typically a water gas shift reactor to achieve good performance. Finally, the highly corrosive nature of phosphoric acid requires the use of expensive materials in the stack (especially the graphite separator plates).

1.5.4 Molten Carbonate Fuel Cell (MCFC)

The electrolyte in this fuel cell is usually a combination of alkali carbonates, which is retained in a ceramic matrix of $LiAlO_2$. The fuel cell operates at 600 to 700 °C where the alkali carbonates form a highly conductive molten salt, with carbonate ions providing ionic conduction. At the high operating temperatures in MCFCs, Ni (anode) and nickel oxide (cathode) are adequate to promote reaction. Noble metals are not required for operation, and many common hydrocarbon fuels can be reformed internally.

The focus of MCFC development has been larger stationary and marine applications, where the relatively large size and weight of MCFC and slow start-up time are not an issue. MCFCs are under development for use with a wide range of conventional and renewable fuels. MCFC-like technology is also considered for DCFC. After the PAFC, MCFCs have been demonstrated most extensively in stationary applications, with dozens of demonstration projects either under way or completed. While the number of MCFC developers and the investment level are reduced compared to a decade ago, development and demonstrations continue.

Advantages: The relatively high operating temperature of the MCFC (650 °C) results in several benefits: no expensive electro-catalysts are needed as the nickel electrodes provide sufficient activity, and both CO and certain hydrocarbons are fuels for the MCFC, as they are converted to hydrogen within the stack (on special reformer plates) simplifying the BoP and improving system efficiency to the high forties to low fifties. In addition, the high temperature waste heat allows the use of a bottoming cycle to further boost the system efficiency to the high fifties to low sixties.

Disadvantages: The main challenge for MCFC developers stems from the very corrosive and mobile electrolyte, which requires use of nickel and high-grade stainless steel as the cell hardware (cheaper than graphite, but more expensive than ferritic steels). The higher temperatures promote material problems, impacting mechanical stability and stack life.

Also, a source of CO_2 is required at the cathode (usually recycled from anode exhaust) to form the carbonate ion, representing additional BoP components. High contact resistances and cathode resistance limit power densities to around 100 – 200 mW/cm^2 at practical operating voltages.

1.5.5 Solid Oxide Fuel Cell (SOFC)

The electrolyte in this fuel cell is a solid, nonporous metal oxide, usually Y_2O_3-stabilized ZrO_2. The cell operates at 600-1000 °C where ionic conduction by oxygen ions takes place. Typically, the anode is Co-ZrO_2 or Ni-ZrO_2 cermet, and the cathode is Sr-doped $LaMnO_3$.

Early on, the limited conductivity of solid electrolytes required cell operation at around 1000 °C, but more recently thin-electrolyte cells with improved cathodes have allowed a reduction in operating temperature to 650 – 850 °C. Some developers are attempting to push SOFC operating temperatures even lower. Over the past decade, this has allowed the development of compact and high-performance SOFC which utilized relatively low-cost construction materials.

Concerted stack development efforts, especially through the U.S. DOE's SECA program, have considerably advanced the knowledge and development of thin-electrolyte planar SOFC. As a consequence of the performance improvements, SOFCs are now considered for a wide range of applications, including stationary power generation, mobile power, auxiliary power for vehicles, and specialty applications.

Advantages: The SOFC is the fuel cell with the longest continuous development period, starting in the late 1950s, several years before the AFC. Because the electrolyte is solid, the cell can be cast into various shapes, such as tubular, planar, or monolithic. The solid ceramic construction of the unit cell alleviates any corrosion problems in the cell. The solid electrolyte also allows precise engineering of the three-phase boundary and avoids electrolyte movement or flooding in the electrodes. The kinetics of the cell are relatively fast, and CO is a directly useable fuel as it is in the MCFC. There is no requirement for CO_2 at the cathode as with the MCFC. The materials used in SOFC are modest in cost. Thin-electrolyte planar SOFC unit cells have been demonstrated to be cable of power densities close to those achieved with PEFC. As with the MCFC, the high operating temperature allows use of most of the waste heat for cogeneration or in bottoming cycles. Efficiencies ranging from around 40 percent (simple cycle small systems) to over 50 percent (hybrid systems) have been demonstrated, and the potential for 60 percent+ efficiency exists as it does for MCFC.

Disadvantages: The high temperature of the SOFC has its drawbacks. There are thermal expansion mismatches among materials, and sealing between cells is difficult in the flat plate configurations. The high operating temperature places severe constraints on materials selection and results in difficult fabrication processes. Corrosion of metal stack components (such as the interconnects in some designs) is a challenge. These factors limit stack-level power density (though significantly higher than in PAFC and MCFC), and thermal cycling and stack life (though the latter is better than for MCFC and PEFC).

1.6 Characteristics

The interest in terrestrial applications of fuel cells is driven primarily by their potential for high efficiency and very low environmental impact (virtually no acid gas or solid emissions).

Efficiencies of present fuel cell plants are in the range of 30 to 55 percent based on the lower heating value (LHV) of the fuel. Hybrid fuel cell/reheat gas turbine cycles that offer efficiencies greater than 70 percent LHV, using demonstrated cell performance, have been proposed. Figure 1-4 illustrates demonstrated low emissions of installed PAFC units compared to the Los Angeles Basin (South Coast Air Quality Management District) requirements, the strictest requirements in the U.S. Measured emissions from the PAFC unit are < 1 ppm of NO_X, 4 ppm of CO, and <1 ppm of reactive organic gases (non-methane) (5). In addition, fuel cells operate at a constant temperature, and the heat from the electrochemical reaction is available for cogeneration applications. Table summarizes the impact of the major constituents within fuel gases on the various fuel cells. The reader is referred to Sections 3 through 7 for detail on trace contaminants.

Another key feature of fuel cells is that their performance and cost are less dependent on scale than other power technologies. Small fuel cell plants operate nearly as efficiently as large ones, with equally low emissions, and comparable cost.[1] This opens up applications for fuel cells where conventional power technologies are not practical. In addition, fuel cell systems can be relatively quiet generators.

To date, the major impediments to fuel cell commercialization have been insufficient longevity and reliability, unacceptably high cost, and lack of familiarity of markets with fuel cells. For fuel cells that require special fuels (such as hydrogen) the lack of a fuel infrastructure also limits commercialization.

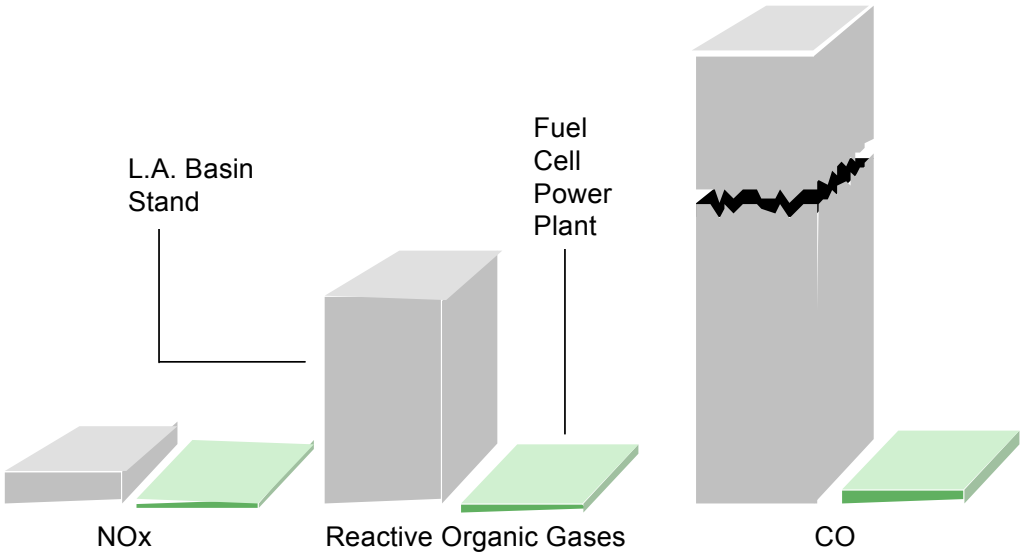

Figure 1-4 Relative Emissions of PAFC Fuel Cell Power Plants Compared to Stringent Los Angeles Basin Requirements

[1]. The fuel processor efficiency is size dependent; therefore, small fuel cell power plants using externally reformed hydrocarbon fuels would have a lower overall system efficiency.

Other characteristics that fuel cells and fuel cell plants offer are:

- Direct energy conversion (no combustion)
- No moving parts in the energy converter
- Quiet
- Demonstrated high availability of lower temperature units
- Siting ability
- Fuel flexibility
- Demonstrated endurance/reliability of lower temperature units
- Good performance at off-design load operation
- Modular installations to match load and increase reliability
- Remote/unattended operation
- Size flexibility
- Rapid load following capability

General negative features of fuel cells include

- Market entry cost high; N^{th} cost goals not demonstrated.
- Endurance/reliability of higher temperature units not demonstrated.
- Unfamiliar technology to the power industry.
- No infrastructure.

Table 1-2 Summary of Major Fuel Constituents Impact on PEFC, AFC, PAFC, MCFC, and SOFC

Gas Species	PEFC	AFC	PAFC	MCFC	SOFC
H_2	Fuel	Fuel	Fuel	Fuel	Fuel
CO	Poison (reversible) (50 ppm per stack)	Poison	Poison (<0.5%)	Fuel[a]	Fuel
CH_4	Diluent	Poison	Diluent	Diluent[b]	Fuel[a]
CO_2 & H_2O	Diluent	Poison	Diluent	Diluent	Diluent
S as (H_2S & COS)	No Studies to date (11)	Poison	Poison (<50 ppm)	Poison (<0.5 ppm)	Poison (<1.0 ppm)

[a] In reality, CO, with H_2O, shifts to H_2 and CO_2, and CH_4, with H_2O, reforms to H_2 and CO faster than reacting as a fuel at the electrode.

[b] A fuel in the internal reforming MCFC.

1.7 Advantages/Disadvantages

The fuel cell types addressed in this handbook have significantly different operating regimes. As a result, their materials of construction, fabrication techniques, and system requirements differ. These distinctions result in individual advantages and disadvantages that govern the potential of

the various cells to be used for different applications. Developers use the advantages of fuel cells to identify early applications and address research and development issues to expand applications (see Sections 3 through 7).

1.8 Applications, Demonstrations, and Status

The characteristics, advantages, and disadvantages summarized in the previous section form the basis for selection of the candidate fuel cell types to respond to a variety of application needs. The major applications for fuel cells are as stationary electric power plants, including cogeneration units; as motive power for vehicles, and as on-board electric power for space vehicles or other closed environments. Derivative applications will be summarized.

1.8.1 Stationary Electric Power

One characteristic of fuel cell systems is that their efficiency is nearly unaffected by size. This means that small, relatively high efficient power plants can be developed, thus avoiding the higher cost exposure associated with large plant development. As a result, initial stationary plant development has been focused on several hundred kW to low MW capacity plants. Smaller plants (several hundred kW to 1 to 2 MW) can be sited at the user's facility and are suited for cogeneration operation, that is, the plants produce electricity and thermal energy. Larger, dispersed plants (1 to 10 MW) are likely to be used for distributed generation. The plants are fueled primarily with natural gas. Once these plants are commercialized and price improvements materialize, fuel cells will be considered for large base-load plants because of their high efficiency. The base-load plants could be fueled by natural gas or coal. The fuel product from a coal gasifier, once cleaned, is compatible for use with fuel cells. Systems integration studies show that high temperature fuel cells closely match coal gasifier operation.

Operation of complete, self-contained, stationary plants continues to be demonstrated using PEFC, AFC, PAFC, MCFC, and SOFC technology. Demonstrations of these technologies that occurred before 2000 were addressed in previous editions of the Fuel Cell Handbook and in the literature of the period. U.S. manufacturer experience with these various fuel cell technologies has produced timely information. A case in point is the 200 kW PAFC on-site plant, the PC-25, that was the first to enter the commercial market (see Figure 1-5).

Figure 1-5 PC-25 Fuel Cell

The plant was developed by UTC Fuel Cells, a division of United Technologies Corporation (UTC). The plants are built by UTC Fuel Cells. The Toshiba Corporation of Japan and Ansaldo SpA of Italy are partners with UTC Fuel Cells. The on-site plant is proving to be an economic and beneficial addition to the operating systems of commercial buildings and industrial facilities because it is superior to conventional technologies in reliability, efficiency, environmental impact, and ease of siting. Because the PC-25 is the first available commercial unit, it serves as a model for fuel cell application. Because of its attributes, the PC-25 is being installed in various applications, such as hospitals, hotels, large office buildings, manufacturing sites, wastewater treatment plants, and institutions to meet the following requirements:

- On-site energy
- Continuous power – backup
- Uninterrupted power supply
- Premium power quality
- Independent power source

Characteristics of the plant are as follows:

- Power Capacity 0 to 200 kW with natural gas fuel (-30 to 45 °C, up to 1500 m)
- Voltage and Phasing 480/277 volts at 60 Hz ; 400/230 volts at 50 Hz

• Thermal Energy (Cogeneration)	740,000 kJ/hour at 60°C (700,000 Btu/hour heat at 140 °F); module provides 369,000 kJ/hour at 120°C (350,000Btu/hour at 250 °F) and 369,000 kJ/hour at 60 °C
• Electric Connection	Grid-connected for on-line service and grid-independent for on-site premium service
• Power Factor	Adjustable between 0.85 to 1.0
• Transient Overload	None
• Grid Voltage Unbalance	1 percent
• Grid Frequency Range	+/-3 percent
• Voltage Harmonic Limits	<3 percent
• Plant Dimensions	3 m (10 ft) wide by 3 m (10 ft) high by 5.5 m (18 ft) long, not including a small fan cooling module (5)
• Plant Weight	17,230 kg (38,000 lb)

UTC Fuel Cells: Results from the operating units as of August, 2002 are as follows: total fleet operation stands at more than 5.3 million hours. The plants achieve 40 percent LHV electric efficiency, and overall use of the fuel energy approaches 80 percent for cogeneration applications (6). Operations confirm that rejected heat from the initial PAFC plants can be used for heating water, space heating, and low pressure steam. One plant has completed over 50,000 hours of operation, and a number of plants have operated over 40,000 hours (6). Fourteen additional plants have operated over 35,000 hours. The longest continuous run stands at 9,500 hours for a unit purchased by Tokyo Gas for use in a Japanese office building (9). This plant ended its duration record because it had to be shut down because of mandated maintenance. It is estimated at this time that cell stacks can achieve a life of 5 to 7 years. The fleet has attained an average of over 95 percent availability. The latest model, the PC-25C, is expected to achieve over 96 percent. The plants have operated on natural gas, propane, butane, landfill gas (10,11), hydrogen (12), and gas from anaerobic digestors (13). Emissions are so low (see Figure 1-4) that the plant is exempt from air permitting in the South Coast and Bay Area (California) Air Quality Management Districts, which have the most stringent limits in the U.S. The sound pressure level is 62 dBA at 9 meters (30 feet) from the unit. The PC-25 has been subjected to ambient conditions varying from -32 °C to +49 °C and altitudes from sea level to 1600 meters (~1 mile). Impressive ramp rates result from the solid state electronics. The PC-25 can be ramped at 10 kW/sec up or down in the grid connected mode. The ramp rate for the grid independent mode is idle to full power in ~one cycle or essentially one-step instantaneous from idle to 200 kW. Following the initial ramp to full power, the unit can adjust at an 80 kW/sec ramp up or down in one cycle.

The fuel cell stacks are made and assembled into units at an 80,000 ft^2 facility located in South Windsor, Connecticut, U.S. Low cost/high volume production depends on directly insertable sub-assemblies as complete units and highly automatic processes such as robotic component handling and assembly. The stack assembly is grouped in a modified spoke arrangement to allow for individual manufacturing requirements of each of the cell components while bringing them in a continuous flow to a central stacking elevator (14).

Ballard Generation Systems: Ballard Generation Systems, a subsidiary of Ballard Power Systems, produces a PEFC stationary on-site plant. It has these characteristics:

- Power Capacity 250 kW with natural gas fuel
- Electric Efficiency 40% LHV
- Thermal Energy 854,600 kJ/hour at 74 °C (810,000 Btu/hour at 165 °F)
- Plant Dimensions 2.4 m (8 ft) wide by 2.4 m (8 ft) high by 5.7 m (18.5 ft) long
- Plant Weight 12,100 kg (26,700 lb)

Ballard completed 10- and 60-kW engineering prototype stationary fuel cell power generators in 2001. Ballard, Shell Hydrogen, and Westcoast Energy established a private capital joint venture to help build early stage fuel cell systems. Ballard launched the Nexa™, a portable 1.2 kW power module, in September 2001. Ballard is also selling carbon fiber products for gas diffusion layers for proton exchange membrane fuel cells. Highlights of Ballard's fuel cell sales are shown below.

FuelCell Energy (FCE): FCE reached 50 MW manufacturing capacity and plans to expand its manufacturing capacity to 400 MW in 2004. The focus of the utility demonstrations and FCE's fuel cell development program is the commercialization of 300 kilowatt, 1.5 megawatt, and 3 megawatt MCFC plants.

- Power Capacity 3.0 MW net AC
- Electric efficiency 57% (LHV) on natural gas
- Voltage and Phasing Voltage is site dependent, 3 phase 60 Hz
- Thermal energy ~4.2 million kJ/hour (~4 million Btu/hour)
- Availability 95%

Siemens Westinghouse Power Corporation (SWPC): The Siemens Westinghouse SOFC is planning two major product lines with a series of product designs in each line. The first product will be a 250 kW cogeneration system operating at atmospheric pressure. This will be followed by a pressurized SOFC/gas turbine hybrid of approximately 0.5 MW. After the initial production, larger systems are expected as well. Also, a system capable of separating CO_2 from the exhaust is planned as an eventual option to other products.

The commercialization plan is focused on an initial offering of a hybrid fuel cell/gas turbine plant. The fuel cell module replaces the combustion chamber of the gas turbine engine. Figure 1-6 shows the benefit behind this combined plant approach. Additional details are provided in Section 7. As a result of the hybrid approach, the 1 MW early commercial unit is expected to attain ~60% efficiency LHV when operating on natural gas.

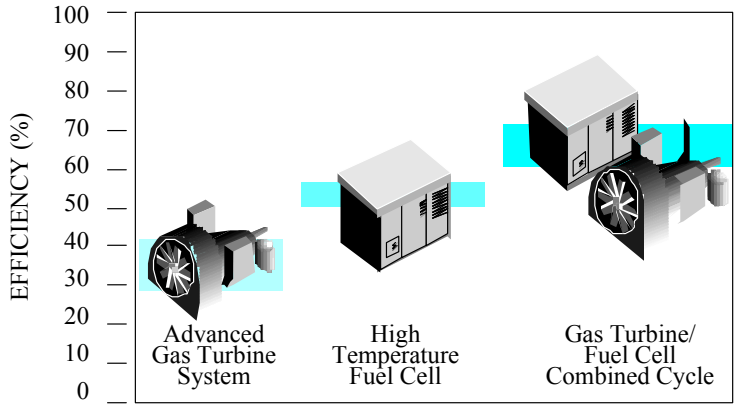

Figure 1-6 Combining the SOFC with a Gas Turbine Engine to Improve Efficiency

Siemens Westinghouse is planning a number of tests on power plants that are prototypes of future products. All systems employ the tubular SOFC concept and most are combined with gas turbines in a hybrid configuration. Capacities of these systems are 250 kilowatts atmospheric, 300 kilowatt class hybrid, and 1 megawatt class hybrid. They are to operate at various sites in the U.S., Canada, and Europe.

An eventual market for fuel cells is the large (100 to 300 MW), base-loaded, stationary plants operating on coal or natural gas. Another related, early opportunity may be in re-powering older, existing plants with high-temperature fuel cells (19). MCFCs and SOFCs coupled with coal gasifiers have the best attributes to compete for the large, base load market. The rejected heat from the fuel cell system can be used to produce steam for the existing plant's turbines. Studies showing the potential of high-temperature fuel cells for plants of this size have been performed (see Section 8). These plants are expected to attain from 50 to 60% efficiency based on the HHV of the fuel. Coal gasifiers produce a fuel gas product requiring cleaning to the stringent requirements of the fuel cells' electrochemical environment, a costly process. The trend of environmental regulations has also been towards more stringent cleanup. If this trend continues, coal-fired technologies will be subject to increased cleanup costs that may worsen process economics. This will improve the competitive position of plants based on the fuel cell approach. Fuel cell systems will emit less than target emissions limits. U.S. developers have begun investigating the viability of coal gas fuel to MCFCs and SOFCs (20,21,22). An FCE 20 kW MCFC stack was tested for a total of 4,000 hours, of which 3,900 hours was conducted at the Plaquemine, LA, site on coal gas as well as pipeline gas. The test included 1,500 hours of operation using 9,142 kJ/m^3 syngas from a slip stream of a 2,180 tonne/day Destec entrained gasifier. The fuel processing system incorporated cold gas cleanup for bulk removal of H_2S and other contaminants, allowing the 21 kW MCFC stack to demonstrate that the FCE technology can operate on either natural gas or coal gas.

A series of standards is being developed to facilitate the application of stationary fuel cell technology power plants. Standard development activities presently underway are

- Fuel Cell Power Systems ANSI/CSA America FC1-2004 (published)

- Stationary Fuel Cell Power Systems -Safety — IEC TC 105 Working Group #3
- Stationary Fuel Cell Power Systems -Installation — IEC TC 105 Working Group #5
- Interconnecting Distributed Resources — IEEE P1547.1, P1547.2, P1547.3, P1547.4
- Test Method for the Performance of Stationary Fuel Cell Power Plants — IEC TC 105 Working Group #4

1.8.2 Distributed Generation

Distributed generation involves small, modular power systems that are sited at or near their point of use. The typical system is less than 30 MW, used for generation or storage, and extremely clean. Examples of technologies used in distributed generation include gas turbines and reciprocating engines, biomass-based generators, solar power and photovoltaic systems, fuel cells, wind turbines, micro-turbines, and flywheel storage devices. See Table 1-3 for size and efficiencies of selected systems.

Table 1-3 Attributes of Selected Distributed Generation Systems

Type	Size	Efficiency, %
Reciprocating Engines	50 kW – 6 MW	33 – 37
Micro turbines	10 kW – 300 kW	20 – 30
Phosphoric Acid Fuel Cell (PAFC)	50 kW – 1 MW	40
Solid Oxide Fuel Cell (SOFC)	5 kW – 3 MW	45 – 65
Proton Exchange Membrane Fuel Cell (PEM)	<1 kW – 1 MW	34 – 36
Photovoltaics (PV)	1 kW – 1 MW	NA
Wind Turbines	150 kW – 500 kW	NA
Hybrid Renewable	<1 kW – 1 MW	40 – 50

The market for distributed generation is aimed at customers dependent on reliable energy, such as hospitals, manufacturing plants, grocery stores, restaurants, and banking facilities. There is currently over 15 GW of distributed power generation operating in the U.S. Over the next decade, the domestic market for distributed generation, in terms of installed capacity to meet the demand, is estimated to be 5-6 GW per year. The projected global market capacity increases are estimated to be 20 GW per year (23). Several factors have played a role in the rise in demand for distributed generation. Utility restructuring is one of the factors. Energy suppliers must now take on the financial risk of capacity additions. This leads to less capital-intensive projects and shorter construction periods. Also, energy suppliers are increasing capacity factors on existing plants rather than installing new capacity, which places pressure on reserve margins. This increases the possibility of forced outages, thereby increasing the concern for reliable service. There is also a demand for capacity additions that offer high efficiency and use of renewables as the pressure for enhanced environmental performance increases (23).

There are many applications for distributed generation systems. They include:

- Peak shaving - Power costs fluctuate hour by hour depending upon demand and generation, therefore customers would select to use distributed generation during relatively high-cost, on-peak periods.
- Combined heat and power (CHP) (Cogeneration) –The thermal energy created while converting fuel to electricity would be utilized for heat in addition to electricity in remote areas, and electricity and heat for sites that have a 24 hour thermal/electric demand.
- Grid support – Strategic placement of distributed generation can provide system benefits and preclude the need for expensive upgrades and provide electricity in regions where small increments of new baseload capacity is needed.
- Standby power – Power during system outages is provided by a distributed generation system until service can be restored. This is used for customers that require reliable back-up power for health or safety reasons, companies with voltage-sensitive equipment, or where outage costs are unacceptably high.
- Remote/Standalone – The user is isolated from the grid either by choice or circumstance. The purpose is for remote applications and mobile units to supply electricity where needed.

Distributed generation systems have small footprints, are modular and mobile making them very flexible in use. The systems provide benefits at the customer level and the supplier level, as well as the national level. Benefits to the customer include high power quality, improved reliability, and flexibility to react to electricity price spikes. Supplier benefits include avoiding investments in transmission and distribution (T&D) capacity upgrades by locating power where it is most needed and opening new markets in remote areas. At the national level, the market for distributed generation establishes a new industry, boosting the economy. The improved efficiencies also reduce greenhouse gas emissions.

However, a number of barriers and obstacles must be overcome before distributed generation can become a mainstream service. These barriers include technical, economic, institutional, and regulatory issues. Many of the proposed technologies have not yet entered the market, and will need to meet performance and pricing targets before entry. Questions have also risen on requirements for connection to the grid. Lack of standardized procedures creates delays and discourages customer-owned projects. Siting, permitting, and environmental regulations can also delay and increase the costs of distributed generation projects.

In 1998, the Department of Energy created a Distributed Power Program to focus on market barriers and other issues that have prohibited the growth of distributed generation systems. Under the leadership of the National Renewable Energy Laboratory (NREL), a collaboration of national laboratories and industry partners have been creating new standards and are identifying and removing regulatory barriers. The goals of the program include 1) strategic research, 2) system integration, and 3) mitigation of regulatory and institutional barriers (24).

Fuel cells, one of the emerging technologies in distributed generation, have been hindered by high initial costs. However, costs are expected to decline as manufacturing capacity and capability increase and designs and integration improve. The fuel cell systems offer many potential benefits as a distributed generation system. They are small and modular, and capital

costs are relatively insensitive to scale. This makes them ideal candidates for diverse applications where they can be matched to meet specific load requirements. The systems are unobtrusive, with very low noise levels and negligible air emissions. These qualities enable them to be placed close to the source of power demand. Fuel cells also offer higher efficiencies than conventional plants. The efficiencies can be enhanced by using the quality waste heat derived from the fuel cell reactions for combined heat and power and combined-cycle applications.

Phosphoric acid fuel cells have successfully been commercialized. Second generation fuel cells include solid oxide fuel cells and molten carbonate fuel cells. Research is ongoing in areas such as fuel options and new ceramic materials. Different manufacturing techniques are also being sought to help reduce capital costs. Proton exchange membrane fuel cells are still in the development and testing phase.

1.8.3 Vehicle Motive Power

Since the late 1980s, there has been a strong push to develop fuel cells for use in light-duty and heavy-duty vehicle propulsion. A major drive for this development is the need for clean, efficient cars, trucks, and buses that operate on conventional fuels (gasoline, diesel), as well as renewable and alternative fuels (hydrogen, methanol, ethanol, natural gas, and other hydrocarbons). With hydrogen as the on-board fuel, these would be zero-emission vehicles. With on-board fuels other than hydrogen, the fuel cell systems would use an appropriate fuel processor to convert the fuel to hydrogen, yielding vehicle power trains with very low acid gas emissions and high efficiencies. Further, such vehicles offer the advantages of electric drive and low maintenance because of few moving parts. This development is being sponsored by various governments in North America, Europe, and Japan, as well as by major automobile manufacturers worldwide. As of May 1998, several fuel cell-powered cars, vans, and buses operating on hydrogen and methanol have been demonstrated.

In the early 1970s, K. Kordesch modified a 1961 Austin A-40 two-door, four-passenger sedan to an air-hydrogen fuel cell/battery hybrid car (23). This vehicle used a 6-kW alkaline fuel cell in conjunction with lead acid batteries, and operated on hydrogen carried in compressed gas cylinders mounted on the roof. The car was operated on public roads for three years and about 21,000 km.

In 1994 and 1995, H-Power (Belleville, New Jersey) headed a team that built three PAFC/battery hybrid transit buses (24,25). These 9 meter (30 foot), 25 seat (with space for two wheel chairs) buses used a 50 kW fuel cell and a 100 kW, 180 amp-hour nickel cadmium battery.

The major activity in transportation fuel cell development has focused on the polymer electrolyte fuel cell (PEFC). In 1993, Ballard Power Systems (Burnaby, British Columbia, Canada) demonstrated a 10 m (32 foot) light-duty transit bus with a 120 kW fuel cell system, followed by a 200 kW, 12 meter (40 foot) heavy-duty transit bus in 1995 (26). These buses use no traction batteries. They operate on compressed hydrogen as the on-board fuel. In 1997, Ballard provided 205 kW (275 HP) PEFC units for a small fleet of hydrogen-fueled, full-size transit buses for demonstrations in Chicago, Illinois, and Vancouver, British Columbia. Working in collaboration with Ballard, Daimler-Benz built a series of PEFC-powered vehicles, ranging from passenger

cars to buses (27). The first such vehicles were hydrogen-fueled. A methanol-fueled PEFC A-class car unveiled by Daimler-Benz in 1997 had a 640 km (400 mile) range. Plans were to offer a commercial vehicle by 2004. A hydrogen-fueled (metal hydride for hydrogen storage), fuel cell/battery hybrid passenger car was built by Toyota in 1996, followed in 1997 by a methanol-fueled car built on the same (RAV4) platform (28).

In February 2002, UTC Fuel Cells and Nissan signed an agreement to develop fuel cells and fuel cell components for vehicles. Renault, Nissan's alliance partner, is also participating in the development projects. UTC Fuel Cells will provide proprietary ambient-pressure proton exchange membrane fuel cell technology.

Ballard's fuel cell engine powered DaimlerChrysler's NECAR 5 fuel cell vehicle in a 13-day, 3,000-mile endurance test across the United States. The drive provided Ballard and DaimlerChrysler with testing experience in a variety of conditions.

Toyota Motor Corp. and Honda Motor Co. announced they would advance their initial vehicle introduction plans for fuel cell vehicles to late in 2002 from 2003. Honda achieved a significant milestone for its product launch by receiving both CARB and EPA certification of its zero emission FCX-V4 automobile. This was the first vehicle to receive such certification. Ballard's fuel cell powered this Honda vehicle.

Other major automobile manufacturers, including General Motors, Volkswagen, Volvo, Chrysler, Nissan, and Ford, have also announced plans to build prototype polymer electrolyte fuel cell vehicles operating on hydrogen, methanol, or gasoline (29). IFC and Plug Power in the U.S., and Ballard Power Systems of Canada (15), are involved in separate programs to build 50 to 100 kW fuel cell systems for vehicle motive power. Other fuel cell manufacturers are involved in similar vehicle programs. Some are developing fuel cell-powered utility vehicles, golf carts, etc. (30,31).

1.8.4 Space and Other Closed Environment Power

The application of fuel cells in the space program (1 kW PEFC in the Gemini program and 1.5 kW AFC in the Apollo program) was demonstrated in the 1960s. More recently, three 12 kW AFC units were used for at least 87 missions with 65,000 hours flight time in the Space Shuttle Orbiter. In these space applications, the fuel cells used pure reactant gases. IFC produced a H_2/O_2 30 kW unit for the Navy's Lockheed Deep Quest vehicle. It operates at depths of 1500 meters (5000 feet). Ballard Power Systems has produced an 80 kW PEFC fuel cell unit for submarine use (methanol fueled) and for portable power systems.

1.8.5 Auxiliary Power Systems

In addition to high-profile fuel cell applications such as automotive propulsion and distributed power generation, the use of fuel cells as auxiliary power units (APUs) for vehicles has received considerable attention (see Figure 1-7). APU applications may be an attractive market because they offer a true mass-market opportunity that does not require the challenging performance and low cost required for propulsion systems for vehicles. In this section, a discussion of the technical performance requirements for such fuel cell APUs, as well as the status of technology and implications for fuel cell system configuration and cost is given.

Participants	Application	Size range	Fuel /Fuel Cell type	Nature of Activity
BMW, International Fuel Cells (a)	passenger car, BMW 7-series	5kW net	Hydrogen, Atmospheric PEM	Demonstration
Ballard, Daimler-Chrysler (b)	Class 8 Freightliner heavy-duty Century Class S/T truck cab	1.4 kW net for 8000 BTU/h A/C unit	Hydrogen, PEM	Demonstration
BMW, Delphi, Global Thermoelectric (c)	passenger car	1-5kW net	Gasoline, SOFC	Technology development program

(a) "Fuel Cell Auxiliary Power Unit – Innovation for the Electric Supply of Passenger Cars?" J. Tachtler et al. BMW Group, SAE 2000-01-0374, Society of Automotive Engineers, 2000.
(b) "Freightliner unveils prototype fuel cell to power cab amenities", O. B. Patten, Roadstaronline.com news, July 20, 2000.
(c) Company press releases, 1999.

Figure 1-7 Overview of Fuel Cell Activities Aimed at APU Applications

Auxiliary power units are devices that provide all or part of the non-propulsion power for vehicles. Such units are already in widespread use in a range of vehicle types and for a variety of applications, in which they provide a number of potential benefits (see Figure 1-8). Although each of these applications could provide attractive future markets for fuel cells, this section will focus on application to on-road vehicles (specifically trucks).

Vehicles Types	Loads Serviced	Potential Benefits
• Heavy-duty & utility trucks • Airplanes • Trains • Yachts & Ships • Recreational vehicles • Automobiles & light trucks (not commercial yet)	• Space conditioning • Refrigeration • Lighting and other cabin amenities • Communication and information equipment • Entertainment (TV, radio)	• Can operate when main engine unavailable • Reduce emissions and noise while parked • Extend life of main engine • Improve power generation efficiency when parked

Figure 1-8 Overview of APU Applications

In 1997, the Office of Naval Research initiated an advanced development program to demonstrate a ship service fuel cell power generation module. The ship service generator supplies the electrical power requirements of the ship. This program would provide the basis for a new fuel cell-based design as an attractive option for future Navy surface ships. This program would provide the Navy with a ship service that is more efficient, and incorporates a distributed power system that would remain operating even if the ship's engine is destroyed.

Fuel cells can serve as a generator, battery charger, battery replacements and heat supply. They can adapt to most environments, even locations in Arctic and Antarctic regions. One effort, in collaboration with the Army Research Office, has demonstrated a prototype fuel cell designed to replace a popular military standard battery. The target application is the Army's BA-5590 primary (i.e., use-once-and-dispose) lithium battery. The Army purchases approximately 350,000 of these batteries every year at a cost of approximately $100 per battery, including almost $30

per battery for disposal. Fuel cells, on the other hand, are not thrown away after each use but can be re-used hundreds of times. Mission weight savings of factors of 10 or more are projected. The prototype fuel cell, which has the same size and delivers the same power as a battery, has been tested in all orientations and under simulated adverse weather conditions, and was enthusiastically received by Army senior management.

System Performance Requirements

A key reason for interest in fuel cell APU applications is that there may be a good fit between APU requirements and fuel cell system characteristics. Fuel cells are efficient and quiet, and APUs do not have the load following requirements and physical size and weight constraints associated with propulsion applications. However, in order to understand the system requirements for fuel cell APUs, it is critical to understand the required functionality (refer to Figure 1-8) as well as competing technologies. To provide the functionality of interest, and to be competitive with internal combustion engine (ICE) driven APUs, fuel cell APUs must meet various requirements; an overview is provided in Figure 1-9.

Key Parameter	*Typical Requirements*	*Expected fuel cell performance*
Power output	12 – 42 V DC is acceptable for most applications, 110 / 220 V AC may be desirable for powering power tools etc.	DC power output simplifies the power conditioning and control for fuel cells
System Capacity	1 – 5 kW for light duty vehicles and truck cabins up to 15 kW for truck refrigeration	Fits expected range for PEFCs and probably also advanced SOFCs
System Efficiency	More than 15-25% based on LHV	Efficiency target should be achievable, even in smallest capacity range
Operating life and reliability	Greater than about 5,000 hours stack life, with regular service intervals less than once every 1,000 hours	Insufficient data available to assess whether this is a challenge or not

Figure 1-9 Overview of typical system requirements

Fuel cell APUs will likely have to operate on gasoline, and for trucks preferably on diesel fuel, in order to match the infrastructure available, and preferably to be able to share on-board storage tanks with the main engine. The small amount of fuel involved in fueling APUs would likely not justify the establishment of a specialized infrastructure (e.g. a hydrogen infrastructure) for APUs alone. Similarly, fuel cell APUs should be water self-sufficient, as the need to carry water for the APU would be a major inconvenience to the operator, and would require additional space and associated equipment.

In addition to the requirement for stationary operation, fuel cell APUs must be able to provide power rapidly after start-up, and must be able to follow loads. While the use of batteries to

accomplish this is almost a given, a system start-up time of about ten minutes or less will likely be required to arrive at a reasonable overall package.

Finally, fuel cell APUs are quiet and clean. These attributes may well be the key competitive advantages that fuel cell APUs have over conventional APUs, and hence their performance may more than match that of internal combustion engines' APUs.

Technology Status

Active technology development efforts in both PEFC and planar SOFC technology, driven primarily by interest in distributed generation and automotive propulsion markets, have achieved significant progress. For distributed power applications, refined and even early commercial prototypes are being constructed. However, in the case of planar SOFC a distinction must be made between different types of SOFC technologies. Neither the tubular nor the electrolyte-supported SOFC technology is suitable for APU applications due to their very high operating temperature, large size and heavy weight. Only the electrode-supported planar SOFC technology may be applicable to APU applications. Since it has only been developed over the past decade, as opposed to several decades for PEFC and other SOFC technologies, it is not developed as far, although it appears to be catching up quickly (See Figure 1-10).

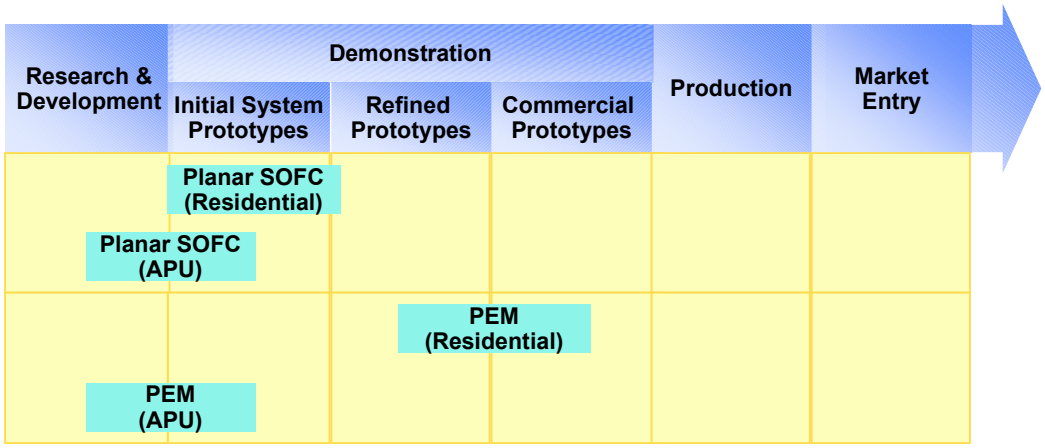

Figure 1-10 Stage of development for fuel cells for APU applications

Fuel cell APU applications could benefit significantly from the development of distributed generation systems, especially from residential-scale systems, because of the similarity in size and duty cycle. However, distributed generation systems are designed mostly for operation on natural gas, and do not face as stringent weight and volume requirements as APU applications. As a result, fuel cell APUs are in the early system prototype stage.

Several developers, including Nuvera, Honeywell, and Plug Power are actively developing residential PEFC power systems. Most of the PEFC system technology can be adapted for APU application, except that a fuel processor capable of handling transportation fuels is required. However, most of the players in the residential PEFC field are also engaged in developing PEFC

systems for automotive propulsion applications, and are targeting the ability to use transportation fuels for PEFC systems.

Relatively few developers of SOFC technology have paid attention to non-stationary markets. All are focused on small-to medium-sized distributed generation and on-site generation markets. Only Global Thermoelectric (Calgary, Canada) has been active in the application of its technology to APUs. A detailed conceptual design and cost estimate of a 5-kW SOFC-based truck APU concluded that, provided continued improvement in several technology areas, planar SOFCs could ultimately become a realistic option for this mass-market application.

System Configuration and Technology Issues

Based on system requirements discussed above, fuel cell APUs will consist of a fuel processor, a stack system and the balance of plant. Figure 1-11 lists the components required in SOFC and PEFC systems. The components needed in a PEFC system for APU applications are similar to those needed in residential power. The main issue for components of PEFC systems is to minimize or eliminate the use of external supplied water. For both PEFC and SOFC systems, start-up batteries (either existing or dedicated units) will be needed, since external electric power is not available.

Detailed cost and design studies for both PEFC and SOFC systems at sizes ranging from 5kW to 1 MW point to the fundamental differences between PEFC and SOFC technology that impact the system design and, by implication, the cost structure. These differences will be discussed in the following paragraphs.

The main components in a SOFC APU are the fuel cell stack, the fuel processor, and the thermal management system. In addition, there are several balance of plant components, which are listed in Figure 11. The relatively simple reformer design is possible because the SOFC stack operates at high temperatures (around 800°C) and is capable of both carbon monoxide and certain hydrocarbons as fuel. Since both the anode and cathode exhaust at temperatures of 600-850°C, high temperature recuperators are required to maintain system efficiency. A recuperator consists of expensive materials (high temperature reducing and oxidizing atmosphere), making it an expensive component in the system. However, if hydrocarbons are converted inside the stack, this leads to a less exothermic overall reaction so that the stack cooling requirements are reduced.

Further system simplification would occur if a sulfur-free fuel was used or if the fuel cell were sulfur tolerant; in that case, the fuel could be provided directly from the reformer to the fuel cell. In order to minimize system volume, (and minimize the associated system weight and start-up time) integration of the system components is a key design issue. By recycling the entire anode tailgas to provide steam, a water management system can be avoided, though a hot gas recirculation system is required.

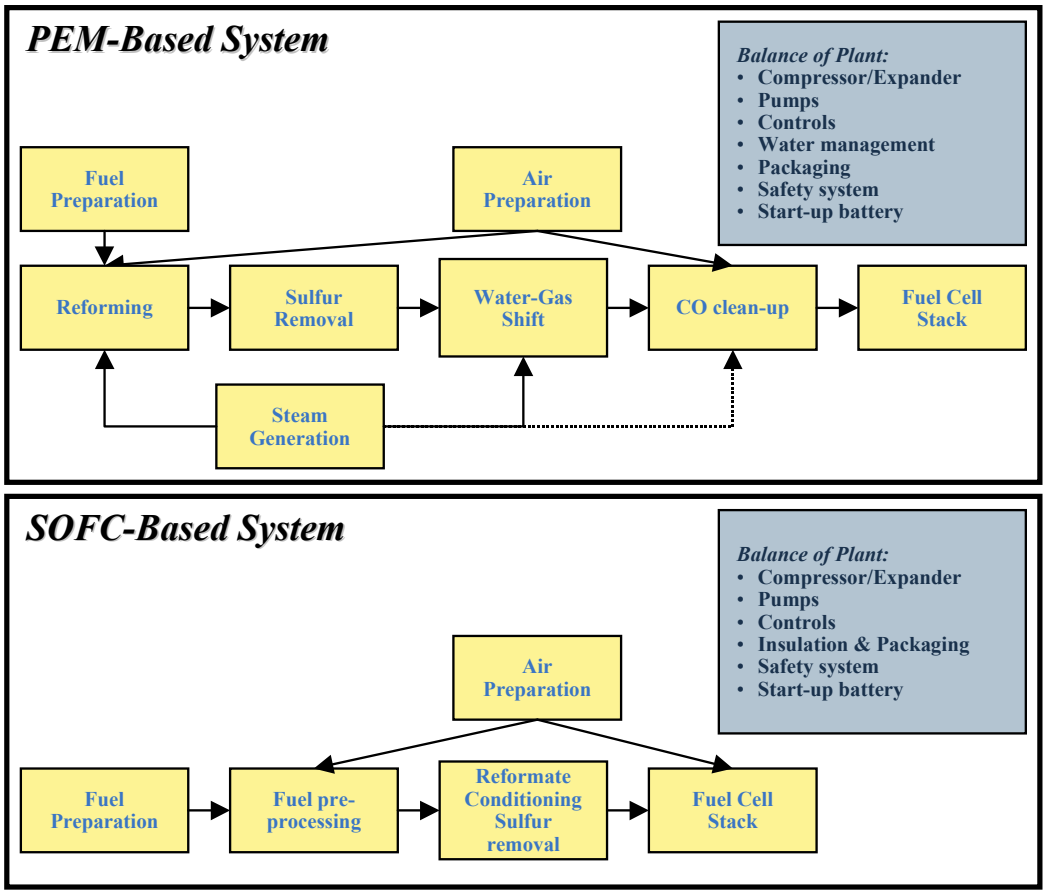

Figure 1-11. Overview of subsystems and components for SOFC and PEFC systems

Figure 1-12 shows a simplified layout for an SOFC-based APU. The air for reformer operation and cathode requirements is compressed and then split between the unit operations. The external water supply shown in Figure 1-12 will most likely not be needed; the anode recycle stream provides water. Unreacted anode tail gas is recuperated in a tail gas burner. Additional energy is available in a SOFC system from enthalpy recovery from tail gas effluent streams that are typically 400-600 °C. Current thinking is that reformers for transportation fuel based SOFC APUs will be of the exothermic type (i.e. partial oxidation or autothermal reforming), as no viable steam reformers are available for such fuels.

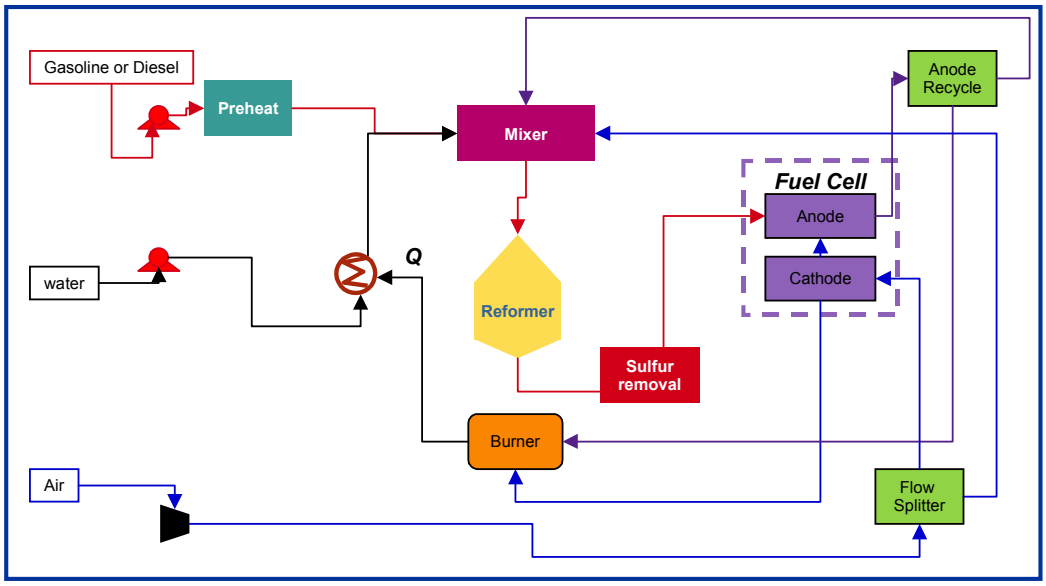

Figure 1-12. Simplified process flow diagram of pre-reformer/SOFC system

Due to the operating requirements of PEFC stack technology, shift reactors and a carbon monoxide removal step are required to produce reformate of sufficient quality. Similarly, the stack operating temperature and its humidity requirements require a water management system as well as radiators for heat rejection. Some developers use pressurized systems to benefit from higher reactant partial pressures on both anode and cathode. Fuel processing for PEFC APU systems is identical to that needed in residential power or propulsion applications. The additional issue for PEFC is the minimization of steam needed for the fuel processor system. Since an APU is a mobile and/or remote unit, the need for external sources of water should be minimized. The reformate stream is further diluted by additional steam, if that water is not removed prior to the fuel cell stack.

Another design integration issue in PEFC systems is water management to hydrate the electrolyte and provide the necessary steam for reforming and water-gas shift operations. Additional steam may be required for the CO clean-up device. Some reformate-based PEFC systems are run under pressure to increase the partial pressure of reactants for the PEFC anode and cathode, increasing efficiency. Pressure operation also aids in heat integration for the internal generation of steam at pressures greater than atmospheric (i.e. steam generated at temperatures greater than 100°C). PEFC system integration involves combining a reformer (either exothermic or endothermic at ~850-1000 °C), shift reactors (exothermic, 150-500 °C), CO-cleanup (primarily exothermic, 50-200 °C), and the fuel cell stack (exothermic, 80 °C). Each reaction zone operates at a significantly different temperature, thus providing a challenge for system integration and heat rejection. To alleviate some of these drawbacks and further reduce the cost of the PEFC systems, developers are investigating the possibility of using higher temperature membranes (e.g. operating slightly above 100 °C). This would increase the carbon monoxide tolerance, potentially simplifying the fuel processor design, and simplify the heat rejection.

The load requirements for auxiliary power applications require smaller fuel cell stacks. The heat losses for a SOFC stack operating at a smaller power duty are a larger proportion of the gross rating than in a stationary power application. Insulation required for specified skin temperature requirements could conceivably result in a large fraction of the total system volume. Integration of the high temperature components is important in order to reduce the system volume and insulation requirements. SOFC APU systems will require inexpensive, high performance insulation materials to decrease both system volume and cost.

Cost Considerations

As for any new class of product, total cost of ownership and operation of fuel cells will be a critical factor in their commercialization, along with the offered functionality and performance. This total cost of ownership typically has several components for power systems such as fuel cells. These components include fuel cost, other operating costs such as maintenance cost, and the first cost of the equipment. This first cost has a significant impact on fuel cells' competitiveness.

The main component of a fuel cell's first cost is the manufacturing cost, which is strongly related to the physical configuration and embodiment of the system, as well as to the manufacturing methods used. System configuration and design, in turn, are directly related to the desired system functionality and performance, while the manufacturing methods are strongly linked to the anticipated production volume.

Arthur D. Little carried out cost structure studies for a variety of fuel cell technologies for a wide range of applications, including SOFC tubular, planar, and PEFC technologies. Because phenomena at many levels of abstraction have a significant impact on performance and cost, they developed a multi-level system performance and cost modeling approach (see Figure 1-13). At the most elementary level, it includes fundamental chemical reaction/reactor models for the fuel processor and fuel cell as one-dimensional systems.

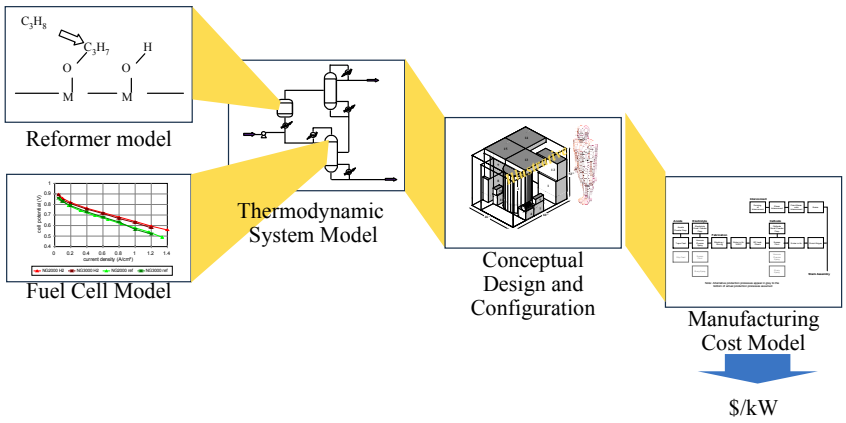

Figure 1-13 Multilevel system modeling approach

Each detailed sub-model feeds into the thermodynamic system model, and provides sizing information directly to the conceptual design. The thermodynamic system model provides a

technical hub for the multi-level approach. It provides inputs on the required flow rates and heat duties in the system. Sizing information, together with information from the thermodynamic model, then flows to the conceptual design.

SOFC Cost Structure

The main difference in SOFC stack cost compared to PEFC cost relates to the simpler system configuration of the SOFC system. This is mainly due to the fact that SOFC stacks do not contain the high-cost precious metals that PEFCs contain. This is off-set in part by the relatively complex manufacturing process required for the SOFC electrode/electrolyte plates and by the somewhat lower power density in SOFC systems. Low-temperature operation (enabled with electrode-supported planar configuration) enables the use of low-cost metallic interconnects that can be manufactured with conventional metal forming operations.

The balance of plant contains all the direct stack support systems, reformer, compressors, pumps, and recuperating heat exchangers. Its cost is low by comparison to the PEFC because of the simplicity of the reformer. However, the cost of the recuperating heat exchangers partially offsets that.

To provide some perspective on the viability of SOFCs in APU applications from a cost perspective, NETL sponsored a cost estimate of a small-scale (5 kW), simple-cycle SOFC anode-supported system, operated on gasoline. The estimated manufacturing cost (see Figure 1-14) could well be close to that estimated for comparable PEFC systems, while providing somewhat higher system efficiency.

While the stack, insulation, and stack balance in this simple-cycle system is a key component; the balance of plant is also an important factor. The stack cost mainly depends on the achievable power density. Small systems like these will likely not be operated under high pressure. While this simplifies the design and reduces cost for compressors and expanders (which are not readily available at low cost for this size range in any case), it might also negatively affect the power density achievable.

A key challenge with small-scale SOFC systems is to overcome heat loss. The higher the heat loss the more recuperation is required to maintain the fuel cell within an acceptable temperature range, and hence to ensure good performance.

The large fraction of cost related to balance of plant issues is mainly due to the very small scale of this system, which results in a significant reverse economy of scale. While design work is still ongoing, it is anticipated that the cost structure of this system will reduce the cost of balance of plant further, and further improve the competitiveness of these systems.

SOFC System Cost Structure:

Manufacturing Costs: $350-550/kW

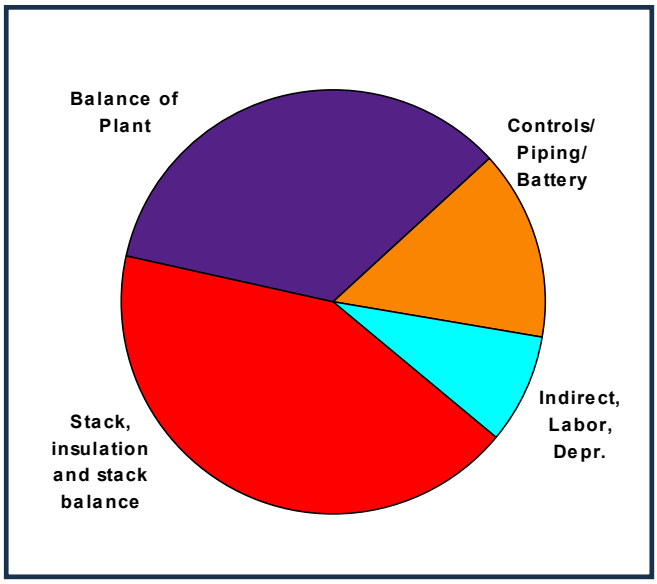

Figure 1-14. Projected cost structure of a 5kWnet APU SOFC system. Gasoline fueled POX reformer, Fuel cell operating at 300mW/cm2, 0.7 V, 90 % fuel utilization, 500,000 units per year production volume.

Outlook and Conclusions

In conclusion, both PEFC and SOFC have the potential to meet allowable cost targets, provided successful demonstrations prove the technology. It is critical however, that for these technologies to be commercially successful, especially in small-capacity markets, high production volumes will have to be reached. APU applications might provide such markets. It is similarly critical that the technologies be demonstrated to perform and achieve the projected performance targets and demonstrate long life. These are the challenges ahead for the fuel cell industry in the APU market segment.

1.8.6 Derivative Applications

Because of the modular nature of fuel cells, they are attractive for use in small portable units, ranging in size from 5 W or smaller to 100 W power levels. Examples of uses include the Ballard fuel cell, demonstrating 20 hour operation of a portable power unit (32), and an IFC military backpack. There has also been technology transfer from fuel cell system components. The best example is a joint IFC and Praxair, Inc., venture to develop a unit that converts natural gas to 99.999% pure hydrogen based on using fuel cell reformer technology and pressure swing adsorption process.

1.9 References

1. A.J. Appleby, F.R. Foulkes, *Fuel Cell Handbook*, Van Nostrand Reinhold, New York, NY, 1989.

2. *Report of the DOE Advanced Fuel-Cell Commercialization Working Group*, Edited by S.S. Penner, DOE/ER/0643, prepared by the DOE Advanced Fuel Cell Working Group (AFC2WG) or the United States Department of Energy under Contract No. DEFG03-93ER30213, March 1995.
3. K. Kordesch, J. Gsellmann, S. Jahangir, M. Schautz, in *Proceedings of the Symposium on Porous Electrodes: Theory and Practice,* Edited by H.C. Maru, T. Katan, M.G. Klein, The Electrochemical Society, Inc., Pennington, NJ, p. 163, 1984.
4. A. Pigeaud, H.C. Maru, L. Paetsch, J. Doyon, R. Bernard, in *Proceedings of the Symposium on Porous Electrodes: Theory and Practice,* Edited by H.C. Maru, T. Katan, M.G. Klein, The Electrochemical Society, Inc., Pennington, NJ, p. 234, 1984.
5. J.M. King, N. Ishikawa, "Phosphoric Acid Fuel Cell Power Plant Improvements and Commercial Fleet Experience," Nov. 96 Fuel Cell Seminar.
6. www.utcfuelcells.com.
7. Communications with IFC, August 24, 2000.
8. K. Yokota, et al., "GOI 11 MW FC Plant Operation Interim Report," in *Fuel Cell Program and Abstracts*, 1992 Fuel Cell Seminar, Tucson, AZ, November 29-December 2, 1992.
9. ONSI Press Release, "Fuel Cell Sets World Record; Runs 9,500 Hours Nonstop," May 20, 1997.
10. Northeast Utilities System Press Release, "Converting Landfill Gas into Electricity is an Environmental Plus," June 24, 1996.
11. "Groton's Tidy Machine," Public Power, March-April 1997.
12. ONSI Press Release, "World's First Hydrogen Fueled Fuel Cell Begins Operation in Hamburg, Germany," November 7, 1997.
13. "Anaerobic Gas Fuel Cell Shows Promise," Modern Power Systems, June 1997.
14. E.W. Hall, W.C. Riley, G.J. Sandelli, "PC25™ Product and Manufacturing Experience," IFC, Fuel Cell Seminar, November 1996.
15. www.ballard.com, 1998.
16. www.fuelcellenergy.com.
17. Information supplied by ERC for the Fuel Cell Handbook.
18. M.M. Piwetz, J.S. Larsen, T.S. Christensen, "Hydrodesulfurization and Pre-reforming of Logistic Fuels for Use in Fuel Cell Applications," *Fuel Cell Seminar Program and Abstracts*, Courtesy Associates, Inc., November 1996.
19. Westinghouse Electric Corporation, Bechtel Group, Inc., "Solid Oxide Fuel Cell Repowering of Highgrove Station Unit 1, Final Report," prepared for Southern California Edison Research Center, March 1992.
20. ERC, "Effects of Coal-Derived Trace Species on the Performance of Molten Carbonate Fuel Cells," topical report prepared for U.S. DOE/METC, DOE/MC/25009-T26, October 1991.
21. N. Maskalick, "Contaminant Effects in Solid Oxide Fuel Cells," in *Agenda and Abstracts*, Joint Contractors Meeting, *Fuel Cells and Coal-Fired Heat Engines Conference*, U.S. DOE/METC, August 3-5, 1993.
22. D.M. Rastler, C. Keeler, C.V. Chang, "Demonstration of a Carbonate on Coal Derived Gas," Report 15, in *An EPRI/GRI Fuel Cell Workshop on Technology Research and Development*. Stonehart Associates, Madison, CT, 1993.
23. Distributed Generation, Securing America's Future with Reliable, Flexible Power," U.S. Department of Energy, Office of Fossil Energy, National Energy Technology Center, October 1999.

24. U. S. Department of Energy's Office of Energy Efficiency and Renewable Energy webpage, http://www.eren.doe.gov/distributedpower Giovando, CarolAnn, "Distributed resources carve out a niche in competitive markets," *Power*, July/August 2000, pp. 46 – 57.
25. K.V. Kordesch, "City Car with H_2-Air Fuel Cell and Lead Battery," *6th Intersociety Energy Conversion Engineering Conference*, SAE Paper No. 719015, 1971.
26. A. Kaufman, "Phosphoric Acid Fuel Cell Bus Development," *Proceedings of the Annual Automotive Technology Development Contractors' Coordination Meeting*, Dearborn, MI, October 24-27, 1994, SAE Proceedings Volume P-289, pp. 289-293, 1995.
27. R.R. Wimmer, "Fuel Cell Transit Bus Testing & Development at Georgetown University," *Proceedings of the Thirty Second Intersociety Energy Conversion Engineering Conference*, July 27-August 1, 1997, Honolulu, HI, pp. 825-830, 1997.
28. N.C. Otto, P.F. Howard, "Transportation Engine Commercialization at Ballard Power Systems," *Program and Abstracts 1996 Fuel Cell Seminar*, November 17-20, 1996, Orlando, FL, pp. 559-562.
29. F. Panik, "Fuel Cells for Vehicle Application in Cars - Bringing the Future Closer," J. Power Sources, 71, 36-38, 1998.
30. S. Kawatsu, "Advanced PEFC Development for Fuel Cell Powered Vehicles," J. Power Sources, 71, 150-155, 1998.
31. *Fuel-Cell Technology: Powering the Future*, Electric Line, November/December 1996.
32. M. Graham, F. Barbir, F. Marken, M. Nadal, "Fuel Cell Power System for Utility Vehicle," *Program and Abstracts 1996 Fuel Cell Seminar*, November 17-20, 1996, Orlando, FL, pp. 571-574.
33. P.A. Lehman, C.E. Chamberlin, "Design and Performance of a Prototype Fuel Cell Powered Vehicle," *Program and Abstracts 1996 Fuel Cell Seminar*, November 17-20, 1996, Orlando, FL, pp. 567-570.
34. J. Leslie, "Dawn of the Hydrogen Age," Wired (magazine), October 1997.

2. FUEL CELL PERFORMANCE

The purpose of this section is to describe the chemical and thermodynamic relations governing fuel cells and how operating conditions affect their performance. Understanding the impacts of variables such as temperature, pressure, and gas constituents on performance allows fuel cell developers to optimize their design of the modular units and it allows process engineers to maximize the performance of systems applications.

A logical first step in understanding the operation of a fuel cell is to define its ideal performance. Once the ideal performance is determined, losses arising from non-ideal behavior can be calculated and then deducted from the ideal performance to describe the actual operation.

2.1 The Role of Gibbs Free Energy and Nernst Potential

The maximum electrical work (W_{el}) obtainable in a fuel cell operating at constant temperature and pressure is given by the change in Gibbs free energy (ΔG) of the electrochemical reaction:

$$W_{el} = \Delta G = -nFE \qquad (2\text{-}1)$$

where n is the number of electrons participating in the reaction, F is Faraday's constant (96,487 coulombs/g-mole electron), and E is the ideal potential of the cell.

The Gibbs free energy change is also given by the following state function:

$$\Delta G = \Delta H - T\Delta S \qquad (2\text{-}2)$$

where ΔH is the enthalpy change and ΔS is the entropy change. The total thermal energy available is ΔH. The available free energy is equal to the enthalpy change less the quantity $T\Delta S$ which represents the unavailable energy resulting from the entropy change within the system.

The amount of heat that is produced by a fuel cell operating reversibly is $T\Delta S$. Reactions in fuel cells that have negative entropy change generate heat (such as hydrogen oxidation), while those with positive entropy change (such as direct solid carbon oxidation) may extract heat from their

surroundings if the irreversible generation of heat is smaller than the reversible absorption of heat.

For the general cell reaction,

$$\alpha A + \beta B \rightarrow cC + \delta D \qquad (2\text{-}3)$$

the standard state Gibbs free energy change of reaction is given by:

$$\Delta G^\circ = c\underline{G}_C^\circ + \delta\underline{G}_D^\circ - \alpha\underline{G}_A^\circ - \beta\underline{G}_B^\circ \qquad (2\text{-}4)$$

where $\underline{G}_i^\circ$ is the partial molar Gibbs free energy for species i at temperature T. This potential can be computed from the heat capacities (C_p) of the species involved as a function of T and from values of both ΔS° and ΔH° at a reference temperature, usually 298K. Empirically, the heat capacity of a species, as a function of T, can be expressed as

$$C_p = a + bT + cT^2 \qquad (2\text{-}5)$$

where a, b, and c are empirical constants. The specific enthalpy for any species present during the reaction is given by

$$\underline{H}_i = \underline{H}_i^\circ + \int_{298}^{T} C_{pi}\,dT \qquad (2\text{-}6)$$

and, at constant pressure the specific entropy at temperature T is given by

$$\underline{S}_i = \underline{S}_i^\circ + \int_{298}^{T} \frac{C_{pi}}{T}\,dT \qquad (2\text{-}7)$$

It then follows that

$$\Delta H = \sum_i n_i \underline{H}_i \Big|_{out} - \sum_i n_i \underline{H}_i \Big|_{in} \qquad (2\text{-}8)$$

and

$$\Delta S = \sum_i n_i \underline{S}_i \Big|_{out} - \sum_i n_i \underline{S}_i \Big|_{in} \qquad (2\text{-}9)$$

The coefficients a, b, and c, as well as H° and S°, are available from standard reference tables, and may be used to calculate ΔH and ΔS. From these values it is then possible to calculate ΔG and E at temperature T.

Instead of using the coefficients a, b, and c, it is modern practice to rely on tables, such as JANAF Thermochemical Tables (1) to provide Cp, ΔH, ΔS, and ΔG over a range of temperatures for all species present in the reaction.

The Gibbs free energy change of reaction can be expressed by the equation:

$$\Delta G = \Delta G^\circ + RT \ln \frac{f_C^c \, f_D^\delta}{f_A^\alpha \, f_B^\beta} \qquad (2\text{-}10)$$

where ΔG° is the Gibbs free energy change of reaction at the standard state pressure (1 atm) and at temperature T, and f_i is the fugacity of species i. Substituting Equation (2-1) in Equation (2-10) gives the relation

$$E = E^\circ + \frac{RT}{n\boldsymbol{F}} \ln \frac{f_C^c \, f_D^\delta}{f_A^\alpha \, f_B^\beta} \qquad (2\text{-}11)$$

or more generally,

$$E = E^\circ + \frac{RT}{n\boldsymbol{F}} \ln \frac{\Pi\,[\text{reactant fugacity}]}{\Pi\,[\text{product fugacity}]} \qquad (2\text{-}12)$$

which is the general form of the Nernst equation. The reversible potential of a fuel cell at temperature T, E°, is calculated from ΔG° for the cell reaction at that temperature.

Fuel cells generally operate at pressures low enough that the fugacity can be approximated by the partial pressure.

2.2 Ideal Performance

The Nernst potential, E, gives the ideal open circuit cell potential. This potential sets the upper limit or maximum performance achievable by a fuel cell.

The overall reactions for various types of fuel cells are presented in Table 2-1. The corresponding Nernst equations for those reactions are provided in Table 2-2.

Table 2-1 Electrochemical Reactions in Fuel Cells

Fuel Cell	Anode Reaction	Cathode Reaction
Polymer Electrolyte and Phosphoric Acid	$H_2 \rightarrow 2H^+ + 2e^-$	$\frac{1}{2} O_2 + 2H^+ + 2e^- \rightarrow H_2O$
Alkaline	$H_2 + 2(OH)^- \rightarrow 2H_2O + 2e^-$	$\frac{1}{2} O_2 + H_2O + 2e^- \rightarrow 2(OH)^-$
Molten Carbonate	$H_2 + CO_3^= \rightarrow H_2O + CO_2 + 2e^-$ $CO + CO_3^= \rightarrow 2CO_2 + 2e^-$	$\frac{1}{2} O_2 + CO_2 + 2e^- \rightarrow CO_3^=$
Solid Oxide	$H_2 + O^= \rightarrow H_2O + 2e^-$ $CO + O^= \rightarrow CO_2 + 2e^-$ $CH_4 + 4O^= \rightarrow 2H_2O + CO_2 + 8e^-$	$\frac{1}{2} O_2 + 2e^- \rightarrow O^=$

CO - carbon monoxide	e^- - electron	H_2O - water
CO_2 - carbon dioxide	H^+ - hydrogen ion	O_2 - oxygen
$CO_3^=$ - carbonate ion	H_2 - hydrogen	OH^- - hydroxyl ion

The Nernst equation provides a relationship between the ideal standard potential (E°) for the cell reaction and the ideal equilibrium potential (E) at other partial pressures of reactants and products. For the overall cell reaction, the cell potential increases with an increase in the partial pressure (concentration) of reactants and a decrease in the partial pressure of products. For example, for the hydrogen reaction, the ideal cell potential at a given temperature can be increased by operating at higher reactant pressures, and improvements in fuel cell performance have, in fact, been observed at higher pressures. This will be further demonstrated in Chapters 3 through 7 for the various types of fuel cells.

The reaction of H_2 and O_2 produces H_2O. When a carbon-containing fuel is involved in the anode reaction, CO_2 is also produced. For MCFCs, CO_2 is required in the cathode reaction to maintain an invariant carbonate concentration in the electrolyte. Because CO_2 is produced at the anode and consumed at the cathode in MCFCs, and because the concentrations in the anode and cathode feed streams are not necessarily equal, the CO_2 partial pressures for both electrode reactions are present in the second Nernst equation shown in Table 2-2.

Table 2-2 Fuel Cell Reactions and the Corresponding Nernst Equations

Cell Reactions*	Nernst Equation
$H_2 + ½O_2 \rightarrow H_2O$	$E = E° + (RT/2F) \ln [P_{H_2} / P_{H_2O}] + (RT/2F) \ln [P_{O_2}^{½}]$
$H_2 + ½O_2 + CO_{2(c)} \rightarrow H_2O + CO_{2(a)}$	$E = E° + (RT/2F) \ln [P_{H_2} / P_{H_2O} (P_{CO_2})_{(a)}] + (RT/2F) \ln [P_{O_2}^{½} (P_{CO_2})_{(c)}]$
$CO + ½O_2 \rightarrow CO_2$	$E = E° + (RT/2F) \ln [P_{CO} / P_{CO_2}] + (RT/2F) \ln [P_{O_2}^{½}]$
$CH_4 + 2O_2 \rightarrow 2H_2O + CO_2$	$E = E° + (RT/8F) \ln [P_{CH_4} / P_{H_2O}^2 P_{CO_2}] + (RT/8F) \ln [P_{O_2}^2]$

(a) - anode
(c) - cathode
E - equilibrium potential
F - Faraday's constant
P - gas pressure
R - universal gas constant
T - temperature (absolute)

* The cell reactions are obtained from the anode and cathode reactions listed in Table 2-1.

The ideal standard potential (E^o) at 298K for a fuel cell in which H_2 and O_2 react is 1.229 volts with liquid water product, or 1.18 volts with gaseous water product. This value is shown in numerous chemistry texts (2) as the oxidation potential of H_2. The potential is the change in Gibbs free energy resulting from the reaction between hydrogen and oxygen. The difference between 1.229 volts and 1.18 volts represents the Gibbs free energy change of vaporization of water at standard conditions.

Figure 2-1 shows the relation of E to cell temperature. Because the figure shows the potential of higher temperature cells, the ideal potential corresponds to a reaction where the water product is in a gaseous state (i.e., E^o is 1.18 volts).

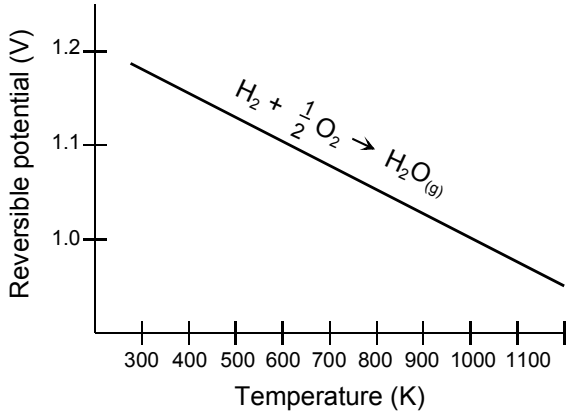

Figure 2-1 H_2/O_2 Fuel Cell Ideal Potential as a Function of Temperature

The impact of temperature on the ideal voltage, E, for the oxidation of hydrogen is also shown in Table 2-3 for the various types of fuel cells. Each case assumes gaseous products as its basis.

Table 2-3 Ideal Voltage as a Function of Cell Temperature

Temperature	25°C (298K)	80°C (353K)	100°C (373K)	205°C (478K)	650°C (923K)	800°C (1073K)	1100°C (1373K)
Cell Type		PEFC	AFC	PAFC	MCFC	ITSOFC	TSOFC
Ideal Voltage	1.18	1.17	1.16	1.14	1.03	0.99	0.91

The open circuit voltage of a fuel cell is also strongly influenced by the reactant concentrations. The maximum ideal potential occurs when the reactants at the anode and cathode are pure. In an air-fed system or if the feed to the anode is other than pure dry hydrogen, the cell potential will be reduced. Similarly, the concentration of reactants at the exit of the cell will be lower than at the entrance. This reduction in partial pressure leads to a Nernst correction that reduces the open circuit voltage locally, often by as much as 250 mV in higher-temperature cells. Because the electrodes should be highly conductive and the electrode within one cell consequently has close to uniform voltage, depressed open circuit voltage affects the operation of the entire cell. This significantly impacts the achievable cell operating voltage and consequently system efficiency of especially the higher-temperature fuel cells.

The ideal performance of a fuel cell depends on the electrochemical reactions that occur between different fuels and oxygen as summarized in Tables 2-1 and 2-2. Low-temperature fuel cells (PEFC, AFC, and PAFC) require noble metal electro-catalysts to achieve practical reaction rates at the anode and cathode, and H_2 is the only acceptable fuel. With high-temperature fuel cells (MCFC, ITSOFC, and TSOFC), the requirements for catalysis are relaxed, and the number of potential fuels expands. While carbon monoxide severely poisons noble metal anode catalysts such as platinum (Pt) in low-temperature fuel cells, it is a reactant in high-temperature fuel cells (operating temperatures of 300 °C and higher) where non-noble metal catalysts such as nickel (Ni) can be used.

Note that H_2, CO, and CH_4 are shown in Table 2-1 as potentially undergoing direct anodic oxidation. In actuality, direct electrochemical oxidation of the CO and CH_4 usually represents only a minor pathway to oxidation of these species. It is common systems analysis practice to assume that H_2, the more readily oxidized fuel, is produced by CO and CH_4 reacting, at equilibrium, with H_2O through the water gas shift and steam reforming reactions, respectively. A simple reaction pathway analysis explains why direct oxidation is rarely the major reaction pathway under most fuel cell operating conditions:

- The driving force for anodic oxidation of CO and CH_4 is lower than that for the oxidation of hydrogen, as reflected in the higher open circuit voltage of the hydrogen oxidation.
- The kinetics of hydrogen oxidation on the anode are significantly faster than that of CO or CH_4 oxidation.

- There is vastly more surface area available for catalytic reforming and shift reaction throughout the anode of a practical fuel cell than there is surface area in the three-phase-boundary for electrochemical oxidation.
- Mass-transfer of CO, CH_4, and even more so of higher hydrocarbons, to the three-phase boundary and through the porous anode is more than ten times slower than that of hydrogen, leading to a more significant impact of concentration polarization.

Nevertheless, direct oxidation can be important under certain conditions, such as at the entrance of a cell. The degree to which an anode supports direct oxidation will then impact the degree of pre-reforming of the fuel that is required, which in turn typically impacts balance of plant complexity and cost. This is why there remains strong interest in the development of direct oxidation anodes.

The H_2 that can be produced from CO and CH_4, along with any H_2 in the fuel supply stream, is referred to as equivalent H_2. The temperature and catalyst of state-of-the-art SOFCs and MCFCs provide the proper environment for the water gas shift reaction to produce H_2 and CO_2 from CO and H_2O. If only H_2 and CO are fed to the fuel cell, it is known as an external reforming (ER) cell. In an internal reforming (IR) fuel cell, the reforming reaction to produce H_2 and CO_2 from CH_4 and H_2O occurs inside the stack. In some IR fuel cells, reforming takes place on the anode (on-anode reforming) while in others a reforming catalyst is placed in proximity to the anode to promote the reaction (in-cell reforming).

2.3 Cell Energy Balance

The discussion above can be used to formulate a mass and energy balance around a fuel cell to describe its electrical performance. The energy balance around the fuel cell is based on the energy absorbing/releasing processes (e.g., power produced, reactions, heat loss) that occur in the cell. As a result, the energy balance varies for the different types of cells because of the differences in reactions that occur according to cell type.

In general, the cell energy balance states that the enthalpy flow of the reactants entering the cell will equal the enthalpy flow of the products leaving the cell plus the sum of three terms: (1) the net heat generated by physical and chemical processes within the cell, (2) the dc power output from the cell, and (3) the heat loss from the cell to its surroundings.

Component enthalpies are readily available on a per mass basis from data tables such as JANAF (1). Product enthalpy usually includes the heat of formation in published tables. A typical energy balance determines the cell exit temperature knowing the reactant composition, the feed stream temperatures, H_2 and O_2 utilization, the expected power produced, and a percent heat loss. The exit constituents are calculated from the fuel cell reactions as illustrated in Example 9-3, Chapter 9.

2.4 Cell Efficiency

The thermal efficiency of a fuel conversion device is defined as the amount of useful energy produced relative to the change in enthalpy, ΔH, between the product and feed streams.

$$\eta = \frac{\text{Useful Energy}}{\Delta H} \qquad (2\text{-}13)$$

Conventionally, chemical (fuel) energy is first converted to heat, which is then converted to mechanical energy, which can then be converted to electrical energy. For the thermal to mechanical conversion, a heat engine is conventionally used. Carnot showed that the maximum efficiency of such an engine is limited by the ratio of the absolute temperatures at which heat is rejected and absorbed, respectively (3).

Fuel cells convert chemical energy directly into electrical energy. In the ideal case of an electrochemical converter, such as a fuel cell, the change in Gibbs free energy, ΔG, of the reaction is available as useful electric energy at the temperature of the conversion. The ideal efficiency of a fuel cell, operating reversibly, is then

$$\eta_{ideal} = \frac{\Delta G}{\Delta H} \qquad (2\text{-}14)$$

The most widely used efficiency of a fuel cell is based on the change in the standard free energy for the cell reaction

$$H_2 + \tfrac{1}{2} O_2 \rightarrow H_2O_{(1)} \qquad (2\text{-}15)$$

given by

$$\Delta G_r^\circ = \underline{G}_{H_2O(\ell)}^\circ - \underline{G}_{H_2}^\circ - \frac{1}{2}\underline{G}_{O_2}^\circ \qquad (2\text{-}16)$$

where the product water is in liquid form. At standard conditions of 25°C (298°K) and 1 atmosphere, the thermal energy (ΔH) in the hydrogen/oxygen reaction is 285.8 kJ/mole, and the free energy available for useful work is 237.1 kJ/mole. Thus, the thermal efficiency of an ideal fuel cell operating reversibly on pure hydrogen and oxygen at standard conditions is:

$$\eta_{ideal} = \frac{237.1}{285.8} = 0.83 \qquad (2\text{-}17)$$

For other electrochemical reactions, different ideal efficiencies apply. Curiously, for direct electrochemical oxidation of carbon ΔG is larger than ΔH, and consequently the ideal efficiency is slightly greater than 100% when using this definition of ideal efficiency.

For convenience, the efficiency of an actual fuel cell is often expressed in terms of the ratio of the operating cell voltage to the ideal cell voltage. As will be described in greater detail in the sections following, the actual cell voltage is less than the ideal cell voltage because of losses associated with cell polarization and ohmic losses. The thermal efficiency of a hydrogen/oxygen fuel cell can then be written in terms of the actual cell voltage:

$$\eta = \frac{\text{Useful Energy}}{\Delta H} = \frac{\text{Useful Power}}{(\Delta G/0.83)} = \frac{\text{Volts}_{actual} \text{ x Current}}{\text{Volts}_{ideal} \text{ x Current}/0.83} = \frac{(0.83)(V_{actual})}{E_{ideal}} \qquad (2\text{-}18)$$

As mentioned previously, the ideal voltage of a cell operating reversibly on pure hydrogen and oxygen at 1 atm pressure and 25ºC is 1.229 V. Thus, the thermal efficiency of an actual fuel cell operating at a voltage of V_{cell}, based on the higher heating value of hydrogen, is given by

$$\eta = 0.83 \text{ x } V_{cell} / E_{ideal} = 0.83 \text{ x } V_{cell} / 1.229 = 0.675 \text{ x } V_{cell} \qquad (2\text{-}19)$$

The foregoing has assumed that the fuel is completely converted in the fuel cell, as is common in most types of heat engines. This efficiency is also referred to as the voltage efficiency. However, in fuel cells, the fuel is typically not completely converted. To arrive at the net cell efficiency, the voltage efficiency must be multiplied by the fuel utilization. An excellent review of the impact of this phenomenon is provided by Winkler (4).

Because the reactant activities in gas-fueled fuel cells drop as the utilization rises, and because the cell voltage cannot be higher than the lowest local potential in the cell, utilization considerations further limit the efficiency. Figure 2-2 shows the impact of fuel utilization on the Nernst voltage, voltage efficiency, and maximum overall cell efficiency for operating conditions typical for an SOFC (800 °C, 50% initial hydrogen concentration). Figure 2-2 shows that to achieve 90% fuel utilization, the Nernst voltage drops by over 200 mV. As a consequence, the maximum cell efficiency (on a higher heating value basis) is not 62%, as predicted based on the ideal potential, but 54%. Of course, practical cell operating effects and cell non-idealities further reduce this efficiency in real life.

These effects are somewhat less profound at lower operating temperatures, such as those found in lower temperature SOFC, MCFC, or in low-temperature fuel cells.

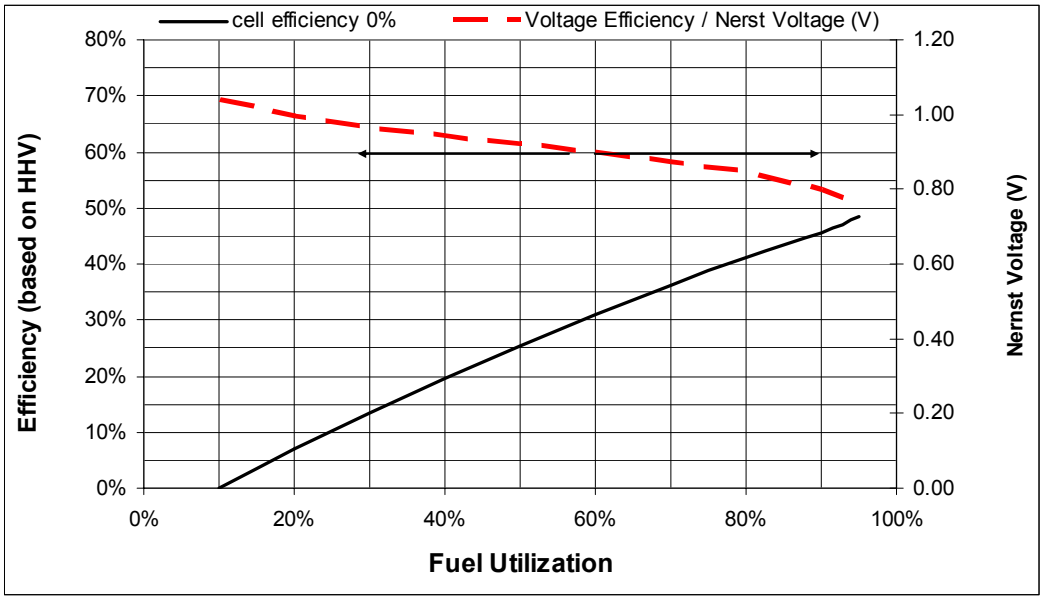

Figure 2-2 Effect of fuel utilization on voltage efficiency and overall cell efficiency for typical SOFC operating conditions (800 °C, 50% initial hydrogen concentration).

2.5 Actual Performance

The actual cell potential is decreased from its ideal potential because of several types of irreversible losses, as shown in Figure 2-3[2]. These losses are often referred to as polarization, overpotential or overvoltage, though only the ohmic losses actually behave as a resistance. Multiple phenomena contribute to irreversible losses in an actual fuel cell:

- Activation-related losses. These stem from the activation energy of the electrochemical reactions at the electrodes. These losses depend on the reactions at hand, the electro-catalyst material and microstructure, reactant activities (and hence utilization), and weakly on current density.
- Ohmic losses. Ohmic losses are caused by ionic resistance in the electrolyte and electrodes, electronic resistance in the electrodes, current collectors and interconnects, and contact resistances. Ohmic losses are proportional to the current density, depend on materials selection and stack geometry, and on temperature.
- Mass-transport-related losses. These are a result of finite mass transport limitations rates of the reactants and depend strongly on the current density, reactant activity, and electrode structure.

In the V-I diagram, especially for low-temperature fuel cells, the effects of the three loss categories are often easy to distinguish, as illustrated in Figure 2-3.

[2] Activation region and concentration region are more representative of low-temperature fuel cells.

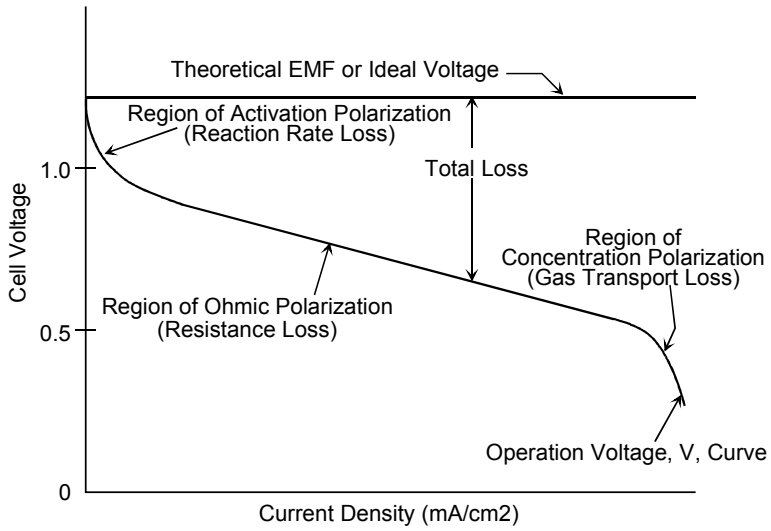

Figure 2-3 Ideal and Actual Fuel Cell Voltage/Current Characteristic

In high-temperature fuel cells, the activation-related losses are often much less significant, and hence the characteristic concave portion of the V-I curve is hard to distinguish. In addition, as transport-related losses play a more important role, the convex portion of the curve often extends further to the left.

Although it is tempting to characterize all losses in the cell as an equivalent resistance, only the ohmic losses actually behave that way, by definition. The ohmic loss depends only on cell geometry, the materials used, and the operating temperature. The other losses depend strongly on reactant concentrations (and hence fuel utilization) and thus they change within cells operated at finite fuel utilization. Attempts to include these types of polarization into the cell resistance more often than not lead to confusion and misinterpretation. This consideration has several ramifications for fuel cell engineers attempting to utilize single-cell data for stack or system design:

- Activation and concentration polarization data presented are generally only valid for that particular cell and operating geometry.
- A mathematical model will generally be required to interpret activation and concentration polarization data and translate it into data useful for stack engineers.
- Detailed reactant concentration information (including utilization) is essential for interpretation of activation and concentration polarization data. In practice, sound interpretation for translation to practical cell designs, sizes, and operating conditions is only possible when data is acquired with very low utilization (typically less than 5%), and for many reactant inlet partial pressures.
- Much of the single-cell data presented and published is taken at finite utilization. While useful for qualitative comparisons between cells, this data is generally not usable for further stack engineering.

Below the three types of losses are discussed in greater detail.

Activation Losses: Activation losses are caused by sluggish electrode kinetics. There is a close similarity between electrochemical and chemical reactions in that both involve an activation energy that must be overcome by the reacting species. In reality, activation losses are the result of complex surface electrochemical reaction steps, each of which have their own reaction rate and activation energy. Usually, the rate parameters and activation energy of one or more rate-limiting reaction steps controls the voltage drop caused by activation losses on a particular electrode under specific conditions. However, in the case of electrochemical reactions with $\eta_{act} \geq$ 50-100 mV, it is possible to approximate the voltage drop due to activation polarization by a semi-empirical equation, called the Tafel equation (5). The equation for activation polarization is shown by Equation (2-20):

$$\eta_{act} = \frac{RT}{\alpha n F} \ln \frac{i}{i_o} \qquad (2\text{-}20)$$

where α is the electron transfer coefficient of the reaction at the electrode being addressed, and i_o is the exchange current density. Tafel plots, such as in Figure 2-4, provide a visual understanding of the activation polarization of a fuel cell. They are used to measure the exchange current density, given by the extrapolated intercept at $\eta_{act} = 0$ which is a measure of the maximum current that can be extracted at negligible polarization (3), and the transfer coefficient (from the slope).

The usual form of the Tafel equation that can be easily expressed by a Tafel Plot is

$$\eta_{act} = a + b \ln i \qquad (2\text{-}21)$$

where $a = (-RT/\alpha nF) \ln i_o$ and $b = RT/\alpha nF$. The term b is called the Tafel slope, and is obtained from the slope of a plot of η_{act} as a function of ln i. There exists a strong incentive to develop electro-catalysts that yield a lower Tafel slope for electrochemical reactions so that increases in current density result only in nominal increases in activation polarization.

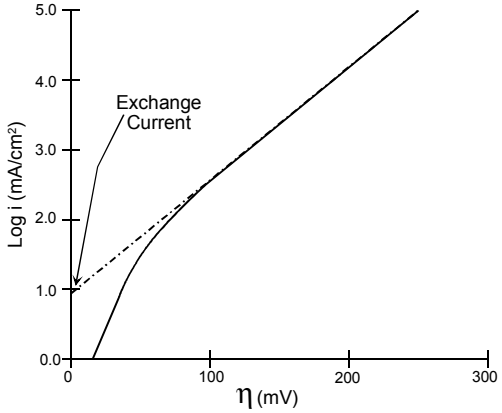

Figure 2-4 Example of a Tafel Plot

The simplified description presented here did not consider processes that give rise to activation polarization, except for attributing it to sluggish electrode kinetics. Processes involving absorption of reactant species, transfer of electrons across the double layer, desorption of product species, and the nature of the electrode surface all contribute to activation polarization.

Ohmic Polarization: Ohmic losses occur because of resistance to the flow of ions in the electrolyte and resistance to flow of electrons through the electrode. The dominant ohmic losses through the electrolyte are reduced by decreasing the electrode separation and enhancing the ionic conductivity of the electrolyte. Because both the electrolyte and fuel cell electrodes obey Ohm's law, the ohmic losses can be expressed by the equation

$$\eta_{ohm} = iR \qquad (2\text{-}22)$$

where i is the current flowing through the cell, and R is the total cell resistance, which includes electronic, ionic, and contact resistance:

$$R = R_{electronic} + R_{ionic} + R_{contact}$$

Any of these components can dominate the ohmic resistance, depending on the cell type. For example, in planar electrolyte-supported SOFC the ionic resistance usually dominates; in tubular SOFC the electronic bulk resistance usually dominates, and in planar thin-electrolyte SOFC contact resistances often dominate.

The ohmic resistance normalized by the active cell area is the Area Specific Resistance (ASR). ASR has the units Ωcm^2. The ASR is a function of the cell design, material choice, manufacturing technique, and, because material properties change with temperature, operating conditions. The ASR is a key performance parameter, especially in high-temperature fuel cells, where the ohmic losses often dominate the overall polarization of the cell.

Experimentally, there are several ways to determine the ohmic cell resistance. If the V-I curve has a substantial linear portion (in the center), the slope of this curve usually closely approximates the ASR of the cell. Only in such a linear portion of the V-I curve the ohmic resistance is dominant, and hence the determination of the ASR valid. Sometimes, a more accurate way to determine the ohmic resistance is from impedance spectroscopy. In an impedance spectrum of a fuel cell, the ohmic resistance is the real value of the impedance of the point for which the imaginary impedance is zero (Figure 2-5). As can be seen in the example, the ohmic resistance is invariant with gas concentration. The part of the impedance that is related to mass transport and kinetics, however, changes markedly with anode feed composition.

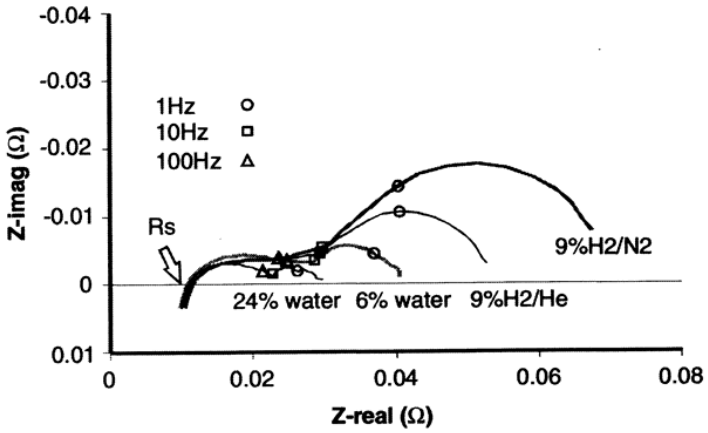

Figure 2-5 Example of impedance spectrum of anode-supported SOFC operated at 850 °C (6). Rs is Ohmic resistance. Two measurements were with hydrogen/water vapor mixtures, and the other in diluted hydrogen.

Finally, the electronic portions of the ohmic resistance could also be measured directly using a four-point probe or with a through-measurement.

Given a certain cell design and operating temperature, the bulk material contributions to R (and hence the ASR) can also be calculated. Based on the detailed cell geometry, the length of both the ionic and electronic current paths and cross-sectional area for current conduction can be measured. Together with the resistivities of the materials used, they yield the bulk ASR. The contact resistance cannot be calculated from fundamental data, and is usually determined by difference between the measured total resistance and the computed bulk resistance.

When using literature data for ASR, it is critical to verify the definition of ASR. Some researchers have defined "ASR"s to include the activation and concentration polarization as well as the ohmic polarization.

Mass Transport-Related Losses: As a reactant is consumed at the electrode by electrochemical reaction, it is often diluted by the products, when finite mass transport rates limit the supply of fresh reactant and the evacuation of products. As a consequence, a concentration gradient is

formed which drives the mass transport process. In a fuel cell with purely gas-phase reactants and products (such as an SOFC), gas diffusion processes control mass transfer. In other cells, multi-phase flow in the porous electrodes can have a significant impact (e.g. in PEFC). In hydrogen fuel cells, the evacuation of product is often more limiting than the supply of fuel, given the difference between the diffusivities of hydrogen and water (vapor).

While at low current densities and high bulk reactant concentrations mass-transport losses are not significant, under practical conditions (high current densities, low fuel and air concentrations), they often contribute significantly to loss of cell potential.

For gas-phase fuel cells, the rate of mass transport to an electrode surface in many cases can be described by Fick's first law of diffusion:

$$i = \frac{nFD\,(C_B - C_S)}{\delta} \qquad (2\text{-}23)$$

where D is the diffusion coefficient of the reacting species, C_B is its bulk concentration, C_S is its surface concentration, and δ is the thickness of the diffusion layer. The limiting current (i_L) is a measure of the maximum rate at which a reactant can be supplied to an electrode, and it occurs when $C_S = 0$, i.e.,

$$i_L = \frac{nFDC_B}{\delta} \qquad (2\text{-}24)$$

By appropriate manipulation of Equations (2-23) and (2-24),

$$\frac{C_S}{C_B} = 1 - \frac{i}{i_L} \qquad (2\text{-}25)$$

The Nernst equation for the reactant species at equilibrium conditions, or when no current is flowing, is

$$E_{i=0} = E^\circ + \frac{RT}{nF} \ln C_B \qquad (2\text{-}26)$$

When current is flowing, the surface concentration becomes less than the bulk concentration, and the Nernst equation becomes

$$E = E^\circ + \frac{RT}{n\boldsymbol{F}} \ln C_S \qquad (2\text{-}27)$$

The potential difference (ΔE) produced by a concentration change at the electrode is called the concentration polarization:

$$\Delta E = \eta_{conc} = \frac{RT}{n\boldsymbol{F}} \ln \frac{C_S}{C_B} \qquad (2\text{-}28)$$

Upon substituting Equation (2-25) in (2-28), the concentration polarization is given by the equation

$$\eta_{conc} = \frac{RT}{n\boldsymbol{F}} \ln\left(1 - \frac{i}{i_L}\right) \qquad (2\text{-}29)$$

In this analysis of concentration polarization, the activation polarization is assumed to be negligible. The charge transfer reaction has such a high exchange current density that the activation polarization is negligible in comparison with the concentration polarization (most appropriate for the high temperature cells).

Cumulative Effect of the Losses: The combined effect of the losses for a given cell and given operating conditions can be expressed as polarizations. The total polarization at the electrodes is the sum of η_{act} and η_{conc}, or

$$\eta_{anode} = \eta_{act,a} + \eta_{conc,a} \qquad (2\text{-}30)$$

and

$$\eta_{cathode} = \eta_{act,c} + \eta_{conc,c} \qquad (2\text{-}31)$$

The effect of polarization is to shift the potential of the electrode ($E_{electrode}$) to a new value ($V_{electrode}$):

$$V_{electrode} = E_{electrode} \pm |\eta_{electrode}| \qquad (2\text{-}32)$$

For the anode,

$$V_{anode} = E_{anode} + |\eta_{anode}| \qquad (2\text{-}33)$$

and for the cathode,

$$V_{cathode} = E_{cathode} - |\eta_{cathode}| \qquad (2\text{-}34)$$

The net result of current flow in a fuel cell is to increase the anode potential and to decrease the cathode potential, thereby reducing the cell voltage. Figure 2-6 illustrates the contribution to polarization of the two half cells for a PAFC. The reference point (zero polarization) is hydrogen. These shapes of the polarization curves are typical of other types of fuel cells as well.

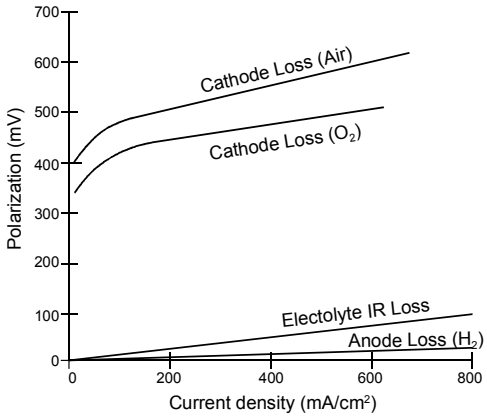

Figure 2-6 Contribution to Polarization of Anode and Cathode

Summing of Cell Voltage: The cell voltage includes the contribution of the anode and cathode potentials and ohmic polarization:

$$V_{cell} = V_{cathode} - V_{anode} - iR \qquad (2\text{-}35)$$

When Equations (2-33) and (2-34) are substituted in Equation (2-35)

$$V_{cell} = E_{cathode} - |\eta_{cathode}| - (E_{anode} + |\eta_{anode}|) - iR \qquad (2\text{-}36)$$

or

$$V_{cell} = \Delta E_e - |\eta_{cathode}| - |\eta_{anode}| - iR \qquad (2\text{-}37)$$

where $\Delta E_e = E_{cathode} - E_{anode}$. Equation (2-37) shows that current flow in a fuel cell results in a decrease in cell voltage because of losses by electrode and ohmic polarizations. The goal of fuel cell developers is to minimize the polarization so that V_{cell} approaches ΔE_e. This goal is approached by modifications to fuel cell design (improvement in electrode structures, better electro-catalysts, more conductive electrolyte, thinner cell components, etc.). For a given cell design, it is possible to improve the cell performance by modifying the operating conditions (e.g., higher gas pressure, higher temperature, change in gas composition to lower the gas impurity concentration). However, for any fuel cell, compromises exist between achieving higher performance by operating at higher temperature or pressure and the problems associated with the stability/durability of cell components encountered at the more severe conditions.

2.6 Fuel Cell Performance Variables

The performance of fuel cells is affected by operating variables (e.g., temperature, pressure, gas composition, reactant utilization, current density), cell design and other factors (impurities, cell life) that influence the ideal cell potential and the magnitude of the voltage losses described above. The equations describing performance variables, which will be developed in Chapters 3 through 7, address changes in cell performance as a function of major operating conditions to allow the reader to perform quantitative parametric analysis. The following discussion provides basic insight into the effects of some operating parameters.

Current Density: The effects on performance of increasing current density were addressed in the previous section that described how activation, ohmic, and concentration losses occur as the current is changed. Figure 2-7 is a simplified depiction of how these losses affect the shape of the cell voltage-current characteristic. As current is initially drawn, sluggish kinetics (activation losses) cause a decrease in cell voltage. At high current densities, there is an inability to diffuse enough reactants to the reaction sites (concentration losses) so the cell experiences a sharp performance decrease through reactant starvation. There also may be an associated problem of diffusing the reaction products from the cell.

Ohmic losses predominate in normal fuel cell operation. These losses can be expressed as iR losses where i is the current and R is the summation of internal resistances within the cell, Equation (2-22). As is readily evident from the equation, the ohmic loss and hence voltage change is a direct function of current (current density multiplied by cell area).

Figure 2-7 presents the most important trade-off in choice of the operating point. It would seem logical to design the cell to operate at the maximum power density that peaks at a higher current density (right of the figure). However, operation at the higher power densities will mean operation at lower cell voltages or lower cell efficiency. Setting
operation near the peak power density can cause instability in control because the system will have a tendency to oscillate between higher and lower current densities around the peak. It is usual practice to operate the cell to the left side of the power density peak and at a point that yields a compromise between low operating cost (high cell efficiency that occurs at high voltage/low current density) and low capital cost (less cell area that occurs at low voltage/high current density). In reality, the precise choice of the operating point depends on complex system trade-offs, usually aided by system studies that allow the designer to take into account effects of operating voltage and current density on parasitic power consumption, sizing of balance of plant components, heat rejection requirements, and other system design considerations.

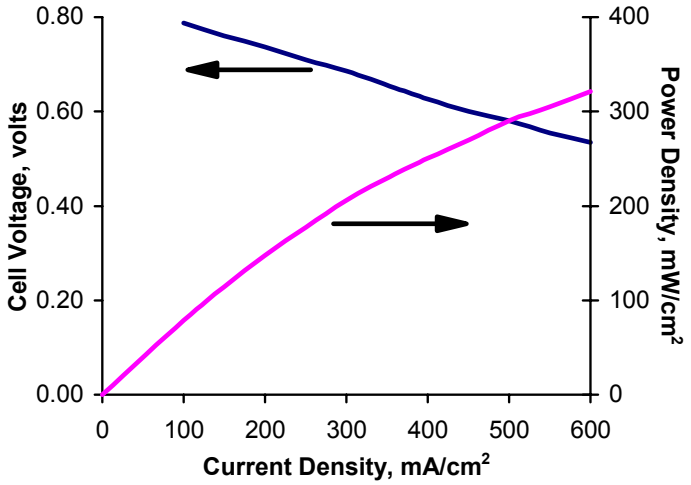

Figure 2-7 Voltage/Power Relationship

It is interesting to observe that the resulting characteristic provides the fuel cell with a benefit that is unique among other energy conversion technologies: the fuel cell efficiency increases at part load conditions.[3] Even though other components within the fuel cell system operate at lower component efficiencies as the system's load is reduced, the combination of increased fuel cell efficiency and lower supporting component efficiencies can result in a rather flat trace of total system efficiency as the load is reduced. This is in contrast with many heat engine-based energy conversion technologies that typically experience a significant drop-off in efficiency at part-load. This gives the fuel cell system a fuel cost advantage for applications where a significant amount of part-load operation is required.

---

[3]. Constraints can limit the degree of part load operation of a fuel cell. For example, a PAFC is limited to operation below approximately 0.85 volts because of entering into a corrosion region.

Temperature and Pressure: The effect of temperature and pressure on the ideal potential (E) of a fuel cell can be analyzed on the basis of changes in the Gibbs free energy with temperature and pressure.

$$\left(\frac{\partial E}{\partial T}\right)_P = \frac{\Delta S}{nF} \qquad (2\text{-}38)$$

or

$$\left(\frac{\partial E}{\partial P}\right)_T = \frac{-\Delta V}{nF} \qquad (2\text{-}39)$$

Because the entropy change for the H_2/O_2 reaction is negative, the reversible potential of the H_2/O_2 fuel cell decreases with an increase in temperature (by 0.84 mV/°C, assuming reaction product is liquid water). For the same reaction, the volume change is negative; therefore, the reversible potential increases with an increase in pressure (with the square root of the pressure, assuming pressure is equal on both electrodes).

However, temperature has a strong impact on a number of other factors:

- Electrode reaction rates. Typically, electrode reactions follow Arrhenius behavior. As a consequence, these losses decline exponentially with increasing temperature, usually more than off-setting the reduction in ideal potential. The higher the activation energy (and hence usually the losses) the greater the impact of temperature. The impact of total pressure depends on the pressure dependence of rate-limiting reaction steps.
- Ohmic losses. The impact of temperature on cell resistance is different for different materials. For metals, the resistance usually increases with temperature, while for electronically and ionically conductive ceramics it decreases exponentially (Arrhenius-form). For aqueous electrolytes, the impact is limited though high temperatures can lead to dehydration of the electrolyte (e.g. PEFC) and loss of conductivity. As a rule of thumb, for high-temperature fuel cells, the net effect is a significant reduction in resistance, while for low-temperature fuel cells the impact over the operating range is limited.

Mass transport processes are not strongly affected by temperature changes within the typical operating temperature and pressure ranges of most fuel cell types.

An increase in operating pressure has several beneficial effects on fuel cell performance because the reactant partial pressure, gas solubility, and mass transfer rates are higher. In addition, electrolyte loss by evaporation is reduced at higher operating pressures. Increased pressure also tends to increase system efficiencies. However, there are compromises such as thicker piping and additional expense for pressurization. Section 8.1.1 addresses system aspects of pressurization. The benefits of increased pressure must be balanced against hardware and materials problems, as well as parasitic power costs. In particular, higher pressures increase material problems in MCFCs (see Section 6.1), pressure differentials must be minimized to prevent reactant gas leakage through

the electrolyte and seals, and high pressure favors carbon deposition and methane formation in the fuel gas.

Reactant Utilization and Gas Composition: Reactant utilization and gas composition have major impacts on fuel cell efficiency. It is apparent from the Nernst equations in Table 2-2 that fuel and oxidant gases containing higher partial pressures of electrochemical reactants produce a higher cell voltage. Utilization (U) refers to the fraction of the total fuel or oxidant introduced into a fuel cell that reacts electrochemically. In low-temperature fuel cells, determining the fuel utilization is relatively straightforward when H_2 is the fuel, because it is the only reactant involved in the electrochemical reaction,[4] i.e.

$$U_f = \frac{H_{2,in} - H_{2,out}}{H_{2,in}} = \frac{H_{2,\text{ consumed}}}{H_{2,in}} \qquad (2\text{-}40)$$

where $H_{2,in}$ and $H_{2,out}$ are the flow rates of H_2 at the inlet and outlet of the fuel cell, respectively. However, hydrogen can be consumed by various other pathways, such as by chemical reaction (i.e., with O_2 and cell components) and loss via leakage out of the cell. These pathways increase the apparent utilization of hydrogen without contributing to the electrical energy produced by the fuel cell. A similar type of calculation is used to determine the oxidant utilization. For the cathode in MCFCs, two reactant gases, O_2 and CO_2, are utilized in the electrochemical reaction. The oxidant utilization should be based on the limiting reactant. Frequently O_2, which is readily available from make-up air, is present in excess, and CO_2 is the limiting reactant.

A significant advantage of high-temperature fuel cells such as MCFCs is their ability to use CO as a fuel. The anodic oxidation of CO in an operating MCFC is slow compared to the anodic oxidation of H_2; thus, the direct oxidation of CO is not favored. However, the water gas shift reaction

$$CO + H_2O \rightleftharpoons H_2 + CO_2 \qquad (2\text{-}41)$$

reaches equilibrium rapidly in MCFCs at temperatures as low as 650°C (1200°F) to produce H_2.[5] As H_2 is consumed, the reaction is driven to the right because both H_2O and CO_2 are produced in equal quantities in the anodic reaction. Because of the shift reaction, fuel utilization in MCFCs can exceed the value for H_2 utilization, based on the inlet H_2 concentration. For example, for an anode gas composition of 34% H_2, 22% H_2O, 13% CO, 18% CO_2, and 12% N_2, a fuel utilization of 80% (i.e., equivalent to 110% H_2 utilization) can be achieved even though this would require 10% more H_2 (total of 37.6%) than is available in the original fuel. The high fuel utilization is possible because the shift reaction provides the necessary additional H_2 that is oxidized at the anode. In this case, the fuel utilization is defined by

---

4. Assumes no gas cross-over or leakage out of the cell.
5. Example 9-5 in Section 9 illustrates how to determine the amount of H_2 produced by the shift reaction.

$$U_f = \frac{H_{2,\,consumed}}{H_{2,in} + CO_{in}} \qquad (2\text{-}42)$$

where the H_2 consumed originates from the H_2 present at the fuel cell inlet ($H_{2,in}$) and any H_2 produced in the cell by the water gas shift reaction (CO_{in}).

Gas composition changes between the inlet and outlet of a fuel cell, caused by the electrochemical reaction, lead to reduced cell voltages. This voltage reduction arises because the cell voltage adjusts to the lowest electrode potential given by the Nernst equation for the various gas compositions at the exit of the anode and cathode chambers. Because electrodes are usually good electronic conductors and isopotential surfaces, the cell voltage can not exceed the minimum (local) value of the Nernst potential. In the case of a fuel cell with the flow of fuel and oxidant in the same direction (i.e., co-flow), the minimum Nernst potential occurs at the cell outlet. When the gas flows are counterflow or crossflow, determining the location of the minimum potential is not straightforward.

The MCFC provides a good example to illustrate the influence of the extent of reactant utilization on the electrode potential. An analysis of the gas composition at the fuel cell outlet as a function of utilization at the anode and cathode is presented in Example 9-5. The Nernst equation can be expressed in terms of the mole fraction of the gases (X_i) at the fuel cell outlet:

$$E = E^o + \frac{RT}{2\mathcal{F}} \ln \frac{X_{H_2} X_{O_2}^{1/2} X_{CO_2,cathode} P^{1/2}}{X_{H_2O,anode} X_{CO_2,anode}} \qquad (2\text{-}43)$$

where P is the cell gas pressure. The second term on the right side of Equation (2-43), the so-called Nernst term, reflects the change in the reversible potential as a function of reactant utilization, gas composition, and pressure. Figure 2-8 illustrates the change in reversible cell potential as a function of utilization using Equation (2-43).

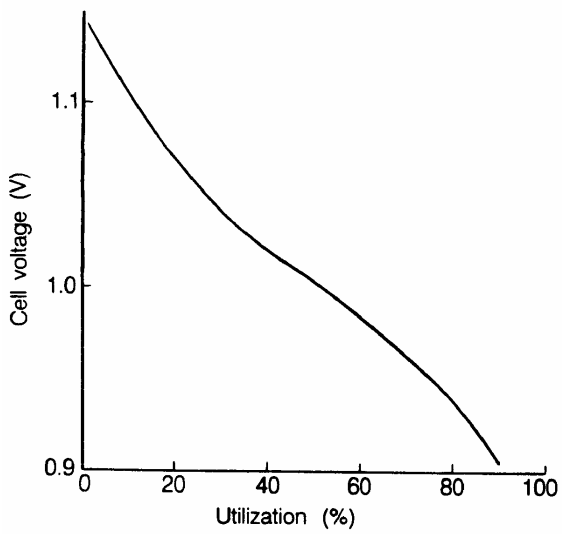

Figure 2-8 The Variation in the Reversible Cell Voltage as a Function of Reactant Utilization

(Fuel and oxidant utilizations equal) in a MCFC at 650°C and 1 atm. Fuel gas: 80% H_2/20% CO_2 saturated with H_2O at 25°C; oxidant gas: 60% CO_2/30% O_2/10% inert)

The reversible potential at 650°C (1200°F) and 1 atmosphere pressure is plotted as a function of reactant utilization (fuel and oxidant utilizations are equal) for inlet gas compositions of 80% H_2/20% CO_2 saturated with H_2O at 25°C (77°F) (fuel gas[6]) and 60% CO_2/30% O_2/10% inerts (oxidant gas); gas compositions and utilizations are listed in Table 2-4. Note that the oxidant composition is based on a gas of 2/1 CO_2 to O_2. The gas is not representative of the cathode inlet gas of a modern system, but is used for illustrative purposes only. The mole fractions of H_2 and CO in the fuel gas decrease as the utilization increases, and the mole fractions of H_2O and CO_2 show the opposite trend. At the cathode, the mole fractions of O_2 and CO_2 decrease with an increase in utilization because they are both consumed in the electrochemical reaction. The reversible cell potential plotted in Figure 2-8 is calculated from the equilibrium compositions for the water gas shift reaction at the cell outlet. An analysis of the data in the figure indicates that a change in utilization from 20% to 80% will cause a decrease in the reversible potential of about 0.158 V. These results show that MCFCs operating at high utilization will suffer a large voltage loss because of the magnitude of the Nernst term.

An analysis by Cairns and Liebhafsky (7) for a H_2/air fuel cell shows that a change in the gas composition that produces a 60 mV change in the reversible cell potential near room temperature corresponds to a 300 mV change at 1200°C (2192°F). Thus, gas composition changes are more significant in high temperature fuel cells.

[6]. Anode inlet composition is 64.5% H_2/6.4% CO_2/13% CO/16.1% H_2O after equilibration by water gas shift reaction.

Table 2-4 Outlet Gas Composition as a Function of Utilization in MCFC at 650°C

Gas		Utilization[a] (%)			
	0	25	50	75	90
Anode[b]					
X_{H2}	0.645	0.410	0.216	0.089	0.033
X_{CO2}	0.064	0.139	0.262	0.375	0.436
X_{CO}	0.130	0.078	0.063	0.033	0.013
X_{H2O}	0.161	0.378	0.458	0.502	0.519
Cathode[c]					
X_{CO2}	0.600	0.581	0.545	0.461	0.316
X_{O2}	0.300	0.290	0.273	0.231	0.158

a - Same utilization for fuel and oxidant. Gas compositions are given in mole fractions.
b - 80% H_2/20% CO_2 saturated with H_2O at 25°C. Fuel gas compositions are based on compositions for water gas shift equilibrium.
c - 30% O_2/60% CO_2/10% inert gas. Gas is not representative of a modern system cathode inlet gas, but used for illustrative purposes only.

2.7 Mathematical Models

Mathematical models are critical for fuel cell scientists and developers as they can help elucidate the processes within the cells, allow optimization of materials, cells, stacks, and systems, and support control systems. Mathematical models are perhaps more important for fuel cell development than for many other power technologies because of the complexity of fuel cells and fuel cell systems, and because of the difficulty in experimentally characterizing the inner workings of fuel cells. Some of the most important uses of mathematical fuel cell models are:

- To help understand the internal physics and chemistry of fuel cells. Because experimental characterization is often difficult (because of physical access limitations and difficulty in controlling test parameters independently), models can help understand the critical processes in cells.
- To focus experimental development efforts. Mathematical models can be used to guide experiments and to improve interpolations and extrapolations of data. The rigor of modeling often forces the explicit position of a scientific hypothesis and provides a framework for testing the hypothesis.
- To support system design and optimization. Fuel cell systems have so many unit operations and components that system models are critical for effective system design.
- To support or form the basis of control algorithms. Because of the complexity of fuel cell systems, several developers have used fully dynamic models of fuel cell systems as the basis for their control algorithms.

- To evaluate the technical and economic suitability of fuel cells in applications. Models can be used to determine whether a fuel cell's unique characteristics will match the requirements of a given application and evaluate its cost-effectiveness.

Each of these applications for fuel cell models has a specific requirement with respect to the level of detail and rigor in the model and its predictive capability. In many higher level applications, the predictive requirements are modest. In some cases, the operational characteristics of the fuel cell are not even a degree a freedom. In such cases, relatively simple models are satisfactory and appropriate. It is possible to encapsulate the mass and energy balances and performance equations for a fuel cell within a spreadsheet application. Such spreadsheet models are often useful for quick trade-off considerations.

On the other end of the spectrum, models intended to improve understanding of complex physical and chemical phenomena or to optimize cell geometries and flow patterns are necessarily very sophisticated, and usually have intensive computational requirements.

As expected, given this wide range of potential uses and the variety of fuel cell types, an equally wide variety of fuel cell models has been developed. While fundamentally the constitutive equations such as those described earlier in this chapter underlie all models, their level of detail, level of aggregation, and numerical implementation method vary widely. A useful categorization of fuel cell models is made by level of aggregation, as shown in Figure 2-9.

As implied in the figure, the outputs of the more detailed fundamental models can be used in lower-order models. This flow of information is, in fact, a critical application for high fidelity models. Recently, much work has been done in the development of algorithms to integrate or embed high-fidelity models into system analysis simulation tools.

Despite the availability of quite sophisticated fuel cell models with well-written code and convenient user interfaces, the fuel cell developer or engineer must be a critical user. As mentioned above, obtaining experimental data on the behavior of fuel cells (especially internally and at the micro-level) can be difficult, time-consuming, and expensive. Unfortunately this has lead to a dearth of accurate and detailed data of sufficient quality and quantity to allow thorough validation of the mathematical models. Much of the data on fuel cell performance reported in the literature is, while phenomenologically often interesting, insufficiently accurate and accompanied by far too little detail on the test conditions to be usable for model validation. In particular, with much of the cell and stack taken at modest utilization, it is almost impossible to infer kinetic data without spatially resolved data on current density, temperature and species concentrations. As a consequence, the validity of fuel cell models must be critically considered for each use. The user of the model must be thoroughly familiar with the assumptions and limitations embedded in the models.

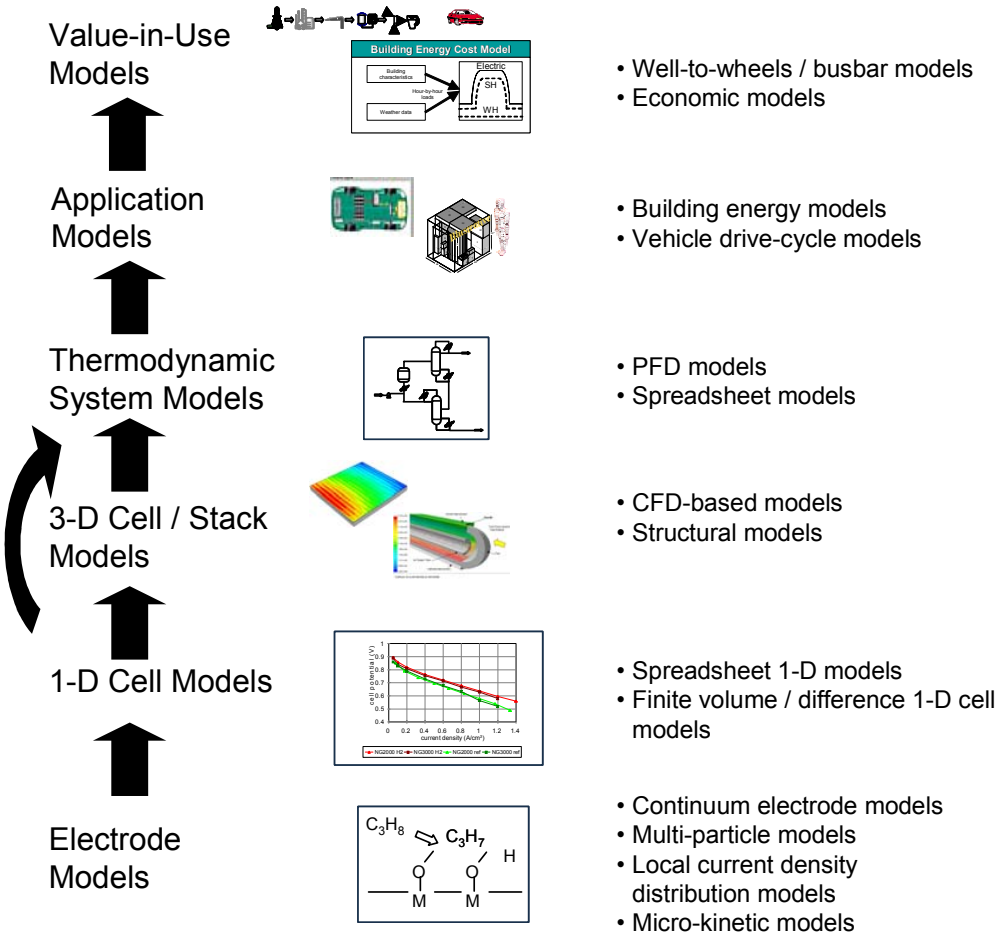

Figure 2-9 Overview of Levels of Fuel Cell Models.

The sub-sections following describe examples of each type of model and provide some insight into their uses. Khaleel (8) and Fleig (9) provide useful overviews of the active developers in fuel cell modeling at different levels of aggregation, in particular for SOFC applications.

2.7.1 Value-in-Use Models

Value-in-use models are mathematical models that allow the user to predict how the unique features of fuel cells will create value or benefits in a given application. Since such models are usually highly application-specific, two examples are provided rather than an exhaustive review. A typical model of this type would be an economic model that helps the user to predict the cost savings resulting from the installation of a fuel cell CHP system in a building. Inputs usually include building specifications and use, climate information, performance and cost characteristics of the fuel cell CHP system, and applicable utility rate structures. Generally, only a high-level description of the fuel cell system is embedded, representing the efficiency and emissions versus load curves. The models are then used, for example, to evaluate the cost-effectiveness of a fuel cell CHP system or compare it with other CHP options. DOE has

supported the development of a number of models of this kind (10), while national laboratories and private companies have developed their own versions of this type of software.

Another well-known type of value-in-use model is the well-to-wheels analysis, in which the energy consumption, environmental impact, and sometimes cost of different transportation options are compared considering all steps from the primary resource to the vehicle. This type of model is commonly used to evaluate hydrogen PEFC vehicles. Argonne National Laboratories' GREET model (11) is the most widely used of these models.

A critical subset of value-in-use models is that used to help establish the manufacturing cost of fuel cells. Several developers have created detailed manufacturing cost models for PEFC and SOFC over the past years (12, 13, 14), the results of which are widely used both in value-in-use models and for business planning. These models typically consider the individual processing steps required to produce particular cell and stack geometries at a given production volume (usually high production volumes). Based on estimates of the material costs, capital cost, and labor requirements for each process step, an estimate of the stack cost is developed. Costs of other components and sub-systems are determined based on a combination of vendor quotes and other manufacturing sub-models.

2.7.2 Application Models

Fuel cell application models are used to assess the interactions between the fuel cell power system and the application environment. The most common use is in vehicle applications where the dynamic interactions between the power system and the vehicle are too complex to analyze without the help of a mathematical model. Several commercial providers of dynamic vehicle modeling software have developed Fuel Cell modules (e.g. Gamma Technologies' GT Power, MSC Software's MSC.EASY5 and others). The best-published vehicle simulator of this type is ADVISOR (Advanced VehIcle SimulatOR) developed by the National Renewable Energy Laboratory and now commercialized by AVL (15). The model assesses the performance and fuel economy of conventional, electric, hybrid, and fuel cell vehicles. The user can evaluate component and vehicle specifications such as electric motors, batteries, engines, and fuel cells. ADVISOR simulates the vehicle's performance under different driving conditions. Industry partnerships contributed state-of-the-art algorithms to ensure the accuracy of the model. For example, detailed electrical analysis is made possible by co-simulation links to Avant's Saber and Ansoft's SIMPLORER. Transient air conditioning analysis is possible by co-simulation with C&R Technologies' SINDA/FLUINT. Michelin provided data for a tire rolling resistance model, and Maxwell provided data for an ultracapacitor energy storage model.

2.7.3 Thermodynamic System Models

Fuel cell system models have been developed to help understand the interactions between various unit operations within a fuel cell system. Most fuel cell system models are based on thermodynamic process flow simulators used by the process industry (power industry, petroleum industry, or chemical industry) such as Aspen Plus, HYSIS, and ChemCAD. Most of these codes are commercially distributed, and over the past years they have offered specific unit operations to assist modeling fuel cell stacks (or at least a guide for putting together existing unit operations to represent a fuel cell stack) and reformers. Others (16) have developed more sophisticated 2-D

models to help with dynamic or quasi-dynamic simulations. The balance of plant components usually can be readily modeled using existing unit operations included in the packages.

These types of models are used routinely by fuel cell developers, and have become an indispensable tool for system engineers. The accuracy of the basic thermodynamic models is quite good, but because the fuel cell sub-models are typically lumped parameter models or simply look-up tables, their accuracy depends heavily on model parameters that have been developed and validated for relevant situations. Aspen Plus is described below as an example, followed by a description of GCTools, an Argonne National Laboratory modeling set that offers an alternative to codes from the commercial software industry.

Unit Operations Models for Process Analysis using ASPEN

DOE's National Energy Technology Laboratory has been engaged in the development of systems models for fuel cells for over 15 years. The models were originally intended for use in applications of stationary power generation designs to optimize process performance and to evaluate process alternatives. Hence, the models were designed to work within DOE's ASPEN process simulator and later ported to the commercial version of this product, ASPEN Plus. ASPEN is a sophisticated software application developed to model a wide variety of chemical processes. It contains a library of unit operations models that simulate process equipment and processing steps, and it has a chemical component data bank that contains physical property parameters that are used to compute thermodynamic properties, including phase and chemical equilibrium.

The first general purpose fuel cell model was a Nernst-limited model designed to compute the maximum attainable fuel cell voltage as a function of the cell operating conditions, inlet stream compositions, and desired fuel utilization. Subsequently, customized unit operations models were developed to simulate the operation of solid oxide (internal reforming), molten carbonate (both external and internal reforming), phosphoric acid, and polymer electrolyte fuel cells (PEFC). These fuel cell models are lumped parameter models based on empirical performance equations. As operation deviates from the setpoint conditions at a "reference" state, a voltage adjustment is applied to account for perturbations. Separate voltage adjustments are applied for current density, temperature, pressure, fuel utilization, fuel composition, oxidant utilization, oxidant composition, cell lifetime, and production year. These models were developed in a collaborative effort by DOE's National Energy Technology Laboratory and the National Renewable Energy Laboratory.

In recent years, participants in the SECA core program have developed a stack sub-model for ASPEN that adequately represents intermediate temperature SOFC.

Stand-alone fuel cell power systems have been investigated, as well as hybrid systems using a wide variety of fuels and process configurations. Some of the systems analyses studies that have been conducted using these fuel cell models are described in Chapter 8.

Argonne's GCTool

Argonne National Laboratory developed the General Computational Toolkit (GCTool) specifically for designing, analyzing, and comparing fuel cell systems and other power plant

configurations, including automotive, space-based, and stationary power systems. A library of models for subcomponents and physical property tables is available, and users can add empirical models of subcomponents as needed. Four different types of fuel cell models are included: polymer electrolyte, molten carbonate, phosphoric acid, and solid oxide. Other process equipment models include heat exchangers, reactors (including reformers), and vehicle systems. The physical property models include multiphase chemical equilibrium. Mathematical utilities include a nonlinear equation solver, a constrained nonlinear optimizer, an integrator, and an ordinary differential equation solver.

GCTool has been used to analyze a variety of PEFC systems using different fuels, fuel storage methods, and fuel processing techniques. Examples include compressed hydrogen, metal hydride, glass microsphere, and sponge-iron hydrogen storage systems. Fuel processing alternatives have included reformers for methanol, natural gas, and gasoline using either partial oxidation or steam reforming.

Researchers have examined atmospheric and pressurized PEFC automotive systems. These analyses included the identification of key constraints and operational analysis for off-design operation, system dynamic and transient performance, and the effects of operation at extreme temperatures.

2.7.4 3-D Cell / Stack Models

Fuel cell stack models are used to evaluate different cell and stack geometries and to help understand the impact of stack operating conditions on fuel cell stack performance. Given the wide range of possible stack geometries and the wide range of operating parameters that influence stack operation, optimization of stack design under specific application requirements is difficult without the help of a model that represents the key physico-chemical characteristics of stacks. A number of three-dimensional stack models has been developed for this purpose. In all of these models, the stack geometry is discretized into finite elements, or volumes, that can be assigned the properties of the various stack components and sub-components. At a minimum, the models must represent electrochemical reactions, ionic and electronic conduction, and heat and mass transfer within the cell. As with system models, most of these models rely on existing modeling platforms although in the case of stack models, an advanced 3-D modeling platform is generally required.

- Computational Fluid Dynamics (CFC) – based Fuel Cell Codes. These are based on commercial CFD codes (e.g. StarCD, Fluent, AEA Technologies' CFX) that have been augmented to represent electrochemical reactions and electronic and ionic conduction. In many cases, refinements in the treatment of catalytic chemical reactions and flow through porous media are also incorporated to represent various electrode processes. In addition to evaluating basic fuel cell performance (current density, temperature and species concentration profiles) these models can help understand the impact of different manifolding arrangements.
- Computational Structural Analysis – based codes. These are based on publicly or commercially available 3-dimensional structural analysis codes (e.g. ANSYS, Nastran, Abacus). Typically, these must be augmented to represent ionic conduction, fluid flow, and electrochemical and chemical reactions. While these codes do not provide as much insight

into the impact of complex flows as the CFD-based codes, they are usually more efficient (run faster) than CFD-based codes and can be used to assess mechanical stresses in the stack; a key issue in some of the high-temperature fuel cell technologies.

Because many of the basic elements describing the core cell performance in all of these approaches is similar, approaches developed for one type of stack model can be ported to another. Below the approach taken by NETL and Fluent is described, which is similar to the approach taken for PEFC cells developed by Arthur D. Little (17), which also applied that approach to SOFC using a structural code (ABACUS (18, 19)). Pacific Northwest National Laboratory (PNNL) has developed several 3-D stack models based on a CFD code (StarCD) and structural codes (MARC). In Europe, Forschungs-Zentrum Julich has developed its own 3-D codes. These models have been applied to a range of cell geometries, though in recent years the focus has been on planar cells.

NETL's 3-D Analysis

The National Energy Technology Laboratory (NETL) developed a 3-dimensional computational fluid dynamics (CFD) model to allow stack developers to reduce time-consuming build-and-test efforts. As opposed to systems models, 3-dimensional CFD models can address critical issues such as temperature profiles and fuel utilization; important considerations in fuel cell development.

CFD analysis computes local fluid velocity, pressure, and temperature throughout the region of interest for problems with complex geometries and boundary conditions. By coupling the CFD-predicted fluid flow behavior with the electrochemistry and accompanying thermodynamics, detailed predictions are possible. Improved knowledge of temperature and flow conditions at all points in the fuel cell lead to improved design and performance of the unit.

In this code, a 1-dimensional electrochemical element is defined, which represents a finite volume of active unit cell. This 1-D sub-model can be validated with appropriate single-cell data and established 1-D codes. This 1-D element is then used in FLUENT, a commercially available product, to carry out 3-D similations of realistic fuel cell geometries. One configuration studied was a single tubular solid oxide fuel cell (TSOFC) including a support tube on the cathode side of the cell. Six chemical species were tracked in the simulation: H_2, CO_2, CO, O_2, H_2O, and N_2. Fluid dynamics, heat transfer, electrochemistry, and the potential field in electrode and interconnect regions were all simulated. Voltage losses due to chemical kinetics, ohmic conduction, and diffusion were accounted for in the model. Because of a lack of accurate and detailed in situ characterization of the SOFC modeled, a direct validation of the model results was not possible. However, the results are consistent with input-output observations on experimental cells of this type.

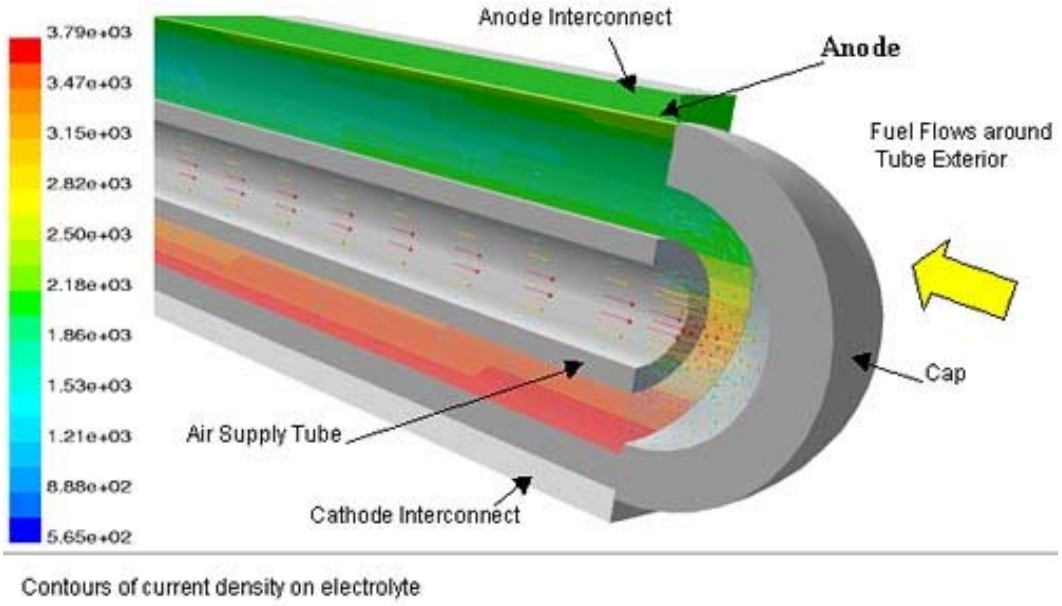

Figure 2-10 Conours of Current Density on Electrolyte

Current density is shown on the electrolyte and air-flow velocity vectors are shown for the cap-end of the tubular fuel cell. Cathode and support tube layers have been removed for clarity. Results indicate that current density and fuel consumption vary significantly along the electrolyte surface as hydrogen fuel is consumed and current flows around the electrodes between interconnect regions. Peak temperature occurs about one-third of the axial distance along the tube from the cap end.

NETL's CFD research has demonstrated that CFD-based codes can provide detailed temperature and chemical species information needed to develop improved fuel cell designs. The output of the FLUENT-based fuel cell model has been ported to finite element-based stress analysis software to model thermal stresses in the porous and solid regions of the cell. In principle, this approach can be used for other types of fuel cells as well, as demonstrated by Arthur D. Little and NETL (16,18)

Further enhancement of the design tool is continuing. The next steps are to validate the model with experimental data and then extend the model to stack module and stack analysis. NETL now operates SOFC test facilities to generate detailed model validation data using well-characterized SOFC test specimens. These steps should make it possible to create a model that accurately predicts the performance of cells and stacks so that critical design information, such as the distribution of cell and stack stresses, can be provided to the fuel cell design engineer.

2.7.5 1-D Cell Models

1-D cell models are critical for constructing 3-D models, but they are also highly useful in interpreting and planning button cell experiments. In 1-D models, all of the critical phenomena in a cell are considered in a 1-D fashion. Generally they incorporate the following elements:

- Transport phenomena:
  - Convective mass transport of reactants and products to/from the surface of the electrodes
  - Mass transport of reactants and products through the porous electrodes
  - Conduction of electronic current through the electrodes and current collectors
  - Conduction of ions through the electrolyte and electrodes (where applicable)
  - Conduction, convection, and radiation of heat throughout the cell
- Chemical reactions:
  - Electrochemical reactions at or near the triple phase boundary (TPB)
  - Internal reforming and shift reactions taking place inside the anode

Figure 2-11 shows an example for a PEFC cell.

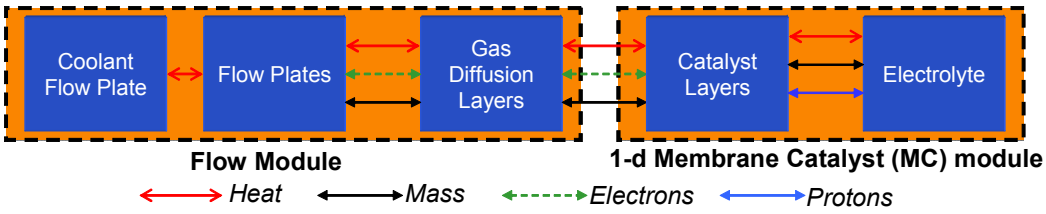

Figure 2-11 Typical Phenomena Considered in a 1-D Model (17)

A large number of 1-D models have been developed. Some are based on numerical discretization methods (e.g. finite element or finite difference methods), while others are analytical in nature. An example of the former was given in the description of the NETL 3-D model. An example of an analytical approach is provided by Chick and Stevenson (20).

2.7.6 Electrode Models

Given the importance of electrode polarization in overall cell performance, electrode sub-models are critical in the development of all other fuel cell models. As described in an excellent review by Fleig ((9), Figure 2-12), one can distinguish four levels of electrode models:

- *Continuum electrode approach*. In this approach the electrode is represented as a homogeneous zone for diffusion, electrochemical reaction, and ion- and electron-conduction. Because this approach ignores the specific processes occurring at the TPB and the impact of the microstructure of the electrode, this approach yields models that must be calibrated for each specific electrode design and for each set of operating conditions. With this approach it is impossible to distinguish between rate-determining steps in the electrochemically active zone, though the relative importance of mass transfer versus kinetic processes can be expressed crudely.
- *Multi-particle approach*. This approach recognizes that electrodes are typically made up of many particles that have different (at least two) phases with different characteristics. Issues of connectivity, percolation, and other mass-transfer-related factors can be addressed with this approach, but the details of the electrochemical reaction steps at the TPB are lumped

together. From a numerical perspective, one or more resistor networks are added to the continuum model.

- *Local current density distribution approach*. A refinement on the multi-particle approach, this approach considers that current-densities are not necessarily homogeneous within the particles, which can strongly impact electrode resistances. Often this approach is executed using a finite element method.
- *Micro-kinetics approach*. In this approach, the individual reaction steps at or near the TPB are considered. Although analytical solutions (in Buttler-Volmer form) can be found if a single rate-determining step is considered, generally a numerical solution is necessary for multi-step reactions. This approach can be embedded in the multi-particle or local-current density approaches, or directly used in a 1-D model with simpler assumptions for the transport phenomena. This is the only approach that can give insight into the rate-determining electrochemical processes that take place in the cell. When optimizing electro-catalysts or studying direct oxidation of hydrocarbons, this type of model can be very enlightening.

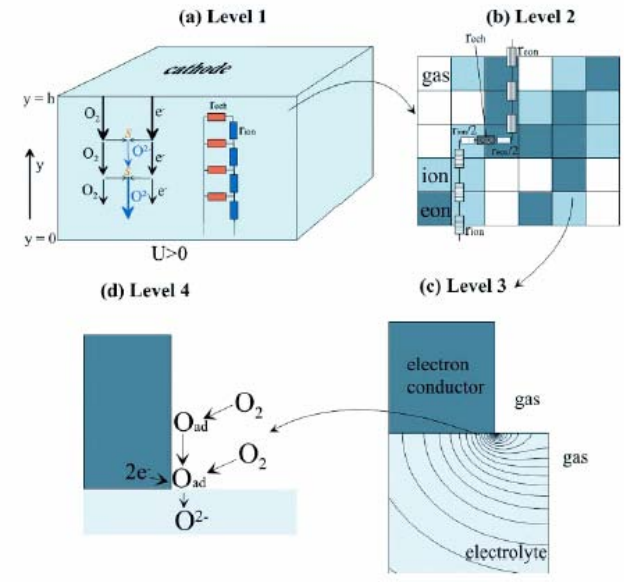

Figure 2-12 Overview of types of electrode models (9)

2.8 References

1 M.W. Chase, et al., "JANAF Thermochemical Tables," Third Edition, American Chemical Society and the American Institute of Physics for the National Bureau of Standards (now National Institute of Standards and Technology), 1985.

2 P.W. Atkins, "Physical Chemistry," 3rd Edition, W.H. Freeman and Company, New York, NY, 1986.

3 "Fuel Cell Handbook," J. Appleby and F. Foulkes, Texas A&M University, Van Nostrand Reinhold, New York (out of print), republished by Krieger Publishing Co., Melbourne, FL, 1989.

4 Winkler, W., *Thermodynamics*, in *High Temperature Solid Oxide Fuel Cells: Fundamentals, Design and Applications*, S.C. Singhal and K. Kendall, Editors. 2003, Elsevier Ltd.: Oxford, UK. p. 53 - 82.
5 S.N. Simons, R.B. King and P.R. Prokopius, in *Symposium Proceedings Fuel Cells Technology Status and Applications*, Figure 1, p. 46, Edited by E.H. Camara, Institute of Gas Technology, Chicago, IL, 45, 1982.
6 P. V. Hendriksen, S. Koch, M. Mogensen, Y. L. Liu, and P. H. Larsen, in *Solid Oxide Fuel Cells VIII*, eds S. C. Singhal and M. Dokiya, The Electrochemical Society Proceedings, Pennington, NJ, PV2003-07, 2003, p. 1147
7 E.J. Cairns and H.A. Liebhafsky, *Energy Conversion,* p. 9**,** 63, 1969.
8 Khaheel, M.A. *Modeling and Simulation SECA Core Program*. in *Modeling and Simulation Team Integration Meeting*. 2003: US DOE. http://www.seca.doe.gov/events/2002/model_simulation/pnnl_m_khaleel.pdf
9 Fleig, J., Solid Oxide Fuel Cell Cathodes: Polarization Mechanisms and Modeling of the Electrochemical Performance. Annual Review of Materials Research, 2003. **33**: p. 361 - 382.
10 U.S. Department of Energy, Office of Building Technology, State and Community Programs, Tools Directory web site, current URL: http://www.eere.energy.gov/buildings/tools_directory/
11 Development and Use of GREET 1.6 Fuel-Cycle Model for Transportation Fuels and Vehicle Technologies, Center for Transportation Research, Energy Systems Division, Argonne National Laboratory, Report ANL/ESD/TM-163, June 2001.
12 Carlson, E., *Assessment of Planar Solid Oxide Fuel Cell Technology*. 1999, US Department of Energy: Cambridge, MA, USA.
13 Koslowske, M., *A Process Based Cost Model for Multi-Layer Ceramic Manufacturing of Solid Oxide Fuel Cells*, in *Materials Science*. 2003, Worcester Polytechnic Institute: Worcester, MA, USA. p. 42.
14 Carlson, E. and S. Mariano, *Cost Analysis of Fuel Cell System for Transportation*. 2000, Arthur D. Little for US DOE OTT: Cambridge, MA, USA.
15 ADVISOR: A Systems Analysis Tool for Advanced Vehicle Modeling, Markel, T., et al., Journal of Power Sources, 2002, available from the following URL: http://www.ctts.nrel.gov/analysis/advisor.html
16 J. Pålsson, A. Selimovic, and L. Sjunnesson, *J. Power Sources*, **86**, (2000), 442 - 448
17 Sriramulu, S. and J. Thijssen. in *Fuel Cell Seminar*. 2000. Portland, OR: US DOE.
18 Thijssen, J. and S. Sriramulu, *Structural Limitations in the Scale-Up of Anode-Supported SOFCs*. 2002, Arthur D. Little for US DOE: Cambridge, MA, USA.
19 Fulton, C., et al. *Structural Limitations in the Scale-Up of Anode-Supported SOFCs*. in *Fuel Cell Seminar*. 2002. Palm Springs, CA: US Department of Energy.
20 Chick, L.A., J.W. Stevenson, and R. Williford. *Spreadsheet Model of SOFC Electrochemical Performance*. in *SECA Training Workshop*. 2003. Morgantown, WV: US DOE NETL. http://www.netl.doe.gov/publications/proceedings/03/seca-model/Chick8-29-03.pdf

3. POLYMER ELECTROLYTE FUEL CELLS

Polymer electrolyte membrane fuel cells (PEFC)[7] are able to efficiently generate high power densities, thereby making the technology potentially attractive for certain mobile and portable applications. Especially the possible application of PEFC as a prime mover for automobiles has captured the imagination of many. PEFC technology differentiates itself from other fuel cell technologies in that a solid phase polymer membrane is used as the cell separator/electrolyte. Because the cell separator is a polymer film and the cell operates at relatively low temperatures, issues such as sealing, assembly, and handling are less complex than most other fuel cells. The need to handle corrosive acids or bases is eliminated in this system. PEFCs typically operate at low temperatures (60^{o} to 80 ^{o}C), allowing for potentially faster startup than higher temperature fuel cells. The PEFC is seen as the main fuel cell candidate technology for light-duty transportation applications. While PEFC are particularly suitable for operation on pure hydrogen, fuel processors have been developed that will allow the use of conventional fuels such as natural gas or gasoline. A unique implementation of the PEFC allows the direct use of methanol without a fuel processor; it is the direct methanol fuel cell (DMFC). The DMFC is seen as the leading candidate technology for the application of fuel cells to cameras, notebook computers, and other portable electronic applications.

3.1 Cell Components

Typical cell components within a PEFC stack include:

- the ion exchange membrane
- an electrically conductive porous backing layer
- an electro-catalyst (the electrodes) at the interface between the backing layer and the membrane
- cell interconnects and flowplates that deliver the fuel and oxidant to reactive sites via flow channels and electrically connect the cells (Figure 3-1).

PEFC stacks are almost universally of the planar bipolar type. Typically, the electrodes are cast as thin films that are either transferred to the membrane or applied directly to the membrane. Alternatively, the catalyst-electrode layer may be deposited onto the backing layer, then bonded to the membrane.

7. Polymer electrolyte membrane fuel cells are referred to by several acronyms; a common one is PEM, which stands for Proton Exchange Membrane.

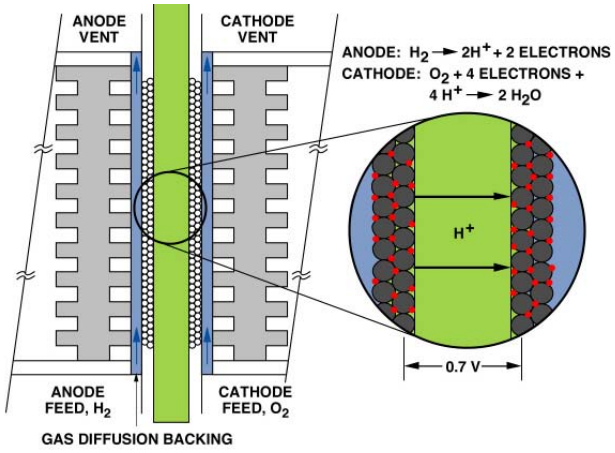

(a)

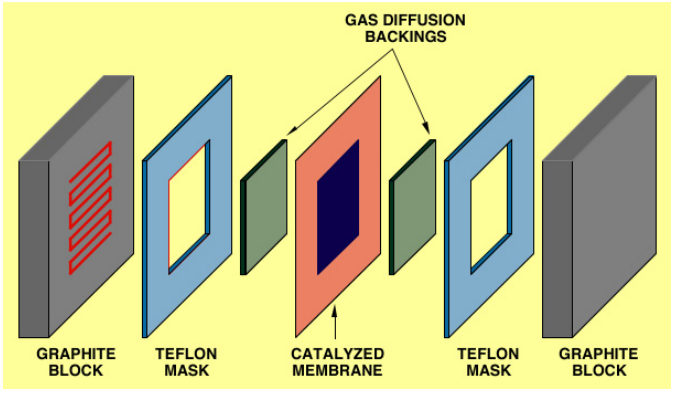

(b)

Figure 3-1 (a) Schematic of Representative PEFC (b) Single Cell Structure of Representative PEFC(1)

3.1.1 State-of-the-Art Components

Membrane

Organic-based cation exchange membranes in fuel cells were originally conceived by William T. Grubb (2) in 1959. That initial effort eventually led to development of the perfluorosulfonic acid polymer used in today's systems. The function of the ion exchange membrane is to provide a conductive path, while at the same time separating the reactant gases. The material is an electrical insulator. As a result, ion conduction takes place via ionic groups within the polymer structure. Ion transport at such sites is highly dependent on the bound and free water associated with those sites.

An accelerated interest in polymer electrolyte fuel cells has led to improvements in both cost and performance. Development has reached the point where both motive and stationary power

applications are nearing an acceptable cost for commercial markets. Operation of PEFC membrane electrode assemblies (MEAs) and single cells under laboratory conditions similar to transportation or stationary applications have operated for over 20,000 hrs continuously with degradation rates of 4 to 6 μV/hr (or about 0.67 to 1.0 percent per 1000 hrs), which approaches the degradation rates needed for stationary applications (about 0.1 percent per 1000 hrs is used as a rule of thumb). Complete fuel cell systems have been demonstrated for a number of transportation applications including public transit buses and passenger automobiles. For stationary applications, a number of demonstration systems have been developed and numerous systems have been installed, mostly in the 2 to 10 kW range. However, although these systems have collectively logged millions of kWhrs (3), developers have not yet demonstrated system or stack life of more than 8,000 hours with realistic catalyst loadings and realistic operating conditions, and then with degradation rates of several percent per 1000 hrs. Consequently, PEFC developers and researchers are focused on achieving critical improvements in extending stack life, simpler system integration, and reduction of system cost. This is true both for stationary and mobile applications.

Manufacturing details of Plug Power's cell and stack design are proprietary, but the literature provides some information on the cell and stack design. Example schematics for the cross-section and a current collecting plate are shown in Figure 3-2 (4, 5). An approach for sealing the cell with flat gaskets is shown (Label 402) but there are many alternatives with gaskets and plates having different shapes and grooves, respectively. The plate shows the flow path for one of the reactants from the inlet to the outlet manifold. The other side of the plate (not shown) would have channels either for coolant flow or the other reactant.

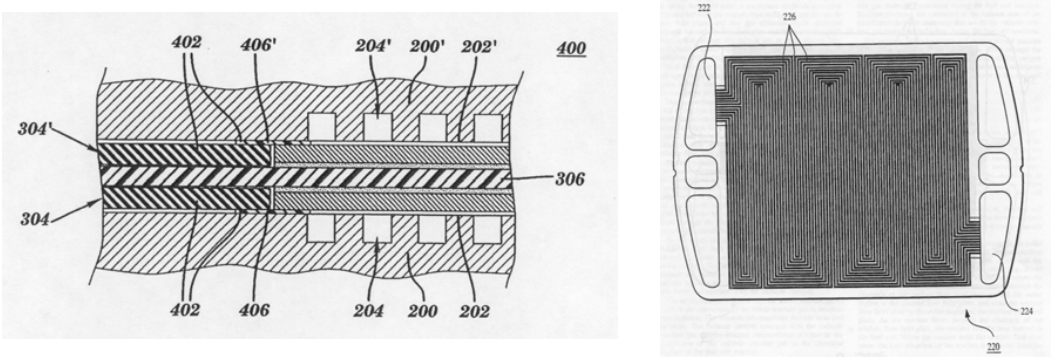

Figure 3-2 PEFC Schematic (4, 5)

The standard electrolyte material in PEFCs belongs to the fully fluorinated Teflon®-based family similar to that produced by E.I. DuPont de Nemours for space application in the mid-1960s. The membrane is characterized by its equivalent weight (inversely proportional to the ion exchange capacity). A typical equivalent weight range is 800 to 1100 milliequivalents per dry gram of polymer. The type used most often in the past was a melt-extruded membrane manufactured by DuPont and sold under the label Nafion® No. 117. The perfluorosulfonic acid family of

membranes exhibits exceptionally high chemical and thermal stability, and is stable against chemical attack in strong bases, strong oxidizing and reducing acids, Cl_2, H_2, and O_2 at temperatures up to 125°C (6). Nafion consists of a fluoropolymer backbone, similar to Teflon®, upon which sulfonic acid groups are chemically bonded (7,29). Nafion membranes have exhibited long life in selected applications, operating conditions, and electrochemical applications. In selected fuel cell tests and water electrolysis systems, lifetimes of over 50,000 hours have been demonstrated. The Dow Chemical Company produced an electrolyte membrane, the XUS 13204.10, that contained a polymeric structure similar to that of Nafion, except that the side chain length was shortened (8). As a result, the membrane properties were significantly impacted, including a higher degree of water interactions within the membrane. This translated to lower electrical resistance and permited higher current densities than the Nafion membrane, particularly when used in thinner form (9). These short side-chain membranes exhibited good performance and stability, but are no longer supplied by Dow. Furthermore, due to Nafion's expense and other engineering issues, new alternative membranes are being developed by a number of different companies.

Progress in manufacturing techniques has been made. Although melt-extruded films were the norm, the industry is moving to a solution-cast film process to reduce costs and improve manufacturing throughput efficiency. In this process, the ionic form of the polymer is solubilized in alcoholic solution, such as propanol, and then fabricated into a film of desired thickness. The conversion of the non-ionic polymer to an ionic phase, ready for use in a fuel cell, is carried out prior to the solubilization step.

Another advancement in membrane technology is that of using an internal support layer to enhance the mechanical strength of the membrane film, especially as the membrane thickness is decreased. The Primea 55 and 56 series membranes manufactured by W.L. Gore are examples of such internally-supported membranes.

Porous Backing Layer

The polymer membrane is sandwiched between two sheets of porous backing media (also referred to as gas diffusion layers or current collectors). The functions of the backing layer[8] are to: (1) act as a gas diffuser; (2) provide mechanical support, (3) provide an electrical pathway for electrons, and (4) channel product water away from the electrodes. The backing layer is typically carbon-based, and may be in cloth form, a non-woven pressed carbon fiber configuration, or simply a felt-like material. The layer incorporates a hydrophobic material, such as polytetrafluoroethylene. The function of polytetrafluoroethylene is to prevent water from "pooling" within the pore volume of the backing layer so that gases freely contact the catalyst sites. Furthermore, it facilitates product water removal on the cathode as it creates a non-wetting surface within the passages of the backing material.

One PEFC developer (10) devised an alternative plate structure that provides passive water control. Product water is removed by two mechanisms: (1) transport of liquid water through the porous bipolar plate into the coolant, and (2) evaporation into the reactant gas streams. The cell is similar in basic design to other PEFCs with membrane, catalysts, substrates, and bipolar plate components. However, there is a difference in construction and composition of the bipolar plate:

8. Commonly referred to as the gas diffusion layer (GDL) even though it has additional functions.

it is made of porous graphite. During operation, the pores are filled with liquid water that communicates directly with the coolant stream. Product water flows from the cathode through the pores into the coolant stream (a small pressure gradient between reactant and the coolant stream is needed). The water in the coolant stream is then routed to a reservoir. Removal of water by the porous membrane results in the reactant flow stream being free of any obstructions (liquid water). The flooded pores serve a second purpose of supplying water to the incoming reactant gases and humidifying those gases. This prevents drying of the membrane, a common failure mode, particularly at the anode. Control of the amount of area used to humidify the inlet gases has eliminated the need to pre-humidify the reactant gases.

Reasons for removing the water through the porous plate are: (1) there is less water in the spent reactant streams; (2) this approach reduces parasitic power needs of the oxidant exhaust condenser; (3) the cell can operate at high utilizations that further reduce water in the reactant streams; (4) higher temperatures can be used with higher utilizations so that the radiator can be smaller,[9] and (5) the control system is simplified. In fact, in-stack water conservation is even more important in arid climates, where there may exist a significant challenge to achieve water balance at the system level without supplying water or refrigerating the exhaust stream.

Hand-in-hand with water management goes the thermal management of the stack. Temperatures within the stack must be kept within a narrow range in order to avoid local dehydration and hot-spots as well as local dead zones. This is particularly challenging when one recognizes the narrow temperature zone and the relatively small temperature difference between the cell operating temperature and the ambient temperature.

Electrode-Catalyst Layer

In intimate contact with the membrane and the backing layer is the catalyst layer. This catalyst layer, integral with its binder, forms the electrode. The catalyst and binder electrode structure is applied either to the membrane or to the backing layer. In either case, the degree of intimacy of the catalyst particles and the membrane is critical for optimal proton mobility. The binder performs multiple functions. In one case, it “fixes” the catalyst particles within a layered structure, while a second function is to contribute to the overall architecture of the electrode. This architecture has a direct bearing on performance.

There are two schools of thought on the electrode composition, in particular, the binder. In the original hydrophobic, porous, gaseous electrodes developed by Union Carbide and later advanced by General Electric, the Dow Chemical Company, and others, the binder was polytetrafluoroethylene: a non-wetting component within the electrode itself. The second school of electrode science developed a hydrophyllic electrode in which the binder was perfluorosulfonic acid. The driver for this development was to enhance the membrane/catalyst contact to minimize the platinum loading requirements (11). In most state-of-the-art PEFC membrane electrode assemblies (MEAs), the catalyst is largely embedded in a solution of electrolyte monomer, which provides high solubility for protons as well as oxygen, and thus effective use of the platinum catalyst surface.

---

9. Higher average temperature operaton is possible because of the reduction of hot spots within the cell. Water will evaporate through the porous plate in the vicinity of a hot spot. Conversely, a local cool spot can produce a concentration of water. This water is quickly removed through the porous plate.

The catalyst is platinum-based for both the anode and cathode. To promote hydrogen oxidation, the anode uses either pure platinum metal catalyst or, as is common in most modern PEFC catalysts, a supported platinum catalyst, typically on carbon or graphite for pure hydrogen feed streams. For other fuels, such as reformate (containing H_2, CO_2, CO, and N_2), the desired catalyst is an alloy of platinum containing ruthenium. Oxygen reduction at the cathode may use either the platinum metal or the supported catalyst.

Because of the the expense of the platinum catalyst, there have been numerous efforts to minimize the use of platinum in the catalyst layer. The platinum particle size has been extensively optimized, and general agreement is that a ~3.5 nm particle size on suitable carbon support is close to optimal: the activity per unit mass of platinum is near optimal under these conditions. In parallel, there have been numerous efforts to substitute other materials for platinum. Most of these attempts focused either on gold or on platinum alloys (usually with transition metals). So far, these efforts have not demonstrated a decisive cost advantage over pure platinum catalysts.

Typically, electrodes can be cast as thin films and transferred to the membrane or applied directly to the membrane. Alternatively, the catalyst-electrode layer may be deposited onto the gas diffusion layer (GDL), then bonded to the membrane. Low platinum loading electrodes (≤ 1.0 mg Pt/cm^2 total on the anode and the cathode) are regularly used, and have performed as well as earlier, higher platinum loading electrodes (2.0 to 4.0 mg Pt/cm^2). These electrodes, which have been produced using a high-volume manufacturing process, have achieved nearly 600 mA/cm^2 at 0.7 V on reformate. A number of companies globally are developing such electrodes. An example of electrode performance is shown in Figure 3-3. The figure depicts the performance of a standard 100 cm^2 7-layer membrane electrode assembly (MEA) manufactured by the 3M Corporation operating on hydrogen and reformate at 70 °C (12). Recent advances in MEA performance and durability have led to tests with reformate in excess of 10,000 hours with the 3M 7-layer MEA. This MEA is produced using high-speed, continuous, automated assembly equipment.

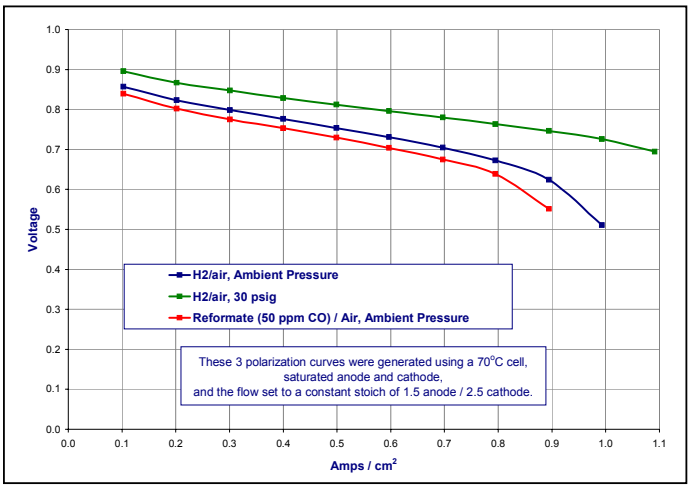

Figure 3-3 Polarization Curves for 3M 7 Layer MEA (12)

The electrochemical reactions of the PEFC are similar to those of the PAFC[10]: molecular hydrogen at the anode is oxidized to provide protons, while at the same time freeing two electrons that pass through an external "electrical" circuit to reach the cathode. The voltages at each electrode, due to the hydrogen oxidation potential and the oxygen reduction potential, form a voltage gradient of approximately 1 volt (depending on conditions) at open circuit, i.e., zero current draw. It is this potential that drives the proton through the membrane. As the proton is "pulled" through the membrane, it drags with it a certain number of water molecules. The proton reacts with oxygen to form water at the catalyst sites on the cathode.

Because of the intrinsic nature of the materials used, the PEFC operates at temperatures between 0 °C to 90 °C, typically in the 60 °C to 80 °C range. When compared to other fuel cells, PEFC technology has been capable of very high current densities: while most technologies can operate up to approximately 1 amp/cm^2, polymer electrolyte membrane fuel cells have operated at up to 4 amps/cm^2 (13). Stack level power densities under pra 2 ctical operating conditions (cathode stoichiometry less than 3, anode utilization more than 85%, pressure less than 3 bar, and catalyst loadings less than 1 mg/cm^2) with reformate of around 50 mW/cm^2 at 0.7 V and of around 400 – 600 mW/cm^2 when operating with hydrogen are feasible (14, 15, 16, 17). This performance is due primarily to the impressive ionic conductivity of PEFC membranes and the high electrical conductivity of the materials used in the gas diffusion layers and bipolar plates (mostly carbon or metals). Other desirable attributes include fast start capability and rapid response to load changes. Because of the high power density capability, smaller, lighter-weight stacks are possible (18). Other beneficial attributes of the cell include no corrosive fluid hazard and lower sensitivity to orientation. As a result, the PEFC is thought to be best suited for vehicular power applications.

The low operating temperature of a PEFC has both advantages and disadvantages. Low temperature operation is advantageous because the cell can start from ambient conditions

10. Equations 5-1, 5-2, and 5-3 for the PAFC apply as well to the PEFC.

quickly, especially when pure hydrogen fuel is available. It is a disadvantage in carbon monoxide-containing fuel streams, because carbon will attack the platinum catalyst sites, masking the catalytic activity and reducing cell performance.[11] The effect is reversible by flowing a CO-free gas over the electrode. To minimize CO poisoning, operating temperatures must be greater than 120 °C, at which point there is a reduction in chemisorption and electro-oxidation. Due to CO affecting the anode, only a few ppm of CO can be tolerated at 80 °C. Because reformed and shifted hydrocarbons contain about one percent CO, a mechanism to eliminate CO in the fuel gas is needed. This can be accomplished with preferential oxidation (PROX) that selectively oxidizes CO over H_2 using a precious metal catalyst. The low operating temperature also means that little, if any, heat is available from the fuel cell for endothermic reforming (19, 20).

As this discussion suggests, there is a considerable advantage at the stack level to the use of pure hydrogen rather than reformate, but in most PEFC applications this must be traded off against the challenges in storing hydrogen and the limited availability of hydrogen. Although considerable effort has been expended to develop liquid-fueled PEFC for transportation applications, most believe that on-board storage of hydrogen will be necessary for practical vehicles (21).

To overcome the challenges of operating on reformate, attempts have been made to develop so-called high-temperature PEFC, which would operate in the 120 °C to 160°C range. New or modified ion exchange membranes would be needed to allow this, because Nafion dehydrates rapidly at such temperatures unless high (greater than 10 bar) pressures are applied. One candidate material is polybenzimidizole (PBI) (22). The higher operating temperature eliminates CO poisoning by eliminating CO occlusion of the platinum sites. Also, this operating regime provides higher quality heat for possible use in stationary combined heat/power (CHP) applications. Because PBI requires significantly lower water content to facilitate proton transport, an additional benefit is that water management is dramatically simplified (23, 24). However, to achieve acceptable ionic conductivity, the membrane must be impregnated with phosphoric acid, which is apparently not very tightly bound to the polymer backbone. As a result, similar precautions are necessary as in a PAFC (avoiding liquid water, corrosion protection). The conductivity of PBI can approach the target of 10 S/cm set for high temperature membranes.

Other approaches to high-temperature membranes are based on the modification of Nafion. Reports indicate that some of the modified materials achieve conductivities close to that of Nafion 112, while allowing operation up to 120 °C at low hydration levels (25,14 ,16 ,17) Both temperature and pressure significantly influence cell performance. Present cells operate at 80 °C over a range of 0.0010 to 1.0 MPa (~0.1 to 150 psig). Nominally, 0.285 MPa (25 psig) (18) is used for some transportation applications although some developers (26) pursue ambient-pressure technology. Using appropriate current collectors and supporting structure, polymer electrolyte fuel cells and electrolysis cells should be capable of operating at pressures up to 3000 psi and differential pressures up to 500 psi (27).

11. Referred to as poisoning in catalysis literature.

Water and Thermal Management

Due to operation at less than 100 °C and atmospheric pressure, water is produced as a liquid. A critical requirement is to maintain high water content in the electrolyte to ensure high ionic conductivity. Maintaining high water content is particularly critical when operating at high current densities (approximately 1 A/cm^2) because mass transport issues associated with water formation and distribution limit cell output. The ionic conductivity of the electrolyte is higher when the membrane is fully saturated: this impacts the overall efficiency of the fuel cell. Without adequate water management, an imbalance will occur between water production and water removal from the cell.

Water content is determined by balance of water[12] during operation. Contributing factors to water transport are the water drag through the cell, back-diffusion from the cathode, and the diffusion of water in the fuel stream through the anode. Water transport is not only a function of the operating conditions[12] but also the characteristics of the membrane and the electrodes. Water drag refers to the amount of water that is pulled by osmotic action along with the proton (28). One estimate is that between 1 to 2.5 molecules are dragged with each proton (29). As a result, transported water can be envisioned as a hydrated proton, $H(H_2O)n$. During operation, a concentration gradient may form whereby the anode is drier than the cathode. Under these conditions, there is back-diffusion of water from the cathode to the anode. Membrane thickness is also a factor in that the thinner the membrane, the greater the transport of water back to the anode. The objective of the stack engineer is to ensure that all parts of the cell are sufficiently hydrated, and that no excessive flooding occurs (29, 30, 31, 32). Adherence of the membrane to the electrode will be adversely affected if dehydration occurs. Intimate contact between the electrodes and the electrolyte membrane is important because there is no free liquid electrolyte to form a conducting bridge. Because this type of degradation is largely irreversible, operation under dry conditions will severely impact membrane lifetime (33).

Reliable forms of water management have been developed based on continuous flow field design and appropriate operating adjustments. For this reason, flow field designs often feature serpentine channels or unstructured flow passages. The flow-plates (which also serve as bipolar plates) are typically made of graphite, an injection-molded and cured carbon material, or a metal. If more water is exhausted than produced, then humidification of the incoming anode gas becomes important (31). If there is too much humidification, however, the electrode floods, which causes problems with gas diffusion to the electrode. A temperature rise between the inlet and outlet of the flow field increases evaporation to maintain water content in the cell. There also have been attempts to control the water in the cell using external wicking connected to the membrane to either drain or supply water by capillary action.

Much progress has been made towards PEFC commercialization. Figure 3-4, from Gore Fuel Cell Technologies, demonstrates the company's newest commercial offering, PRIMEA® Series 56 MEA that has demonstrated over 15,000 hours of cell operation (34).

12. A smaller current, larger reactant flow, lower humidity, higher temperature, or lower pressure will result in a water deficit. A higher current, smaller reactant flow, higher humidity, lower temperature, or higher pressure will lead to a water surplus.

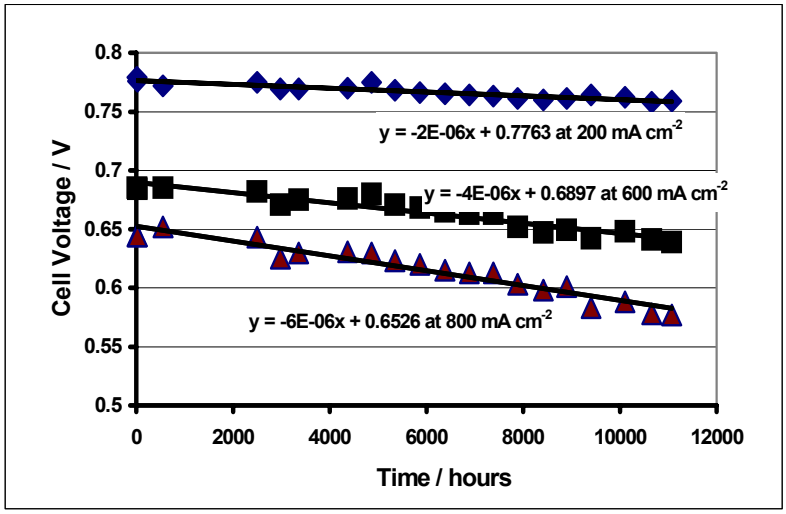

Figure 3-4 Endurance Test Results for Gore Primea 56 MEA at Three Current Densities

To improve effectiveness of the platinum catalyst, a soluble form of the polymer is incorporated into the pores of the carbon support structure. This increases the interface between the electrocatalyst and the solid polymer electrolyte. Two methods are used to incorporate the polymer solution within the catalyst. In Type A, the polymer is introduced after fabrication of the electrode; in Type B, it is introduced before fabrication.

Most PEFCs presently use cast carbon composite plates for current collection and distribution, gas distribution, and thermal management. Cooling is accomplished using a circulating fluid, usually water that is pumped through integrated coolers within the stack. The temperature rise across the cell is kept to less than 10 °C. In one configuration, water-cooling and humidification are in series, which results in the need for high quality water. The cooling unit of a cell can be integrated to supply reactants to the MEA, remove reaction products from the cell, and seal off the various media against each other and the outside. Metal (usually coated) plates are used as an alternative by some developers.

The primary contaminants of a PEFC are carbon monoxide (CO) and sulfur (S). Carbon dioxide (CO_2) and unreacted hydrocarbon fuel act as diluents. Reformed hydrocarbon fuels typically contain at least 1 percent CO. Even small amounts of CO in the gas stream, however, will preferentially adsorb on the platinum catalyst and block hydrogen from the catalyst sites. Tests indicate that as little as 10 ppm of CO in the gas stream impacts cell performance (35, 36). Fuel processing can reduce CO content to several ppm, but there are system costs associated with increased fuel purification. Platinum/ruthenium catalysts with intrinsic tolerance to CO have been developed. These electrodes have been shown to tolerate CO up to 200 ppm (37). Although much less significant than the catalyst poisoning by CO, anode performance is adversely affected by the reaction of CO_2 with adsorbed hydrides on platinum. This reaction is the electrochemical equivalent of the water gas shift reaction.

Other contaminants of concern include ammonia (membrane deterioration), alkali metals (catalyst poisoning, membrane degradation), particles, and heavy hydrocarbons (catalyst poisoning and plugging). Both the anode and cathode flows must be carefully filtered for these contaminants, as even ppb-level concentration can lead to premature cell and stack failure.

A number of technical and cost issues face polymer electrolyte fuel cells at the present stage of development (35, 38, 39, 40, 41). These concern the cell membrane, cathode performance, and cell heating limits. The membranes used in present cells are expensive, and available only in limited ranges of thickness and specific ionic conductivity. Lower-cost membranes that exhibit low resistivity are needed. This is particularly important for transportation applications characterized by high current density operation. Less expensive membranes promote lower-cost PEFCs, and thinner membranes with lower resistivities could contribute to power density improvement (41). It is estimated that the present cost of membranes could fall (by a factor of 5) if market demand increased significantly (to millions of square meters per year) (33).

The DOE has set platinum loading targets at 0.4 mg/cm^2 total, a maximum to allow achieving the automotive cost targets. This will require a significantly higher catalyst effectiveness (present loadings are on the order of 1 mg/cm^2 total) while achieving the other improvements in performance required.

Improved cathode performance, when operating on air at high current densities, is needed. At high current densities, there is a limiting gas permeability and ionic conductivity within the catalyst layer. A nitrogen blanket forming on the gas side of the cathode is suspected of creating additional limitations (1). There is a need to develop a cathode that lessens the impact of the nitrogen blanket, allows an increase in cell pressure, and increases ionic conductivity.

Local heat dissipation limits stack operation with air at a current density of approximately 2 A/cm^2. Single cells have shown the capability to operate at higher current densities on pure oxygen. It may be possible to increase current density and power density through better cooling schemes.

3.1.2 Component Development

The primary focus of ongoing research has been to improve performance and reduce cost. The principal areas of development are improved cell membranes, CO removal from the fuel stream, and improved electrode design. There has been a move toward operation with zero humidification at ambient pressure, increased cell temperature, and direct fuel use. DuPont now produces a membrane of 2 mils or less thickness that performs (at lower current densities) similar to the Dow Chemical Company membrane, the XUS 13204.10 depicted in the top curve of Figure 3-5 (42). There is ongoing work to investigate alternative membranes and MEAs that not only exhibit durability and high performance, but also can be manufactured inexpensively in high volume.

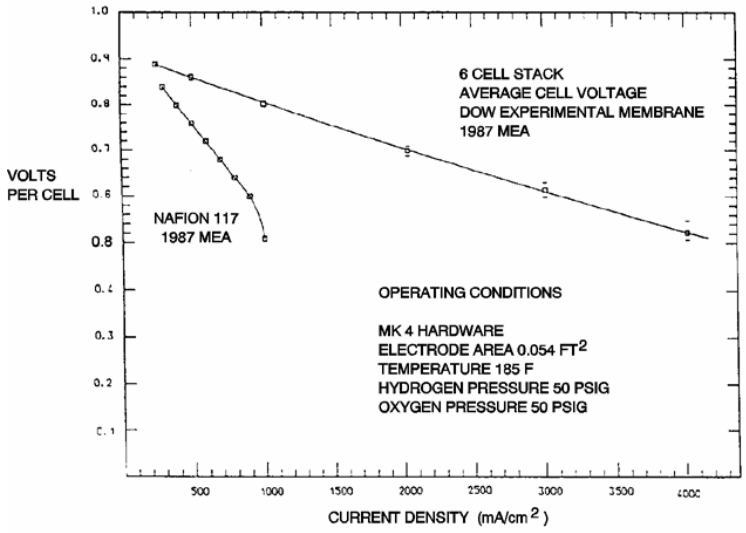

Figure 3-5 Multi-Cell Stack Performance on Dow Membrane (9)

PEFCs were originally made with an unimpregnated electrode/Nafion electrolyte interface. This was later replaced by a proton conductor that was impregnated into the active layer of the electrode. This allowed reduced catalyst loading to 0.4 mg/cm^2 while obtaining high power density (27). The standard "Prototech" electrodes contained 10 percent Pt on carbon supports. Using higher surface area carbon-supported catalysts, researchers have tested electrodes with even lower platinum loading, but having performance comparable to conventional electrodes. Los Alamos National Laboratory has tested a cathode with 0.12 mg Pt/cm^2 loading, and Texas A&M University has tested a cathode with 0.05 mg Pt/cm^2 loading. Another example of low catalyst loadings is the work carried out at DLR (43) in which loadings as low as 0.07 mg/cm^2 were applied to the membrane using a dry process. The binder was a Teflon-like material.

Another approach has been developed to fabricate electrodes with loading as low as 0.1 mg Pt/ cm^2 (44). The electrode structure was improved by increasing the contact area between the electrolyte and the platinum clusters. The advantages of this approach were that a thinner catalyst layer of 2 to 3 microns and a uniform mix of catalyst and polymer were produced. For example, a cell with a Pt loading of 0.07 to 0.13 mg/cm^2 was fabricated. The cell generated 3 A/cm^2 at > 0.4V on pressurized O_2, and 0.65 V at 1 A/cm^2 on pressurized air (44, 45).

Stable performance was demonstrated over 4,000 hours with Nafion membrane cells having 0.13 mg Pt/cm^2 catalyst loading and cell conditions of 2.4 atmospheres H_2, 5.1 atmospheres air, and 80 °C (4,000 hour performance was 0.5 V at 600 mA/cm^2). Water management was stable, particularly after thinner membranes of somewhat lower equivalent weight became available. Some performance losses may have been caused by slow anode catalyst deactivation, but the platinum catalyst "ripening" phenomenon was not considered to contribute significantly to the long-term performance losses observed in PEFCs (1).

Other research has focused on developing low-cost, lightweight, graphite carbon-based materials that can be used in place of expensive, high-purity graphite bipolar plates. Plated metals, such as aluminum and stainless steel, are also under consideration for this application, despite contact resistance and durability concerns. Conductive plastic and composite bipolar plates have met with significant success in the laboratory, and have even reached commercial production. The time line for development of a vinyl ester configuration is shown in Reference (46) for a material that has reached almost 100 S/cm.

Selective oxidation is able to decrease CO in a methanol reformed gas (anode fuel supply stream) from 1% to approximately 10 ppm using a platinum/alumina catalyst. The resulting performance of the anode catalyst, though satisfactory, is impacted even by this low amount of CO. Research at Los Alamos National Laboratory has demonstrated an approach to remedy this problem by bleeding a small amount of air or oxygen into the anode compartment.

Figure 3-6 shows that performance equivalent to that obtained on pure hydrogen can be achieved using this approach. It is assumed that this approach would also apply to reformed natural gas that incorporate water gas shift to obtain CO levels of 1% entering the fuel cell. This approach results in a loss of fuel, that should not exceed 4 percent provided the reformed fuel gas can be limited to 1 percent CO(1). Another approach is to develop a CO-tolerant anode catalyst such as the platinum/ruthenium electrodes currently under consideration. Platinum/ruthenium anodes have allowed cells to operate, with a low-level air bleed, for over 3,000 continuous hours on reformate fuel containing 10 ppm CO (27).

There is considerable interest in extending PEFC technology to direct methanol and formaldehyde electro-oxidation (47, 48) using Pt-based bi-metallic catalyst. Tests have been conducted with gas diffusion-type Vulcan XC-72/Toray support electrodes with Pt/Sn (0.5 mg/cm^2, 8 percent Sn) and Pt/Ru (0.5 mg/cm^2, 50 percent Ru). The electrodes have Teflon content of 20 percent in the catalyst layer.

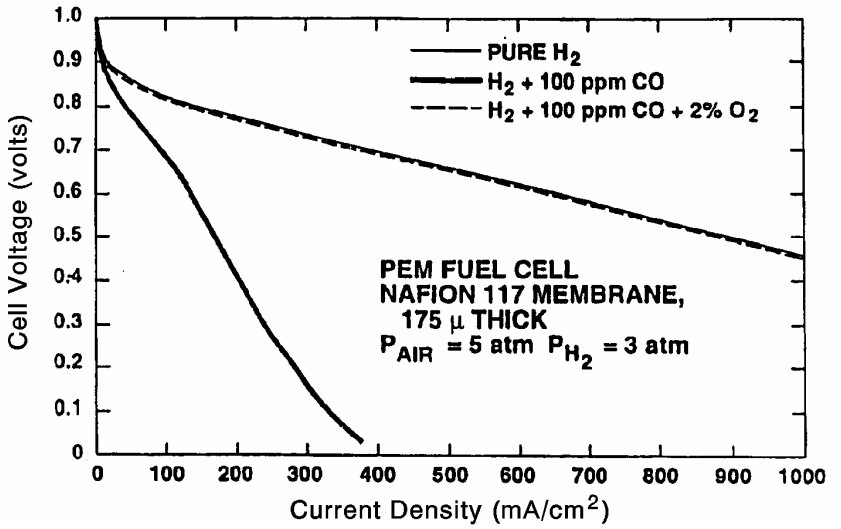

Figure 3-6 Effect on PEFC Performance of Bleeding Oxygen into the Anode Compartment (1)

3.2 Performance

A summary of the performance levels achieved with PEFCs since the mid-1960s is presented in Figure 3-7. Because of changes in operating conditions involving pressure, temperature, reactant gases, and other parameters, a wide range of performance levels can be obtained. The performance of the PEFC in the U.S. Gemini Space Program was 37 mA/cm^2 at 0.78 V in a 32-cell stack that typically operated at 50 °C and 2 atmospheres (49). Current technology yields performance levels that are vastly superior. Results from Los Alamos National Laboratory show that 0.78 V at about 200 mA/cm^2 (3 atmospheres H_2 and 5 atmospheres air) can be obtained at 80 °C in PEFCs containing a Nafion membrane and electrodes with a platinum loading of 0.4 mg/cm^2. Further details on PEFC performance with Nafion membranes are presented by Watkins, et al. (50). In recent years, the development effort has been focused on maintaining power density while reducing platinum loading, broadening temperature and humidity operating envelopes, and other improvements that will reduce cost (25,51,14 ,16 ,11).

Operating temperature has a significant influence on PEFC performance. An increase in temperature decreases the ohmic resistance of the electrolyte and accelerates the kinetics of the electrode reactions. In addition, mass transport limitations are reduced at higher temperatures. The overall result is an improvement in cell performance. Experimental data (55, 52, 53) suggest a voltage gain in the range of 1.1 - 2.5 mV for each degree (°C) of temperature increase. Operating at higher temperatures also reduces the chemisorption of CO. Improving the cell performance through an increase in temperature, however, is limited by the vapor pressure of water in the ion exchange membrane due to the membrane's susceptibility to dehydration and the subsequent loss of ionic conductivity.

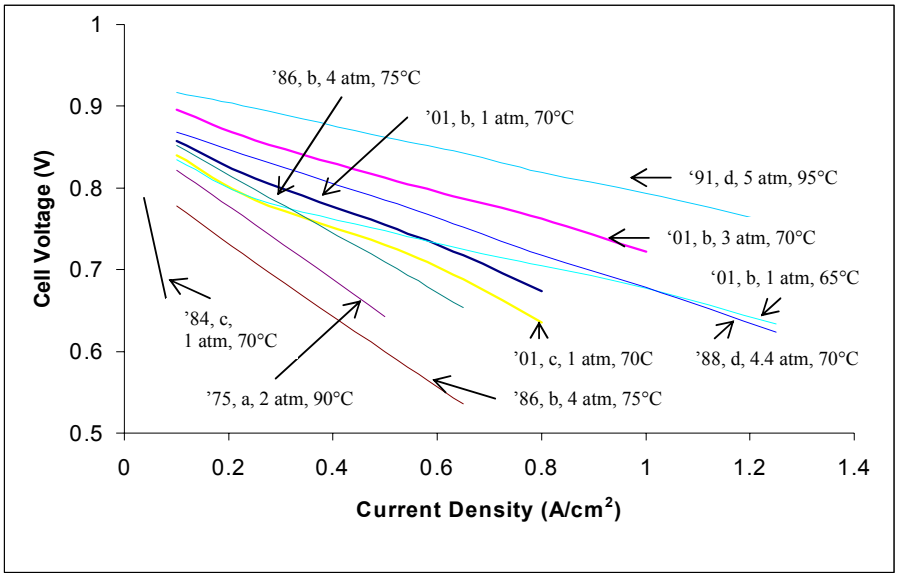

Figure 3-7 Evolutionary Changes in PEFCs Performance [(a) H_2/O_2, (b) H_2/Air, (c) Reformate Fuel/Air, (d) H_2/unkown)] [24, 10, 12, 54, 55]

Operating pressure also impacts cell performance. The influence of oxygen pressure on the performance of a PEFC at 93 °C is illustrated in Figure 3-8 (56). An increase in oxygen pressure from 30 to 135 psig (3 to 10.2 atmospheres) produces an increase of 42 mV in the cell voltage at 215 mA/cm^2. According to the Nernst equation, the increase in the reversible cathode potential that is expected for this increase in oxygen pressure is about 12 mV, which is considerably less than the measured value. When the temperature of the cell is increased to 104 °C, the cell voltage increases by 0.054 V for the same increase in oxygen pressure. Additional data suggest an even greater pressure effect. A PEFC at 50 °C and 500 mA/cm^2 (55) exhibited a voltage gain of 83 mV for an increase in pressure from 1 to 5 atmospheres. Another PEFC at 80 °C and 431 mA/cm^2 (52) showed a voltage gain of 22 mV for a small pressure increase from 2.4 to 3.4 atmospheres. These results demonstrate that an increase in the pressure of oxygen results in a significant reduction in polarization at the cathode. Performance improvements due to increased pressure must be balanced against the energy required to pressurize the reactant gases. The overall system must be optimized according to output, efficiency, cost, and size.

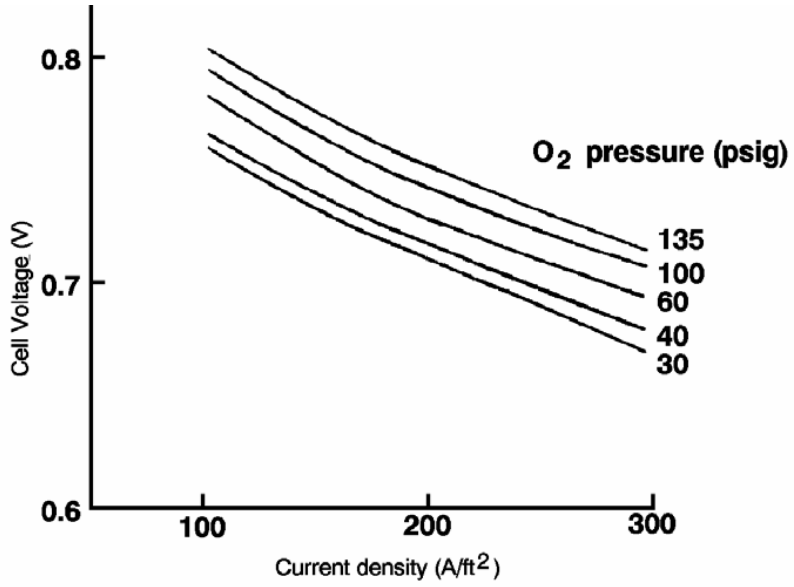

Figure 3-8 Influence of O_2 Pressure on PEFC Performance (93°C, Electrode Loadings of 2 mg/cm^2 Pt, H_2 Fuel at 3 Atmospheres) [(56) Figure 29, p. 49]

Lifetime performance degradation is a key performance parameter in a fuel cell, but the causes of degradation are not fully understood. The sources of voltage decay are kinetic (or activation) loss, ohmic (or resistive) loss, loss of mass transport, and loss of reformate tolerance (42).

Presently, the major focus of R&D on PEFC technology is to develop a fuel cell for terrestrial transportation, which requires the development of low-cost cell components. Hydrogen is considered the primary fuel for transportation applications, while reformed natural gas is the prime candidate for stationary applications. For automotive applications, the focus has shifted to

improving durability under realistic conditions, relaxing temperature and humidity requirements, and reducing cost, all while maintaining power densities. For reformate-fueled stacks, achieving better tolerance to CO and sulfur are critical factors. Because the operating temperature of PEFCs is much lower than PAFCs, poisoning of the anode electro-catalyst by CO from steam reformed methanol is a concern. The performance achieved with a proprietary anode in a PEFC with four different concentrations of CO in the fuel gas is shown in Figure 3-9. The graph shows that at higher current densities, the poisoning effect of CO is increased. At these higher current densities, the presence of CO in the fuel causes the cell voltage to become unstable and cycle over a wide range. Additional data (36) have suggested that the CO tolerance of a platinum electro-catalyst can be enhanced by increasing either temperature or pressure, which is one of the main reasons for pursuing high temperature PEFC membranes.

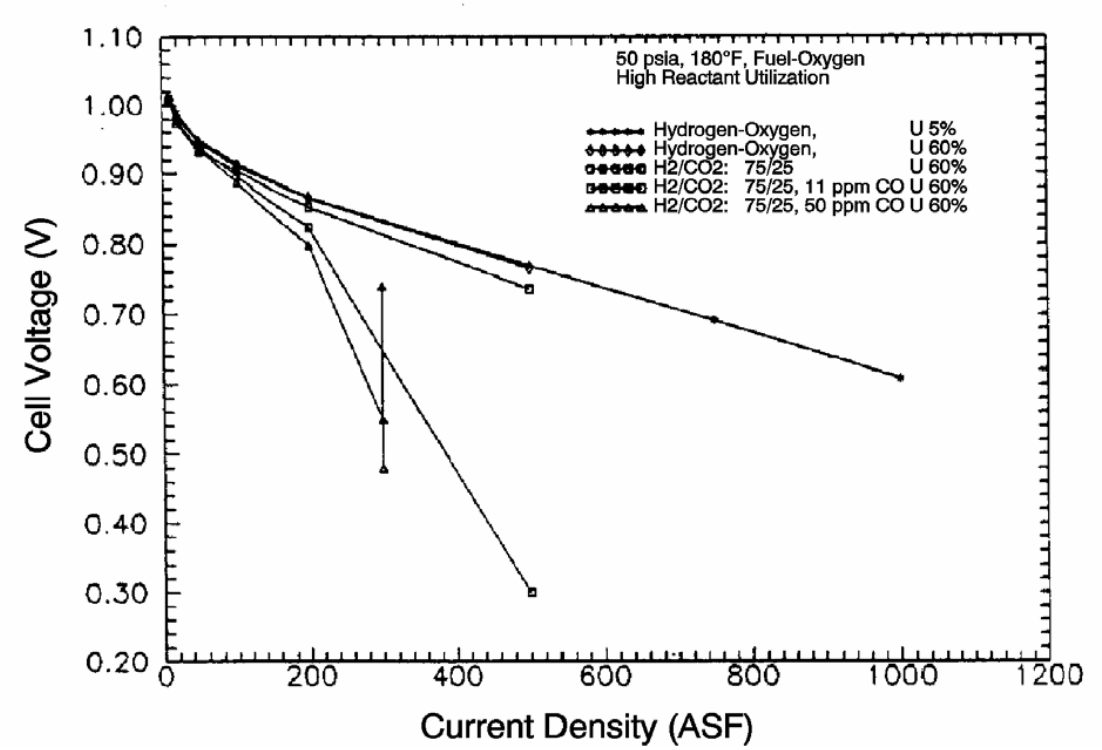

Figure 3-9 Cell Performance with Carbon Monoxide in Reformed Fuel (56)

3.3 PEFC Systems

PEFC stacks require tight control of fuel and air feed quality, humidity level, and temperature for sustained high-performance operation. To provide this, PEFC stacks must be incorporated in a sophisticated system. Naturally, the architecture of these systems depends strongly on whether they are fueled by hydrogen or by a hydrocarbon fuel.

3.3.1 Direct Hydrogen PEFC Systems

Direct hydrogen PEFC systems require extensive thermal and water management to ensure that the PEFC stack operates under the desired design conditions (Figure 3-10). Key components are

heat exchangers, humidifiers, and condensers. To understand the challenge of designing such a system, contrast the operating conditions of a PEFC stack (60 °C to 80 °C and 40 to 100 percent RH) with the environment such systems must work in. Automotive design standards require that engines to operate at temperatures up to 60 °C (start in a sunny spot). Thus, very little driving temperature difference will be available between the PEFC cooling medium and the ambient, requiring a large radiator surface area. If such conditions occur in an arid region, significant amounts of water are lost from the exhaust unless sophisticated water recovery systems (such as sorbent wheels or refrigerated systems) are used.

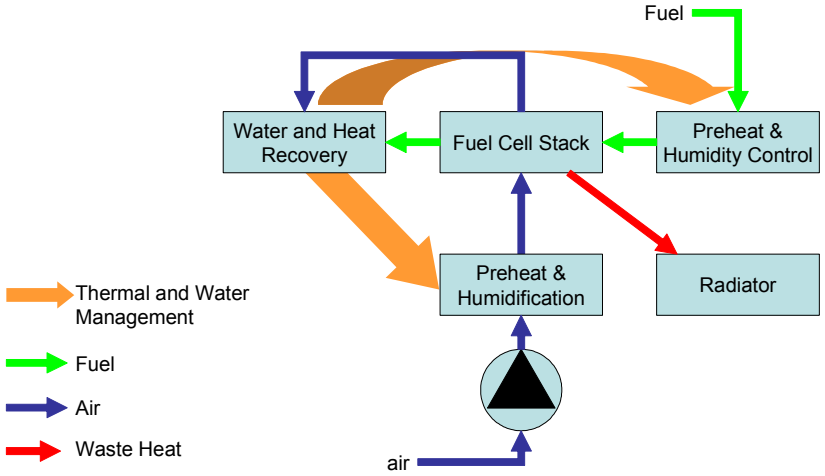

Figure 3-10 Typical Process Flow Diagram Showing Major Components of Direct Hydrogen PEFC System.

A key part of the direct hydrogen PEFC system is the hydrogen storage tank. A wide range of hydrogen storage methods is being considered (compressed hydrogen storage, liquid storage, storage in metal hydrides, and chemical storage). Each of these options offers distinct advantages, but also represents a compromise between energy density, weight, impact on energy efficiency, and cost. Special safety considerations must be made in all cases. As a consequence, the size and weight of the balance of plant components for these systems are important factors in the overall power system weight and volume. Automotive fuel cell developers have made tremendous strides in reducing the volume of direct hydrogen PEFC systems. Nevertheless, significant additional volume and weight reduction are required to match the power density of internal combustion engines.

3.3.2 Reformer-Based PEFC Systems

Reformer-based PEFC systems avoid the complexities and compromises of hydrogen storage, but instead the system must be designed to handle hydrocarbon fuels (similar considerations apply for alcohol fuels). This requires four major additional unit operations (Figure 3-11), collectively referred to as fuel processing:

- Fuel preheat and vaporization. Necessary to prepare the fuel to meet the reformer's feed requirements. Often, this unit operation is physically integrated with the reformer.

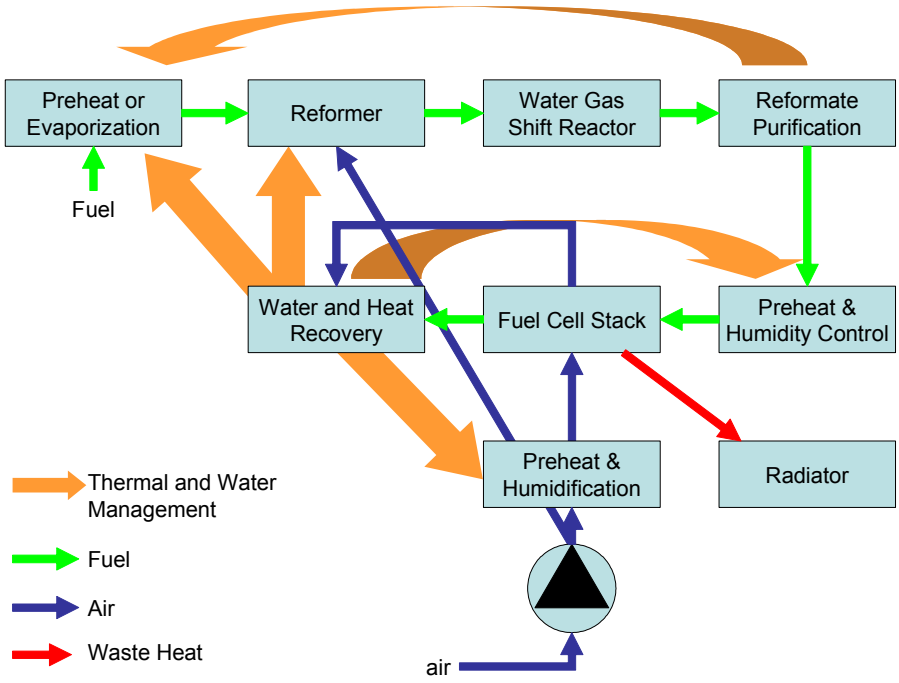

Figure 3-11 Schematic of Major Unit Operations Typical of Reformer-Based PEFC Systems.

- Reformer. This unit chemically converts hydrocarbon or alcohol to synthesis gas (a mixture of hydrogen and carbon monoxide). The two most practical oxidants are steam and air. If air is used, the reformer is referred to as a partial oxidation (POX) reformer; if steam is used, a steam reformer (SR), and if a mix of air and steam is used, an autothermal reformer (ATR). The choice of reformer type depends on a number of factors. Typically, POX reformers are smaller, cheaper, respond faster, and are suitable for a wide range of fuels. Steam reformers enable a higher system efficiency. ATRs and catalytic POX reformers (CPOX) share some of the advantages of each type:
  - Water Gas Shift Reactor (WGSR). The WGSR reacts carbon monoxide with water vapor to form hydrogen and carbon dioxide. This reactor is critical in PEFC systems (as well as PAFC), since the stack is unable to convert carbon monoxide.
  - Reformate purification. This is necessary because the PEFC stacks are sensitive to even trace concentrations of contaminants. Especially CO and sulfur are problematic species, and must be reduced to levels of around 10 and 1 ppm or less, respectively. Sulfur removal is, in actuality, done upstream in the process (just before or just after the reformer), but CO removal must be done just prior to stack entry.

A number of approaches can be used to purify reformate fuel (including pressure swing adsorption, membrane separation, methanation, and selective oxidation). Selective or preferential oxidation (PROX) is usually the preferred method for CO removal in the relatively small fuel cell systems because of the parasitic system loads and energy required by other methods. In selective oxidation, the reformed fuel is mixed with air or oxygen either before the

fuel is fed to the cell or within the stack itself. Current selective oxidation technology can reduce CO levels to <10 ppm. Another approach involves the use of a selective oxidation catalyst that is placed between the fuel stream inlet and the anode catalyst. Since the stack cannot tolerate even 10 ppm, air is usually bled into the anode directly to manage CO. Research to find approaches and materials that better tolerate impurities in the fuel continues today.

These unit operations add weight and volume, and reduce the efficiency of the system (fuel processor "efficiencies" typically range from 75 to 90 percent, but similar losses occur in the production of hydrogen from fossil fuels). In addition to the unit operations however, it is important to realize that their presence also impacts the size, performance, and cost of the fuel cell stack:

- The hydrogen in the anode feed of reformate-based systems is typically diluted with CO_2 and (in case of POX or ATR) nitrogen. As a consequence, the hydrogen mole fraction at the anode inlet is rarely higher than 0.3 (vs. 75 percent in the case of a direct hydrogen system). This decreases the ideal potential of the cells and increases the concentration-related losses.
- The presence of trace CO and sulfur and large quantities of CO_2 affects the performance of the anode electro-catalyst. As a consequence, more platinum must be used (typically 0.4 to 1 mg/cm^2 more), and even then the power density is typically 30 to 40 percent lower than with hydrogen-based systems.

The choice between a direct hydrogen and a reformate-based system depend on the application. For light duty vehicles, most experts now prefer direct hydrogen systems (hence the focus of the U.S. DOE program), while for stationary applications natural gas reformer-based PEFC systems are favored.

3.3.3 Direct Methanol Fuel Cell Systems

Specially optimized PEFCs can be fed with methanol (or fuels with similar chemical structure), creating a so-called direct methanol fuel cell (DMFC). Conceptually, this could lead to a very simple system with a fuel that has a relatively high energy density and is a liquid under ambient conditions. Performance levels achieved with a DMFC using air is now in the range of 180 to 250 mA/cm^2 (29) but because cell voltages typically range between 0.25 to 0.4 V, the power density ranges between 40 to 100 mW/cm^2. This low cell voltage is caused by a few common problems with the DMFC, several of which result from the cross-over of neutral methanol from the anode to the cathode side:

- High anode overpotential has been shown to be caused by absorption of partial de-composition products of methanol (e.g. CO)
- High cathode overpotential, caused by poisoning of the cathode electro-catalyst by cross-over methanol and its decomposition products

This performance still requires platinum loadings that are almost ten times higher (around 3 to 5 mg/cm^2) than needed in high-performance direct hydrogen PEFC. When feeding concentrated methanol directly, the cross-over can be as high as 30 to 50 percent compared with the amount oxidized electrochemically. If the concentration is reduced, the cross-over is reduced but so is the current density (due to reduced activity of the reactants). Obviously, the methanol crossed over is

lost, affecting efficiency and hence the heat generation. Research has focused on finding more advanced electrolyte materials to combat fuel crossover and more active anode catalysts to promote methanol oxidation. Significant progress has been made over the past few years in both of these key areas. Gottesfeld provides a good overview of the recent advances in DMFC technology (1).

Other developers have focused on miniaturizing the balance of plant components necessary to control water balance and minimize methanol loss or even developing reformer-based portable systems (57).

Another, less-well-reported disadvantage is that a large amount of water is transported across the membrane (has an aqueous methanol solution on one side and air on the other). This transport must be mitigated by sometimes complex water recovery systems that detract significantly from the conceptual simplicity of the DMFC. These limitations bar DMFCs from application in automobiles or stationary aplications until the cross-over is reduced by at least an order of magnitude. Some developers are focusing on membranes and MEAs that reduce water cross-over (58). Despite the challenges mentioned, there is significant interest in DMFCs for portable power applications in the 1 W to 1 kW capacity range.

Improvements in solid polymer electrolyte materials have extended the operating temperature of direct methanol PEFCs from 60 °C to almost 100 ^{o}C. Electro-catalyst developments have focused on materials with higher activity. Researchers at the University of Newcastle upon Tyne have reported over 200 mA/cm^2 at 0.3 V at 80 °C with platinum/ruthenium electrodes having platinum loading of 3.0 mg/cm^2. The Jet Propulsion Laboratory in the U.S. has reported over 100 mA/cm^2 at 0.4 V at 60 ^{o}C with platinum loading of 0.5 mg/cm^2. Recent work at Johnson Matthey has clearly shown that platinum/ruthenium materials possess substantially higher activity than platinum alone (59).

All fuel cells exhibit kinetic losses that cause the electrode reactions to deviate from their theoretical ideal. This is particularly true for a direct methanol PEFC. Eliminating the need for a fuel reformer, however, makes methanol and air PEFCs an attractive alternative to PEFCs that require pure hydrogen as a fuel. The minimum performance goal for direct methanol PEFC commercialization is approximately 200 mW/cm^2 at 0.5 to 0.6 V.

Figure 3-12 shows examples of performance typically achievable by developers.

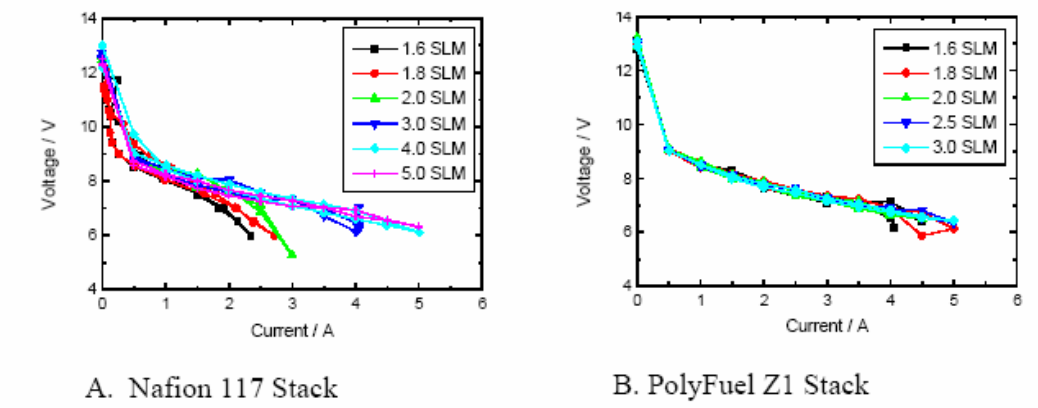

Figure 3-12 Comparison of State-of-the-Art Single Cell Direct Methanol Fuel Cell Data (58)

Developers in the U.S., Japan, and Europe have developed impressively integrated DMFC systems. Although energy density must still improve to broadly compete with state-of-the-art lithium-ion batteries in consumer applications, several developers have announced products for niche consumer or industrial applications within the next few years. If successful, this could represent the earliest commercialization of fuel cells beyond space applications.

3.4 PEFC Applications

3.4.1 Transportation Applications

The focus for PEFC applications of PEFC today is on prime power for cars and light trucks. PEFC is the only type of fuel cell considered for prime motive power in on-road vehicles (as opposed to APU power, for which SOFC is also being developed). PEFC systems fueled by hydrogen, methanol, and gasoline have been integrated into light duty vehicles by at least twelve different carmakers. Early prototypes of fuel cell vehicles (Honda and Toyota) have been released to controlled customer groups in Japan and the U.S. However, all automakers agree that the widespread application of PEFC to transportation will not occur until well into the next decade:

- Volume and weight of fuel cell systems must be further reduced
- Life and reliability of PEFC systems must be improved
- PEFC systems must be made more robust in order to be operable under the entire range of environmental conditions expected of vehicles
- Additional technology development is required to achieve the necessary cost reductions
- A hydrogen infrastructure, and the accompanying safety codes and standards must be developed.

3.4.2 Stationary Applications

Several developers are also developing PEFC systems for stationary applications. These efforts are aimed at very small-scale distributed generation (~1 to 10 kW AC). The vast majority of systems are designed for operation on natural gas or propane. Hundreds of demonstation units have been sited in programs in the U.S., Europe, and Japan. Typical performance characteristics are given by Plug Power (60). Considerable progress has been made in system integration and in achieving stand-alone operation. System efficiency typically ranges from 25 to 32 percent (based on LHV). By recovering the waste heat from the cooling water, the overall thermal efficiency can be raised to about 80 percent, but the water temperature (about 50 to 70 °C) is rather modest for many CHP applications. System operating life has been extended to about 8,000 hrs for a single system with a single stack, with degradation of about 5 percent per 1,000 hours.

3.5 References

1. S. Gottesfeld, “The Polymer Electrolyte Fuel Cell: Materials Issues in a Hydrogen Fueled Power Source,” LANL, undated.
2. W.T. Grubb, *Proceedings of the 11th Annual Battery Research and Development Conference*, PSC Publications Committee, Red Bank, NJ, p. 5, 1957; U.S. Patent No. 2,913,511, 1959.
3. Communication with Plug Power, August 2002.
4. W.D. Ernst, Patent No. 5,912,088, Plug Power Inc., June 15, 1999.
5. G.S. Eisman, et al., Patent No. 6,280,865, Plug Power Inc., August 28, 2001.
6. W.G.F. Grot, G.E. Munn, P.N. Walmsley, paper presented at the 141st National Meeting of the Electrochemical Society, Inc., Abstract No. 154, Houston, TX, May 7-11, 1972.
7. T. Ralph, "Proton Exchange Membrane Fuel Cells: Progress in Cost Reduction of the Key Components," *Platinum Metals Review*, 41, pp. 102-113, 1997.
8. B.R. Ezzell, B. Carl, and W. Mod, Ion Exchange Membranes for the Chlor Alkali Industry, AIChE Symp. Series, Houston, TX, March 1985, Pg. 49
9. K. Prater, "The Renaissance of the Solid Polymer Fuel Cell," Ballard Power Systems, Inc., Journal of Power Sources, p. 29, 1990.
10. D.J. Wheeler, J.S. Yi, R. Fredley, D. Yang, T. Patterson Jr., L. VanDine, “Advacements in Fuel cell Stack Technology at International Fuel Cells,” International Fuel Cells (now UTC Fuel Cells*), Journal of New Materials for Electrochemical Systems*, 4, 2001.
11. Peter M. Schutz, A Preliminary Investigation of Radiation Catalysts in Fuel Cells, Master of Science Thesis, Virginia Polytechnic University, Blacksburg, Va., August, 1979 Pg. 59.
12. 3M Product Bulletin, date unknown.
13. D. S. Watkins, et al., Abstracts 37th International Power Sources Symposium (The Electrochemical Society) p. 782, 1988.
14. Lousenberg, D., et al. *Diferentiated Membranes and Dispersions for Commercial PEM Fuel Cell and Electrolysis Systems*. in *2003 Fuel Cell Seminar*. 2003. Miami Beach, FL, USA: Department of Energy.
15. Teather, E. and J. Staser. *MEA Improvements for Sub-humidified Fuel Cell Operation*. In *2003 Fuel Cell Seminar*. 2003. Miami Beach, FL, USA: Department of Energy.
16. Cleghorn, S., et al. *New MEAs for Low Cost System Design*. in *2003 Fuel Cell Seminar*. 2003. Miami Beach, FL, USA: Department of Energy.
17. Peter M. Schutz, A Preliminary Investigation of Radiation Catalysts in Fuel Cells, Master of Science Thesis, Virginia Polytechnic University, Blacksburg, Va., August, 1979 Pg. 59.

18. J. C. Amphlett, M. Farahani, R. F. Mann, B. A. Peppley, P. R. Roberge, in *Proceedings of the 26th Intersociety Energy Conversion Engineering Conference*, August 4-9, 1991, Volume 3, Conversion Technologies/Electrochemical Conversion, American Nuclear Society, La Grange, Illinois, p. 624, 1991.
19. M. Krumpelt, K. M. Myles, No. 8, An EPRI/GRI Fuel Cell Workshop on Technology Research and Development, April 13-14, 1993, Stonehart Associates, Madison, Connecticut, 1993.
20. M. Krumpelt, R. Kumar, J. Miller, C. Christianson, in *1992 Fuel Cell Seminar Program and Abstracts*, The Fuel Cell Seminar Organizing Committee, November 29 - December 2, 1992, Tucson, Arizona, p. 35, 1992.
21. W. Teagan, J. Bentley, "Status: ADL/EPYX Fuel Processing Technology," Joint DOE/EPRI/GRI Workshop on Fuel Cell Technology, San Francisco, CA, May 18-20, 1998.
22. R. F. Savinell, J. S. Wainright, M. Litt, "High Temperature Polymer Electrolyte Fuel Cells," The Electrochemical Society, Journal 98-27, p.81.
23. W.D. Ernst, "PEM Technology Development at Plug Power," *2000 Fuel Cell Seminar Program and Abstracts*, Portland Oregon, sponsored by Fuel Cell Seminar Organizing Committee, October 30 – November 2, 2000.
24. Gordon Research Conference, Rhode Island, July 29 - August 3, 2001.
25. Debe, M., et al. *Activities of Low Pt Loading, Carbon-Less, Ultra-Thin Nanostructured Filmbased Electrodes for PEM Fuel Cells and Roll-Good Fabricated MEA Performances in Single Cells and Stacks*. in *2003 Fuel Cell Seminar*. 2003. Miami Beach, FL, USA: Department of Energy.
26. Wheeler, D., T. Clark, and S. Motupally. *PEM Fuel CEll Programs at UTC Fuel Cells*. in *2003 Fuel Cell Seminar*. 2003. Miami Beach, FL, USA: Department of Energy.
27. T.G. Coker, A.B. LaConti, L.J. Nuttall, in *Proceedings of the Symposium on Membranes and Ionic and Electronic Conducting Polymers*, edited by E.G. Yeager, B. Schumm, K. Mauritz, K. Abbey, D. Blankenship, J. Akridge, The Electrochemical Society, Inc., Pennington, NJ, p. 191, 1983.
28. N. Giordano, et al., in *Proceedings 26th Intersociety Energy Conversion Engineering Conference*, August 4-9, 1991, Volume 3, Conversion Technologies/Electrochemical Conversion, American Nuclear Society, La Grange, Illinois, p. 624, 1991.
29. T.A. Zawodzinski, et al., *Journal of Electrochemical Society*, p. 140, 1042, 1993.
30. T.E. Springer, et al., *Journal of Electrochemical Society*, p. 138, 2335, 1991.
31. D.M. Bernardi, *Journal of Electrochemical Society*, p. 137, 3344, 1990.
32. T.E. Springer, M. S. Wilson, S. Gottesfeld, "Modeling and Experimental Diagnostics in Polymer Electrolyte Fuel Cells," submitted to J. ElectroChem. Soc., LA-UR-93-1469 Los Alamos National Laboratory, New Mexico, 1993.
33. R. Baldwin, M. Pham, A. Leonida, J. McElroy, and T. Nalette, Hydrogen-Oxygen Proton Exchange Membrane Fuel Cells and Electrolyzers, Proceedings of the Space Electrochemical Research and Technology (SERT), NASA LEWIS Research Center, Cleveland, Ohio, April, 1989.
34. S. Cleghorn, J. Kolde, W. Liu, "Catalyst Coated Composite Membranes," Chapter 49, *Fuel Cell Reference Book,* to be published, Wiley-VCH, 2002.

35. S. Gottesfeld, “Polymer Electrolyte Fuel Cells: Transportation and Stationary Application,” No. 10, in *An EPRI/GRI Fuel Cell Workshop on TechnologyResearch and Development,* April 13-14, 1993, Stonehart Associates, Madison, Connecticut, 1993.
36. "Investigation of Design and Manufacturing Methods for Low-Cost Fabrication of High Efficiency, High Power Density PEM Fuel Cell Power Plant," prepared by International Fuel Cells, Final Report FCR-11320A, June 10, 1991.
37. D. Wilkinson, D. Thompsett, "Materials and Approaches for CO and CO_2 Tolerance for Polymer Electrolyte Membrane Fuel Cells," *Proceedings of the Second International Symposium on New Materials for Fuel Cell and Modern Battery Systems*, pp. 266-285, (Montreal, Quebec, Canada, July 6-10, 1997).
38. “Information Sheet,” prepared by the U.S. Department of Energy, Office of Propulsion Systems, Proton Exchange Membrane Fuel Cell Program, DE93000009, November 1992.
39. K. Sikairi, K. Tsurumi, S. Kawaguchi, M. Watanabe, P. Stonehart, in *1992 Fuel Cell Seminar Program and Abstracts*, Tucson, AZ, November 29 - December 2, 1992, sponsored by Fuel Cell Organizing Committee, p. 153, 1992.
40. S. Srinivasan, O.A. Velev, A. Parthasarathy, A.C. Ferriera, S. Mukerjee, M. Wakizoe, Y.W. Rho, Y.T. Kho, A.J. Appleby, in *1992 Fuel Cell Seminar Program and Abstracts*, Tucson, Arizona November 29 - December 2, 1992, sponsored by Fuel Cell Organizing Committee, p. 619, 1992.
41. F.N. Buchi, B. Gupta, M. Rouilly, P.C. Hauser, A. Chapiro, G.G. Scherer, in *27th Intersociety Energy Conversion Engineering Conference Proceedings*, Volume 3, Conversion Technologies/Electrochemical Conversions, San Diego, CA, August 3-7, 1992, published by Society of Automotive Engineers, Inc., Warrendale, PA, 419, 1992.
42. T.A. Zawodzinski, T.A. Springer, F. Uribe, S. Gottesfeld, "Characterization of Polymer Electrolytes for Fuel Cell Applications," Solid State Tonics 60, pp. 199-211, North-Holland, 1993.
43. E. Gulzow, M. Schulze, N. Wagner, et al., J. of Power Sources Vol. 86 pages 352-362, 2000.
44. M.S. Wilson, T.E. Springer, T.A. Zawodzinski, S. Gottesfeld, in *26th Intersociety Energy Conversion Engineering Conference Proceedings*, Volume 3, Conversion Technologies/Electrochemical Conversion, Boston, Massachusetts, August 4-9, 1991, published by Society of Automotive Engineers, Inc., Warrendale, PA, 1991.
45. C. Derouin, T. Springer, F. Uribe, J. Valerio, M. Wilson, T. Zawodzinski, S. Gottesfeld, in *1992 Fuel Cell Seminar Program and Abstracts*, Tucson AZ, November 29 - December 2, 1992, sponsored by Fuel Cell Organizing Committee, p. 615, 1992.
46. J.G. Clulow, F.E. Zappitelli, C.M. Carlstrom, J.L. Zemsky, D.M. Buskirk, M.S. Wilson, “Development of Vinyl Ester/ Graphite Composite Bipolar Plates,” Fuel Cell Technology: Opportunites and Challenges, 2002 AIChE Spring National Meeting, March 10-14, 2002.
47. P.D. Naylor, P.J. Mitchell, P.L. Adcock, in *1992 Fuel Cell Seminar Program and Abstracts*, Tucson, AZ, November 29 - December 2, 1992, sponsored by Fuel Cell Organizing Committee, 575, 1992.
48. S.R. Narayanan, E. Vamos, H. Frank, S. Surampudi, G. Halpert, in *1992 Fuel Cell Seminar Program and Abstracts*, Tucson, AZ, November 29 - December 2, 1992, sponsored by Fuel Cell Organizing Committee, p. 233, 1992.
49. A.J. Appleby, E.B. Yeager, *Energy*, pg. 11, 137, 1986.

50. D. Watkins, K. Dircks, E. Epp, A. Harkness, *Proceedings of the 32nd International Power Sources Symposium*, The Electrochemical Society, Inc., Pennington, NJ, p. 590, 1986.
51. Koehler, J., et al. *Advanced MEA Technology for Hydrogen and Reformate Application*. in *2003 Fuel Cell Seminar*. 2003. Miami Beach, FL, USA: Department of Energy.
52. J.C. Amphlett, et al., "The Operation of a Solid Polymer Fuel Cell: A Parametric Model," Royal Military College of Canada, no date.
53. K. Ledjeff, et al., "Low Cost Membrane Fuel Cell for Low Power Applications," Fraunhofer-Institute for Solar Energy Systems, *Program and Abstracts, 1992 Fuel Cell Seminar*.
54. J. R. Huff, "Status of Fuel Cell Technologies," *Fuel Cell Seminar Abstracts, Fuel Cell Seminar*, October 26-29, 1986, Tucson, AZ.
55. J. Srmivason, et al., "High Energy Efficiency and High Power Density Proton Exchange Membrane Fuel Cells - Electrode Kinetics and Mass Transport," Journal of Power Sources, p. 36, 1991
56. A. LaConti, G. Smarz, F. Sribnik, "New Membrane-Catalyst for Solid Polymer Electrolyte Systems," Final Report prepared by Electro-Chem Products, Hamilton Standard for Los Alamos National Laboratory under Contract No. 9-X53-D6272-1, 1986.
57. Pavio, J. *Performance and Design of a Reformed Hydrogen Fuel Cell System*. in *2003 Fuel Cell Seminar*. 2003. Miami Beach, FL, USA: Department of Energy.
58. Cox, P., S.-Y. Cha, and A. Attia. *PolyFuel's Z1 Membrane and Catalyst Coatings to Improve the Fuel Cell Performance in Portable Power Applications*. in *2003 Fuel Cell Seminar*. 2003. Miami Beach, FL, USA: Department of Energy.
59. M. Hogarth, G. Hards, "Direct Methanol Fuel Cells: Technological Advances and Further Requirements," *Platinum Metals Review*, 40, pp. 150-159, 1996.
60. Feitelberg, A. *On the Efficiency of PEM Fuel Cell Systems and Fuel Processors*. in *2003 Fuel Cell Seminar*. 2003. Miami Beach, FL, USA: Department of Energy.

4. ALKALINE FUEL CELL

The Alkaline Fuel Cell (AFC) was one of the first modern fuel cells to be developed, beginning in 1960. The application at that time was to provide on-board electric power for the Apollo space vehicle. Desirable attributes of the AFC include excellent performance compared to other candidate fuel cells due to its active O_2 electrode kinetics and flexibility to use a wide range of electro-catalysts. The AFC continues to be used: it now provides on-board power for the Space Shuttle Orbiter with cells manufactured by UTC Fuel Cells.

The AFC developed for space application was based, in large part, on work initiated by F.T. Bacon (1) in the 1930s. By 1952, construction and performance testing of a 5-kW alkaline fuel cell, operating on H_2 and O_2, was completed. The fuel cell developed by Bacon operated at 200 to 240 ^oC with 45 percent KOH electrolyte. Pressure was maintained at 40 to 55 atm to prevent the electrolyte from boiling. At this relatively high temperature and pressure, performance of the cell was quite good (0.78 volts at 800 mA/cm^2). The anode consisted of a dual-porosity Ni electrode (two-layer structure with porous Ni of 16 μm maximum pore diameter on the electrolyte side and 30 μm pore diameter on the gas side). The cathode consisted of a porous structure of lithiated NiO. The three-phase boundary in the porous electrodes was maintained by a differential gas pressure across the electrode, since a wetproofing agent was not available at that time, i.e., PTFE (polytetrafluoroethylene) as a wetproofing material did not exist, and it would not have been stable in the high temperature alkaline solution (2).

The kinetics of O_2 reduction in alkaline electrolytes are more favorable than in phosphoric acid electrolyte. Consider a Pt cathode (0.25 mg/cm^2) in 30 percent KOH at 70 °C and in 96 percent phosphoric acid at 165 °C. The cathode potentials (vs. RHE - Reversible Hydrogen Electrode) at 100 mA/cm^2 in these two electrolytes are 0.868 and 0.730 V, respectively, according to data reported by Appleby (Figure 2.15-1 in Reference 3). Various explanations have been advanced for the higher O_2 reduction rates in alkaline electrolytes (4). The practical consequence of the higher performance of Pt cathodes in alkaline electrolytes is that AFCs are capable of higher efficiencies than PAFCs at a given current density, or higher power densities at the same efficiency. Bockris (2) estimates that the efficiency of AFCs fueled by pure H_2 is about 60 percent HHV, and that of PAFCs is about 50 percent HHV.

The high performance of the alkaline cell relative to phosphoric acid and other cells leads to the plausibility of developing the technology for terrestrial application. The leading developer of alkaline technology for space application, UTC Fuel Cells, investigated adaptating the

technology to terrestrial, stationary power applications using air as an oxidant in the early 1970s. The predominant drawback with terrestrial applications is that CO_2 in any hydrocarbon fuel or in the air reacts with the ion carrier in the electrolyte. During the 1970s, a high pressure drop platinum/palladium separator was used in the fuel processor to obtain a pure stream of H_2 from reformed hydrocarbon fuels (primarily natural gas for stationary power plants). Similarly, a soda-lime scrubber treated the inlet ambient air stream to minimize CO_2 entering the cell. The expense of the separator and scrubber was deemed uneconomical for commercial development of stationary power plants. Augmenting the issue was a slow build-up of K_2CO_3 due to the minuscule amount of CO_2 escaping the soda-lime scrubber. There was also an issue of component life for stationary power applications. Alkaline cell life (now 2,600 hours on H_2/O_2, but 5,000 hour R&D underway) is suitable for space missions, but too brief for terrestrial, stationary power plants. As a result of the CO_2 issue, UTC Fuel Cells, which uses an immobilized electrolyte, now focuses their alkaline program completely toward space applications with H_2/O_2 as fuel and oxidant.

Union Carbide Corp. (UCC) developed AFCs for terrestrial mobile applications starting in the late 1950s, lasting until the early 1970s. UCC systems used liquid caustic electrolytes; the electrodes were either pitch-bonded carbon plates or plastic-bonded carbon electrodes with a nickel current collector. UCC also built fuel cell systems for the U.S. Army and the U.S. Navy, an alkaline direct hydrazine powered motorcycle, and the "Electrovan" of General Motors. Finally, Professor Karl V. Kordesch built his Austin A-40 car, fitted with UCC fuel cells with lead acid batteries as hybrid. It was demonstrated on public roads for three years. The years of research and development are very well summarized in reference (5) *Brennstoffbatterien*.

Based on the UCC technology, other developers are now pursuing terrestrial applications of alkaline technology due to its high performance, particularly for motive power. The majority of these developers use circulating electrolytes with an external, commercial type soda-lime absorber that promises to resolve the problem of CO_2 in the air stream. The quantity of CO_2 can be limited to a small amount with a circulating electrolyte, versus a continual build-up with an immobilized electrolyte. Life expectancy increases (~5,000 hour life is ample for personal automobile engine life) because the cell is nearly inactive when switched off**.** Hence, only the true operating hours count for the total lifetime. During normal operation, the electrolyte circulates continuously, which has several advantages over an immobilized system: 1) no drying-out of the cell occurs because the water content of the caustic electrolyte remains quite constant everywhere inside the stack; 2) heat management by dedicated heat exchanger compartments in the stack becomes unnecessary - the electrolyte itself works as a cooling liquid inside each cell; 3) accumulated impurities, such as carbonates, are concentrated in the circulating stream and can easily be removed (comparable to a function of oil in today's gasoline engines); 4) the OH^- concentration gradient is highly diminished, and 5) the electrolyte prevents the build-up of gas bubbles between electrodes and electrolyte as they are washed away.

Other attributes are that the alkaline cell could have high reactivity without the need for noble metal catalysts on the cell electrodes; this represents a cost savings (6). Additionally, the radiator of the alkaline cell system should be smaller than the radiator in the competitive PEFC system because of higher alkaline cell temperature and its higher performance.

In stacks using circulating electrolytes, parasitic currents might occur. All cells are connected via the electrolyte stream to all other cells, producing high voltages between the electrodes. Parasitic current not only lowers the stack performance, but can also harm the electrodes. Fortunately, this issue can be resolved easily by using a special electrode frame design with long, narrow electrolyte channels.

Some developers have investigated a direct methanol alkaline cell to circumnavigate hydrocarbon fuel separator issues. These cells exhibit a reduced performance, and have not been as thoroughly investigated as the hydrogen-fueled cells.

The unusual economics for remote power applications (i.e., space, undersea, and military applications) result in the cell itself not being strongly constrained by cost. The consumer and industrial markets, however, require the development of low-cost components if the AFC is to successfully compete with alternative technologies. Much of the recent interest in AFCs for mobile and stationary terrestrial applications has addressed the development of low-cost cell components. In this regard, carbon-based porous electrodes play a prominent role (6). It remains to be demonstrated whether alkaline cells will prove commercially viable for the transportation sector. Reference (7) provides an in-depth view of the development history and the potential of alkaline technology for terrestrial application.

Figures 4-1 and 4-2 depict the operating configuration of the H_2/O_2 alkaline fuel cell (8) and a H_2/air cell (9). In both, the half-cell reactions are:

$$H_2 + 2OH \rightarrow 2H_2O + 2e \quad \text{(Anode)} \tag{4-1}$$

$$\tfrac{1}{2}O_2 + H_2O + 2e \rightarrow 2OH \quad \text{(Cathode)} \tag{4-2}$$

Hydroxyl ions, OH^-, are the conducting species in the electrolyte. The equivalent overall cell reaction is:

$$H_2 + \tfrac{1}{2}O_2 \rightarrow H_2O + \text{electric energy} + \text{heat} \tag{4-3}$$

Since KOH has the highest conductance among the alkaline hydroxides, it is the preferred electrolyte.

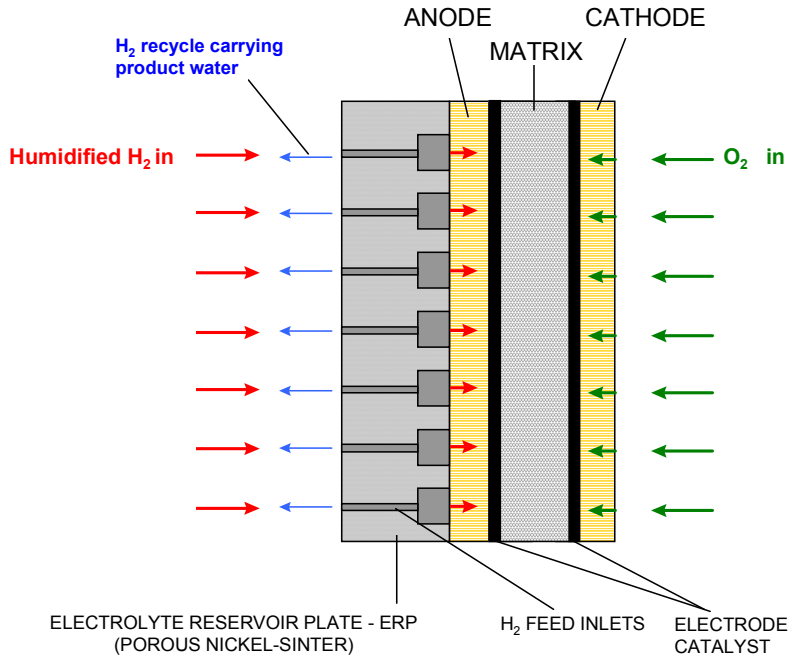

Figure 4-1 Principles of Operation of H_2/O_2 Alkaline Fuel Cell, Immobilized Electrolyte (8)

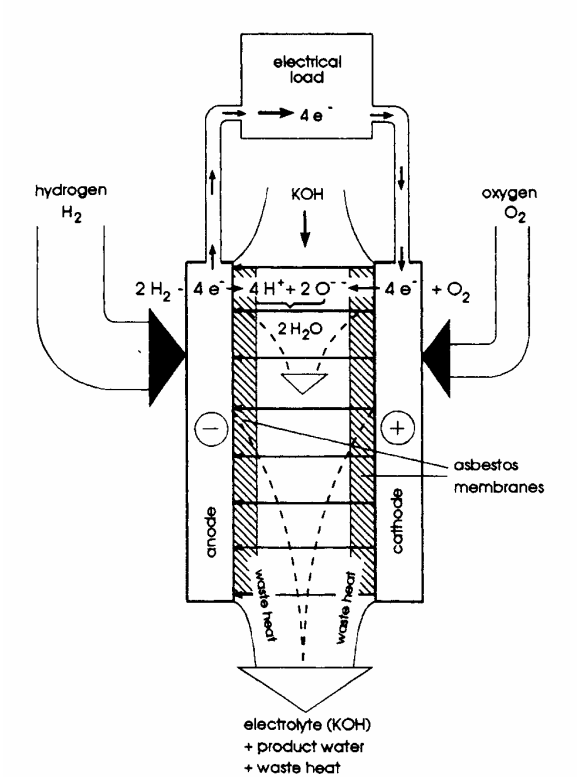

Figure 4-2 Principles of Operation of H_2/Air Alkaline Fuel Cell, Circulating Electrolyte (9)

4.1 Cell Components

4.1.1 State-of-the-Art Components

The concentration of KOH in an immobilized electrolyte typically used in the space program varies from 35 to 50 wt percent KOH for low temperature (<120 °C) operation to 85 wt percent KOH in cells designed for operation at high temperature (~260 °C). The electrolyte is retained in a matrix (usually asbestos), and a wide range of electro-catalysts can be used (e.g., Ni, Ag, metal oxides, spinels, and noble metals) to promote reaction.

The cylindrical AFC modules used in the U.S. Apollo Space Program had a 57 cm diameter, a 112 cm height, weighed about 110 kg, produced a peak power of 1.42 kW at 27 to 31 V, and operated at an average power of 0.6 kW. These cells operated on pure H_2 and O_2 and concentrated electrolyte (85 percent KOH) at a moderate pressure (4 atmospheres reactant gas pressure) without electrolyte boiling. With this concentrated electrolyte, cell performance was not as high as in the less-concentrated electrolyte; consequently, the operating temperature was increased to 260 ^{o}C. The typical performance of this AFC cell was 0.85 V at 150 mA/cm^2, comparing favorably to the performance of the Bacon cell operating at about 10 times higher pressure.

The state-of-the-art alkaline fuel cell stacks in the Space Shuttle Orbiter are rectangular with a width of 38 cm, a length of 114 cm, and a height of 35 cm. They weigh 118 kg, produce a peak power of 12 kW at a minimum of 27.5 V (end of life), and operate at an average power of 7 kW. They operate in the same pressure range as the Apollo cells (4 atmospheres), but at a lower temperature (85 to 95 °C) and higher current density (0.88 V at 470 mA/cm^2; UTC Fuel Cells has demonstrated 3.4 W/cm^2 at 0.8 V and 4,300 mA/cm^2, Reference (8)). The electrodes contain high loadings of noble metals: 80 percent Pt – 20 percent Pd anodes are loaded at 10 mg/cm^2 on Ag-plated Ni screen; 90 percent Au – 10 percent Pt cathodes are loaded at 20 mg/cm^2 on Ag-plated Ni screen. Both are bonded with PTFE to achieve high performance at the lower temperature of 85 ot 95 ^{o}C. A wide variety of materials (e.g., potassium titanate, ceria, asbestos, zirconium phosphate gel) have been used in the micro-porous separators for AFCs. The electrolyte is 35 percent KOH and is replenished via a reservoir on the anode side. Gold-plated magnesium is used for the bipolar plates. Sheibley and Martin (10) provide a brief survey of the advanced technology components in AFCs for space applications.

An advanced cell configuration for underwater application was developed using high surface area Raney nickel anodes loaded at 120 mg/cm^2 (1 to 2 percent Ti) and Raney silver cathodes loaded at 60 mg/cm^2 containing small amounts of Ni, Bi, and Ti (11).

The efforts of Union Carbide Corporation have formed the basis for most of today's terrestrial applications of AFCs with circulating liquid electrolytes. Companies like Da Capo Fuel Cell Ltd. (which bought ZeTek Power (formerly Zevco and Elenco)), Astris Energy, and Apollo Energy System Inc. are developing circulating electrolyte cells for motive and backup power primarily based on that technology. A typical configuration (Apollo, Figure 4-2) uses carbon-based plastic-bonded gas diffusion electrodes with a current collector (nickel) inside. Due to the ease of preparation, the electrodes in present stacks use noble metals loaded to less than 0.5mg/cm^2. The 0.3 cm thick cells are stacked in a monopolar order and are commonly

connected in series via edge connectors. Neither membranes nor bipolar plates are needed. The stacks operate at 75 °C, using a 9N KOH electrolyte. The gases are fed at ambient pressure; either pure hydrogen or cracked ammonia is used. Lifetime testing (12) has not been finished, but is >1,000 hours at intermittent operation (a few hours per day).

Several types of catalysts are used or are being considered for the electrodes: 1) noble metals (expensive but simple, and acceptable for low volume stack preparation); 2) "classic" non-noble metals (silver for the cathode and Raney nickel for the anode), and 3) spinels and perovskites (often referred to as alternative catalysts, these are being developed because they cost less than the noble metal catalysts).

4.1.2 Development Components

Immobilized electrolyte AFCs, used mostly in space or closed environments, and circulating electrolyte AFCs, used for terrestrial application, face separate and unique development challenges.

H_2/O_2 alkaline technology using immobilized electrolytes is considered to be fully developed. Confidence in the present cell technology is best represented by the fact that there is no back-up electric power on the Space Shuttle Orbiter. Further improvement of the present H_2/O_2 design is not considered to be cost effective with one exception: maintenance cost can be decreased directly by increasing the cell stack life of the Orbiter power plant.

The life-limiting event in the present Orbiter cell is KOH corrosion of the cell frame (cell support). Present stack life is 2,600 hours. The cell stacks have demonstrated capability to reach this life in 110 flights and a total of ~87,000 hours in the Orbiter (July 2002). Present practice is to refurbish the power unit at 2,600 hours by installing a new stack, and cleaning and inspecting the balance of equipment. The stack life is being improved to 5,000 hours by elongating the path length associated with KOH-induced corrosion of the cell frame. A 10 cell short stack has demonstrated the new 5,000 hours concept. The concept is now being qualified in a complete power plant, presently being tested (13).

Electrode development in circulating electrolyte AFCs has concentrated on 1) multi-layered structures with porosity characteristics optimized for flow of liquid electrolytes and gases (H_2 and air), and 2) catalyst development. Another area for concern is the instability of PTFE, which causes weeping of the electrodes. Most developers use noble metal catalysts; some use non-noble catalysts. Spinels and perovskites are being developed in an attempt to lower the cost of the electrodes. Development of low-cost manufacturing processes includes powder mixing and pressing of carbon-based electrodes, sedimentation and spraying, and high-temperature sintering.

AFC electrolyte development has been restricted to KOH water solutions with concentrations ranging from 6 to12N. Still, use of less expensive NaOH has been considered. Minimal cost advantages appear to be far outweighed by performance reductions due to wetting angle and lower conductivity. However, NaOH as an electrolyte increases the lifetime of electrodes when CO_2 is present, because sodium carbonate, although less soluble than potassium carbonate, forms much smaller crystals, which do not harm the carbon pores.

Other approaches to increasing life and reducing weight and cost include investigating epoxy resins, polysulfone and ABS (acrylonitrile-butadiene-styrene). Framing techniques under development include injection molding, filter pressing, and welding (14, 15).

Immobilized electrolyte AFCs are highly sensitive to carbon dioxide (CO_2). Non-hydrocarbon hydrogen fuel or pure H_2 can be fed directly to the anode. For example, a carbon-free fuel gas such as cracked ammonia (25 percent N_2, 75 percent H_2, and residual NH_3) can be fed directly to the cell. Due to the high diffusion rate of hydrogen compared to nitrogen, only a very small decrease in potential is observed with hydrogen content greater than 25 percent (at medium current densities). Gas purification is necessary when H_2 is produced from carbon-containing fuel sources (e.g., methanol, gasoline, propane and others). There are many approaches to separate CO_2 from gaseous or liquid streams. Physical separation and chemical separation are the most common methods used. However, CO_2 removal by these methods requires more than one process step to reduce the CO_2 to the limits required by the fuel cell. Two additional methods include cryogenic separation and biological fixation. If liquid hydrogen is used as the fuel for the alkaline fuel cell, a system of heat exchangers can be used to condense the CO_2 out of the air for the oxidant stream. This technique has a potential weight advantage over the soda-lime scrubber. Low-temperature distillation is commonly used for the liquefaction of CO_2 from high purity sources. A new, potentially efficient technique that is being investigated uses capillary condensation to separate gases by selective wicking. Biological separation is promising, but must overcome the challenge of reactivation after shutdown periods.

Another promising CO_2 separation method is membrane separation. This has the advantages of being compact, no moving parts, and the potential for high energy efficiency. Polymer membranes transport gases by solution diffusion, and typically have a low gas flux and are subject to degradation. These membranes are relatively expensive. The main drawbacks of membrane separation are the significant pressure differential that may be required across the membrane and its high cost. The need for a high pressure gradient can be eliminated by using a membrane in which a potential is applied over the membrane. This approach is sometimes referred to as the "sacrificial cell" technique. Another approach is to use a membrane with steam reforming of liquid fuels. Little additional energy is needed to pressurize the liquid fuel and water to the pressure required for separation.

Alkaline cell developers continue to investigate CO_2 separation methods that show economic promise. However, circulating electrolyte is the technology of choice for terrestrial applications.

4.2 Performance

Performance of AFCs since 1960 has undergone many changes, as evident in the performance data in Figure 4-3. H_2/air performance is shown as solid lines, and H_2/O_2 performance is shown as dashed lines. The early AFCs operated at relatively high temperature and pressure to meet the requirements for space applications. More recently, a major focus of the technology is for terrestrial applications in which low-cost components operating at near-ambient temperature and pressure with air as the oxidant are desirable. This shift in fuel cell operating conditions resulted in the lower performance shown in Figure 4-3**.** The figure shows, using dotted lines, H_2/O_2 performance for: 1) the Orbiter with immobilized electrolyte (8), and 2) a circulating electrolyte cell (12).

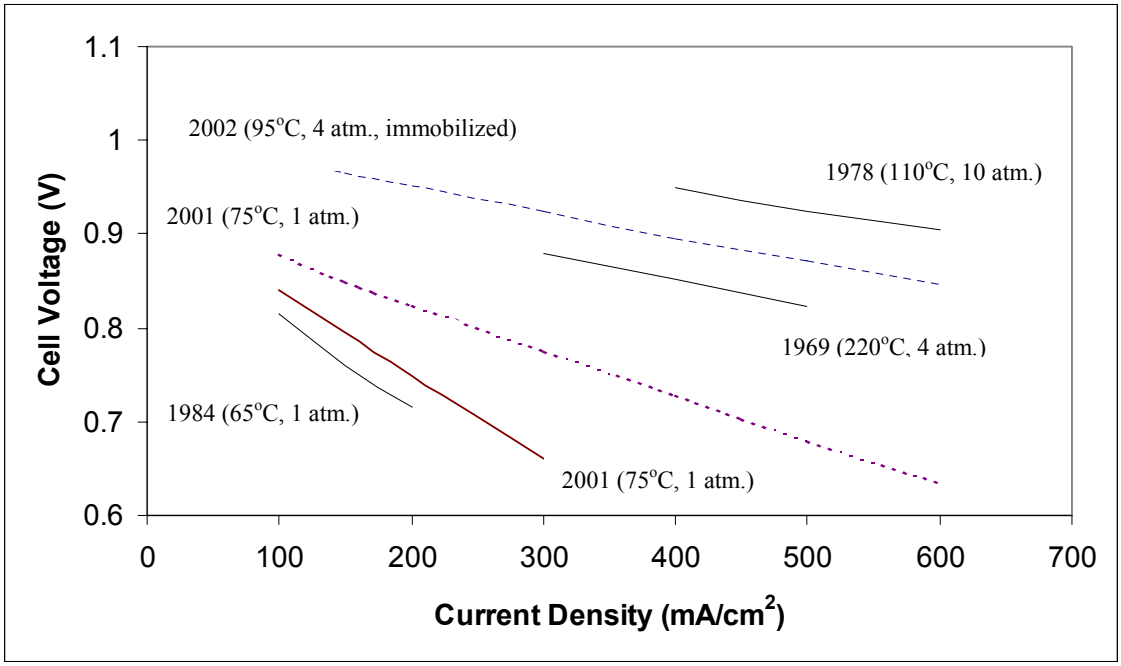

Figure 4-3 Evolutionary Changes in the Performance of AFCs (8, 12, & 16)

The data described in the following paragraphs pertains to the H_2/air cell. Unfortunately, H_2/air performance data is rather dated; there has been a noticeable lack of recent H_2/air data.

4.2.1 Effect of Pressure

AFCs experience the typical enhanced performance with an increase in cell operating pressure. Figure 4-4 plots the increase in reversible e.m.f. (electromotive force) of alkaline cells with pressure over a wide range of temperatures (17). The actual increase in cell open circuit voltage is somewhat less than shown because of the greater gas solubility with increasing pressure that produces higher parasitic current.

At an operating temperature (T), the change in voltage (ΔV_P) as a function of pressure (P) can be expressed fairly accurately using the expression:

$$\Delta V_P \text{ (mV)} = 0.15T \text{ (°K)} \log(P_2/P_1) \qquad (4\text{-}4)$$

over the entire range of pressures and temperatures shown in Fig. 4-4. In this expression, P_2 is the desired performance pressure and P_1 is the reference pressure at which performance is known.

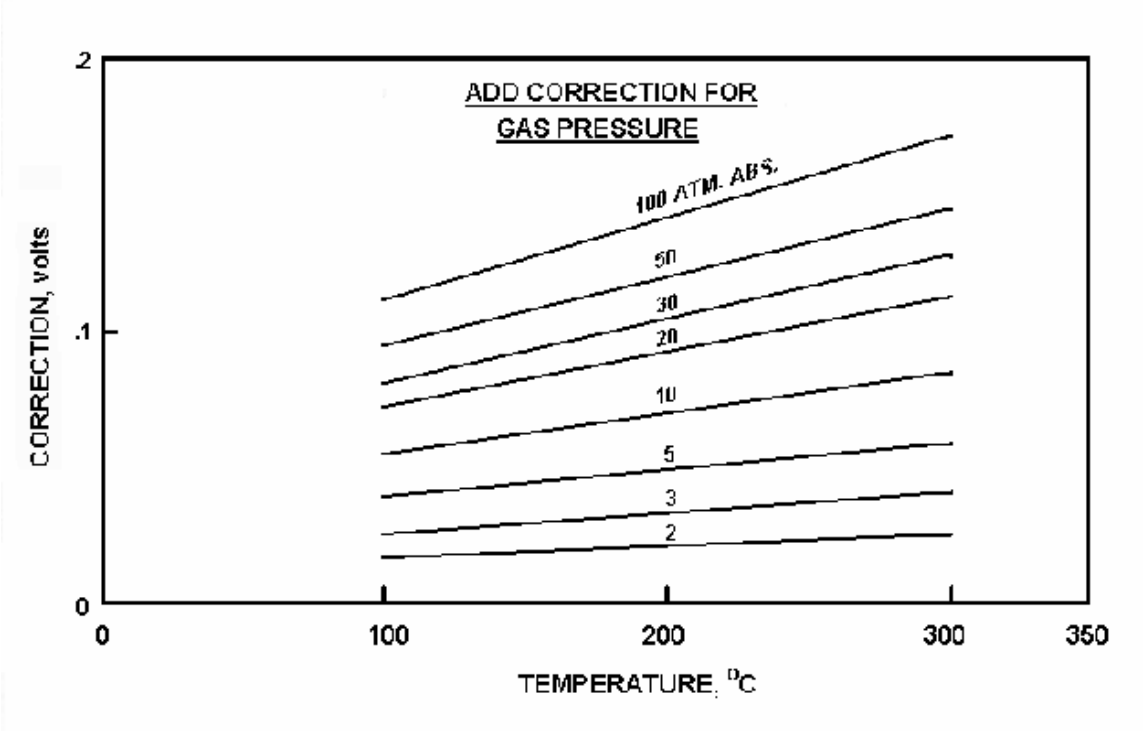

Figure 4-4 Reversible Voltage of the Hydrogen-Oxygen Cell (14)

To achieve faster kinetics, operating temperatures greater than 100 °C, accompanied by higher pressures, are used. Spacecraft fuel cells have operated for over 5,000 hours at 200 °C at 5 atm achieving HHV efficiencies exceeding 60 percent (18, 19). It should be noted that a pressure increase beyond about 5 atm produces improvements that are usually outweighed by a significant weight increase required to sustain the higher operating pressure. For space applications, weight is critical. Also, this increase in performance can only be realized in applications where compressed gases are available (such as in space vehicles or submarines). In all other cases, compressors are needed. Compressors are not only noisy, but incur parasitic power that lowers the system efficiency (20). An increase of overall efficiency when using compressors in simple cycles is very unlikely.

4.2.2 Effect of Temperature

Section 2.1 describes that the reversible cell potential for a fuel cell consuming H_2 and O_2 decreases by 49 mV under standard conditions in which the reaction product is water vapor. However, as is the case in PAFCs, an increase in temperature improves cell performance because activation polarization, mass transfer polarization, and ohmic losses are reduced.

The improvement in performance with cell temperature of catalyzed carbon-based (0.5 mg Pt/cm^2) porous cathodes is illustrated in Figure 4-5 (21). As expected, the electrode potential at a given current density decreases at lower temperatures, and the decrease is more significant at higher current densities. In the temperature range of 60 to 90 °C, the cathode performance increases by about 0.5 mV/°C at 50 to 150 mA/cm^2.

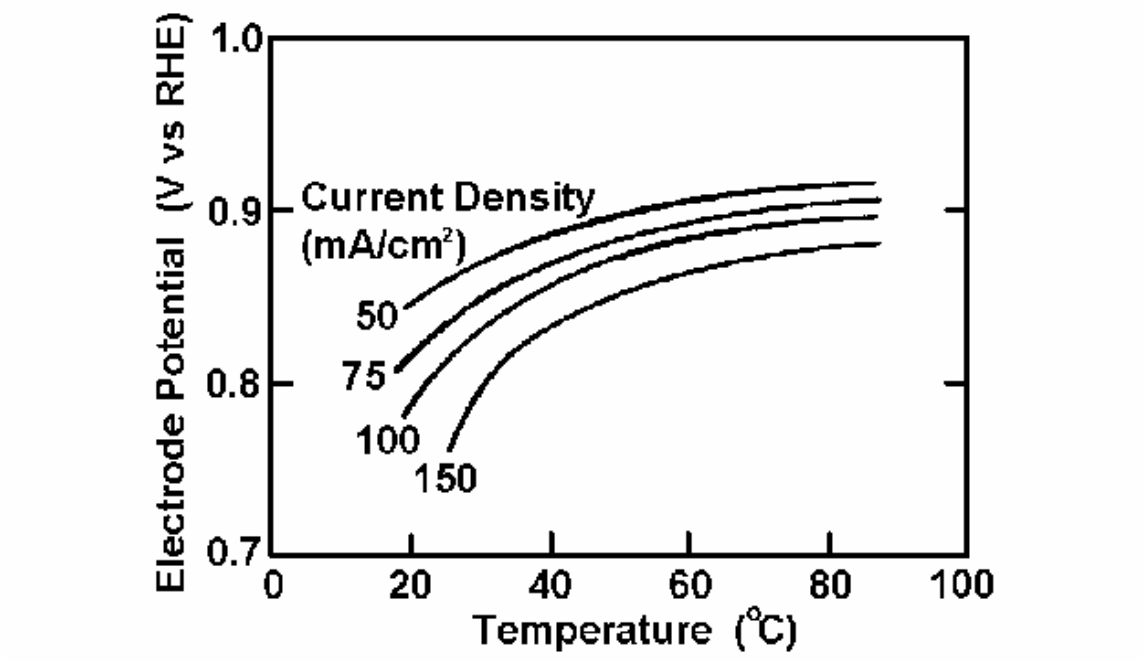

Figure 4-5 Influence of Temperature on O_2, (air) Reduction in 12 N KOH.
Source: Fig. 10, p. 324, Reference (21).

Early data by Clark, et al. (22) indicated a temperature coefficient for AFCs operating between 50 to 70 °C of about 3 mV/°C at 50 mA/cm^2, and cells with higher polarization had higher temperature coefficients under load. Later measurements by McBreen, et al. (23) on H_2/air single cells (289 cm^2 active area, carbon-based Pd anode and Pt cathode) with 50 percent KOH showed that the temperature coefficient above 60 °C was considerably lower than that obtained at lower temperatures, as shown in Figure 4-6. The McBreen data suggest the following expressions for evaluating the change in voltage (ΔV_T) as a function of temperature (T) at 100 mA/cm^2:

$$\Delta V_t\,(mV) = 4.0\,(T_2\text{-}T_1) \qquad \text{for } T < 63\ °C \qquad (4\text{-}5)$$

or

$$\Delta V_t\,(mV) = 0.7\,(T_2\text{-}T_1) \qquad \text{for } T > 63\ °C \qquad (4\text{-}6)$$

Alkaline cells exhibit reasonable performance when operating at low temperatures (room temperature up to about 70 °C). This is because the conductivity of KOH solutions is relatively high at low temperatures. For instance, an alkaline fuel cell designed to operate at 70 °C will reduce to only half power level when its operating temperature is reduced to room temperature (24).

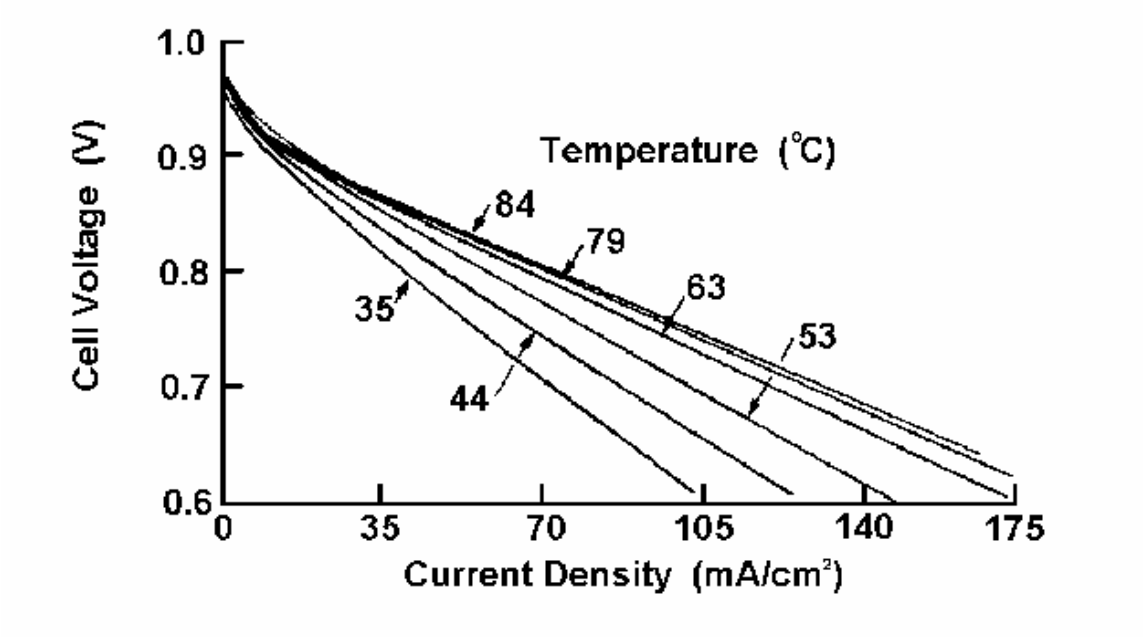

Figure 4-6 Influence of Temperature on the AFC Cell Voltage
Source: Figure 6, p. 889, reference (23).

4.2.3 Effect of Impurities

Carbon dioxide was the only impurity of concern in the data surveyed. AFCs with immobilized electrolytes suffer a considerable performance loss with reformed fuels containing CO_2 and from the presence of CO_2 in air (typically ~350 ppm CO_2 in ambient air). The negative impact of CO_2 arises from its reaction with OH

$$CO_2 + 2OH \rightarrow CO_3^{=} + H_2O \qquad (4\text{-}7)$$

producing the following effects: 1) reduced OH concentration, interfering with kinetics; 2) electrolyte viscosity increase, resulting in lower diffusion rate and lower limiting currents; 3) precipitation of carbonate salts in the porous electrode, reducing mass transport; 4) reduced oxygen solubility, and 5) reduced electrolyte conductivity.

In the case of circulating liquid electrolytes, the situation is not as critical, but is still significant. The influence of CO_2 on air cathodes (0.2 mg Pt/cm^2 supported on carbon black) in 6N KOH at 50 °C can be ascertained by analysis of the performance data presented in Figure 4-7 (25). To obtain these data, the electrodes were operated continuously at 32 mA/cm^2, and current-voltage performance curves were periodically measured. Performance in both CO_2-free air and CO_2-containing air showed evidence of degradation with time. However, with CO_2-free air the performance remained much more constant after 2,000 to 3,000 hours of operation. Later tests, however, showed that this drop in performance was caused purely by mechanical destruction of

the carbon pores by carbonate crystals. Improved electrodes can withstand even high amounts of CO_2 (5 percent) over many thousands of hours, as proven recently by DLR (Deutsches Zentrum fuer Luft- und Raumfahrt) (26).

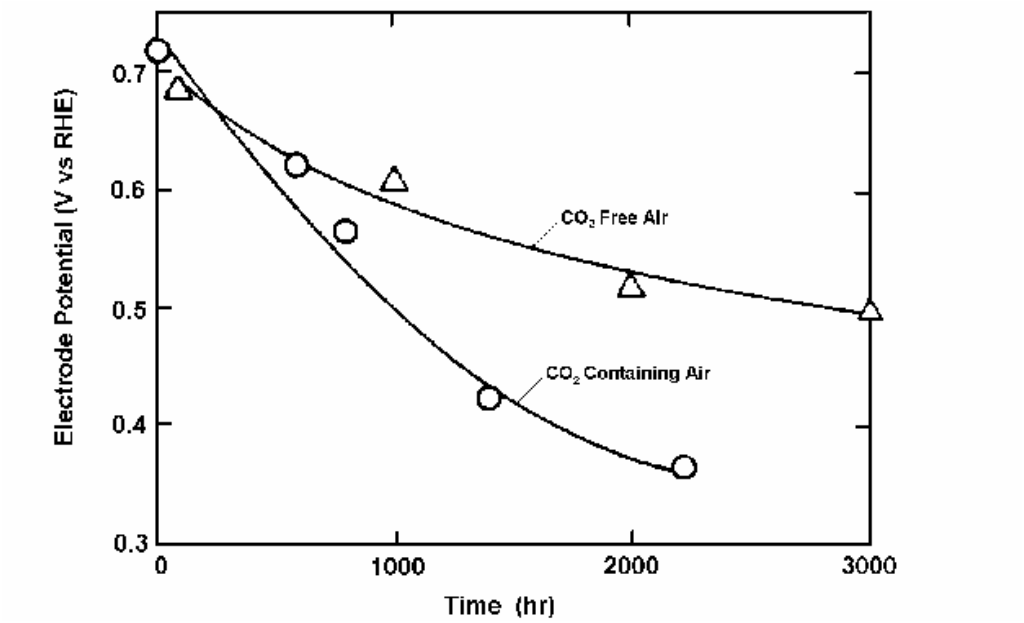

Figure 4-7 Degradation in AFC Electrode Potential with CO_2 Containing and CO_2 Free Air Source: Figure 2, p. 381, Reference (25)

High concentrations of KOH are also detrimental to the life of O_2 electrodes operating with CO_2-containing air, but operating the electrode at higher temperature is beneficial because it increases the solubility of CO_2 in the electrolyte. Hence, modifying the operating conditions can prolong electrode life. Extensive studies by Kordesch, et al. (25) indicate that the operational life of air electrodes (PTFE-bonded carbon electrodes on porous nickel substrates) with CO_2-containing air in 9N KOH at 65 °C ranges from 1,600 to 3,400 hours at a current density of 65 mA/cm^2. The life of these electrodes with CO_2-free air tested under similar conditions ranged from 4,000 to 5,500 hours. It was reported (2) that a lifetime of 15,000 hours was achieved with AFCs, with failure caused at that time by corrosion of the cell frames.

4.2.4 Effects of Current Density

As in the case with PAFCs, voltage obtained from an AFC is affected by ohmic, activation, and concentration losses. Figure 4-8 presents data obtained in the 1960s (22) that summarizes these effects, excluding electrolyte ohmic (iR) losses, for a catalyzed reaction (0.5 to 2.0 mg noble metal/cm^2) with carbon-based porous electrodes for H_2 oxidation and O_2 reduction in 9N KOH at 55 to 60 °C. The electrode technology was similar to that employed in the fabrication of PAFC electrodes.

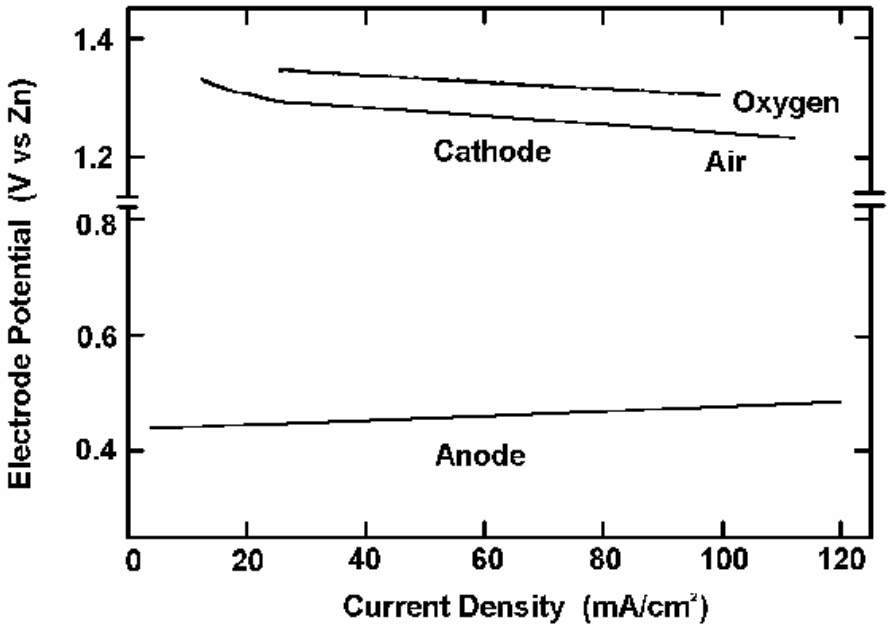

Figure 4-8 iR-Free Electrode Performance with O_2 and Air in 9 N KOH at 55 to 60°C. Catalyzed (0.5 mg Pt/cm^2 Cathode, 0.5 mg Pt-Rh/cm^2 Anode) Carbon-based Porous Electrodes (22)

The results in Figure 4-8 yield the following current density equations for cells operating in 9N KOH at 55 to 60 °C:

$$\Delta V_J \text{ (mV)} = -0.18\Delta J \qquad \text{for J = 40 to 100 mA/cm}^2 \text{ operating in } O_2 \qquad (4\text{-}8)$$

or

$$\Delta V_J \text{ (mV)} = -0.31\Delta J \qquad \text{for J = 40 to 100 mA/cm}^2 \text{ operating in air} \qquad (4\text{-}9)$$

where J is in mA/cm^2. The performance of a single cell with supported noble metal electro-catalyst (0.5 mg Pt-Rh/cm^2 anode, 0.5 mg Pt/cm^2 cathode) in 12N KOH at 65 ^{o}C is shown in Figure 4-9 (21). These results, reported in 1986, are comparable to those obtained in 1965. The iR-free electrode potentials (vs. RHE) at 100 mA/cm^2 in Figure 4-9 are 0.9 V with O_2 and 0.85 V with air. One major difference between the early cathodes and the cathodes in current use is that the limiting current for O_2 reduction from air has been improved (i.e., 100 to 200 mA/cm^2 improved to >250 mA/cm^2).

These results yield the following equations for cells operating in 12N KOH at 65 ^{o}C:

$$\Delta V_J \text{ (mV)} = -0.25\Delta J \qquad \text{for J = 50 to 200 mA/cm}^2 \text{ operating in } O_2 \qquad (4\text{-}10)$$

or

$$\Delta V_J \text{ (mV)} = -0.47\Delta J \qquad \text{for J = 50 to 200 mA/cm}^2 \text{ operating in air.} \qquad (4\text{-}11)$$

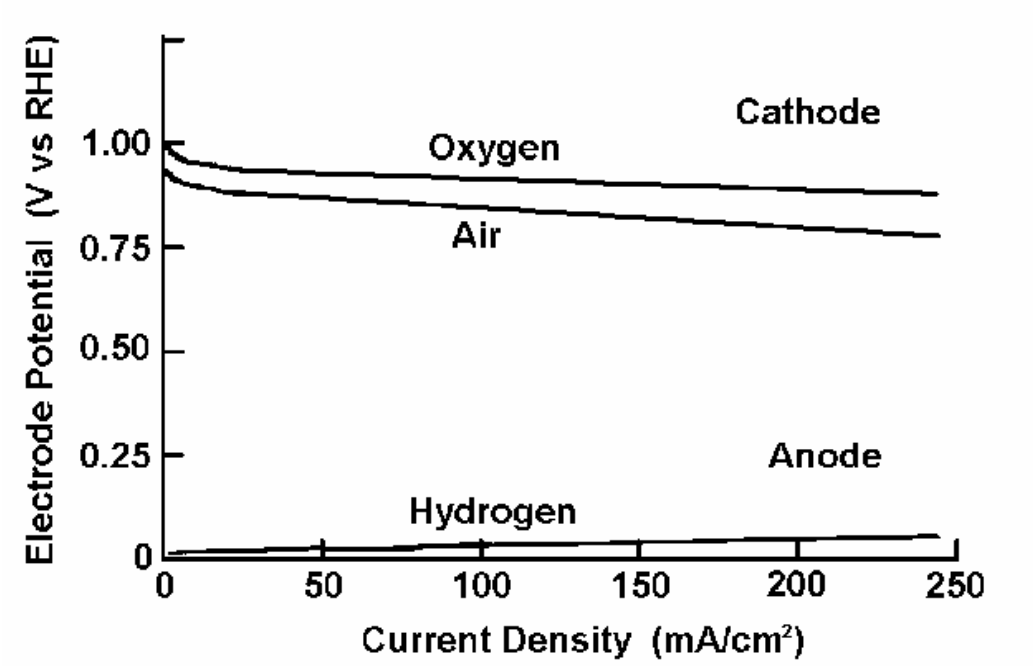

Figure 4-9 iR Free Electrode Performance with O_2 and Air in 12N KOH at 65 °C. Catalyzed (0.5 mg Pt/cm^2 Cathode, 0.5 mg Pt-Rh/cm^2 Anode), Carbon-based Porous Electrodes (21).

4.2.5 Effects of Cell Life

The UTC Fuel Cells H_2/O_2 alkaline technology exhibits a degradation of ~25 mV/1,000 hours (13). AFC cell stacks have demonstrated sufficiently stable operation for at least 5,000 hours, with degradation rates of 20 mV per 1,000 hours or less (24). Siemens reported a total of >8,000 operating hours with approximately 20 units (27). For large scale utility applications, economics demand operating times exceeding 40,000 hours, which presents perhaps the most significant obstacle to commercialization of AFC devices for stationary electric power generation.

4.3 Summary of Equations for AFC

The preceding sections described parametric performance based on various referenced data at different cell conditions. The following set of equations can be used to predict performance only if no better data or basis for estimate is available. Unfortunately, a noticeable lack of recent, published H_2/air data is available to predict performance trends. The equations presented below can be used in conjunction with the measured H_2/air performance shown in Figure 4-10 (12) as a basis for predicting performance at various operating conditions. The Space Shuttle Orbiter performance is included in Figure 4-10 as a reference point for H_2/O_2 performance (8); however, the trend equations should not be used for H_2/O_2 cells to predict operation at other conditions.

Parameter	Equation	Comments	
Pressure	ΔV_P (mV) = 0.15 T (^oK) log (P_2/P_1)	1 atm < P < 100 atm 100 ^oC < T < 300 °C	(4-4)
Temperature	ΔV_T (mV) = 4.0 (T_2-T_1)	for T < 63 °C, at 100 mA/cm^2	(4-5)
	ΔV_T (mV) = 0.7 (T_2-T_1)	for T > 63 °C, at 100 mA/cm^2	(4-6)
Current Density	ΔV_J (mV) = -0.18ΔJ	for J = 40 to 100 mA/cm^2 operating in O_2 with 9N KOH at 55-60 °C.	(4-8)
	ΔV_J (mV) = -0.31ΔJ	for J = 40 ti 100 mA/cm^2 operating in air with 9N KOH at 55-60 °C.	(4-9)
	ΔV_J (mV) = -0.25ΔJ	for J = 50 to 200 mA/cm^2 operating in O_2 with 12N KOH at 65 °C.	(4-10)
	ΔV_J (mV) = -0.047ΔJ	for J = 50 to 200 mA/cm^2 operating in air with 12N KOH at 65 °C.	(4-11)
Life Effects	$\Delta V_{Lifetime}$ (mV) = 20 µV per 1,000 hours or less		(4-12)

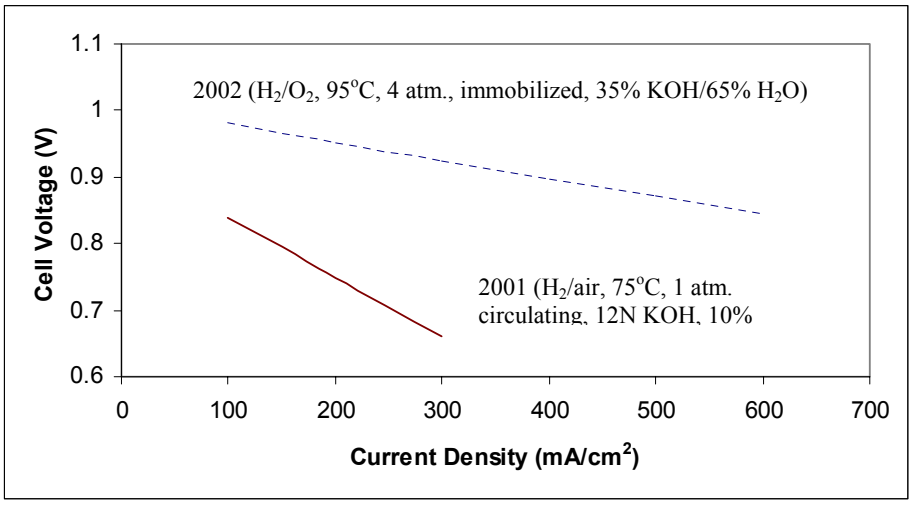

Figure 4-10 Reference for Alkaline Cell Performance

4.4 References

1. F.T. Bacon, *Electrochim. Acta,* 14, 569, 1969.
2. J.O'M Bockris and A.J. Appleby, *Energy*, 11, 95, 1986.
3. A.J. Appleby, *Energy*, 11, 13, 1986.
4. K.F. Blurton and E. McMullin, *Energy Conversion,* 9, 141, 1969.
5. K.V. Kordesch, *Brennstoffbatterien*, Springer-Verlag, New York, 1984.
6. V. Hacker, P. Enzinger, M. Muhr, K. Kordesh, J. Gsellman, M. Cifrain, P. Prenninger, K. Meitz, R. Aronsson, "Advantages of Alkaline Fuel Cell Systems for Mobile Applications," *2000 Fuel Cell Seminar Program and Abstracts*, Portland, OR; sponsored by the Fuel Cell Seminar Organizing Committee, October 30 – November 2, 2000.
7. G.F. McLean, T. Niet, S. Prince-Richard, N.Djilali, "An assessment of alkaline fuel cell technology," University of Victoria, in *International Journal of Hydrogen Energy,* p. 507 – 526, 27 (2002).
8. Communication with UTC Fuel Cells, July, 2002.
9. K. V. Kordesch, G. Simader, "Fuel Cells and Their Applications," Wiley, Weinheim – New York – Tokyo 1996.
10. D.W. Sheibley and R.A. Martin, *Prog. Batteries Solar Cells*, 6, 155, 1987.
11. K. Strasser, *J. Power Sources* 29, 152-153, 1990.
12. M. Cifrain, K. Kordesch, J. Gsellmann, T. Hejze, R. R. Aronson, "Alkaline Fuel Cells with Circulating Electrolytes," Poster presented at *Fuel Cell Seminar 2000,* Portland, Oregon, October 30-November 2, 2000.
13. Meeting with UTC Fuel Cells, June 2002.
14. K. Strasser, *J. Electrochem. Soc.* 127, 2173-2177, 1980.
15. H. van den Broeck, G. van Bogaert, G. Vennekens, L. Vermeeren, F. Vlasselaer, J. Lichtenberg, W. Schlösser, A. Blanchart, *Proc. 22nd IECEC Meeting*, 1005, Philadelphia, 1987.
16. J. Huff, paper presented at the 1986 "Status of Fuel Cell Technologies," *Fuel Cell Seminar Abstracts, Fuel Cell Seminar*, Tucson, AZ, October 26-29, 1986.
17. A.M. Adams, F.T. Bacon and R.G.H. Watson, *Fuel Cells* (W. Mitchell, ed.), Academic Press, New York, 138,1963.
18. S.S. Penner, ed., *Assessment of Research Needs for Advanced Fuel Cells*, DOE/ER/300.60-T1, US DOE, 1985.
19. Fuel Cell Seminar Abstracts, Long Beach, CA; sponsored by the National Fuel Cell Coordinating Group, October 23-26, 1988.
20. J. Larminie, A. Dicks, *"Fuel Cell Systems Explained,"* Wiley, Chichester (GB) 2000.
21. K. Tomantschger, F. McClusky, L. Oporto, A. Reid and K. Kordesch, *J. Power Sources*, 18, 317, 1986.
22. M.B. Clark, W.G. Darland and K.V. Kordesch, *Electrochem. Tech.,* 3, 166, 1965.
23. J. McBreen, G. Kissel, K.V. Kordesch, F. Kulesa, E.J. Taylor, E. Gannon and S. Srinivasan, in *Proceedings of the 15th Intersociety Energy Conversion Engineering Conference*, Volume 2, American Institute of Aeronautics and Astronautics, New York, NY, 886, 1980.
24. J.M.J. Blomen and M.N. Mugerwa ed., *Fuel Cell Systems*, Plenum Press, New York and London, 251, 1993.
25. K. Kordesch, J. Gsellmann and B. Kraetschmer, in *Power Sources*, 9, Edited by J. Thompson, Academic Press, New York, NY, 379, 1983.

26. E. Guelzow, M. Schulze, "Long Time Operation of AFC Electrodes with CO_2 Containing Gases," *8th Ulm ElectroChemical Talks*, Neu-Ulm, Germany, Abstracts p. 68, June 20-21, 2002.
27. K. Strasser, L. Blume and W. Stuhler, *Fuel Cell Seminar Program and Abstracts*, Long Beach, CA; sponsored by the National Fuel Cell Coordinating Group, October 23-26, 1988.

5. PHOSPHORIC ACID FUEL CELL

The phosphoric acid fuel cell (PAFC) was the first fuel cell technology to be commercialized. The number of units built exceeds any other fuel cell technology, with over 85 MW of demonstrators that have been tested, are being tested, or are being fabricated worldwide. Most of the plants are in the 50 to 200 kW capacity range, but large plants of 1 MW and 5 MW have been built. The largest plant operated to date achieved 11 MW of grid quality ac power (1, 2). Major efforts in the U.S. are concentrated on the improvement of PAFCs for stationary, dispersed power plants and on-site cogeneration power plants. The major industrial participants are UTC Fuel Cells in the U.S. and Fuji Electric Corporation, Toshiba Corporation, and Mitsubishi Electric Corporation in Japan.

Figure 5-1 depicts the operating configuration of the phosphoric acid cell. The electrochemical reactions occurring in PAFCs are

$$H_2 \rightarrow 2H^+ + 2e^- \qquad (5\text{-}1)$$

at the anode, and

$$\tfrac{1}{2}O_2 + 2H^+ + 2e^- \rightarrow H_2O \qquad (5\text{-}2)$$

at the cathode. The overall cell reaction is

$$\tfrac{1}{2}O_2 + H_2 \rightarrow H_2O \qquad (5\text{-}3)$$

The electrochemical reactions occur on highly dispersed electro-catalyst particles supported on carbon black. Platinum (Pt) or Pt alloys are used as the catalyst at both electrodes.

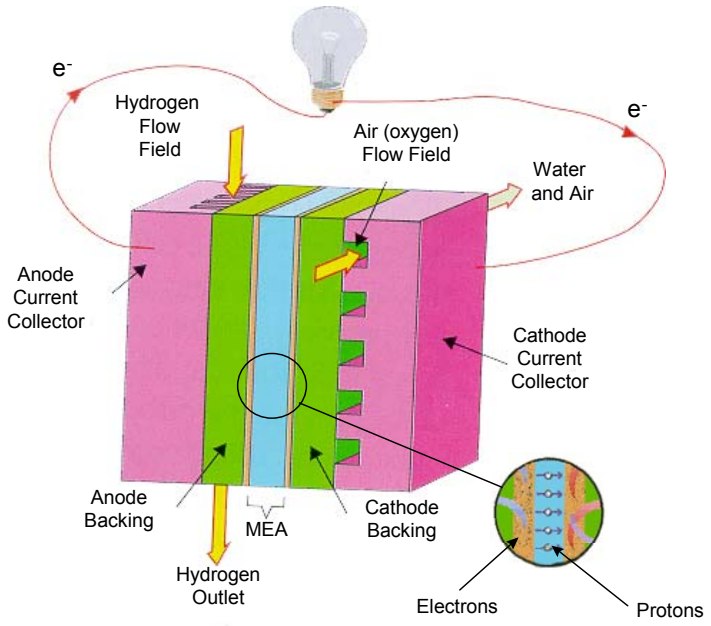

Figure 5-1 Principles of Operation of Phosphoric Acid Fuel Cell (Courtesy of UTC Fuel Cells)

5.1 Cell Components

5.1.1 State-of-the-Art Components

There have been only minor changes in cell design in recent years. The major U.S. manufacturer, UTC Fuel Cells, has concentrated on improving cell stability and life, and in improving the reliability of system components at reduced cost.

The evolution of cell components from 1965 to the present day for PAFCs is summarized in Table 5-1. In the mid-1960s, the conventional porous electrodes were polytetrafluoroethylene (PTFE) - bonded Pt black, and the loadings were about 9 mg Pt/cm^2. During the past two decades, Pt supported on carbon black has replaced Pt black in porous PTFE-bonded electrode structures as the electro-catalyst. A dramatic reduction in Pt loading has also occurred; the loadings[13] are currently about 0.10 mg Pt/cm^2 in the anode and about 0.50 mg Pt/cm^2 in the cathode.

The operating temperatures and acid concentrations of PAFCs have increased to achieve higher cell performance; temperatures of about 200 °C (392 °F) and acid concentrations of 100 percent H_3PO_4 are commonly used today. Although the present practice is to operate at atmospheric pressure, the operating pressure of PAFCs surpassed 8 atm in the 11 MW electric utility demonstration plant, confirming an increase in power plant efficiency. However, a number of

[13]. Assuming a cell voltage of 750 mV at 205 mA/cm^2 (approximate 11 MW design, 8 atmospheres) and the current Pt loadings at the anode and cathode, ~54 g Pt is required per kilowatt of power generated.

issues remain whether to design and operate PAFC units at atmospheric vs. pressurized conditions.

Primarily, small, multi-kW PAFC power units that were the focus of initial commercial applications led to atmospheric pressure operation. Although pressurization increased efficiency (lower fuel cost), it complicated the power unit - resulting in higher capital cost. The economic trade-off favored simpler, atmospheric operation for early commercial units.

Another important issue, independent of power unit size, is that pressure promotes corrosion. Phosphoric acid electrolyte (H_3PO_4) produces a vapor. This vapor, which forms over the electrolyte, is corrosive to cell locations other than the active cell area. These cell locations are at a mixed voltage (open circuit and cell voltage), that can be over ~0.8V/cell. That is the limit above which corrosion occurs (active area limited to operation under ~0.8 V/cell). An increase in cell total pressure causes the partial pressure of the H_3PO_4 vapor to increase, causing increased corrosion in the cell. Cell temperature must also be increased with pressurized conditions to produce steam for the steam reformer (3).

A major breakthrough in PAFC technology that occurred in the late 1960s was the development of carbon black and graphite for cell construction materials; this and other developments are reviewed by Appleby (4) and Kordesch (5). Carbon black and graphite were sufficiently stable to replace the more expensive gold-plated tantalum cell hardware used at the time. The use of high-surface-area graphite to support Pt permitted a dramatic reduction in Pt loading without sacrificing electrode performance. It was reported (4) that "without graphite, a reasonably inexpensive acid fuel cell would be impossible, since no other material combines the necessary properties of electronic conductivity, good corrosion resistance, low density, surface properties (especially in high area form) and, above all, low cost." However, carbon corrosion and Pt dissolution become an issue at cell voltages above ~0.8 V. Consequently, low current densities at cell voltage above 0.8 V and hot idle at open circuit potential should be avoided.

The porous electrodes used in PAFCs have been described extensively in patent literature (6); see also the review by Kordesch (5). These electrodes contain a mixture of electro-catalyst supported on carbon black and a polymeric binder, usually PTFE (30 to 50 wt percent). The PTFE binds the carbon black particles together to form an integral, but porous, structure that is supported on a porous graphite substrate. The graphite structure serves as a support for the electro-catalyst layer, as well as the current collector. A typical graphite structure used in PAFCs has an initial porosity of about 90 percent, which is reduced to about 60 percent by impregnation with 40 wt percent PTFE. This wet-proof graphite structure contains macropores of 3 to 50 μm diameter (median pore diameter of about 12.5 μm) and micropores with a median pore diameter of about 34 Å for gas permeability. The composite structure, consisting of a carbon black/PTFE layer on the graphite substrate, forms a stable, three-phase interface in the fuel cell, with H_3PO_4 electrolyte on one side (electro-catalyst side) and the reactant gas environment on the other.

Table 5-1 Evolution of Cell Component Technology for Phosphoric Acid Fuel Cells

Component	ca. 1965	ca. 1975	Current Status[a]
Anode	PTFE-bonded Pt black	PTFE-bonded Pt/C	PTFE-bonded Pt/C
		Vulcan XC-72[a]	
	9 mg/cm^2	0.25 mg Pt/cm^2	0.25 mg Pt/cm^2
Cathode	PTFE-bonded Pt black	PTFE-bonded Pt/C	PTFE-bonded Pt/C
		Vulcan XC-72[a]	
	9 mg/cm^2	0.5 mg Pt/cm^2	0.5 mg Pt/cm^2
Electrode Support	Ta mesh screen	Graphite Structure	Graphite Structure
Electrolyte Support	Glass fiber paper	PTFE-bonded SiC	PTFE-bonded SiC
Electrolyte	85 percent H_3PO_4	95 percent H_3PO_4	100 percent H_3PO_4
Electrolyte Reservoir		Porous graphite plate.	Porous graphite plate.
Cooler			1 per ~7 cells; imbedded (*SS)* tubes in graphite plate

a. - Over 40,000 hour component life demonstrated in commercial power plants.

A bipolar plate separates the individual cells and electrically connects them in series in a fuel cell stack. In some designs, the bipolar plate also contains gas channels that feed the reactant gases to the porous electrodes and remove the reaction products and inerts. Bipolar plates made from graphite resin mixtures that are carbonized at low temperature (~900 °C/1,652 °F) are not suitable because of their rapid degradation in PAFC operating environments (7, 8). However, corrosion stability is improved by heat treatment to 2,700 °C (4,892 °F) (8), i.e., the corrosion current is reduced by two orders of magnitude at 0.8 V in 97 percent H_3PO_4 at 190°C (374 °F) and 4.8 atm (70.5 psi). The all-graphite bipolar plates are sufficiently corrosion-resistant for a projected life of 40,000 hours in PAFCs, but they are still relatively costly to produce.

Several designs for the bipolar plate and ancillary stack components are used by fuel cell developers, and these are described in detail (9, 10, 11, 12). A typical PAFC stack contains cells connected in series to obtain the practical voltage level desired for the load. In such an arrangement, individual cells are stacked with bipolar plates between the cells. The bipolar plates used in early PAFCs consisted of a single piece of graphite with gas channels machined on either side to direct the flow of fuel and oxidant. Currently, both bipolar plates of the previous design and new designs consisting of several components are being considered. In the multi-component bipolar plates, a thin impervious plate separates the reactant gases in adjacent cells in the stack, and

separate porous plates with ribbed channels are used to direct gas flow. In a cell stack, the impervious plate is subdivided into two parts, and each joins one of the porous plates. The electrolyte vaporizes so that a portion of H_3PO_4 escapes from the cell in the air stream over time. An electrolyte reservoir plate (ERP), made of porous graphite, provides enough electrolyte to achieve a 40,000-hour cell life goal (there is no electrolyte replacement). The ERP also accommodates increases in electrolyte volume due to an increase in H_2O, so the porous graphite electrodes don't flood. These fluctuations in electrolyte volume occur during start-up and during transient operation. The porous structure, which allows rapid gas transport, is also used to store additional acid to replenish the supply lost by evaporation during the cell operating life.

In PAFC stacks, provisions must be included to remove heat generated during cell operation. In practice, heat has been removed by either liquid (two-phase water or a dielectric fluid) or gas (air) coolants that are routed through cooling channels located (usually about every fifth cell) in the cell stack. Liquid cooling requires complex manifolds and connections, but better heat removal is achieved than with air-cooling. The advantage of gas cooling is its simplicity, reliability, and relatively low cost. However, the size of the cell is limited, and the air-cooling passages must be much larger than the liquid- cooling passages.

Improvements in state-of-the-art phosphoric acid cells are illustrated by Figure 5-2. Performance by the ~1 m^2 (10 ft^2) short stack, (f), results in a power density of nearly 0.31 W/cm^2.

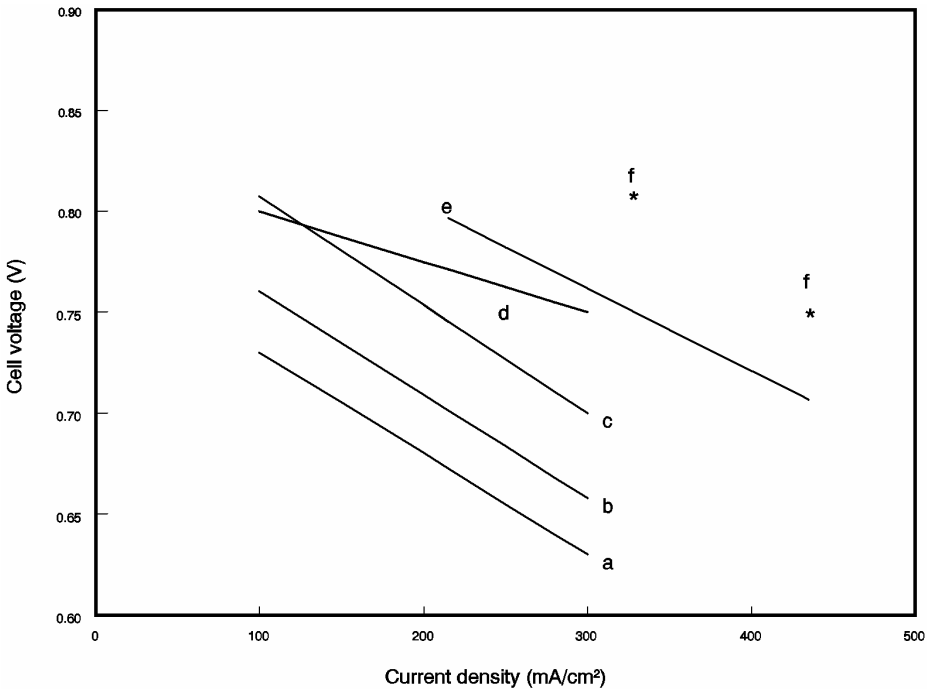

Figure 5-2 Improvement in the Performance of H_2-Rich Fuel/Air PAFCs

a - 1977: 190 °C, 3 atm, Pt loading of 0.75 mg/cm^2 on each electrode (13)
b - 1981: 190 °C, 3.4 atm, cathode Pt loading of 0.5 mg/cm^2 (14)
c - 1981: 205 °C, 6.3 atm, cathode Pt loading of 0.5 mg/cm^2 (14)
d - 1984: 205 °C, 8 atm, electro-catalyst loading was not specified (15)
e - 1992: 205 °C, 8 atm, 10 ft^2 short stack, 200 hrs, electro-catalyst loading not specified (16)
f - 1992: 205 °C, 8 atm, subscale cells, electro-catalyst loading not specified (16)

5.1.2 Development Components

Phosphoric acid electrode/electrolyte technology has reached a level of maturity at which developers commit resources for commercial capacity, multi-unit demonstrations and pre-prototype installations. UTC Fuel Cells has 25 (200 kW) atmospheric pressure power plants that have operated between 30,000 to 40,000 hours. Most cell parts are graphite, and there has been no electrolyte replacement over the cell life of 40,000 hours. Grid-independent units undergo extensive cycling. Cell components are manufactured at scale and in large quantities, demonstrating confidence that predicted performance will be met (3). However, further increases in power density and reduced cost are needed to achieve economic competitiveness with other energy technologies, as expressed in the early 1990s (17, 18). Fuel cell developers continue to address these issues.

In 1992, UTC Fuel Cells' predecessor, International Fuel Cells, completed a government-sponsored, advanced water-cooled PAFC development project to improve the performance and reduce the cost of both its atmospheric and pressurized technology for both on-site and utility

applications (16). The project focused on five major activities: 1) produce a conceptual design of a large stack with a goal of 175 W/ft^2 (0.188 W/cm^2), 40,000 hour useful life, and a stack cost of less than $400/kW; 2) test pressurized Configuration "B" single cells developed in a previous program, but improved with proprietary design advances in substrates, electrolyte reservoir plates, catalysts, seals, and electrolyte matrix to demonstrate the 175 W/ft^2 (0.188 W/cm^2) power density goal; 3) test a pressurized short stack with subscale size, improved component cells, and additional improvements in the integral separators and coolers to confirm the stack design; 4) test a pressurized short stack of improved full-size cell components, nominal 10 ft^2 size (approximately 1 m^2), to demonstrate the 175 W/ft^2 (0.188 W/cm^2) power density goal, and 5) test an advanced atmospheric "on-site" power unit stack with the improved components.

A conceptual design of an improved technology stack, operating at 120 psi (8.2 atm) and 405 °F (207 °C), was produced based on cell and stack development tests. The stack was designed for 355 10 ft^2 (approximately 1 m^2) cells to produce over 1 MW dc power in the same physical envelope as the 670 kW stack used in the 11 MW PAFC plant built for Tokyo Electric Power. The improvements made to the design were tested in single cells and in subscale and full size short stacks.

Table 5-2 summarizes the results. Single cells achieved an initial performance of 0.75 volts/cell at a current density of 400 A/ft^2 (431 mA/cm^2) at 8.2 atm and 207 °C. The power density, 300 W/ft^2 (0.323 W/cm^2), was well above the project goal. Several cells were operated to 600 A/ft^2 (645 mA/cm^2), achieving up to 0.66 volts/cell. The flat plate component designs were verified in a subscale stack prior to fabricating the full size short stack. The pressurized short stack of 10 ft^2 cells achieved a performance of 285 W/ft^2 (0.307 W/cm^2). Although the average cell performance, 0.71 volts/cell at 400 A/ft^2 (431 mA/cm^2), was not as high as the single cell tests, the performance was 65 percent higher than the project goal. Figure 5-3 presents single cell and stack performance data for pressurized operation. The stack was tested for over 3,000 hours. For reference purposes, Tokyo Electric Power Company's 11 MW power plant, operational in 1991, had an average cell performance of approximately 0.75 volts/cell at 190 mA/cm^2 or 0.142 W/cm^2 (19).

Table 5-2 Advanced PAFC Performance

	Average Cell Voltage, V	Current Density mA/cm^2	Power Density W/cm^2
IFC Pressurized:			
Project Goal			0.188
Single Cells	0.75 to 0.66	431 to 645	0.323
	0.71	431	
Full Size Short Stack	0.75	190	0.307
11 MW Reference			0.142
IFC Atmospheric:			
Single Cells	0.75	242	0.182
Full Size Short Stack	0.65	215	0.139
Mitsubishi Electric Atmospheric			
Single Cells	0.65	300	0.195

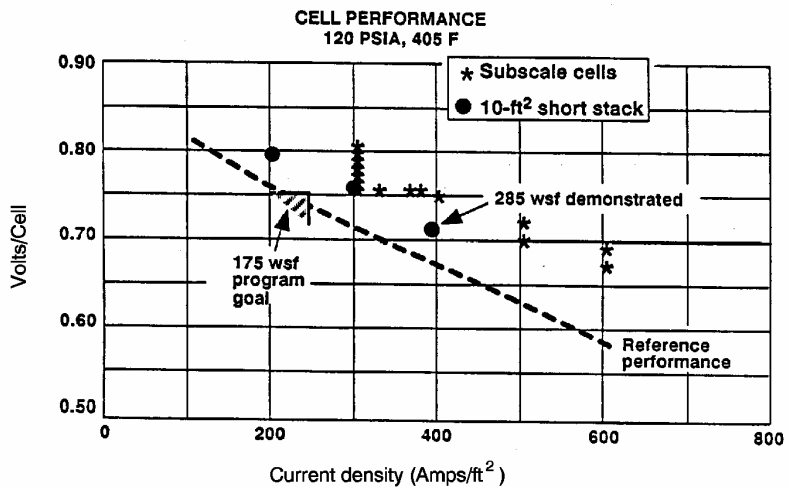

Figure 5-3 Advanced Water-Cooled PAFC Performance (16)

The atmospheric pressure short stack, consisting of 32 cells, obtained an initial performance of 0.65 volts/cell at 200 A/ft^2 (215 mA/cm^2) or 0.139 W/cm^2. The performance degradation rate was less than 4 mV/1,000 hours during the 4,500 hour test. Single cells, tested at atmospheric conditions, achieved a 500 hour performance of approximately 0.75 volts/cell at 225 A/ft^2 (242 mA/cm^2) or 0.182 W/cm^2.

Mitsubishi Electric Corporation investigated alloyed catalysts, processes to produce thinner electrolytes, and increased utilization of the catalyst layer (20). These improvements resulted in an initial atmospheric performance of 0.65 mV at 300 mA/cm^2 or 0.195 W/cm^2, which was higher than the UTC Fuel Cells' performance mentioned above (presented in Table 5-2 for comparison). Note that this performance was obtained using small 100 cm^2 cells and may not yet have been

demonstrated with full-scale cells in stacks. Approaches to increase life are to use series fuel gas flow in the stack to alleviate corrosion, provide well-balanced micropore size reservoirs to avoid electrolyte flooding, and use a high corrosion resistant carbon support for the cathode catalyst. These improvements resulted in the lowest PAFC degradation rate publicly acknowledged: 2 mV/1,000 hours for 10,000 hours at 200 to 250 mA/cm^2 in a short stack with 3,600 cm^2 area cells. UTC Fuel Cells reported a similar degradation rate in 2002 for power units operating up to 40,000 hours (3).

Several important technology development efforts for which details have been published include catalyst improvements, advanced gas diffusion electrode development, and tests on materials that offer better carbon corrosion protection. Transition metal (e.g., iron, cobalt) organic macrocycles[14] from the families of tetramethoxyphenylporphyrins (TMPP), phthalocyanines (PC), tetraazaannulenes (TAA) and tetraphenylporphyrins (TPP) have been evaluated as O_2-reduction electro-catalysts in PAFCs. One major problem with these organic macrocycles is their limited chemical stability in hot concentrated phosphoric acid. However, after heat treatment of the organic macrocycle (i.e., CoTAA, CoPC, CoTMPP, FePC, FeTMPP) on carbon at about 500 to 800 °C (932 to1,472 °F), the pyrolyzed residue exhibits electro-catalytic activity that, in some instances, is comparable to that of Pt and has promising stability, at least up to about 100 °C/212 °F (21). Another successful approach for enhancing the electro-catalysis of O_2 reduction is to alloy Pt with transition metals such as Ti (22), Cr (23), V (24), Zr, and Ta (24). The enhancement in electro-catalytic activity has been explained by a correlation between the optimum nearest-neighbor distance of the elements in the alloy and the bond length in O_2 (25).

Conventional cathode catalysts comprise either platinum or platinum alloys supported on conducting carbon black at 10 wt percent platinum. Present platinum loadings on the anode and cathode are 0.1 mg/cm^2 and 0.5 mg/cm^2, respectively (12, 16). It has been suggested by Ito, et al., that the amount of platinum may have been reduced to the extent that it might be cost effective to increase the amount of platinum loading on the cathode (26). However, a problem exists in that fuel cell stack developers have not experienced satisfactory performance improvements when increasing the platinum loading. Johnson Matthey Technology Centre (J-M) presented data that resulted in improved performance nearly in direct proportion to that expected based on the increase in platinum (27). Initial tests by J-M confirmed previous results - that using platinum alloy catalyst with a 10 wt percent net platinum loading improves performance. Platinum/nickel alloy catalysts yielded a 49 wt percent increase in specific activity over pure platinum. This translated into a 39 mV improvement in the air electrode performance at 200 mA/cm^2.

Johnson Matthey then determined that the platinum loading in the alloyed catalyst could be increased up to 30 wt percent while retaining the same amount of platinum without any decrease in specific activity or performance; the amount of nickel, hence the total amount of alloyed catalyst, decreased. Next, J-M researchers increased the amount of platinum from 10 to 30 wt percent while keeping the same nickel catalyst loading. The total amount of alloyed catalyst increased in this case. Results showed an additional 36 wt percent increase in specific activity, which provided another 41 mV increase at 200 mA/cm^2. The ideal voltage increase would have been 46 mV for this increase in platinum. Thus, the performance increase obtained experimentally was nearly in

[14]. See Reference 21 for literature survey.

direct proportion to the theoretical amount expected. The type of carbon support did not seem to be a major factor, based on using several typical supports during the tests.

The anode of a phosphoric acid fuel cell is subject to a reduction in performance when even low amounts of contaminants are preferentially absorbed on the noble catalysts. Yet, hydrogen-rich fuel gases, other than pure hydrogen, are produced with contaminant levels well in excess of the anode's tolerance limit. Of particular concern are CO, COS, and H_2S in the fuel gas. The fuel stream in a state-of-the-art PAFC anode, operating at approximately 200 °C (392 °F), must contain 1 vol percent or less of CO (12), less than 50 ppmv of COS plus H_2S, and less than 20 ppmv of H_2S (28). Current practice is to place COS and H_2S cleanup systems and CO shift converters prior to the cell (normally in the fuel processor before reforming) to reduce the fuel stream contaminant levels to the required amounts. Giner, Inc. performed experiments to develop a contaminant-tolerant anode catalyst in order to reduce or eliminate the cleanup equipment (29). An anode catalyst, G87A-17-2, was identified that resulted in only a 24 mV loss from reference when exposed to a 75 percent H_2, 1 percent CO, 24 percent CO_2, 80 ppm H_2S gas mixture at 190 °C (374 °F), 85 percent fuel utilization, and 200 mA/cm^2. A baseline anode experienced a 36 mV loss from the reference at the same conditions. At 9.2 atm (120 psi) pressure, the anode loss was only 19 mV at 190 °C (374 °F) and 17 mV at 210 °C (410 °F) (compared with pure H_2) with a gas of 71 percent H_2, 5 percent CO, 24 percent CO_2, and 200 ppm H_2S. Economic studies comparing the tradeoff between decreased cell performance with increased savings in plant cost showed no advantage when the new anode catalyst was used with gas containing 1 percent CO/200 ppm H_2S. A $7/kW increase resulted with the 5 percent CO gas (compared to a 1 percent CO gas) at a 50 MW size. Some savings would result by eliminating the low temperature shift converter. The real value of the catalyst may be its ability to tolerate excessive CO and H_2S concentrations during fuel processor upsets, and to simplify the system by eliminating equipment.

As previously mentioned, state-of-the-art gas diffusion electrodes are configured to provide an electrolyte network and a gas network formed with the mixture of carbon black and PTFE. In the electrodes, carbon black agglomerates, consisting of small primary particles 0.02 to 0.04 μm, are mixed with much larger PTFE particles of ~0.3 μm. The carbon black surface may not be covered completely by the PTFE because of the large size of conventional PTFE particles. The space in the agglomerates or the space between the agglomerates and PTFE may act as gas networks at the initial stage of operation, but fill with electrolyte eventually because of the small contact angle of carbon black, uncovered with PTFE, to electrolyte (<90°), resulting in the degradation of cell performance. Attempts to solve this flooding problem by increasing the PTFE content have not been successful because of the offset in performance resulting from the reduction of catalyst utilization. Higher performance and longer lifetime of electrodes are intrinsically at odds, and there is a limit to the improvement in performance over life by optimizing PTFE content in the state-of-the-art electrode structures. Watanabe, et al. (30) proposed preparing an electrode utilizing 100 percent of catalyst clusters, where the functions of gas diffusion electrodes were allotted completely to a hydrophilic, catalyzed carbon black and a wet-proofed carbon black. The former worked as a fine electrolyte network, and the latter worked as a gas-supplying network in a reaction layer. Higher utilization of catalyst clusters and longer life at the reaction layer were expected, compared to state-of-the-art electrodes consisting of the uniform mixture of catalyzed carbon black and PTFE particles. The iR-free electrode potentials for the reduction of oxygen and

air at 200 mA/cm^2 on the advanced electrode were 10 mV higher than those of the conventional electrode.

There is a trade-off between high power density and cell life performance. One of the major causes of declining cell performance over its life is that electrode flooding and drying, caused by migration of phosphoric acid between the matrix and the electrodes, occurs during cell load cycling. Researchers at Fuji Electric addressed two approaches to improve cell life performance while keeping power density high (31). In one, the wettability of the cathode and anode were optimized, and in the other a heat treatment was applied to the carbon support for the cathode catalyst. During tests, it was observed that a cell with low cathode wettability and high anode wettability was more than 50 mV higher than a cell with the reverse wetting conditions after 40 start/stop cycles.

The use of carbon black with large surface area to improve platinum dispersion on supports was investigated as a method to increase the power density of a cell (32). However, some large surface area carbon blacks are fairly corrosive in hot potassium acid, resulting in a loss of catalytic activity. The corrosivity of the carbon support affects both the rate of catalyst loss and electrode flooding and, in turn, the life performance of a cell. Furnace black has been heat treated at high temperature by Fuji Electric to increase its resistance to corrosion. It was found that corrosion could be reduced and cell life performance improved by heat treating carbon supports at high temperature, at least to around 3,000 °C (5,432 °F).

More recently, UTC Fuel Cells cites improvements to achieve 40,000 hour cell life through better cell temperature control, increasing H_3PO_4 inventory, and incorporating electrolyte reservoir plates in the cell stack (3).

5.2 Performance

There have been only minor changes in documented cell performance since the mid-1980s - mostly due to the operating conditions of the cell. The changes are reported in performance trends shown in this section that were primarily gained from contracts that UTC Fuel Cells had with the Department of Energy or outside institutions. New, proprietary PAFC performance data may likely have been observed by the manufacturer (3).

Cell performance for any fuel cell is a function of pressure, temperature, reactant gas composition, and fuel utilization. In addition, performance can be adversely affected by impurities in both the fuel and oxidant gases.

The sources of polarization in PAFCs (with cathode and anode Pt loadings of 0.5 mg Pt/cm^2, 180 °C, 1 atm, 100 percent H_3PO_4) were discussed in Section 2 and were illustrated as half cell performance in Figure 2-4. From Figure 2-4 it is clear that the major polarization occurs at the cathode, and furthermore, the polarization is greater with air (560 mV at 300 mA/cm^2) than with pure oxygen (480 mV at 300 mA/cm^2) because of dilution of the reactant. The anode exhibits very low polarization (-4 mV/100 mA/cm^2) on pure H_2, and increases when CO is present in the fuel gas. The ohmic (iR) loss in PAFCs is also relatively small, amounting to about 12 mV at 100 mA/cm^2.

Typical PAFCs will generally operate in the range of 100 to 400 mA/cm^2 at 600 to 800 mV/cell. Voltage and power constraints arise from increased corrosion of platinum and carbon components at cell potentials above approximately 800 mV.

5.2.1 Effect of Pressure

Even though pressure operation is not being pursued, it is still of interest for possible future development. It is well known that an increase in the cell operating pressure enhances the performance of PAFCs (11, 33, 34). The theoretical change in voltage (ΔV_P) as a function of pressure (P) is expressed as

$$\Delta V_P(\text{mV}) = \frac{(3)(2.3\,RT)}{2F} \log \frac{P_2}{P_1} \qquad (5\text{-}4)$$

where $\frac{3(2.3RT)}{2F} = 138\ mV$ at 190°C (374 °F). Experimental data (35) reported that the effect of pressure on cell performance at 190°C (374 °F) and 323 mA/cm^2 is correlated by the equation:

$$\Delta V_P\,(\text{mV}) = 146 \log \frac{P_2}{P_1} \qquad (5\text{-}5)$$

where P_1 and P_2 are different cell pressures. The experimental data (35) also suggest that Equation (5-5) is a reasonable approximation for a temperature range of 177 °C $\leq$ T $\leq$ 218 °C (351 °F $\leq$ T $\leq$ 424 °F) and a pressure range of 1 atm $\leq$ P $\leq$ 10 atm (14.7 psi $\leq$ P $\leq$ 147.0 psi). Data from Appleby (14) in Figure 5-2 indicate that the voltage gain observed by increasing the pressure from 3.4 atm (190 °C) to 6.3 atm (205 °C) is about 44 mV. According to Equation (5-5), the voltage gain calculated for this increase in pressure at 190 °C (374 °F) is 39 mV[15], which is in reasonable agreement with experimental data in Figure 5-2. Measurements (33) of ΔV_P for an increase in pressure from 4.7 to 9.2 atm (69.1 to 135.2 psia) in a cell at 190 °C (374 °F) show that ΔV_P is a function of current density, increasing from 35 mV at 100 mA/cm^2 to 42 mV at 400 mA/cm^2 (50 percent O_2 utilization with air oxidant, 85 percent H_2 utilization with pure H_2 fuel). From Equation (5-4), ΔV_p is 43 mV for an increase in pressure from 4.7 to 9.2 atm (69.1 to 135.2 psia) at 190 °C (374 °F), which is very close to the experimental value obtained at 400 mA/cm^2. Other measurements (36) for the same increase in pressure from 4.7 to 9.2 atm (69.1 to 135.2 psia), but at a temperature of 210 °C (410 °F) show less agreement between the experimental data and Equation (5-4).

The improvement in cell performance at higher pressure and high current density can be attributed to a lower diffusion polarization at the cathode and an increase in the reversible cell potential. In addition, pressurization decreases activation polarization at the cathode because of the increased oxygen and water partial pressures. If the partial pressure of water is allowed to increase, a lower acid concentration will result. This will increase ionic conductivity and bring about a higher exchange current density. The net outcome is a reduction in ohmic losses. It was reported (33) that an increase in cell pressure (100 percent H_3PO_4, 169 °C (336 °F)) from 1 to 4.4 atm (14.7 to

[15]. The difference in temperature between 190 and 205 °C is disregarded so Equation (5-5) is assumed to be valid at both temperatures.

64.7 psia) produces a reduction in acid concentration to 97 percent, and a decrease of about 0.001 ohm in the resistance of a small six cell stack (350 cm^2 electrode area).

5.2.2 Effect of Temperature

Figure 2-1 shows that the reversible cell potential for PAFCs consuming H_2 and O_2 decreases as the temperature increases by 0.27 mV/°C under standard conditions (product is water vapor). However, as discussed in Section 2, an increase in temperature has a beneficial effect on cell performance because activation polarization, mass transfer polarization, and ohmic losses are reduced.

The kinetics for the reduction of oxygen on Pt improves[16] as the cell temperature increases. At a mid-range operating load (~250 mA/cm^2), the voltage gain (ΔV_T) with increasing temperature of pure H_2 and air is correlated by

$$\Delta V_T \text{ (mV)} = 1.15 \, (T_2 - T_1) \text{ (°C)} \qquad \textit{(5-6)}$$

Data suggest that Equation (5-6) is reasonably valid for a temperature range of 180 °C $\leq$ T $\leq$ 250 °C (356 °F $\leq$ T $\leq$ 482 °F). It is apparent from this equation that each degree increase in cell temperature should increase performance by 1.15 mV. Other data indicate that the coefficient for Equation (5-6) may be in the range of 0.55 to 0.75, rather than 1.15. Although temperature has only a minimal effect on the H_2 oxidation reaction at the anode, it is important in terms of the amount of CO that can be absorbed by the anode. Figure 5-4 shows that increasing the cell temperature results in increased anode tolerance to CO absorption. A strong temperature effect was also observed using simulated coal gas. Below 200 °C (392 °F), the cell voltage drop was significant. Experimental data suggest that the effect of contaminants is not additive, indicating that there is an interaction between CO and H_2S (37). Increasing temperature increases performance, but elevated temperature also increases catalyst sintering, component corrosion, electrolyte degradation, and evaporation. UTC Fuel Cells operates its phosphoric acid cells at 207 °C (405 °F), which is a compromise that allows reasonable performance at a life of 40,000 hours (3).

[16]. The anode shows no significant performance improvement from 140 to 180° on pure H_2, but in the presence of CO, increasing the temperature results in a marked improvement in performance (see discussion in Section 5.2.4).

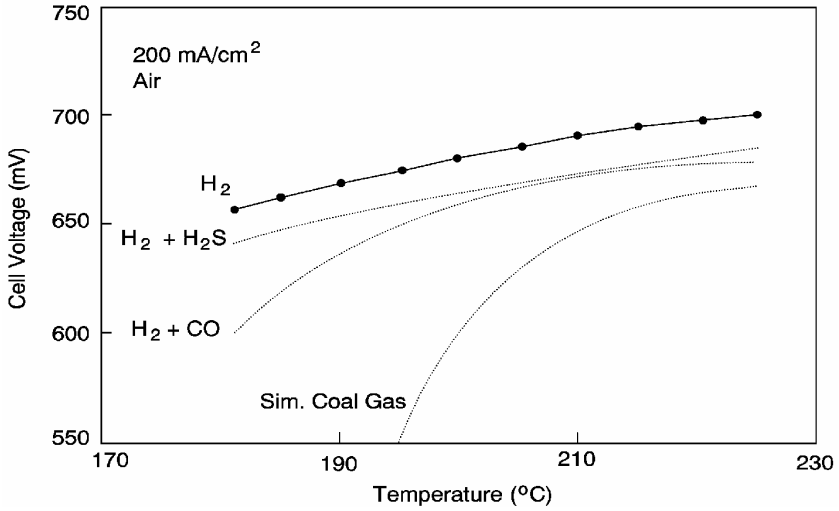

Figure 5-4 Effect of Temperature: Ultra-High Surface Area Pt Catalyst. Fuel: H_2, H_2 + 200 ppm H_2S and Simulated Coal Gas (37)

5.2.3 Effect of Reactant Gas Composition and Utilization

Increasing reactant gas utilization or decreasing inlet concentration results in decreased cell performance due to increased concentration polarization and Nernst losses. These effects are related to the partial pressures of reactant gases and are discussed below.

Oxidant: The oxidant composition and utilization are parameters that affect the cathode performance, as evident in Figure 2-5. Air, which contains ~21 percent O_2, is the obvious oxidant for terrestrial application PAFCs. The use of air with ~21 percent O_2 instead of pure O_2 results in a decrease in the current density of about a factor of three at constant electrode potential. The polarization at the cathode increases with an increase in O_2 utilization. Experimental measurements (38) of the change in overpotential ($\Delta\eta_c$) at a PTFE-bonded porous electrode in 100 percent H_3PO_4 (191 °C, atmospheric pressure) as a function of O_2 utilization is plotted in Figure 5-5 in accordance with Equation (5-7):

$$\Delta\eta_c = \eta_c - \eta_{c,\infty} \qquad (5\text{-}7)$$

where η_c and $\eta_{c,\infty}$ are the cathode polarizations at finite and infinite (i.e., high flow rate, close to 0 percent utilization) flow rates, respectively. The additional polarization attributed to O_2 utilization is reflected in the results, and the magnitude of this loss increases rapidly as the utilization increases. At a nominal O_2 utilization of 50 percent for prototype PAFC power plants, the additional polarization estimated from the results in Figure 5-5 is 19 mV. Based on experimental data (16, 38, 39), the voltage loss due to a change in oxidant utilization can be described by Equations (5-8) and (5-9):

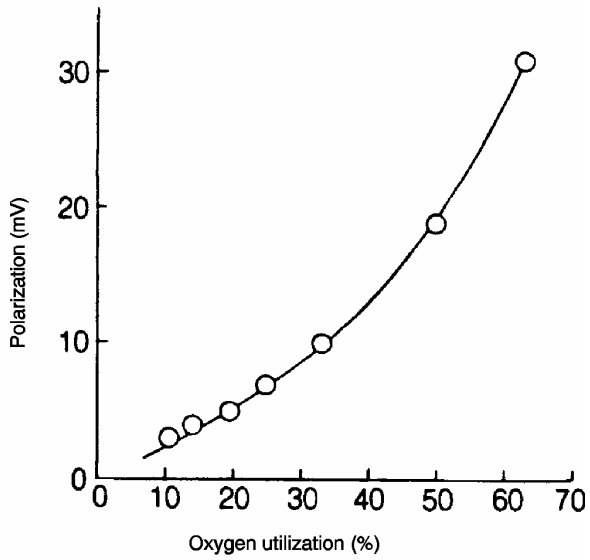

Figure 5-5 Polarization at Cathode (0.52 mg Pt/cm^2) as a Function of O_2 Utilization, which is Increased by Decreasing the Flow Rate of the Oxidant at Atmospheric Pressure 100 percent H_3PO_4, 191°C, 300 mA/cm^2, 1 atm. (38)

$$\Delta V_{Cathode}\,(mV) = 148 \log \frac{(\bar{P}_{O_2})_2}{(\bar{P}_{O_2})_1} \quad 0.04 \le \frac{\bar{P}_{O_2}}{\bar{P}_{Total}} \le 0.20 \qquad (5\text{-}8)$$

$$\Delta V_{Cathode}\,(mV) = 96 \log \frac{(\bar{P}_{O_2})_2}{(\bar{P}_{O_2})_1} \quad 0.20 < \frac{\bar{P}_{O_2}}{\bar{P}_{Total}} < 1.00 \qquad (5\text{-}9)$$

where $\bar{P}_{O_2}$ is the average partial pressure of O_2. The use of two equations over the concentration range more accurately correlates actual fuel cell operation. Equation (5-8) will generally apply to fuel cells using air as the oxidant and Equation (5-9) for fuel cells using an O_2-enriched oxidant.

Fuel: Hydrogen for PAFC power plants will typically be produced from conversion of a wide variety of primary fuels such as CH_4 (e.g., natural gas), petroleum products (e.g., naphtha), coal liquids (e.g., CH_3OH), or coal gases. Besides H_2, CO and CO_2 are also produced during conversion of these fuels (unreacted hydrocarbons are also present). These reformed fuels contain low levels of CO (after steam reforming and shift conversion reactions in the fuel processor) that cause anode CO absorption in PAFCs. The CO_2 and unreacted hydrocarbons (e.g., CH_4) are electrochemically inert and act as diluents. Because the anode reaction is nearly reversible, the fuel composition and hydrogen utilization generally do not strongly influence cell performance. The voltage change due to a change in the partial pressure of hydrogen (which can result from a change in either the fuel composition or utilization) can be described by Equation (5-10) (16, 36, 37):

$$\Delta V_{Anode}(mV) = 55 \log \frac{(\bar{P}_{H_2})_2}{(\bar{P}_{H_2})_1} \qquad (5\text{-}10)$$

where $\bar{P}_{H_2}$ is the average partial pressure of H_2. At 190 °C (374 °F), the presence of 10 percent CO_2 in H_2 should cause a voltage loss of about 2 mV. Thus, diluents in low concentrations are not expected to have a major effect on electrode performance; however, relative to the total anode polarization (i.e., 3 mV/100 mA/cm^2), the effects are large. It has been reported (16) that with pure H_2, the cell voltage at 215 mA/cm^2 remains nearly constant at H_2 utilizations up to 90 percent, and then it decreases sharply at H_2 utilizations above this value.

Low utilizations, particularly oxygen utilization, yield high performance. Low utilizations, however, result in poor fuel use. Optimization of this parameter is required. State-of-the-art utilizations are on the order of 85 percent and 50 percent for the fuel and oxidant, respectively.

5.2.4 Effect of Impurities

The concentrations of impurities entering the PAFC are very low relative to diluents and reactant gases, but their impact on performance is significant. Some impurities (e.g., sulfur compounds) originate from fuel gas entering the fuel processor and are carried into the fuel cell with the reformed fuel, whereas others (e.g., CO) are produced in the fuel processor.

Carbon Monoxide: The presence of CO in a H_2-rich fuel has a significant effect on anode performance because CO affects Pt electrode catalysts. CO absorption is reported to arise from the dual site replacement of one H_2 molecule by two CO molecules on the Pt surface (40, 41). According to this model, the anodic oxidation current at a fixed overpotential, with (i_{CO}) and without (i_{H_2}) CO present, is given as a function of CO coverage (θ_{CO}) by Equation (5-11):

$$\frac{i_{CO}}{i_{H_2}} = (1 - \theta_{CO})^2 \qquad (5\text{-}11)$$

For $[CO]/[H_2] = 0.025$, $\theta_{CO} = 0.31$ at 190°C (35); therefore, i_{CO} is about 50 percent of i_{H_2}.

Both temperature and CO concentration have a major influence on the oxidation of H_2 on Pt in CO containing fuel gases. Benjamin, et al. (35) derived Equation (5-12) for the voltage loss resulting from CO absorption as a function of temperature

$$\Delta V_{CO} = k(T)\,([CO]_2 - [CO]_1) \qquad (5\text{-}12)$$

where k(T) is a function of temperature, and $[CO]_1$ and $[CO]_2$ are the mole fractions CO in the fuel gas. The values of k(T) at various temperatures are listed in Table 5-3. Using Equation (5-12) and the data in Table 5-3, it is apparent that for a given change in CO content, ΔV_{CO} is about 8.5 times larger at 163 °C (325 °F) than at 218 °C (424 °F). The correlation provided by Equation (5-12) was obtained at 269 mA/cm^2; thus, its use at significantly different current densities may not be

appropriate. In addition, other more recent data (37) suggest a value for k(T) of -2.12 at a temperature of 190 °C (374 °F) rather than -3.54.

Table 5-3 Dependence of k(T) on Temperature

T (°C)	T (°F)	k(T)[a] (mV/ percent)
163	325	-11.1
177	351	-6.14
190	374	-3.54
204	399	-2.05
218	424	-1.30

a - Based on electrode with 0.35 mg Pt/cm^2, and at 269 mA/cm^2 (35)

The data in Figure 5-6 illustrate the influence of H_2 partial pressure and CO content on the performance of Pt anodes (10 percent Pt supported on Vulcan XC-72, 0.5 mg Pt/cm^2) in 100 percent H_3PO_4 at 180 °C (356 °F) (11). Diluting the H_2 fuel gas with 30 percent CO_2 produces an additional polarization of about 11 mV at 300 mA/cm^2. The results show that the anode polarization with fuel gases of composition 70 percent H_2/(30-x) percent CO_2/x percent CO (x =0, 0.3, 1, 3 and 5) increases considerably as the CO content increases to 5 percent.

Sulfur Containing Compounds: Hydrogen sulfide and carbonyl sulfide (COS) impurities[17] in fuel gases from fuel processors and coal gasifiers can reduce the effectiveness of fuel cell catalysts. Concentrations of these compounds must also be limited in a power plant's fuel processing section, because the fuel reformer too has catalysts. As a result, sulfur must be removed prior to fuel reforming with the non-sulfur tolerant catalysts now in use in PAFC power plants. It is prudent to be concerned about sulfur effects in the cell, however, because the fuel processor catalyst's tolerance limits may be less than the fuel cell catalyst's or there could be an upset of the fuel processor sulfur guard with sulfur passing through to the cell. The concentration levels of H_2S in an operating PAFC (190 to 210 °C (374 to 410 °F), 9.2 atm (120 psig), 80 percent H_2 utilization, <325 mA/cm^2) that can be tolerated by Pt anodes without suffering a destructive loss in performance are <50 ppm (H_2S + COS) or <20 ppm (H_2S) (42). Rapid cell failure occurs with fuel gas containing more than 50 ppm H_2S. Sulfur does not affect the cathode, and the impact of sulfur on the anodes can be re-activated by polarization at high potentials (i.e., operating cathode potentials). A synergistic effect between H_2S and CO negatively impacts cell performance. Figure 5-7 (37) shows the effect of H_2S concentration on ΔV with and without 10 percent CO present in H_2. The ΔV is referenced to performance on pure H_2 in the case of H_2S alone and to performance on H_2 with 10 percent CO for H_2S and CO. In both cases, at higher H_2S concentrations, the ΔV rises abruptly. This drop in performance occurs above 240 ppm for H_2S alone and above 160 ppm for H_2S with 10 percent CO.

[17]. Anode gases from coal gasifiers may contain total sulfur of 100 to 200 ppm.

Experimental studies by Chin and Howard (43) indicate that H_2S adsorbs on Pt and blocks the active sites for H_2 oxidation. The following electrochemical reactions, Equations (5-13), (5-14), and (5-15) involving H_2S are postulated to occur on Pt electrodes:

$$Pt + HS^- \rightarrow Pt - HS_{ads} + e^- \quad (5\text{-}13)$$

$$Pt - H_2S_{ads} \rightarrow Pt - HS_{ads} + H^+ + e^- \quad (5\text{-}14)$$

$$Pt - HS_{ads} \rightarrow Pt - S_{ads} + H^+ + e^- \quad (5\text{-}15)$$

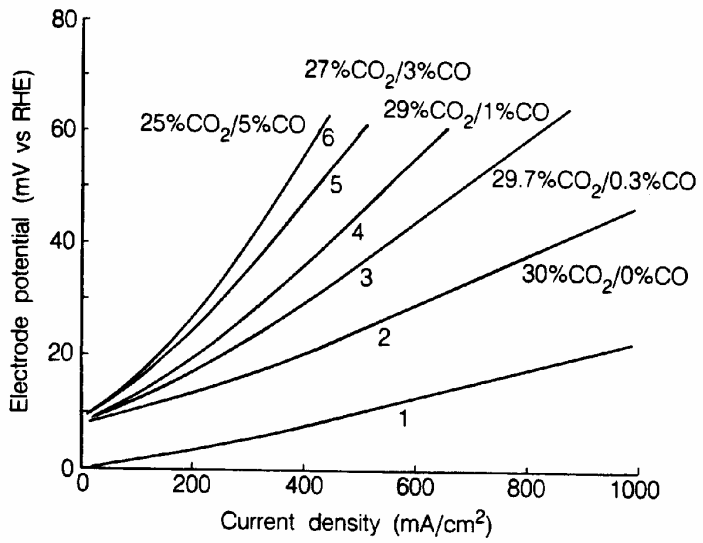

Figure 5-6 Influence of CO and Fuel Gas Composition on the Performance of Pt Anodes in 100 percent H_3PO_4 at 180°C. 10 percent Pt Supported on Vulcan XC-72, 0.5 mg Pt/cm^2. Dew Point, 57°. Curve 1, 100 percent H_2; Curves 2-6, 70 percent H_2 and CO_2/CO Contents (mol percent) Specified (21)

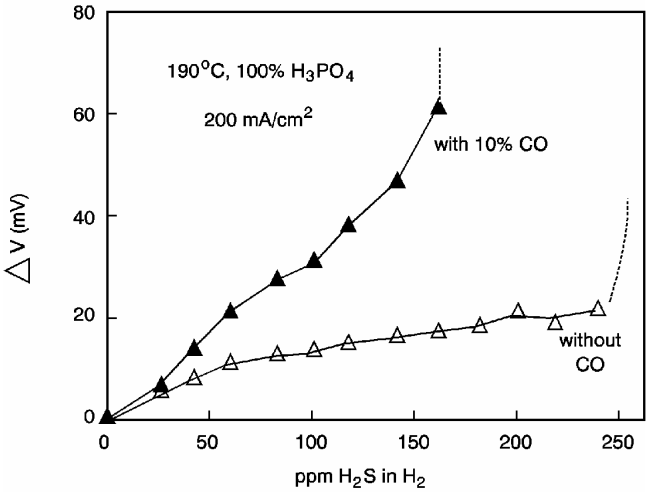

Figure 5-7 Effect of H_2S Concentration: Ultra-High Surface Area Pt Catalyst (37)

Elemental sulfur (in Equation (5-15) is expected on Pt electrodes only at high anodic potentials; at sufficiently high potentials, sulfur is oxidized to SO_2. The extent of catalyst masking by H_2S increases with increasing H_2S concentration, electrode potential, and exposure time. The effect of H_2S, however, decreases with increasing cell temperature.

Other Compounds: The effects of other compounds (such as those containing nitrogen) on PAFC performance has been adequately reviewed by Benjamin, et al. (35). Molecular nitrogen acts as a diluent but other nitrogen compounds (e.g., NH_3, HCN, NO_X) may not be as innocuous. NH_3 in the fuel or oxidant gases reacts with H_3PO_4 to form a phosphate salt, $(NH_4)H_2PO_4$,

$$H_3PO_4 + NH_3 \rightarrow (NH_4)H_2PO_4 \qquad (5\text{-}16)$$

which decreases the rate of O_2 reduction. A concentration of less than 0.2 mol percent $(NH_4)H_2PO_4$ must be maintained to avoid unacceptable performance losses (44). Consequently, the amount of molecular nitrogen must be limited to 4 percent because it will react with hydrogen to form NH_3 (3). The effects of HCN and NO_X on fuel cell performance have not been clearly established.

5.2.5 Effects of Current Density

The voltage that can be obtained from a PAFC is reduced by ohmic, activation, and concentration losses that increase with increasing current density. The magnitude of this loss can be approximated by the following equations:

$$\Delta V_J\,(mV) = -0.53\,\Delta J \qquad \text{for J= 100 to 200 mA/cm}^2 \qquad (5\text{-}17)$$

$$\Delta V_J\,(mV) = -0.39\,\Delta J \qquad \text{for J= 200 to 650 mA/cm}^2 \qquad (5\text{-}18)$$

The coefficients in these equations were correlated from performance data for cells (45) operating at 120 psia (8.2 atm), 405 °F (207 °C) (16) with fuel and oxidant utilizations of 85 percent and 70 percent, respectively[18], an air fed cathode, and an anode inlet composition of 75 percent H_2, and 0.5 percent CO. Similarly, at atmospheric conditions, the magnitude of this loss can be approximated by

$$\Delta V_J \text{ (mV)} = -0.74\ \Delta J \qquad \text{for J= 50 to 120 mA/cm}^2 \qquad \textit{(5-19)}$$

$$\Delta V_J \text{ (mV)} = -0.45\ \Delta J \qquad \text{for J= 120 to 215 mA/cm}^2 \qquad \textit{(5-20)}$$

The coefficients in the atmospheric condition equations were derived from performance data for cells (45) operating at 14.7 psia (1 atm) and 400 °F (204 °C), fuel and oxidant utilizations of 80 percent and 60 percent, respectively[18], an air fed cathode, and an anode inlet composition of 75 percent H_2 and 0.5 percent CO.

5.2.6 Effects of Cell Life

One of the primary areas of research is in extending cell life. The goal is to maintain the performance of the cell stack during a standard utility application (~40,000 hours). Previous state-of-the-art PAFCs (46, 47, 48) showed the following degradation over time:

$$\Delta V_{\text{lifetime}} \text{ (mV)} = -3 \text{ mV/1,000 hours} \qquad \textit{(5-21)}$$

UTC Fuel Cells reports that the efficiency of its latest power plants at the beginning of life is 40 percent LHV. The infant life loss reduces the efficiency quickly to 38 percent, but then there is a small decrease in efficiency over the next 40,000 hours (expected cell life) resulting in an average efficiency over life of 37 percent (3). Assuming that the loss in efficiency is due solely to cell voltage loss, the maximum degradation rate can be determined as:

$$\Delta V_{\text{lifetime}} \text{ (mV)} = -2 \text{ mV/1,000 hours} \qquad \textit{(5-22)}$$

[18]. Assumes graph operating conditions (not provided) are the same as associated text of Ref.15.

5.3 Summary of Equations for PAFC

The preceding sections provide parametric performance based on various referenced data at differing cell conditions. It is suggested that the following set of equations be used unless the reader prefers other data or rationale. Figure 5-8 is provided as reference PAFC performances at ambient pressure and 8.2 atm.

Parameter	Equation	Comments	
Pressure	$\Delta V_P\,(mV) = 146 \log \frac{P_2}{P_1}$	1 atm ≤ P ≤ 10 atm 177 °C ≤ T ≤ 218 °C	(5-5)
Temperature	$\Delta V_T\,(mV) = 1.15\,(T_2 - T_1)$	180 °C ≤ T ≤ 250 °C	(5-6)
Oxidant	$\Delta V_{Cathode}\,(mV) = 148 \log \frac{(\bar{P}_{0_2})_2}{(\bar{P}_{0_2})_1}$	$0.04 \le \frac{\bar{P}_{0_2}}{\bar{P}_{Total}} \le 0.20$	
	$\Delta V_{cathode}\,(mV) = 96 \log \frac{(\bar{P}_{02})_2}{(\bar{P}_{02})_1}$	$0.20 \le \frac{\bar{P}_{0_2}}{\bar{P}_{Total}} < 1.0$	(5-9)
Fuel	$\Delta V_{anode}\,(mV) = 55 \log \frac{(\bar{P}_{H_2})_2}{(\bar{P}_{H_2})_1}$		(5-10)
CO Absorption Impact	$\Delta V_{CO}\,(mV) = -11.1\,([CO]_2 - [CO]_1)$ $\Delta V_{CO}\,(mV) = --6.14\,([CO]_2 - [CO]_1)$ $\Delta V_{CO}\,(mV) = -3.54\,([CO]_2 - [CO]_1)$ $\Delta V_{CO}\,(mV) = -2.05\,([CO]_2 - [CO]_1)$ $\Delta V_{CO}\,(mV) = -1.30\,([CO]_2 - [CO]_1)$	163 °C 177 °C 190 °C 204 °C 218 °C	(5-12)
Current Density	$\Delta V_J\,(mV) = -0.53\,)\Delta J$ for J = 100 to 200 mA/cm^2, P = 8.2 atm		(5-17)
	$\Delta V_J\,(mV) = -0.39\,)\Delta J$ for J = 200 to 650 mA/cm^2, P = 8.2 atm		(5-18)
	$\Delta V_J\,(mV) = -0.74\,)\Delta J$ for J = 50 to 120 mA/cm^2, P = 1 atm		(5-19)
	$\Delta V_J\,(mV) = -0.45\,)\Delta J$ for J = 120 to 215 mA/cm^2, P = 1 atm		(5-20)
Life Effects	$\Delta V_{lifetime}\,(mV) = -2mV/1{,}000$ hrs.		(5-22)

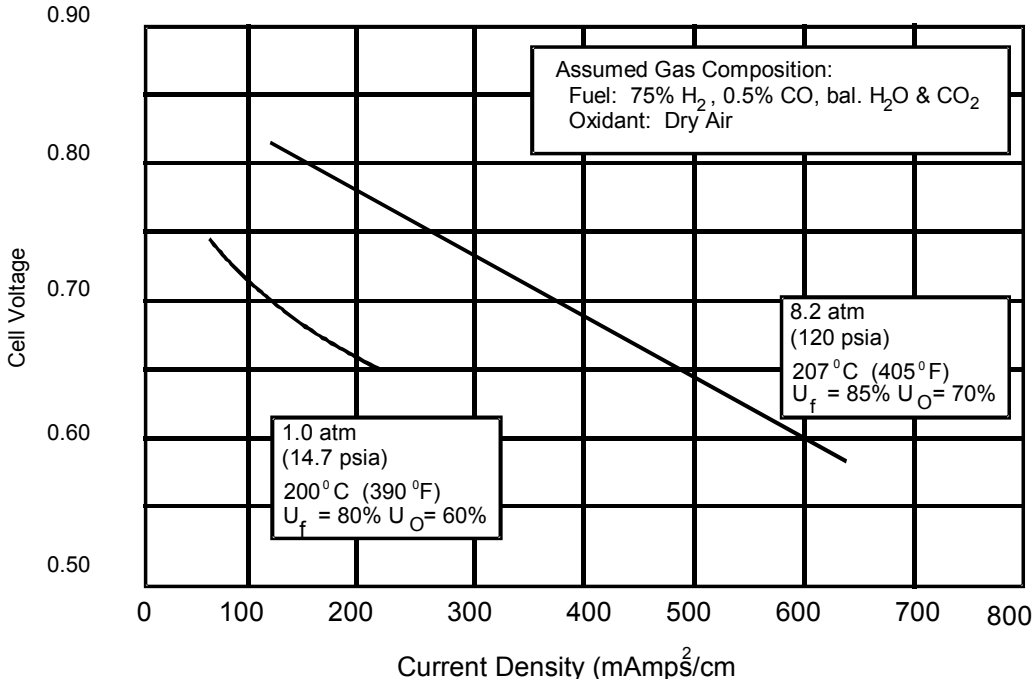

Figure 5-8 Reference Performances at 8.2 atm and Ambient Pressure. Cells from Full Size Power Plant (16)

5.4 References

1. J. Hirschenhofer, "Latest Progress in Fuel Cell Technology," IEEE-Aerospace and Electronic Systems Magazine, 7, November 1992.
2. J. Hirschenhofer, "Status of Fuel Cell Commercialization Efforts," *American Power Conference*, Chicago, IL, April 1993.
3. Meeting with UTC Fuel Cells, June 2002.
4. J. Appleby, in *Proceedings of the Workshop on the Electrochemistry of Carbon*, Edited by S. Sarangapani, J.R. Akridge and B. Schumm, The Electrochemical Society, Inc., Pennington, NJ, p. 251, 1984.
5. K.V. Kordesch, "Survey of Carbon and Its Role in Phosphoric Acid Fuel Cells," BNL 51418, prepared for Brookhaven National Laboratory, December 1979.
6. K. Kinoshita, *Carbon: Electrochemical and Physicochemical Properties*, Wiley Interscience, New York, NY, 1988.
7. L. Christner, J. Ahmad, M. Farooque, in *Proceedings of the Symposium on Corrosion in Batteries and Fuel Cells and Corrosion in Solar Energy Systems,* Edited by C. J. Johnson and S.L. Pohlman, The Electrochemical Society, Inc., Pennington, NJ, p. 140, 1983.
8. P.W.T. Lu, L.L. France, in *Extended Abstracts*, Fall Meeting of The Electrochemical Society, Inc., Volume 84-2, Abstract No. 573, The Electrochemical Society, Inc., Pennington, NJ, p. 837, 1984.

9. M. Warshay, in *The Science and Technology of Coal and Coal Utilization,* Edited by B.R. Cooper, W.A. Ellingson, Plenum Press, New York, NY, p. 339, 1984.
10. P.R. Prokopius, M. Warshay, S.N. Simons, R.B. King, in *Proceedings of the 14th Intersociety Energy Conversion Engineering Conference,* Volume 2, American Chemical Society, Washington, D. C., p. 538, 1979.
11. S.N. Simons, R.B. King, P.R. Prokopius, in *Symposium Proceedings Fuel Cells Technology Status and Applications,* Edited by E. H. Camara, Institute of Gas Technology, Chicago, IL, p. 45, 1982.
12. Communications with IFC, September 2000.
13. A.P. Fickett, in *Proceedings of the Symposium on Electrode Materials and Processes for Energy Conversion and Storage,* Edited by J.D.E. McIntyre, S. Srinivasan and F.G. Will, The Electrochemical Society, Inc. Pennington, NJ, p. 546, 1977.
14. A.J. Appleby, *J. Electroanal, Chem.,* 118**,** 31, 1981.
15. J. Huff, "Status of Fuel Cell Technologies," in *Fuel Cell Seminar Abstracts*, 1986 National Fuel Cell Seminar, Tucson, AZ, October 1986.
16. "Advanced Water-Cooled Phosphoric Acid Fuel Cell Development, Final Report," Report No. DE/MC/24221-3130, International Fuel Cells Corporation for U.S. DOE under Contract DE-AC21-88MC24221, South Windsor, CT, September 1992.
17. N. Giordano, E. Passalacqua, L. Pino, V. Alderucci, P.L. Antonucci, "Catalyst and Electrochemistry in PAFC: A Unifying Approach," in *The International Fuel Cell Conference Proceedings*, NEDO/MITI, Tokyo, Japan, 1992.
18. B. Roland, J. Scholta, H. Wendt, "Phosphoric Acid Fuel Cells - Materials Problems, Process Techniques and Limits of the Technology," in *The International Fuel Cell Conference Proceedings*, NEDO/MITI, Tokyo, Japan, 1992.
19. "Overview of 11 MW Fuel Cell Power Plant," Non-published information from Tokyo Electric Power Company, September 1989.
20. M. Matsumoto, K. Usami, "PAFC Commercialization and Recent Progress of Technology in Mitsubishi Electric," in *The International Fuel Cell Conference Proceedings*, NEDO/MITI, Tokyo, Japan, 1992.
21. J.A.S. Bett, H.R. Kunz, S.W. Smith and L.L. Van Dine, "Investigation of Alloy Catalysts and Redox Catalysts for Phosphoric Acid Electrochemical Systems," FCR-7157F, prepared by International Fuel Cells for Los Alamos National Laboratory under Contract No. 9-X13-D6271-1, 1985.
22. B.C. Beard, P.N. Ross, *J. Electrochem. Soc.,* 133, 1839, 1986.
23. J.T. Glass, G.L. Cahen, G.E. Stoner, E.J. Taylor, *J. Electrochem. Soc.,* 134, 58, 1987.
24. P.N. Ross, "Oxygen Reduction on Supported Pt Alloys and Intermetallic Compounds in Phosphoric Acid," Final Report, EM-1553, prepared under Contract 1200-5 for the Electric Power Research Institute, Palo Alto, CA, September 1980.
25. V. Jalan, J. Giner, in *DECHEMA Monographs,* Volume 102, Edited by J.W. Schultze, VCH Verlagsgesellschaft, Weinheim, West Germany, p. 315, 1986.
26. T. Ito, K. Kato, S. Kamitomai, M. Kamiya, "Organization of Platinum Loading Amount of Carbon-Supported Alloy Cathode for Advanced Phosphoric Acid Fuel Cell," in *Fuel Cell Seminar Abstracts*, 1990 Fuel Cell Seminar, Phoenix, AZ, November 25-28, 1990.
27. J.S. Buchanan, G.A. Hards, L. Keck, R.J. Potter, "Investigation into the Superior Oxygen Reduction Activity of Platinum Alloy Phosphoric Acid Fuel Cell Catalysts," in *Fuel Cell Seminar Abstracts*, Tucson, AZ, November 29-December 2, 1992.

28. K. Kinoshita, F.R. McLarnon, E.J. Cairns, *Fuel Cells, A Handbook*, prepared by Lawrence Berkeley Laboratory for the U.S. Department of Energy under Contract DE-AC03-76F00098, May 1988.
29. N.D. Kackley, S.A. McCatty, J.A. Kosek, "Improved Anode Catalysts for Coal Gas-Fueled Phosphoric Acid Fuel Cells," Final Report DOE/MC/25170-2861, prepared for U.S. Department of Energy under Contract DE-AC21-88MC25170, July 1990.
30. M. Watanabe, C. Shirmura, N. Hara, K. Tsurumi, "An Advanced Gas-Diffusion Electrode for Long-Life and High Performance PAFC," in *The International Fuel Cell Conference Proceedings*, NEDO/MITI, Tokyo, Japan, 1992.
31. M. Aoki, Y. Ueki, H. Enomoto, K. Harashima, "Some Approaches to Improve the Life Performance of Phosphoric Acid Fuel Cell," paper provided to the authors by Fuji Electric Corporate Research and Development, 1992, date of preparation unknown.
32. M. Watanabe, H. Sei, P. Stonehart, *Journal of Electroanalytical Chemistry*. 261, 375, 1989.
33. M. Farooque, "Evaluation of Gas-Cooled Pressurized Phosphoric Acid Fuel Cells for Electric Utility Power Generation," Final Technical Report, NASA CR-168298 prepared by Energy Research Corp. under Contract No. DEN 3-201 for NASA Lewis Research Center, September 1983.
34. J. McBreen, W.E. O'Grady, R. Richter, *J. Electrochem. Soc.,* 131**,** 1215, 1984.
35. T.G. Benjamin, E.H. Camara, L.G. Marianowski, *Handbook of Fuel Cell Performance,* prepared by the Institute of Gas Technology for the United States Department of Energy under Contract No. EC-77-C-03-1545, May 1980.
36. J.M. Feret, "Gas Cooled Fuel Cell Systems Technology Development," Final Report, NASA CR-175047, prepared by Westinghouse Electric Corp. under Contract No. DEN 3-290 for NASA Lewis Research Center, August 1985.
37. V. Jalan, J. Poirier, M. Desai, B. Morrisean, "Development of CO and H_2S Tolerant PAFC Anode Catalysts," in *Proceedings of the Second Annual Fuel Cell Contractors Review Meeting*, 1990.
38. P.W.T. Lu and L. L. France, in *Proceedings of the Symposium on Transport Processes in Electrochemical Systems,* R. S. Yeo, K. Katan and D. T. Chin, The Electrochemical Society, Inc., Pennington, NJ, p. 77, 1982.
39. P.N. Ross, "Anomalous Current Ratios in Phosphoric Acid Fuel Cell Cathodes," LBL-13955; submitted to *J. Electrochem. Soc.*, March 1986.
40. P.Ross, P. Stonehart, *Electrochim. Acta,* 21**,** 441, 1976.
41. W. Vogel, J. Lundquist, P. Ross, P. Stonehart, *Electrochim. Acta,* 20**,** 79, 1975.
42. H.R. Kunz, in *Proceedings of the Symposium on Electrode Materials and Processes for Energy Conversion and Storage,* Edited by J. D. E. McIntyre, S. Srinivasan and F. G. Will, The Electrochemical Society, Inc., Pennington, NJ, p. 607, 1977.
43. D.T. Chin, P.D. Howard, *J. Electrochem. Soc.,* 133, 2447, 1986.
44. S.T. Szymanski, G.A. Gruver, M. Katz, H.R. Kunz, *J. Electrochem. Soc.,* 127, 1440, 1980.
45. F.S. Kemp, IFC, "Status of Development of Water - Cooled Phosphoric Acid Fuel Cells," in *Proceedings of the Second Annual Fuel Cell Contractors Review Meeting*, U.S. DOE/METC, 1990.
46. N. Giordano, "Fuel Cells Activity at CNR, TAE Institute," CNR/TAE, Italy, 1992.
47. "Gas Cooled Fuel Cell Systems Technology Development," Westinghouse/DOE, WAES-TR-92-001, March 1992.
48. K. Harasawa, I. Kanno, I. Masuda, "Fuel Cell R&D and Demonstration Programs at Electric Utilities in Japan," in *Fuel Cell Seminar Abstracts*, Tucson, AZ, November 29-December 2, 1992.

6. MOLTEN CARBONATE FUEL CELL

The molten carbonate fuel cell operates at approximately 650 °C (1200 °F). The high operating temperature is needed to achieve sufficient conductivity of the carbonate electrolyte, yet allow the use of low-cost metal cell components. A benefit associated with this high temperature is that noble metal catalysts are not required for the cell electrochemical oxidation and reduction processes. Molten carbonate fuel cells are being developed for natural gas and coal-based power plants for industrial, electrical utility, and military applications[19]. Currently, one industrial corporation is actively pursuing the commercialization of MCFCs in the U.S.: FuelCell Energy (FCE). Europe and Japan each have at least one developer pursuing the technology: MTU Friedrichshafen, Ansaldo (Italy), and Ishikawajima-Harima Heavy Industries (Japan).

Figure 6-1 depicts the operating configuration of the molten carbonate fuel cell. The half cell electrochemical reactions are

$$H_2 + CO_3^{=} \rightarrow H_2O + CO_2 + 2e^- \qquad (6\text{-}1)$$

at the anode, and

$$\tfrac{1}{2}O_2 + CO_2 + 2e^- \rightarrow CO_3^{=} \qquad (6\text{-}2)$$

at the cathode. The overall cell reaction[20] is

$$H_2 + \tfrac{1}{2}O_2 + CO_2\ (\text{cathode}) \rightarrow H_2O + CO_2\ (\text{anode}) \qquad (6\text{-}3)$$

[19]. MCFCs operate more efficiently with CO_2 containing bio-fuel derived gases. Performance loss on the anode due to fuel dilution is compensated by cathode side performance enhancement resulting from CO_2 enrichment.

[20]. CO is not directly used by electrochemical oxidation, but produces additional H_2 when combined with water in the water gas shift reaction.

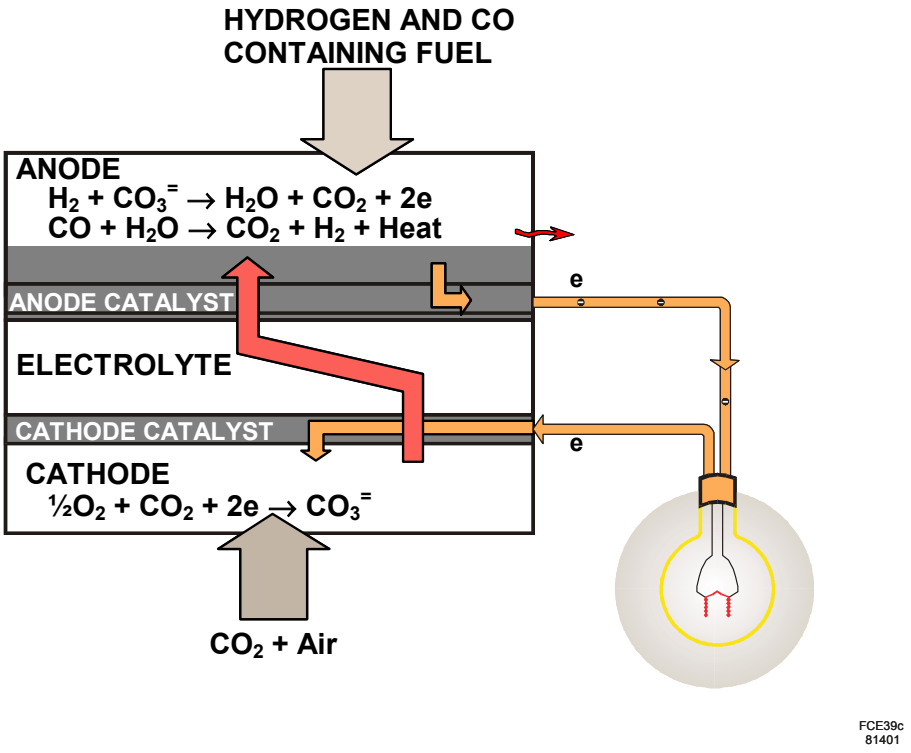

Figure 6-1 Principles of Operation of Molten Carbonate Fuel Cells (FuelCell Energy)

Besides the reaction involving H_2 and O_2 to produce H_2O, Equation 6-3 shows a transfer of CO_2 from the cathode gas stream to the anode gas stream via the $CO_3^{=}$ ion, with 1 mole CO_2 transferred along with two Faradays of charge, or 2 gram moles of electrons. The reversible potential for an MCFC, taking into account the transfer of CO_2, is given by the equation

$$E = E^{\circ} + \frac{RT}{2F} \ln \frac{P_{H_2} P_{O_2}^{1/2}}{P_{H_2O}} + \frac{RT}{2F} \ln \frac{P_{CO_{2c}}}{P_{CO_{2a}}} \qquad (6\text{-}4)$$

where the subscripts a and c refer to the anode and cathode gas compartments, respectively. When the partial pressures of CO_2 are identical at the anode and cathode, and the electrolyte is invariant, the cell potential depends only on the partial pressures of H_2, O_2, and H_2O. Typically, the CO_2 partial pressures are different in the two electrode compartments and the cell potential is affected accordingly.

The need for CO_2 at the cathode requires some schemes that will either 1) transfer the CO_2 from the anode exit gas to the cathode inlet gas ("CO_2 transfer device"), 2) produce CO_2 by combusting the anode exhaust gas, which is mixed directly with the cathode inlet gas, or 3) supply CO_2 from an

alternate source. It is usual practice in an MCFC system that the CO_2 generated at the anode (right side of Equation 6-1) be routed (external to the cell) to the cathode (left side of Equation 6-2).

MCFCs differ in many respects from PAFCs because of their higher operating temperature (650 vs. 200 °C) and the nature of the electrolyte. The higher operating temperature of MCFCs provides the opportunity to achieve higher overall system efficiencies (potential for heat rates below 7,500 Btu/kWh) and greater flexibility in the use of available fuels.[21] On the other hand, the higher operating temperature places severe demands on the corrosion stability and life of cell components, particularly in the aggressive environment of the molten carbonate electrolyte. Another difference between PAFCs and MCFCs lies in the method used for electrolyte management in the respective cells. In a PAFC, PTFE serves as a binder and wet-proofing agent to maintain the integrity of the electrode structure and to establish a stable electrolyte/gas interface in the porous electrode. The phosphoric acid is retained in a matrix of PTFE and SiC between the anode and cathode. There are no high temperature, wetproofing materials available for use in MCFCs that are comparable to PTFE. Thus, a different approach is required to establish a stable electrolyte/gas interface in MCFC porous electrodes, and this is illustrated schematically in Figure 6-2. The MCFC relies on a balance in capillary pressures to establish the electrolyte interfacial boundaries in the porous electrodes (1, 2, 3). At thermodynamic equilibrium, the diameters of the largest flooded pores in the porous components are related by the equation

$$\frac{\gamma_c \cos\theta_c}{D_c} = \frac{\gamma_e \cos\theta_e}{D_e} = \frac{\gamma_a \cos\theta_a}{D_a} \qquad (6\text{-}5)$$

where γ is the interfacial surface tension, θ is the contact angle of the electrolyte, D is the pore diameter, and the subscripts a, c, and e refer to the anode, cathode and electrolyte matrix, respectively. By properly coordinating the pore diameters in the electrodes with those of the electrolyte matrix, which contains the smallest pores, the electrolyte distribution depicted in Figure 6-2 is established. This arrangement permits the electrolyte matrix to remain completely filled with molten carbonate, while the porous electrodes are partially filled, depending on their pore size distributions. According to the model illustrated in Figure 6-2 and described by Equation (6-5), the electrolyte content in each of the porous components will be determined by the equilibrium pore size (<D>) in that component; pores smaller than <D> will be filled with electrolyte, and pores larger than <D> will remain empty. A reasonable estimate of the volume distribution of electrolyte in the various cell components is obtained from the measured pore-volume-distribution curves and the above relationship for D (1, 2).

Electrolyte management, that is, control over the optimum distribution of molten carbonate electrolyte in the different cell components, is critical for achieving high performance and endurance with MCFCs. Various processes (i.e., consumption by corrosion reactions, potential-driven migration, creepage of salt and salt vaporization) occur, all of which contribute to the redistribution of molten carbonate in MCFCs; these aspects are discussed by Maru, et al. (4) and Kunz (5).

---

[21]. *In situ* reforming of fuels in MCFCs is possible as discussed later in the section.

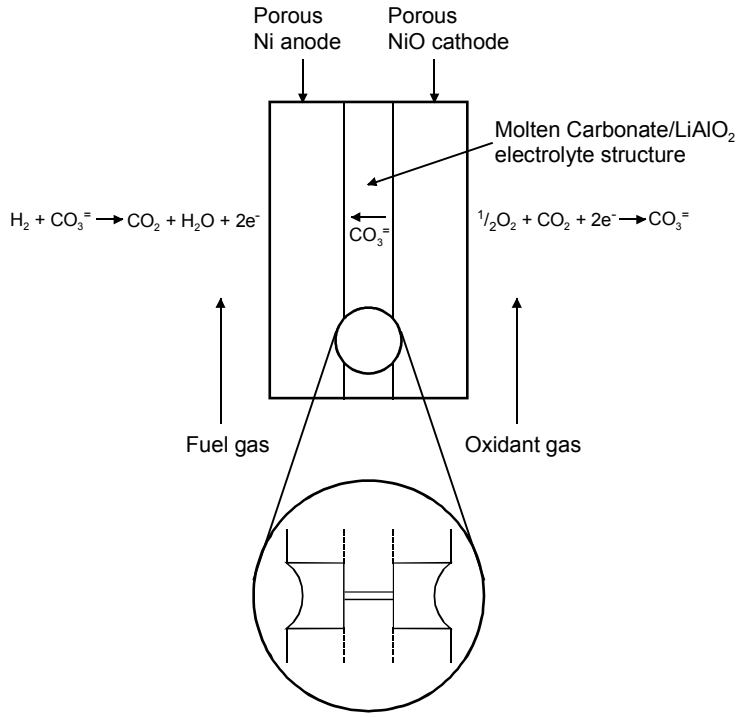

Figure 6-2 Dynamic Equilibrium in Porous MCFC Cell Elements
(Porous electrodes are depicted with pores covered by a thin film of electrolyte)

6.1 Cell Components

6.1.1 State-of-the-Art Componments

The data in Table 6-1 provide a chronology of the evolution in MCFC component technology. In the mid-1960s, electrode materials were, in many cases, precious metals, but the technology soon evolved to use Ni-based alloys at the anode and oxides at the cathode. Since the mid-1970s, the materials for the electrodes and electrolyte (molten carbonate/$LiAlO_2$) have remained essentially unchanged. A major development in the 1980s was the evolution in fabrication of electrolyte structures. Developments in cell components for MCFCs have been reviewed by Maru, et al. (6, 7), Petri and Benjamin (8), and Selman (9). Over the past 28 years, the performance of single cells has improved from about 10 mW/cm^2 to >150 mW/cm^2. During the 1980s, both the performance and endurance of MCFC stacks dramatically improved. The data in Figure 6-3 illustrate the progress that has been made in the performance of single cells, and in the cell voltage of small stacks at 650 °C. Several MCFC stack developers have produced cell stacks with cell areas up to 1 m^2. Tall, full-scale U.S. stacks fabricated to date include several FCE-300 plus cell stacks with ~9000 cm^2 cell area producing >250 kW.

Table 6-1 Evolution of Cell Component Technology for Molten Carbonate Fuel Cells

Component	Ca. 1965	Ca. 1975	Current Status
Anode	• Pt, Pd, or Ni	• Ni-10 Cr	• Ni-Cr/Ni-Al/Ni-Al-Cr • 3-6 μm pore size • 45 to 70 percent initial porosity • 0.20 to .5 mm thickness • 0.1 to1 m^2/g
Cathode	• Ag_2O or lithiated NiO	• lithiated NiO	• lithiated NiO-MgO • 7 to15 μm pore size • 70 to 80 percent initial porosity • 60 to 65 percent after lithiation and oxidation • 0.5 to 1 mm thickness • 0.5 m^2/g
Electrolyte Support	• MgO	• mixture of α-, β-, and γ-$LiAlO_2$ • 10 to 20 m^2/g • 1.8 mm thickness	• γ-$LiAlO_2$, α-$LiAlO_2$ • 0.1 to12 m^2/g • 0.5 to1 mm thickness
Electrolyte[a] (wt percent)	• 52 Li-48 Na • 43.5 Li-31.5 Na-25 K • "paste"	• 62 Li-38 K • hot press "tile" • 1.8 mm thickness	• 62 Li-38 K • 60 Li-40 Na 51 Li-48 Na • tape cast • 0.5 to1 mm thickness

a - Mole percent of alkali carbonate salt

Specifications for the anode and cathode were obtained from References (6), (10), and (11).

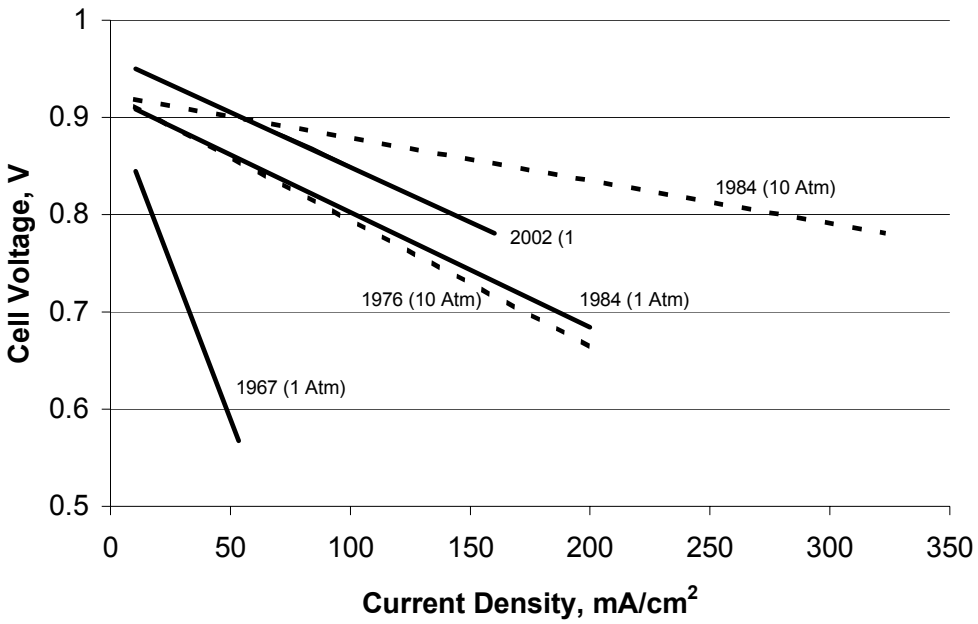

Figure 6-3 Progress in the Generic Performance of MCFCs on Reformate Gas and Air (12, 13)

The conventional process to fabricate electrolyte structures until about 1980 involved hot pressing (about 5,000 psi) mixtures of $LiAlO_2$ and alkali carbonates (typically >50 vol percent in liquid state) at temperatures slightly below the melting point of the carbonate salts (e.g., 490°C for electrolyte containing 62 mol Li_2CO_3-38 mol K_2CO_3). These electrolyte structures (also called "electrolyte tiles") were relatively thick (1 to 2 mm) and difficult to produce in large sizes[22] because large tooling and presses were required. The electrolyte structures produced by hot pressing are often characterized by 1) void spaces (<5 porosity), 2) poor uniformity of microstructure, 3) generally poor mechanical strength, and 4) high iR drop. To overcome these shortcomings of hot pressed electrolyte structures, alternative processes such as tape casting (7) and electrophoretic deposition (14) for fabricating thin electrolyte structures were developed. The greatest success to date with an alternative process has been reported with tape casting, which is a common processing technique used by the ceramics industry. This process involves dispersing the ceramic powder in a solvent[23] that contains dissolved binders (usually an organic compound), plasticizers, and additives to yield the proper slip rheology. The slip is cast over a moving smooth substrate, and the desired thickness is established with a doctor blade device. After drying the slip, the "green" structure is assembled into the fuel cell where the organic binder is removed by thermal decomposition, and the absorption of alkali carbonate into the ceramic structure occurs during cell startup.

[22]. The largest electrolyte tile produced by hot pressing was about 1.5 m^2 in area (7).
[23]. An organic solvent is used because $LiAlO_2$ in the slip reacts with H_2O.

The tape casting and electrophoretic deposition processes are amenable to scale-up, and thin electrolyte structures (0.25-0.5 mm) can be produced. The ohmic resistance of an electrolyte structure[24] and the resulting ohmic polarization have a large influence on the operating voltage of MCFCs (15). FCE has stated that the electrolyte matrix encompasses 70 of the ohmic loss (16) of the cell. At a current density of 160 mA/cm^2, the voltage drop (ΔV_{ohm}) of an 0.18 cm thick electrolyte structure, with a specific conductivity of ~0.3/ohm-cm at 650 °C, was found to obey the relationship (14),

$$\Delta V_{ohm}\,(V) = 0.5t \qquad (6\text{-}6)$$

where ΔV_{ohm} is in volts and t is the thickness in cm. Later data confirm this result (16). With this equation, it is apparent that a fuel cell with an electrolyte structure of 0.25 cm thickness would operate at a cell voltage that is 35 mV higher than that of an identical cell with an electrolyte structure of 0.18 cm thickness because of the lower ohmic loss. Thus, there is a strong incentive for making thinner electrolyte structures to improve cell performance.

The electrolyte composition affects the performance and endurance of MCFCs in several ways. Higher ionic conductivities, and hence lower ohmic polarization, are achieved with Li-rich electrolytes because of the relative high ionic conductivity of Li_2CO_3 compared to that of Na_2CO_3 and K_2CO_3. However, gas solubility and diffusivity are lower, and corrosion is more rapid in Li_2CO_3.

The major considerations with Ni-based anodes and NiO cathodes are structural stability and NiO dissolution, respectively (9). Sintering and mechanical deformation of the porous Ni-based anode under compressive load lead to performance decay by redistribution of electrolyte in a MCFC stack. The dissolution of NiO in molten carbonate electrolyte became evident when thin electrolyte structures were used. Despite the low solubility of NiO in carbonate electrolytes (~10 ppm), Ni ions diffuse in the electrolyte towards the anode, and metallic Ni can precipitate in regions where a H_2 reducing environment is encountered. The precipitation of Ni provides a sink for Ni ions, and thus promotes the diffusion of dissolved Ni from the cathode. This phenomenon becomes worse at high CO_2 partial pressures (17, 18) because dissolution may involve the following mechanism:

$$NiO + CO_2 \rightarrow Ni^{2+} + CO^{=}_3 \qquad (6\text{-}7)$$

The dissolution of NiO has been correlated to the acid/base properties of the molten carbonate. The basicity of the molten carbonate is defined as equal to -log (activity of $O^{=}$) or -log a_{M_2O}, where a is the activity of the alkali metal oxide M_2O. Based on this definition, acidic oxides are associated with carbonates (e.g., K_2CO_3) that do not dissociate to M_2O, and basic oxides are formed with highly dissociated carbonate salts (e.g., Li_2CO_3). The solubility of NiO in binary

[24]. Electrolyte structures containing 45 wt% $LiAlO_2$ and 55 wt% molten carbonate (62 mol% Li_2CO_3-38 mol% K_2CO_3) have a specific conductivity at 650°C of about 1/3 that of the pure carbonate phase (15).

carbonate melts shows a clear dependence on the acidity/basicity of the melt (19, 20). In relatively acidic melts, NiO dissolution can be expressed by

$$NiO \rightarrow Ni^{2+} + O^{=} \qquad (6\text{-}8)$$

In basic melts, NiO reacts with $O^{=}$ to produce one of two forms of nickelate ions:

$$NiO + O^{=} \rightarrow NiO_2^{=} \qquad (6\text{-}9)$$

$$2NiO + O^{=} + \tfrac{1}{2}O_2 \rightarrow 2NiO_2^{-} \qquad (6\text{-}10)$$

A distinct minimum in NiO solubility is observed in plots of log (NiO solubility) versus basicity (-log a_{M_2O}), which can be demarcated into two branches corresponding to acidic and basic dissolution. Acidic dissolution is represented by a straight line with a slope of +1, and a NiO solubility that decreases with an increase in a_{M_2O}. Basic dissolution is represented by a straight line with a slope of either -1 or -½, corresponding to Equations (6-9) and (6-10), respectively. The CO_2 partial pressure is an important parameter in the dissolution of NiO in carbonate melts because the basicity is directly proportional to log P_{CO_2}. An MCFC usually operates with a molten carbonate electrolyte that is acidic.

Based on a 12,000-hour full-size stack tests as well as post-test results, FCE believes that Ni dissolution and subsequent precipitation will not be an issue for the desired 40,000-hour (5-yr) life (21) at atmospheric pressure. But at 10 atm cell pressure, only about 5,000 to 10,000 hours may be possible with currently available NiO cathodes (22). The solubility of NiO in molten carbonates is complicated by its dependence on several parameters: carbonate composition, H_2O partial pressure, CO_2 partial pressure, and temperature. For example, measurements of NiO dissolution by Kaun (23) indicate that solubility is affected by changing the electrolyte composition; a lower solubility is obtained in a Li_2CO_3-K_2CO_3 electrolyte that contains less Li_2CO_3 (i.e., lower solubility in 38 mol Li_2CO_3-62 mol K_2CO_3 than in 62 mol Li_2CO_3-38 mol K_2CO_3 at 650 °C). However, the solubility of Ni increases in the electrolyte with 38 mol Li_2CO_3 when the temperature decreases, whereas the opposite trend is observed in the electrolyte with 62 mol Li_2CO_3. Another study reported by Appleby (24) indicates that the solubility of Ni decreases from 9 to 2 ppm by increasing the Li concentration in Li_2CO_3-K_3CO_3 from 62 to 75 wt percent, and a lower solubility is obtained in 60 mol percent Li_2CO_3-40 mol percent Na_2CO_3 at 650 °C. The compaction of cathodes became evident in MCFC stacks once the anode creep was eliminated when strengthened by oxide dispersion [i.e., oxide dispersion strengthened (ODS) anode].

The bipolar plates used in MCFC stacks are usually fabricated from thin (~15 mil) sheets of an alloy (e.g., Incoloy 825, 310S or 316L stainless steel) that are coated on one side (i.e., the side

exposed to fuel gases in the anode compartment) with a Ni layer. The Ni layer is stable in the reducing gas environment of the anode compartment, and it provides a conductive surface coating with low contact resistance. Pigeaud, et al. describe approaches to circumvent the problems associated with gas leaks and corrosion of bipolar plates (25). Corrosion is largely overcome by applying a coating (about 50 μm thickness) at the vulnerable locations on the bipolar plate. For example, the wet-seal[25] area on the anode side is subject to a high chemical potential gradient because of the fuel gas inside the cell and the ambient environment (usually air) on the outside of the cell, which promotes corrosion (about two orders of magnitude greater than in the cathode wet-seal area (26)). Donado, et al. present a general discussion on corrosion in the wet-seal area of MCFCs (27). A thin aluminum coating in the wet-seal area of a bipolar plate provides corrosion protection by forming a protective layer of $LiAlO_2$ after reaction of Al with Li_2CO_3 (28). Such a protective layer would not be useful in areas of the bipolar plate that must permit electronic conduction because $LiAlO_2$ is an insulating material.

A dense and electronically insulating layer of $LiAlO_2$ is not suitable for providing corrosion resistance to the cell current collectors because these components must remain electrically conductive. The typical materials used for this application are 316 stainless steel and Ni plated stainless steels. However, materials with better corrosion resistance are required for long-term operation of MCFCs. Research is continuing to understand the corrosion processes of high-temperature alloys in molten carbonate salts under both fuel gas and oxidizing gas environments (29, 28) and to identify improved alloys (30) for MCFCs. Stainless steels such as Type 310 and 446 have demonstrated better corrosion resistance than Type 316 in corrosion tests (30).

6.1.2 Development Components

MCFC components are limited by several technical considerations (31), particularly those described in Section 6.1.1. Even though present approaches function properly in full size cells at atmospheric pressure, research is addressing alternate cathode materials and electrolytes, performance improvement, life extension beyond the commercialization goal of five years, and cost reduction (32). The studies described in recent literature provide updated information on promising development of the electrodes, the electrolyte matrix, and the capability of the cell to tolerate trace contaminants in the fuel supply. Descriptions of some of this work follow.

Anode: As stated in Section 6.1.1 and Reference (33), state-of-the-art anodes are made of a Ni-Cr/Ni-Al alloy. The Cr was added to eliminate the problem of anode sintering. However, Ni-Cr anodes are susceptible to creep when placed under the torque load required in the stack to minimize contact resistance between components. The Cr in the anode is also lithiated by the electrolyte; then it consumes carbonate. Developers are trying lesser amounts of Cr (8 percent) to reduce the loss of electrolyte, but some have found that reducing the Cr by 2 percentage points increased creep (34). Several developers have tested Ni-Al alloy anodes that provide creep resistance with minimum electrolyte loss (34, 35, 36). The low creep rate with this alloy is attributed to the formation of $LiAlO_2$ dispersed in Ni (35).

---

[25]. The area of contact between the outer edge of the bipolar plate and the electrolyte structure prevents gas from leaking out of the anode and cathode compartments. The gas seal is formed by compressing the contact area between the electrolyte structure and the bipolar plate so that the liquid film of molten carbonate at operating temperature does not allow gas to permeate through.

Even though alloys of chromium or aluminum strengthened nickel provides a stable, non-sintering, creep-resistant anode, electrodes made with Ni are relatively high in cost. Alloys, such as Cu-Al and $LiFeO_2$, have not demonstrated sufficient creep strength or performance. Because of this, present research is focused on reducing the manufacturing cost of the nickel alloy anodes (37).

There is a need for better sulfur tolerance in MCFCs, especially when considering coal operation. The potential benefit for sulfur tolerant cells is to eliminate cleanup equipment that impacts system efficiency. This is especially true if low temperature cleanup is required, because the system efficiency and capital cost suffer when the fuel gas temperature is first reduced, then increased to the cell temperature level. Tests are being conducted on ceramic anodes to alleviate the problems, including sulfur poisoning, being experienced with anodes (31). Anodes are being tested with undoped $LiFeO_2$ and $LiFeO_2$ doped with Mn and Nb. Preliminary testing, where several parameters were not strictly controlled, showed that the alternative electrodes exhibited poor performance and would not operate over 80 mA/cm^2. At the present time, no alternative anodes have been identified. Instead, future work will focus on tests to better understand material behavior and to develop alternative materials with emphasis on sulfur tolerance.

Cathode*:* An acceptable material for cathodes must have adequate electrical conductivity, structural strength, and low dissolution rate in molten alkali carbonates to avoid precipitation of metal in the electrolyte structure. State-of-the art cathodes are made of lithiated NiO (33, 38) that have acceptable conductivity and structural strength. However, in early testing, a predecessor of UTC Fuel Cells found that the nickel dissolved, then precipitated and reformed as dendrites across the electrolyte matrix. This decreased performance and eventual short-circuting of the cell. Dissolution of the cathode has turned out to be the primary life-limiting constraint of MCFCs, particularly in pressurized operation (35). Developers are investigating approaches to resolve the NiO dissolution issue. For atmospheric cells, developers are looking at increasing the basicity of the electrolyte (using a more basic melt such as $Li/NaCO_3$). Another approach is to lower CO_2 (acidic) partial pressure. To operate at higher pressures (higher CO_2 partial pressure), developers are investigating alternative materials for the cathodes and using additives in the electrolyte to increase its basicity (37).

Initial work on $LiFeO_2$ cathodes showed that electrodes made with this material were very stable chemically under the cathode environment; there was essentially no dissolution (31). However, these electrodes perform poorly compared to the state-of-the-art NiO cathode at atmospheric pressure because of slow kinetics. The electrode shows promise at pressurized operation, so it is still being investigated. Higher performance improvements are expected with Co-doped $LiFeO_2$. It also has been shown that 5 mol lithium-doped NiO with a thickness of 0.02 cm provided a 43 mV overpotential (higher performance) at 160 mA/cm^2 compared to the state-of-the-art NiO cathode. It is assumed that reconfiguring the structure, such as decreasing the agglomerate size, could improve performance.

Another idea for resolving the cathode dissolution problem is to formulate a milder cell environment. This leads to the approach of using additives in the electrolyte to increase its basicity. Small amounts of additives provide similar voltages to those without additives, but larger amounts adversely affect performance (39). Table 6-2 quantifies the limiting amounts of additives.

Table 6-2 Amount in Mol percent of Additives to Provide Optimum Performance (39)

	62 MOL percent Li_2CO_3/K_2CO_2	52 MOL percent Li_2CO_3/NA_2CO_3
$CaCO_3$	0 to 15	0 to 5
$SrCO_3$	0 to 5	0 to 5
$BaCO_3$	0 to 10	0 to 5

Another approach to a milder cell environment is to increase the fraction of Li in the baseline electrolyte or change the electrolyte to Li/Na rather than the baseline 62/38 Li/K melt (29, 39, 40). Within the past 10 years, a lower cost stabilized cathode was developed with a base material cost comparable to the unstabilized cathode (41). A 100 cm^2 cell test of the lower-cost stabilized cathode with a Li/Na electrolyte system completed 10,000 hours of operation.

Electrolyte Matrix: The present electrolyte structure materials are tightly packed, fine α- or γ-$LiAlO_2$ with fiber or particulate reinforcement. Long-term cell testing reveals significant particle growth and γ to α phase transformation, leading to detrimental changes in the pore structure. The particles grow faster at higher temperatures, in low CO_2 gas atmospheres, and in strongly basic melts. The γ phase is stable at > 700 °C, whereas the α phase is stable at 600 to 650 °C. Such particle growth and phase transformations can be explained by a dissolution - precipitation mechanism. The matrix must also be strong enough to counter operating mechanical and thermal stresses, and still maintain the gas seal. Thermal cycling below the carbonate freezing temperature can induce cracking due to thermo-mechanical stress. Ceramic fiber reinforcement is most effective for crack deflection, followed by platelet and sphere forms. However, strong, cost effective, and stable ceramic fibers are not yet commercially available. Long-term, intense material research may be needed to develop such ceramic fibers. If particle sizes are markedly different, the phase transformation is more controlled by the particle sizes, according to Ostwald ripening where small particles preferentially dissolve and re-precipitate onto larger particles. Therefore, a more uniform particle size distribution is needed to maintain a desired pore structure. The industry trend is to switch from γ-$LiAlO_2$ to α-$LiAlO_2$ for better long-term phase and particle-size stabilities. FCE is developing a low-cost $LiAlO_2$, aqueous-base manufacturing system, but must resolve slow drying rate of $LiAlO_2$ and its instability in water (42).

Electrolyte: Present electrolytes have the following chemistry: lithium potassium carbonate, Li_2CO_3/K_2CO_3 (62:38 mol percent) for atmospheric pressure operation and lithium sodium carbonate, $LiCO_3/NaCO_3$ (52:48 o 60:40 mol percent) that is better for improved cathode stability under pressurized operation and life extension. The electrolyte composition affects electrochemical activity, corrosion, and electrolyte loss rate. Evaporation of the electrolyte is a life-limiting issue for the molten carbonate fuel cell. Li/Na electrolyte is better for higher-pressure operation than Li/K because it gives higher performance. This allows the electrolyte matrix to be made thicker for the same performance relative to the Li/K electrolyte. Thicker electrolytes result in a longer time to shorting by internal precipitation. Li/Na also provides

better corrosion resistance to mitigate acidic cathode dissolution. However, it has lower wettability and greater temperature sensitivity. Additives are being investigated to minimize the temperature sensitivity of Li/Na. The electrolyte has a low vapor pressure at operating temperature, and may slowly evaporate. Stack testing has shown that the electrolyte vapor loss is significantly slower than expected. The evaporation loss is projected to have minimal impact on stack life.

***Electrolyte Structure**:* Ohmic losses contribute about a 65 mV loss at the beginning of life, and may increase to as much as 145 mV by 40,000 hours (16). The majority of the voltage loss is in the electrolyte and the cathode components. The electrolyte offers the highest potential for reduction because 70 percent of the total cell ohmic loss occurs there. FCE investigated increasing the porosity of the electrolyte 5 percent to reduce the matrix resistance by 15 percent, and change the melt to Li/Na from Li/K to reduce the matrix resistivity by 40 percent. Work is continuing on the interaction of the electrolyte with the cathode components. At the present time, an electrolyte loss of 25 percent of the initial inventory can be projected with a low surface area cathode current collector and with the proper selection of material.

Another area for electrolyte improvement is the ability to prevent gas crossover from one electrode to the other. FCE produced an improved matrix fabrication process providing low temperature binder burnout. FCE reported in 1997 that it had developed a high performance rugged matrix that increases the gas sealing efficiency by approximately a factor of ten better than the design goal (43).

***Electrolyte Migration**:* There is a tendency for the electrolyte to migrate from the positive end of the stack to the negative end of the stack. This may cause the end cells to lose performance compared to the central cells. The electrolyte loss is through the gasket used to couple the external manifolds to the cell stack. The standard gasket material is porous and provides a conduit for electrolyte transfer. A new gasket design incorporating electrolyte flow barriers inside the gasket (US Patent 5,110,692) plus end cell inventory capability offers the potential for reaching 40,000 hours, if only this mode of failure is considered. Stacks with internal manifolding do not require a gasket, and may not experience this problem (44).

Bipolar Plate: The present bipolar plate consists of a separator, current collectors, and the wet seal. The separator and current collector is Ni-coated 310S/316L and the wet seal is formed by aluminization of the metal. The plate is exposed to the anode environment of one side and the cathode environment on the other. Low oxygen partial pressure on the anode side of the bipolar plate prevents the formation of a protective oxide coating. After reaction with the thin, creeping electrolyte, heat-resistant alloys form a multi-layered corrosion scale. This condition may be accelerated by carbonization, higher temperature, and higher moisture gas environment. On the cathode side, contact electrical resistance increases as an oxide scale builds up. Electrolyte loss due to corrosion and electrolyte creep also contributes to power decay. Single alloy bipolar current collector materials that function well in both anode and cathode environments need to be developed. Although such development has been attempted, high cost and high ohmic resistance prevent it from being successful. Presently, stainless steels, particularly austenitic stainless steels, are the primary construction materials. More expensive nickel-based alloys resist corrosion as well as or only slightly better than austenitic stainless steels. A thermodynamically

stable nickel coating is needed to protect the anode side. Unfortunately, electroless nickel coatings, although dense or uniform in thickness, are expensive and contain detrimental impurities; electrolytic nickel coatings are not sufficiently dense or uniform in thickness. FCE and others have found that cladding with nickel provides excellent corrosion protection. A nickel cladding of 50 μm thickness is projected for >40,000 hours of life (42).

***Coal Gas Trace Species**:* MCFCs to date have been operated on reformed or simulated natural gas and simulated coal gas. Testing conducted with simulated coal gas has involved the expected individual and multi-trace constituents to better understand coal operation (45).

Table 6-3 shows the contaminants and their impact on MCFC operation. The table denotes the species of concern and what cleanup of the fuel gas is required to operate on coal gas. Confidence in operation with coal will require the use of an actual gasifier product. An FCE MCFC stack was installed (fall of 1993) using a slipstream of an actual coal gasifier to further clarify the issues of operation with trace gases (46).

Table 6-3 Qualitative Tolerance Levels for Individual Contaminants in Isothermal Bench-Scale Carbonate Fuel Cells (46, 47, and 48)

CONTAMINANTS (typical ppm in raw coal gas)	REACTION MECHANISM	QUALITATIVE TOLERANCES	CONCLUSIONS
NO NOTICEABLE EFFECTS			
NH_3 (10,000) Cd (5) Hg (1) Sn (3)	$2NH_3 \rightarrow N_2+3H_2$ $Cd+H_2O \rightarrow CdO(s)+H_2$ (Hg Vapor Not Reactive) (Sn(l) Not Volatile)	~1 vol percent NH_3 ~30 ppm Cd 35 ppm Hg No Vapor @ 650°C	No Effects No Cell Deposits No TGA Effects No Cell Deposits
MINOR EFFECTS			
Zn (100) Pb (15)	$Zn+H_2O \rightarrow ZnO(s)+H_2$ $Pb+H_2O \rightarrow PbS(s)+H_2$	<15 ppm Zn 1.0 ppm Pb sat'd vapor	No Cell Deposits at 75 percent Utilization Cell Deposits Possible in Presence of High H_2Se
SIGNIFICANT EFFECTS			
H_2S (15,000) HCl (500) H_2Se (5) As (10)	$xH_2S+Ni \rightarrow NiS_x+xH_2$ $2HCl+K_2CO_3 \rightarrow 2KCl(v)+H_2O/CO_2$ $xH_2Se+Ni \rightarrow NiSe_x+xH_2$ $AsH_3+Ni \rightarrow NiAs(s)+3/2H_2$	<0.5 ppm H_2S <0.1 ppm HCl <0.2 ppm H_2Se <0.1 ppm As	Recoverable Effect Long Term Effects Possible Recoverable Effect Cumulative Long Term Effect

6.2 Performance

Factors affecting the selection of operating conditions are stack size, heat transfer rate, voltage level, load requirement, and cost. The performance curve is defined by cell pressure, temperature, gas composition, and utilization. Typical MCFCs will generally operate in the range of 100 to 200 mA/cm^2 at 750 to 900 mV/cell.

Typical cathode performance curves obtained at 650 °C with an oxidant composition (12.6 percent O_2/18.4 percent CO_2/69 percent N_2) that is anticipated for use in MCFCs, and a common baseline composition (33 percent O_2/67 percent CO_2) are presented in Figure 6-4 (22, 49). The baseline

composition contains O_2 and CO_2 in the stoichiometric ratio that is needed in the electrochemical reaction at the cathode (Equation (6-2)). With this gas composition, little or no diffusion limitations occur in the cathode because the reactants are provided primarily by bulk flow. The other gas composition, which contains a substantial fraction of N_2, yields a cathode performance that is limited dilution by an inert gas.

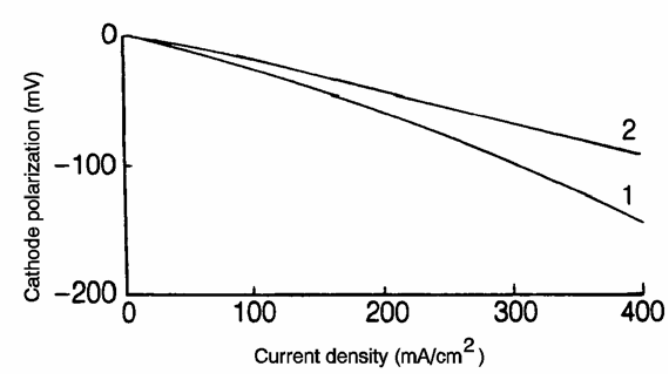

Figure 6-4 Effect of Oxidant Gas Composition on MCFC Cathode Performance at 650°C, (Curve 1, 12.6 percent O_2/18.4 percent CO_2/69.0 percent N_2; Curve 2, 33 percent O_2/67 percent CO_2)

In the 1980s, the performance of MCFC stacks increased dramatically. During the 1990s, cells as large as 1.0 m^2 are being tested in stacks. Most recently, the focus has been on achieving performance in a stack equivalent to single cell performance. Cells with an electrode area of 0.3 m^2 were routinely tested at ambient and above ambient pressures with improved electrolyte structures made by tape-casting processes (22). Several stacks underwent endurance testing in the range of 7,000 to 10,000 hours. The voltage and power as a function of current density after 960 hours for a 1.0 m^2 stack consisting of 19 cells are shown in Figure 6-5. The data were obtained with the cell stack at 650 °C and 1 atmosphere.

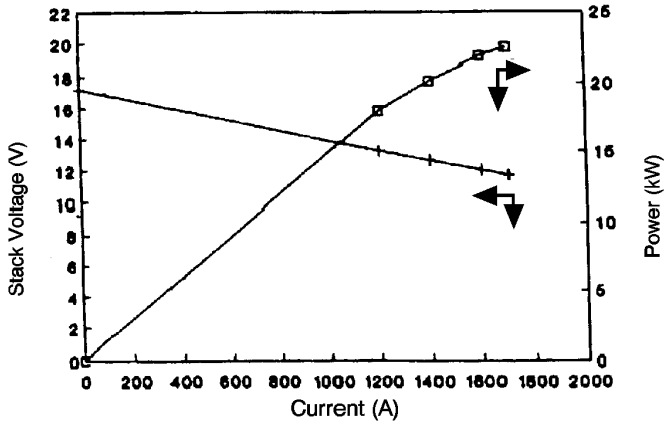

Figure 6-5 Voltage and Power Output of a 1.0/m^2 19 cell MCFC Stack after 960 Hours at 965 °C and 1 atm, Fuel Utilization, 75 percent (50)

The remainder of this section will review operating parameters that affect MCFC performance. Supporting data will be presented, as well as equations derived from empirical analysis.

6.2.1 Effect of Pressure

The dependence of reversible cell potential on pressure is evident from the Nernst equation. For a change in pressure from P_1 to P_2, the change in reversible potential (ΔV_p) is given by

$$\Delta V_p = \frac{RT}{2F} \ln \frac{P_{1,a}}{P_{2,a}} + \frac{RT}{2F} \ln \frac{P_{2,c}^{3/2}}{P_{1,c}^{3/2}} \qquad (6\text{-}11)$$

where the subscripts a and c refer to the anode and cathode, respectively. In an MCFC with the anode and cathode compartments at the same pressure (i.e., $P_1=P_{1,a}=P_{1,c}$ and $P_2=P_{2,a}=P_{2,c}$):

$$\Delta V_p = \frac{RT}{2F} \ln \frac{P_1}{P_2} + \frac{RT}{2F} \ln \frac{P_2^{3/2}}{P_1^{3/2}} = \frac{RT}{4F} \ln \frac{P_2}{P_1} \qquad (6\text{-}12)$$

At 650 °C

$$\Delta V_p \text{ (mV)} = 20 \ln \frac{P_2}{P_1} = \left(46 \log \frac{P_2}{P_1}\right) \qquad (6\text{-}13)$$

Thus, a tenfold increase in cell pressure corresponds to an increase of 46 mV in the reversible cell potential at 650 °C.

Increasing the operating pressure of MCFCs results in enhanced cell voltages because of the increase in the partial pressure of the reactants, increase in gas solubilities, and increase in mass transport rates. Opposing the benefits of increased pressure are the effects of pressure on undesirable side reactions such as carbon deposition (Boudouard reaction):

$$2CO \rightarrow C + CO_2 \qquad (6\text{-}14)$$

and methane formation (methanation)

$$CO + 3H_2 \rightarrow CH_4 + H_2O \qquad (6\text{-}15)$$

In addition, decomposition of CH_4 to carbon and H_2 is possible

$$CH_4 \rightarrow C + 2H_2 \qquad (6\text{-}16)$$

but this reaction is suppressed at higher pressure. According to Le Chatelier's principle, an increase in pressure will favor carbon deposition by Equation (6-14)[26] and methane formation by Equations (6-15) and (6-16) (51). The water-gas shift reaction (52)[27]

$$CO_2 + H_2 \leftrightarrow CO + H_2O \qquad (6\text{-}17)$$

is not affected by an increase in pressure because the number of moles of gaseous reactants and products in the reaction is identical. Carbon deposition in an MCFC is to be avoided because it can lead to plugging of the gas passages in the anode. Methane formation is detrimental to cell performance because the formation of each mole consumes three moles of H_2, which represents a considerable loss of reactant and would reduce power plant efficiency.

The addition of H_2O and CO_2 to the fuel gas modifies the equilibrium gas composition so that the formation of CH_4 is not favored. Increasing the partial pressure of H_2O in the gas stream can

[26]. Data from translation of Russian literature (51) indicate the equilibrium constant is almost independent of pressure.

[27]. Data from translation of Russian literature (52) indicate the equilibrium constant K is a function of pressure. In relative terms, if K (627 °C) = 1 at 1 atm, it decreases to 0.74K at 500 atm and 0.60K at 1000 atmospheres. At the operating pressures of the MCFC, the equilibrium constant can be considered invariant with pressure.

reduce carbon deposition. Measurements (22) on 10 cm x 10 cm cells at 650 °C using simulated gasified coal GF-1 (38 percent H_2/56 percent CO/6 percent CO_2) at 10 atm showed that only a small amount of CH_4 is formed. At open circuit, 1.4 vol percent CH_4 (dry gas basis) was detected, and at fuel utilizations of 50 to 85 percent, 1.2 to 0.5 percent CH_4 was measured. The experiments with a high CO fuel gas (GF-1) at 10 atmospheres and humidified at 163 °C showed no indication of carbon deposition in a subscale MCFC. These studies indicated that CH_4 formation and carbon deposition at the anodes in an MCFC operating on coal-derived fuels can be controlled, and under these conditions, the side reactions would have little influence on power plant efficiency.

Figure 6-6 shows the effect of pressure (3, 5, and 10 atmospheres) and oxidant composition (3.2 percent CO_2/23.2 percent O_2/66.3 percent N_2/7.3 percent H_2O and 18.2 percent CO_2/9.2 percent O_2/65.3 percent N_2/7.3 percent H_2O) on the performance of 70.5 cm^2 MCFCs at 650 °C (53). The major difference as the CO_2 pressure changes is the change in open circuit potential, which increases with cell pressure and CO_2 content (see Equation (6-11)). At 160 mA/cm^2, ΔV_p is -44 mV for a pressure change from 3 to 10 atmospheres for both oxidant compositions.

Because ΔV_p is a function of the total gas pressure, the gas compositions in Figure 6-6 have little influence on ΔV_p. Based on these results, the effect of cell voltage from a change in pressure can be expressed by the equation

$$\Delta V_p\,(\text{mV}) = 84 \log \frac{P_2}{P_1} \qquad (6\text{-}18)$$

where P_1 and P_2 are different cell pressures. Another analysis by Benjamin, et al. (54) suggests that a coefficient less than 84 may be more applicable. The change in voltage as a function of pressure change was expressed as

$$\Delta V_p\,(\text{mV}) = 76.5 \log \frac{P_2}{P_1} \qquad (6\text{-}19)$$

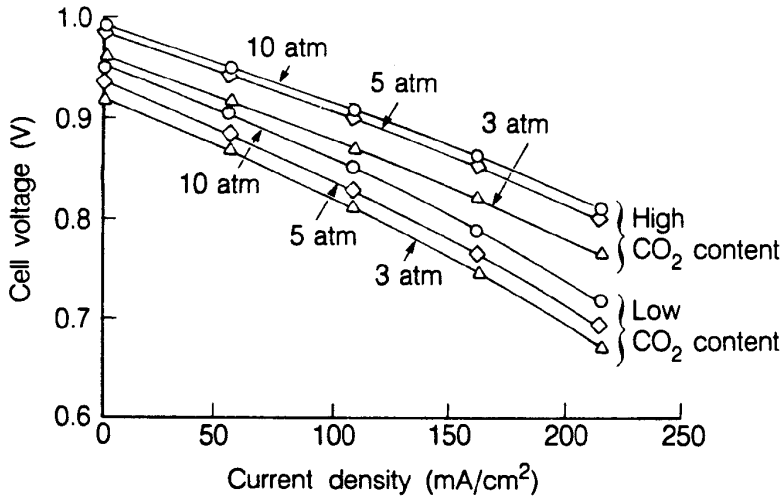

Figure 6-6 Influence of Cell Pressure on the Performance of a 70.5 cm^2 MCFC at 650 °C (anode gas, not specified; cathode gases, 23.2 percent O_2/3.2 percent CO_2/66.3 percent N_2/7.3 percent H_2O and 9.2 percent O_2/18.2 percent CO_2/65.3 percent N_2/7.3 percent H_2O; 50 percent CO_2, utilization at 215 mA/cm^2) (53, Figure 4, Pg. 395)

Equation (6-19) was based on a load of 160 mA/cm^2 at a temperature of 650 °C. It was also found to be valid for a wide range of fuels and for a pressure range of 1 atmosphere ≤ P ≤ 10 atmospheres. Other results (55) support this coefficient. Figure 6-7 shows the influence of pressure change on voltage gain for three different stack sizes. These values are for a temperature of 650 °C and a constant current density of 150 mA/cm^2 at a fuel utilization of 70 percent. The line that corresponds to a coefficient of 76.5 falls approximately in the middle of these values. Further improvements in cell performance will lead to changes in the logarithmic coefficient. Additional data (56, 57, 58) indicate that the coefficient may indeed be less than 76.5, but Equation (6-19) appears to represent the effect of pressure change on performance.

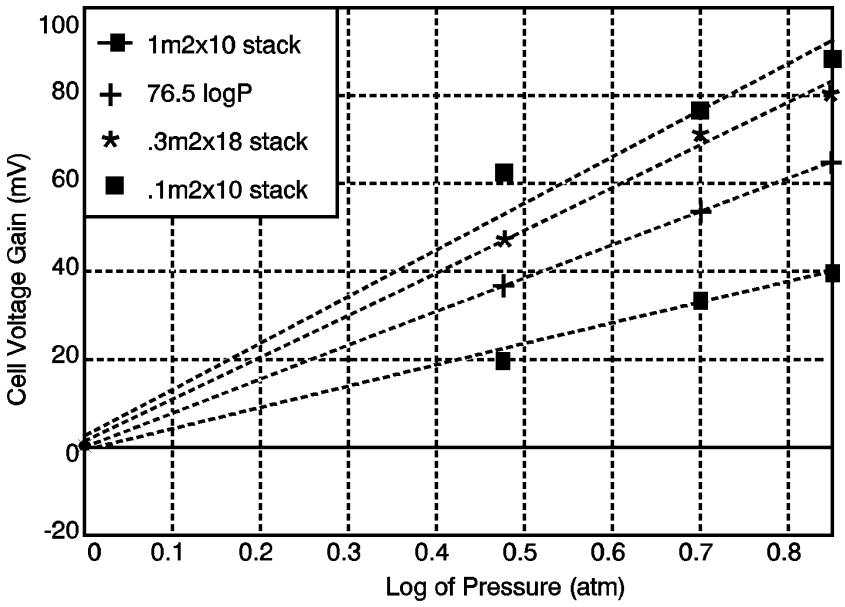

Figure 6-7 Influence of Pressure on Voltage Gain (55)

6.2.2 Effect of Temperature

The influence of temperature on the reversible potential of MCFCs depends on several factors, one of which involves the equilibrium composition of the fuel gas (22, 59, 60, 61).[28] The water gas shift reaction achieves rapid equilibrium[29] at the anode in MCFCs, and consequently CO serves as an indirect source of H_2. The equilibrium constant (K)

$$K = \frac{P_{CO} P_{H_2O}}{P_{H_2} P_{CO_2}} \qquad (6\text{-}20)$$

increases with temperature (see Table 6-4 and Appendix 10.1), and the equilibrium composition changes with temperature and utilization to affect the cell voltage.

The influence of temperature on the voltage of MCFCs is illustrated by the following example. Consider a cell with an oxidant gas mixture of 30 percent O_2/60 percent CO_2/10 percent N_2, and a fuel gas mixture of 80 percent H_2/20 percent CO_2. When the fuel gas is saturated with H_2O vapor at 25 °C, its composition becomes 77.5 percent H_2/19.4 percent CO_2/3.1 percent H_2O.

---

28. For a fixed gas composition of H_2, H_2O, CO, CO_2, and CH_4 there is a temperature, T_b, below which the exothermic Boudouard reaction is thermodynamically favored, and a temperature, T_m, above which carbon formation by the endothermic decomposition of CH_4 is thermodynamically favored; more extensive details on carbon deposition are found elsewhere (22, 59, 60, 61).
29. The dependence of equilibrium constant on temperature for carbon deposition, methanation, and water gas shift reactions is presented in Appendix 10.1.

After considering the equilibrium established by the water gas shift reaction, the equilibrium concentrations can be calculated (see Example 9-5 in Section 9) using Equation (6-20) and the equilibrium constant; see for instance, Broers and Treijtel (62). The equilibrium concentrations are substituted into Equation (6-4) to determine E as a function of T.

Table 6-4 Equilibrium Composition of Fuel Gas and Reversible Cell Potential as a Function of Temperature

Parameter[a]	Temperature (°K)		
	800	900	1000
P_{H_2}	0.669	0.649	0.643
P_{CO_2}	0.088	0.068	0.053
P_{CO}	0.106	0.126	0.141
P_{H_2O}	0.137	0.157	0.172
E^b (V)	1.155	1.143	1.133
K^c	0.2474	0.4538	0.7273

a - P is the partial pressure computed from the water gas shift equilibrium of inlet gas with composition 77.5 percent H_2/19.4 percent CO_2/3.1 percent H_2O at 1 atmosphere.
b - Cell potential calculated using Nernst equation and cathode gas composition of 30 percent O_2/60 percent CO_2/10 percent N_2.
c - Equilibrium constant for water gas shift reaction from Reference (59).

The results of these calculations are presented in Table 6-4. Inspection of the results shows a change in the equilibrium gas composition with temperature. The partial pressures of CO and H_2O increase at higher T because of the dependence of K on T. The result of the change in gas composition, and the decrease in E° with increasing T, is that E decreases with an increase in T. In an operating cell, the polarization is lower at higher temperatures, and the net result is that a higher cell voltage is obtained at elevated temperatures. The electrode potential measurements (9) in a 3 cm^2 cell[30] show that the polarization at the cathode is greater than at the anode, and that the polarization is reduced more significantly at the cathode with an increase in temperature. At a current density of 160 mA/cm^2, cathode polarization is reduced by about 160 mV when the temperature increases from 550 to 650 °C, whereas the corresponding reduction in anode polarization is only about 9 mV (between 600 and 650 °C, no significant difference in polarization is observed at the anode).

Baker, et al. (63) investigated the effect of temperature (575 to 650 °C) on the initial performance of small cells (8.5 cm^2). With steam-reformed natural gas as the fuel and 30 percent

30. Electrolyte is 55 wt% carbonate eutectic (57 wt% Li_2CO_3, 31 wt% Na_2CO_3, 12 wt% K_2CO_3) and 45 wt% $LiA1O_2$, anode is Co + 10% Cr, cathode is NiO, fuel is 80% H_2/20% CO_2 and oxidant is 30% CO_2/70% air.

CO_2/70 percent air as the oxidant, the cell voltage[31] at 200 mA/cm^2 decreased by 1.4 mV/° for a reduction in temperature from 650 to 600 °C, and 2.16 mV/°C for a decrease from 600 to 575 °C. In the temperature range 650 to 700 °C, data analysis (58) indicates a relationship of 0.25 mV/° C. The following equations summarize these results.

$$\Delta V_T\,(mV) = 2.16\,(T_2 - T_1) \qquad 575°C \leq T < 600\ °C \qquad (6\text{-}21)$$

$$\Delta V_T\,(mV) = 1.40\,(T_2 - T_1) \qquad 600°C \leq T < 650\ °C \qquad (6\text{-}22)$$

$$\Delta V_T\,(mV) = 0.25\,(T_2 - T_1) \qquad 650°C < T \leq 700\ °C \qquad (6\text{-}23)$$

The two major contributors responsible for the change in cell voltage with temperature are the ohmic polarization and electrode polarization. It appears that in the temperature range of 575 to 650 °C, about 1/3 of the total change in cell voltage with decreasing temperature is due to an increase in ohmic polarization, and the remainder from electrode polarization at the anode and cathode. Most MCFC stacks currently operate at an average temperature of 650 °C. Most carbonates do not remain molten below 520 °C, and as seen by the previous equations, increasing temperature enhances cell performance. Beyond 650 °C, however, there are diminishing gains with increased temperature. In addition, there is increased electrolyte loss from evaporation and increased material corrosion. An operating temperature of 650 °C thus offers a compromise between high performance and stack life.

6.2.3 Effect of Reactant Gas Composition and Utilization

The voltage of MCFCs varies with the composition of the reactant gases. The effect of reactant gas partial pressure, however, is somewhat difficult to analyze. One reason involves the water gas shift reaction at the anode due to the presence of CO. The other reason is related to the consumption of both CO_2 and O_2 at the cathode. Data (55, 64, 65, 66) show that increasing the reactant gas utilization generally decreases cell performance.

As reactant gases are consumed in an operating cell, the cell voltage decreases in response to the polarization (i.e., activation, concentration) and to the changing gas composition. These effects are related to the partial pressures of the reactant gases.

Oxidant: The electrochemical reaction at the cathode involves the consumption of two moles CO_2 per mole O_2 (see Equation (6-2)), and this ratio provides the optimum cathode performance. The influence of the $[CO_2]/[O_2]$ ratio on cathode performance is illustrated in Figure 6-8 (22). As this ratio decreases, the cathode performance decreases, and a limiting current is discernible. In the

[31]. Cell was operated at constant flow rate; thus, the utilization changes with current density.

limit where no CO_2 is present in the oxidant feed, the equilibrium involving the dissociation of carbonate ions becomes important.

$$CO_3^{=} \leftrightarrow CO_2 + O^{=} \qquad (6\text{-}24)$$

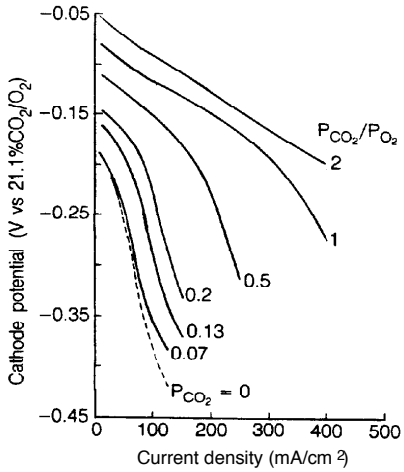

Figure 6-8 Effect of CO_2/O_2 Ratio on Cathode Performance in an MCFC, Oxygen Pressure is 0.15 atm (22, Figure 5-10, Pgs. 5-20)

Under these conditions, the cathode performance shows the greatest polarization because of the composition changes that occur in the electrolyte. The change in the average cell voltage of a ten-cell stack as a function of oxidant utilization is illustrated in Figure 6-9. In this stack, the average cell voltage at 172 mA/cm^2 decreases by about 30 mV for a 30 percentage point increase in oxidant (20 to 50 percent) utilization. Based on this additional data (55, 64, 65), the voltage loss due to a change in oxidant utilization can be described by the following equations:

$$\Delta V_{cathode}\,(mV) = 250 \log \frac{\left(\overline{P}_{CO_2}\ \overline{P}_{O_2}^{\frac{1}{2}}\right)_2}{\left(\overline{P}_{CO_2}\ \overline{P}_{O_2}^{\frac{1}{2}}\right)_1} \qquad \text{for } 0.04 \le \left(\overline{P}_{CO_2}\ \overline{P}_{O_2}^{\frac{1}{2}}\right) \le 0.11 \qquad (6\text{-}25)$$

$$V_{cathode}\,(mV) = 99 \log \frac{\left(\overline{P}_{CO_2}\ \overline{P}_{O_2}^{\frac{1}{2}}\right)_2}{\left(\overline{P}_{CO_2}\ \overline{P}_{O_2}^{\frac{1}{2}}\right)_1} \qquad \text{for } 0.11 < \left(\overline{P}_{CO_2}\ \overline{P}_{O_2}^{\frac{1}{2}}\right) \le 0.38 \qquad (6\text{-}26)$$

where $\overline{P}_{CO_2}$ and $\overline{P}_{O_2}$ are the average partial pressures of CO_2 and O_2 in the system.

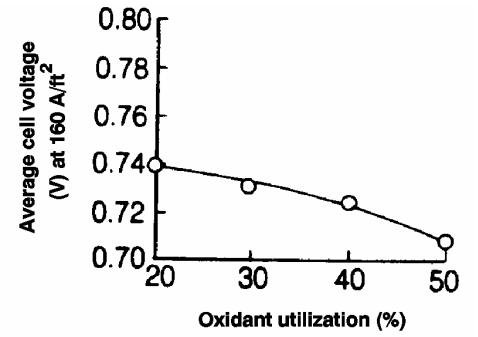

Figure 6-9 Influence of Reactant Gas Utilization on the Average Cell Voltage of an MCFC Stack (67, Figure 4-21, Pgs. 4-24)

Fuel: The data in Table 6-5 from Lu and Selman (68) illustrate the dependence of the anode potential on the composition of five typical fuel gases and two chemical equilibria occurring in the anode compartment.[32] The calculations show the gas compositions and open circuit anode potentials obtained after equilibria by the water gas shift and CH_4 steam reforming reactions are considered. The open circuit anode potential calculated for the gas compositions after equilibration, and experimentally measured, is presented in Table 6-5. The equilibrium gas compositions obtained by the shift and steam reforming reactions clearly show that, in general, the H_2 and CO_2 contents in the dry gas decrease, and CH_4 and CO are present in the equilibrated gases. The anode potential varies as a function of the $[H_2]/[H_2O][CO_2]$ ratio; a higher potential is obtained when this ratio is higher. The results show that the measured potentials agree with the values calculated, assuming that simultaneous equilibria of the shift and the steam reforming reactions reach equilibrium rapidly in the anode compartments of MCFCs.

[32]. No gas phase equilibrium exists between O_2 and CO_2 in the oxidant gas that could alter the composition or cathode potential.

Table 6-5 Influence of Fuel Gas Composition on Reversible Anode Potential at 650 °C (68, Table 1, Pg. 385)

Typical Fuel Gas[a]	Gas Composition (mole fraction) H_2	H_2O	CO	CO_2	CH_4	N_2	-E[b] (mV)
Dry gas							
High Btu (53 °C)	0.80	-	-	0.20	-	-	1116±3[c]
Intermed. Btu (71 °C)	0.74	-	-	0.26	-	-	1071±2[c]
Low Btu 1 (71 °C)	0.213	-	0.193	0.104	0.011	0.479	1062±3[c]
Low Btu 2 (60 °C)	0.402	-	-	0.399	-	0.199	1030±[c]
Very low Btu (60 °C)	0.202	-	-	0.196	-	0.602	1040±[c]
Shift equilibrium							
High Btu (53 °C)	0.591	0.237	0.096	0.076	-	-	1122[d]
Intermed. Btu (71 °C)	0.439	0.385	0.065	0.112	-	-	1075[d]
Low Btu 1 (71 °C)	0.215	0.250	0.062	0.141	0.008	0.326	1054[d]
Low Btu 2 (60 °C)	0.231	0.288	0.093	0.228	-	0.160	1032[d]
Very low Btu (60 °C)	0.128	0.230	0.035	0.123	-	0.484	1042[d]
Shift and Steam-reforming							
High Btu (53 °C)	0.555	0.267	0.082	0.077	0.020	-	1113[d]
Intermed. Btu (71 °C)	0.428	0.394	0.062	0.112	0.005	-	1073[d]
Low Btu 1 (71 °C)	0.230	0.241	0.067	0.138	0.001	0.322	1059[d]
Low Btu 2 (60 °C)	0.227	0.290	0.092	0.229	0.001	0.161	1031[d]
Very low Btu (60 °C)	0.127	0.230	0.035	0.123	0.0001	0.485	1042[d]

a - Temperature in parentheses is the humidification temperature
b - Anode potential with respect to 33 percent O_2/67 percent CO_2 reference electrode
c - Measured anode potential
d - Calculated anode potential, taking into account the equilibrated gas composition

Further considering the Nernst equation, an analysis shows that the maximum cell potential for a given fuel gas composition is obtained when $[CO_2]/[O_2] = 2$. Furthermore, the addition of inert gases to the cathode, for a given $[CO_2]/[O_2]$ ratio, causes a decrease in the reversible potential. On the other hand, the addition of inert gases to the anode increases the reversible potential for a given $[H_2]/[H_2O][CO_2]$ ratio and oxidant composition. This latter result occurs because two moles of product are diluted for every mole of H_2 reactant. However, the addition of inert gases to either gas stream in an operating cell can lead to an increase in concentration polarization.

Figure 6-10 depicts an average voltage loss for the stack of about 30 mV for a 30 percent increase in fuel utilization (30 to 60 percent). This and other data (66) suggest that the voltage loss due to a change in fuel utilization can be described by the following equation:

$$\Delta V_{anode}\,(mV) = 173 \log \frac{\left(\overline{P}_{H_2} / \overline{P}_{CO_2}\,\overline{P}_{H_2O}\right)_2}{\left(\overline{P}_{H_2} / \overline{P}_{CO_2}\,\overline{P}_{H_2O}\right)_1} \qquad (6\text{-}27)$$

where $\overline{P}_{H_2}$, $\overline{P}_{CO_2}$, and $\overline{P}_{H_2O}$ are the average partial pressures of H_2, CO_2, and O_2 in the system.

The above discussion implies that MCFCs should be operated at low reactant gas utilizations to maintain voltage levels, but doing this means inefficient fuel use. As with other fuel cell types, a compromise must be made to optimize overall performance. Typical utilizations are 75 to 85 percent of the fuel.

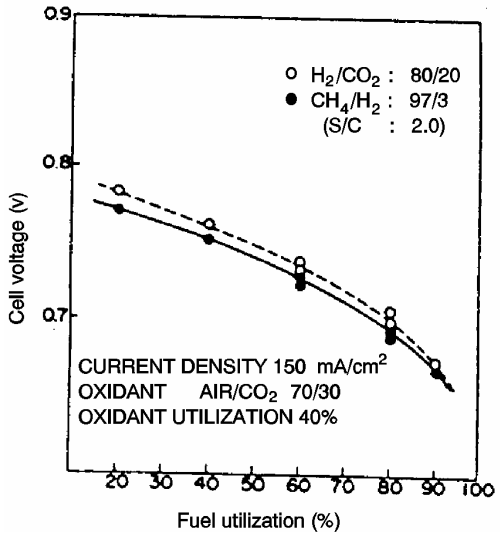

Figure 6-10 Dependence of Cell Voltage on Fuel Utilization (69)

6.2.4 Effect of Impurities

Gasified coal is expected to be the major source of fuel gas for MCFCs, but because coal contains many contaminants in a wide range of concentrations, fuel derived from this source also contains a considerable number of contaminants.[33] A critical concern with these contaminants is the concentration levels that can be tolerated by MCFCs without significant degradation in

[33]. See Table 11.1 for contaminant levels found in fuel gases from various coal gasification processes.

performance or reduction in cell life. A list of possible effects of contaminants from coal-derived fuel gases on MCFCs is summarized in Table 6-6 (70).

Table 6-6 Contaminants from Coal-Derived Fuel Gas and Their Potential Effect on MCFCs (70, Table 1, Pg. 299)

Class	Contaminant	Potential Effect
Particulates	Coal fines, ash	• Plugging of gas passages
Sulfur compounds	H_2S, COS, CS_2, C_4H_4S	• Voltage losses • Reaction with electrolyte via SO_2
Halides	HCl, HF, HBr, $SnCl_2$	• Corrosion • Reaction with electrolyte
Nitrogen compounds	NH_3, HCN, N_2	• Reaction with electrolyte via NO_X
Trace metals	As, Pb, Hg, Cd, Sn Zn, H_2Se, H_2Te, AsH_3	• Deposits on electrode • Reaction with electrolyte
Hydrocarbons	C_6H_6, $C_{10}H_8$, $C_{14}H_{10}$	• Carbon deposition

The typical fuel gas composition and contaminants from an air-blown gasifier that enter the MCFC at 650 °C after hot gas cleanup, and the tolerance level of MCFCs to these contaminants are listed in Table 6-7 (79, 71, 72). It is apparent from this example that a wide spectrum of contaminants is present in coal-derived fuel gas. The removal of these contaminants can add considerably to the efficiency. A review of various options for gas cleanup is presented by Anderson and Garrigan (70) and Jalan, et al. (73).

Sulfur*:* It is well established that sulfur compounds in low parts per million concentrations in fuel gas are detrimental to MCFCs (74, 75, 76, 77, 78). The tolerance of MCFCs to sulfur compounds (74) is strongly dependent on temperature, pressure, gas composition, cell components, and system operation (i.e., recycle, venting, gas cleanup). The principal sulfur compound that has an adverse effect on cell performance is H_2S. At atmospheric pressure and high gas utilization (~75 percent), <10 ppm H_2S in the fuel can be tolerated at the anode (tolerance level depends on anode gas composition and partial pressure of H_2), and <1 ppm SO_2 is acceptable in the oxidant (74). These concentration limits increase when the temperature increases, but they decrease at increasing pressures.

Table 6-7 Gas Composition and Contaminants from Air-Blown Coal Gasifier After Hot Gas Cleanup, and Tolerance Limit of MCFCs to Contaminants

Fuel Gas[a] (mol percent)	Contaminants[b,c]	Content[b,c]	Remarks[b]	Tolerance[c,d] Limit
19.2 CO	Particulates	<0.5 mg/l	Also includes ZnO from H_2S cleanup stage	<0.1 g/l for large particulates >0.3 :m
13.3 H_2	NH_3	2600 ppm		<10,000 ppm
2.6 CH_4	AsH_3	<5 ppm		< 1 ppm
6.1 CO_2	H_2S	<10 ppm	After first-stage cleanup	<0.5 ppm
12.9 H_2O	HCl	500 ppm	Also includes other halides	<10 ppm
45.8 N_2	Trace Metals	<2 ppm <2 ppm <2 ppm <2 ppm	Pb Cd Hg Sn	<1 ppm 30+ ppm 35+ ppm NA
	Zn	<50 ppm	From H_2S hot cleanup	<20 ppm
	Tar	4000 ppm	Formed during desulfurization cleanup stage	<2000 ppm[e]

a - Humidified fuel gas enters MCFC at 650 °C
b - (71, Table 1, Pg. 177)
c - (79)
d - (72)
e - Benzene

The mechanisms by which H_2S affects cell performance have been investigated extensively (75, 76, 77, 78). The adverse effects of H_2S occur because of:

- Chemisorption on Ni surfaces to block active electrochemical sites,
- Poisoning of catalytic reaction sites for the water gas shift reaction, and
- Oxidation to SO_2 in a combustion reaction, and subsequent reaction with carbonate ions in the electrolyte.

The adverse effect of H_2S on the performance of MCFCs is illustrated in Figure 6-11. The cell voltage of a 10 cm x 10 cm cell at 650 °C decreases when 5 ppm H_2S is added to the fuel gas (10 percent H_2/5 percent CO_2/10 percent H_2O/75 percent He), and current is drawn from the cell. The measurements indicate that low concentrations of H_2S do not affect the open circuit potential, but they have a major impact on the cell voltage as current density is progressively increased. The decrease in cell voltage is not permanent;[34] when fuel gas without H_2S is introduced into the cell, the cell voltage returns to the level for a cell with clean fuel. These results can be explained by the chemical and electrochemical reactions that occur involving H_2S and $S^{=}$. A nickel anode at anodic potentials reacts with H_2S to form nickel sulfide:

$$H_2S + CO_3^{=} \rightarrow H_2O + CO_2 + S^{=} \qquad (6\text{-}28)$$

followed by

$$Ni + xS^{=} \rightarrow NiS_x + 2xe^{-} \qquad (6\text{-}29)$$

When the sulfided anode returns to open circuit, the NiS_x is reduced by H_2:

$$NiS_x + xH_2 \rightarrow Ni + xH_2S \qquad (6\text{-}30)$$

Similarly, when a fuel gas without H_2S is introduced to a sulfided anode, reduction of NiS_x to Ni can also occur. Detailed discussions on the effect of H_2S on cell performance are presented by Vogel and co-workers (75, 76) and Remick (77, 78).

The rapid equilibration of the water gas shift reaction in the anode compartment provides an indirect source of H_2 by the reaction of CO and H_2O. If H_2S poisons the active sites for the shift reaction, this equilibrium might not be established in the cell, and a lower H_2 content than predicted would be expected. Fortunately, evidence (77, 78) indicates that the shift reaction is not significantly poisoned by H_2S. In fact, Cr used in stabilized-Ni anodes appears to act as a sulfur tolerant catalyst for the water gas shift reaction (78).

The CO_2 required for the cathode reaction is expected to be supplied by recycling the anode gas exhaust (after combustion of the residual H_2) to the cathode. Therefore, any sulfur in the anode effluent will be present at the cathode inlet unless provisions are made for sulfur removal. In the absence of sulfur removal, sulfur enters the cathode inlet as SO_2, which reacts quantitatively (equilibrium constant is 10^{15} to 10^{17}) with carbonate ions to produce alkali sulfates. These sulfate

[34]. The effects of H_2S on cell voltage are reversible if H_2S concentrations are present at levels below that required to form nickel sulfide.

ions are transported through the electrolyte structure to the anode during cell operation. At the anode, $SO_4^{=}$ is reduced to $S^{=}$, thus increasing the concentration of $S^{=}$ there.

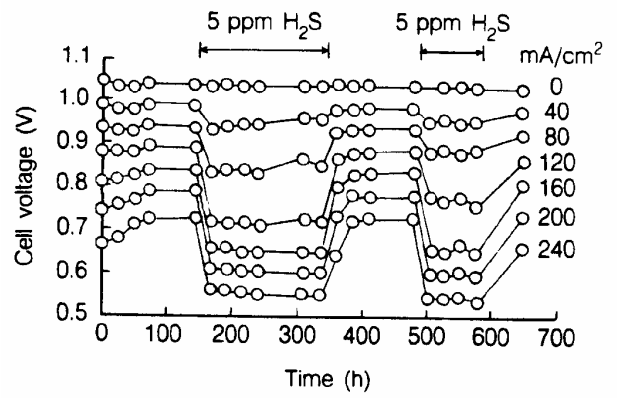

Figure 6-11 Influence of 5 ppm H_2S on the Performance of a Bench Scale MCFC (10 cm x 10 cm) at 650 °C, Fuel Gas (10 percent H_2/5 percent CO_2/10 percent H_2O/75 percent He) at 25 percent H_2 Utilization (78, Figure 4, Pg. 443)

Based on the present understanding of the effect of sulfur on MCFCs, and with the available cell components, it is projected that long-term operation (40,000 hr) of MCFCs may require fuel gases with sulfur[35] levels of the order 0.01 ppm or less, unless the system is purged of sulfur at periodic intervals or sulfur is scrubbed from the cell burner loop (76). Sulfur tolerance would be approximately 0.5 ppm (see Table 6-3) in the latter case. Considerable effort has been devoted to develop low-cost techniques for sulfur removal, and research and development are continuing (80, 81). The effects of H_2S on cell voltage are reversible if H_2S concentrations are present at levels below which nickel sulfide forms.

Halides: Halogen-containing compounds are destructive to MCFCs because they can lead to severe corrosion of cathode hardware. Thermodynamic calculations (82) show that HCl and HF react with molten carbonates (Li_2CO_3 and K_2CO_3) to form CO_2, H_2O, and the respective alkali halides. Furthermore, the rate of electrolyte loss in the cell is expected to increase because of the high vapor pressure of LiCl and KCl. The concentration of Cl^- species in coal-derived fuels is typically in the range 1 to 500 ppm. It has been suggested (83) that the level of HCl should be kept below 1 ppm in the fuel gas, perhaps below 0.5 ppm (47), but the tolerable level for long-term operation has not been established.

***Nitrogen Compounds*:** Compounds such as NH_3 and HCN do not appear to harm MCFCs (70, 79) in small amounts. However, if NO_X is produced by combustion of the anode effluent in the cell burner loop, it could react irreversibly with the electrolyte in the cathode compartment to form nitrate salts. The projection by Gillis (84) for NH_3 tolerance of MCFCs was 0.1 ppm, but Table 6-3 indicates that the level could be 1 vol percent (47).

[35]. Both COS and CS_2 appear to be equivalent to H_2S in their effect on MCFCs (76).

Solid Particulates: These contaminants can originate from a variety of sources, and their presence is a major concern because they can block gas passages and/or the anode surface. Carbon deposition and conditions that can be used to control its formation have been discussed earlier in this section. Solid particles such as ZnO, which is used for sulfur removal, can be entrained in the fuel gas leaving the desulfurizer. The results by Pigeaud (72) indicate that the tolerance limit of MCFCs to particulates larger than 3 μm diameter is <0.1 g/l.

Other Compounds: Experimental studies indicate that 1 ppm As from gaseous AsH_3 in fuel gas does not affect cell performance, but when the level is increased to 9 ppm As, the cell voltage drops rapidly by about 120 mV at 160 mA/cm^2 (71). Trace metals, such as Pb, Cd, Hg, and Sn in the fuel gas, are of concern because they can deposit on the electrode surface or react with the electrolyte (16). Table 6-3 addresses limits of these trace metals.

6.2.5 Effects of Current Density

The voltage output from an MCFC is reduced by ohmic, activation, and concentration losses that increase with increasing current density. The major loss over the range of current densities of interest is the linear iR loss. The magnitude of this loss (iR) can be described by the following equations (64, 85, 86):

$$\Delta V_J(mV) = -1.21\Delta J \qquad \text{for } 50 \leq J \leq 150 \qquad (6\text{-}31)$$

$$\Delta V_J(mV) = -1.76\Delta J \qquad \text{for } 150 \leq J \leq 200 \qquad (6\text{-}32)$$

where J is the current density (mA/cm^2) at which the cell is operating.

6.2.6 Effects of Cell Life

Endurance of the cell stack is a critical issue in the commercialization of MCFCs. Adequate cell performance must be maintained over the desired length of service, quoted by one MCFC developer as being an average potential degradation no greater than 2mV/1,000 hours over a cell stack lifetime of 40,000 hours (29). State-of-the-art MCFCs (55, 64, 66, 87, 88) depict an average degradation over time of

$$\Delta V_{lifetime}(mV) = -5mV/1000 \text{ hours} \qquad (6\text{-}33)$$

6.2.7 Internal Reforming

In a conventional fuel cell system, a carbonaceous fuel is fed to a fuel processor where it is steam reformed to produce H_2 (as well as other products, CO and CO_2, for example), which is then introduced into the fuel cell and electrochemically oxidized. The internal reforming molten carbonate fuel cell, however, eliminates the need for a separate fuel processor for reforming

carbonaceous fuels. This concept is practical in high-temperature fuel cells where the steam reforming reaction[36] can be sustained with catalysts. By closely coupling the reforming reaction and the electrochemical oxidation reaction within the fuel cell, the concept of the internal reforming MCFC is realized. The internal reforming MCFC eliminates the need for the external fuel processor. It was recognized early that the internal reforming MCFC approach provides a highly efficient, simple, reliable, and cost effective alternative to the conventional MCFC system (89). Development to date in the U.S. and Japan continues to support this expectation (85, 90).

There are two alternate approaches to internal reforming molten carbonate cells: indirect internal reforming (IIR) and direct internal reforming (DIR). In the first approach, the reformer section is separate, but adjacent to the fuel cell anode. This cell takes advantage of the close-coupled thermal benefit where the exothermic heat of the cell reaction can be used for the endothermic reforming reaction. Another advantage is that the reformer and the cell environments do not have a direct physical effect on each other. A disadvantage is that the conversion of methane to hydrogen is not promoted as well as in the direct approach. In the DIR cell, hydrogen consumption reduces its partial pressure, thus driving the methane reforming reaction, Equation (6-34), to the right. Figure 6-12 depicts one developer's approach where IIR and DIR have been combined.

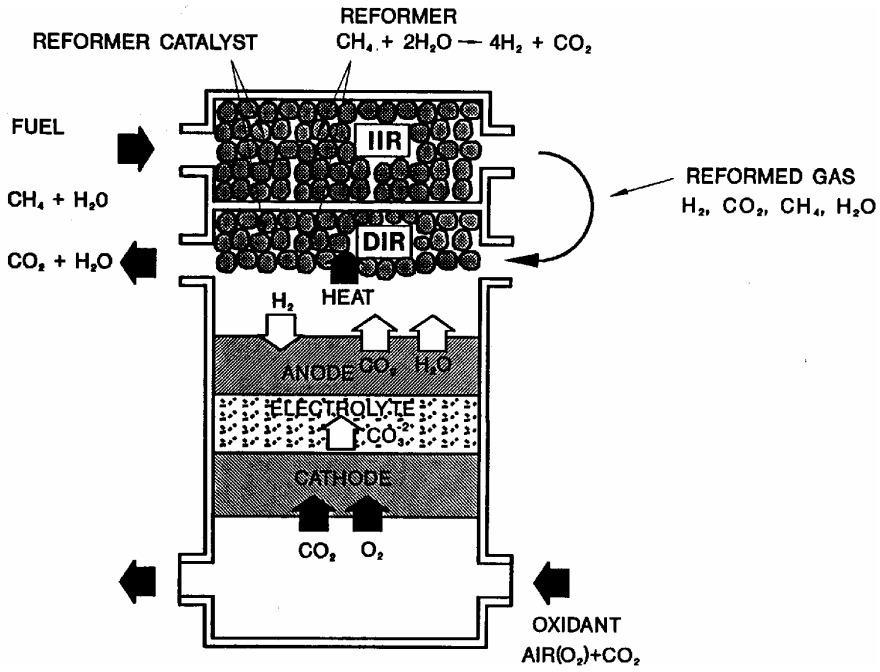

Figure 6-12 IIR/DIR Operating Concept, Molten Carbonate Fuel Cell Design (29)

[36]. Steam reforming of CH_4 is typically performed at 750 to 900 °C; thus, at the lower operating temperature of MCFCs, a high activity catalyst is required. Methanol is also a suitable fuel for internal reforming. It does not require an additional catalyst because the Ni-based anode is sufficiently active.

Methane is a common fuel in internal reforming MCFCs, where the steam reforming reaction

$$CH_4 + H_2O \rightarrow CO + 3H_2 \qquad (6\text{-}34)$$

occurs simultaneously with the electrochemical oxidation of hydrogen in the anode compartment. The steam reforming reaction is endothermic, with $\Delta H_{650°C} = 53.87$ kcal/mol (89), whereas the overall fuel cell reaction is exothermic. In an internal reforming MCFC, the heat required for the reaction in Equation (6-34) is supplied by heat from the fuel cell reaction, thus eliminating the need for external heat exchange that is required by a conventional fuel processor. In addition, the product steam from the reaction in Equation (6-1) can be used to enhance the reforming reaction and the water gas shift reaction to produce additional H_2. The forward direction of the reforming reaction (Equation (6-34)) is favored by high temperature and low pressure; thus, an internal reforming MCFC is best suited to operate near atmospheric pressure.

A supported Ni catalyst (e.g., Ni supported on MgO or $LiAlO_2$) sustains the steam reforming reaction at 650 °C to produce sufficient H_2 to meet the needs of the fuel cell. The interrelationship between the conversion of CH_4 to H_2 and its utilization in an internal reforming MCFC at 650 °C is illustrated in Figure 6-13. At open circuit, about 83 percent of the CH_4 was converted to H_2, which corresponds closely to the equilibrium concentration at 650°C. When current is drawn from the cell, H_2 is consumed and H_2O is produced, and the conversion of CH_4 increases and approaches 100 percent at fuel utilizations greater than about 65 percent. Thus, by appropriate thermal management and adjustment of H_2 utilization with the rate of CH_4 reforming, a similar performance can be obtained in internal reforming MCFC stacks with natural gas and with synthesized reformate gas containing H_2 and CO_2, Figure 6-14. The concept of internal reforming has been successfully demonstrated for more than 15,000 hours in a 5 kW stack (91 and more than 10,000 hours in a 250 kW stack (92) The performance of the 2 kW stack over time can be seen in Figure 6-15 (13).

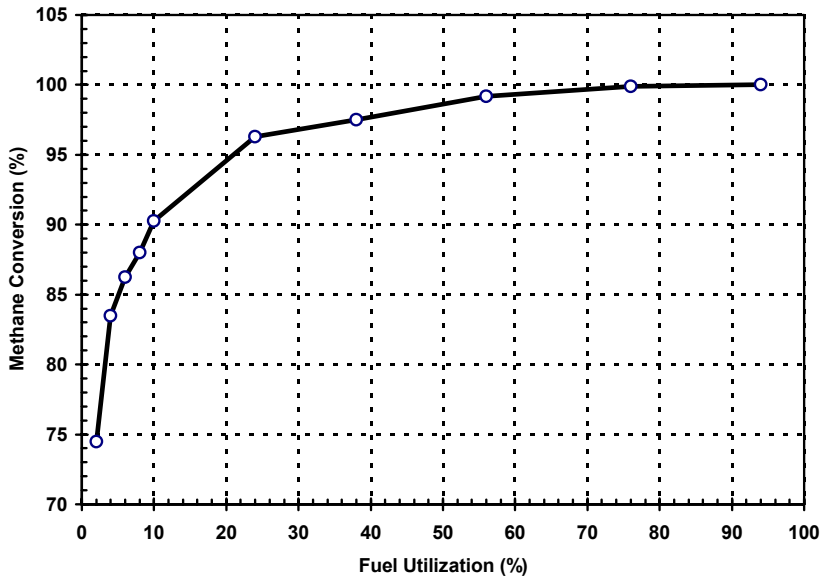

Figure 6-13 CH_4 Conversion as a Function of Fuel Utilization in a DIR Fuel Cell (MCFC at 650 ºC and 1 atm, steam/carbon ratio = 2.0, >99 percent methane conversion achieved with fuel utilization > 65 percent (93)

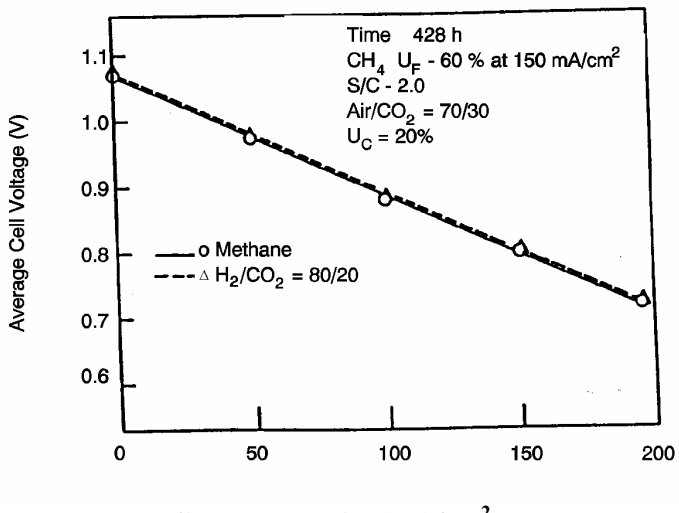

Figure 6-14 Voltage Current Characteristics of a 3kW, Five Cell DIR Stack with 5,016 cm^2 Cells Operating on 80/20 percent H_2/CO_2 and Methane (85)

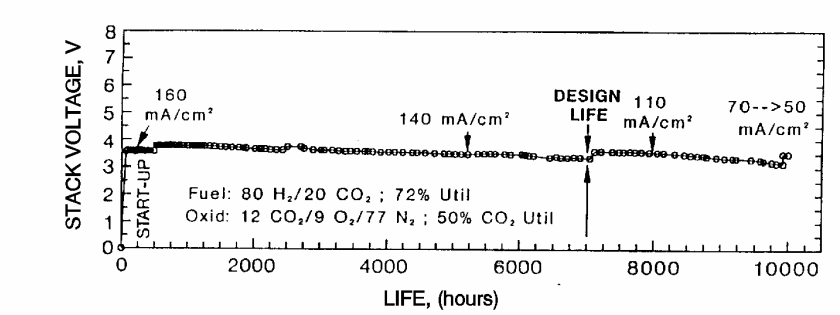

Figure 6-15 Performance Data of a 0.37m^2 2 kW Internally Reformed MCFC Stack at 650 °C and 1 atm (13)

Direct Internal Reforming Catalysts: The anode catalyst is deactivated by the alkali carbonate's electrolyte-containing environment. Making hardware of a non-wetting metal such as nickel has mitigated electrolyte creepage over the hardware surface towards the catalyst. Presently DIR catalyst deactivation is mainly by the vapor phase alkali species. The deactivation mechanism includes electrolyte-accelerated sintering, pore filling/plugging, and surface coverage. Making hardware of a non-wetting metal such as nickel has mitigated electrolyte creepage over the hardware surface towards the catalyst. Alkali-resistant supports such as magnesium oxide, calcium aluminate, and α-alumina have been investigated to reduce vapor phase alkali species effects. Results show that these supports undergo different degrees of decay. Ruthenium and rhodium-based catalysts are more stable, but are too costly (95, 96) FCE has identified a more active and stable DIR catalyst (high activity supported Ni), projecting a catalyst life exceeding 40,000 hours and pursuing further enhancement of catalyst life. Another approach is to apply a getter-type barrier to trap the volatile alkali species before they reach the catalysts. A porous Ni or a SiC membrane was placed between the cell internal catalyst and the electrolyte-containing components. (37)

6.3 Summary of Equations for MCFC

The preceding sections provide parametric performance based on various referenced data at different operating conditions. It is suggested that the following set of equations could be used for performance adjustments unless the reader prefers other data or correlations. Figure 6-16 is provided as reference MCFC performance.

Parameter	Equation	Comments	
Pressure	$\Delta V_p(mV) = 76.5 \log \frac{P_2}{P_1}$	1 atm $\leq$ P $\leq$ 10 atm	(6-19)
Temperature	$\Delta V_T(mV) = 2.16(T_2 - T_1)$	575°C $\leq$ T < 600 °C	(6-21)
	$\Delta V_T(mV) = 1.40(T_2 - T_1)$	600°C $\leq$ T $\leq$ 650 °C	(6-22)
	$\Delta V_T(mV) = 0.25(T_2 - T_1)$	650°C < T $\leq$ 700 °C	(6-23)
Oxidant	$\Delta V_{cathode}(mV) = 250 \log \frac{(\bar{P}_{CO_2}\ \bar{P}_{O_2}^{1/2})_2}{(P_{CO_2}\ P_{O_2}^{1/2})_1}$	$0.04 \leq (\bar{P}_{CO_2}\ \bar{P}_{O_2}^{1/2}) \leq 0.11$	(6-25)
	$\Delta V_{cathode}(mV) = 99 \log \frac{(\bar{P}_{CO_2}\ \bar{P}_{O_2}^{1/2})_2}{(\bar{P}_{CO_2}\ \bar{P}_{O_2}^{1/2})_1}$	$0.11 \leq (\bar{P}_{CO_2}\ \bar{P}_{O_2}^{1/2}) \leq 0.38$	(6-26)
Fuel	$\Delta V_{anode}(mV) = 173 \log \frac{(\bar{P}_{H_2} / \bar{P}_{CO_2}\ \bar{P}_{H_2O}^{1/2})_2}{(\bar{P}_{H_2} / \bar{P}_{CO_2}\ \bar{P}_{O_2}^{1/2})_1}$		(6-27)
Current Density	$\Delta V_J(mV) = -1.21\ \Delta J$	50 $\leq$ J $\leq$ 150mA/cm^2	(6-31)
	$\Delta V_J(mV) = -1.76\ \Delta J$	150 < J $\leq$ 200mA/cm^2	(6-32)
Life Effects	$\Delta V_{lifetime}(mV) = -5mV/1000$ hours		(6-33)

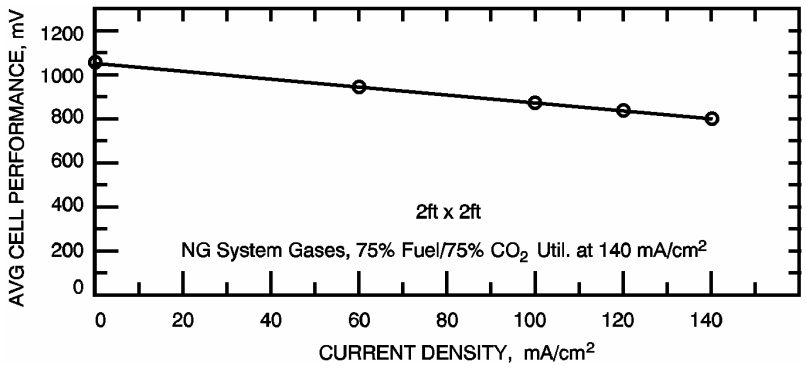

Figure 6-16 Average Cell Voltage of a 0.37m^2 2 kW Internally Reformed MCFC Stack at 650 °C and 1 atm. Fuel, 100 percent CH_4, Oxidant, 12 percent CO_2/9 percent O_2/77 percent N_2

FuelCell Energy presented a computer model for predicting carbonate fuel cell performance at different operating conditions. The model was described in detail at the Fourth International Symposium on Carbonate Fuel Cell Technology, Montreal, Canada, 1997 (97). The model equations are as follows:

The general voltage versus current density relation is:

$$V = E_{Nernst} - (\eta_a + \eta_c) - \eta_{conc} - iz_r \qquad (6\text{-}41)$$

where

$$V_0 = E_0 + \frac{RT}{2F} \ln \left(\frac{P_{H_2,a}}{P_{CO_2,a}\, P_{H_2O,a}} P_{CO_2,c}\ P_{O_2,c}^{1/2} \right) \qquad (6\text{-}42)$$

At low current density ($i<0.04$ A/cm^2)

$$\eta_a = \frac{iRT}{2F} \frac{1}{K_a^0} e^{Ea/T}\, p_{H_2}^{\beta-0.5}\, p_{CO_2}^{-\beta}\, p_{H_2O}^{-\beta} \qquad (6\text{-}43)$$

$$\eta_c = \frac{iRT}{2F} \frac{1}{K_a^0} e^{Ec/T}\, p_{CO_2}^{-b_1'}\, p_{O_2}^{-b_2'} \qquad (6\text{-}44)$$

At high current density ($i < 0.04$A/cm^2)

$$\eta_a = \frac{RT}{2F}\left(a_0 + a_1 \ln p_{H_2} + a_2 \ln p_{CO_2,a} + a_3 \ln p_{H_2O} + a_4/T + a_5 \ln(i)\right) \qquad (6\text{-}45)$$

$$\eta_c = \frac{RT}{2F}\left(b_0 + b_1 \ln p_{CO_2,c} + b_2 \ln p_{o_2} + b_3/T + b_4 \ln i\right) \qquad (6\text{-}46)$$

and

$$\eta = c_6 \ln(1 - i/i_L) \qquad (6\text{-}47)$$

cell resistance

$$Z_r = Z_0 \exp[c(\frac{1}{T_0} - \frac{1}{T})] \qquad (6\text{-}48)$$

A description of the parameters in the model follows:

V	=	Cell voltage, V
$E_\circ$	=	Standard E.M.F., V
R	=	Universal gas constant (8.314 joule/deg-mole)
T	=	Temperature, K
P	=	Partial pressure of gas compositions at anode (a) or cathode (c), atm.
η	=	Polarization, V
i	=	Current density, A/cm^2
z	=	Cell impedance, Ω-cm^2
F	=	Faraday's Constant (96,487 joule/volt - gram equivalent)
a,b,c	=	Parameters determined for experiments

The parameters in the above equations were calibrated from 400 sets of FCE's laboratory-scale test data and were further verified by several large-scale stack experiments. These parameter values may depend on the FCE cell design and characteristics, and may not be directly applicable to other carbonate technologies. Figure 6-17 is a comparison of the measured data match with the model prediction.

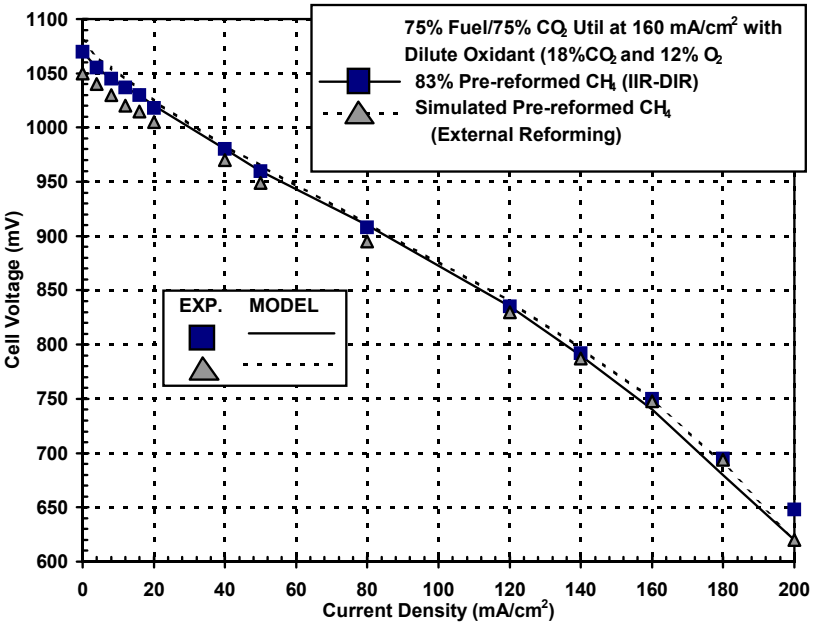

Figure 6-17 Model Predicted and Constant Flow Polarization Data Comparison (98)

6.4 References

1. H.C. Maru, L.G. Marianowski, *Extended Abstracts,* Abstract #31, Fall Meeting of the Electrochemical Society, October 17-22, 1976, Las Vegas, NV, Pg. 82, 1976.R.H.
2. J. Mitteldorf, G. Wilemski, *J. Electrochem. Soc.,* 131, 1784, 1984.
3. R.H. Arendt, *J. Electrochem. Soc.,* 129, 942, 1982.
4. H.C. Maru, A. Pigeaud, R. Chamberlin, G. Wilemski, in *Proceedings of the Symposium on Electrochemical Modeling of Battery, Fuel Cell, and Photoenergy Conversion Systems,* edited by J.R. Selman and H.C. Maru, The Electrochemical Society, Inc., Pennington, NJ, Pg. 398, 1986.
5. H.R. Kunz, *J. Electrochem. Soc.,* 134, 105, 1987.
6. A. Pigeaud, H.C. Maru, L. Paetsch, J. Doyon, R. Bernard, in *Proceedings of the Symposium on Porous Electrodes: Theory and Practices,* edited by H.C. Maru, T. Katan and M.G. Klein, The Electrochemical Society, Inc., Pennington, NJ, Pg. 234, 1984.
7. H.C. Maru, L. Paetsch, A. Pigeaud, in *Proceedings of the Symposium on Molten Carbonate Fuel Cell Technology,* edited by R.J. Selman and T.D. Claar, The Electrochemical Society, Inc., Pennington, NJ, Pg. 20, 1984.
8. R.J. Petri, T.G. Benjamin, in *Proceedings of the 21st Intersociety Energy Conversion Engineering Conference,* Volume 2, American Chemical Society, Washington, DC, Pg. 1156, 1986.
9. R.J. Selman, *Energy,* 11, 153, 1986.
10. M. Farooque, ERC, "Development on Internal Reforming Carbonate Fuel Cell Technology, Final Report," prepared for U.S. DOE/METC, DOE/MC/23274-2941, Pgs. 4-19 - 4-29, October, 1990.
11. FCE correspondence, June 2002
12. R. Huff, "Status of Fuel Cell Technologies," 1986 Fuel Cell Seminar, October 26-29, 1986, Tucson, AZ, 1986.
13. M. Farooque, data from ERC testing, 1992 and 2002.
14. C.E. Baumgartner, V.J. DeCarlo, P.G. Glugla, J.J. Grimaldi, *J. Electrochem. Soc.,* 132, 57, 1985.
15. P.G. Glugla, V.J. DeCarlo, *J. Electrochem. Soc.,* 129, 1745, 1982.
16. C. Yuh, M. Farooque, R. Johnsen, ERC, "Understanding of Carbonate Fuel Cell Resistances in MCFCs," in *Proceedings of the Fourth Annual Fuel Cells Contractors Review Meeting*, U.S. DOE/METC, Pgs. 53 - 57, July, 1992 and FCE correspondence, 2002.
17. C. Baumgartner, *J. Electrochem. Soc.,* 131, 1850, 1984.
18. W.M. Vogel, L.J. Bregoli, H.R. Kunz, S.W. Smith, in *Proceedings of the Symposium on Molten Carbonate Fuel Cell Technology,* edited by R.J. Selman and T.D. Claar, The Electrochemical Society, Inc., Pennington, NJ, Pg. 443, 1984.
19. M.L. Orfield, D.A. Shores, in *Corrosion 86,* Paper No. 88, National Association of Corrosion Engineers, Houston, TX, 1986.
20. D.A. Shores, in *Proceedings of the 22nd Intersociety Energy Conversion Engineering Conference,* Volume 2, American Institute of Aeronautics & Astronautics, New York, NY, Pg. 1023, 1987.
21. Communication with FCE, July 2002.
22. "Development of Improved Molten Carbonate Fuel Cell Technology," Final Report prepared by United Technologies Corp. for the Electric Power Research Institute, Palo Alto, CA, under Contract #RP1085-4, July 1983.

23. T.D. Kaun, in *Proceedings of the Fourth International Symposium on Molten Salts,* edited by M. Blander, D.S. Newman, M.L. Saboungi, G. Mamantov, K. Johnson, The Electrochemical Society, Inc., Pennington, NJ, Pg. 489, 1984.
24. A.J. Appleby, "Advanced Fuel Cells and Their Future Market," *Energy Conservation Strategies,* Progress Series, edited by W.E. Murphy, L.H. Fletcher, American Society of Aeronautics and Astronautics, New York, NY, date unknown.
25. A. Pigeaud, A.J. Skok, P.S. Patel, H.C. Maru, *Thin Solid Films,* 83, 1449, 1981.
26. R.A. Donado, L.G. Marianowski, H.C. Maru, J.R. Selman, *J. Electrochem. Soc.,* 131, 2541, 1984.
27. R.A. Donado, L.G. Marianowski, H.C. Maru, J.R. Selman, *J. Electrochem. Soc.,* 131, 2535, 1984.
28. R.B. Swaroop, J.W. Sim, K. Kinoshita, *J. Electrochem. Soc.,* 125, 1799, 1978.
29. M. Farooque, ERC, "Development on Internal Reforming Carbonate Fuel Cell Technology, Final Report," prepared for U.S. DOE/METC, DOE/MC/23274-2941, Pgs.. 3 - 18, October, 1990.
30. D.A. Shores, P. Singh, in *Proceedings of the Symposium on Molten Carbonate Fuel Cell Technology,* edited by R.J. Selman and T. D. Claar, The Electrochemical Society, Inc., Pennington, NJ, Pg. 271, 1984.
31. G. Kucera, K. Myles, A. Brown, M. Roche, D. Chu, E. Indacochea, "ANL's Research and Development of Alternate Components for MCFCs," *in Proceedings of the Fourth Annual Fuel Cells Contractors Review Meeting*, U.S. DOE/METC, July 1992, Pgs. 31 - 41.
32. M Farooque, H.C. Maru, “Carbonate Fuel Cells Overview,” *in Proceedings of the American Chemical Society Meeting*, August 2001.
33. N. Minh, "High Temperature Fuel Cells," in *CHEMTECH*, journal published by the American Chemical Society, Vol. 21, No. 1, January, Pgs. 32-37, 1991.
34. Y. Yamamasu, T. Kakihara, E. Kasai, T. Morita, IHI, "Component Development and Durability Test of MCFC," in *The International Fuel Cell Conference Proceedings*, NEDO/MITI, Tokyo, Japan, Pgs. 161-164, 1992.
35. H. Urushibata, T. Murahashi, MELCO, "Life Issues of Molten Carbonate Fuel Cell," in *The International Fuel Cell Conference Proceedings*, NEDO/MITI, Tokyo, Japan, Pgs. 223-226, 1992.
36. S. Takashima, K. Ohtsuka, T. Kara, M. Takeuchi, Y. Fukui, H. Fujimura, Hitachi, "MCFC Stack Technology at Hitachi," in *The International Fuel Cell Conference Proceedings*, NEDO/MITI, Tokyo, Japan, Pgs. 265-268, 1992.
37. C. Yuh, M. Farooque, “Carbonate Fuel Cell Materials,” in *Advanced Materials and Processes*, journal published by the American Society of Materials, July, 2002.
38. J. Hirschenhofer, D. Stauffer, R. Engleman, Fuel Cells A Handbook (Revision 3) prepared by Gilbert/Commonwealth, Inc. for the U.S. Department of Energy under Contract No. DE-ACO1-88FE61684, January 1994.
39. K. Tanimoto, Y. Miyazaki, M. Yanagida, S. Tanase, T. Kojima, N. Ohtori, H. Okuyama, T. Kodama, Government Industrial Research Institute, Osaka, "Cell Performance of Molten Carbonate Fuel Cell with Alkali and Alkaline Earth Carbonate Mixtures," in *The International Fuel Cell Conference Proceedings*, NEDO/MITI, Pgs. 185-188, Tokyo, Japan, 1992.

40. K. Ota, S. Mitsushima, K Kato, N. Kamiya, Yokahama National University, "Solubilities of Metal Oxides in Molten Carbonate, " in Proceedings of the Second Symposium on Molten Carbonate Fuel Cell Technology, Volume 90 - 16, The Electrochemical Society, Inc. Pennington, NJ, Pgs. 318-327, 1990.
41. T. Benjamin, et al., "Status of the M-C Power MCFC Commercialization Program," IECEC-97, Honolulu, Hawaii, July 27 - August 1, 1997.
42. A. Yuh, M. Farooque, "Carbonate Fuel Cell Materials," in *Advanced Materials and Processes*, journal published by the American Society of Materials, July, 2002.
43. H. Maru, et al., "ERC Direct Carbonate Fuel Cell Program Overview," DOE Contractor's Review Meeting, Morgantown, WV, August 26-28, 1997.
44. R.O.Petkus, "Successful Test of a 250 kW Molten Carbonate Fuel Cell Power Generator at Miramar," POWER-GEN International '97, Dallas, TX, December 1997.
45. A. Pigeaud, ERC, and G. Wilemski, Physical Sciences, "Effects of Coal-Derived Trace Species on the Performance of Carbonate Fuel Cells," *in Proceedings of the Fourth Annual Fuel Cells Contractors Review Meeting*, U.S. DOE/METC, Pgs. 42-45, July 1992.
46. D. Rastler, EPRI, G. Devore, Destec Engineering, R. Castle, Haldor Topsoe, C. Chi, ERC, "Demonstration of a Carbonate Fuel Cell Stack on Coal-Derived Gas," *in Fuel Cell Seminar.*
47. "Effects of Coal-Derived Trace Species on the Performance of Molten Carbonate Fuel Cells," Topical Report prepared by Energy Research Corporation for US DOE/METC, DOE/MC/25009-T26, October, 1991.
48. A. Pigeaud, et al., "Trace Contaminant Effects and Emissions with Integrated Coal Gasification and Cleanup," 1994 Fuel Cell Seminar, Pgs. 539-542 (1994).
49. L.J. Bregoli and H.R. Kunz, *J. Electrochem. Soc.,* 129, 2711, 1982.
50. Benjamin, et al., "Status of MCFC Technology at M-C Power-1992," 1992 Fuel Cell Seminar Program and Abstracts, 1992.
51. M.G. Gonikberg, *Chemical Equilibria and Reaction Rates at High Pressures,* Translated from Russian by M. Artment, edited by S. Monson, published for the National Science Foundation, Washington, D.C., by the Israel Program for Scientific Translations Jerusalem, Israel, Pg. 58, 1963.
52. M.G. Gonikberg, *Chemical Equilibria and Reaction Rates at High Pressures,* Translated from Russian by M. Artment, edited by S. Monson, published for the National Science Foundation, Washington, DC, by the Israel Program for Scientific Translations, Jerusalem, Israel, Pg. 133, 1963.
53. H.R. Kunz, L.A. Murphy, in *Proceedings of the Symposium on Electrochemical Modeling of Battery, Fuel Cell, and Photoenergy Conversion Systems,* edited by J.R. Selman and H.C. Maru, The Electrochemical Society, Inc., Pennington, NJ, Pg. 379, 1986.
54. T.G. Benjamin, E.H. Camara, L.G. Marianowski, *Handbook of Fuel Cell Performance,* prepared by the Institute of Gas Technology for the United States Department of Energy under Contract No. EC-77-C-03-1545, May 1980.
55. Research and Development on Fuel Cell Power Generation Technology FY1990 Annual Report, NEDO, April 1991.
56. M. Hosalaetal, "IHI Large Site Molten Carbonate Fuel Cell Advancements," *Fuel Cell Program and Abstracts* 1990 Fuel Cell Seminar, Phoenix, AR, November 25-28, 1990.
57. W.H. Johnson, "Molten Carbonate Fuel Cell Technology Improvement," Quarterly Technical Progress Report No. 23 for the Period Ending May, 1990, prepared for US DOE/METC, DOE/MC/23270-2923, September 1990.

58. D.B. Stauffer, et al., "An Aspen/SP MCFC Performance User Block," G/C Report No. 2906, July 1991.
59. J.R. Rostrup-Nielsen, in *Catalysis Science and Technology,* edited by J.R. Anderson and M. Boudart, Springer-Verlag, Berlin, German Democratic Republic, Pg. 1, 1984.
60. H.A. Leibhafsky, E.J. Cairns, *Fuel Cells and Fuel Batteries,* John Wiley and Sons, Inc., New York, NY, Pg. 654, 1968.
61. T.D. Tawari, E. Pigeaud, H.C. Maru, in *Proceedings of the Fifth Annual Contractors Meeting on Contaminant Control in Coal-Derived Gas Streams,* DOE/METC-85/6025, edited by D.C. Cicero and K.E. Markel, U.S. Department of Energy, Morgantown, WV, Pg. 425, January 1986.
62. G.H.J. Broers, B.W. Triejtel, *Advanced Energy Conversion,* 5, 365, 1965.
63. A. Baker, S. Gionfriddo, A. Leonida, H. Maru, P. Patel, "Internal Reforming Natural Gas Fueled Carbonate Fuel Cell Stack," Final Report prepared by Energy Research Corporation for the Gas Research Institute, Chicago, IL, under Contract No. 5081-244-0545, March, 1984.
64. M. Farooque, Data from ERC testing, 1992.
65. S. Kaneko, et al., "Research on On-Site Internal Reforming Molten Carbonate Fuel Cell," 1989 International Gas Research Conference, 1989.
66. M. Farooque, "Development of Internal Reforming Carbonate Fuel Cell Stack Technology," Final Report, DOE/MC/23274-2941, October 1991.
67. J.M. King, A.P. Meyer, C.A. Reiser, C.R. Schroll, "Molten Carbonate Fuel Cell System Verification and Scale-up," EM-4129, final report prepared by United Technologies Corp. for the Electric Power Research Institute, Research Project 1273-1, July 1985.
68. S.H. Lu, J.R. Selman, in *Proceedings of the Symposium on Molten Carbonate Fuel Cell Technology,* edited by R.J. Selman, T.D. Claar, The Electrochemical Society, Inc., Pennington, NJ, Pg. 372, 1984.
69. T. Tanaka, et al., "Research on On-Site Internal-Reforming Molten Carbonate Fuel Cell," 1989 International Gas Research Conference, Pg. 252, 1989.
70. G.L. Anderson, P.C. Garrigan, in *Proceedings of the Symposium on Molten Carbonate Fuel Cell Technology,* edited by R.J. Selman, T.D. Claar, The Electrochemical Society, Inc., Pennington, NJ, Pg. 297, 1984.
71. A. Pigeaud, in *Proceedings of the Sixth Annual Contractors Meeting on Containment Control in Coal-Derived Gas Streams,* DOE/METC-86/6042, edited by K.E. Markel and D.C. Cicero, U.S. Department of Energy, Morgantown, WV, Pg. 176, July 1986.
72. A. Pigeaud, "Study of the Effects of Soot, Particulate and Other Contaminants on Molten Carbonate Fuel Cells Fueled by Coal Gas," Progress Report prepared by Energy Research Corporation for U.S. Department of Energy, Morgantown, WV, under Contract No. DE-AC21-84MC21154, June 1987.
73. V. Jalan, M. Desai, C. Brooks, in *Proceedings of the Symposium on Molten Carbonate Fuel Cell Technology,* edited by R. J. Selman, T. D. Claar, The Electrochemical Society, Inc., Pennington, NJ, Pg. 506, 1984.
74. L.J. Marianowski, *Prog. Batteries & Solar Cells,* 5, 283, 1984.
75. W.V. Vogel and S.W. Smith, *J. Electrochem. Soc.,* 129, 1441, 1982.
76. S.W. Smith, H.R. Kunz, W.M. Vogel and S.J. Szymanski, in *Proceedings of the Symposium on Molten Carbonate Fuel Cell Technology,* edited by R.J. Selman and T.D. Claar, The Electrochemical Society, Inc., Pennington, NJ, Pg. 246, 1984.

77. R.J. Remick, E.H. Camara, paper presented at the Fall Meeting for The Electrochemical Society, Inc., New Orleans, LA, October 7-12, 1984.
78. R.J. Remick, in *Proceedings of the Fourth Annual Contractors Meeting on Contaminant Control in Hot Coal-Derived Gas Streams,* DOE/METC-85/3, edited by K. E. Markel, U.S. Department of Energy, Morgantown, WV, Pg. 440, May 1984.
79. M.C. Williams, D.A. Berry, "Overview of the DOE-Funded Fuel Cell Contaminants R&D Program," Fuel Cell Seminar Program and Abstracts, 1990 Fuel Cell Seminar, Phoenix, AR, November 25-28, 1990.
80. P.S. Patel, S.M. Rich, H.C. Maru, in *Proceedings of the Fourth Annual Contractors Meeting on Contaminant Control in Hot Coal-Derived Gas Streams,* DOE/METC-85/3, edited by K. E. Markel, U.S. Department of Energy, Morgantown, WV, Pg. 425, May 1984.
81. G.L. Anderson, F.O. Berry, G.D. Harmon, R.M. Laurens, R. Biljetina, in *Proceedings of the Fifth Annual Contractors Meeting on Contaminant Control in Coal-Derived Gas Streams,* DOE/METC-85/6025, edited by D.C. Cicero, K.E. Markel, U.S. Department of Energy, Morgantown, WV, Pg. 87, January 1986.
82. T.P. Magee, H.R. Kunz, M. Krasij, H.A. Cole, "The Effects of Halides on the Performance of Coal Gas-Fueled Molten Carbonate Fuel Cell," Semi-Annual Report, October 1986 - March 1987, prepared by International Fuel Cells for the U.S. Department of Energy, Morgantown, WV, under Contract No. DE-AC21-86MC23136, May 1987.
83. G.N. Krishnan, B.J. Wood, G.T. Tong, M.A. Quinlan, in *Proceedings of the Fifth Annual Contractors Meeting on Contaminant Control in Coal-Derived Gas Streams,* DOE/METC-85/6025, edited by D.C. Cicero and K.E. Markel, U.S. Department of Energy, Morgantown, WV, Pg. 448, January 1986.
84. E.A. Gillis, *Chem. Eng. Prog.,* 88, October 1980.
85. T. Tanaka, et al., "Development of Internal Reforming Molten Carbonate Fuel Cell Technology," in *Proceedings of the 25th IECEC*, American Institute of Chemical Engineers, New York, NY, August 1990.
86. M. Miyazaki, T. Okada, H. Ide, S. Matsumoto, T. Shinoki, J. Ohtsuki, "Development of an Indirect Internal Reforming Molten Carbonate Fuel Cell Stack," in the 27th Intersociety Energy Conversion Engineering Conference Proceedings, San Diego, CA, August 3-7, 1992, Pg. 290, 1992.
87. W.H. Johnson, "International Fuel Cells MCFC Technical Accomplishment," in *Proceedings of the Second Annual Fuel Cells Contractor's Review Meeting*, US DOE/METC, May 1990.
88. T. Benjamin, G. Rezniko, R. Donelson, D. Burmeister," IMHEX^{R} MCFC Stack Scale-Up," in the *Proceedings of the 27th Intersociety Energy Conversion Engineering Conference*, Vol. 3, San Diego, CA, Aug. 3-7, 1992, Pg. 290, 1992.
89. H.C. Maru, B.S. Baker, *Prog. Batteries & Solar Cells*, 5, 264, 1984.
90. M. Faroogue, G. Steinfield, H. Maru, "Comparative Assessment of Coal-Fueled Carbonate Fuel Cell and Competing Technologies," in *Proceedings of the 25th IECEC*, Vol. 3, American Institute of Chemical Engineers, New York, NY, 1990.
91. H.C. Maru and M. Farooque, FCE, “Molten Carbonate Fuel Cell Product Design Improvement,” Prepared for U.S. DOE/DARPA, Annual Report, DE-FC21-95MC31184, Pages 5-9, December 1999.
92. H.C. Maru and M. Farooque, FCE, “Molten Carbonate Fuel Cell Product Design Improvement,” Prepared for U.S. DOE/DARPA, Annual Report, DE-FC21-95MC31184, Pages 4-10, December 2000.

93. ERC correspondence, laboratory data, March 1998.
94. M. Farooque, data from ERC testing, 1992
95. S. Katikaneni, C. Yuh, S. Abens and M. Farooque, "Catalysis Today, 2002".
96. S. Katikaneni, C. Yuh and M. Farooque, "The Direct Carbonate Fuel Cell Technology: Advances in Fuel Processing and Internal Reforming," ACS Fuel Chemistry, 46(2) 685-688, Preprints, 2001.
97. J. Ding, et al., "A Computer Model for Direct Carbonate Fuel Cells," Proceedings of the Fourth International Symposium on Carbonate Fuel Cells, 191st Electrochemical Society Meeting, Montreal, May 1997.
98. J. Ding, P. S. Patel, M. Farooque, H. C. Maru, in Carbonate Fuel Cell Technology IV, (eds. J. R. Selman, et al.), The Electrochemical Society, Inc., New Jersey, Pg. 127-138, 1997.

7. SOLID OXIDE FUEL CELLS

Solid oxide fuel cells (SOFCs) have an electrolyte that is a solid, non-porous metal oxide, usually Y_2O_3-stablilized ZrO_2. The cell operates at 600-1000 ^oC where ionic conduction by oxygen ions takes place. Typically, the anode is a Ni-ZrO_2 cermet and the cathode is Sr-doped $LaMnO_3$. There is no liquid electrolyte with its attendant material corrosion or electrolyte management problems. The high temperature of the SOFC, however, places stringent requirements on its materials. The development of suitable low cost materials and the low-cost fabrication of ceramic structures are presently the key technical challenges facing SOFCs.

The cell is constructed with two porous electrodes that sandwich an electrolyte. Air flows along the cathode. When an oxygen molecule contacts the cathode/electrolyte interface, it acquires electrons from the cathode. The oxygen ions diffuse into the electrolyte material and migrate to the other side of the cell where they contact the anode. The oxygen ions encounter the fuel at the anode/electrolyte interface and react catalytically, giving off water, carbon dioxide, heat, and electrons. The electrons transport through the external circuit, providing electrical energy.

Solid oxide fuel cells (SOFC) allow conversion of a wide range of fuels, including various hydrocarbon fuels. The relatively high operating temperature allows for highly efficient conversion to power, internal reforming, and high quality by-product heat for cogeneration or for use in a bottoming cycle. Indeed, both simple-cycle and hybrid SOFC systems have demonstrated among the highest efficiencies of any power generation system, combined with minimal air pollutant emissions and low greenhouse gas emissions. These capabilities have made SOFC an attractive emerging technology for stationary power generation in the 2 kW to 100s MW capacity range.

More recently, (planar) SOFC systems with high power densities operating at lower temperatures (700 to 850 °C instead of 900 to 1000 °C as was previously the norm) have been developed. Combined with the ability of SOFC to use conventional fossil fuels, this could help reduce the cost of the fuel cell because less-expensive materials of construction could be used at lower temperatures. This would improve the economy of applications ranging from small-scale stationary power (down to ~2 kW) to auxiliary power units for vehicles and mobile generators for civilian as well as military applications. There is even the possibility that SOFC could eventually be used for part of the prime power in vehicles. The present challenge for developers is to produce robust, high-performance stack technologies based on suitable low-cost materials and fabrication methods. Derivatives from SOFC technology, such as oxygen sensors used in automobiles, are already in widespread commercial use.

This chapter provides an overview of the key features and characteristics of SOFC, along with descriptions of the main types of SOFC and their performance. Those readers interested in greater detail, as well as an excellent history of SOFC development, are referred to Singhal and Kendall (1), and other references listed at the end of this chapter.

7.1 Cell Components

The major components of an individual SOFC cell include the electrolyte, the cathode, and the anode. Fuel cell stacks contain an electrical interconnect, which links individual cells together in series or parallel. The electrolyte is made from a ceramic such as yttria-stabilized zirconia (YSZ) and functions as a conductor of oxide ions. Oxygen atoms are reduced into oxide ions on the porous cathode surface by electrons, and then flow through the ceramic electrolyte to the fuel-rich porous anode where the oxide ions react with fuel (hydrogen), giving up electrons. The interconnect serves to conduct the electrons through an external circuit.

7.1.1 Electrolyte Materials

As indicated by their name, SOFCs use solid oxide ceramics, typically perovskites, as the electrolyte. Nernst (2) realized in the 1890s that certain perovskites, stabilized zirconias, conducted ions in a certain temperature range. Baur and Preis (3) demonstrated in 1943 that such electrolytes could be used as (oxygen) ion conductors in fuel cells. Currently, yttrium stablilized zirconia (3, 8, or 10 percent yttria, abbreviated to YSZ) is the most commonly used electrolyte for SOFC. YSZ provides high conductivity at temperatures above 700 °C (Figure 7-1, (4, 5, 6)), while exhibiting negligible electronic conductivity at these temperatures (above 1500 °C it becomes an electronic conductor). In a fuel cell operating with a current density of 250 mA/cm^2 at 1000 °C and an electrolyte of 200 μm thickness, the resistance loss in the electrolyte would be 50 mV. However, for mechanical reasons it is desirable to operate the SOFC at lower temperatures. To operate at 800 °C, the electrolyte thickness would have to be reduced by about an order of magnitude to maintain a similar ohmic loss in the electrolyte.

Colloidal fabrication and co-sintering processes have emerged, whereby YSZ membranes are produced as thin films (~10 μm) on porous electrode structures. These thin-film membranes improve performance and reduce operating temperatures of SOFCs. To enable these colloidal processes to be successful, finer YSZ powders are needed. These applications require nano-scale powders with BET surface areas of 100 to 120 m^2/g and the use of suspensions ranging from 10 to 40 percent solid content (7, 8).

Alternative electrolytes have been considered and are being developed. As shown in Figure 7-1, scandium-doped zirconia (SDZ) is more conductive than YSZ, permitting a further reduction of the operating temperature by 50 to 100 °C. Gadolinium-doped ceria is even more conductive, but is partially reduced in hydrogen at temperatures above 600 °C; formation of Ce^{+3} ions generates electron holes that make ceria electronically conductive, thus short-circuiting the cell.

A substantially more conductive material that is stable in air and hydrogen was discovered by Goodenough (9). Lanthanum gallate with strontium doping on the A-site of the perovskite and magnesium on the B-site could be used at temperatures as low as 600 °C even on a thick electrolyte. Laboratory fuel cells with this electrolyte have been tested, but the typical

challenges of matching the thermal expansion coefficients, mechanical strength, and chemical compatibilities need further development.

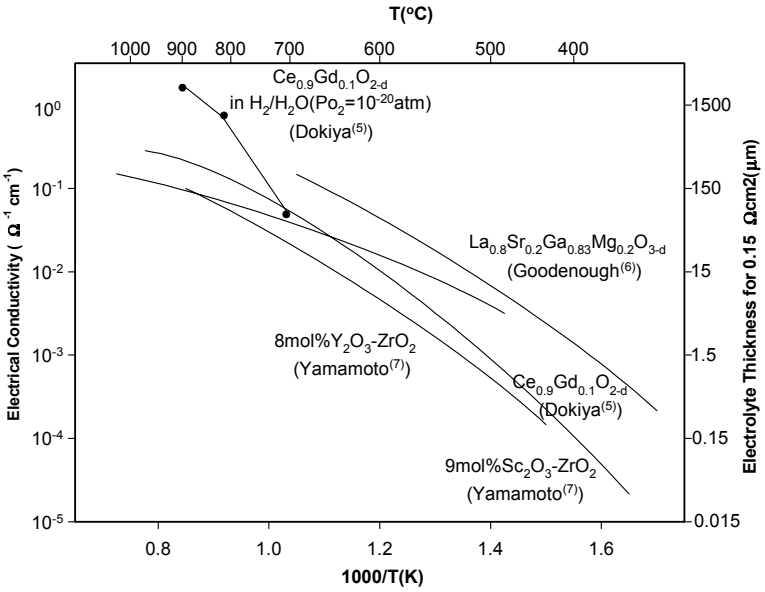

Figure 7-1 Electrolyte Conductivity as a Function of Temperature (4, 5, 6)

All of the above-mentioned solid electrolytes are oxygen conductors. An automatic consequence of this is that, as in molten carbonate fuel cells, the products of electrochemical reactions all end up on the anode side. While is beneficial for internal reforming and water gas shift reaction (which utilizes the water produced as a reactant), it dilutes the fuel, and at high utilization it can significantly reduce the Nernst potential.

It has been shown that solid electrolytes can be made to conduct protons (10, 11, 12, 13). While these electrolytes are still in a very early stage of development, such proton conductors might eventually overcome some of the limitations of cells as oxygen ion conductors.

7.1.2 Anode Materials

Although a wide range of materials has been considered as anode materials for SOFC (14), most developers today use a cermet of nickel and YSZ. Early on in the development of SOFC, precious metals such as platinum and gold were used, as well as pure transition metals such as nickel and iron. Because of the physical and chemical instability of these materials, other materials such as nickel aluminide were tested.

Finally, in 1970, Spacil (15) recognized that a composite of nickel and YSZ particles could provide a stable and highly active anode. The composition of the anode, particle sizes of the powders, and the manufacturing method are key to achieving high electrical conductivity, adequate ionic conductivity, and high activity for electrochemical reactions and reforming and shift reactions. Reduction of the NiO powder in the virgin anode mixture to Ni results in the desired porosity. For the more recent anode-supported cells, it also achieves good mechanical properties and maintains geometric stability during manufacture and operation. For example, by

using a combination of coarse and fine YSZ powder, mechanical strength can be ensured while also achieving the desired contact between the Ni phase and the YSZ phase. In some modern cell designs, a graded anode is used to achieve coarse porosity and high mechanical strength in most of the anode, and fine micro-porosity in the anode zone immediately adjacent to the electrolyte. Despite the relative success of the Ni-YSZ anode, it has drawbacks:

- Sensitivity to sulfur and other contaminants. Strong reversible poisoning of the anode occurs at feed concentrations ranging from about 1 ppm H_2S when operating at 1000 °C down to less than 50 ppb when operating at 750 °C (See Figure 7-2a (16, 17)). These concentrations require desulfurization of the anode feed, even if it is produced from low-sulfur fuels such as natural gas or ultra-low sulfur diesel or gasoline (See Figure 7-2b). No data is available publicly on the impact of other species (water or hydrocarbons) or different sulfur species on sulfur tolerance, or on the effect after long periods of time (e.g. 40,000 hours or more). Another strong anode poison reported is HCl. Poisoning by these species is reversible after exposure at low concentrations, but irreversible after exposure at concentrations above about 200 ppm.
- Oxidation reduction intolerance. Ni-YSZ anodes are made by mixing NiO with YSZ and then reducing the NiO to Ni. However, if the anode is subsequently exposed to air, especially at elevated temperatures, the Ni re-oxidizes readily. Because of the large volume change during the reduction/oxidation of the anode, the anode's structure and strength are severely compromised. Effectively, the anodes must be kept under reducing conditions at all times.
- The thermal expansion coefficient of the anode is substantially higher than the electrolyte and cathode. In anode-supported designs, this can lead to mechanical and dimensional stability problems, especially during thermal cycling.
- Poor activity for direct oxidation of hydrocarbons and propensity for carbon formation when exposed to hydrocarbons. To improve the activity for direct oxidation and reduce the anode's propensity for carbon formation, copper – ceria anodes are being developed.

Even though these drawbacks can typically be mitigated by appropriate system design, many consider that better anodes will be needed. To improve the sulfur tolerance and reduction oxidation tolerance of the anodes, several groups are working on oxide-based anodes. Researchers at PNNL have demonstrated sulfur tolerance up to 100 ppm, at least for short times. In addition, as expected, the oxide-based anodes provide excellent oxidation/reduction stability. However, activity for hydrogen oxidation must still be improved to be competitive with Ni-YSZ anodes. In addition, though little experimental data exists, one would expect that these anodes must be modified to provide adequate activity for reforming and water gas shift reactions.

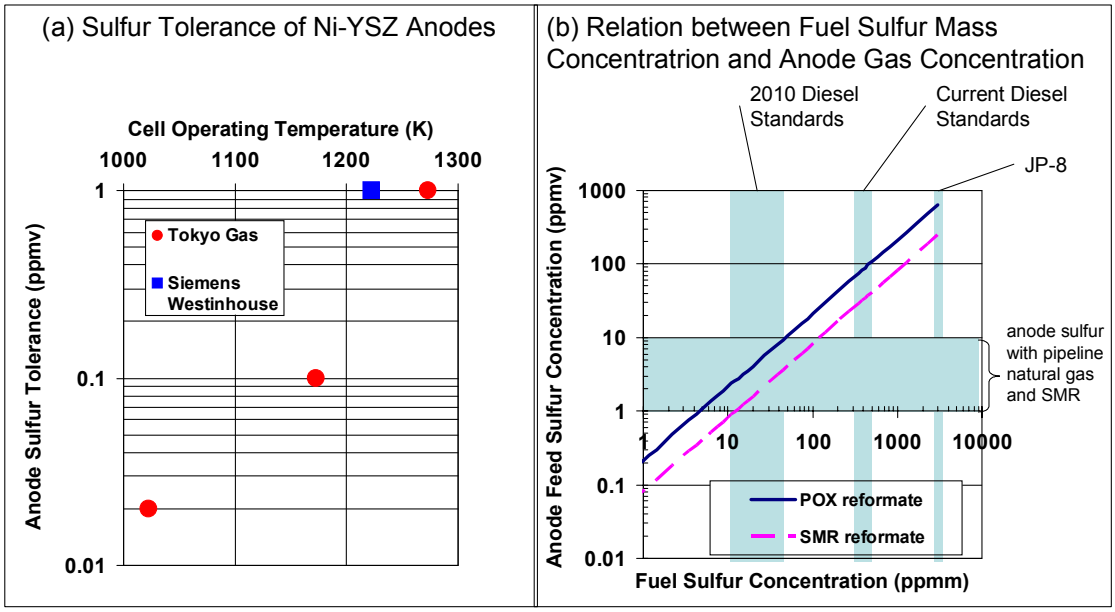

Figure 7-2 (a) Sulfur Tolerance of Ni-YSZ Anodes (16, 17) and (b) Relationship between Fuel Sulfur and Anode Sulfur Concentration.

7.1.3 Cathode Materials

Most cathode materials used in SOFC today are lanthanum-based perovskite materials (structure ABO_3). During early development, platinum and other noble metals, and even magnetite (14), were used as cathode materials for SOFC. They are no longer pursued actively because of chemical and physical instability, incompatibility with most electrolytes, and, in the case of platinum, cost. Currently, most cathodes are based on doped lanthanum manganites. In high-temperature SOFC (operating temperature ~1000 °C), strontium-doped $LaMnO_3$ (LSM) is used. The choice of this material is a compromise between a number of factors:

- Chemical stability and relatively low interactions with electrolyte. With YSZ electrodes, many La-based compounds form the insulating $La_2Zr_2O_7$. With ceria-based electrolytes, this issue is not a concern and other cathode materials are considered (e.g. $(La,Sr)(Co,Fe)O_3$ or LSCF).
- Adequate electronic and ionic conductivity. Though the conductivities are adequate, the ionic conductivity of LSM is significantly lower than YSZ, and its electronic conductivity is a fraction of any of the metals or even of lanthanum chromite. Consequently, ionic and electronic resistance can become a significant factor, especially in cell designs that incorporate long current paths through the cathode. For lower-temperature cells, conductivity of LSM is inadequate, and other materials, such as strontium-doped lanthanum ferrite (LSF) are considered.
- Relatively high activity.
- Manageable interactions with ceramic interconnects (notably lanthanum chromite). Though some interdiffusion occurs, this does not represent a major problem.
- Thermal expansion coefficients that closely match those of YSZ.

Accordingly, the good compatibility with YSZ and the high electro-catalytic activity make LSM the cathode material of choice of SOFCs operating around 1000 °C.

For intermediate-temperature operation (700 to 800 °C), a composite layer (typically 20 to 40 µm thick) of YSZ and LSM is often used to overcome the modest ion conductivity at lower temperatures (18, 19, 20). Alternatively, LSCF or LSF are also pursued for such applications.

A serious challenge in the use of LSM as a cathode material in intermediate temperature SOFC stems from the use of metallic interconnects. Many of these metals contain chromium, which forms a stable protective oxide (chromia) layer with reasonable conductivity (see Section 7.1.4 on interconnects for more details). However, chromia vapors can lead to serious poisoning of the cathode (21, 22). Although one might attribute this problem more to the interconnect material than to the cathode, the poisoning effect was found to depend strongly on the electrolyte/cathode material combination.

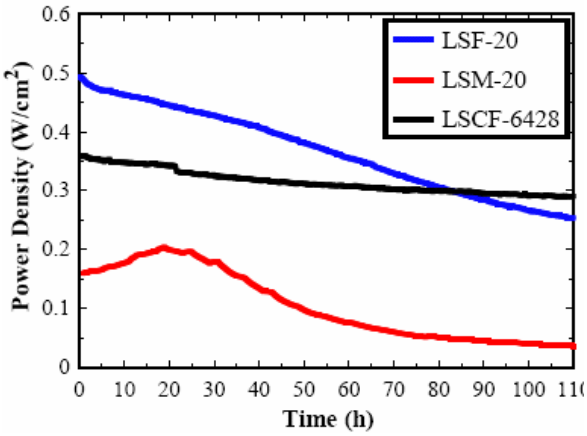

Figure 7-3 Impact of Chromia Poisoning on the Performance of Cells with Different Electrolytes (From (21))

For low-temperature operation (below 700 °C), the use of LSM as the cathode material represents significant potential loss, and other materials are being pursued.

7.1.4 Interconnect Materials

Broadly, interconnect materials for SOFC fall into two categories: conductive ceramic (perovskite) materials for operation at high temperature (900 to 1000 °C) and metallic alloys for lower temperature operation. Though the shape of SOFC interconnects depends heavily on the cell and stack design, the materials choice is almost entirely determined by physical and chemical stability under operating conditions.

The ceramic interconnects used in higher temperature SOFCs are primarily doped lanthanum and yttrium chromites (dopants typically include Mg, Sr, Ca, Ca/Co). These perovskites are unique in that they exhibit high electronic conductivity and resist reduction under exposure to syngas at high temperatures. Electronic conductivity of these materials increases with temperature (making them unsuitable for use at low temperatures). At 1,000 °C the conductivities of these materials

range from 1 to around 30 S/cm, with an activation energy of 12 to 19 kJ/mol, depending on dopant and dopant level. The dopant levels also control thermo-mechanical properties and compatibility with electrode or electrolyte materials. Lanthanum chromite-based interconnects have shown to be stable in cells for as much as 69,000 hrs (23). However, one problem with ceramic interconnects is that they are rigid and weak, similar to the ceramic cells: there is no flexibility in any of the components to ensure good contact pressure. In some designs that use ceramic interconnects, a contact felt (23) or conductive contact paste is used. Unfortunately, the reliability of this component is not as good as the interconnect.

In the past ten years, with the development of thin-electrolyte anode-supported SOFC operation at lower temperatures (lower than 800 °C), the prospect of using metallic interconnects arose. However, even at temperatures ranging from 650 to 800 °C, typical state-of-the-art anode-supported SOFC operating conditions and design requirements for metallic interconnects are challenging. For example:

- High operating temperature in excess of the drop-off in creep strength for many common metals and thermal cycling. At the same time, the interconnect must maintain uniform contact (usually requiring some pressure) with the electrodes.
- Exposure (at least on one side) to strongly oxidizing environment, while at the same time requiring low contact resistance with the electrodes. This is a challenge because many of the stable oxides that protect high-temperature alloys from corrosion (see Figure 7-4) such as alumina and silica) have very low conductivities. The most commonly-used stable oxide that does have some electronic conductivity (chromia) leads to evaporation and electrode poisoning.

Early on, metallic interconnects for cells operating at around 900 °C included high-chrome alloys (notably the Cr5Fe1Y_2O_3 developed by Plansee A.G. and Siemens (24, 25). Aside from potential for electrode poisoning, the high chrome content results in a high materials cost. Because these alloys are typically formed using powder metallurgy followed by machining, processing results in an expensive interconnect.

Lower operating temperatures would allow the use of ferritic steels, that could reduce the materials cost, and ferritic steels are typically easier to process with low-cost processing techniques. The corrosion resistance of steel depends on the formation of stable oxide layers on the surface (Figure 7-5). After extensive testing of commercial compositions, it was concluded that none possessed the corrosion resistance required, especially to withstand the thermal cycling requirements while still providing adequate contact resistance. Efforts were undertaken to develop more suitable compositions, which led to the development of several special alloys. Many developers now use the Krupp formulation Crofer22 APU.

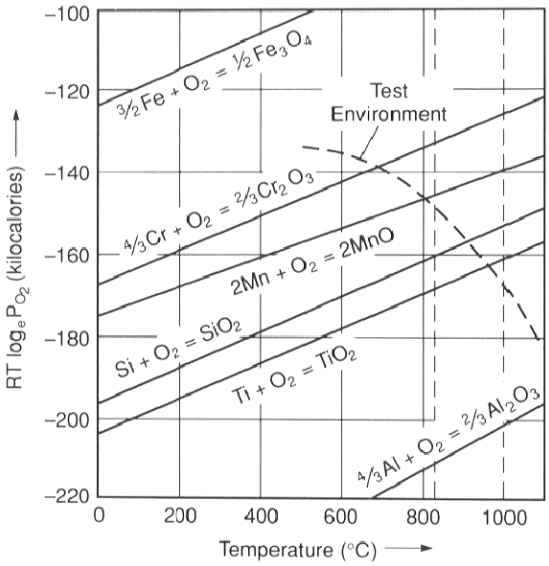

Figure 7-4 Stability of Metal Oxides in Stainless Steels (26, 27)

To ensure good contact resistance (primarily with the cathode) and minimize evaporation of chromia, many developers use interconnect coatings of strontium-doped lanthanum cobaltite or manganite, which have proven effective for at least several thousand hours.

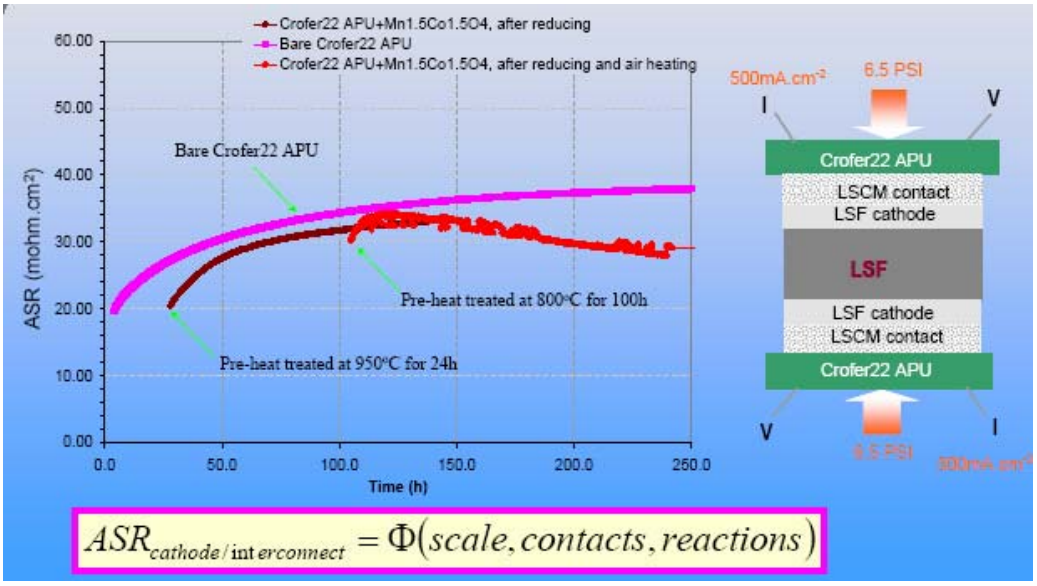

Figure 7-5 Impact of LSCM Contact Layer on Contact Resistance in Cell with Metal Interconnect (from (28)).

With these improvements, interconnects can be made that function in intermediate temperature SOFCs, although several additional improvements may still require attention to allow the construction of commercially viable products:

- Further improvement in contact resistance, especially after long exposure and thermal cycling
- Further improvements in corrosion resistance, especially after long exposure and thermal cycling
- Improved performance and mechanical stability of the coatings
- Low-cost manufacturing methods for materials, shapes, and coatings
- Improved creep strength to increase design flexibility for cells

SOFC anodes are fabricated from composite powdered mixtures of electrolyte materials (YSZ, GDC, or SDC) and nickel oxide. The nickel oxide is subsequently reduced to nickel metal prior to operation. The NiO/YSZ anode material is suited for applications with YSZ material, whereas NiO/SDC and NiO/GDC anode materials are best used with ceria-based electrolyte materials. Typical anode materials have nickel content of approximately 40 volume percent after reduction of the nickel oxide to nickel. Depending upon the application, powders have surface areas of 15 to 20 m^2/g for screen-printing and 5 to 10 m^2/g for tape casting.

7.1.5 Seal Materials

The challenges of sealing the oxidant from fuel in planar SOFC stacks is significant, hence a sub-section is devoted to potential seal materials here. The function of SOFC seals includes:

- Prevent mixing of fuel and oxidant
- In some configurations, prevent mixing of reactants with the ambient environment
- In some configurations, provide mechanical bonding of components
- In some designs, provide electrical insulation between stack components

Seal materials must be chemically and physically stable at operating conditions. In some applications (e.g. in on-road vehicles), the seal must also be able to withstand acceleration forces associated with vibration and shock. Finally, seal materials must be low in cost and amenable to low-cost stack manufacturing methods.

These requirements are tough to meet simultaneously. For example, the chemical stability of a material may be acceptable under either oxidizing or reducing environments. However, mechanistic characterizations have shown that when relatively thin pieces of material are exposed to both atmospheres, rapid deterioration occurs.(29). Seal designs are highly specific to particular cell and stack designs and, consequently, seal designs are often proprietary. Some tubular and monolithic designs require no seals at all. Planar designs typically require multiple seals per repeat unit, and even in planar designs the length of the seals can vary by two or three orders of magnitude for a given area cell depending on design. A number of possible seal types is shown in Figure 7-6 for a rectangular planar cell with metal interconnects.

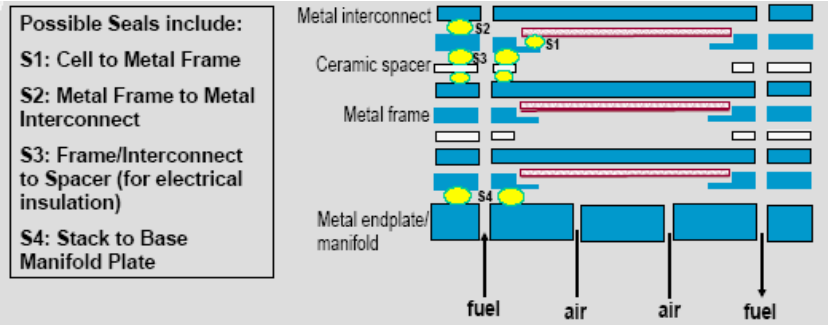

Figure 7-6 Possible Seal Types in a Planar SOFC (from (29))

The requirements, material choices, and general sealing concepts are common to most planar SOFC stack designs. Fundamentally, two different types of seals are being developed for SOFC: bonded and compressive seals.

Bonded Seals

Bonded seals can be rigid or compliant. A hermetic seal is achieved through adhesive forces between the seal material and both surfaces against which the seal is to work. Naturally, the seal material must have good adhesive properties (good wettability of the material to be sealed). Some are designed to remain flexible over the operating range of the cell, while others are meant to be rigid. To use the rigid type of seal, the thermal expansion coefficient of the seal material and all other components must be closely matched. If the seal is compliant, the thermal expansion coefficient matching requirements are somewhat relaxed. The bonding temperature for this type of seal should lie between the operating temperature and the stability limit for the other cell materials. There are several common sub-types of bonded seals currently under consideration for SOFC applications. Glass and glass-ceramic seals are perhaps the most common. This type of seal is attractive because:

- Viscous/wetting behavior of glass facilitates hermetic sealing
- They are inexpensive and easy to manufacture and apply
- Wide range of compositions of glass and ceramics allows tailoring some of the key properties (e.g. thermal expansion coefficient glass transition temperature)
- Glass-ceramics can be designed to avoid viscous flow and uncontrolled progressive crystallization during operation

However, glass-ceramic seals also exhibit disadvantages:

- They are brittle, leading to seal and even cell failures during cool-down;
- Despite control, few glass systems allow a match of thermal expansion coefficient to other important cell materials (typically alkaline earth-alumina-silica glasses). In any case, the cell materials don't match each other close enough to allow a rigid seal in larger cells
- Many glasses interact with adjacent cell components, especially with the interconnects
- Some of the constituents of glass volatilize during operation (e.g. silica, borate, and alkali metals). These constituents will likely foul or poison the electrode catalyst or interact in an undesirable manner with other cell components

Metal brazes, which use a molten metal filler to ensure sealing, provide some attractive features:

- Molten metal facilitates hermetic sealing
- Easy to fabricate
- Properties can be tailored by judicious choice of composition

However, several factors limit their application in SOFC:

- Brazes are electrically conductive, making them unsuitable of most seal types
- Few braze materials are compatible with SOFC operating conditions. Noble metals are considered too expensive in most SOFC stack designs. Silver is less expensive, but its use in a dual (oxidizing and reducing) environment can lead to chemical instability

In addition to the benefits listed above, bonded seals result in compact structures, as no load-frame or other means to apply pressure is required. However, in cells with metal interconnects, the mismatch in thermal expansion may be too great for the use of rigid seals. For example, Figure 7-7 shows that in a typical cell 10 cm across, the relative movement of the edges of the interconnect with respect to the edges of the anode is almost 100 μm. Compare that with the typical thickness of the seal (around 200 μm) and consider that the shear stresses on the seal would build up to around 17 MPa (30): far too much for the rigid glass or glass-ceramic seals to withstand. To date, no compliant bonded seals have been identified or developed.

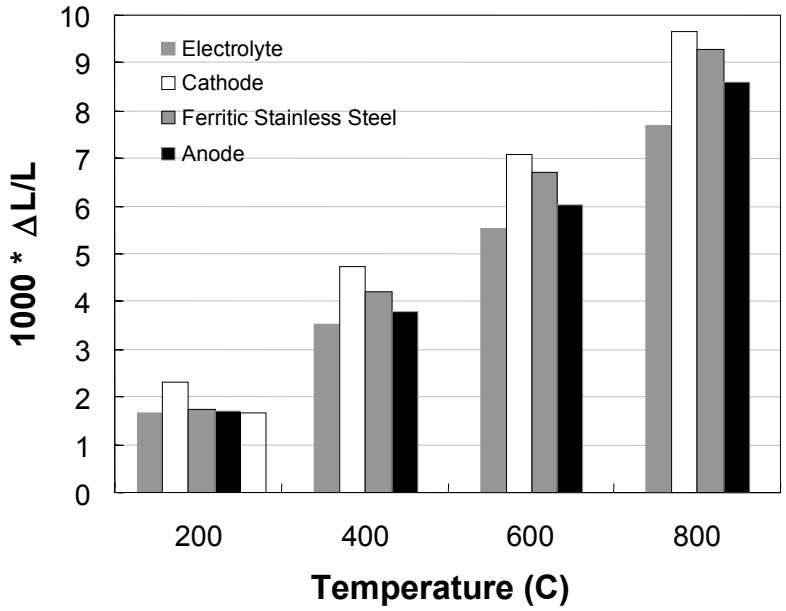

Figure 7-7 Expansion of Typical Cell Components in a 10 cm x 10 cm Planar SOFC with Ni-YSZ anode, YSZ Electrolyte, LSM Cathode, and Ferritic Steel Interconnect.

Compressive Seals

A hermetic seal is achieved by pressing the seal material between the surfaces to be sealed. The seal material must be elastic over the operating temperature range, and sufficiently soft to fill the micro-roughness on the surfaces to be sealed. Compressive seals offer several advantages (29):

- Mechanically "de-couple" adjacent stack components, thus reducing thermal stress during cycling
- Thermal expansion matching requirements between cell components may be somewhat relaxed (though electrical contact considerations may still require this)
- Some are easy and inexpensive to fabricate

However, there are also barriers to overcome (29):

- Difficult to achieve a hermetic seal with some materials unless "soft seat" interlayer is provided
- Few materials and structures are compliant and provide a hermetic seal at the operating temperatures
- A load frame is required to provide compression to all seals. This type of hardware is potentially bulky and expensive. If (portions of the) load frame must be kept at lower temperatures than the stack itself, packaging and insulation is significantly complicated, especially if multiple stacks are to be combined for larger-capacity systems
- Other stack components must be designed to withstand prolonged pressure. This can be a challenge, given that creep strength of the metals used in the interconnect is typically very low (in the 700 to 800 °C operating temperature range typical for state-of-the-art planar cells)
- To the extent that electrical contact between cell components depends on controlled pressure, balancing these pressure requirements with those of the seal can be a challenge for the cell designer

Recently, mica and hybrid mica seals have been developed as a viable technology. Mica seals were found to have many desirable characteristics, such as the ability to withstand thermal cycling, but exhibited unacceptable leak rates. When a thin layer of glass is inserted on either side of the seal to fill the voids between the seal and the other stack components, the leak rate was substantially reduced while other desirable properties were retained.

Figure 7-8 shows the leak rate can be reduced to about 0.05 to 0.2 sccm/cm (which translates into less than 1 percent of the fuel for typical 10 cm x 10 cm cells) for at least several dozen cycles.

While this progress is encouraging, the long-term physical and chemical stability of all seal types considered for SOFC still require additional improvement.

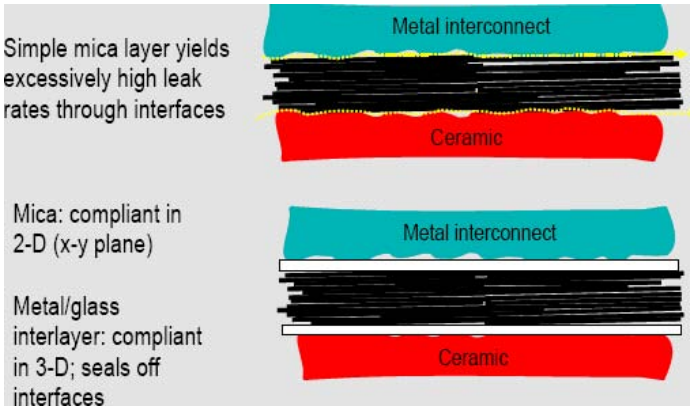

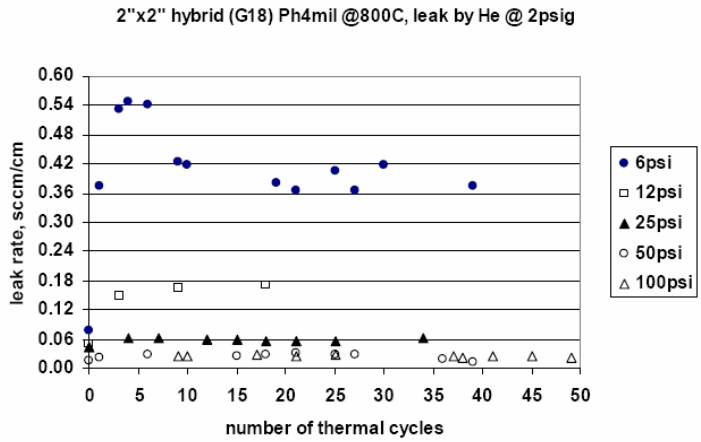

Figure 7-8 Structure of Mica and Mica-Glass Hybrid Seals and Performance of Hybrid Seals (29)

7.2 Cell and Stack Designs

Two types of cell designs are being pursued for SOFC: tubular cells and planar cells. The interest in tubular cells is unique to SOFC: all other types of fuel cells focus exclusively on planar designs. In SOFC, the benefit of a simple sealing arrangement potentially outweighs the disadvantages of low volumetric power density and long current path that are inherent in tubular cell geometries.

7.2.1 Tubular SOFC

Although the Siemens Westinghouse design of tubular SOFC is by far the best-known and most developed, two other types of tubular SOFCs, shown in Figure 7-9 illustrate ways in which the cells are interconnected. Numerous other designs have been proposed, but are no longer pursued (14).

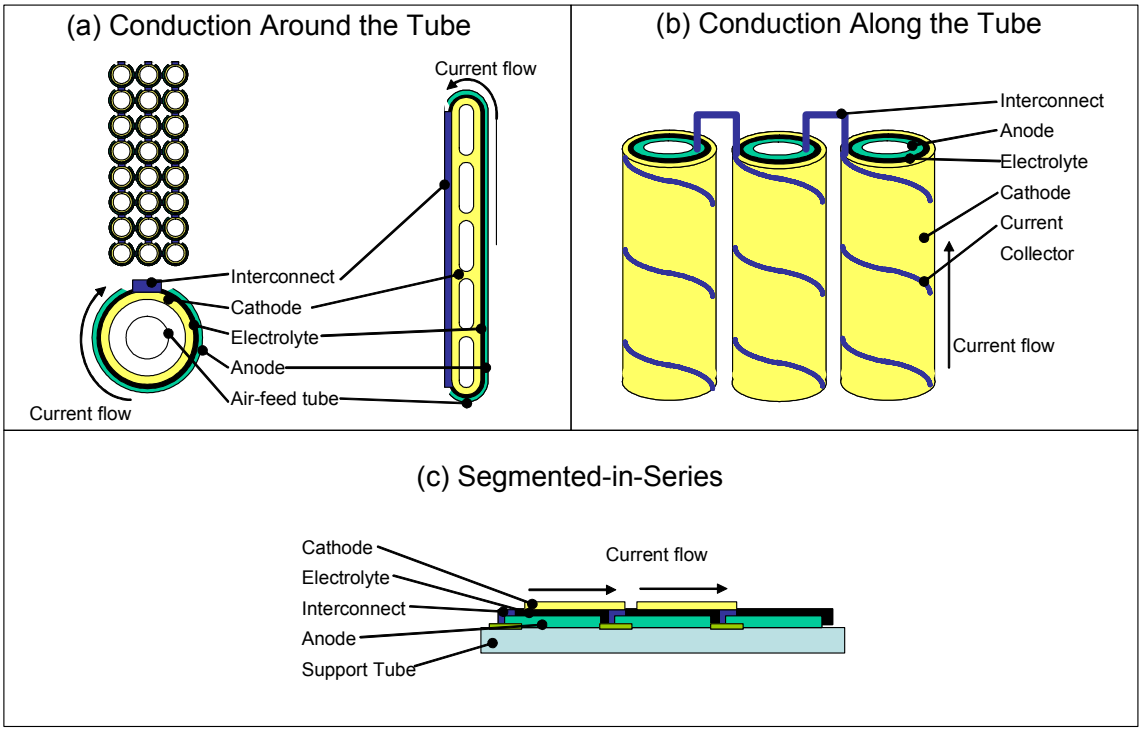

Figure 7-9 Three Types of Tubular SOFC: (a) Conduction around the Tube (e.g. Siemens Westinghouse and Toto (31)); (b) Conduction along the Tube (e.g. Acumentrics (32)); (c) Segmented in Series (e.g. Mitsubishi Heavy Industries, Rolls Royce (33, 34)).

Inevitable in tubular designs is conduction of the current in the plane of the electrolyte over significant distances:

- In the Siemens Westinghouse technology, this current is conducted tangentially around the tube. Toto, in Japan, follows an almost identical approach. Each tube contains one cell. Tubes are connected either in series or in parallel. In a refinement on this approach to shorten the current path and increase volumetric power density, the tube can be flattened and ribs added
- In micro-tubular SOFC technology (e.g. Acumentrics), current is conducted axially along the tube. Interconnections are made at the end of the tube using various proprietary interconnection systems that connect cells within the stack. To minimize the in-plane resistance on the cathode side, a metallic current collector (typically silver) is applied. Acumentrics has shown the technology to be capable of repeated thermal cycling. Typical tube dimensions and performance are shown in Figure 7-10. The cells have been integrated into 2 kW stacks.

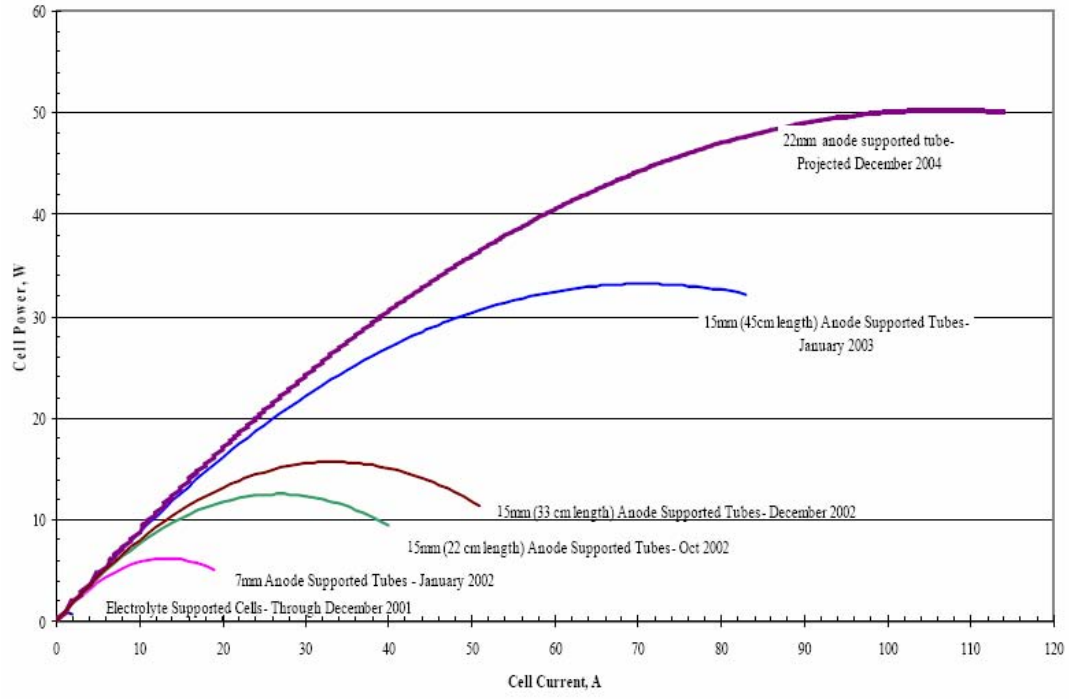

Figure 7-10 Cell Performance and Dimensions of Accumentrics Technology (32).

- In segmented-in-series tubular SOFC technology, the tube's active cell area is segmented and connected in series. As a consequence, the length over which in-plane conduction occurs can be controlled by the cell segmentation pattern. Another consequence of segmentation in series is that the voltage per tube is higher, and hence the total current lower, requiring less heavy-duty interconnections between tubes. Mitsubishi Heavy Industries has developed this approach with cylindrical tubes and constructed both atmospheric and pressurized 10 kW stacks, achieving power densities of around 140 mW/cm^2 (35, 36). Rolls Royce is developing a version with flattened tubes (34).

The remainder of this section on tubular SOFC focuses on the cell design furthest advanced in its development: the Siemens Westinghouse tubular SOFC technology.

Tubular SOFC Cell Manufacturing Method

A schematic cross-section of the Siemens Westinghouse cell is shown in Figure 7-11. Air is fed through an alumina feed tube, while fuel is supplied externally. The cell length has been gradually increased from 30 cm to about 150 cm. The cell has a diameter of 1.27 cm. Figure 7-12 shows a bundle of eighteen cells that features 3 cells in series with 6 cells in parallel. To ensure good contact between tubes, nickel felt is used. Because the current flows tangentially to the electrodes, a relatively large ohmic loss exists, especially in the cathode, which places an upper limit on the tube diameter.

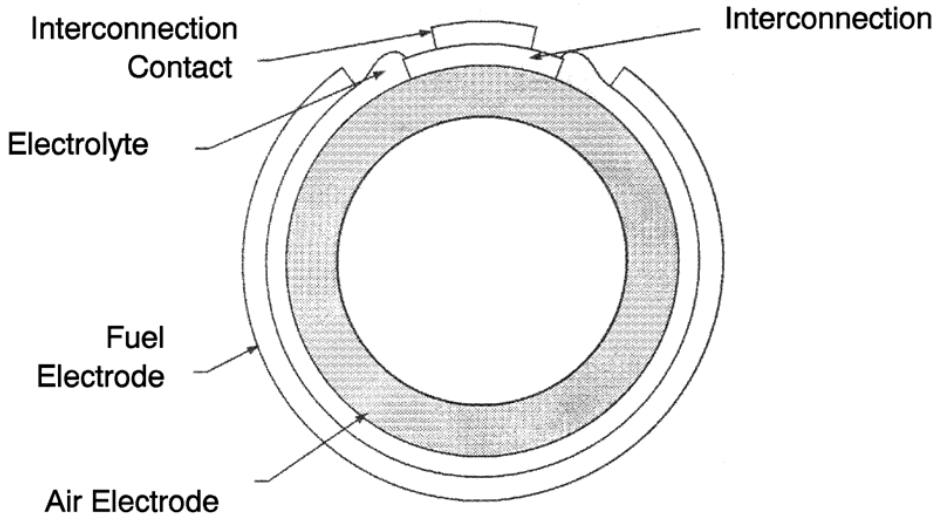

Figure 7-11 Schematic cross-section of cylindrical Siemens Westinghouse SOFC Tube.

To make a tubular SOFC, the cathode tube is fabricated first by extrusion and sintering. As shown in Table 7-1, it has a porosity of 30 to 40 percent to permit rapid transport of reactant and product gases to the cathode/electrolyte interface where the electrochemical reactions occur. The electrolyte is applied to the cathode tubes by electrochemical vapor deposition (EVD), which for many years has been the heart of Siemens Westinghouse technology (37). In this technique, metal chloride vapor is introduced on one side of the tube surface, and O_2/H_2O is introduced on the other side. The gas environments on both sides of the tube act to form two galvanic couples, as described in Equations 7-1, 7-2, and 7-3.

$$MeCl_y + \tfrac{1}{2}yO^{=} \rightarrow MeO_{y/2} + \tfrac{1}{2}yCl_2 + ye^{-} \quad (7\text{-}1)$$

$$\tfrac{1}{2}O_2 + 2e^{-} \rightarrow O^{=} \quad (7\text{-}2)$$

$$H_2O + 2e^{-} \rightarrow H_2 + O^{=} \quad (7\text{-}3)$$

The net result is the formation of a dense, uniform metal oxide layer in which the deposition rate is controlled by the diffusion rate of ionic species and the concentration of electronic charge carriers. This procedure is used to fabricate the solid YSZ electrolyte.

The anode consists of metallic Ni and YSZ. The latter inhibits sintering of the metal particles, with thermal expansion comparable to the other cell materials. The anode structure is fabricated with a porosity of 20-40 percent to facilitate mass transport of reactant and product gases.

Table 7-1 Evolution of Cell Component Technology for Tubular Solid Oxide Fuel Cells

Component	Ca. 1965	Ca. 1975	At Present [a]
Anode	• Porous Pt	• Ni/ZrO_2 cermet[a]	• Ni/ZrO_2 cermet[b] • Deposit slurry, EVD fixed[c] • 12.5 X 10^{-6} cm/cm °C CTE • ~150 µm thickness • 20 to 40 percent porosity
Cathode	• Porous Pt	• Stabilized ZrO_2 impregnated with praseodymium oxide and covered with SnO doped In_2O_3	• Doped lanthanum manganite • Extrusion, sintering • ~2 mm thickness • 11 X 10^{-6} cm/cm °C CTE from room temperature to 1000 °C • 30 to 40 percent porosity
Electrolyte	• Yttria stabilized ZrO_2 • 0.5-mm thickness	• Yttria stabilized ZrO_2	• Yttria stabilized ZrO_2 (8 mol percent Y_2O_3) • EVD[d] • 10.5 X 10^{-6} cm/cm °C CTE from room temperature to 1000 °C • 30 to 40 µm thickness
Cell Interconnect	• Pt	• Mn doped cobalt chromite	• Doped lanthanum chromite • Plasma spray • 10 X 10^{-6} cm/cm °C CTE • ~100 µm thickness

a - Specification for Siemens Westinghouse SOFC
b - Y_2O_3 stabilized ZrO_2
c - "Fixed EVD" means additional ZrO_2 is grown by EVD to fix (attach) the nickel anode to the electrolyte. This process is expected to be replaced.
d - EVD = electrochemical vapor deposition

The cell interconnect (doped lanthanum chromite) must be impervious to fuel and oxidant gases, and must possess good electronic conductivity. The interconnect is exposed to both the cathode and anode environments. Thus, it must be chemically stable under O_2 partial pressures of about 1 to 10^{-18} atmospheres at 1,000 °C. The interconnect material is applied to the cathode tube as a narrow strip (see Figure 7-9, Figure 7-11) prior to depositing the electrolyte by masking the rest of the tube. Similarly, the interconnect strip is masked when the electrolyte is applied.

The other cell components should permit only electronic conduction, and interdiffusion of ionic species in these components at 1,000 °C should not affect their electronic conductivity. Other restrictions on the cell components are that they must be stable in the gaseous environments in the cell and they must be capable of withstanding thermal cycling. The materials listed in Table 7-1 appear to meet these requirements.

The resistivities of typical cell components at 1,000 °C under fuel cell gaseous environments (38) are 10 ohm-cm (ionic) for the electrolyte (8-10 mol percent Y_2O_3 doped ZrO_2), 1 ohm-cm (electronic) for the cell interconnect (doped $LaCrO_3$), 0.01 ohm-cm (electronic) for the cathode (doped $LaMnO_3$), and 3 x 10^{-6} ohm-cm (electronic) for the anode (Ni/ZrO_2 cermet). It is apparent that the solid oxide electrolyte is the least conductive of the cell components, followed by the cell interconnect. Furthermore, an operating temperature of about 1,000 °C is necessary if the ionic conductivity of the solid electrolyte (i.e., 0.02/ohm-cm at 800 °C and 0.1/ohm-cm at 1,000 °C) is to be within an order of magnitude of that of aqueous electrolytes. The solid electrolyte in SOFCs must be only about 25 to 50 μm thick if its ohmic loss at 1,000 °C is to be comparable to the electrolyte in PAFCs (39). Fortunately, thin electrolyte structures of about 40 μm thickness can be fabricated by EVD, as well as by tape casting and other ceramic processing techniques.

Operation of SOFCs requires individual cell components that are thermally compatible so that stable interfaces are established at 1,000 °C, i.e., CTEs for cell components must be closely matched to reduce thermal stress arising from differential expansion between components. Fortunately, the electrolyte, interconnect, and cathode listed in Table 7-1 have reasonably close CTEs (i.e., ~10^{-5} cm/cm °C from room temperature to 1,000 °C). An anode made of 100 percent nickel would have excellent electrical conductivity. However, the CTE of 100 percent nickel would be 50 percent greater than the ceramic electrolyte and the cathode tube, which causes a thermal mismatch. This thermal mismatch has been resolved by mixing ceramic powders with Ni or NiO. The trade-off in the amounts of Ni (to achieve high conductivity) and ceramic (to better match the CTE) is approximately 30/70 Ni/YSZ by volume (40).

Schematic representations of the gas manifold design and cross section of a typical tube bundle (41) are presented in Figure 7-12. In this design, the tubular cathode is formed by extrusion. The electrolyte and cell interconnect are deposited by electrochemical vapor deposition (EVD) and plasma spraying, respectively, on the cathode. The anode is subsequently formed on the electrolyte by slurry deposition. A major advantage of this design is that relatively large single tubular cells can be constructed in which the successive active layers can be deposited without chemical or material interference with previously-deposited layers. The support tube is closed at one end, which eliminates gas seals between cells.

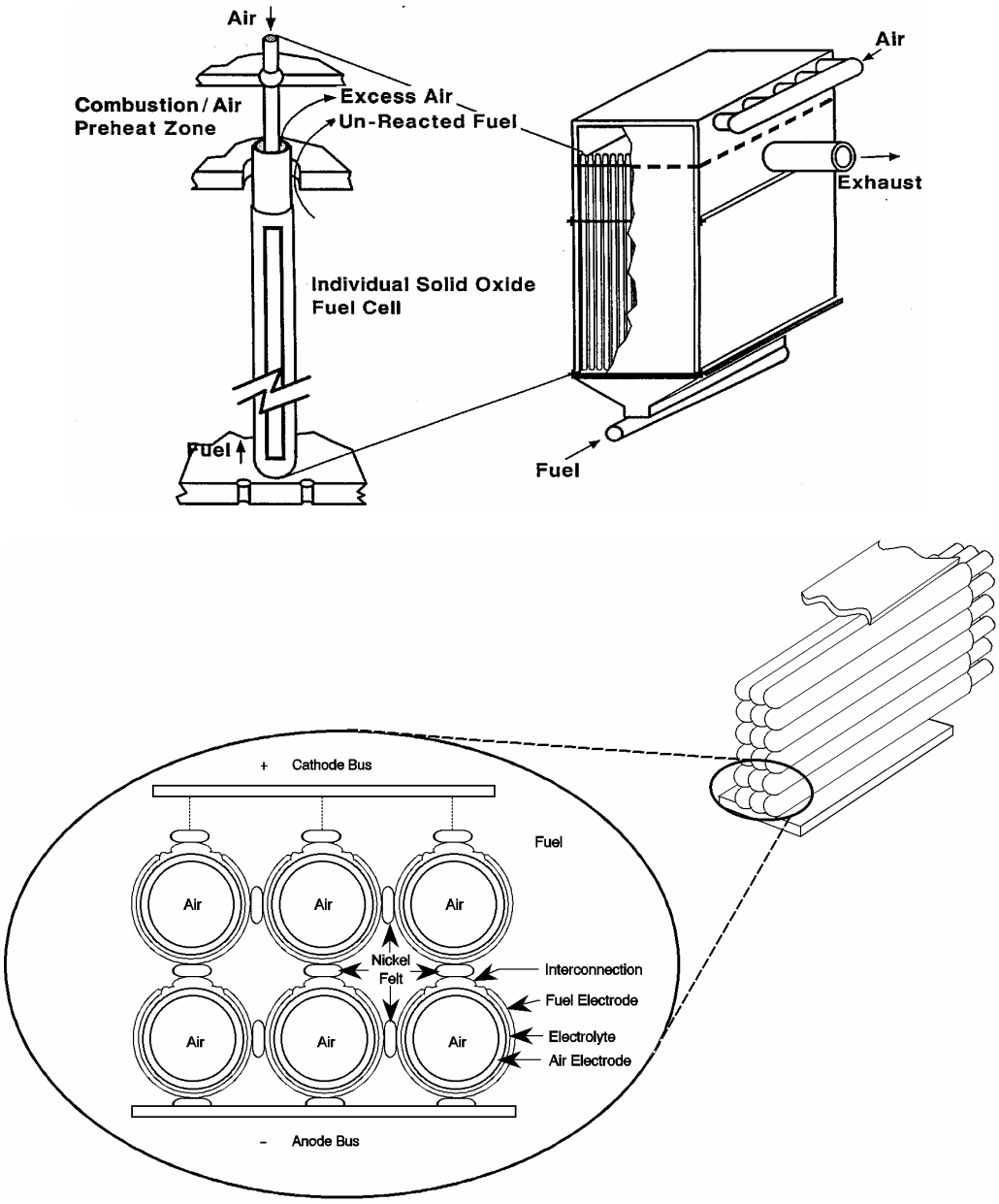

Figure 7-12 Gas Manifold Design for a Tubular SOFC and Cell-to-Cell Connections in a Tubular SOFC (41)

The oxidant is introduced via a central $A1_2O_3$ injector tube and fuel gas is supplied to the exterior of the closed-end cathode tube. In this arrangement, the $A1_2O_3$ tube extends to the closed end of the tube, and the oxidant flows back past the cathode surface to the open end. The fuel flows past the anode on the exterior of the cell and in a parallel direction (co-flow) to the oxidant gas. The spent gases are exhausted into a common plenum, where any remaining fuel reacts. The heat generated preheats the incoming oxidant stream and drives an expander. One

attractive feature of this arrangement is that it eliminates the need for leak-free gas manifolding of the fuel and oxidant streams. However, the seal-less tubular design results in a relatively long current path around the circumference of the cell.

For the current YSZ electrolyte to provide sufficient oxygen conductivity, it must be heated to a high temperature (900 to 1,000 °C). This means that expensive, high temperature alloys must be used to house the fuel cell, increasing its cost substantially. These costs could be reduced if the operating temperature was lowered to between 600 to 800 °C, allowing the use of less expensive structural materials such as stainless steel. A lower operating temperature would also ensure a greater overall system efficiency and a reduction in the thermal stress in the ceramic structure, leading to a longer service life for the fuel cell.

To lower the operating temperature, either the conductivity of the YSZ must be improved by thinner electrolytes, or alternative electrolytic materials must be developed that can replace YSZ. A concerted effort is being made by researchers around the world to find a better solution.

7.2.1.1 Performance

This section provides empirical information that can be used to estimate the performance of SOFCs based on various operating parameters. The SOFCs being developed, particularly the planar types, have unique designs, are constructed of various materials, and are fabricated by different techniques. This development process will result in further evolution of the performance trends summarized here. The electrochemical reactions associated with hydrogen fuel are expressed in equations (7-4) to (7-6):

$$H_2 + O^{=} \rightarrow H_2O + 2e^- \tag{7-4}$$

at the anode, and

$$\tfrac{1}{2}O_2 + 2e^- \rightarrow O^{=} \tag{7-5}$$

at the cathode. The overall cell reaction is

$$H_2 + \tfrac{1}{2}O_2 \rightarrow H_2O \tag{7-6}$$

The corresponding Nernst equation for the reaction in equation 7-6 is

$$E = E^\circ + \frac{RT}{2F} \ln \frac{P_{H_2} P_{O_2}^{1/2}}{P_{H_2O}} \tag{7-7}$$

In addition to hydrogen, carbon monoxide (CO) and other hydrocarbons such as methane (CH_4) can be used as fuels. It is feasible that the water gas shift reaction involving CO ($CO + H_2O \rightarrow H_2 + CO_2$) and the steam reforming of CH_4 ($CH_4 + H_2O \rightarrow 3H_2 + CO$) in the high temperature environment of SOFCs produce H_2 that is easily oxidized at the anode. The direct oxidation of CO in fuel cells is also well established. Because of the increased number of chemical species and competing reactions, however, derivation of cell performance as a function of temperature,

pressure, and composition effects is not straightforward. Data by Crucian, et al. (42), presents results for the direct oxidation of hydrocarbons on copper/ceria.

The thermodynamic efficiency of SOFCs operating on H_2 and O_2 at open circuit voltage is lower than that of MCFCs and PAFCs because of the lower free energy at higher temperatures. On the other hand, the higher operating temperature of SOFCs is beneficial in reducing polarization resistance.

The voltage losses in SOFCs are governed by ohmic losses in the cell components. The contribution to ohmic polarization (iR) in a tubular cell (assuming uniform current distribution in the electrolyte) is 45 percent from the cathode, 18 percent from the anode, 12 percent from the electrolyte, and 25 percent from the interconnect when these components have thicknesses of 2.2, 0.1, 0.04 and 0.085 mm, respectively, and specific resistivities (ohm-cm) at 1,000 °C of 0.013, 3 x 10^{-6}, 10, and 1, respectively. The cathode iR dominates the total ohmic loss despite the higher specific resistivities of the electrolyte and cell interconnection because of the short conduction path through these components and the long current path in the plane of the cathode.

In an effort to further improve performance, power density, and cost, Siemens Westinghouse initiated the development of a variant on its technology with a flattened tube (also schematically shown in Figure 7-9a). By shortening the current path the power density, on an active area basis, is substantially increased. In addition, the volumetric power density is increased (Figure 7-13), (42).

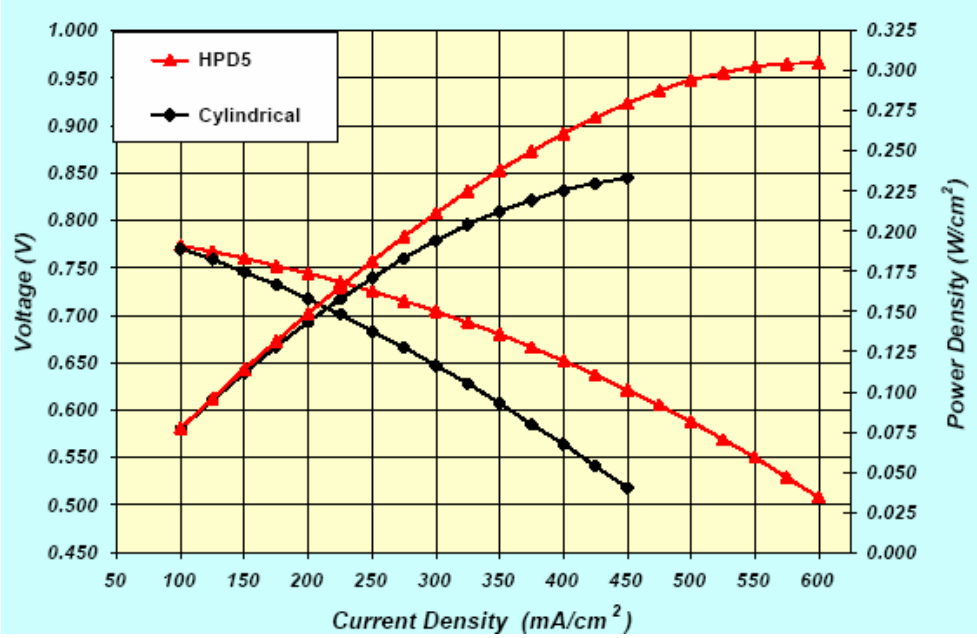

Figure 7-13 Performance Advantage of Sealless Planar (HPD5) over Conventional Siemens Westinghouse Technology (42)

Effect of Pressure

SOFCs, like PAFCs and MCFCs, show enhanced performance by increasing cell pressure. The following equation approximates the effect of pressure on cell performance at 1,000 °C:

$$\Delta V_p(mV) = 59 \log \frac{P_2}{P_1} \tag{7-8}$$

where P_1 and P_2 are different cell pressures. The above correlation was based on the assumption that overpotentials are predominately affected by gas pressures and that these overpotentials decrease with increased pressure.

Siemens Westinghouse, in conjunction with Ontario Hydro Technologies, tested air electrode supported (AES) cells at pressures up to 15 atmospheres on both hydrogen and natural gas (42). Figure 7-14 illustrates the performance at various pressures:

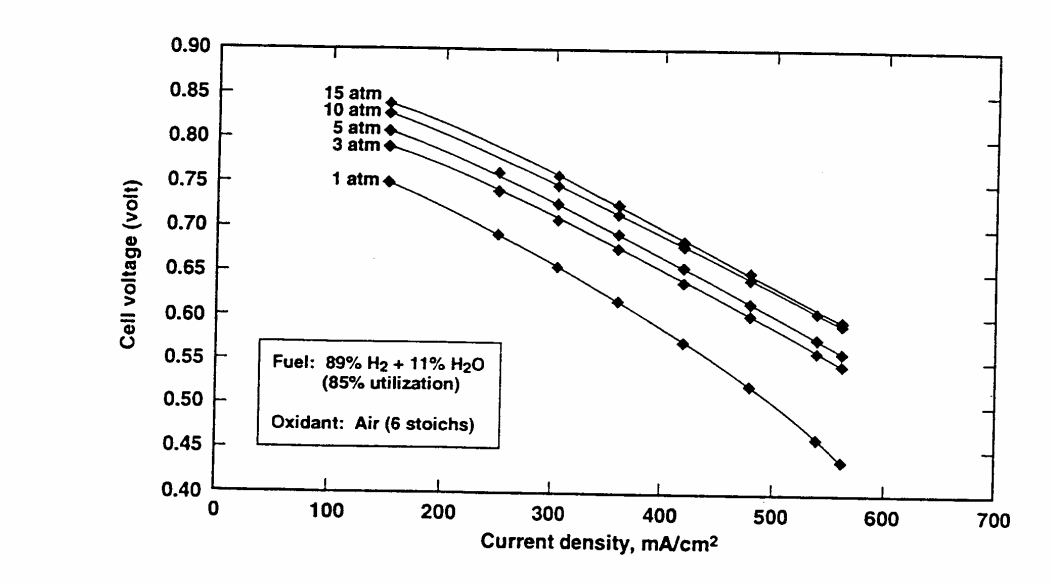

Figure 7-14 Effect of Pressure on AES Cell Performance at 1,000 °C (2.2 cm diameter, 150 cm active length)

Effect of Temperature

The dependence of SOFC performance on temperature is illustrated in Figure 7-15 for a two-cell stack using air (low utilization) and a fuel of 67 percent H_2/22 percent CO/11 percent H_2O (low utilization). The sharp decrease in cell voltage as a function of current density at 800 °C is a manifestation of the high ohmic polarization (i.e., low ionic conductivity) of the solid electrolyte at this temperature. The ohmic polarization decreases as the operating temperature increases to

1,050 °C, and correspondingly, the current density at a given cell voltage increases. The data in Figure 7-15 show a larger decrease in cell voltage with decreasing temperature between 800 to 900 °C than that between 900 to 1,000 °C at constant current density. This and other data suggest that the voltage gain with respect to temperature is a strong function of temperature and current density. One reference (43) postulates the voltage gain as:

$$\Delta V_T(mV) = 1.3(T_2 - T_1)(°C) \quad (7\text{-}9)$$

for a cell operating at 1,000 °C, 160 mA/cm^2, and a fuel composition of 67 percent H_2/22 percent CO/11 percent H_2O. In light of the strong functionality with respect to current density, it might be more appropriate to describe the voltage gain with the following relationship:

$$\Delta V_T(mV) = K(T_2 - T_1)(°C) * J \quad (7\text{-}10)$$

where J is the current density in mA/cm^2.

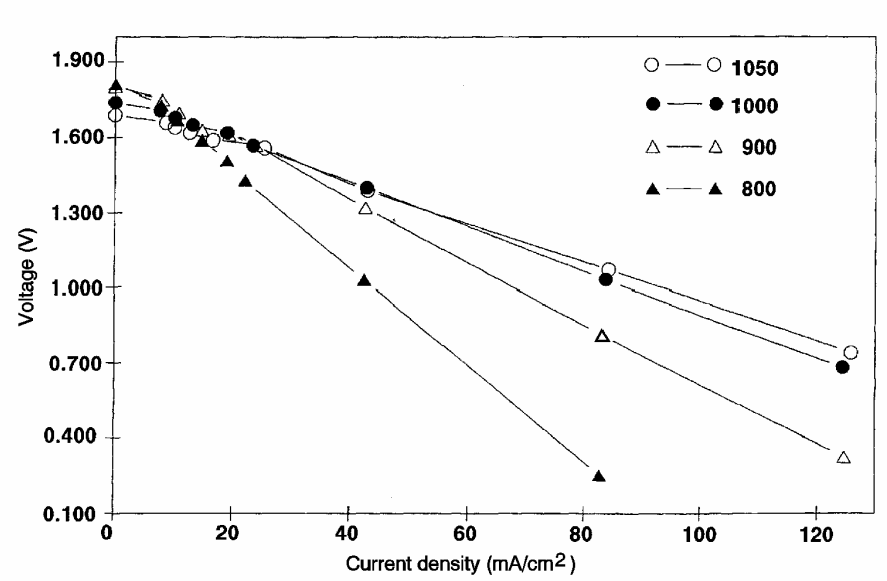

Figure 7-15 Two-Cell Stack Performance with 67 percent H_2 + 22 percent CO + 11 percent H_2O/Air

The following values of K have been deduced from several references using a fuel composition of 67 percent H_2/22 percent CO/11 percent H_2O, and an air oxidant.

Table 7-2. K Values for ΔV_T

K	Temperature (°C)	Ref.
0.008	~1000	43
0.006	1000 - 1050	44
0.014	900 - 1000	
0.068	800 - 900	
0.003	900 - 1000	45
0.009	800 - 900	

By inspection, there is a reasonably large range in the value of K between these references. As the SOFC technology matures, these differences may reconcile to a more cohesive set of values. In the interim, the following expressions may help the reader if no other information is available:

$$\Delta V_T(mV) = 0.008(T_2 - T_1)(°C) * J(mA/cm^2) \qquad 900\ °C \le T \le 1050\ °C \qquad (7\text{-}11)$$

$$\Delta V_T(mV) = 0.040(T_2 - T_1)(°C) * J(mA/cm^2) \qquad 800\ °C \le T \le 900\ °C \qquad (7\text{-}12)$$

$$\Delta V_T(mV) = 1.300(T_2 - T_1)(°C) * J(mA/cm^2) \qquad 650\ °C \le T \le 800\ °C \qquad (7\text{-}13)$$

Equations (7-11) and (7-12) are for a fuel composed of 67 percent H_2/22 percent CO/11 percent H_2O. Experiments using different fuel combinations, such as 80 percent H_2/20 percent CO_2 (45) and 97 percent H_2/3 percent H_2O (49, 51), suggest that these correlations may not be valid for other fuels. Equation (7-13) is based on the average value of the data shown in Figure 7-13, i.e., an anode-supported PSOFC with a thin electrolyte using hydrogen as a fuel and air as an oxidant. This approach is indicative of the current development path being pursued in SOFC technology: planar, electrode-supported cells featuring thin (<10 μm) electrolytes of YSZ. It has been noted that new electrode and electrolyte materials are also under development.

Figure 7-16 presents a set of performance curves for a fuel of 97 percent H_2/3 percent H_2O at various temperatures (43). Voltage actually increases with decreasing temperature for current densities below approximately 65 mA/cm^2. Other data (46) show that this inverse relationship can extend to current densities as high as 200 mA/cm^2.

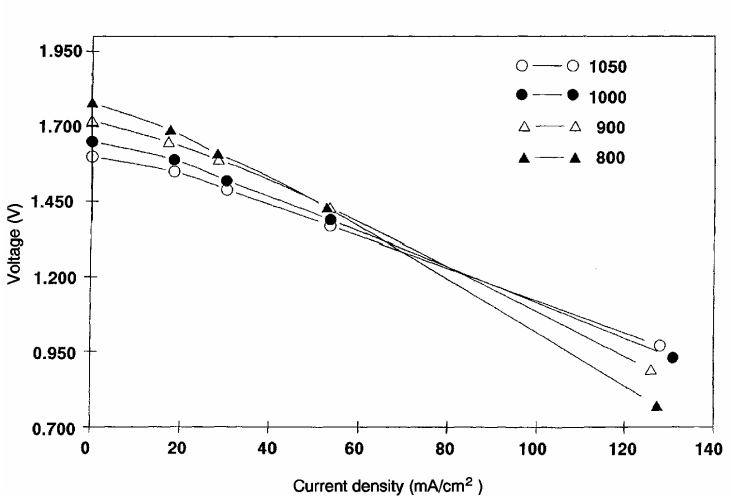

Figure 7-16 Two Cell Stack Performance with 97% H_2 and 3% H_2O/Air (43)

Effect of Reactant Gas Composition and Utilization

Because SOFCs operate at high temperature, they are capable of internally reforming fuel gases (i.e., CH_4 and other light hydrocarbons) without the use of a reforming catalyst (i.e., anode itself is sufficient), and this attractive feature of high temperature operation has been experimentally verified. Another important aspect is that recycle of CO_2 from the spent fuel stream to the inlet oxidant is not necessary because SOFCs utilize only O_2 at the cathode.

Oxidant: The performance of SOFCs, like that of other fuel cells, improves with pure O_2 rather than air as the oxidant. With a fuel of 67 percent H_2/22 percent CO/11 percent H_2O at 85 percent utilization, the cell voltage at 1,000 °C shows an improvement with pure O_2 over that obtained with air (see Figure 7-19). In the figure, the experimental data are extrapolated by a dashed line to the theoretical Nernst potential for the inlet gas compositions (45). At a target current density of 160 mA/cm^2 for the tubular SOFC operating on the above-mentioned fuel gas, a difference in cell voltage of about 55 mV is obtained. The difference in cell voltage with pure O_2 and air increases as the current density increases, which suggests that concentration polarization plays a role during O_2 reduction in air. More recent data for planar cells at 800 ^{o}C are presented in Figure 7-17. These data suggest that concentration polarization at open circuit conditions is not a significant factor with the new generation of cells. However, as expected, the differences in voltage between air and oxygen increases with increasing current density.

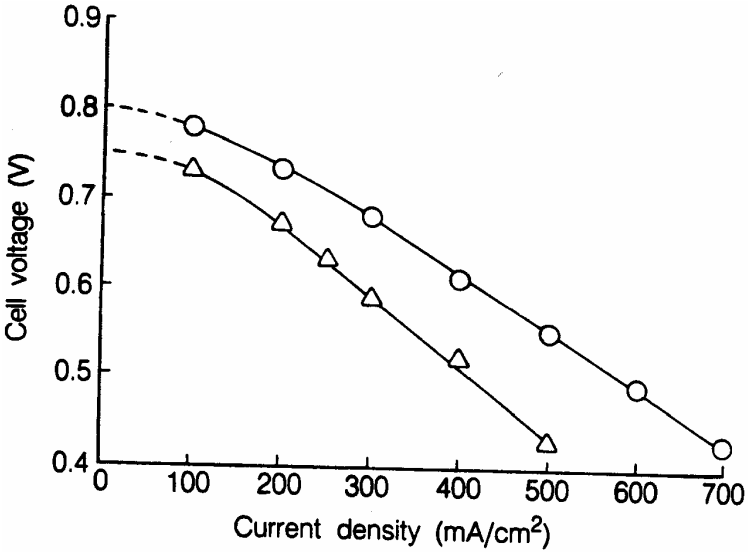

Figure 7-17 Cell Performance at 1,000 °C with Pure Oxygen (o) and Air (Δ) Both at 25 percent Utilization (Fuel (67 percent H_2/22 percent CO/11 percent H_2O) Utilization is 85 percent)

Based on the Nernst equation, the theoretical voltage gain due to a change in oxidant utilization at T = 1,000 °C is

$$\Delta V_{Cathode} = 63 \log \frac{(\bar{P}_{O_2})_2}{(\bar{P}_{O_2})_1} \qquad (7\text{-}14)$$

where $\bar{P}_{O_2}$ is the average partial pressure of O_2 in the system. Data (43) suggest that a more accurate correlation of voltage gain is described by

$$\Delta V_{Cathode} = 92 \log \frac{(\bar{P}_{O_2})_2}{(\bar{P}_{O_2})_1} \qquad (7\text{-}15)$$

Fuel: The influence of fuel gas composition on the theoretical open circuit potential of SOFCs is illustrated in Figure 7-18, following the discussion by Sverdrup, et al. (39). The oxygen/carbon (O/C) atom ratio and hydrogen/carbon (H/C) atom ratio, which define the fuel composition, are plotted as a function of the theoretical open circuit potential at 1,000 °C. If hydrogen is absent from the fuel gas, H/C = 0. For pure CO, O/C = 1; for pure CO_2, O/C = 2. The data in the figure show that the theoretical potential decreases from about 1 V to about 0.6 V as the amount of O_2 increases and the fuel gas composition changes from CO to CO_2. The presence of hydrogen in the fuel produces two results: (1) the potential is higher, and (2) the O/C ratio corresponding to complete oxidation extends to higher values. These effects occur

because the equilibrium composition obtained by the water gas shift reaction in gases containing hydrogen (H_2O) and carbon (CO) produces H_2, but this reaction is not favored at higher temperatures. In addition, the theoretical potential for the H_2/O_2 reaction exceeds that for the CO/O_2 reaction at temperatures of about 800 °C. Consequently, the addition of hydrogen to the fuel gas will yield a higher open circuit potential in SOFCs. Based on the Nernst equation, the theoretical voltage gain due to a change in fuel utilization at T = 1,000 °C is

$$\Delta V_{Anode} = 126 \log \frac{(\overline{P}_{H_2} / \overline{P}_{H_2O})_2}{(\overline{P}_{H_2} / \overline{P}_{H_2O})_1} \qquad (7\text{-}16)$$

where $\overline{P}_{H_2}$ and $\overline{P}_{H_2O}$ are the average partial pressures of H_2 and H_2O in the fuel gas.

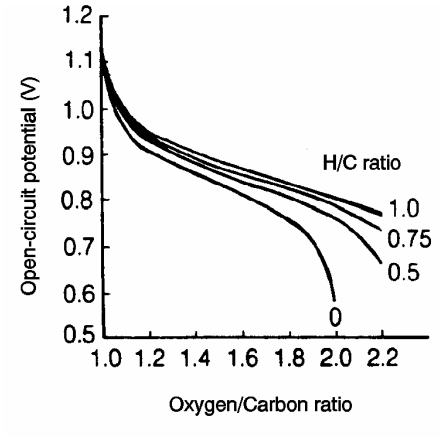

Figure 7-18 Influence of Gas Composition of the Theoretical Open-Circuit Potential of SOFC at 1,000 °C

The fuel gas composition has a major effect on the cell voltage of SOFCs. The performance data (47) obtained from a 15-cell stack (1.7 cm^2 active electrode area per cell) of the tubular configuration at 1,000 °C illustrates the effect of fuel gas composition. With air as the oxidant and fuels of composition 97 percent H_2/3 percent H_2O, 97 percent CO/3 percent H_2O, and 1.5 percent H_2/3 percent CO/75.5 percent CO_2/20 percent H_2O, the current densities achieved at 80 percent voltage efficiency were ~220, ~170, and ~100 mA/cm^2, respectively. The reasonably close agreement in the current densities obtained with fuels of composition 97% H_2/3% H_2O and 97 percent CO/3 percent H_2O indicates that CO is a useful fuel for SOFCs. However, with fuel gases that have only a low concentration of H_2 and CO (i.e., 1.5 percent H_2/3 percent CO/75.5 percent CO_2/20 percent H_2O), concentration polarization becomes significant and the performance is lower.

A reference fuel gas used in experimental SOFCs had a composition of 67 percent H_2/22 percent CO/11 percent H_2O. With this fuel (85 percent utilization) and air as the oxidant (25 percent utilization), individual cells (~1.5 cm diameter, 30 cm length and ~110 cm^2 active surface area) delivered a peak power of 22 W (48). Figure 7-19 (45) shows the change in cell voltage with

fuel utilization for a SOFC that operates on this reference fuel and pure O_2 or air as oxidant (25 percent utilization). The cell voltage decreases with an increase in the fuel utilization at constant current density. Insufficient data are available in the figure to determine whether temperature has a significant effect on the change in cell voltage with utilization. However, the data do suggest that a larger voltage decrease occurs at 1,000 °C than at 800 or 900 °C. Based on this and other data (48, 49), the voltage gain at T = 1,000 °C and with air is defined by Equation (7-17):

$$\Delta V_{Anode} = 172 \log \frac{(\bar{P}_{H_2} / \bar{P}_{H_2O})_2}{(\bar{P}_{H_2} / \bar{P}_{H_2O})_1} \qquad (7\text{-}17)$$

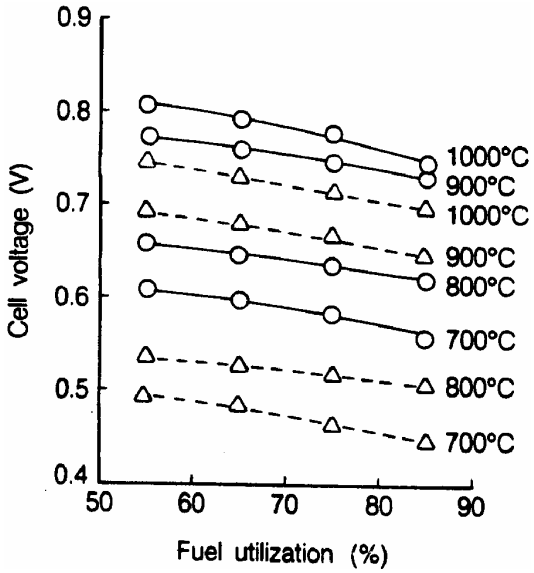

Figure 7-19 Variation in Cell Voltage as a Function of Fuel Utilization and Temperature (Oxidant (o - Pure O_2; Δ - Air) Utilization is 25 percent . Current Density is 160 mA/cm^2 at 800, 900 and 1,000 °C and 79 mA/cm^2 at 700 °C)

Effect of Impurities

Hydrogen sulfide (H_2S), hydrogen chloride (HCl) and ammonia (NH_3) are impurities typically found in coal gas. Some of these substances may harm the performance of SOFCs. Early experiments (57) used a simulated oxygen-blown coal gas containing 37.2 percent CO/34.1 percent H_2/0.3 percent CH_4 /14.4 percent CO_2/13.2 percent H_2O/0.8 percent N_2. These experiments showed no degradation in the presence of 5,000 ppm NH_3. An impurity level of 1 ppm HCl also showed no detectable degradation. H_2S levels of 1 ppm resulted in an immediate performance drop, but this loss soon stabilized into a normal linear degradation. Figure 7-2020 shows the performance of the experimental cell over time (50). Additional experiments showed that removing H_2S from the fuel stream returned the cell to nearly its original level. It was also found that maintaining an impurity level of 5,000 ppm NH_3 and 1 ppm HCl, but decreasing the H_2S level to 0.1 ppm eliminated any detrimental effect due to the presence of sulfur, even though, as mentioned above, 1 ppm H_2S caused virtually no degradation.

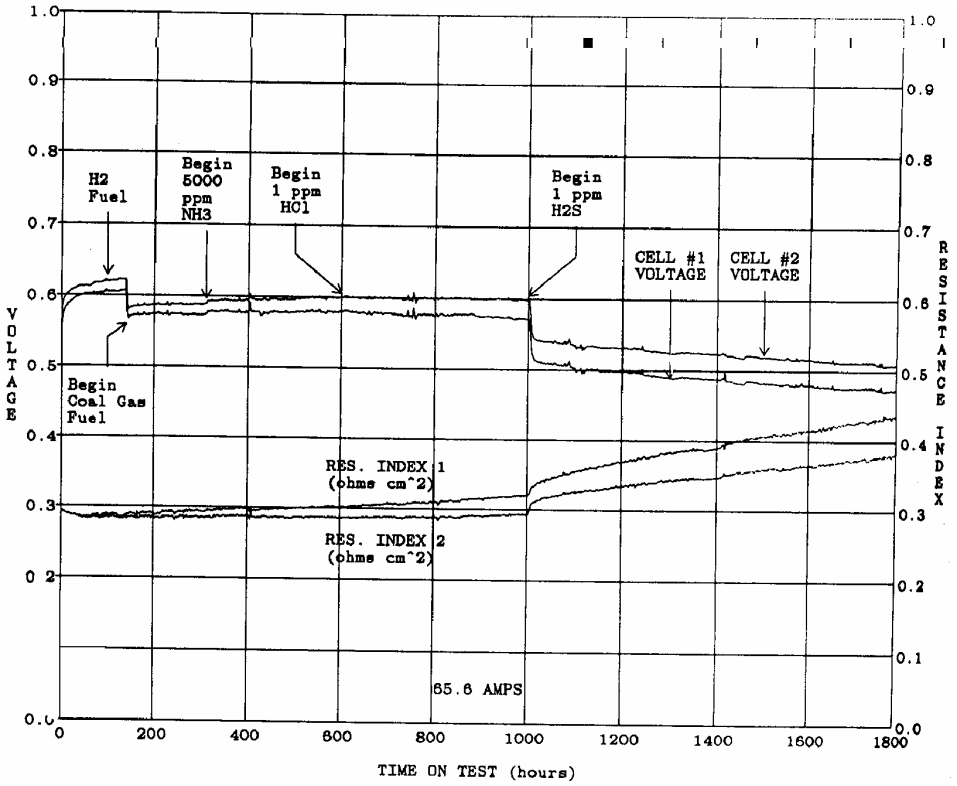

Figure 7-20 SOFC Performance at 1,000 °C and 350 mA/cm^2, 85 percent Fuel Utilization and 25 percent Air Utilization (Fuel = Simulated Air-Blown Coal Gas Containing 5,000 ppm NH_3, 1 ppm HCl and 1 ppm H_2S)

Silicon (Si), which also can be found in coal gas, has been studied (50) as a contaminant. It is believed to accumulate on the fuel electrode in the form of silica (SiO_2). The deposition of Si throughout the cell has been found to be enhanced by high (~50%) H_2O content in the fuel. Si is transported by the following reaction:

$$SiO_2\ (s) + 2H_2O\ (g) \rightarrow Si(OH)_4\ (g) \qquad (7\text{-}18)$$

As CH_4 reforms to CO and H_2, H_2O is consumed. This favors the reversal of Equation (7-18), which allows SiO_2 to be deposited downstream, possibly on exposed nickel surfaces. Oxygen-blown coal gas, however, has a H_2O content of only ~13 percent, and this is not expected to allow for significant Si transport.

Effect of Current Density

The voltage level of a SOFC is reduced by ohmic, activation, and concentration losses, which increase with increasing current density. The magnitude of this loss is described by the following equation that was developed from information in the literature (44, 51, 52 ,53, 54, 55):

$$\Delta V_j(mV) = -0.73\Delta J \qquad (T = 1000\ ^\circ C) \qquad (7\text{-}19)$$

where J is the current density (mA/cm^2) at which the cell is operating. Air electrode-supported (AES) cells by Siemens Westinghouse exhibit the performance depicted in Figure 7-.

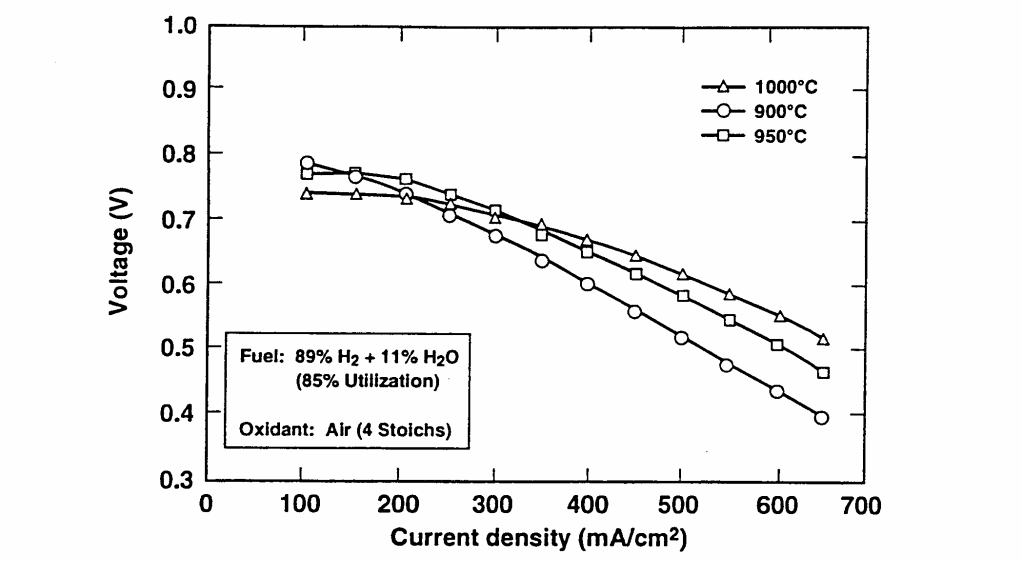

Figure 7-21 Voltage-Current Characteristics of an AES Cell (1.56 cm Diameter, 50 cm Active Length)

Effect of Cell Life

The endurance of the cell stack is of primary concern for SOFCs. As SOFC technology has continued to approach commercialization, research in this area has increased and improvements made. The Siemens Westinghouse state-of-the-art tubular design has been validated by continuous electrical testing of over 69,000 hours with less than 0.5 percent voltage degradation per 1,000 hours of operation. This tubular design is based on the early calcia-stabilized zirconia porous support tube (PST). In the current technology, the PST has been eliminated and replaced by a doped lanthanum manganite air electrode tube. These air electrode-supported (AES) cells have shown a power density increase of approximately 33 percent over the previous design. Siemens Westinghouse AES cells have shown less than 0.2 % voltage degradation per 1,000 hours in a 25 kW stack operated for over 44,000 hours (23,56), and negligible degradation in the 100 kW stack operated in the Netherlands and Germany (>16,000 hours).

Summary of Equations for Tubular SOFC

The preceding discussion provided parametric performance based on various referenced data at different operating conditions. It is suggested that the following set of equations could be used for performance adjustments unless the reader prefers other data or correlations.

Parameter	Equation	Comments	
Pressure	$\Delta V_p(mV) = 59 \log \frac{P_2}{P_1}$	1 atm ≤ P ≤ 10 atm	(7-8)
Temperature	$\Delta V_T(mV) = 0.008(T_2 - T_1)(°C) * J$[1]	900 °C ≤ T ≤ 1050 °C	(7-11)
	$\Delta V_T(mV) = 0.04(T_2 - T_1)(°C) * J$[1]	800 °C ≤ T ≤ 900 °C	(7-12)
	$\Delta V_T(mV) = 1.3(T_2 - T_1)(°C) * J$	650 °C ≤ T ≤ 800 °C	(7-13)
Oxidant	$\Delta V_{Cathode}(mV) = 92 \log \frac{(\bar{P}_{O_2})_2}{(\bar{P}_{O_2})_1}$	$0.16 \leq \frac{\bar{P}_{O_2}}{\bar{P}_{Total}} \leq 0.20$	(7-15)
Fuel	$\Delta V_{Anode} = 172 \log \frac{(\bar{P}_{H_2}/\bar{P}_{H_2O})_2}{(\bar{P}_{H_2}/\bar{P}_{H_2O})_1}$	$0.9 \leq \bar{P}_{H_2}/\bar{P}_{H2O} \leq 6.9$ T = 1000 °C, with air	(7-17)
Current Density	$\Delta V_J(mV) = -0.73\Delta J$	50 < J < 400 mA/cm^2 P = 1 atm., T = 1000 °C	(7-19)

7.2.2 Planar SOFC

A variety of planar SOFC sub-types are distinguished according to construction:

Structural support for membrane/electrolyte assembly:

- Electrolyte-supported. Early planar cells were mostly electrolyte-supported. This requires a relatively thick electrolyte (>100 but typically around 200 µm, with both electrodes at about 50 µm) which leads to high resistance, requiring high-temperature operation. Sulzer Hexis and Mitsubishi Heavy Industries (MHI) are actively pursuing this technology and have scaled-up the technology into 1 and 15 kW systems, respectively. Power density at 0.7 V is reported to be about 140 mW/cm^2 for the Sulzer stacks (57, 58, 59, 60, 61) and about 190 to 220 mW/cm^2 for the MHI stacks (62, 63, 64, 65), both under commercially-relevant operating conditions.
- Cathode-supported. This allows for a thinner electrolyte than electrolyte-supported cells, but mass transport limitations (high concentration polarization) and manufacturing challenges (it is difficult to achieve full density in a YSZ electrolyte without oversintering an LSM cathode) make this approach inferior to anode-supported thin-electrolyte cells.
- Anode-Supported. Advances in manufacturing techniques have allowed the production of anode-supported cells (supporting anode of 0.5 to 1 mm thick) with thin electrolytes. Electrolyte thicknesses for such cells typically range from around 3 to 15 µm (thermomechanically, the limit in thickness is about 20 to 30 µm (the cathode remains around 50 µm thick), given the difference in thermal expansion between the anode and the electrolyte). Such cells provide potential for very high power densities (up to 1.8 W/cm^2 under laboratory conditions, and about 600 to 800 mW/cm^2 under commercially-relevant conditions).

[1] Where J = mA/cm^2, for fuel composition of 67% H_2/22% CO/11% H_2O

- Metal interconnect-supported. Lawrence Berkeley National Laboratory (66), Argonne National Laboratory, and Ceres (67) have pioneered metal-supported cells to minimize mass transfer resistance and the use of (expensive) ceramic materials. In such cells, the electrodes are typically 50 µm thick and the electrolyte around 5 to15 µm. While the benefits are obvious, the challenges are to find a materials combination and manufacturing process that avoids corrosion and deformation of the metal and interfacial reactions during manufacturing as well as operation.

Interconnect material:

- Ceramic (lanthanum or yttrium chromite) suitable for high-temperature operation (900 to 1000 °C). These materials, while chemically stable and compatible with the MEA from a chemical and thermal expansion perspective, are mechanically weak and costly.
- Cr-based or Ni-based superalloy for intermediate-high temperature operation (800 to 900 °C). These materials are chemically stable at 900 °C, but they require additional coatings to prevent Cr-poisoning of the electrodes. In addition, they are expensive and difficult to form.
- Ferritic steel (coated or uncoated) for intermediate temperature operation (650 to 800 °C). While uncoated steels are chemically unstable, especially during thermal cycling, coated steels provide corrosion resistance as well as acceptable conductivity when new. However, thermal cycling performance still requires improvement.

Shape of the cell.

- Rectangular, with gases flowing in co-flow, counter-flow, or cross-flow.
- Circular, typically with gases flowing out from the center in co-flow, and mixing and burning at the edge of the cells. Spiral flow arrangements and counter-flow arrangements have also been proposed.

Method for creating flow-channels:

- Flat ceramic cell with channels in interconnect or flow-plate.
- Corrugated ceramic with flat interconnects.

Manifolding arrangement:

- External manifolding.
- Internal manifolding, through the electrolyte.
- Internal manifolding through the interconnect, but not through the electrolyte.

Figure 7-22 shows a sample of recently-pursued planar SOFC approaches. The anode-supported technology with metal interconnects will be described in some detail below. Mitsubishi tested a 15 kW system with its all-ceramic MOLB design for almost 10,000 hours with degradation rates below 0.5 percent per 1,000 hrs, but without thermal cycles, and with power densities ranging from 190 to 220 mW/cm^2 (under practical operating conditions). Because the interconnect is flat and relatively thin (the flow-passage is embedded in the MEA), less of the expensive $LaCrO_3$ is required than if the flow-passages were in the interconnect. Nevertheless, cost reduction is still one of the main priorities for this stack technology. Thermal cycling is also thought to be a challenge with the system, which is targeted to small-scale distributed stationary power generation applications.

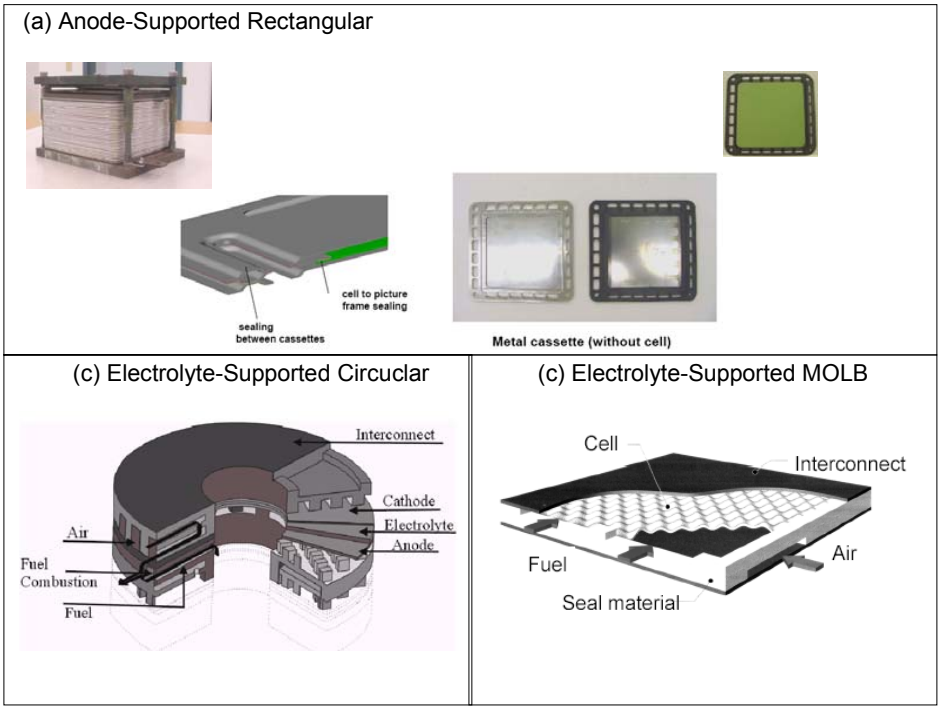

Figure 7-22 Overview of Types of Planar SOFC: (a) Planar Anode-Supported SOFC with Metal Interconnects(68); (b) Electrolyte-Supported Planar SOFC Technology with Metal Interconnect (57,58,69); (c) Electrolyte-Supported Design with "egg-crate" electrolyte shape and ceramic interconnect (62,63,64,65).

Sulzer Hexis built 110 1 kW demonstration units based on its electrolyte-supported technology with superalloy interconnects. The latest version of the units, integrated into a hot water/heating appliance, has shown a degradation rate of around 1 to 2 percent per 1000 hrs in continuous operation, and about 2x higher with thermal cycling (69).

The planar anode-supported SOFC with metal interconnects has benefited from support for fundamental science and stack development under DOE's SECA Program. The SECA Program is focused on developing technology required for competitive SOFC stack technologies that can be mass-customized for a wide range of applications, including stationary power generation, mobile power generation, military power applications, and transportation applications such as auxiliary power units (APUs). By commercializing SOFC stacks for a number of applications simultaneously, stack production could be increased more rapidly and, consequently, manufacturing cost reduced more quickly. The SECA Program has two interrelated components: (1) the core program in which universities, national laboratories, and private industry develop fundamental component and materials technologies for SOFC stacks that can be licensed with stack developers, and (2) a vertical program with teams of private stack developers with other parties to develop and demonstrate stacks that meet the SECA goals (70). Particularly useful, and broadly shared amongst the international SOFC development community, are the stack performance goals developed by SECA.

Table 7-3 SECA Program Goals for SOFC Stacks (70)

	PHASE I	PHASE II	PHASE III
POWER RATING (NET)	3kW - 10 kW	3kW - 10 kW	3kW - 10 kW
COST	$800/kW	$600/kW	$400/kW
EFFICIENCY (AC or DC/LHV)	Mobile – 25 to 45% Stationary – 35 to 55%	Mobile – 30 to 50% Stationary – 40 to 60%	Mobile – 30 to 50% Stationary – 40 to 60%
STEADY STATE TEST @ NORMAL OPERATING CONDITIONS	1500 hours 80% availability ΔPower ≤ 2% degradation/500 hours at a constant stack voltage.	1500 hours 85% availability ΔPower ≤ 1% degradation/500 hours at a constant stack voltage.	1500 hours 95% availability ΔPower ≤ 0.1% degradation/500 hours at a constant stack voltage.
TRANSIENT TEST	10 cycles ΔPower ≤ 1% degradation after 10 cycles at a constant stack voltage.	50 cycles ΔPower ≤ 0.5% degradation after 50 cycles at a constant stack voltage.	100 cycles ΔPower ≤ 0.1% degradation after 100 cycles at a constant stack voltage.
TEST SEQUENCE	1) Steady State Test - 1000 hours 2) Transient Test 3) Steady State Test - 500 hours	1) Steady State Test - 1000 hours 2) Transient Test 3) Steady State Test - 500 hours	1) Steady State Test – 1000 hours 2) Transient Test 3) Steady State Test - 500 hours
FUEL TYPE	For the complete duration of the Steady State and Transient Tests, operate the Prototype on either a commercial commodity, natural gas, gasoline, or diesel fuel (s) or a representative fuel based on respectively methane, iso-octane, or hexadecane corresponding to the proposed primary application (s). If multiple applications using different fuels are proposed split the total test time equally among the different fuel types.	For the complete duration of the Steady State and Transient Tests, operate the Prototype on either a commercial commodity natural gas, gasoline, or diesel fuel (s) corresponding to the proposed primary application (s). Utilize external or internal primary fuel reformation or oxidation. If multiple applications using different fuels are proposed split the total test time equally among the different fuel types.	For the complete duration of the Steady State and Transient Tests, operate the Prototype on either a commercial commodity natural gas, gasoline, or diesel fuel (s) corresponding to the proposed primary application (s). Utilize external or internal primary fuel reformation or oxidation. If multiple applications using different fuels are proposed split the total test time equally among the different fuel types.
MAINTENANCE INTERVALS	Design aspects should not require maintenance at intervals more frequent than 1000 operating hours.	Design aspects should not require maintenance at intervals more frequent than 1000 operating hours.	Design aspects should not require maintenance at intervals more frequent than 1000 operating hours.
DESIGN LIFETIME	≥ 40,000 operating hours for stationary applications and 5,000 hours for transportation applications for military uses.	≥ 40,000 operating hours for stationary applications and 5,000 hours for transportation applications for military uses.	≥ 40,000 operating hours for stationary applications and 5,000 hours for transportation applications for military uses.

Over the past ten years, this technology has developed from a scientific concept to cell technologies that can achieve 1.8 W/cm^2 under idealized laboratory conditions, and stacks that can achieve initial power densities of 300 to 500 mW/cm^2. The power density of this technology has allowed the engineering of integrated systems for small-scale stationary power and APU applications, making the hypothesis that these stack technologies can be customized for a wide range of high-volume applications.

7.2.2.1 Single Cell Performance

A significant advance in the development of intermediate temperature PSOFCs has been the use of metallic "bipolar" interconnects in conjunction with thin electrolytes. Although originally conceptualized in the early 1990s, development of the anode-supported planar SOFC with metallic interconnects was significantly accelerated by the US DOE's SECA Program. The benefits of the anode-supported approach with metallic interconnects were readily recognized (see summary in **Table 7-4**):

- Sintering and Creep – Milder temperatures result in less sintering and creep of the stack materials. This helps maintain geometric stability and high surface area for reaction.
- Thermally Activated Processes – Thermally activated processes such as chromium vaporization, elemental inter-diffusion and migration, metallic corrosion, and ceramic aging become problematic at higher temperatures. The lower the operating temperature is maintained, the less damage these processes will cause to the fuel cell.
- Thermal Stress – Reduced width of the operating temperature band reduces thermal expansion and contraction stresses during cycling, thus maintaining geometric stability.
- Increase in Nernst potential.
- Heat Loss – Reduced heat loss from the more compact stack at lower operating temperature.
- Material Flexibility – The range of potential construction materials is somewhat greater at lower temperatures. In particular, certain metals can be incorporated in SOFC stack designs.
- Balance of Plant – The BOP costs may be less if lower cost materials can be used in the recuperators. In addition, the stack temperatures will be closer to typical reformer and sulfur removal reactor operating temperatures; this further reduces the load on the thermal management system. However, it must be remembered that the main factor driving the heat duty of the thermal management system is the amount of cooling air required for stable stack operation, which in turn depends on the internal reforming capability of the stack and on the acceptable temperature rise across the stack.
- Start-up time may be reduced. Lighter weight and high thermal conductivity of the metal interconnects may allow more rapid heat-up to operating temperature.

Some negative effects also result from reducing the operating temperature of the SOFC:

- A proven interconnect material for operating in the intermediate temperature range (650 to 800 ^{o}C) does not yet exist.
- Sulfur resistance decreases with temperature. However, recent work has shown that addition of certain materials provides adequate sulfur tolerance at lower temperatures.
- Lower temperatures generally require a planar configuration to minimize resistance losses. This is accomplished using ultra-thin electrode and electrolyte membranes. In turn, effective seals for the planar configuration are needed.

Table 7-4 Recent Technology Advances on Planar Cells and Potential Benefits

	Technology Advance	Potential Benefit
Design	Electrode supported **thin electrolyte** unit cells – e.g., anode	• Lower resistance of electrolyte • Increased power density
System	**Lower temperature** of operation	• Use of metallic Interconnects and manifolding possible
Materials	**Metallic interconnect plates**	• Lower cost • Lower resistance interconnect • Mechanical solution to thermal expansion of stack
Materials	More conductive electrolyte materials: Sc – Zr Oxides Ce – Gd Oxides	• Reduced voltage drop across electrolyte

An example of a stack geometry is shown in Figure7-22a (68). The cassette-type repeat unit with a plain rectangular ceramic cell, a metal picture frame with cavities for manifolding, and a matching separator plate is not uncommon among developers of planar anode-supported SOFC with metal interconnects. Units such as the one shown typically result in a pitch of 5 to 10 unit cells per inch. The bipolar plate has several functions, including providing a gas barrier between the anode and cathode, providing a series electrical connector between the anode and cathode, and flow field distribution.

Individual cell assemblies, each including an anode, electrolyte, and cathode are stacked with metal interconnecting plates between them. The metal plates are shaped to permit the flow of fuel and air to the membranes. The electrolyte and interconnect layers are made by tape casting. The electrodes are applied by the slurry method, by screen-printing, by plasma spraying, or by tape-casting/tape calendaring. Fuel cell stacks are formed by layers of unit cells, much like other fuel cell technologies. Tests of single cells and two-cell stacks of SOFCs with a planar configuration (5cm diameter) have demonstrated power densities up to 1.8 W/cm^2 (Figure 7-23) under ideal conditions.

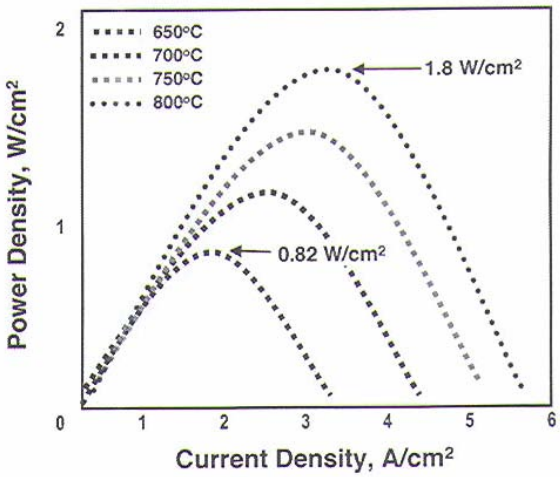

Figure 7-23 Representative State-of-the-Art Button Cell Performance of Anode-Supported SOFC (1)

To reduce resistivity of the electrolyte, development has focused on reducing its thickness from 150 µm to about 10 µm. Wang, et al. (71), at the University of Pennsylvania, fabricated thin-film YSZ electrolytes between 3 and 10 µm. Wang reported significant improvement in cell performance with mixed conducting-doped YSZ electrodes; Tb- and Ti-doped YSZs increased power densities between 15 to 20 percent. Other examples of this approach are also available in the literature (72, 73,74 ,75 ,76).

Ball and Stevens (74) report that gadolinium-doped ceria is a good candidate for use as an alternative electrolyte when compared to zirconia, due to its higher conductivity at lower temperatures. However, doped ceria has a number of disadvantages, such as electronic conductivity and reduced strength. Results indicate that an increase in strength can be produced in the ceria by addition of zirconia particles that is dependent on the particle size and heat treatment.

Research at the University of Texas at Austin (72) sought to develop electrolytes that have higher conductivity than YSZ. Goodenough and Huang (77) identified a system of LaSrGaMgO (LSGM) as a superior oxide-ion electrolyte with performance at 800 °C comparable to YSZ at 1,000 °C. LSGM lacks the toughness of YSZ, which makes it more difficult to fabricate as an ultra-thin film, but its superior ionic conductivity allows thicker films to be used. Figure 7-24 illustrates the performance of a single cell based on LSGM electrolyte.

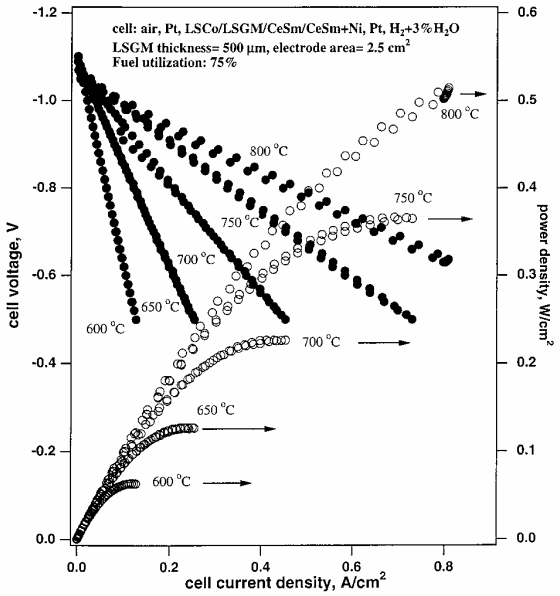

Figure 7-24 Single Cell Performance of LSGM Electrolyte (50 μm thick)

Barnett, Perry, and Kaufmann (75) found that fuel cells using 8 μm thick yttria-stabilized zirconia (YSZ) electrolytes provide low ohmic loss. Furthermore, adding thin porous yttria-doped ceria (YDC) layers on either side of the YSZ yielded much-reduced interfacial resistance at both LSM cathodes and Ni-YSZ anodes. The cells provided higher power densities than previously reported below 700 °C, e.g., 300 and 480 mW/cm^2 at 600 and 650 °C, respectively (measured in 97 percent H_2 and 3 percent H_2O and air), and also provided high power densities at higher temperatures, e.g., 760 mW/cm^2 at 750 °C. Other data (Figure 7-25) from the University of Utah (73) show power densities of 1.75 W/cm^2 with H_2/air and 2.9 W/cm^2 with H_2/O_2 at 800 °C for an anode-supported cell. However, no data is presented with regard to electrodes or electrolyte thickness or composition.

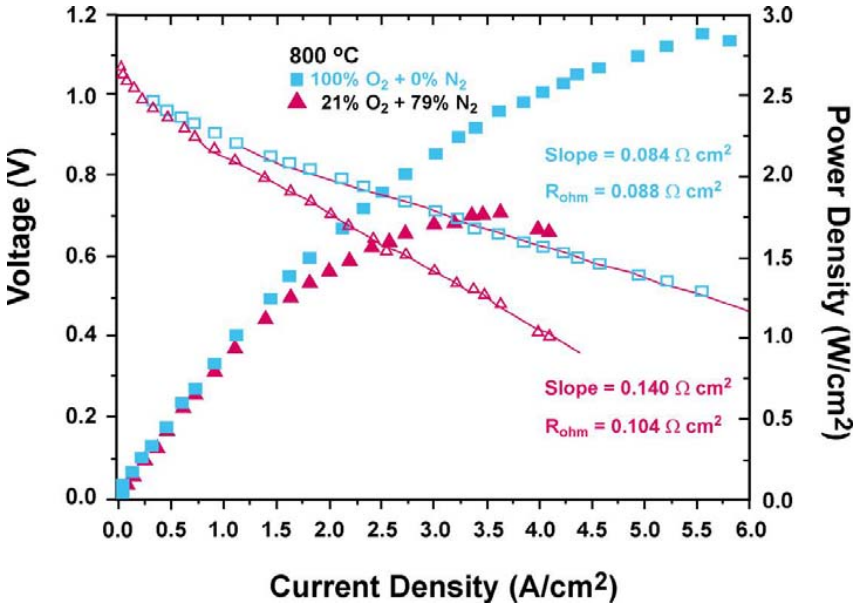

Figure 7-25 Effect of Oxidant Composition on a High Performance Anode-Supported Cell

7.2.2.2 Stack Performance

A number of planar cell stack designs have been developed based on planar anode-supported SOFC with metal interconnects. Typically, cells for full-scale stacks are about 10 to 20 cm mostly square or rectangular (though some are round). Stacks with between 30 and 80 cells are the state-of-the-art. Figure 7-26 shows examples of state-of-the art planar anode-supported SOFC stacks and selected performance data (68,78, 79). The stacks shown are the result of three to seven generations of full-scale stack designs by each of the developers. The capacities of these stacks (2 to 12 kW operated on reformate and at 0.7 V cell voltage) is sufficient for certain small-scale stationary and mobile (APU) applications.

It is still difficult to compare performance figures for the stacks, as performance is reported for different (often vaguely described) operating conditions. However, it has been estimated that if the data were corrected for fuel composition and fuel utilization, the power density on a per unit area basis for these stacks is around 300 to 400 mW/cm^2. The differences in performance are modest compared with the differences in performance between this generation and previous generations of stacks.

These three stack technologies can be considered to be among the most advanced of the planar anode-supported SOFC stacks. Interestingly, their stack architectures are rather similar:

- All are rectangular cells, with a cassette-type multi-component repeat unit design
- All use integrated manifolds that do not pierce the ceramics
- All use some form of stack compression, although presumably the Jülich stack requires this for contact, not sealing (a glass seal is used)

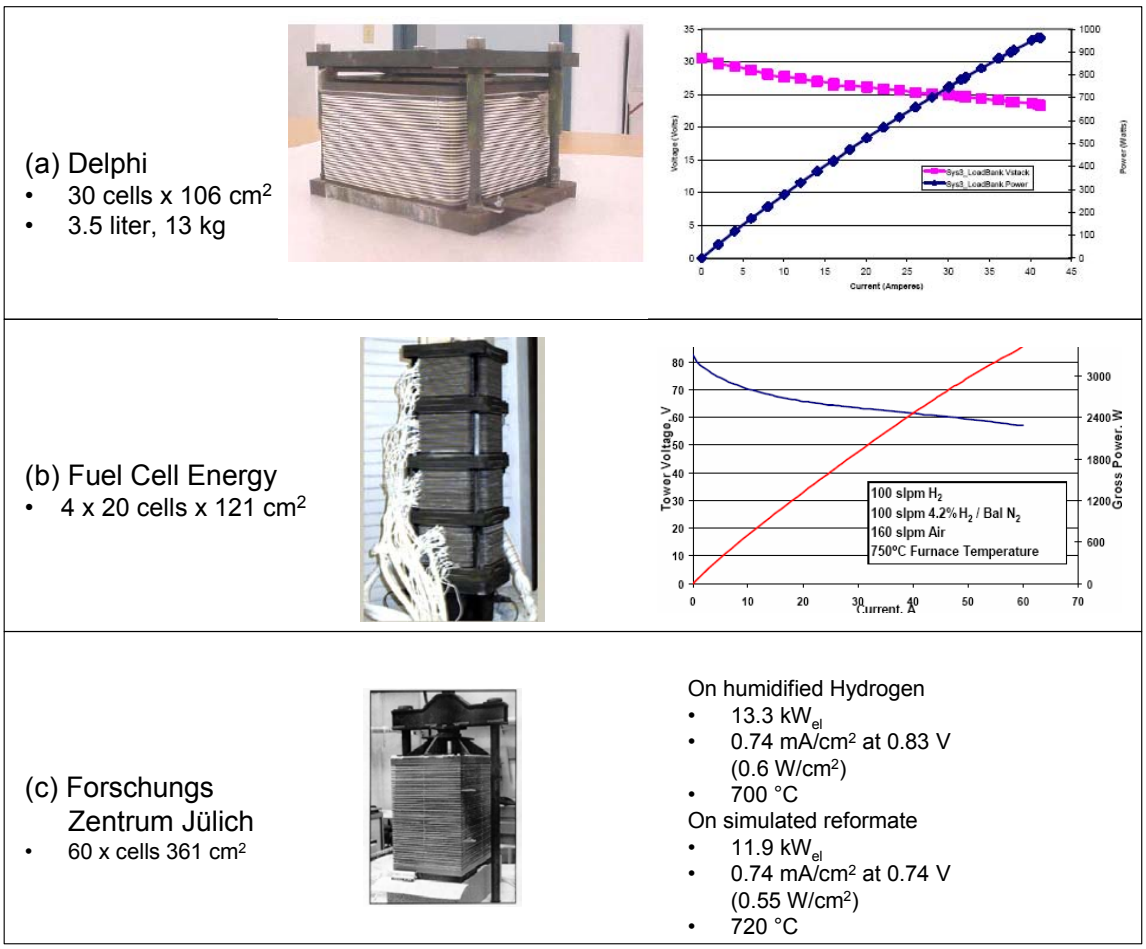

Figure 7-26 Examples of State-of-the-Art Planar Anode-Supported SOFC Stacks and Their Performance Characteristics (68,79,78)

The stack performance lags behind the impressive performance demonstrated at the cell level. Results reported by Delphi are typical (Figure 7-27). Of course, the very high numbers for single cells (1.8 W/cm^2) were obtained with pure reactants, humidified hydrogen as a fuel, and with very low utilization. But still, if the performance in single cells were corrected for the operating conditions prevalent in a full cell at about 80 percent utilization with real reformate (data in Figure 7-27 represent a more modest level of utilization and idealized fuels), a power density of between 600 and 800 mW/cm^2 may be expected. However, measured power densities in multi-cell stacks (note Figure 7-27 shows only single-cell stacks) for such conditions range from 300 to 400 mW/cm^2. Most of this discrepancy stems from high contact resistance caused by deterioration of the electrodes and the electrical interface with the interconnects.

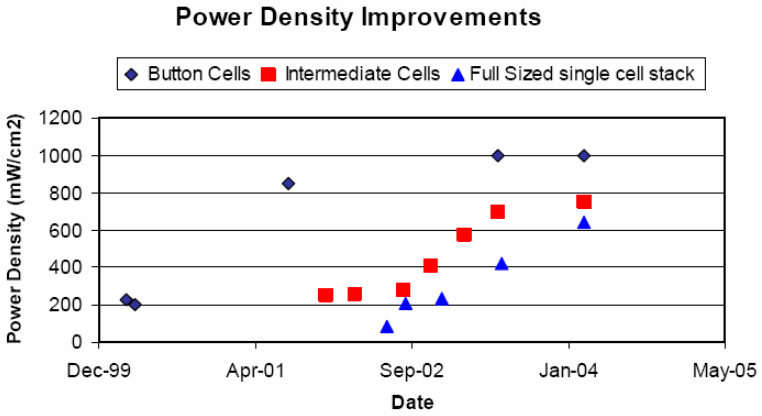

Figure 7-27 Trend in Cell and Single-Cell-Stack Performance in Planar SOFC (68)

Degradation rates observed by various groups for this type of stack range from about 0.8 to about 3 percent per 1,000 hours, though experiments with coated ferritic steel interconnects reportedly achieve still lower degradation rates. The longest operating experience is currently around 6,000 to 7,000 hours per stack. The effect of thermal cycling varies strongly from system to system, but it appears that about 5 to 10 thermal cycles are achievable. The effects of more thermal cycles combined with long-term operation are not well-characterized in the public literature. With respect to degradation rate, both chromia poisoning and interfacial resistances are issues that require further improvement. Because of the thin metal foils used in some of the designs, the effect of changes in chromium content of the bulk foil metal over long periods of time must be taken into account, and could influence corrosion behavior in a non-linear fashion (80).

Although these are significant problems, they have been well-characterized. Structured public-private R&D programs are now under way in the U.S., Europe, and Japan to overcome these hurdles in the coming years.

7.2.3 Stack Scale-Up

Although some SOFC applications require systems no larger than the 2 to 10 kW to which many tubular and planar SOFC have been scaled-up, most stationary applications, especially those with the greatest potential impact on global energy use, will require systems ranging from about 200 kW for medium-scale distributed generation to several hundred MW for utility-scale power stations. Table 7-5 lists the major SOFC system manufacturers worldwide; this list does not include research institutes, universities, and manufacturers of solely ceramic components (1).

Tubular SOFC systems have been scaled-up and integrated into systems with capacities up to 250 kW (Figure 7-28). This is accomplished by combining individual tubes into 3x8 tube modules with capacities of around 2 kW. These modules, in turn, are combined to form the stack. Mitsubishi Heavy Industries scaled-up its tubular segmented-in-series system to 10 kW (pressurized and atmospheric) and its all-ceramic planar design up to 15 kW. The planar design follows a scale-up approach that involves small ~2 kW units which are combined into larger stack units. Planar anode-supported stacks with metallic interconnects have been scaled-up to about 12 kW in a single stack.

Figure 7-28 Siemens Westinghouse 250 kW Tubular SOFC Installation (31)

The question then arises how these stack technologies could be used to create systems with capacities ranging from 200 kW to at least 20 MW. One approach would be to simply combine ~5 kW stacks in a modular fashion into a larger system. However, as recent studies have implied, this would lead to rather complex manifolding arrangements of very large numbers of cells (a 1 MW system would require at least 200 5 kW stacks). Although feasible, the complexity, cost, and pressure loss associated with such massive modularization are not trivial.

Scaling up cells and individual single stacks may have limits based on fundamental considerations:

- The larger the cells, the more severe the effects of CTE mismatches.
- As cells are scaled up, pressure drop will increase unless flow channels are made higher. Higher flowchannels will increase the cell resistance and, in most designs, increase the material intensity of the stack.
- Scaling up the cells for certain applications makes it more difficult to mass-customize stack technology for a broad range of applications with different capacity requirements.
- Increasing the number of cells has its limits because of mechanical stability concerns.
- As the number of cells increases, minor imperfections in cell geometry (e.g. flatness) will lead to maldistributions of the contact or sealing pressure inside the stacks.
- Manifolding the gas flow evenly to all cell levels will become difficult.

An alternative approach would be to build integrated stack units out of planar cells, for example using a windowpane design (Figure 7-29). Earlier in the development of planar SOFC, when developers of electrolyte-supported planar SOFC were focused on large-capacity applications, several players suggested this approach. It appears likely that cost, simplicity, and reliability advantages will ultimately drive developers of larger-scale systems.

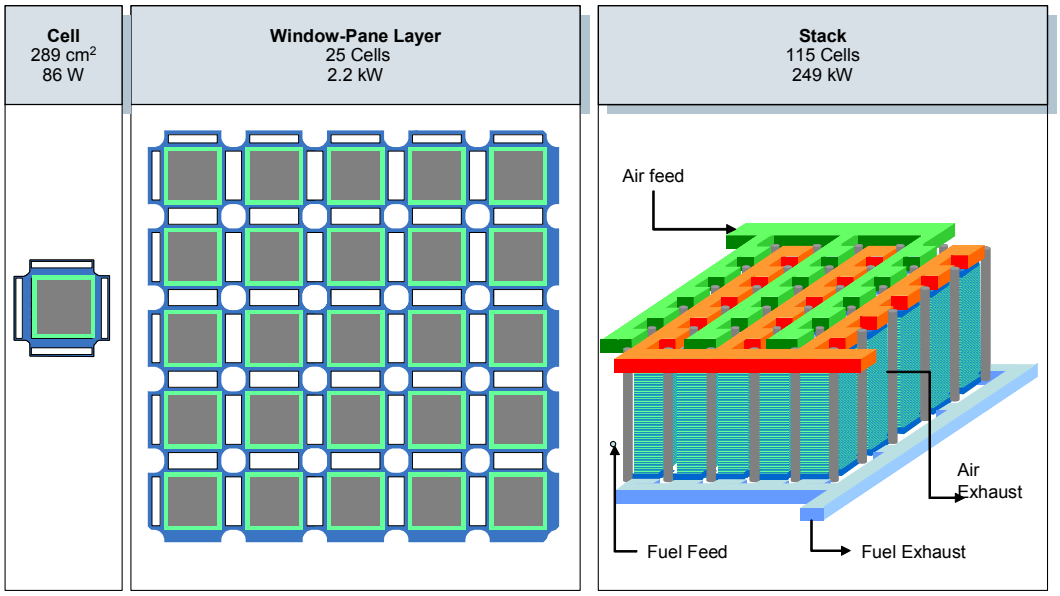

Figure 7-29 Example of Window-Pane-Style Stack Scale-Up of Planar Anode-Supported SOFC to 250 kW

Table 7-5 SOFC Manufacturers and Status of Their Technology

Manufacturer	Country	Achieved	Year	Attributes and status
Acumentrics Corp.	USA	2 kW	2002	Microtubular SOFCs, 2kW for uninterruptible power
Adelan	UK	200 W	1997	Microtubular, rapid start-up and cyclable
Ceramic Fuel Cells Ltd	Australia	5 kW 25 kW	1998 2000	Planar SOFC, laboratory stack testing, 600 operating hours for 5 kW stack, developing 40 kW fuel cell system
Delphi/Battelle	USA	5 kW	2001	Developing 5 kW units based on planar cells
Fuel Cell Technologies (with Siemens Westinghouse Power Corporation)	Canada	5 kW 2 kW	2002 2002	5 kW prototype SOFC under test, 40 percent electrical efficiency. Several Field trails planned in Sweden, USA, Japan, etc.
General Electric Power Systems (formerly Honeywell and Allied Signal)	USA	0.7 kW 1 kW	1999 2001	Planar SOFCs, atmospheric and hybrid systems
Global Thermoelectric	Canada	1 kW	2000	Planar SOFCs, 5000 hours fuel cell test
MHI/Chubu Electric	Japan	4 kW 15 kW	1997 2001	Planar SOFC, laboratory stack testing, 7500 operating hours
MHI/Electric Power Development Co.	Japan	10 kW	2001	Tubular SOFC, pressurized operation, 10 kW laboratory testing for 700 hours
Rolls-Royce	UK	1 kW	2000	Planar SOFC, laboratory testing, developing 20 kW stack for hybrid systems
Siemens Westinghouse Power Corporation	USA	25 kW 110 kW 220 kW	1995 1998 2000	Tubular SOFC, several units demonstrated on customer sites. More than 16,000 single stack operating hours, first hybrid SOFC demonstration
SOFCo (McDermott Technologies and Cummins Power Generation	USA	0.7 kW	2000	Planar SOFC, laboratory testing, 1000 operating hours, developing 10 kW versatile SOFC unit
Sulzer Hexis	Switzerland	1 kW	1998-2002	Planar SOFC, field trails of many testing
Tokyo Gas	Japan	1.7 kW	1998	Planar design, laboratory testing
TOTO/Kyushu Electric Power/Nippon Steel	Japan	2.5 kW	2000	Tubular SOFC, laboratory testing, developing 10 kW system for 2005

7.3 System Considerations

System design depends strongly on fuel type, application, and required capacity, but the stack has several important impacts on the system design and configuration:

- The stack operating temperature range, degree of internal reforming, operating voltage, and fuel utilization determine the air cooling flow required, as well as level of recuperation required. This determines specifications for the blower or compressors and the thermal management system.
- The stack geometry and sealing arrangement typically determine stack pressure drop and maximum operating pressure, which can influence the system design especially in hybrid systems.
- The stack's sulfur tolerance determines the specifications of the desulfurization system.
- The degree of internal reforming that the stack can accept influences the choice and design of the reformer.

7.4 References

1. Singhal, S.C. and K. Kendall, eds., "High Temperature Solid Oxide Fuel Cells: Fundamentals, Design and Applications". 1st ed. 2003, Elsevier Ltd.: Oxford, UK.
2. Nernst, W., Verfahren zur Erzeugung von Elektrischen Glühlicht. 1897: Deutschland., DRP 104 872
3. Baur, E. and H. Preis, Zeitung für Elektrochemie, 1937. 43: p. 727 - 732.
4. Wang, S., T. Kobayashi, M. Dokiya, and T. Hashimoto, J. Electrochemical Society, p. 3606, v. 147 (10), (2000).
5. Huang, K., R.S. Tichy, and J. B. Goodenough, J. American Ceramics Society, p. 2565, v. 81 (10), (1998).
6. Arachi, Y., H. Sakai, O. Yamamoto, Y. Takeda, and N. Imanishi, Solid State Ionics, p. 133, v. 122, (1999).
7. NexTech Materials, Ltd. Website, http://www.fuelcellmaterials.com
8. Swartz, S.L., "Low Cost Manufacturing of Multi-Layer Ceramic ***Fuels***," paper presented at Solid State Energy Conversion Alliance 2nd Annual Workshop Proceedings, March 2001, http://www.netl.doe.gov/publications/proceedings/01/seca/swartz.pdf
9. Goodenough, J.B. and K. Huang, "Lanthanum Gallate as a New SOFC Electrolyte", ProceedingstheFuelCells'97ReviewMeeting. http://www.netl.doe.gov/publications/procedings/97/97fc/FC5-5.pdf
10. Bonanos, N., B. Ellis, and M.N. Mahood, Solid State Ionics, 1991. 44: p. 305 - 311.
11. Iwahara, H., et al., Journal of the Electrochemical Society, 1993. 137(2): p. 462 - 465.
12. Kuzin, B., et al. in 5th International Symposium on Solid Oxide Fuel Cells (SOFC-V). 1997: Electrochemical Society.
13. Coors, G.W., R. Sidwell, and F. Anderson. Sixth European Solid Oxide Fuel Cell Forum. 2004. Luzern, der Schweiz: European Fuel Cell Forum.
14. Möbius, H.-H., History, in High Temperature Solid Oxide Fuel Cells: Fundamentals, Design and Applications, S.C. Singhal and K. Kendall, Editors. 2003, Elsevier Ltd.: Oxford, UK. p. 23 - 51.
15. Spacil, H.S. 1970: U.S. Pat No. 3,558,360.
16. Singhal, S.C., et al., Anode Development for Solid Oxide Fuel Cells. 1986, United States Department of Energy: Pittsburgh, PA.

17. Matsuzaki, Y. and I. Yasuda, The Poisoning Effect of Sulfur-Containing Impurity Gas on a SOFC Anode: Part I. Dependence on Temperature, Time, and Impurity Concentration. Solid State Ionics, 2000. **132**: p. 261 - 269.
18. Virkar, A.V., et al., Solid State Ionics, 2000. **131**: p. 189 - 198.
19. Juhl, M., et al., Journal of Power Sources, 1996. **61**: p. 173.
20. Ghosh, D., et al. in Solid Oxide Fuel Cells VII. 2001: The Electrochemical Society.
21. Simner, S.P. and J.W. Stevenson. Cathode - Chromia Interactions. in *SECA 2004 Annual Meeting and Core Program Review*. 2004. Boston: US DOE NETL.
22. Taniguchi, S., et al., Journal of Power Sources, 1995. **55**: p. 73 - 79.
23. Singhal, S.C., "Recent Progress in Tubular Solid Oxide Fuel Cell Technology," Proceedings of the Fifth International Symposium on Solid Oxide Fuel Cells (SOFC – V), The Electrochemical Society, Inc., Pennington, NJ, 1997.
24. Köck, W., et al. in Solid Oxide Fuel Cells IV. 1995: The Electrochemical Society Proceedings, 841.
25. Blum, L., et al. in Solid Oxide Fuel Cells IV. 1995: The Electrochemical Society Proceedings, 163.
26. Report to DOE FETC, "Assessment of Planar Solid Oxide Fuel Cell Technology", Reference 39463-02, Arthur D. Little, Inc., October 1999.
27. Lai, G.Y., "High Temperature Corrosion of Engineering Alloys," ASM 1990.
28. Yang, G., et al. Advanced Metallic Interconnect Development. in SECA 2004 Annual Meeting and Core Program Review. 2004. Boston: US DOE NETL.
29. Stevenson, J.W. SOFC Seals: Material Status. in SECA Seal Meeting. 2003. Albequerque, NM, USA: US DOE NETL.
30. Thijssen, J. and S. Sriramulu, Structural Limitations in the Scale-Up of Anode-Supported SOFCs. 2002, Arthur D. Little for US DOE: Cambridge, MA, USA.
31. George, R. and A. Casanova. Developments in Siemens Westinghouse SOFC Program. in 2003 Fuel Cell Seminar. 2003. Miami Beach, FL, USA: Department of Energy.
32. Besette, N. Status of the Acumentrics SOFC Program. in SECA 2004 Annual Meeting and Core Program Review. 2004. Boston: US DOE NETL.
33. Nakanishi, A., et al. Development of MOLB Type SOFC. in Eighth International Symposium on Solid Oxide Fuel Cells (SOFC VIII). 2003. Paris, France: The Electrochemical Society, Inc.
34. Agnew, G.D., et al. Scale-Up of a Multi-Functional Solid Oxide Fuel Cell to Multi-Tens of Kilowatt Level (MF-SOFC). in Eighth International Symposium on Solid Oxide Fuel Cells (SOFC VIII). 2003. Paris, France: The Electrochemical Society, Inc.
35. H. Mori, N. Hisatome, K. Ikeda, K. Tomida, in Solid Oxide Fuel Cells VI (SOFC - VI) (M. D. S. C. Singhal, ed.), The Electrochemical Society, Honolulu, Hawaii, 1999, p. 52
36. J. Iritani, N. Komiyama, K. Nagata, K. Ikeda, K. Tomida, in Solid Oxide Fuel Cells VII (SOFC - VII) (S. C. S. H. Yokokawa, ed.), The Electrochemical Society, Tsukuba, Japan, 2001, p. 63 .
37. Isenberg, A.O., Proceedings of the Symposium on Electrode Materials on Processes for Energy Conversion and Storage, edited by J.D.E. McIntyre, S. Srinivasan, and F.G. Will, The Electrochemical Society, Inc., Pennington, NJ, p. 682, 1977.
38. Fee, D.C., S.A. Zwick, J.P. Ackerman, in Proceedings of the Conference on High Temperature Solid Oxide Electrolytes, held at Brookhaven National Laboratory, BNL 51728, compiled by F.J. Salzano, October, 1983.

39. Sverdrup, E.F., C.J. Warde, and A.D. Glasser, in "From Electrocatalysis to Fuel Cells," edited by G. Sandstede, University of Washington Press, Seattle, WA, 1972.
40. Minh, N.Q., "Ceramic Fuel Cells," J. Am. Ceram. Soc., p. 76 [3], 563-88, 1993.
41. Courtesy of Siemens Westinghouse.
42. Vora, S.D. SECA Program at Siemens Westinghouse. in SECA 2004 Annual Meeting and Core Program Review. 2004. Boston: US DOE NETL.
43. Singhal, S.C., "Recent Progress in Tubular Solid Oxide Fuel Cell Technology," Proceedings of the Fifth International Symposium on Solid Oxide Fuel Cells (SOFC – V), The Electrochemical Society, Inc., Pennington, NJ, 1997.
44. Ide, H., et al., "Natural Gas Reformed Fuel Cell Power Generation Systems – A Comparison of Three System Efficiencies," Proceedings of the 24th Intersociety Energy Conversion Engineering Conference, The Institute of Electrical and Electronic Engineers, Washington, D.C., 1989.
45. Data from Allied – Signal Aerospace Company, 1992.
46. Zeh, C., private communication, 2nd Edition of Handbook, April, 1987.
47. Khandkar, A., S. Elangovan, "Planar SOFC Development Status," Proceedings of the Second Annual Fuel Cells Contractors Review Meeting, U.S. DOE/METC, May, 1990.
48. Warde, C.J., A.O. Isenberg, and J.T. Brown, "High Temperature Solid Electrolyte Fuel Cells Status and Programs at Westinghouse," in Program and Abstracts, ERDA/EPRI Fuel Cell Seminar, Palo Alto, CA, June, 1976.
49. Dollard, W.J., and J.T. Brown, "Overview of the Westinghouse Solid Oxide Fuel Cell Program," Fuel Cell Abstracts, 1986 Fuel Cell Seminar, Tucson, AZ, October, 1986.
50. Uchuyama, F., et al., "ETL Multi-Layer Spray Coating for SOFC Component," The International Fuel Cell Conference Proceedings, NEDO/MITI, Tokyo, Japan, 1992.
51. Maskalick, N., "Contaminant Effects in Solid Oxide Fuel Cell," Proceedings of the Fourth Annual Fuel Cells Contractors Review Meeting, U.S. DOE/METC, July, 1992.
52. Minh, N., et al, "Monolithic Solid Oxide Fuel Cell Development: Recent Technical Progress," Fuel Cell Seminar Program and Abstracts, Fuel Cell Seminar, Tuscon, AZ, November, 1992.
53. Yashida, Y., et al, "Development of Solid Oxide Fuel Cell," paper provided by Mitsubishi Heavy Industries, Ltd.
54. Khandkar, A., et al., "Planar SOFC Technology Status and Overview," Ceramatec, Inc., Fuel Cell Seminar Program and Abstracts, 1992 Fuel Cell Seminar, Tuscon, AZ, November, 1992.
55. "Research and Development on Fuel Cell Power Generation Technology," FY 1990 Annual Report, NEDO, April, 1991.
56. Nakanishi, T., "Substrate Type, Planar Solid Oxide Fuel Cell," Fuji Electric, Fuel Cell Seminar Program and Abstracts, 1992 Fuel Cell Seminar, Tucson, AZ, November, 1992.
57. Forbes, C., Private Communication, (2002).
58. R. Diethelm, Th. Gamper, M. Keller, R. Kruschwitz, D. Lenel, in Electrochemical Society, Vol. 97-18, 1997, p. 79.
59. R. Diethelm, in Electrochemical Society, Vol. 99-19, 1999, p. 60.
60. K. Honegger, M. Keller, and G.M. Christie, in Electrochemical Society, Vol. 99-19, 1999, p. 1019.
61. E. Batawi, A. Schuler, M. Keller, and C. Voisard, in Electrochemical Society, Vol. 2001-16, 2001, p. 140.

62. E. Batawi, W. Kraussler, M. Janousek, B. Boggwiler and R. Diethelm, in Electrochemical Society, Vol. 99-19, 1999, p. 731.
63. Y. Sakaki, M. Hattori, H. Miyamoto, H. Aiki, K. Takenobou, in Solid Oxide Fuel Cells VII (SOFC - VII) (S. C. S. H. Yokokawa, ed.), The Electrochemical Society, Tsukuba, Japan, 2001, p. 72 .
64. T. Satake, K. Watanabe, F. Nanjo, K. Takenobu, in USPTO, Mitsubishi Jukogyo Kabushiki Kaisha, United States, 1996.
65. M. Hattori, M. Iio, Y. Sakaki, in Seventh International Symposium on Solid Oxide Fuel Cells (SOFC - VII) (S. C. S. H. Yokokawa, ed.), The Electrochemical Society, Tsukuba, Japan, 2001, p. 1061 .
66. Nakanishi, A., et al. Development of MOLB Type SOFC. in Eighth International Symposium on Solid Oxide Fuel Cells (SOFC VIII). 2003. Paris, France: The Electrochemical Society, Inc.
67. Visco, S.J., et al. Developmet of Low-Cost Alloy Supported SOFCs. in Eighth International Symposium on Solid Oxide Fuel Cells (SOFC VIII). 2003. Paris, France: The Electrochemical Society, Inc.
68. Brandon, N., et al. Metal Supported IT-SOFCs for Operation at 500-600C. in 2003 Fuel Cell Seminar. 2003. Miami Beach, FL, USA: Department of Energy.
69. Schuler, A. An Intermediate Report on the Way to a Near-Series Sulzer Hexis Fuel Cell System. in Sixth European Solid Oxide Fuel Cell Forum. 2004. Luzern, der Schweiz: European Fuel Cell Forum.
70. Shaffer, S. Development Update on Delphi's Solid Oxide Fuel Cell System. in SECA 2004 Annual Meeting and Core Program Review. 2004. Boston: US DOE NETL.
71. Surdoval, W., S.C. Singhal, and G.L. McVay. The Solid State Energy Conversion Alliance (SECA) - A U.S. Department of Energy Initiative to Promote the Development of Mass Customized Solid Oxide Fuel Cells for Low-Cost Power. in SOFC VII. 2000. Tsukuba, Japan: The Electrochemical Society Proceedings.
72. Wang, C., W.L. Worrell, S. Park, J.M. Vohs, and R.J. Gorte, "Fabrication and Performance of Thin Film YSZ SOFCs Between 600 and 800°C," paper presented at the JointFuelCellTechnologyReviewConference,1999 http://www.netl.doe.gov/publications/proceedings/99/99fuelcell/fc7-1.pdf
73. Goodenough, J.B. and K. Huang, "Lanthanum Gallate as a New SOFC Electrolyte", Proceedings of the Fuel Cells '97 Review Meeting.
74. Surdoval, W.A., "SECA Core Technology Program," presented at Solid State Energy Conversion Alliance 3rd Annual Workshop Proceedings, March 2002. http://www.netl.doe.gov/publications/proceedings/02/SECA/SECA3Surdoval.pdf
75. Ball, R.J. and R. Stevens, "Novel Composite Electrolytes for Solid Oxide Fuel Cell Applications", paper presented at the 26th Annual International Conference on Advanced Ceramics and Composites, Cocoa Beach, FL, January 13 – 18, 2002.
76. Barnett, S., E. Perry, and D. Kaufmann, "Application of Ceria Layers to Increase Low Temperature SOFC Power Density", Proceedings of the Fuel Cells '97 Review Meeting. http://www.netl.doe.gov/publications/proceedings/97/97fc/FC6-6.pdf
77. Bhide, S.V., W. Meng, and A.V. Virkar, "Stability of Mixed Perovskite Proton Conductors," paper presented at Joint Fuel Cell Technology Review Conference, 1999.
78. Goodenough, J., "Solid Oxide Fuel Cells with Gallate Electrolytes," summary data on research supported by EPRI, 1998.

79. Steinberger-Wilckens, R., et al. Progress in SOFC Stack Development at Forschungszentrum Jülich. in Sixth European Solid Oxide Fuel Cell Forum. 2004. Luzern, der Schweiz: European Fuel Cell Forum.
80. Patel. Thermally Integrated High Power Density SOFC Generator. in SECA 2004 Annual Meeting and Core Program Review. 2004. Boston: US DOE NETL.
81. Huczkowski, P., et al. Growth Rate and Electrical Conductivity of Oxide Scales on Ferritic Steels Proposed as Interconnect Materials for SOFC. in Sixth European Solid Oxide Fuel Cell Forum. 2004. Luzern, der Schweiz: European Fuel Cell Forum.

8. FUEL CELL SYSTEMS

Although a fuel cell produces electricity, a fuel cell power system requires the integration of many components beyond the fuel cell stack itself, for the fuel cell will produce only dc power and utilize only certain processed fuel. Various system components are incorporated into a power system to allow operation with conventional fuels, to tie into the ac power grid, and often, to utilize rejected heat to achieve high efficiency. In a rudimentary form, fuel cell power systems consist of a fuel processor, fuel cell power section, power conditioner, and potentially a cogeneration or bottoming cycle to utilize the rejected heat. A simple schematic of these basic systems and their interconnections is presented in Figure 8-1.

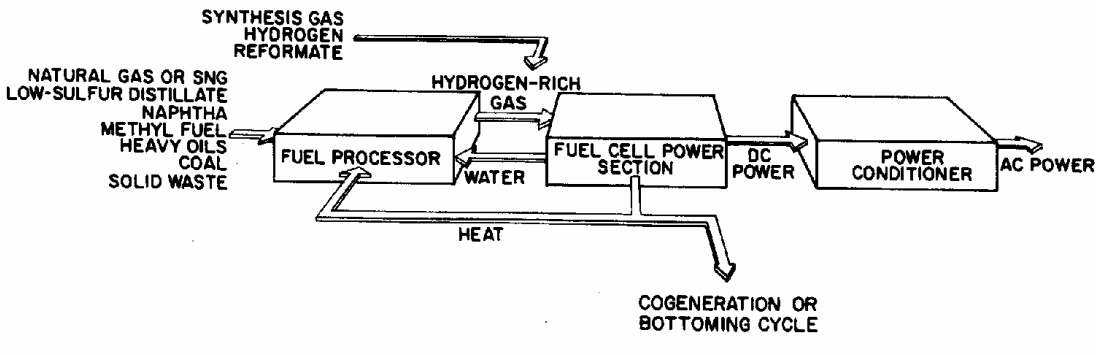

Figure 8-1 A Rudimentary Fuel Cell Power System Schematic

The cell and stacks that compose the power section have been discussed extensively in the previous sections of this handbook. Section 8.1 addresses system processes such as fuel processors, rejected heat utilization, the power conditioner, and equipment performance guidelines. System optimization issues are addressed in Section 8.2. System design examples for present day and future applications are presented in Sections 8.3 and 8.4, respectively. Section 8.5 discusses research and development areas that are required for future systems. Section 8.5 presents some advanced fuel cell network designs, and Section 8.6 introduces hybrid systems that integrate fuel cells with other generating technologies.

8.1 System Processes

The design of a fuel cell system involves more than the optimizing of the fuel cell section with respect to efficiency or economics. It involves minimizing the cost of electricity (or heat and electric products as in a cogeneration system) within the constraints of the desired application. For most applications, this requires that the fundamental processes be integrated into an efficient plant with low capital cost. Often these objectives are conflicting, so compromises, or design decisions, must be made. In addition, project-specific objectives, such as desired fuel, emission levels, potential uses of rejected heat (electricity, steam, or heat), desired output levels, volume or weight criteria (volume/kW or weight/kW), and tolerance for risk all influence the design of the fuel cell power system.

8.1.1 Fuel Processing

Fuel processing is defined in this Handbook as the conversion of a commercially available gas, liquid, or solid fuel to a fuel gas reformate suitable for the fuel cell anode reaction. Fuel processing encompasses the cleaning and removal of harmful species in the fuel, the conversion of the fuel to the fuel gas reformate, and downstream processing to alter the fuel gas reformate according to specific fuel cell requirements. Examples of these processes are:

- Fuel Cleaning – Removal of sulfur, halides, and ammonia to prevent fuel processor and fuel cell catalyst degradation.
- Fuel Conversion – Converting a fuel (primarily hydrocarbons) to a hydrogen-rich gas reformate.
- Reformate Gas Alteration – Converting carbon monoxide (CO) and water (H_2O) in the fuel gas reformate to hydrogen (H_2) and carbon dioxide (CO_2) via the water-gas shift reaction; selective oxidation to reduce CO to a few ppm, or removal of water by condensing to increase the H_2 concentration.

A fuel processor is an integrated unit consisting of one or more of the above processes, as needed for the fuel cell requirements[37] and the fuel, that function together to be cost effective for the application. Design considerations may include high thermal efficiency, high hydrogen yield (for some fuel cells hydrogen plus carbon monoxide yield), multi-cycling, compactness, low weight, and quick starting capability, depending on the application.

Figure 8-2 depicts the Processing steps needed for a low temperature cell.[38] Most fuel processors make use of the chemical and heat energy left in the fuel cell effluent to provide heat for fuel processing thus enhancing system efficiency.

37. Primarily determined by the cell's operating temperature.
38. Requires relatively complex fuel processing.

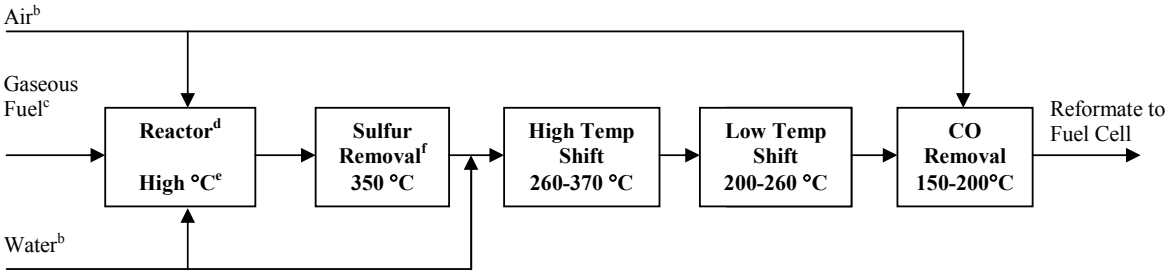

a) - For MCFC & SOFC, no high temperature shift, low temperature shift, or CO removal required.
   - For PAFC and circulating AFC, no CO removal required after low temperature shift.
   - For PEFC, all components required except that for high temperature CO removal eliminated or reduced in complexity.
b) Possible to use residual air, water, and heat of fuel effluent from fuel cell and other downstream components.
c) Vaporizer required for liquid fuels.
d) Non-catalytic POX fuel processor does not require water.
e) Temperature dependent on fuel, sulfur content of fuel, and type of reactor.
f) Can be located prior to, within, or after the reactor; liquid desulfurizer located prior to the vaporizer.

Figure 8-2 Representative Fuel Processing Steps & Temperatures

Fuel conversion and alteration catalysts are normally susceptible to deactivation by impurities,[39] thus the fuel cleaning process takes place upstream or within the fuel conversion process. The fuel conversion and reformate gas alteration processes can take place either external to the fuel cell or within the fuel cell anode compartment. The former is referred to as an external reforming fuel cell and the latter is referred to as an internal reforming fuel cell. Cells are being developed to directly react commercially available gas and liquid fuels, but the chemically preferred reaction of present fuel cells is via hydrogen-rich gas. This discussion will address external reforming fuel processors only. Descriptions of internal reforming are contained within the specific fuel cell sections. The system calculation section provides examples of heat and material balances for both externally and internally reforming fuel cells.

Fuel processors are being developed to allow a wide range of commercial fuels suitable for stationary, vehicle, and military applications. Technology from large chemical installations has been successfully transferred to small, compact fuel cells to convert pipeline natural gas, the fuel of choice for small stationary power generators. Several hundred multi-kWe commercial fuel cell units are operating that contain fuel processors (see Section 1.6). Cost is an issue, as it is with the entire fuel cell unit, for widespread commercial application. Scaling of existing fuel processing technology to larger fuel cell power plants will reduce the specific cost of the fuel processor.

Natural gas fuel reforming for fuel cells is essentially mature. Recent fuel processor research and development has focused on fuels for transportation and military applications.

39. Referred to as poisoning in catalysis literature. Ni-based fuel processing catalysts are poisoned by "physiadsorbtion" of S onto the Ni surface, thus reducing performance. Pt catalysts are less susceptible to S poisoning because S does not physiadsorb as strongly as it does on Ni; thus affecting performance less.

The issue with transportation is how to match a plausible commercial fuel infrastructure with the requirements of the fuel cell unit to be competitive. Economics drive the fuel of choice toward existing infrastructure, such as gasoline. Fuel cell requirements drive the fuel toward methanol or a "fuel cell friendly" gasoline. Environmental concerns drive the fuel of choice toward pure hydrogen[40]. Gasoline is a complex fuel, requiring high conversion temperature, and it has high levels of impurities that affect catalytic activity (see Appendix A). Methanol fuel processors (regarded by some as a necessary step towards an eventual liquid transportation fuel) are easier to develop than processors capable of converting gasoline. However, use of methanol or hydrogen would require major changes to the fuel supply infrastructure. Processors for both methanol and gasoline have been tested up to the 50 kWe level for vehicle application. What fuel to use onboard the vehicle is open to question at this time, but recent research in the fuel cell community points toward a modified gasoline tailored for fuel cell use that could be supplied through the existing fuel infrastructure (1).

The U.S. military has a substantial fuel supply infrastructure in place. The two predominant fuel types in this infrastructure are diesel and jet fuel, a kerosene. It is highly improbable that the U.S. military would change these fuels to accommodate fuel cells. Use of a fuel more suitable to the fuel cell would limit the technology's military use (there is R&D activity for fuel cell power packs to provide man-portable soldier power using hydrogen cartridges, or other hydrogen-containing forms, as well as methanol). Diesel and jet fuel are two of the most difficult conventional fuels to convert to a hydrogen-rich gas. They contain large amounts of sulfur that deactivate catalysts and require high conversion temperature. Fuel processors that convert diesel and jet fuel to a hydrogen-rich gas are in the early stages of development. The technology has been demonstrated at a 500 W size; 50 kWe units are being developed. Argonne National Laboratory (ANL) has operated a 3 kWe autothermal reformer with direct injection of diesel-like hydrocarbons – hexadecane and dodecane. Experiments with real diesel are anticipated shortly (2).

Fuel Processing Issues

Major issues that influence the development of a fuel processor are 1) choice of commercially available fuels suitable for specific applications; 2) fuel flexibility; 3) catalyst tolerance; 4) fuel cell size, and 5) vaporization of heavy hydrocarbons. Heavy hydrocarbons, such as diesel, require vaporization temperatures much in excess of 350 to 400 °C, at which temperature some of the heavier fuels pyrolyze.

Fuel Choice and Flexibility: The fuel cell is a power generation technology that is in the early stages of commercial use. As a result, it is paramount to target applications that have the potential for widespread use (to attract adequate financial investment) with the simplest technology development (to minimize development cost). There is a strong relation between viable applications and the infrastructure of available fuels.

40. The US FreedomCAR program is focused primarily towards hydrogen and secondarily towards "gasoline" as the onboard fuel.

High-value niche markets drove early fuel cell technology development. These included the use of fuel cells for on-board electric power in space vehicles, and to demonstrate that fuel cells are an efficient, environmentally-friendly technology for stationary on-site commercial power.

The technology of choice for on-board electric power on mid-length space vehicle missions (several days to a year), including the important man-moon mission, was the fuel cell. This was because the use of batteries for more than a couple of days proved too heavy, combustion engines and gas turbines required too heavy a fuel supply, and the use of a nuclear reactor was only suitable for missions of a year or more. There was a simple choice of fuel for space fuel cells: it was hydrogen because it doesn't require a fuel processor other than storage and pressurization, it is relatively lightweight when stored under pressure, and it was the best fuel for the early-developed alkaline fuel cell. Fuel flexibility was not an issue.

It was logical to exploit fuel cell space development for terrestrial use. The initial terrestrial application was to increase power generation efficiency (in reaction to the oil crisis of the early 1970s) and to improve the environment by lowering fossil-fueled power generation exhaust emission. Although coal-derived gas was recognized as a viable fuel, early fuel cell development was based on conveniently accessible pipeline gas prior to turing attention to coal-derived gas. One of the major fuel cell sponsors at the time was the natural gas industry.

Pipeline gas consists primarily of methane that is relatively easy to purify. The technology to convert methane to a H_2-rich gas existed for large chemical plants. Developers had only to adapt existing technology to small fuel cell units, not easy due to several magnitudes of scale-down. Owners of stationary power plants usually desire fuel flexibility. Fortunately, the fuel processor on these early plants could convert a light distillate, such as naphtha, with minor changes (e.g., add a vaporizer, change-out the fuel nozzles).

Once the niche markets were exploited to start fuel cells on their development path, it became necessary to target widespread potential applications while keeping technology development as simple as possible. General application areas of present interest to the fuel cell community are multi-kWe residential, commercial, and light industrial stationary power, transportation prime and auxiliary power, and military uses.

In summary, these are the applications and coupled fuel choices of interest to fuel cell technology to date:

- H_2 is preferable for a closed environment such as space vehicle application. There are sources of H_2-rich gases, such as an off-gas at a chemical plant, that require only fuel cleaning. Fuel flexibility is not applicable in either case.
- The fuel choice for small, stationary power plants is pipeline gas due to its availability for multiple commercial, light-industrial, and residential applications. Some users request that the fuel processor convert at least one additional fuel, i.e., a light distillate.
- Light vehicles are a key commercial target due to the large number of potential units; the fuel choice is open to question. Some proponents support the use of on-board hydrogen. There is a strong argument for liquid fuels due to on-board volume restrictions and existing fuel supply infrastructure. Candidate liquid fuels for light vehicles could be available gasoline or

a new gasoline, if driven by the infrastructure. Methanol may have an edge if it proves too difficult to process gasoline, provided the use of methanol compares favorably on a cost and environmental basis with present internal combustion engine (ICE) gasoline. Fuel flexibility in processors should be considered because of the indecision on fuel type and because the public is accustomed to a selection of different octane liquid fuels and diesel.

- The present infrastructure fuel for heavy vehicles is high sulfur diesel (now ~500 ppm sulfur by weight) but this may change to a nearly sulfur-free diesel as proposed by the EPA. Beginning June 1, 2006, refiners must produce a diesel containing a maximum of 15 ppm sulfur (3). The fuel for this sector could also be a gasoline if such a fuel cell system could compete.
- On-board vehicle auxiliary power is increasing dramatically to satisfy consumer convenience demands. Fuel selection for these applications parallel light and heavy vehicle fuels.
- The military will continue with its fuel infrastructure of high sulfur diesel (up to 1,000 ppm sulfur by weight) and jet fuel (JP-8, up to 300 ppm by weight). Sulfur specification will remain high because the military has to consider worldwide fuel sources. High sulfur diesel and JP-8 are close in characteristics, so no fuel flexibility is required. However, there is a possibility that some parts of the military or the Coast Guard (a military service within the DOT) could use fuels more compatible to the fuel cell in limited applications.
- As environmental regulation becomes more stringent for megawatt-size power stations and fuel cells are scaled larger in size, there is the possibility to use the U.S.'s most plentiful, indigenous fuel, coal. The term, coal, covers a broad spectrum of solid fuels that complicate fuel processing, particularly cleanup.
- There is the possibility of using other available fuels such as light distillates, ethanol, anaerobic digester gas, biomass, and refuse-derived fuel.

The market that has the greatest impact on fuel processor development at this time is in the light vehicle application sector, due to the potential large number of units. Some fuel processor developers are focusing on the development of methanol fuel processing either as the fuel of choice or as a development step toward processing gasoline. Others consider that it is best to develop a vehicle that uses the most environmentally attractive fuel, hydrogen. There are numerous opinions reagarding fuel and infrastructure best-suited for the light vehicle transportation market.

Methanol is unquestionably the easiest of the potential liquid fuels to convert to hydrogen for vehicle use. Methanol disassociates to carbon monoxide and hydrogen at temperatures below 400 °C and can be catalytically steam reformed at 250 °C or less. This provides a quick start advantage. Methanol can be converted to hydrogen with efficiencies of >90 percent. But methanol is produced primarily from natural gas, requiring energy, and it is less attractive than gasoline on a well-to-wheels efficiency basis (5, 6).

Gasoline has many advantages over methanol, but conversion to H_2 requires temperatures in excess of 650 °C and produces greater amounts of CO, methane (CH_4), and possibly coke. Without catalyst, the conversion temperature is 1,000 °C or higher. High temperatures require special materials of construction and significant preheating. Petroleum-derived fuels contain more sulfur and trace amounts of metal that could be harmful to the fuel cell. Natural gas is not

good for transportation because of its low relative energy density and 700 °C or higher processing temperature (7).

ExxonMobil has presented a position paper (8) for liquid fuels that addresses the pros and cons of methanol versus gasoline. Paraphrased excerpts from this are:

- Fuels that are most directly suited to the fuel cell are the most difficult and costly to produce and distribute. Gasoline and methanol are the leading candidates to power fuel cell engines. Both the gasoline and methanol fuel cell vehicles should be more fully developed prior to making a commercial decision on fuel choice.
- Due to methanol's corrosivity and its affinity for water, it cannot be readily distributed in today's fuel infrastructure. Methanol burns with a nearly invisible flame. Available luminosity additives won't reform in the low-temperature methanol steam reformers. Methanol is more acutely toxic than gasoline. Additives that are likely to be needed for safety and health reasons will impact the fuel processor's performance and cost.
- Gasoline fuel processing has the ability to utilize the existing infrastructure, a major advantage. It is inherently more flexible than the low temperature methanol processor, allowing multiple fuel use in the same system. The gasoline processor is also more tolerant of contaminants or additives contained in the fuel. Due to the higher energy density of gasoline, the gasoline system offers the potential for up to twice the vehicle range of the methanol system. Today's mid-sized passenger cars are about 15 to 18 percent "well-to-wheels" energy efficient as indicated in Figure 8-3.[41] Despite the increased vehicle efficiency of a methanol fuel-based system, the resultant "well-to-wheel" efficiency would be only 20 to 28 percent, lower than either gasoline hybrids or gasoline fuel cell vehicles.
- A customized gasoline for fuel cells could offer better performance and be produced at lower cost because many of conventional gasoline's more expensive ingredients would not be required. Naphtha is a common refinery stream that is an inexpensive alternative to conventional gasoline. Although its octane is too low for today's ICE, naphtha is ideal for fuel cells and could be supplied to retail stations within the existing gasoline infrastructure.

Fuel Cell and Fuel Processor Catalyst Tolerance: There are major fuel requirements for the gas reformates that must be addressed. These requirements result from the effects of sulfur, carbon monoxide, and carbon deposition on the fuel cell catalyst. The activity of catalysts for steam reforming and autothermal reforming can be affected by sulfur poisoning and coke formation; this commonly occurs with most fuels used in fuel cells of present interest. Other fuel constituents can also prove detrimental to various fuel cells. Examples of these are halides, hydrogen chloride, and ammonia.

---

41. Editor's note - The gasoline-fueled ICE well-to-wheel efficiency values apply to today's technology and are averaged over the entire driving cycle. Advanced IC engine/vehicles are more efficient over the entire operating cycle than 18% (up to 20 some odd %). This implies that future IC engine/vehicle efficiency for light vehicles can be in excess of the 15 to 18% quoted in the ExxonMobil paper. Vehicle miles per gallon increase when the ICE is combined with a battery in developmental vehicles with very low drag coefficients. For example, the 60+ mpg for the Honda Insight, 40 to 50+ mpg for the Toyota Prius, 70+ mpg for the Ford Prodigy, and ~80 mpg for the GM Precept. The overall well-to-wheel efficiency over a standard city/highway driving cycle for a four passenger, production hybrid vehicle has been estimated to be about 25-30%, close to a fuel cell vehicle. The fuel cell engines for lightweight vehicles are likely to be hybrids, and therefore the projected efficiencies must be carefully considered.

There are discrepancies in the tolerance for harmful species specified by fuel cell developers, even for similar type fuel cells. These discrepancies are probably due to electrode design, microstructure differences, or in the way developers establish tolerance. In some cases, the presence of certain harmful species causes immediate performance deterioration. More often, the degradation occurs over a long period of time, depending on the developer's permissible exposure to the specific harmful species. Here, the developer establishes an estimated cell life based on economics. The permissible amount of the harmful constituent is then determined based on economic return vs. fuel cell life expectancy.

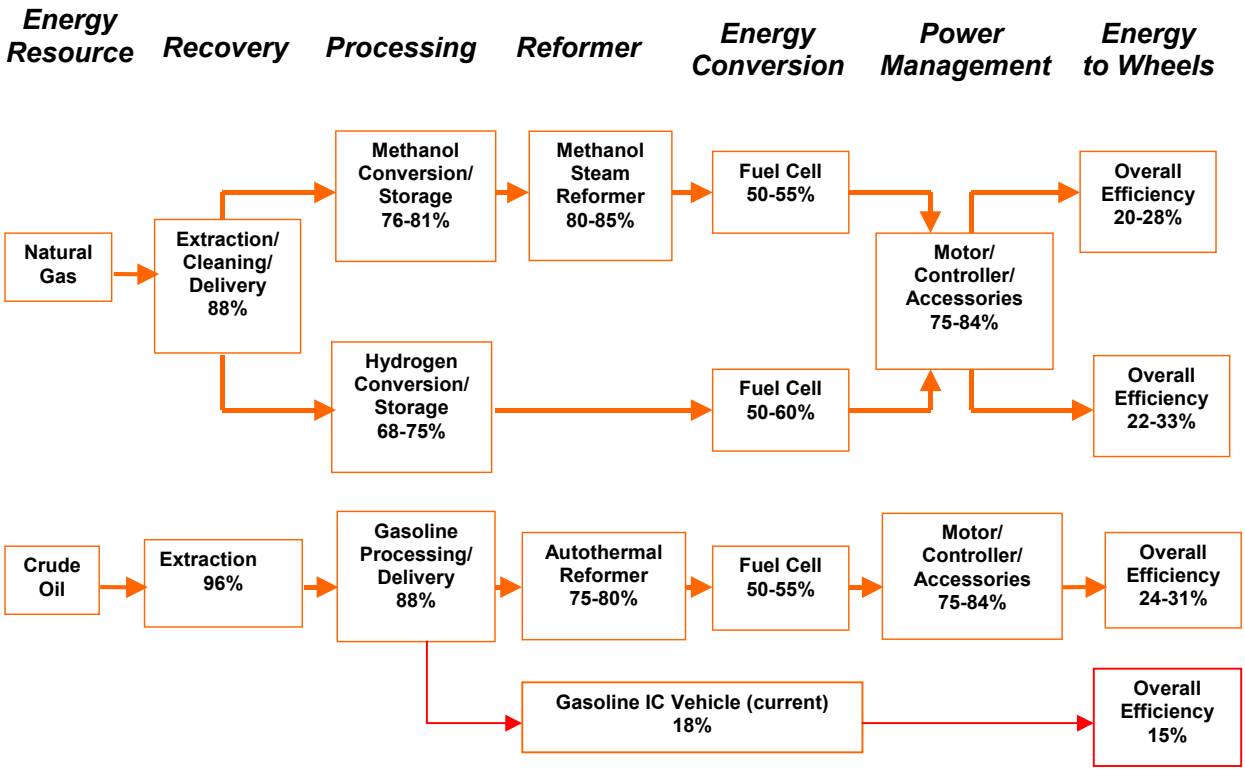

Figure 8-3 "Well-To-Wheel" Efficiency for Various Vehicle Scenarios (9)

Sulfur Effects

Present gasolines contain approximately 300 ppm by weight of sulfur. New government standards will reduce the sulfur concentration to an average of 30 ppm and a maximum of 80 ppm by 2006; however fuel gas produced from these gasolines may contain as high as 3-8 ppm of H_2S. No. 2 fuel oil contains 2,200 to 2,600 ppm of sulfur by weight. Even pipeline gas contains sulfur-containing odorants (mercaptans, disulfides, or commercial odorants) for leak detection. Metal catalysts in the fuel reformer can be susceptible to sulfur poisoning, requiring that the sulfur in the fuel reformate be removed. Some researchers have advised limiting the sulfur content of the fuel from a steam reformer to less than 0.1 ppm, but note that the limit may be higher in an autothermal reformer (10).

Sulfur poisons catalytic sites in the fuel cell also. The effect is aggravated when there are nickel or iron-containing components, including catalysts that are sensitive to sulfur and noble metal catalysts such as found in low temperature cell electrodes. Sulfur tolerances are described in the specific fuel cell sections of this handbook.[42] In summary, the sulfur tolerances of the cells of interest, by percent volume in the cleaned and altered fuel reformate gas to the fuel cells from published data, are:

- PEFC - <50 ppm sulfur as H_2S (11), poisoning is cumulative and not reversible.
- PAFC - <50 ppm sulfur as H_2S + COS or <20 ppm sulfur as H_2S at the anode. Poisoned anodes can be re-activated by polarization at high potentials.
- MCFC - <0.5 ppm sulfur as H_2S (at the cathode) equates to <10 ppm at the anode because of fuel exhaust being sent to the cathode in an MCFC (same amount of sulfur, more gas at the cathode), poisoning is reversible.
- SOFC - <1 ppm sulfur as H_2S, poisoning is reversible for the tubular SOFC. H_2S levels of 1 ppm result in an immediate performance drop, but this loss soon stabilizes into a normal linear degradation. Tests show that high temperature planar SOFCs with all-ceramic components can tolerate up to 3,000 ppm of sulfur. Sulfur, in H_2S form, has been used as a fuel for an external reforming, all-ceramic SOFC operating at 1,000 °C (12). However, developers want to reduce the cell temperature to allow less expensive metal components, primarily interconnects, and improve cycle efficiency. There is a requirement to lower sulfur significantly if metal parts are used in an SOFC. For planar SOFCs, claims for sulfur tolerance vary among the developers. The range of sulfur has been published as 10 to 35 ppm. Planar SOFC sulfur tolerance probably will be secondary to the fuel processor catalyst that, as mentioned, may be as low as 0.1 ppm.

42. There is ambiguity in the way sulfur is reported in fuel cell literature that has caused confusion in the amount that can be tolerated. Reports often fail to distinguish whether the sulfur is measured by weight, as it would be before vaporization of a liquid fuel, or by volume, as it would be in a gas fuel or fuel gas reformate. An approximate rule of thumb is that the amount (by volume) of sulfur in a vaporized fuel is one-tenth the amount of sulfur measured by weight in the liquid fuel. 300 ppm sulfur (by weight) in the liquid fuel equates to 30 ppm sulfur (by volume) when the fuel is converted to a gaseous reformate.

Carbon Monoxide Effects

Carbon monoxide, a fuel in high temperature cells (MCFC and SOFC), is preferentially absorbed on noble metal catalysts that are used in low temperature cells (PAFC and PEFC) in proportion to the H_2:CO partial pressure ratio. A particular level of carbon monoxide yields a stable performance loss. The coverage percentage is a function of temperature, and that is the sole difference between PEFC and PAFC (13). Cell limits are:

- PEFC – Consensus tolerance is <50 ppm into the anode.
- PAFC – Major US manufacturer set tolerance limit as <1.0 percent into the anode.
- MCFC – CO and H_2O shift to H_2 and CO_2 in the cell as the H_2 is consumed by the cell reaction due to a favorable temperature and catalyst.
- SOFC – CO can be a fuel. However, if the fuel gas contains H_2O, the shift reaction ($CO + H_2O \rightarrow H_2 + CO_2$) is chemically favored.

Carbon Deposition Effects

The processing of hydrocarbons always has the potential to form coke (soot). If the fuel processor is not properly designed or operated, coking is likely to occur (7). Carbon deposition not only represents a loss of carbon for the reaction, but more importantly results in deactivation of catalysts in the processor and the fuel cell due to deposition at the active sites. Thermodynamic equilibrium provides a first approximation of the potential for coke formation. The governing equations are:

$C + CO_2 \leftrightarrow 2CO$	(Boudouard)	(8-1)
$C + 2H_2 \leftrightarrow CH_4$	(carbon-hydrogen)	(8-2)
$C + H_2O \leftrightarrow CO + H_2$	(carbon-steam or gasification)	(8-3)

The possible formation of carbon using a particular fuel can be determined by the simultaneous solution of the above equations using their equilibrium coefficients.[43] No solid graphitic carbon exists at low temperatures (~600 °C) in binary mixtures containing at least 2 atoms of oxygen or 4 atoms of hydrogen per atom of carbon (14).

Fuel Cell Unit Size: The size of the fuel cell is a characteristic that impacts fuel processor selection. There is a lower level of power output at which it is no longer advantageous to incorporate a fuel processor. The decision is also application-specific. It is likely that releasing H_2 by chemical reaction from a solid compound when mixed with water is economical for small portable units (below 100 W). An H_2 storage cartridge can be replaced in seconds (15). Actually the power level at which the tradeoff is likely to occur changes as processing and storage technology advances. One fuel processor developer has produced a 100 W partial oxidation (POX) methane reactor the size of a coffee can. The unit includes a reforming zone, shift reactors, and all heat exchangers. H_2 is 36 percent (assume dry) and the CO level can be reduced to 1 percent. The unit runs on methane, propane, and ethanol (16). Another research project is investigating methanol reformers for sub-watt fuel cell power sources for the Army.

43. Carbon is slightly less likely to be deposited than equilibrium coefficient calculations indicate, due to kinetics.

Fuel Processing Techniques

The generic term most often applied to the process of converting liquid or gaseous light hydrocarbon fuels to hydrogen and carbon monoxide is “reforming”. There are a number of methods to reform fuel. The three most commercially developed and popular methods are 1) steam reforming, 2) partial-oxidation reforming, and, 3) autothermal reforming.

Steam reforming (SR) provides the highest concentration of hydrogen and can obtain a conversion efficiency. Partial oxidation (POX) is a fast process, good for starting, fast response, and a small reactor size. Non-catalytic POX operates at temperatures of appro ximately 1,400 °C, but adding a catalyst (catalytic POX or CPOX) can reduce this temperature to as low as 870 °C. Combining steam reforming closely with CPOX is termed autothermal reforming (ATR).

Steam Reforming: Historically, steam reforming has been the most popular method of converting light hydrocarbons to hydrogen. The fuel is heated and vaporized, then injected with superheated steam into the reaction vessel. The steam-to-carbon molar ratio is usually in the neighborhood of 2.5:1 but developers strive for lower ratios to improve cycle efficiency. Excess steam is used to force the reaction to completion as well as to inhibit soot formation. Like most light hydrocarbons, heavier fuels can be reformed through high temperature reaction with steam. Steam reforming is usually carried out using nickel-based catalysts. Cobalt and noble metals are also active, but more expensive. The catalytic activity depends on metal surface area. For nickel, the crystals sinter quickly above the so-called Tamman temperature (590 °C), approaching a maximum size related to the pore diameter of the support. The crystal growth results in loss of surface area and activity (17). The steam reformer can operate with or without a catalyst. Most commercial applications of steam reforming use a catalyst to enhance reaction rates at decreased temperatures. Lower temperatures favor high CO and hydrogen concentration. The reforming catalyst also promotes the water-gas shift reaction. Steam reforming is endothermic, thus favored by high temperatures. But it is a slow reaction and requires a large reactor (4). As a result, rapid start and transients cannot be achieved by steam reforming due to its inherently slower indirect heating (18). Steam reforming suits pipeline gas and light distillate stationary fuel cell power generation well.

The exothermic water-gas shift reaction occurs in the steam reformer reactor. The combined reaction, steam reforming and water gas shift, is endothermic. As such, an indirect high temperature heat source is needed to operate the reactor. This heat source usually takes the form of an adjacent, high-temperature furnace that combusts a small portion of the fuel or the fuel effluent from the fuel cell. Efficiency improves by using rejected heat from other parts of the system. Note that the intrinsic water-gas shift in the reactor may not lower the CO content to the fuel cell requirement, and additional shifting will be needed for lower temperature fuel cells.

Steam reforming of higher hydrocarbons can be used to produce methane suitable for use in high temperature internal reforming fuel cells. Steam pre-reforming of hydrocarbons, as a process step in the manufacture of hydrogen, ammonia, methanol, carbon monoxide, and syngas, is an established technology. All higher hydrocarbons are converted over a nickel-based catalyst into a gas mixture containing hydrogen, methane, and carbon oxides. Establishment of methanation and shift reaction equilibria at the process conditions determines the composition of

the pre-reformed gas. By proper design of fuel processing systems, a wide variety of fuels may be converted to a suitable reformate. This reformate can then be used to promote internal reforming for high temperature fuel cell systems. For each type of fuel, optimum operating parameters such as temperature, steam/carbon ratio, and catalyst must be established (19).

Partial Oxidation: A substoichiometric amount of air or oxygen is used to partially combust the fuel. Partial oxidation is highly exothermic, and raises the reactants to a high temperature. The resulting reaction products, still in a reduced state, are then quenched through the introduction of superheated steam. The addition of steam promotes the combined water-gas shift and steam reforming reactions, which further cools the gas. In most cases, and with sufficient pre-heating of the reactants, the overall reaction is exothermic and self-sustaining. For some applications however, particularly small-scale configurations, a catalyst can be used to increase reaction rates at lower reaction temperatures. As with steam reforming, additional, water-gas shift may be necessary to satisfy the fuel cell requirements.

POX reactor temperatures vary widely. Noncatalytic processes for gasoline reforming require temperatures in excess of 1,000 °C. These temperatures require the use of special materials and significant preheating and integration of process streams. The use of a catalyst can substantially reduce the operating temperature, allowing the use of more common construction materials such as steel. Lower temperature conversion leads to less carbon monoxide (an important considera-tion for low temperature fuel cells), so that the shift reactor can be smaller. Lower temperature conversion will also increase system efficiency.

For some heavy hydrocarbon fuels, typical values range from as low as 870 °C for catalytic POX upwards to 1,400 °C for non-catalytic POX. For sulfur-bearing diesel fuel, a catalytic POX reactor will usually operate at approximately 925 °C. This relatively elevated temperature is needed to overcome catalyst degradation due to the presence of sulfur. Non-catalytic POX reactors operate at around 1,175 °C on diesel fuel.

Advantages of POX that make this type of fuel conversion suitable for transportation power are:

- POX does not need indirect heat transfer (across a wall), so the processor is more compact and lightweight (7).
- Contrary to widely-held opinion, POX and ATR are capable of higher reforming efficiencies than are steam reformers (20).

Partial oxidation should be reacted so that the overall reaction is exothermic, but at a low oxygen-to-fuel ratio to favor higher hydrogen yields.

It is a widely-held opinion that POX leads to lower efficiency than steam reforming due to the POX reaction being exothermic. However, a thorough examination of the thermodynamics shows that POX and ATR have higher reforming efficiencies than steam reformers. This raises the question why there is a need to use steam reforming or an ATR if the POX's efficiency is higher. The minimum allowable oxygen to carbon (O/C) ratio is 1 for the POX process. This generates high heat that leads to undesirable high temperatures (low H_2, CO_2 selectivity, materials of construction constraints, etc.). The steam reformer and ATR allow lower O/C ratios, keep the temperature down, and result in higher CO_2 and H_2 selectivity (more H_2 yield per mole of fuel).

Autothermal Reforming: The coupling of SR with POX is termed autothermal reforming (ATR). Some define ATR as a SR reaction and a POX reaction that take place over microscopic distances at the same catalytic site, thus avoiding complex heat exchange (21). Others have the less restrictive definition that ATR occurs when there is no wall between a combined SR reaction and catalytic POX reaction. ATR is carried out in the presence of a catalyst that controls the reaction pathways and thereby determines the relative extents of the POX and SR reactions. The SR reaction absorbs part of the heat generated by the POX reaction, limiting the maximum temperature in the reactor. The net result can be a slightly exothermic process.

Autothermal reforming provides a fuel processor compromise that operates at a lower O/C and lower temperature than the POX; is smaller, quicker starting, and quicker responding than the SR, and results in high H_2 concentration. A catalytic POX reaction must be used to reduce the temperature to a value compatible with the SR temperature.

Other Reforming Combinations: There have been fuel processor configurations where a non-catalytic POX is placed in series with a steam reformer. Without catalyst, the POX reaction must be at a higher temperature than the steam reformer reaction. These reactions must take place in separate compartments with heat exchange and a wall between them (18). This configuration is not considered within the definition of autothermal reforming.

State-of-the-Art Components

Developers have brought fuel processing technology to the point where conversion of all fuels of interest to fuel cells have been demonstrated to a degree. Natural gas steam reforming is used in commercial fuel cell units. There has been equal success with steam reforming light distillates, although these fuels are not commonly used. Tests have been performed on reactors and complete small fuel processors using methanol, gasoline, and diesel, all suitable for vehicle use. These tests have not advanced to operation over prolonged periods. However, there have been tests that indicate these fuels can be processed in POX and ATR reactors with high levels of sulfur. Water-gas shift and methods to lower CO even to a few ppm have been developed, but the final CO cleanup processes are in an early stage of development. All fuel processors need additional engineering development to reduce volume, weight, and cost to allow widespread fuel cell power unit use. The state-of-the-art information below is based primarily on U.S. or closely-related fuel cell programs.

Generic Fuel Conversion: Considering the spectrum of fuel conversion from steam reforming to partial oxidation should convey a basic understanding of the reforming processes. An elegant, general equation published by the ANL describes fuel conversion throughout the spectrum. Autothermal reforming falls within this spectrum so that the equation encompasses processes of interest to fuel cells. The equation does not apply to complete combustion, but that conversion process is not relevant to fuel cells (20, 22, 23). The general, idealized equation is:

$$C_nH_mO_p + x(O_2 + 3.76N_2) + (2n - 2x - p)H_2O = nCO_2 + (2n - 2x - p + m/2)H_2 + 3.76xN_2 \qquad (8\text{-}4)$$

where x is the molar ratio of oxygen-to-fuel. This ratio is very important because it determines:

- The minimum amount of water that is required to completely convert the carbon in the fuel to carbon dioxide ($2n - 2x - p$). Excess water is used in practice to ensure the conversion, resulting in water in the reformate (right side of the equation). Typically, one or two moles of water for every mole of oxygen are used.
- The maximum hydrogen yield ($2n - 2x - p + m/2$)
- The maximum concentration (percentage) of hydrogen in the reformate $\{[2n - 2x - p + m/2]/[n + (2n - 2x - p + m/2) + 3.76x]$ all times 100$\}$
- The heat of reaction $\{\Delta H_r = n(\Delta H_{f,CO_2}) - (2n - 2x - p)\Delta H_{f,H_2O} - \Delta H_{f,fuel}\}$.

Decreasing the oxygen-to-fuel ratio, x, results in increasing demand for water (water-to-fuel ratio), with commensurate increases in the yield and concentration of hydrogen in the reformate gas. When $x = 0$, the equation reduces to the strongly endothermic steam reforming reaction. The reaction becomes less endothermic with increasing oxygen. It becomes thermoneutral[44] at $x = x_0$ (0.44 for methane). Above this point, the reaction becomes increasingly exothermic. At $x = 1$ with methane, the pure POX reaction, the feed contains sufficient oxygen to convert all of the carbon in the fuel to CO_2. No water needs to be added. The equation is a mix of the steam reforming reaction and the POX reaction at values of x between 0 and n.

Beyond $x = [n - (p/2)] = n$ (when $p = 0$), where water is a product, the heat of reaction is determined by the phase of the product water. At still higher values, the excess oxygen oxidizes the hydrogen to produce water. Finally, at stoichiometric combustion, all carbon and hydrogen are converted to carbon dioxide and water. Here, $x = Xc = [n - (p/2) + (m/4)]$. The value of x reduces to 2 with CH_4 as the fuel.

Equation 8-4 depicts a total reaction where the fuel input is converted to carbon dioxide. Actually, the initial reforming step is carried out at elevated temperatures, where a mixture of carbon monoxide and carbon dioxide is formed. In the subsequent reformate conversion step, the carbon monoxide is converted via the water-gas shift to carbon dioxide:

$$CO + H_2O \leftrightarrow H_2 + CO_2 \qquad (8\text{-}5)$$

44. The thermoneutral point (of oxygen-to-carbon ratio) is where the enthalpy of the reaction is zero, ($\Delta H_{f,298} = 0$).

There may be additional, downstream inputs of water/steam and oxygen/air for water-gas shift and selective oxidation to further reduce CO, if needed.

When the function of a fuel processor is to convert a fuel to hydrogen, the fuel conversion efficiency is

$$\text{Efficiency} = \frac{\text{Lower Heating Value of Anode Fuel(s) Produced}}{\text{Lower Heating Value of Fuel Used}} \qquad (8\text{-}6)$$

The fuel conversion efficiency for methane conversion to hydrogen is 93.9 percent at the thermoneutral point, $x = 0.44$ (an ATR reaction) and 91.7 percent at $x = 0$ (the SR reaction). The difference between the two efficiency values is exactly equivalent to the loss represented by the latent heat of vaporization of the H_2O that escapes with the combustions products in the SR burner exhaust. The concentration of hydrogen is 53.9 percent at $x = 0.44$ (ATR) and 80 percent at $x = 0$ (SR).

Equation 8-4 and related heats of reaction can be manipulated to show that the maximum efficiency is a state point function, regardless of path (steam reforming, partial oxidation, or autothermal reforming), and is achieved at the thermoneutral point. In practice, x is set slightly higher than the thermoneutral point so that additional heat is generated to offset heat losses from the reformer. Table 8-1 presents efficiencies at the thermoneutral point for various hydrocarbon fuels.

Table 8-1 Calculated Thermoneutral Oxygen-to-Fuel Molar Ratios (x_o) and Maximum Theoretical Efficiencies (at x_o) for Common Fuels (23)

$C_nH_mO_p$	n	m	p	$\Delta H_{f,fuel}$ (kcal/gmol)	m/2n	X_o, $\Delta H_r = 0$	Efficiency (percent)
Methanol $CH_3OH(l)$	1	4	1	-57.1	2	0.230	96.3
Methane CH_4	1	4	0	-17.9	2	0.443	93.9
Iso-Octane $C_8H_{18}(l)$	8	18	0	-62.0	1.125	2.947	91.2
Gasoline $C_{7.3}H_{14.8}O_{0.1}(l)$	7.3	14.8	0.1	-53.0	1.014	2.613	90.8

Because the components and design of a fuel processor depend on the fuel type, the following discussion is organized by the fuel being processed.

Hydrogen Processing: When hydrogen is supplied directly to the fuel cell, the fuel processing section is no more than a storage and delivery system. However, in general applications, hydrogen must be generated from other fuels and processed to meet the system requirements.

Natural Gas Processing: The major constituents of pipeline gas are methane, ethane, propane, CO_2, and, in some cases, N_2. Sulfur-containing odorants (mercaptans, disulfides, or commercial odorants) are added for leak detection. Because neither fuel cells nor commercial reformer

catalysts are sulfur tolerant, the sulfur must be removed. This is usually accomplished with a zinc oxide sulfur polisher and the possible use of a hydrodesulfurizer, if required. The zinc oxide polisher is able to remove the mercaptans and disulfides. However, some commercial odorants, such as Pennwalt's Pennodorant 1013 or 1063, contain THT (tetrahydrothiophene), more commonly known as thiophane, and require the addition of a hydrodesulfurizer before the zinc oxide sorbant bed. The hydrodesulfurizer will, in the presence of hydrogen, convert the thiophane into H_2S that is easily removed by the zinc oxide polisher. The required hydrogen is supplied by recycling a small amount of the natural gas reformed product. Although a zinc oxide reactor can operate over a wide range of temperatures, a minimum bed volume is achieved at temperatures of 350 to 400 °C (660 to 750 °F).

The CH_4 in the natural gas is usually converted to H_2 and CO in a SR reactor. Steam reforming reactors yield the highest percentage of hydrogen of any reformer type. The basic SR reactions for methane and a generic hydrocarbon are:

$$CH_4 + H_2O \leftrightarrow CO + 3H_2 \quad (8\text{-}7)$$

$$C_nH_m + nH_2O \leftrightarrow nCO + (m/2 + n)\, H_2 \quad (8\text{-}8)$$

$$CO + H_2O \leftrightarrow CO_2 + H_2 \quad (8\text{-}9)$$

In addition to natural gas, steam reformers can be used on light hydrocarbons such as butane and propane, and on naphtha with a special catalyst. Steam reforming reactions are highly endothermic and need a significant heat source. Often the residual fuel exiting the fuel cell is burned to supply this requirement. Fuels are typically reformed at temperatures of 760 to 980 °C (1,400 to 1,800 °F).

A typical steam reformed natural gas reformate is presented in Table 8-2.

Table 8-2 Typical Steam Reformed Natural Gas Reformate

Mole Percent	Reformer Effluent	Shifted Reformate
H_2	46.3	52.9
CO	7.1	0.5
CO_2	6.4	13.1
CH_4	2.4	2.4
N_2	0.8	0.8
H_2O	37.0	30.4
Total	100.0	100.0

A POX reformer also can be used to convert gaseous fuels, but does not produce as much hydrogen as the steam reformers. For example, a methane-fed POX reformer would produce only about 75 percent of the hydrogen (after shifting) that was produced by an SR. Therefore, partial oxidation reformers are typically used only on liquid fuels that are not well suited for steam reformers. Partial oxidation reformers rank second after steam reformers with respect to their hydrogen yield. For illustration, the overall POX reaction (exothermic) for methane is

$$CH_4 + ½O_2 \rightarrow CO + 2H_2 \quad (8\text{-}10)$$

When natural gas fuels are used in a PAFC or a PEFC, the reformate must be water-gas shifted because of the high CO levels in the reformate gas. A PAFC stack can tolerate about 1 percent CO in the cell before having an adverse effect on cell performance due to catalyst poisoning. The allowable CO level in the fuel gas for a PEFC is considerably lower. The shift conversion is often performed in two or more stages when CO levels are high. A first high-temperature stage allows high reaction rates, while a low-temperature converter allows for a higher conversion. Excess steam is used to enhance the CO conversion. A single-stage shift reactor is capable of converting 80 to 95 percent of the CO (24). The water gas shift reaction is mildly exothermic, so multiple stage systems must have interstage heat exchangers. Feed temperatures of high- and low-temperature shift converters range from approximately 260 to 370 °C (500 to 700 °F) and 200 to 260 °C (400 to 500 °F), respectively. Hydrogen formation is enhanced by low temperature, but is unaffected by pressure.

When used in a PEFC, the reformate must pass through a preferential CO catalytic oxidizer, even after being shifted in a shift reactor. Typically, the PEFC can tolerate a CO level of only 50 ppm. Work is being performed to increase the CO tolerance level in PEFC.

At least two competing reactions can occur in the preferential catalytic oxidizer:

$$CO + ½O_2 \rightarrow CO_2 \quad (8\text{-}11)$$
$$H_2 + ½O_2 \rightarrow H_2O \quad (8\text{-}12)$$

The selectivity of these competing reactions depends upon the catalyst and determines the quantity of required oxygen (25).

Liquid Fuel Processing: Liquid fuels such as distillate, naphtha, diesel oils, and heavy fuel oil can be reformed in partial oxidation reformers. All commercial POX reactors employ noncatalytic POX of the feed stream by oxygen in the presence of steam with reaction temperatures of approximately 1,300 to 1,500 °C (2,370 to 2,730 °F) (24). For illustration, the overall POX reaction for pentane is

$$C_5H_{12} + 5/2O_2 \rightarrow 5CO + 6H_2 \quad (8\text{-}13)$$

The overall reaction is exothermic, and largely independent of pressure. The process is usually performed at 20 to 40 atmospheres to yield smaller equipment (24). A typical fuel composition for a fuel oil fed POX reformer is presented in Table 8-3. The CO contained in this reformate may need to be converted with a shift converter or selective catalytic converter, depending upon the specific fuel cell being fed.

Table 8-3 Typical Partial Oxidation Reformed Fuel Oil Reformate (24)

Mole Percent (dry, basis)	Reformer Effluent
H_2	48.0
CO	46.1
CO_2	4.3
CH_4	0.4
N_2	0.3
H_2S	0.9
Total	100.0

Alcohols are steam-reformed at lower temperatures (<600 °C) while alkanes[45] and unsaturated hydrocarbons require slightly higher temperatures. Cyclic hydrocarbons and aromatics have also been reformed at relatively low temperatures, however a different mechanism appears to be responsible for their reforming. Blended fuels like gasoline and diesel, that are mixtures of a broad range of hydrocarbons, require temperatures of >700 °C maximum hydrogen production. Methanol, one of the fuels being considered for transportation applications, can be converted into hydrogen by steam reforming:

$$CH_3OH = CO + 2H_2 \quad (8\text{-}14)$$
$$CO + H_2O = CO_2 + H_2 \quad (8\text{-}15)$$

The equivalent overall result of these two specific reactions is:

$$CH_3OH + H_2O = CO_2 + 3H_2 \quad (8\text{-}16)$$

The optimum choice of operating conditions is close to a steam to methanol ratio of 1.5 and a temperature range of 250 °C to 399 °C. Pressure does not influence the reaction rate, but very high pressures limit the equilibrium conversion, which otherwise is better than 99 percent at the preferred range of 5 to 15 bars. The Cu/Zn/Al and Cu/Zn/Cr based catalysts have been used in industrial units for many years (17).

Coal Processing: The numerous coal gasification systems available today can be reasonably classified as one of three basic types: 1) moving-bed, 2) fluidized-bed, and 3) entrained-bed. All three of these types use steam and either air or oxygen to partially oxidize coal into a gas product. The moving-bed gasifiers produce a low temperature (425 to 650 °C; 800 to 1,200 °F) gas containing devolatilization products such as methane and ethane, and hydrocarbons including naphtha, tars, oils, and phenol. Entrained-bed gasifiers produce a gas product at high temperature (>1,260 °C; >2,300 °F composed almost entirely of hydrogen, carbon monoxide, and carbon dioxide. The fluidized-bed gasifier product gas falls between these two other reactor types in composition and temperature (925 to 1,040 °C; 1,700 to 1,900 °F).

45. Alkanes are saturated hydrocarbons, i.e., no double carbon bonds. Examples are CH_4, C_2H_6, C_3H_8, and C(n)H(2n+2). Alkenes have carbon-carbon double bonds such as ethene C_2H_4 and C(n)H(2n).

The heat required for gasification is supplied by the partial oxidation of coal. Overall, the gasification reactions are exothermic, so waste heat boilers often are used at the gasifier effluent. The temperature, and therefore composition, of the product gas depends upon the amount of oxidant and steam, as well as the design of the reactor.

Gasifiers typically produce contaminants that must be removed before entering the fuel cell anode. These contaminants include H_2S, COS, NH_3, HCN, particulates, tars, oils, and phenols. The contaminant levels depend on both the fuel composition and the gasifier employed. There are two families of cleanup that remove the sulfur impurities: hot and cold gas cleanup systems. Cold gas cleanup technology is commercial, has been proven over many years, and provides the system designer with several choices. Hot gas cleanup technology is still developmental and would likely need to be joined with low temperature cleanup systems to remove the non-sulfur impurities in a fuel cell system. For example, tars, oils, phenols, and ammonia could all be removed in a low temperature water quench followed by gas reheat.

A typical cold gas cleanup process following an entrained gasifier would include the following subprocesses: heat exchange (steam generation and regenerative heat exchange), particulate removal (cyclones and particulate scrubbers), COS hydrolysis reactor, ammonia scrubber, acid gas (H_2S) scrubbers (Sulfinol, SELEXOL), sulfur recovery (Claus and SCOT processes), and sulfur polishers (zinc oxide beds). All of these cleanup systems increase process complexity and cost, while decreasing efficiency and reliability. In addition, many of these systems have specific temperature requirements that necessitate the addition of heat exchangers or direct contact coolers.

For example, a COS hydrolysis reactor operates at about 180 °C (350 °F), the ammonia and acid scrubbers operate in the vicinity of 40 °C (100 °F), while the zinc oxide polisher operates at about 370 °C (700 °F). Thus, gasification systems with cold gas cleanup often become a maze of heat exchange and cleanup systems.

Typical compositions for several oxygen-blown coal gasification products are shown in Table 8-4.

Table 8-4 Typical Coal Gas Compositions for Selected Oxygen-Blown Gasifiers

Gasifier Type	Moving-Bed	Fluidized-Bed	Entrained-Bed			
Manufacturer	**Lurgi (20)**	**Winkler**	**Destec**	**Koppers-Totzek**	**Texaco**	**Shell**
Coal	Illinois No. 6	Texas Lignite	Appalachian Bit.	Illinois No. 6	Illinois No. 6	Illinois No. 6
Mole Percent						
Ar	trace	0.7	0.8	0.9	0.9	1.1
CH_4	3.3	4.6	0.6	-	0.1	-
C_2H_4	0.1	-	-	-	-	-
C_2H_6	0.2	-	-	-	-	-
CO	5.8	33.1	45.2	43.8	39.6	63.1
CO_2	11.8	15.5	8.0	4.6	10.8	1.5
COS	trace	-	-	0.1	-	0.1
H_2	16.1	28.3	33.9	21.1	30.3	26.7
H_2O	61.8	16.8	9.8	27.5	16.5	2.0
H_2S	0.5	0.2	0.9	1.1	1.0	1.3
N_2	0.1	0.6	0.6	0.9	0.7	4.1
NH_3+ HCN	0.3	0.1	0.2	-	-	-
Total	100.0	100.0	100.0	100.0	100.0	100.0

Reference Sources: (26, 27)
Note: All gasifier effluents are based on Illinois No. 6, except the Winkler, which is based on a Texas Lignite, and the Destec, which is based on an Appalachian Bituminous.

Other Solid Fuel Processing: Solid fuels other than coal can be utilized in fuel cell systems. For example, biomass and RDF (refuse-derived-fuels) can be integrated into a fuel cell system as long as the gas product is processed to meet the requirements of the fuel cell. The resulting systems would be very similar to the coal gas system with appropriate gasifying and cleanup systems. However, because biomass gas products can be very low in sulfur, the acid cleanup systems may simply consist of large sulfur polishers.

State-of-the-Art Components - Cleaning and Reformate Gas Alteration (Removal Of Contaminants): Besides their basic fuel reforming function, fuel processors require the removal of impurities that degrade the fuel processor or fuel cell performance. Sulfur is the major contaminant encountered. Carbon monoxide reduction for low temperature fuel cells and avoidance of carbon deposition are also addressed. A typical processing chain for a low temperature fuel cell will have a hydrodesulfurizer, a halogen guard, a zinc oxide sulfur absorber, a catalytic reformer, a high temperature shift converter, a second halogen guard, and low temperature shift converter. Figure 8-2 provides insight into how these may be arranged. The function of all these components, except the reformer, is to remove impurities. For the PEFC, an additional device is necessary to remove essentially all CO, such as a preferential oxidizer (28).

Sulfur Reduction: There are high temperature and low temperature methods to remove sulfur from a fuel reformate. Low temperature cleanup, such as hydrodesulfurizing (limited to fuels

with boiling end points below 205 °C), is less difficult and lower in cost so should be used where possible, certainly with low temperature fuel cells. Sulfur species in the fuel are converted to H_2S, if necessary, then the H_2S is trapped on zinc oxide. A minimum bed volume of the zinc oxide reactor is achieved at temperatures of 350 to 400 °C. Thermodynamic and economic analyses show that it is appropriate to use high temperature cleanup with high temperature fuel cells.

There is a vast difference between removing sulfur from a gaseous fuel and a liquid fuel. The sulfur in a liquid fuel is usually removed after it is converted to a gas. This by removing the sulfur in the reforming reactor at high temperature, or by incorporating sulfur resistant catalysts. Sulfur resistant catalysts are being developed, but none are mature enough for present use. ANL is developing catalysts to reform gasoline, and have demonstrated that their catalyst can tolerate sulfur. The ANL catalyst has been shown to tolerate (100s of hours) sulfur present in natural gas in an engineering scale reformer.

At least one developer has a liquid-phase fuel desulfurizer cartridge that will be used to remove sulfur prior to fuel vaporization. Other developers remove the sulfur immediately after vaporization and prior to reforming. Hydrogen must be recirculated to the removal device to convert the sulfur species to H_2S so that it can be entrapped on zinc oxide. Zinc oxide beds are limited to operation at temperatures below 430 °C to minimize thermal cracking of hydrocarbons that can lead to coke formation. Thermodynamics also favor lower temperatures. At higher temperatures, the H_2S cannot be reduced to levels low enough for shift catalyst or to reach fuel cell limits. For sulfur removal in the reformer, the presence of significant concentrations of steam in the fuel gas has a negative impact on the reaction equilibrium, leading to a higher concentration of H_2S than could be achieved with a dry fuel gas.

Carbon Monoxide Reduction: The use of CO as a fuel in high temperature cells and water-gas shift reactions to lower carbon monoxide to conditions suitable for a PAFC or a PEFC have been previously described. Fuel gas reformate contains 0.5 to 1 percent by volume of CO even after the shift reactions. Present PEFCs operate below 100 °C. At these temperatures, even small amounts of CO are preferentially adsorbed on the anode platinum (Pt) catalysts. This blocks access of H_2 to the surface of the catalyst, degrading cell performance (29). Reformate for PEFC stacks must contain very low (<50 ppm) CO to minimize Pt absorption to a reasonable value to maintain sufficient active sites for the oxidation of H_2. This can be achieved in two ways, by air injection into the anode at up to about 4 percent of the reformate feed rate or by reducing CO concentration prior to the cell: even at 50 ppm, catalyst poisoning by CO must be mitigated by the injection of some air at the anode. For the latter approach, a preferential oxidizer (PROX) is used to reduce CO concentration prior to the cell. It has highly dispersed supported Pt or Pt-Ru (ruthenium) catalyst. Such catalysts act on the principle of selective adsorption of CO onto the active Pt or Pt-Ru (relative to H_2), leading to CO being selectively oxidized by stoichiometric amounts of air co-fed to the catalyst bed. As the CO is oxidized, the gas temperature rises, which decreases the selectivity of CO adsorption on the catalyst and also increases the kinetics of the reverse water-gas shift reaction. In practice, the PROX process is carried out in stages to permit cooling between stages. The PROX is a relatively large unit that operates at 100 to 180 °C (22). Preferential gas cleanup by selective oxidation results in 0.1 to 2 percent H_2 lost (30).

Carbon Deposition Avoidance: The processing of hydrocarbons always has the potential to form coke. Coke formation is influenced by the composition of the fuel, the catalyst, and the process conditions (e.g., partial pressure of steam). Coke causes the greatest problems in gas flow paths and on catalyst. Carbon deposition not only represents a loss of carbon for the reaction, but more importantly also results in deactivation of the catalyst due to deposition at the active sites. Thermal cracking[46] in over-heated preheaters and manifolds can easily form carbon. If the fuel conversion reactor is not properly designed or operated, coking is likely to occur. Thermo dynamic equilibrium provides a first approximation of the potential for coke formation. Free carbon in hydrocarbon fuels forms according to the three equations, (8-1), (8-2), and (8-3). Figures 8-4 and 8-5 show the effect of increasing steam on carbon deposition for methane and octane, respectively. Increasing steam, hydrogen, and carbon dioxide concentrations alleviates carbon deposition. Low contents of aromatics and alkenes help to maintain the activity of the catalyst (10). No carbon deposits at low temperatures (~600 °C) in mixtures containing at least two atoms of oxygen and four atoms of hydrogen per atom of carbon. At these conditions, all carbon is present as CO_2 or CH_4 (7).

Higher hydrocarbon fuels show a greater tendency for carbon formation than does methane. One method to alleviate carbon deposition problems in the fuel processor is to use special catalysts either containing alkali or based on an active magnesia support. With a highly active catalyst, the limit permitted on the final boiling point of the hydrocarbon feedstock is related mainly to the possibility of desulfurizing the feed to below 0.1 ppm, rather than to the reactivity of the hydrocarbons. With proper desulfurization, it has been possible to convert light oil into syngas with no trace of higher hydrocarbons in the reformate gas (17).

Coke formation resulting from higher hydrocarbon fuels can also be eliminated with an adiabatic pre-reformer. The adiabatic reformer is a simple fixed bed reactor. By adiabatic pre-reforming, all higher hydrocarbons are converted at low temperature (below ~500 °C) with steam into methane, hydrogen, and carbon oxides at conditions where carbon formation does not occur. It is possible to use a high pre-heating temperature (650 °C or above) for internal reforming in MCFC and SOFC without the risk of carbon formation. For natural gas containing only minor amounts of higher hydrocarbons, adiabatic pre-reforming at a steam to carbon ratio as low as 0.25 mole/atom has been demonstrated. For heavier feedstocks such as naphtha, operation at a steam to carbon ratio of 1.5 has been proven in industry. Pilot tests have been carried out at a steam to carbon ratio of 1.0 with reformate recycle.

46. Thermal cracking is the breaking of a hydrocarbon carbon-carbon bond through the free-radical mechanism. Cracking may result in the formation of lower chained hydrocarbons, the original "cracked" hydrocarbon, or further cracking of the hydrocarbon to soot.

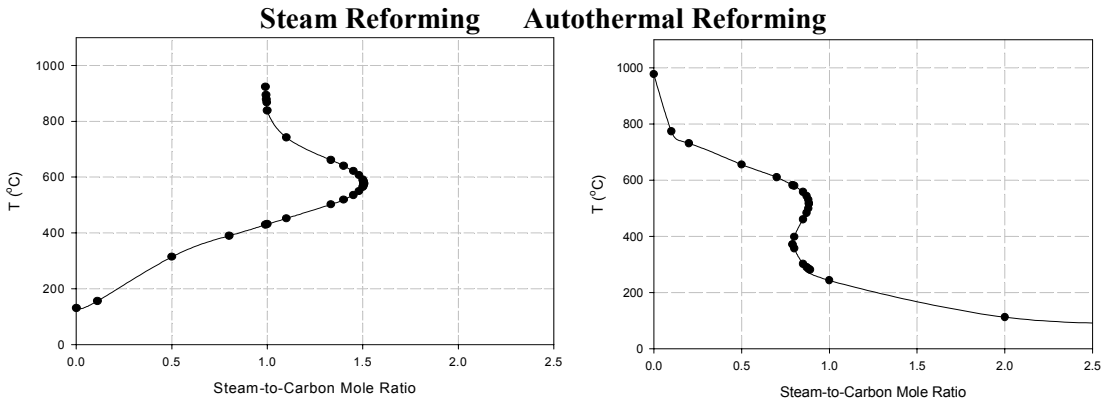

Figure 8-4 Carbon Deposition Mapping of Methane (CH_4)
(Carbon-Free Region to the Right of Curve)

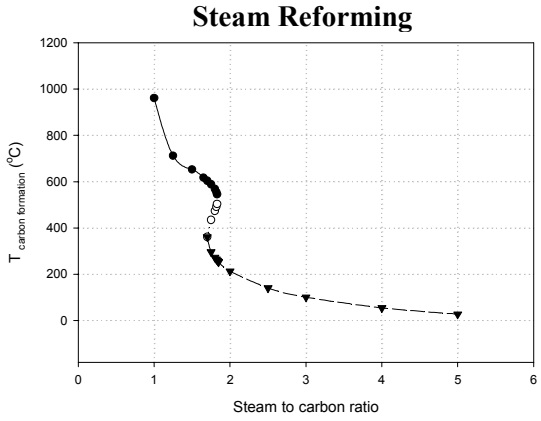

Figure 8-5 Carbon Deposition Mapping of Octane (C_8H_{18})
(Carbon-Free Region to the Right and Above the Curve)

Coking can be also be avoided by operating at high temperatures and at high oxygen-to-carbon ratios, where the ratio is based on the total atoms of oxygen contained in the steam and air feeds. For a given O/C ratio in the feed, it is preferable that the oxygen comes from water. Thus, for a given O/C, SR is preferred over ATR, which is preferred over POX; "preferred" meaning that coke formation can be avoided while still operating at a lower temperature (20, 23, 31).

Other Impurities Reduction: Halides in fuels such as naphtha have deleterious effects on steam reforming and low temperature shift, thus halogen guards must be included in fuel processing.

There are many types of coal with different compositions, including harmful species. One common constituent, HCl, will cause formation of stable chlorides and corrosion in a MCFC. There has not been much work in SOFC yet on this topic. It is doubtful whether low temperature cells will be fueled by coal.

Research & Development Components

There are two major areas where fuel processor developers are focusing their research and development efforts, catalyst development and process/engineering development. A smaller, long term effort on novel processing schemes is in the early stages of investigation.

Catalyst Development. Performance targets for the fuel processor for transportation fuel cell systems will require that the reforming catalysts used in these processors exhibit a higher activity and better thermal and mechanical stability than reforming catalysts currently used in the production of H_2 for large-scale manufacturing processes. To meet these targets, reforming catalysts will have to process the feed at a space velocity of 200,000/hr (based on the volumetric flow of the feed in the gaseous state at 25 °C and 1 atm) with a fuel conversion of >99 percent and a H_2 selectivity of >80 percent (moles of H_2 in product/moles of H_2 "extractable" from the feed), and have a lifetime of 5,000 hr. Given the potential market for transportation applications, many of the major catalyst producers, such as Johnson-Matthey, Engelhard Corporation, and dmc^2 division of OM Group, Inc., have begun to develop new reforming catalysts (32). An ANL program is focused on improving long-term stability (minimize deactivation), an important, immediate goal, reducing coke formation for higher hydrocarbons, and improving catalyst sulfur tolerance while addressing cost issues. A major issue is to demonstrate that the catalyst can operate for 40,000+ hours in stationary applications and 4,000+ hours in transportation applications. It is believed that no one has successfully demonstrated these targets. Another issue is that coke formation will be problematic with higher hydrocarbons, especially diesel. Most industrial reforming catalysts are operated steam-rich to minimize coke formation. However, this increases the size of the reformer as well as the energy needed to vaporize the water. This option may not be viable for reformers used with fuel cells. Finally, <20 ppb of S is the target for use with nickel steam reforming catalyst. Most fuels being considered contain either sulfur at the ppm level, such as gasoline, or added as an odorant for safety reasons, such as to natural gas. The ability of the catalyst to process fuels containing ppm levels of sulfur would be beneficial. The ANL catalysts are based on solid oxide fuel cell technology, where a transition metal is supported on an oxide- ion-conducting substrate, such as ceria, zirconia, or lanthanum gallate, that has been doped with a small amount of a non-reducible element, such as gadolinium, samarium, or zirconium. Platinum was the transition metal used in the first generation of the ANL catalyst. Because of concerns over the cost associated with using a precious metal-based catalyst, work has begun on reducing the cost of the catalyst either by replacing Pt with a less expensive non-noble metal or by using a combination of a noble metal, at a considerably lower metal loading, and with a base metal without sacrificing performance. Work is proceeding on catalysts based on Ni, Rh, and combinations of Ni and Rh. Süd-Chemie, Inc. currently produces reforming catalysts based on this technology under a licensing agreement with Argonne (32).

There is also a need to develop better water gas shift catalysts (7, 33, 34), especially catalysts that operate at temperatures ranging from 200 to 300 ^{o}C. Commercial shift catalysts based on FeCr and CuZn oxides are available, but are not designed for the rapid startups and frequent exposure to oxidizing conditions that will be experienced during normal operation of fuel processors developed for transportation applications. These commercial catalysts have fixed size, high density, and are susceptible to contaminant poisoning by ingredients found in

infrastructure fuels. Of primary concern is the need to reduce these catalysts in a well-controlled manner that minimizes temperature rise in order to achieve maximum catalyst activity and to prevent the exposure of the catalyst in the reduced state to oxidizing conditions. For example, the CuZn catalysts will sinter if exposed to >270 ^{o}C and are pyrophoric when exposed to air in the reduced state. Present commercial catalysts are developed for process plant service where transient conditions are not a concern. There is a need for highly active catalysts that can be supported on a low density monolith that do not require reduction in order to be active and are stable when exposed to oxidizing conditions. ANL is developing a more robust shift catalyst that will work better under transient operating conditions than present catalysts developed for process plant service. The advantage of this catalyst over standard catalysts is that it is air stable, which is needed for many start-up and shutdown cycles. There is a trade-off of a moderate reduction in activity (35).

There is also a need to demonstrate that the low-temperature, PROX catalysts have high selectivity toward CO and long term stability.

Process/Engineering Development Numerous engineering and process issues are being addressed by fuel processor developers (20, 31, 36). Several major issues are:

- As the size of the catalyst bed increases, the segregation within an ATR reactor bed toward over-oxidation and catalyst overheating in the front of the bed, and air starvation and carbon formation in the back end of the bed are important to consider. Maintaining a good temperature distribution in the bed, especially with a large reactor, is identified as one of the challenges facing this approach.
- Fuel processor tests have been on the order of 40 hours, although the fuel processors have been tested for 1,000 hours on natural gas. There is a need is to show similar results at realistic operating conditions and further engineering development to enhance the catalyst activity and make the fuel processor lighter and smaller.
- There is a need to investigate improved and simplified fuel processor designs. Examples are combining the reformer and the desulfurizer in a single stage to reduce weight and volume, producing an integrated vaporizer design, and designing for a wide variation of fuel vaporization temperatures to allow fuel flexible operation.
- Transient issues are important in transport applications and should be addressed early by testing. The challenge is to demonstrate the operation at high sulfur content over the full operating envelope of the vehicle – start-up, transients, shutdown, sulfur spikes in the fuel, etc. using the same processor.

Novel Processing Schemes: Various schemes have been proposed to separate the hydrogen-rich fuel in the reformate for cell use or to remove harmful species. At present, the separators are expensive, brittle, require large pressure differential, and are attacked by some hydrocarbons. There is a need to develop thinner, lower pressure drop, low cost membranes that can withstand separation from their support structure under changing thermal loads. Plasma reactors offer independence of reaction chemistry and optimum operating conditions that can be maintained over a wide range of feed rates and H_2 composition. These processors have no catalyst and are compact. However, results are preliminary and have only been tested at a laboratory scale.

Other: Although not R&D, it should prove beneficial for fuel cell developers to provide fuel tolerance specifications to fuel processor developers. Tolerances should be established by standard definition, determination methods, and measurement procedures. This would aid the fuel processor developer to deliver products compatible with various fuel cell units. Of particular importance are sulfur and CO limits.

8.2 Power Conditioning

Power conditioning is an enabling technology that is necessary to convert DC electrical power generated by a fuel cell into usable AC power for stationary loads, automotive applications, and interfaces with electric utilities. The purpose of this section is to explore power conditioning approaches for the following applications:

- Fuel cell power conversion to supply a dedicated load
- Fuel cell power conversion to supply backup power (UPS) to a load connected to a local utility
- Fuel cell power conversion to supply a load operating in parallel with the local utility (utility interactive)
- Fuel cell power conversion to connect directly to the local utility
- Power conversion for automotive fuel cell applications
- Power conversion architectures for a fuel cell turbine hybrid interfaced to local utility

Figure 8-6 shows a block diagram of a representative fuel cell power plant. Natural gas flows to a fuel processor, where the methane is reformed to hydrogen-rich gas. The hydrogen gas reacts in the power producing section, which consists of a fuel cell. The DC power generated by the fuel cell must be converted to AC power; one of the power conditioning approaches identified above would be selected, based on the specific application.

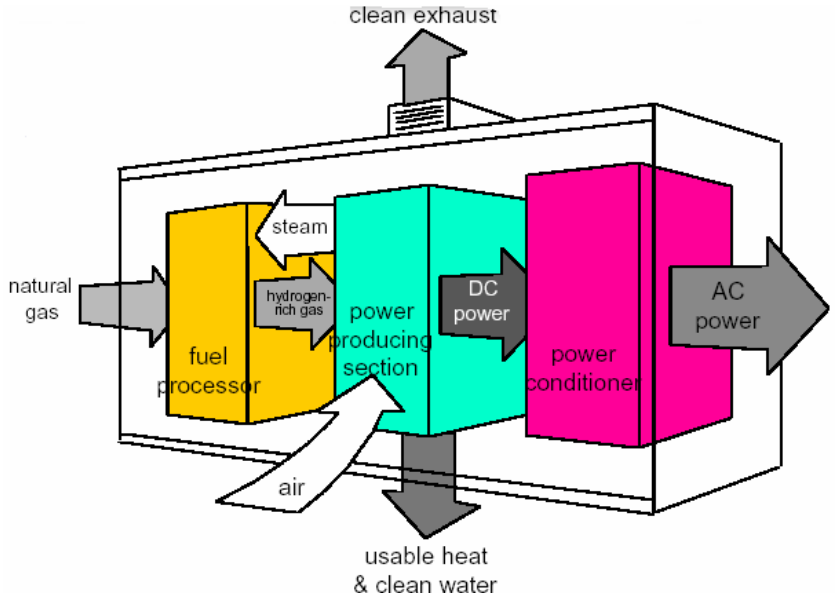

Figure 8-6 Block diagram of a fuel cell power system

8.2.1 Introduction to Fuel Cell Power Conditioning Systems

Various power conversion "building" blocks, such as DC-DC converters and DC-AC inverters, are employed in fuel cell power conditioning systems. Figure 8-7 shows a typical variation of the output voltage of a fuel cell stack in response to changes in load current. Since the DC voltage generated by a fuel cell stack varies widely and is low in magnitude (<50V for a 5 to 10kW system, <350V for a 300kW system), a step up DC-DC converter is essential to generate a regulated higher voltage DC (400V typical for 120/240V AC output). The DC-DC converter is responsible for drawing power from the fuel cell, and therefore should be designed to match fuel cell ripple current specifications. Further, the DC-DC converter should not introduce any negative current into the fuel cell. A DC-AC inverter is essential to provide the DC to useful AC power at 60Hz or 50Hz frequency. An output filter connected to the inverter filters the switching frequency harmonics and generates a high quality sinusoidal AC waveform suitable for the load.

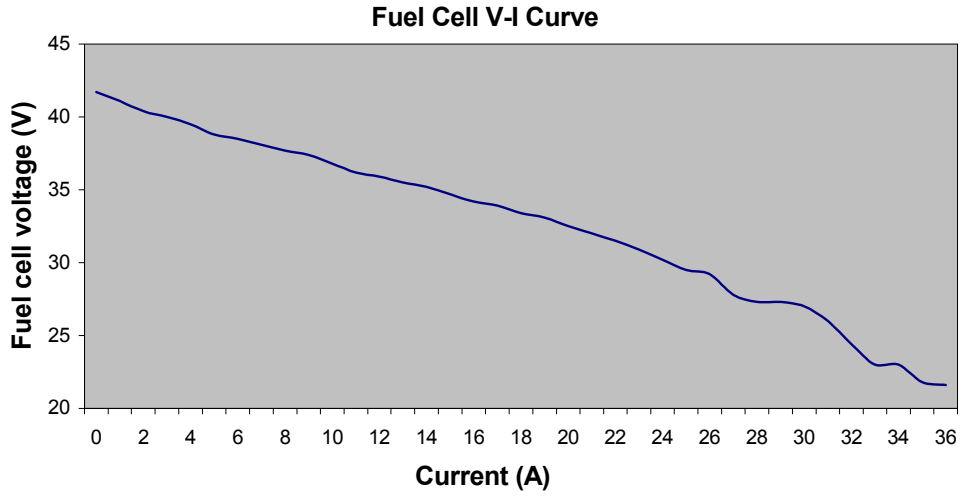

Figure 8-7a Typical fuel cell voltage / current characteristics [1]

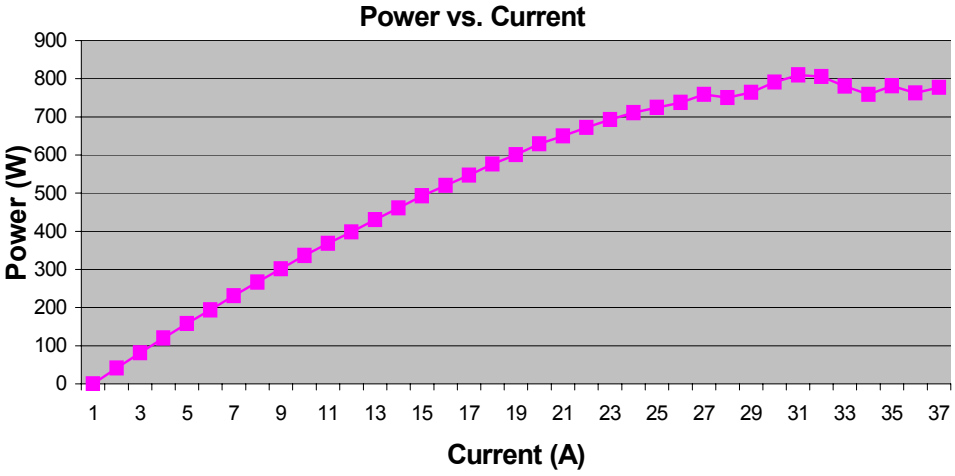

Figure 8-7b Fuel cell power vs. current curve [1]

8.2.2 Fuel Cell Power Conversion for Supplying a Dedicated Load [2,3,4]

Fuel cell power conversion for a 10kW stand-alone load is a representative example for distributed generation. Figure 8-7 shows the variation of fuel cell output voltage vs. load; fuel cell output DC voltage exhibits nearly 2:1 voltage range (Figure 8-7a). The power conversion unit must be capable of operating in this range and, in particular, be able to deliver rated power while regulating output voltage. Output from the power conversion unit is expected to be high quality power with less than 5 percent total harmonic distortion (THD). For domestic loads, a 5:1 or better peak to average power capability for tripping breakers and starting motors is desired. This puts an additional constraint on the design of the power conditioning unit for stand-alone loads. Table 8-5 shows a typical specification for a stand-alone fuel cell power conditioning unit.

.

Table 8-5: Specifications of a typical fuel cell power conditioning unit for stand-alone domestic (U.S.) loads

Continuous output power:	10 kW continuous
Output Phase (s):	Split single-phase, each output rated for 0 to 5,000 VA, not to exceed 10,000 VA total
Output voltage:	120V, 240V Sinusoidal AC. Output voltage tolerance no wider than ±6 percent over the full allowed line voltage and temperature ranges, from no-load to full-load. Frequency 60±0.1 Hz.
Output frequency:	60Hz (U.S.) or 50Hz (Europe) with enough precision to run AC clock accuracy
Fuel Cell Current Ripple: (Fuel cell dependent)	▪ 120 Hz ripple: < 15 percent from 10 to 100 percent load ▪ 60 Hz ripple: < 10 percent from 10 to 100 percent load ▪ 10 kHz and above: < 60 percent from 10 to 100 percent load
Output THD:	< 5 percent
Protection:	Over current, over voltage, short circuit, over temperature, and under voltage. No damage caused by output short circuit. The inverter must shut down if the input voltage dips below the minimum input of 42 V. Inverter should not self-reset after a load-side fault. IEEE Standard 929 is a useful reference.
Acoustic Noise:	No louder than conventional domestic refrigerator. Less than 50 dBA sound level measured 1.5 m from the unit.
Environment:	Suitable for indoor installation in domestic applications, 10 °C to 40 °C possible ambient range.
Electromagnetic Interference	Per FCC 18 Class A -- industrial
Efficiency:	Greater than 90 percent for 5kW resistive load
Safety:	The system is intended for safe, routine use in a home or small business by non-technical customers.
Life:	The system should function for at least ten years with routine maintenance when subjected to normal use in a 20 °C to 30 °C ambient environment.

Currently, fuel cells supply only average power from the fuel cell. Thus, peak power must be supplied from some other energy source such as a battery or supercapacitor [5,6]. The power conditioning unit must therefore provide means for interfacing a battery and also ensure its charge maintenance. Figure 8-8 shows a block diagram of a typical fuel cell powered unit for supplying a load along with a battery interface. Figures 8-9 through 8-11 show three possible block diagrams and circuit topologies of power conversion units for this application.

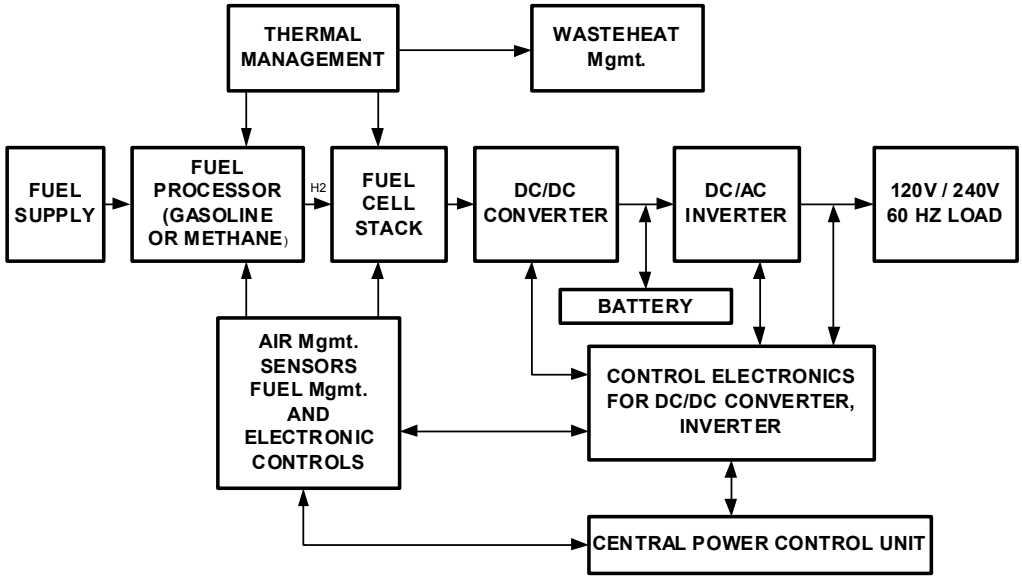

Figure 8-8 Block diagram of a typical fuel cell powered unit for supplying a load (120V/240V)

Power conditioning unit with line frequency transformer: Figure 8-9a shows the block diagram and Figure 8-9b shows the circuit topology of the power conditioning unit. In Figure 8-9b, the fuel cell output DC (say 29V to 39V) is converted to a regulated DC output (say 50V) by means of a simple DC-DC boost converter. The output of the DC-DC converter is processed via a pulse width modulation (PWM) DC-AC inverter to generate a low voltage sinusoidal AC of ± 35 V AC (rms), a line frequency isolation transformer with a turns ratio of 1:3.5 is then employed to generate 120V/240V AC output as shown. A 42 to 48V battery is connected to the output terminals of the DC-DC converter to provide additional power at the output terminals for motor startups, etc. During steady state, the DC-DC converter regulates its output to 50V and the battery operates in a float mode. The fuel cell and the DC-DC converter are rated for steady state power (say 10kW), while the DC-AC inverter section is rated to supply the motor-starting VA. Assuming a motor-starting current of 3 to 5 times the rated value, the DC-AC inverter rating will be in the 15kVA to 25kVA range. The DC-DC boost converter is operated in current mode control. During a motor startup operation, the current mode control goes into saturation and limits the maximum current supplied from the cell. During this time, the additional energy from the battery is utilized. During steady state operation, the fuel cell energy is used to charge the battery when the output load is low.

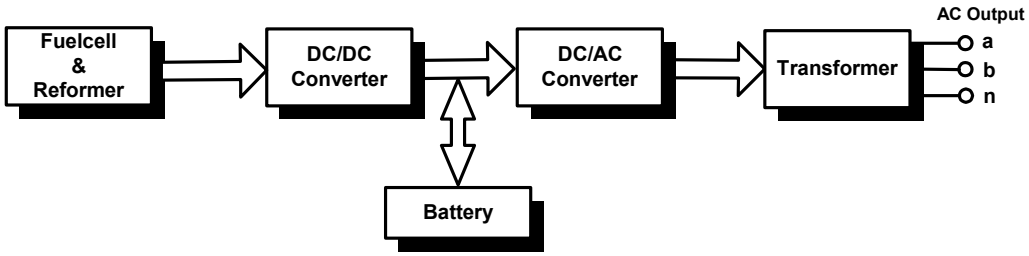

Figure 8-9a Block diagram of the power conditioning unit with line frequency transformer

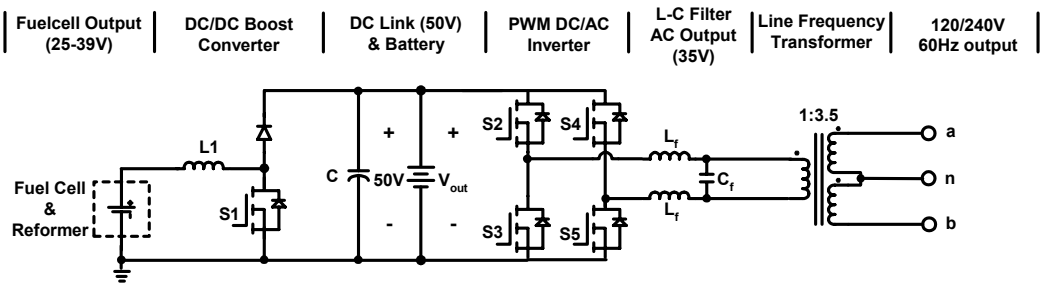

Figure 8-9b Circuit topology of the power conditioning unit with line frequency transformer

Efficiency calculation (approximate): Referring to Figure 8-9a, assume:
DC-DC converter efficiency = η_1
DC-AC inverter efficiency = η_2
Line frequency isolation transformer efficiency = η_3
The overall conversion efficiency of the power conditioning unit $\eta = \eta_1 * \eta_2 * \eta_3$
Assuming η_1 = 0.95 (95 percent) ; η_2 = 0.95 (95 percent); η_3 = 0.98 (98 percent), then η = 0.88 (88 percent).

The main limitation of this system is the low voltage of the entire power conditioning unit, which results in higher current and lower overall efficiency. Another disadvantage is the presence of a line frequency isolation transformer, which is large in size and weight (10kg/kw). Figure 8-9b shows the circuit topology of the power conditioning unit.

Power conditioning unit with high frequency isolation transformer: Figure 8-10a shows a similar power conditioning block diagram. In this design, the low frequency isolation transformer has been eliminated by employing an additional DC-DC conversion stage. The 50V to 400V DC-DC conversion stage includes a high frequency isolation transformer. The fuel cell and the first DC-DC converter are rated for steady state conditions. The second DC-DC converter, along with the DC-AC inverter, is rated for steady state and transient conditions. Figure 8-10b shows the circuit topology of the power conditioning unit. This approach suffers from three power conversion stages in the power flow path, which contributes to reduced efficiency.

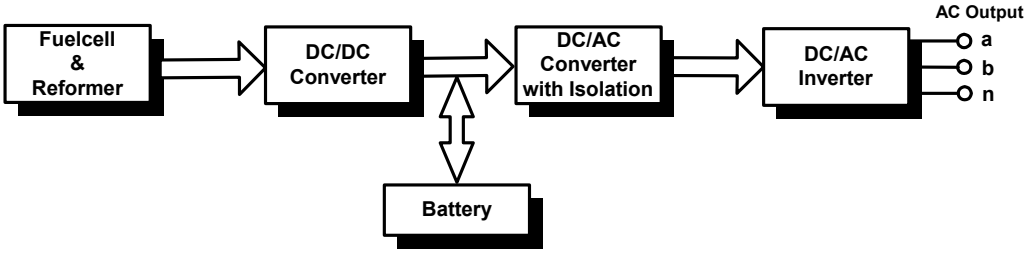

Figure 8-10a Block diagram of the power conditioning unit with high frequency isolation transformer within the DC-DC converter stage

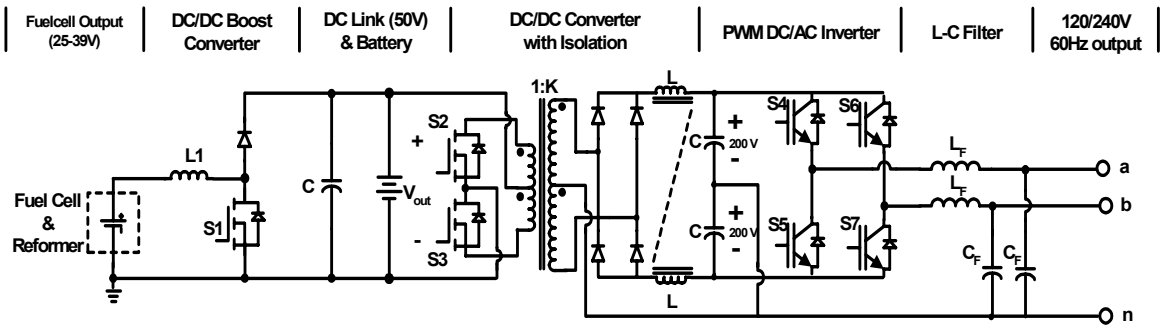

Figure 8-10b Circuit topology of the power conditioning unit with high frequency isolation transformer within the DC-DC converter stage (3,4)

Figure 8-11a shows a power conditioning unit with fewer power conversion stages in series. In this approach, a push-pull type boost converter with a 1:10 gain employing a high-frequency isolation transformer is used. The output of the push-pull DC-DC converter is set to 400V with ± 200V. The DC-DC converter output is connected to two half bridge dual voltage DC-AC inverters to obtain 120/240V AC output. It is economical to install a ± 200V battery at the output of the DC-DC converter stage and regulate the push-pull DC-DC converter output to ±200V. The fuel cell and the push-pull DC-DC converter are rated to supply steady state load (10kW), while the DC-AC inverter stage is rated to supply the steady state as well as transient load demands such as motor starting, etc. Figure 8-11b illustrates the possible circuit topology for this approach. Assuming conversion efficiency of the DC-DC and DC-AC stages to be 96 percent each, an overall efficiency of 92 percent can be realized with this approach. Figure 8-12 shows the fuel cell power conditioner control system block diagram for powering a load. The DC-DC and DC-AC control blocks are controlled separately. The power consumed by the load is first computed by the reference signal generator block, and suitable reference signals for the DC-AC inverter and the fuel cell controller are generated. The DC-DC converter controller regulates the dc-link and draws power from the fuel cell. This block has the appropriate protection circuitry and limits to protect both the fuel cell and the dc-link against over-current and over-voltage, respectively. Fuel cell accessory loads are supplied via the dc-link. The battery also provides start-up power for this unit.

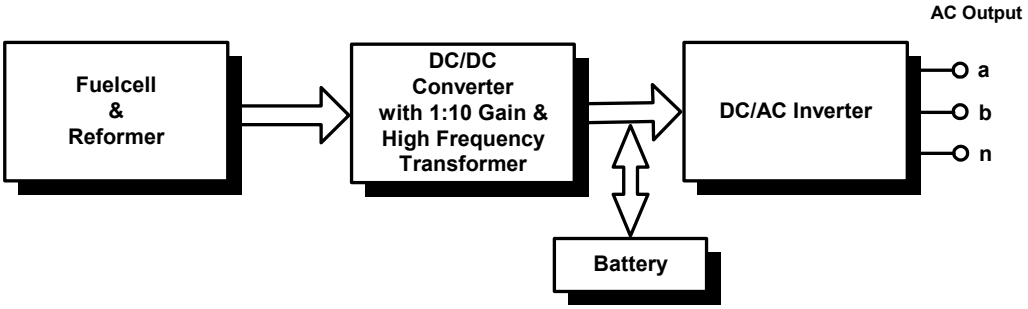

Figure 8-11a Block diagram of the power conditioning unit with fewer power conversion stages in series path of the power flow

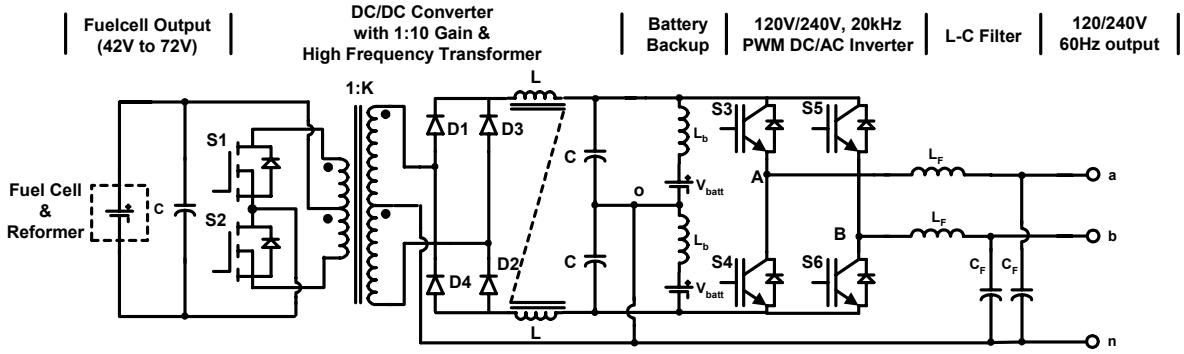

Figure 8-11b Circuit topology of the power conditioning unit with fewer power conversion stages in series path of the power flow

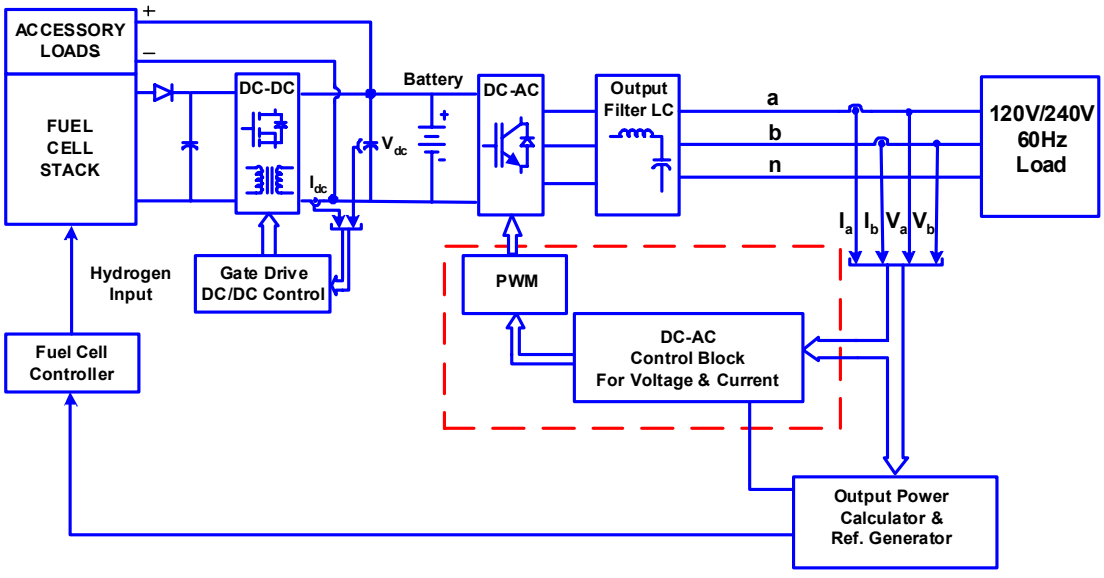

Figure 8-12 Fuel cell power conditioner control system for powering dedicated loads

8.2.3 Fuel Cell Power Conversion for Supplying Backup Power to a Load Connected to a Local Utility

Conventional uninterruptible power supply (UPS) systems employ engine generators and/or batteries as their main sources to provide electric power for critical functions or loads when the normal supply, i.e. utility power, is not available [7]. A typical UPS system consists of rechargeable batteries such as sealed lead-acid or nickel cadmium (Ni-Cd). However, these batteries contain toxic heavy metals such as cadmium, mercury, and lead that may cause serious environmental problems if they are discarded without special care [7]. Further, unlike batteries, fuel cells provide continuous power for as long as reactants are supplied. This feature is especially useful whenever the duration of the power outage is uncertain.

Among the various kinds of fuel cells, proton exchange membrane fuel cells (PEFC) are compact and lightweight. They provide a high output power density at room temperature, and are easy to start-up and shut down in system operation [1,8,9].

In this section, design considerations for a 1-kW fuel cell powered line-interactive UPS system with one hour of backup power employing modular (fuel cell and power converter) blocks is discussed. Figure 8-13 shows two commercially available PEFC fuel cells (25 to 39V, 500W) [1] along with suitable DC-DC and DC-AC power electronic converter modules. Commercially available supercapacitors [5] supply transient power at the output terminals. Two possible power-conditioning architectures are investigated.

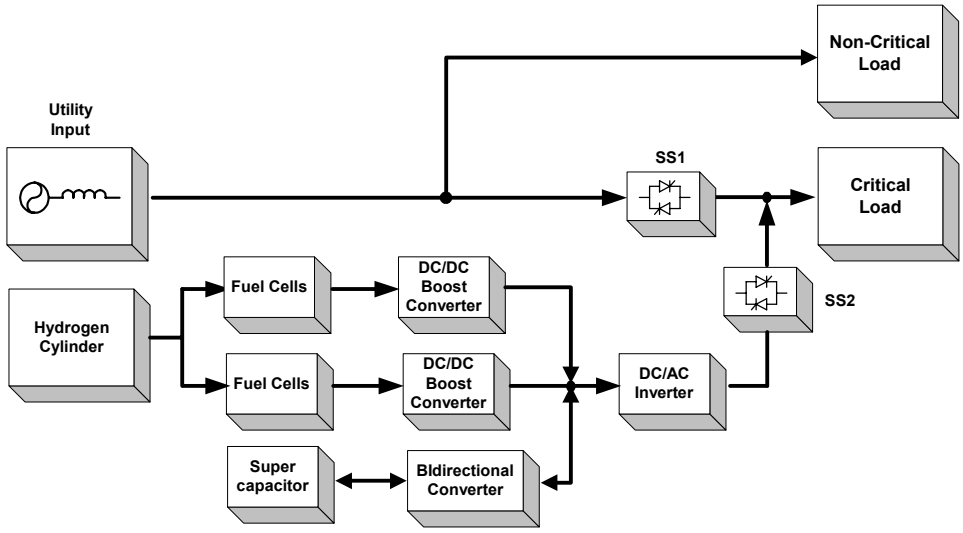

Figure 8-13 Diagram of a modular fuel cell power conversion unit for supplying backup power to a load connected to a local utility [10,11]

Figure 8-13 shows a diagram of a line interactive UPS whose main function is to provide backup power to a load connected to a local utility. The load is connected via two static transfer switches

SS1 and SS2 either to the utility or to the fuel cell source. Normally the fuel cell inverter side static switch SS2 is rated for inverter output. However, the utility side SS1 is rated for 1500 percent for approximately 15 milliseconds to provide current to open the down stream or load side circuit breaker in case of a short circuit [7]. Two commercially available 500W fuel cell stacks are considered in this example design. The use of a supercapacitor is explored to supply inrush current to the load (2kW for 20 seconds). A static bypass switch is configured to disconnect the utility in case of its failure or out of specified voltage range for the load. In steady state, the fuel cell power source is assumed to be in hot standby mode, i.e. supply 10 percent of its capacity; this allows the fuel cell subsystem to be ready to supply the load during a utility shutdown. It is assumed that pure hydrogen is available to supply the rated output power (1kW) for a 1hr utility outage. Figure 8-14 and Figure 8-15 show two possible circuit topologies for this application. The approach in Figure 8-15 is more suitable, as it employs modular DC-DC converters to interface each fuel cell output to a 400V dc-link. A 42V supercapacitor module [5,6] is connected to the dc-link via a bi-directional DC-DC converter. The bi-directional DC-DC converter module allows quick discharge and charging of the supercapacitor modules to supply inrush current demanded by the load.

Table 8-6 Example specifications for the 1kW fuel cell powered backup power (UPS) unit [10,11]

Continuous output power:	1 kW continuous for 1hr
Peak power:	2kW for 20 seconds
Output Phase (s):	Single-phase, not to exceed 1,000 VA total
Output voltage:	120V, Sinusoidal AC. Output voltage tolerance no wider than ±6 percent over the full allowed line voltage and temperature ranges, from no-load to full-load. Frequency 60±0.1 Hz.
Output frequency:	60Hz (U.S.) or 50Hz (Europe) with enough precision to run AC clock accuracy
Transfer time (typical/max):	4/6 milliseconds
Load power factor (PF) range & crest factor (CF):	PF: 0.6 to 1; CF: 3
Fuel Cell Current Ripple: (Fuel cell dependent)	▪ 120 Hz ripple: < 15 percent from 10 to 100 percent load ▪ 60 Hz ripple: < 10 percent from 10 to 100 percent load
Output THD:	< 5 percent
Protection:	Over current, over voltage, short circuit, over temperature, and under voltage. No damage caused by output short circuit. The inverter must shut down if the input voltage dips below the minimum specified fuel cell voltage (29V). Inverter should not self-reset after a load-side fault. IEEE Standard 929 is a useful reference.
Acoustic Noise:	No louder than conventional domestic refrigerator. Less than 50 dBA sound level measured 1.5 m from the unit.
Environment:	Suitable for indoor installation in domestic applications, 10 °C to 40 °C possible ambient range.
Electromagnetic Interference	Per FCC 18 Class A -- industrial
Efficiency:	Greater than 90 percent
Safety:	The system is intended for safe, routine use in a home or small business by non-technical customers.
Life:	The system should function for at least ten years with routine maintenance when subjected to normal use in a 20 °C to 30 °C ambient environment.

Table 8-7 Specifications of 500W PEFC fuel cell stack (available from Avista Labs [1])

Power Output (Continuous)	500 W
Output Voltage	25 to 39 DC
Fuel Source	Hydrogen
Fuel Consumption	7.0L/min @500W(<1.0L/min @ no load)
System Start Time	7 minutes @room temperature
Turndown Ratio	500W to no load, infinity
Operating Temperature Range	41 °F to 95 °F (5 °C to 35 °C)
Dimension (W x D x H)	22.3" x 24.2" x 13.6" (0.056m x 0.0615m x0.0345m)
Weight	97 lbs w/cartridges (44kg w/cartridge)

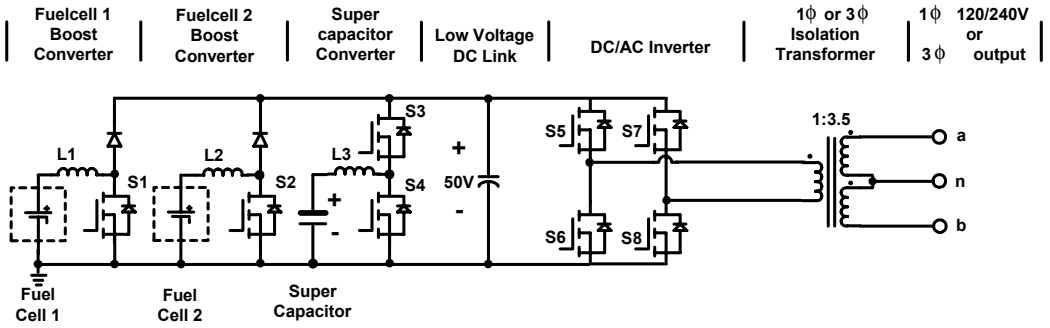

Figure 8-14 Modular power conditioning circuit topology employing two fuel cells to supply a load via a line frequency isolation transformer [10,11]

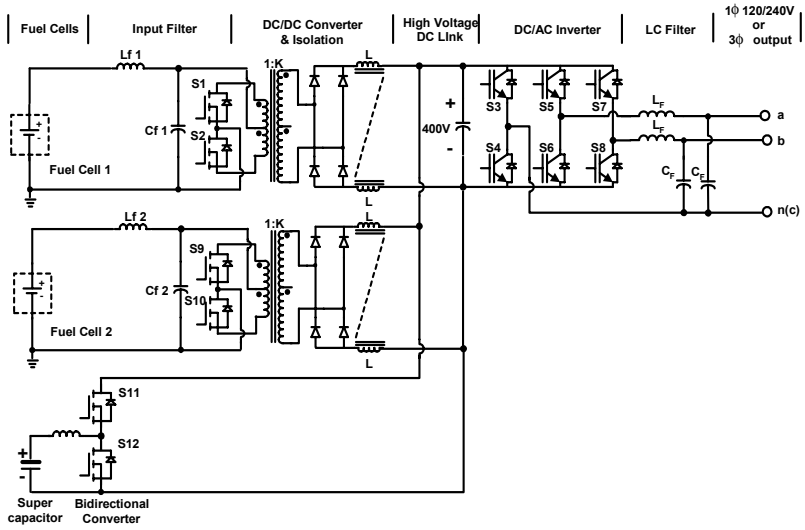

Figure 8-15 Modular power conditioning circuit topology employing two fuel cells using a higher voltage (400V) dc-link [10,11]

8.2.4 Fuel Cell Power Conversion for Supplying a Load Operating in Parallel With the Local Utility (Utility Interactive)

Figure 8-16 shows the block diagram of a fuel cell power conversion scheme supplying a load in parallel with the utility. In this configuration, the peak power (as well as the inrush current) demanded by the load is provided by the utility. By paralleling the fuel cell power output to the utility, the following advantages can be realized:

- Power conversion rating is same as the fuel cell
- Peak power (as well as the inrush current) demanded by the load is provided by the utility
- A constant fuel cell power level can be set.

While in the utility connect mode, the voltage is set by the utility and current control is used to manage the power flow from the fuel cell.

In the event of a utility failure, the fuel cell system does not have the ability to supply inrush current to loads such as for motor starting etc. Special circuit breakers to isolate loads up to the capacity of the fuel cell are necessary. Furthermore, the utility interconnection must conform to IEEE Standard P1547 to prevent energizing a section of the utility by the fuel cell source under utility fault conditions (islanding).

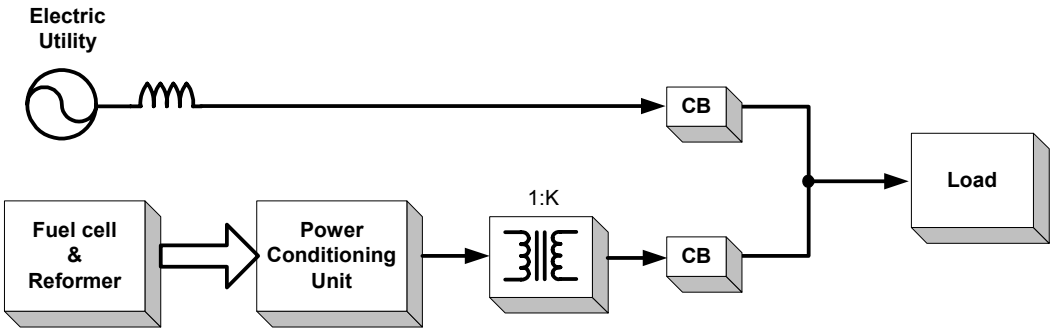

Figure 8-16 Fuel cell supplying a load in parallel with the utility

8.2.5 Fuel Cell Power Conversion for Connecting Directly to the Local Utility

Fuel cell power systems can be configured with the purpose of connecting directly to the utility to supply power as shown in Figure 8-17. IEEE Standard P1547 [12] outlines the criteria and requirements for interconnecting distributed resources such as a fuel cell power plant with the electric power system. It provides requirements relevant to the performance, operation, testing, safety considerations, and maintenance of the interconnection. Islanding should be avoided at any cost: that is a condition in which a fuel cell power plant energizes a portion of the electric power system when the utility power is disconnected. In other words, the fuel cell power connected to the utility must be disconnected immediately in case of utility failure. In general, a fuel cell power converter that has to be interfaced with the utility should meet the following requirements:

- When a distributed resource such as a fuel cell is synchronized with the utility, it should not cause the area electric power system voltage to fluctuate more than ±5 percent

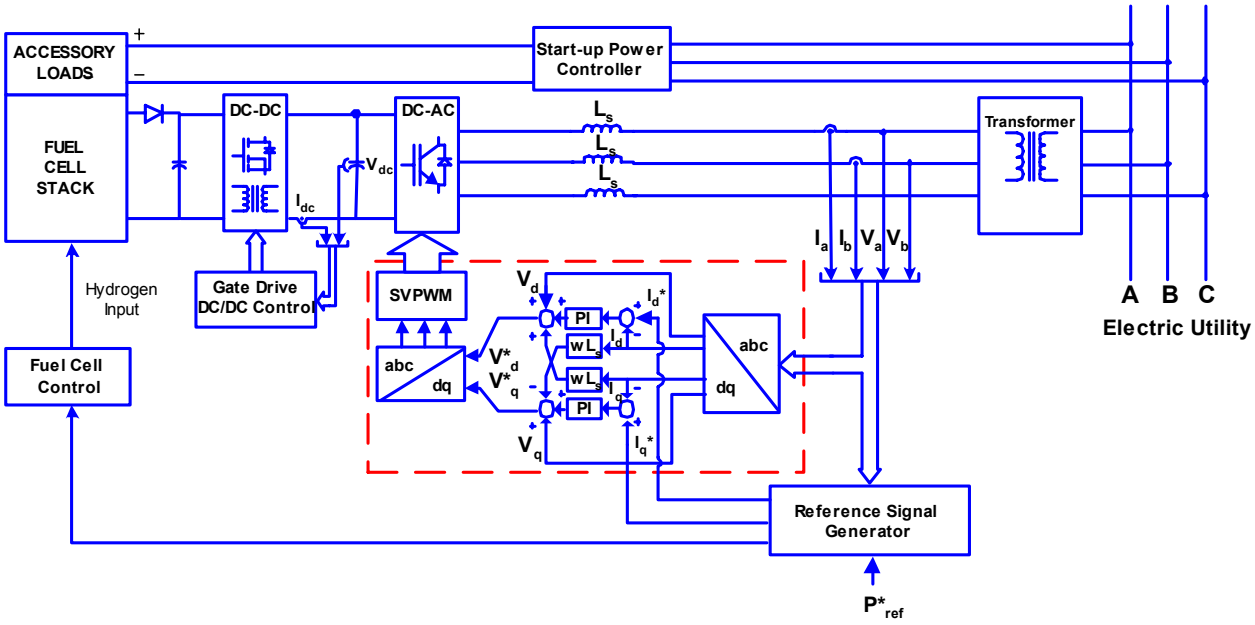

Figure 8-17 Fuel cell power conditioner control system for supplying power to the utility (utility interface)

- The paralleling device (static switch / mechanical circuit breaker) should be capable of withstanding twice the nominal peak utility voltage
- Unintentional islanding: the fuel cell power conditioner must detect islanding and cease to energize the area electric power system within 2 seconds of the formation of an island.

Figure 8-17 shows the fuel cell power conditioner control system for supplying power to the utility. The DC-DC converter and the DC-AC inverter are controlled separately. The required electric power to be injected into the utility grid is set by P^*_{ref} signal, the signal generator block then generates appropriate reference signals for the DC-AC inverter and the fuel cell controller to generate more power. The DC-AC inverter control block shows a "d-q" control with space vector PWM. A line frequency isolation transformer is shown to match the output AC voltage of the fuel cell unit with that of the utility. Utility power can be utilized initially to perform the fuel cell startup operation. Upon satisfactory startup, current control of the fuel cell power conditioning unit can be utilized to set the power level to be supplied to the utility. Higher power fuel cell systems in the 50kW to 500kW range [13,14,15] are characteristic of commercial installations such as industrial facilities, hospitals, hotels, fast food outlets, etc. At these power levels, 480V three phase AC output is preferred (in the U.S.). It should be noted that a minimum dc-link voltage of 784V DC is essential to generate 480V AC output from a three phase power electronic inverter. The fuel cell voltage must be sufficiently high, or a suitable DC-DC converter can be employed to increase the dc-link voltage. If the fuel cell stack voltage can be boosted to 800V DC, then a transformer-less system can be envisioned. It should be emphasized that using an isolation transformer in higher voltage/higher power fuel cell systems interconnected to a utility offers an effective means of meeting the requirements of domestic and

international safety standards for electronic equipment. In the United States, for example, such standards are set by the Occupational Safety and Health Administration (OSHA), with product testing performed according to appointed laboratories, such as Underwriters Laboratories (UL). Throughout Europe, safety standards are established by the International Electro-technical Commission (IEC).

8.2.6 Power Conditioners for Automotive Fuel Cells

An announcement by the Secretary of Energy stated that $1.5 billion U.S. government subsidies would be re-allocated to develop fuel cell technologies for automotive applications. For the automotive fuel cell market to directly impact the stationary fuel cell market, fuel cell vehicles must achieve commercial success. A number of requirements are necessary to effectively commercialize fuel cell vehicles [16,17]. Most important are the need to further develop hydrogen-reforming technologies and the availability of low cost, reliable power conditioning systems. In view of this, it is motivating to explore common power conditioning systems that have dual use - both for stationary and automotive fuel cell applications. Development of common standards will be beneficial for the overall fuel cell market.

Figure 8-18 shows a typical fuel cell vehicle system block diagram [16]. A fuel cell vehicle system consists of three main components: (a) fuel processor; (b) fuel cell stack, and (c) power conditioning unit (DC-DC or DC-AC) to power a traction motor (AC or DC). A fuel cell system designed for vehicular propulsion must have weight, volume, power density, start-up, and transient response similar to the present internal combustion engine-based vehicles. Proton exchange membrane (PEFC) fuel cells are gaining importance as the fuel cell for vehicular applications [16,17] because of their low operating temperature, relatively high power density, specific power longevity, efficiency, and relatively high durability. One problem in PEFC-based technology is that the carbon (CO) concentration in fuel should be reduced to less than 10 parts per million (PPM); higher CO content in hydrogen contributes to deterioration of the cell performance.

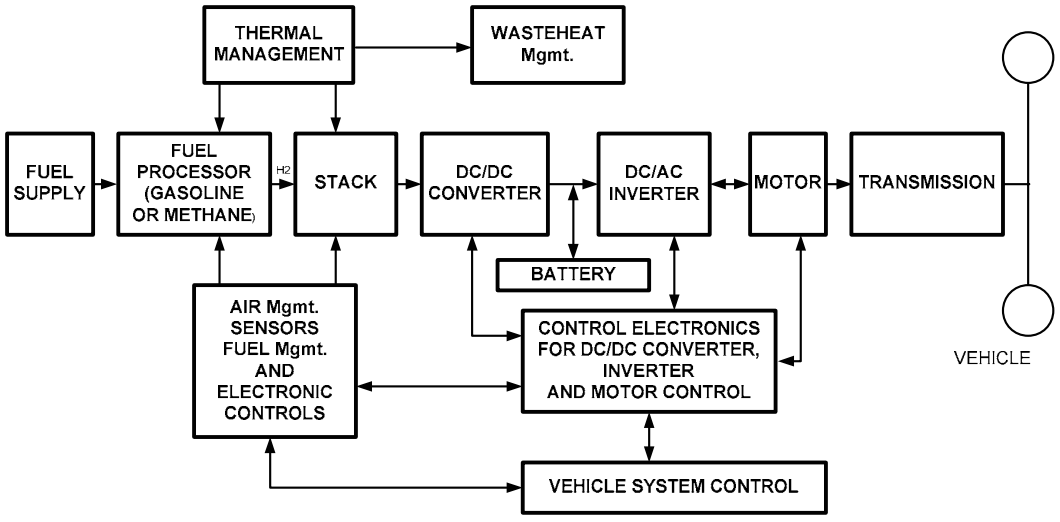

Figure 8-18 A typical fuel cell vehicle system [16]

Fuel cell vehicle configurations: Fuel cell vehicles can be classified as fuel cell electric and fuel cell hybrid vehicles [16,17]. A fuel cell electric vehicle uses a fuel cell system as the power source without the use of the battery. A fuel cell hybrid vehicle consists of a battery or a supercapacitor [16] in addition to the fuel cell system. This configuration enables most efficient use of both the fuel cell and battery for vehicle propulsion. The battery (or supercapacitor) provides power during start-up and acceleration, and the fuel cell supplies the steady state load. A range extender-type fuel cell vehicle can also be designed with a low power fuel cell whose only function is to charge the batteries. In this case, the battery is designed to provide full power and the fuel cell is employed as an on-board battery charger.

Power conditioning system for the fuel cell hybrid vehicle: Figure 8-19 shows a typical topology of a power conditioning unit for a fuel cell hybrid vehicle powering a three phase variable speed AC traction motor load. The bi-directional converter S2 and S3 can be eliminated if a 42V battery is employed. Figure 8-20 shows the fuel cell converter control system block diagram. The reference signal from the vehicle power controller is used to generate the current reference (I_{ref}) as shown. The current reference I_{ref} is used to control the hydrogen input to the fuel cell stack. Also, I_{ref} regulates the current output of the DC-DC boost converter, which powers the DC-AC inverter stage. The power required to power fuel cell accessory loads are powered from the battery. The battery power is also used for system start-up to bring the fuel cell stack voltage to a nominal value.

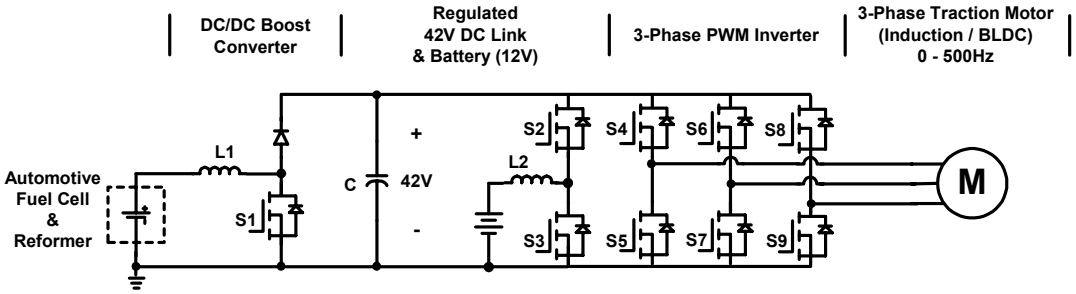

Figure 8-19 Power conditioning unit for fuel cell hybrid vehicle

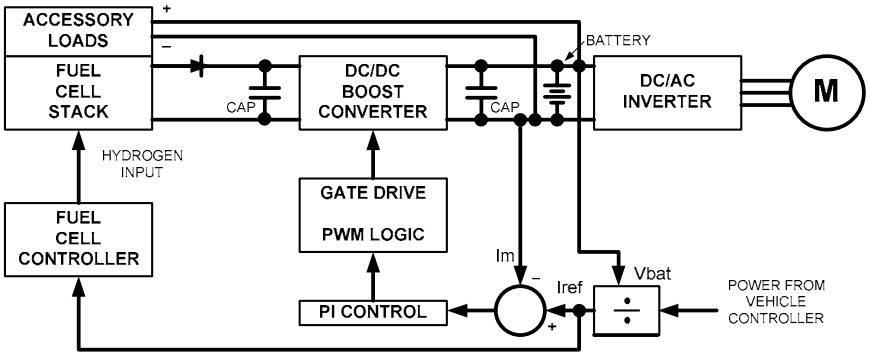

Figure 8-20 Fuel cell power conditioner control system [16]

It is important to note that the vehicle power train for the fuel cell powered system is similar to that of battery powered vehicles. The power conditioning system requirements for vehicles include low EMI, high efficiency, low cost, and suitable for intermittent use over a 10 to 15 year lifetime.

8.2.7 Power Conversion Architecture for a Fuel Cell Turbine Hybrid Interfaced With a Local Utility

Systems studies to date indicate that fuel cell/turbine hybrids could realize a 25 percent increase in efficiency and 25 percent reduction in cost for a comparably sized fuel cell [14,15]. The synergy realized by fuel cell/turbine hybrids derives primarily from using the rejected thermal energy and combustion of residual fuel from a fuel cell to drive the gas turbine. This leveraging of the thermal energy makes the high-temperature molten carbonate (MCFC) and solid oxide fuel cells (SOFC) ideal candidates for hybrid systems. Use of a recuperator contributes to thermal efficiency by transferring heat from the gas turbine exhaust to the fuel and air. Integrating a pressurized SOFC with a micro-turbine generator to yield a system with a nominal capacity of 250kW has shown a power generating efficiency approaching 60 percent [14,15]. During normal steady state operation, the SOFC will produce about 80 percent of the electrical power and the micro-turbine will produce the remaining 20 percent. Effectively, for this design the fuel cell supplants the combustor of the micro-turbine, providing the added benefit of eliminating combustion and combustion by-product formation.

Figure 8-21 shows the block diagram for the power conditioning unit of the example 250kW fuel cell turbine hybrid system. Three 100kW SOFC stacks, each generating 200V are connected in series to generate 600V DC. A DC-DC boost converter is employed to convert the 600V DC generated by SOFC to 750V dc-link. The 750V dc-link is then connected to the 360kVA three-phase PWM inverter to generate 480V, 60Hz output. The micro-turbine, on the other hand, typically operates at high speed (96,000 rpm rated speed) and is connected to a 3-phase brush-less permanent magnet generator [18]. The local utility supplies the necessary startup power for both the SOFC and the micro-turbine.

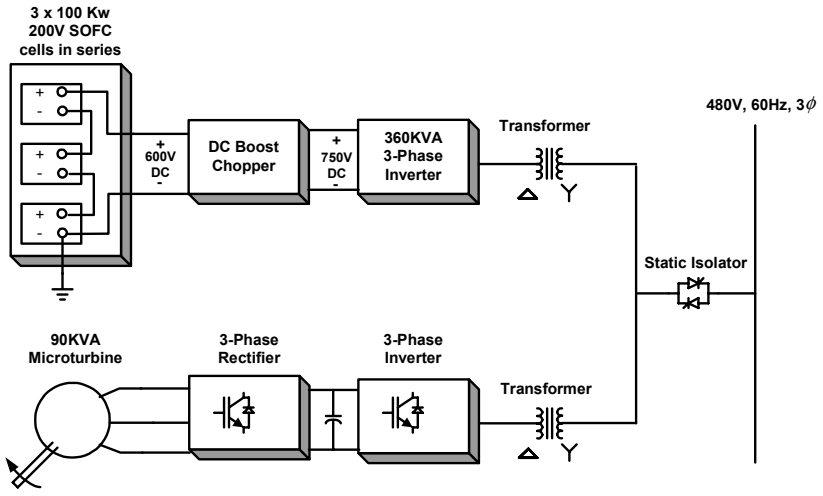

Figure 8-21 Power conditioning unit for the 250kW fuel cell turbine hybrid system

The electric power generated by the micro-turbine generator is at higher frequency (1.6kHz at rated speed) and is converted to DC via a 3-phase PWM rectifier. The DC power is then converted to AC by means of a 3-phase PWM inverter unit. The AC electrical outputs of both the SOFC and the micro-turbine are combined, as shown, and connected to the utility. A line frequency isolation transformer is employed at the output terminals of both the SOFC and the micro-turbine power conditioning units. Each transformer provides isolation as well as voltage matching with the utility. The hybrid power generating system is connected to the utility via a static isolator to facilitate rapid disconnection in the event of a fault.

Shared dc-link power conditioning unit [19]: Figure 8-22 shows an alternative power conditioning unit for the fuel cell turbine hybrid system. In this approach a common dc-link system is envisioned. The SOFC DC-DC converter and the micro-turbine PWM rectifier stages output are paralled together to form a common dc-link. The main advantage of this approach is that only one common DC-AC power conditioning unit is necessary. This architecture has the potential to reduce the cost of the power conditioning unit of a hybrid system.

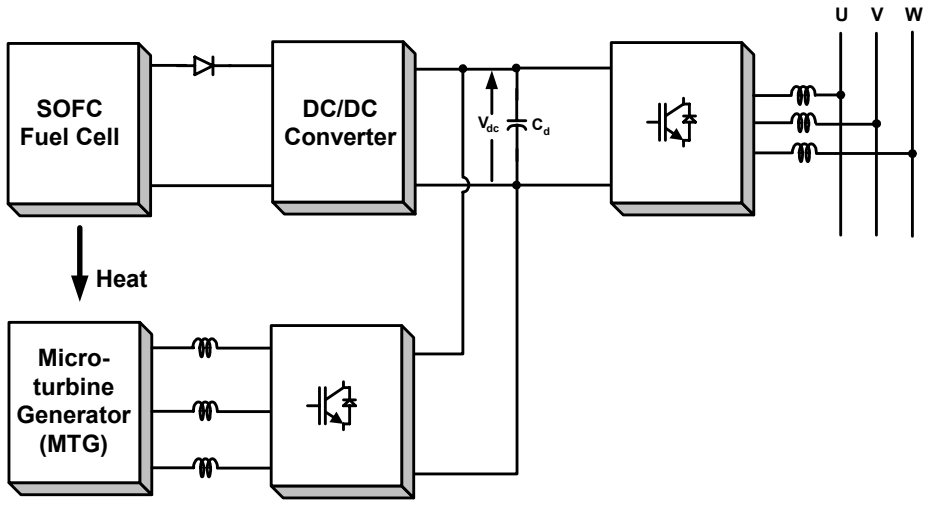

Figure 8-22 Alternative power conditioning unit for the fuel cell turbine hybrid system with shared dc-link [19]

Power conditioning units for MW-range fuel cell turbine hybrid systems [19]: FuelCell Energy Inc. (FCE) is developing an ultra-high efficiency fuel cell/turbine hybrid power plant [20]. The power system is based on an innovative cycle utilizing an indirectly heated gas turbine to supplement fuel cell generated power. System development is being conducted under the Department of Energy through the Office of Fossil Energy, and managed by the National Energy Technology Laboratory (NETL). The project objectives include the design of a 40 MW system using an internally reformed fuel cell being commercialized by FCE [20].

The power conditioning unit for multi-megawatt fuel cell hybrid systems operates at medium voltage levels (2300V, 4160V, 6600V or 11000V in the U.S.). Medium voltage power conditioner units employing integrated gate-commutated thyristor (IGCT) type devices and/or

modular systems employing high voltage insulated gate bipolar transistors (IGBTs) are possible candidates.

Figure 8-23 shows a possible power conditioning topology employing high voltage IGCT devices. It is envisioned that two fuel cell turbine hybrid systems with common dc-link are connected in series via their respective DC-DC converter stages to form a high voltage dc-link (6,000V). A neutral point clamped (NPC) type PWM inverter with 12 IGCT devices is employed to generate 4,160V three-phase AC voltage that is suitable for utility interface. Commercial IGCT based NPC inverters are widely available for powering variable speed medium voltage induction motors [21,22]. The stated technology is, therefore, viable.

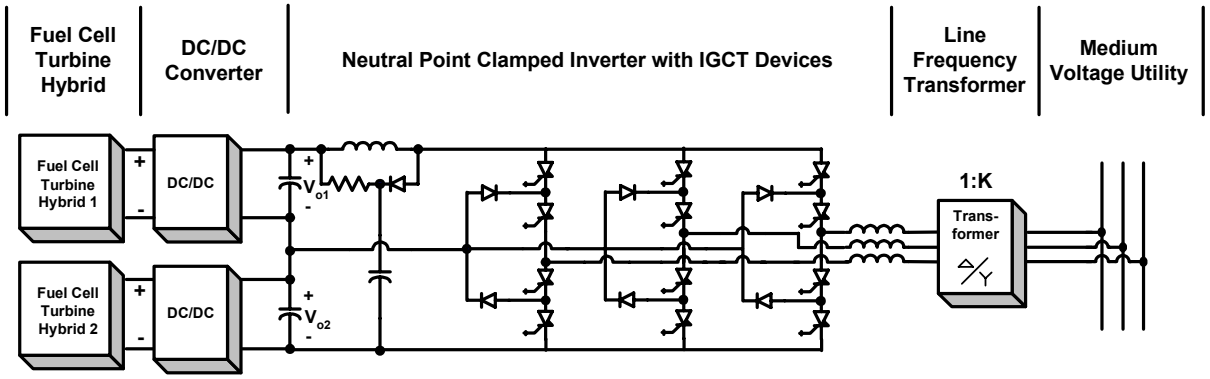

Figure 8-23 Possible medium voltage power conditioning topology for megawatt range hybrid fuel cell systems [19]

8.2.8 Fuel Cell Ripple Current

An important variable in the design of the power conditioner for a fuel cell is the amount of ripple current the fuel cell can withstand. Since reactant utilization is known to impact the mechanical nature of a fuel cell, it is suggested [23] that the varying reactant conditions surrounding the cell (due to ripple current) govern, at least in part, the lifetime of the cells. Both the magnitude and frequency of the ripple current is important. For fuel cells powering single phase loads (60Hz), the ripple current of concern is twice the output frequency, i.e. 120Hz. A limit of 0.15 per unit (i.e. 15 percent of its rated current) from 10 to 100 percent load is specified [2]. In case of single phase inverters with dual output voltage (120V/240V), there is a possibility of 60Hz ripple current in the fuel cell under unbalanced loading conditions (i.e. one output phase loaded and the other unloaded). A limit of 0.1 per unit is specified for 60Hz ripple current from 10 to 100 percent load [2]. Further, the magnitude of the low frequency ripple current drawn from the fuel cell by the DC-DC converter is largely dependent on the voltage loop response characteristics. Also the dc-link capacitor size determines the 120Hz voltage ripple on the dc-link, which in turn has an impact on the input current drawn from the fuel cell. It should be noted that switching frequency components in the DC-DC converter can be easily filtered via a small high frequency capacitive filter. For balanced three phase AC loads at the inverter output, the possibility of low frequency components in the fuel cell input current is low.

Corrective measures for limiting fuel cell ripple current: The following corrective measures are suggested for limiting the fuel cell ripple current (especially for power conditioners with single phase AC output):

- Install an input filter, as in Figure 8-15, to filter the 120Hz component of the ripple current to 0.15 per unit: this approach contributes to additional size, weight, and cost of the unit.
- Increase the size of the dc-link capacitor in the DC-AC inverter: size, weight, and cost are of concern.
- Reduce the response time of the voltage loop of the DC-DC converter: this will affect the regulation of the dc-link and impact the quality of inverter AC output, and possibly increase the size of the output AC filter.

8.2.9 System Issues: Power Conversion Cost and Size

400V DC is required to produce 120V/240V AC. If a fuel cell can produce 400V DC, then only an inverter stage is required, resulting in lowest cost for power conditioning. Present day commercially available fuel cells produce low voltage (12V to 100V). Therefore, either a line frequency transformer to increase the AC voltage or a DC-DC converter to boost the DC voltage is required, adding to cost, weight, and volume. Figure 8-24 shows a representative cost per kW of the power conditioning unit, as the voltage and current values are varied for a certain power level. It is clear from this figure that extremes of voltage at low power and high current at high power levels does not result in an optimum design. In general, higher voltage levels are required at higher power outputs to minimize the cost of power conditioning hardware. The other issue is power density and size of power conditioning unit. Using higher switching frequency for power conversion should result in smaller size. However, the switching losses are higher and a design compromise becomes necessary. Employing power semiconductor devices with lower losses combined with active cooling methods should yield an optimum size. Power integrated circuits can also be considered for further size reduction and become viable, if the fuel cell systems are produced in high volume.

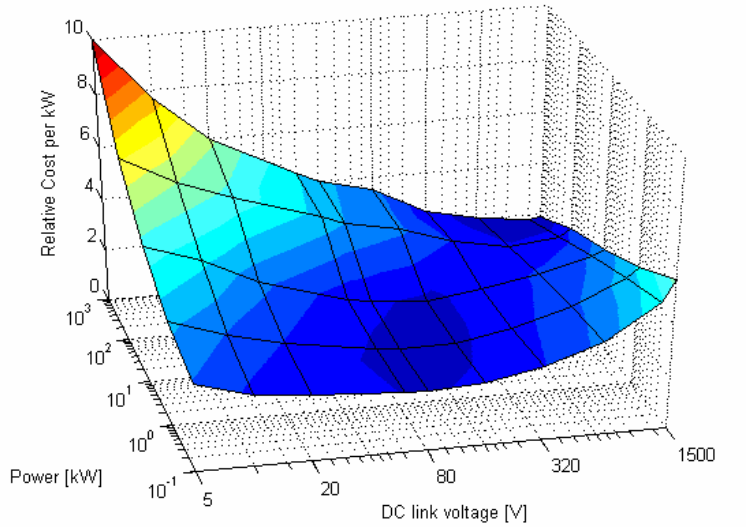

Figure 8-24 Representative cost of power conditioning as a function of power and dc-link voltage

8.2.10 REFERENCES

1. Avistalabs, "SR-12 Modular PEM Generator Operator's Manual", 2000.
2. DOE Future Energy Challenge 2001, Low Cost Fuel Cell Inverter Design competition.
3. "Analysis and Design of a Low Cost Fuel Cell Inverter for Fuel Cell Systems," Texas A&M University, Report to DOE, August 2001.
4. R. Gopinath, S.S. Kim, P. Enjeti, et al., "Development of a Low Cost Fuel Cell Inverter With DSP Control", IEEE PESC Conference Record, June 2002.
5. Montena, "http://www.montena.com/", PC2500 Ultracapacitor Datasheet.
6. J. L. Durán-Gómez, P. Enjeti, and A. von Jouanne, "An Approach to Achieve Ride-Through of an Adjustable Speed Drive with Flyback Converter Modules Powered by Super Capacitors", *IEEE Transactions on Industry Applications,* Vol. 38, No. 2, March/April 2002, pp. 514-522.
7. A. Kusko, "Emergency/Standby Power Systems", McGraw-Hill Book Company, 1989, ISBN: 0-07-035688-0.
8. E.Santi, et al., "A Fuel Cell Based Domestic Uninterruptible Power Supply", IEEE Applied Power Electronics Conference and Exposition, APEC '02 Proceedings, pp. 605-613, 2002.
9. Sukumara, G.V., Parthasarathy, A., and Shankar, V.R, "Fuel Cell Based Uninterrupted Power Sources", Power Electronics and Drive Systems, Proceedings Volume: 2, pp. 728 – 733, 1997.
10. W. Choi, P. Enjeti, "Design of a Modular Fuel Cell Based UPS System", paper submitted to IEEE APEC'03.
11. P. Enjeti and J. Howze, "A 2kW Fuel Cell Based UPS System", Texas State Energy Conservation Office and DOE sponsored project, Texas A&M University, 2002.
12. IEEE Standard P1547 Document: http://www.ieee.org
13. "220kW Solid Oxide Fuel Cell / Microturbine Generator Hybrid Proof of Concept Demonstration Report", March 2001, California Energy Commission.
14. McDermott Technology, Inc. and Northern Research and Engineering Corporation , "Fuel Cell/Micro-Turbine Combined Cycle", Final Report for U.S. Department of Energy, December 1999.
15. Siemens Westinghouse Power Corporation, "A High Efficiency PSOFC/ATS-Gas Turbine Power System", Final Report for U.S. Department of Energy, February 2001.
16. K. Rajashekara, "Propulsion System Strategies for Fuel Cell Vehicles", Fuel Cell Power for Transportation 2000 Conference, SAE 2000 World Congress, March 2000, Ref: 2000-01-0369.
17. T. Matsumoto, et al., "Development of Fuel Cell Hybrid Vehicle", Fuel Cell Power for Transportation 2002 Conference, SAE 2002 World Congress, March 2000, Ref: 2002-01-0096.
18. 30kW Capstone Microturbine Generator, http://www.capstone.com
19. P. Enjeti, P. Krein, J. Lai, "Power Conditioning Approaches to Fuel Cells and Gas Turbine Hybrids", NTU short course (Sponsored by DOE), March 2002.
20. H.G. Ayagh, J.M. Daly, et al. "Critical Components for Direct Fuel Cell/Turbine Ultra-Efficiency system", Presented at Turbine Power Systems Conference and Conditioning Monitoring Workshop, Galveston, TX, Feb 2002. Authors affiliation: Fuel Cell Energy Inc. Danbury, CT.

21. P. Lataire, “White Paper on the New ABB Medium Voltage Drive System, Using IGCT Power Semiconductors and Direct Torque Control”, EPE journal, Vol. 7, No. ¾, December 1998, pp. 40-45.
22. J.P. Lyons. V. Vlatkovic, P.M. Espelage, F.H. Boettner, E. Larsen, (*GE*), “Innovation IGCT Main Drives”, IEEE IAS, Conf. Rec. 1999.
23. Randall S. Gemmen, “Analysis for the Effect of Inverter Ripple Current on Fuel Cell Operating Condition”, ASME 2001 International Mechanical Engineering Congress and Exposition, November 11, 2001, New York.

8.3 System Optimization

The design and optimization of a fuel cell power system is very complex because of the number of required systems, components, and functions. Many possible design options and trade-offs affect unit capital cost, operating cost, efficiency, parasitic power consumption, complexity, reliability, availability, fuel cell life, and operational flexibility. Although a detailed discussion of fuel cell optimization and integration is not within the scope of this section, a few of the most common system optimization areas are examined.

From Figure 8-25, it can be seen that the fuel cell itself has many trade-off options. A fundamental trade-off is determining where along the current density voltage curve the cell should operate. As the operating point moves up in voltage by moving (left) to a lower current density, the system becomes more efficient but requires a greater fuel cell area to produce the same amount of power. That is, by moving up the voltage current density line, the system will experience lower operating costs at the expense of higher capital costs. Many other parameters can be varied simultaneously to achieve the desired operating point. Some of the significant fuel cell parameters that can be varied are pressure, temperature, fuel composition and utilization, and oxidant composition and utilization. The system design team has a fair amount of freedom to manipulate design parameters until the best combination of variables is found.

8.3.1 Pressure

Fuel cell pressurization is typical of many optimization issues, in that there are many interrelated factors that can complicate the question of whether to pressurize the fuel cell. Pressurization improves process performance at the cost of providing the pressurization. Fundamentally, the question of pressurization is a trade-off between the improved performance (and/or reduced cell area) and the reduced piping volume, insulation, and heat loss compared to the increased parasitic load and capital cost of the compressor and pressure-rated equipment. However, other factors can further complicate the issue. To address this issue in more detail, pressurization for an MCFC system will be examined.

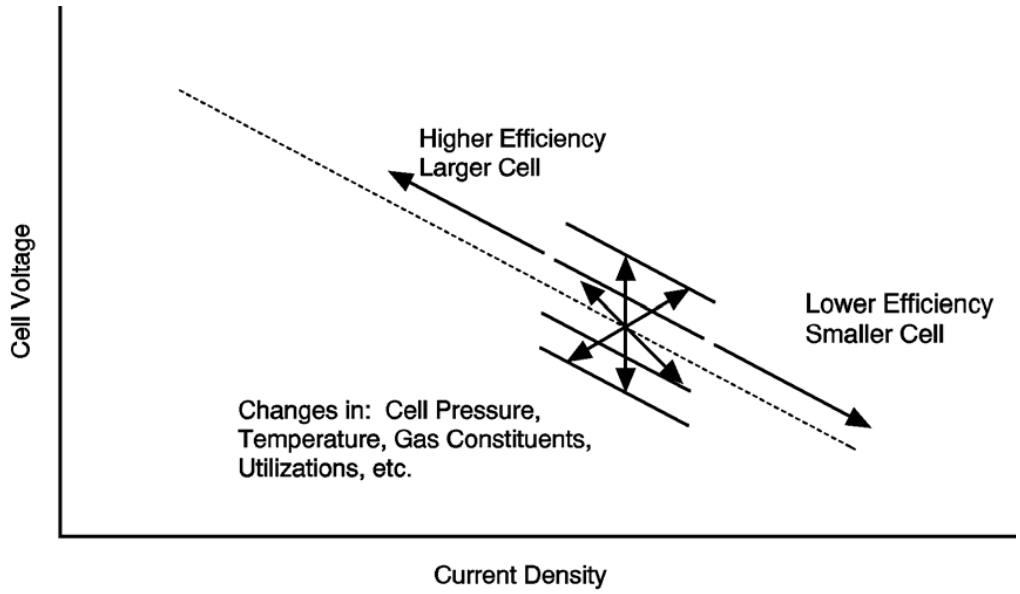

Figure 8-25 Optimization Flexibility in a Fuel Cell Power System

In an MCFC power system, increased pressure can result in increased cathode corrosion. Cathode corrosion is related to the acidity of the cell, which increases with the partial pressure of CO_2, and therefore with the cell pressure. Such corrosion is typified by cathode dissolution and nickel precipitation, which can ultimately result in a shorted cell, causing cell failure (1). Thus, the chosen pressure of the MCFC has a direct link to the cell life, economics, and commercial viability.

Increasing the pressure in a MCFC system can also increase the likelihood of soot formation and decrease the extent of methane reforming. Both are undesirable. Furthermore, the effect of contaminants on the cell and their removal from a pressurized MCFC system have not been quantified. The increased pressure also will challenge the fuel cell seals (1).

The selection of a specific fuel cell pressure will affect numerous design parameters and considerations such as the current collector width, gas flow pattern, pressure vessel size, pipe and insulation size, blower size and design, compressor auxiliary load, and the selection of a bottoming cycle and its operating conditions.

These issues do not eliminate the possibility of a pressurized MCFC system, but they do favor the selection of more moderate pressures. For external reforming systems sized near 1 MW, the current practice is a pressurization of 3 atmospheres.

The performance of an internal reforming MCFC also would benefit from pressurization, but unfortunately, the increase is accompanied by other problems. One problem that would need to be overcome is the increased potential for poisoning the internal reforming catalyst resulting from the

increase in sulfur partial pressure. The current practice for internal reforming systems up to 3 MW is atmospheric operation.

Pressurization of an SOFC yields a smaller gain in fuel cell performance than either the MCFC or PAFC. For example, based on the pressure relationships presented earlier, changing the pressure from one to ten atmospheres would change the cell voltage by ~150, ~80, and ~60 mV for the PAFC, MCFC, and SOFC, respectively. In addition to the cell performance improvement, pressurization of SOFC systems allows the thermal energy leaving the SOFC to be recovered in a gas turbine, or gas turbine combined cycle, instead of just a steam bottoming cycle. Siemens Westinghouse is investigating the possibilities associated with pressurizing the SOFC for cycles as small as 1 to 5 MW.

Large plants benefit the most from pressurization, because of the economy of scale on equipment such as compressors, turbines, and pressure vessels. Pressurizing small systems is not practical, as the cost of the associated equipment outweighs the performance gains.

Pressurization in operating PAFC systems demonstrates the economy of scale at work. The IFC 200 kWe and the Fuji Electric 500 kWe PAFC offerings have been designed for atmospheric operation, while larger units operate at pressure. The 11 MWe plant at the Goi Thermal Power Station operated at a pressure of 8.2 atmospheres (2), while a 5 MWe PAFC unit (NEDO/ PAFCTRA) operates at slightly less than 6 atmospheres (3). NEDO has three 1 MWe plants, two of which are pressurized while one is atmospheric (3).

Although it is impossible to generalize at what size a plant would benefit by pressurization, when plants increase in size to approximately 1 MW and larger, the question of pressurization should be evaluated.

8.3.2 Temperature

Although the open circuit voltage decreases with increasing temperature, the performance at operating current densities increases with increasing temperature due to reduced mass transfer polarizations and ohmic losses. The increased temperature also yields higher quality rejected heat. An additional benefit to an increased temperature in the PAFC is an increased tolerance to CO levels, a catalyst poison. The temperatures at which the various fuel cells can operate are, however, limited by material constraints. The PAFC and MCFC are both limited by life shortening corrosion at higher temperatures. The SOFC has material property limitations. Again, the fuel cell and system designers should evaluate what compromise will work best to meet their particular requirements.

The PAFC is limited to temperatures in the neighborhood of 200 ºC (390 ºF) before corrosion and lifetime loss become significant. The MCFC is limited to a cell average temperature of approximately 650 ºC (1200 ºF) for similar reasons. Corrosion becomes significant in an MCFC when local temperatures exceed 700 ºC (1290 ºF). With a cell temperature rise on the order of 100 ºC (210 ºF), an average MCFC temperature of 650 ºC (1200 ºF) will provide the longest life, highest performance compromise. In fact, one reference (4) cites "the future target of the operating temperature must be 650 °C $\pm$30 °C (1290 °F $\pm$55 °F)."

The high operating temperature of the SOFC puts numerous requirements (phase and conductivity stability, chemical compatibility, and thermal expansion) on material selection and development (5). Many of these problems could be alleviated with lower operating temperatures. However, a high temperature of approximately 1000 °C (1830 ºF), i.e., the present operating temperature, is required in order to have sufficiently high ionic conductivities with the existing materials and configurations (5).

8.3.3 Utilization

Both fuel and oxidant utilizations[47] involve trade-offs with respect to the optimum utilization for a given system. High utilizations are considered to be desirable (particularly in smaller systems) because they minimize the required fuel and oxidant flow, for a minimum fuel cost and compressor/blower load and size. However, utilizations that are pushed too high result in significant voltage drops. One study (6) cites that low utilizations can be advantageous in large fuel cell power cycles with efficient bottoming cycles because the low utilization improves the performance of the fuel cell and makes more heat available to the bottoming cycle. Like almost all design parameters, the selection of optimum utilization requires an engineering trade-off that considers the specifics of each case.

Fuel Utilization: High fuel utilization is desirable in small power systems, because in such systems the fuel cell is usually the sole power source. However, because the complete utilization of the fuel is not practical, except for pure H_2 fuel, and other requirements for fuel exist, the selection of utilization represents a balance between other fuel/heat requirements and the impact of utilization on overall performance.

Natural gas systems with endothermic steam reformers often make use of the residual fuel from the anode in a reformer burner. Alternatively, the residual fuel could be combusted prior to a gas expander to boost performance. In an MCFC system, the residual fuel often is combusted to maximize the supply of CO_2 to the cathode while at the same time providing air preheating. In an SOFC system, the residual fuel often is combusted to provide high-temperature air preheating.

The designer has the ability to increase the overall utilization of fuel (or the oxidant) by recycling a portion of the spent stream back to the inlet. This increases the overall utilization while maintaining a lower per pass utilization of reactants within the fuel cell to ensure good cell performance. The disadvantage of recycling is the increased auxiliary power and capital cost of the high temperature recycle fan or blower.

One study by Minkov, et al. (6) suggests that low fuel and oxidant utilizations yield the lowest COE in large fuel cell power systems. By varying the fuel cell utilization, the electric power generation split between the fuel cell, steam turbine, and gas turbine are changed. The low fuel utilization decreases the percentage of power from the fuel cell while increasing the fuel cell performance. The increased power output from the gas turbine and steam turbine also results in their improved performance and economy of scale. The specific analysis results depend upon the assumed stack costs. The optimal power production split between the fuel cell and the gas and steam turbines is approximately 35 percent, 47 percent, and 17 percent for a 575 MW MCFC

[47]. Utilization - the amount of gases that are reacted within the fuel cell compared to that supplied.

power plant. The associated fuel utilization is a relatively low 55 percent. It remains to be seen whether this trend will continue to hold for the improved cells that have been developed since this 1988 report was issued.

Oxidant Utilization: In addition to the obvious trade-off between cell performance and compressor or blower auxiliary power, oxidant flow and utilization in the cell often are determined by other design objectives. For example, in the MCFC and SOFC cells, the oxidant flow is determined by the required cooling. This tends to yield oxidant utilizations that are fairly low (~25 percent). In a water-cooled PAFC, the oxidant utilization based on cell performance and a minimized auxiliary load and capital cost is in the range of 50 to 70 percent.

8.3.4 Heat Recovery

Although fuel cells are not heat engines, heat is still produced and must be removed. Depending upon the size of the system, the temperature of the available heat, and the requirements of the particular site, this thermal energy can be either rejected, used to produce steam or hot water, or converted to electricity via a gas turbine or steam bottoming cycle or some combination thereof.

Cogeneration: When small quantities of heat and/or low temperatures typify the waste heat, the heat is either rejected or used to produce hot water or low-pressure steam. For example, in a PAFC where the fuel cell operates at approximately 205 °C (400 °F), the highest pressure steam that could be produced would be something less than 14 atmospheres (205 psia). This is obviously not practical for a steam turbine bottoming cycle, regardless of the quantity of heat available. At the other end of the spectrum is the TSOFC, which operates at ~1000 °C (~1800 °F) and often has a cell exhaust temperature of approximately 815 °C (1500 °F) after air preheating. Gas temperatures of this level are capable of producing steam temperatures in excess of 540 °C (1000 °F), which makes it more than suitable for a steam bottoming cycle. However, even in an SOFC power system, if the quantity of waste heat is relatively small, the most that would be done with the heat would be to make steam or hot water. In a study performed by Siemens Westinghouse of 50 to 2000 kW TSOFC systems, the waste heat was simply used to generate 8 atmospheres (100 psig) steam (7).

Bottoming Cycle Options: Whenever significant quantities of high-temperature rejected heat are available, a bottoming cycle can add significantly to the overall electric generation efficiency. Should the heat be contained within a high-pressure gas stream, then a gas turbine potentially followed by a heat recovery steam generator and steam turbine should be considered. If the hot gas stream is at low pressure, then a steam bottoming cycle is logical.

If a steam bottoming cycle is appropriate, many design decisions need to be made, including the selection of the turbine cycle (reheat or non-reheat) and the operating conditions. Usually, steam turbines below 100 MW are non-reheat, while turbines above 150 MW are reheat turbines. This generalization is subject to a few exceptions. In fact, a small (83 MW) modern reheat steam turbine went into operation (June 1990) as a part of a gas turbine combined cycle repowering project (8).

8.3.5 Miscellaneous

Compressor Intercooling: Whether a compressor should be intercooled or not depends on the trade-off between the increased efficiency of the intercooled compressor and its increased capital cost. In general, intercooling is required for large compressors with pressure ratios that exceed approximately 5:1 (9). The designer also should consider whether the heat is advantageous to the process. For example, when near the 5:1 pressure ratio, it may not be appropriate to intercool if the compressed stream will subsequently require preheating as it would with the process air stream of an MCFC or SOFC system.

Humidification/Dehumidification: Water often is added or removed in fuel cell systems to promote or prevent certain chemical reactions. For some reactions, excess water can help to drive the reaction, while too much requires larger equipment and can even reduce the yield of a reaction or decrease the performance of a fuel cell. Excess water often is utilized to increase the yield of reforming reactions and the water gas shift.

In a natural gas fueled PAFC, water is condensed out of the fuel stream going to the fuel cell to increase the partial pressure of hydrogen. In coal gasification MCFC, water often is added to the fuel stream prior to the fuel cell to prevent soot formation. The addition of excess steam not only prevents soot formation, but also causes a voltage drop of approximately 2 mV per each percentage point increase in steam content (10). The use of zinc ferrite hot gas cleanup can aggravate the soot formation problem because of the catalytic effect of the sorbent on carbon formation, and requires even higher moisture levels (11).

Maintaining the proper quantity of water within a PEFC is very important for proper operation. Too much, and the cell will flood; too little, and the cell membrane will dehydrate. Either will severely degrade cell performance. The proper balance is achieved only by considering water production, evaporation, and humidification levels of the reactant gases. Achieving the proper level of humidification is also important. With too much humidification, the reactant gases will be diluted, with a corresponding drop in performance. The required humidification level is a complex function of the cell temperature, pressure, reactant feed rates, and current density. Optimum PEFC performance is achieved with a fully saturated, yet unflooded membrane (12).

8.3.6 Concluding Remarks on System Optimization

System design and optimization encompass many questions, issues, and trade-offs. In the process of optimizing a power plant design, the engineer will address the selection of fundamental processes, component arrangements, operating conditions, fuel cell and bottoming cycle technologies and associated power production split, system integration, and capital and life cycle costs. The design will be governed by criteria such as output, weight, fuel basis, emissions, and cost objectives. Site and application specific criteria and conditions may strongly influence the cycle design criteria and resulting design.

The objective of this system optimization discussion was not to present a detailed review of the subject of optimization, but simply to present select issues of system optimization as they apply to fuel cell power systems.

8.4 Fuel Cell System Designs

The following five cycles are examples of current fuel cell offerings that reflect manufacturers' anticipated commercialization plans. These cycles are based on information available in relevant literature and may differ from the ultimate size of the commercial offering.

8.4.1 Natural Gas Fueled PEFC System

A natural gas PEFC power plant configuration is shown in Figure 8-26 and is a slight simplification of a cycle published in 1997 by a Ballard Researcher (13). In light of the PEFC sensitivity to CO, CO_2 and methane, the fuel processing represents a significant portion of the cycle. Natural gas fuel enters a fuel compressor and a fuel cleanup device. (The reference document does not describe the cleanup device, but it is assumed to be a sulfur polisher to prevent poisoning of the fuel cell catalyst.) The cleaned gas is mixed with water in a vaporizer, which evaporates the liquid water into water vapor with waste heat from the reformer. This humidified fuel is reformed in the steam reformer. Because natural gas reformate is high in CO, the reformate is sent to a shift converter and selective oxidizer to reduce the CO to 10 to 50 ppm. This hydrogen rich/carbon monoxide lean fuel is fed to the PEFC stack where it reacts electrochemically with compressed air.

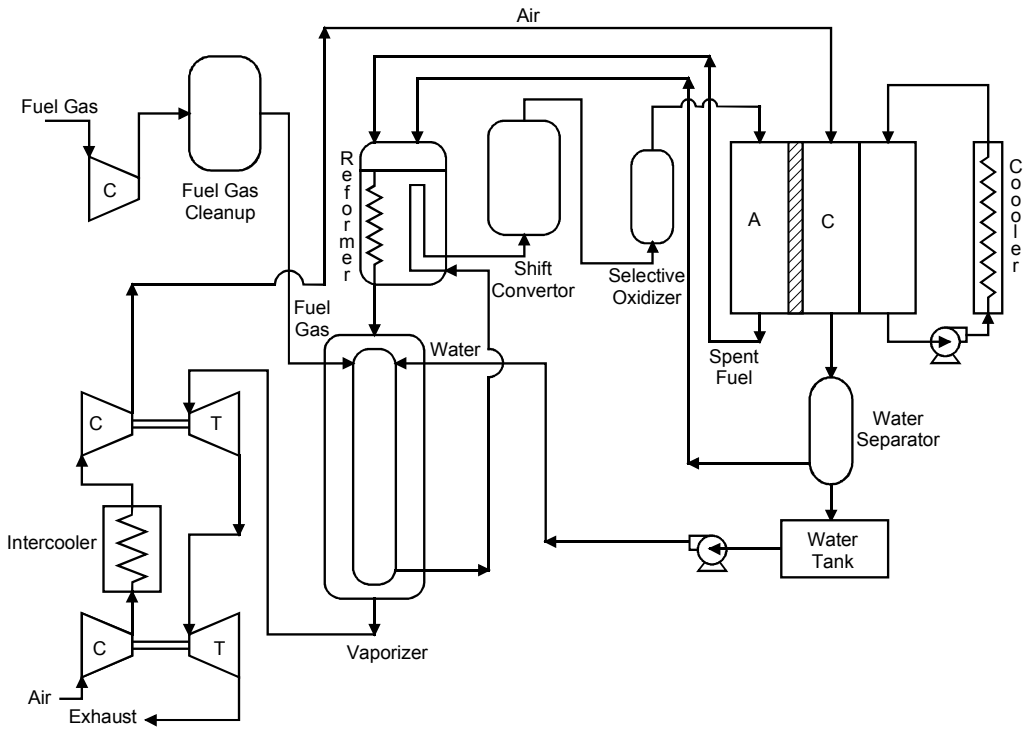

Figure 8-26 Natural Gas Fueled PEFC Power Plant

Ambient air is compressed in a turbocharger, powered by the expansion of the hot pressurized exhaust gases. Following this first compression stage, the air is intercooled by a fin fan air cooler and fed into a second turbocharger. The high-pressure air is fed directly to the PEFC

stack. The fuel cell water product is liberated to the oxidant gas stream. The spent oxidant stream exits the fuel cell where a water separator removes much of this water, which is subsequently used to humidify the fuel gas prior to the entering the reformer. The spent oxidant and fuel streams are combusted in the reformer burner to provide heat for the endothermic reforming reactions. The reformer exhaust also provides heat to the vaporizer. Finally, the residual heat and pressure of this exhaust stream are used in the turbochargers to drive the air compressor.

The fuel cell itself liberates heat that can be utilized for space heating or hot water. The reference article did not list any operating conditions of the fuel cell or of the cycle. The PEFC is assumed to operate at roughly 80 ºC. Another recent article (14) published by Ballard shows numerous test results that were performed at 3 to 4 atmospheres where fuel utilizations of 75 to 85 percent have been achieved. Performance levels for an air fed PEFC are now in the range of 180 to 250 mW/cm^2. Ballard Power Systems has performed field trials of 250 kW systems with select utility partners. Commercial production of stationary power systems is anticipated for the year 2002. Similarly sized transportation cycles also are anticipated for commercial production in the same year.

8.4.2 Natural Gas Fueled PAFC System

IFC has been marketing the PC25, a 200 kW atmospheric PAFC unit, since 1992. Details of this commercial cycle are proprietary and not available for publication. In order to discuss an example PAFC cycle, a pressurized (8 atm) 12 MW system will be presented (15). This cycle is very similar to the 11 MW IFC PAFC cycle that went into operation in 1991 in the Tokyo Electric Power Company system at the Goi Thermal Station, except that two performance enhancements have been incorporated. Limited data are available regarding the Goi power plant. However, it is understood that the average cell voltage is 750 mV and the fuel utilization is 80 percent (16). The enhanced 12 MW cycle presented here utilizes values of 760 mV and 86 percent. This enhanced cycle (Figure 8-27) is discussed below with selected gas compositions presented in Table 8-8.

Natural gas (stream 100) is supplied at pressure and contains sulfur odorants for leak detection. A small hydrogen-rich recycle stream (stream 117) is mixed with the natural gas to hydrolyze the sulfur compounds to facilitate sulfur removal. The fuel stream (stream 102) is heated to 299 ºC (570 ºF) before entering the sulfur removal device. Superheated steam (stream 1) is mixed with the heated fuel to provide the required moisture for the reforming and the water gas shift reactions. The humidified stream (stream 105) is heated to approximately (705 ºC) 1300 ºF before entering the reformer. The effluent fuel stream (stream 107) leaves the reformer at approximately 760 ºC (1400 ºF) and is cooled in the heat exchanger used to preheat the humidified natural gas stream. This stream (stream 108) enters the high temperature shift converter (HTSC) at approximately 360 ºC (680 ºF), while leaving (stream 109) at about 415 ºC (780 ºF). The HTSC effluent is cooled in two heat exchangers before proceeding to the low temperature shift converter. A two-stage approach is utilized, allowing the HTSC to proceed at a faster rate, while the LTSC yields higher hydrogen concentrations.

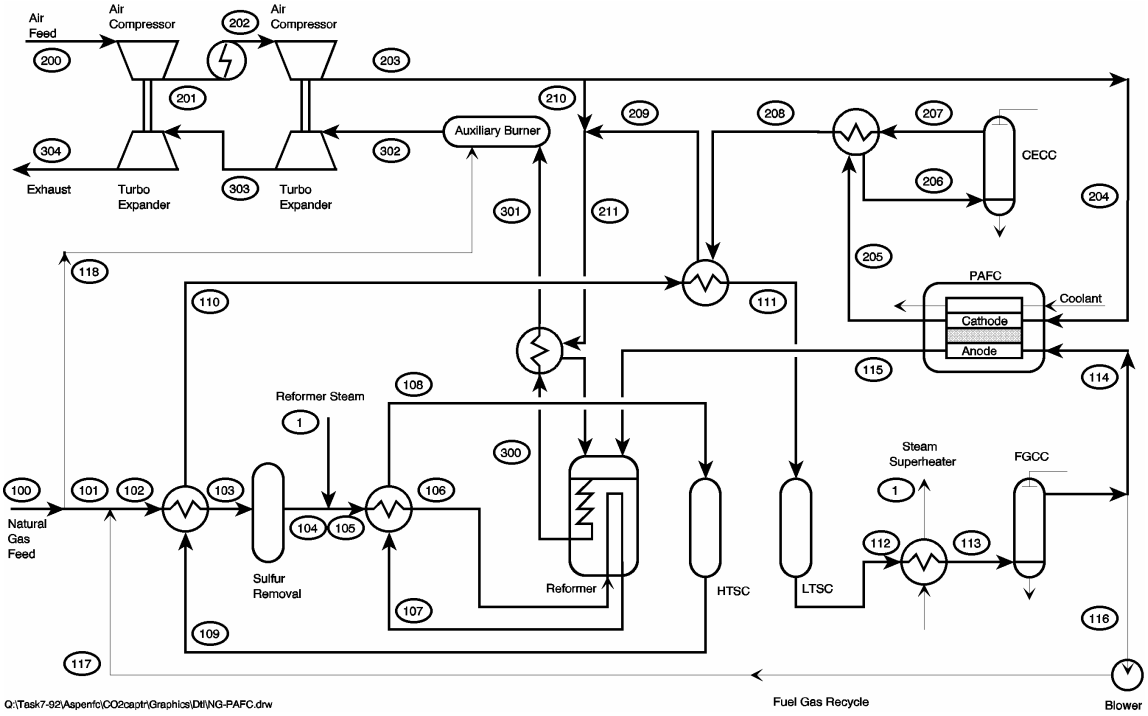

Figure 8-27 Natural Gas fueled PAFC Power System

Table 8-8 Stream Properties for the Natural Gas Fueled Pressurized PAFC

Strm No.	Description	Temp. C	Press. atm	Mole Flow Kgmol/hr	Mass Flow kg/hr	MW	Ar %	CH4 %	C2H6 %	CO %	CO2 %	H2 %	H2O %	N2 %	O2 %	Total %
1	Reformer Steam	243.3	10.00	418.8	7,545	18.02							100.0			100.0
100	NG Feed	15.6	13.61	115.1	1,997	17.34		90.0	5.0					5.0		100.0
106	Reformer Feed	712.8	9.93	562.6	9,846	17.50		18.3	1.0	trace	1.0	4.0	74.5	1.1		100.0
107	Reformer Effluent	768.3	9.59	755.9	9,846	13.03		2.4	trace	7.1	6.5	46.3	37.0	0.8		100.0
112	LTSC Effluent	260.0	8.72	755.9	9,846	13.03		2.4		0.5	13.1	52.9	30.4	0.8		100.0
114	Anode Feed	60.6	8.55	506.6	5,557	10.97		3.3		0.7	18.3	74.5	2.0	1.1		100.0
115	Anode Exhaust	207.2	7.95	181.4	4,901	27.02		9.3		1.9	51.2	28.8	5.7	3.1		100.0
118	NG to Aux Burner	15.6	13.61	1.59	27.5	17.34		90.0	5.0					5.0		100.0
200	Air Feed	15.6	1.00	1,156.5	33,362	28.85	0.9				trace		1.1	77.2	20.7	100.0
204	Cathode Feed	192.8	8.27	1,120.8	32,332	28.85	0.9				trace		1.1	77.2	20.7	100.0
205	Cathode Exhaust	207.2	8.09	1,283.4	32,987	25.70	0.8				trace		26.3	67.5	5.4	100.0
208	Cath. Gas to Heat Exch.	151.7	7.85	1,045.3	28,697	27.45	1.0				trace		9.5	82.8	6.7	100.0
209	Cath. Gas to Ref. Burner	243.9	7.81	1,045.3	28,697	27.45	1.0				trace		9.5	82.8	6.7	100.0
211	Cath. Gas to Heat Exch.	242.2	7.81	1,081.0	29,727	27.50	1.0				trace		9.2	82.6	7.1	100.0
301	Reformer Exhaust	380.6	7.71	1,234.6	34,629	28.05	0.9				9.2		15.9	72.8	1.2	100.0
302	Aux. Burner Exhaust	410.6	7.68	1,236.2	34,656	28.03	0.9				9.3		16.1	72.7	1.0	100.0
304	Exhaust	180.0	1.03	1,236.2	34,656	28.03	0.9				9.3		16.1	72.7	1.0	100.0

The LTSC effluent (stream 112) is utilized to superheat the steam required for the reformer and water gas shift reactions. The saturated steam sent to the superheater is supplied by the fuel cell water cooling circuit. The cooled stream (stream 113) is further cooled in a fuel gas contact

cooler (FGCC) to remove the excess moisture levels. This raises the partial pressure of hydrogen in the fuel before entering the fuel cell. Some of the hydrogen-rich fuel is recycled back, as mentioned previously, to the incoming natural gas, while the majority of the fuel (stream 114) proceeds to the fuel cell anode. Approximately 86 percent of the hydrogen in the fuel stream reacts in the fuel cell, where the hydrogen donates an electron and the resulting proton migrates to the cathode, where it reacts with oxygen in the air to form water. Key cell operating parameters are summarized in Table 8-9. The overall performance is summarized in Table 8-10. The spent fuel is combusted in the reformer burner and supplies heat for the endothermic reforming reactions.

Table 8-9 Operating/Design Parameters for the NG fueled PAFC

Operating Parameters	Value
Volts per Cell (V)	0.76
Current Density (mA/cm^2)	320
No of stacks	12
Cell Operating Temp. (ºC)	207
Cell Outlet Pressure (atm)	8.0
Overall Fuel Utilization (percent)	86.2
Overall Oxidant Utilization (percent)	70.0
DC to AC Inverter efficiency	97.0 percent
Auxiliary Load	4.2 percent

Table 8-10 Performance Summary for the NG fueled PAFC

Performance Parameters	Value
LHV Thermal Input (MW)	25.42
Gross Fuel Cell Power (MW) Fuel Cell DC Power Inverter Loss Fuel Cell AC Power	 13.25 (0.40) 12.85
Auxiliary Power	0.54
Net Power	12.31
Electrical Efficiency (percent LHV)	48.4
Electrical Efficiency (percent HHV)	43.7
Heat Rate (Btu/kWh, LHV)	7,050

Note: The net HHV efficiency for the Goi Thermal Power Station is 41.8 percent (HHV) (1).

Ambient air (stream 200) is compressed in a two-stage compressor with intercooling to conditions of approximately 193 ºC (380 ºF) and 8.33 atmospheres (122.4 psia). The majority of the compressed air (stream 203) is utilized in the fuel cell cathode; however, a small amount of air is split off (stream 210) for use in the reformer burner. The spent oxidant (stream 205) enters a recuperative heat exchange before entering a cathode exhaust contact cooler, which removes moisture to be reused in the cycle. The dehumidified stream (stream 207) is again heated, mixed with the small reformer air stream, and sent to the reformer burner (stream 211). The reformer burner exhaust (stream 300) preheats the incoming oxidant and is sent to the auxiliary burner, where a small amount of natural gas (stream 118) is introduced. The amount of natural gas required in the auxiliary burner is set so the turbine shaft work balances the work required at the compressor shaft. The cycle exhaust (stream 304) is at approximately 177 ºC (350 ºF).

Some of the saturated steam generated by the fuel cell cooling water is utilized to meet the reformer water requirements. Approximately 3,800 kg/hr (8,400 lb/hr) of 12.2 atmospheres (180 psi) saturated steam is available for other uses.

Cycle performance is summarized in Table 8-10. The overall net electric conversion efficiency is 43.7 percent based on HHV input, or 48.4 percent on LHV.

8.4.3 Natural Gas Fueled Internally Reformed MCFC System

Fuel Cell Energy is developing initial market entry MCFC power systems, with mature megawatt class units projected to be available in 2004. These units will be produced in various sizes. Preliminary cycle information was received from FCE for a nominal 3 MW power plant. This cycle is presented in Figure 8-28 and is described below.

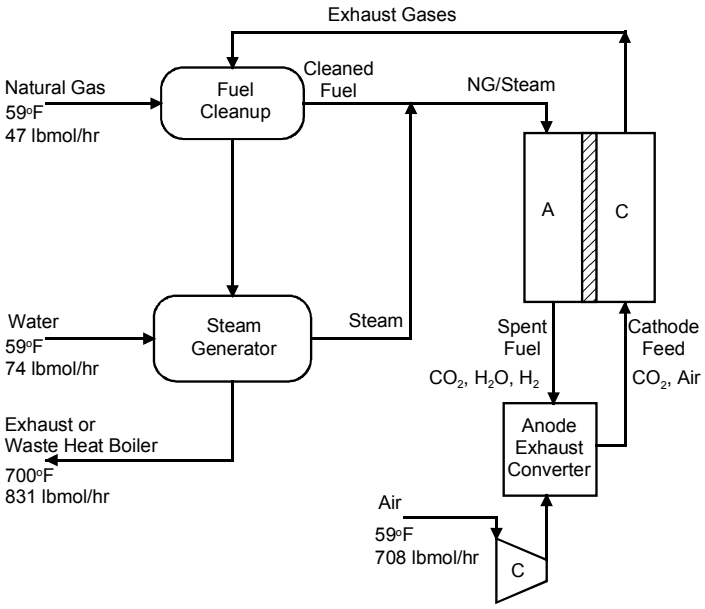

Figure 8-28 Natural Gas Fueled MCFC Power System

Natural gas is cleaned of its sulfur contaminants in a fuel cleanup device. Steam is added to the fuel stream prior to being fed to the internally reforming fuel cell. The fuel reacts electrochemically with the oxidant within the fuel cell to produce 3 MW of dc power.

The spent fuel is completely combusted in the anode exhaust converter. This flue gas mixture is fed directly to the fuel cell cathode. The cathode exhaust has significant usable heat, which is utilized in the fuel cleanup and in steam generation. The residual heat can be utilized to heat air, water, or steam for cogeneration applications. Design parameters for the IR-MCFC are presented in Table 8-11. Overall performance values are presented in Table 8-12.

Table 8-11 Operating/Design Parameters for the NG Fueled IR-MCFC

Operating Parameters	Value
Volts per Cell (V)	unknown
Current Density (mA/cm^2)	unknown
Operating Temperature (^{o}C)	unknown
Cell Outlet Pressure (atm)	1.0
Fuel Utilization (percent)	78.percent
Oxidant Utilization (percent)	75.percent
Inverter Efficiency	95.percent

Table 8-12 Overall Performance Summary for the NG Fueled IR-MCFC

Performance Parameters	Value
LHV Thermal Input (MW)	4.8
Gross Fuel Cell Power (MW) Fuel Cell DC Power Inverter Loss Fuel Cell AC Power	 3.0 (0.15) 2.85
Auxiliary Power (MW)	0.05
Net Power (MW)	2.80
Electrical Efficiency (percent LHV)	58 percent
Heat Rate (Btu/kWh, LHV)	5,900

8.4.4 Natural Gas Fueled Pressurized SOFC System

This natural gas fuel cell power system is based on a pressurized TSOFC combined with a combustion turbine developed by Siemens Westinghouse[48] (17). Most TSOFC power plant concepts developed to date have been based on atmospheric operation. However, as shown in Section 7, the cell voltage increases with cell pressure. Thus, operating with an elevated pressure will yield increased power and efficiency for a given cycle. In addition, the use of a pressurized SOFC will also allow integration with a combustion turbine. The combustion turbine selected for integration by Siemens Westinghouse is the unique 1.4 MW Heron reheat combustion turbine, a proposed product of Heron (18).

A flow diagram for the natural gas fueled 4.5 MW class cascaded[49] TSOFC power cycle is presented in Figure 8-29. A brief process description is given below, followed by a performance summary. Selected state point values are presented in Table 8-13.

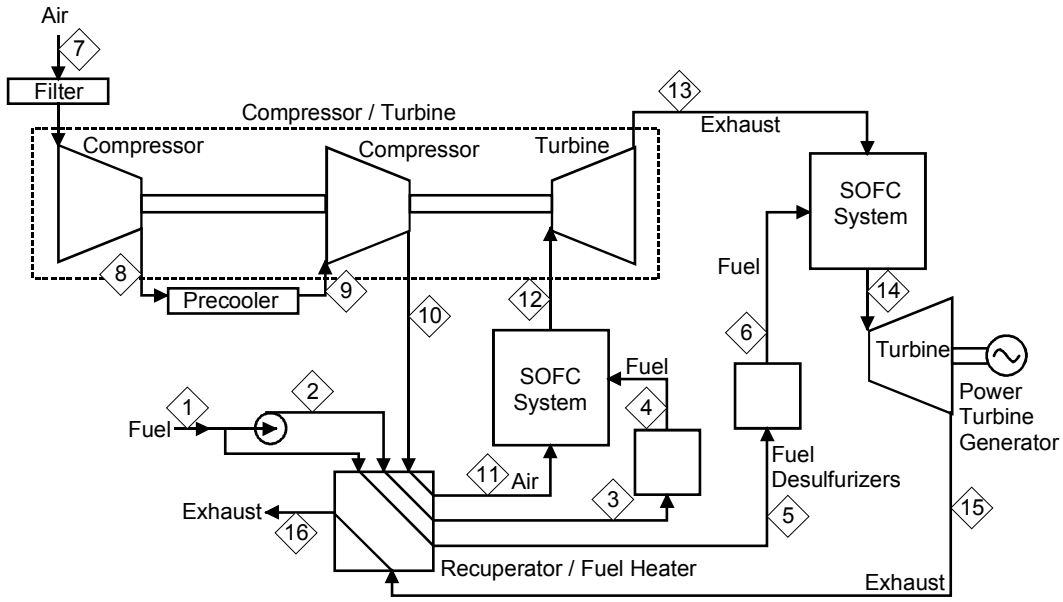

Figure 8-29 Schematic for a 4.5 MW Pressurized SOFC

---

48. The referenced Siemens Westinghouse publication presented the cycle concept and overall performance values. Neither specific stream information nor assumptions were presented. The stream data and assumptions presented here were developed by Parsons. The stream data were developed using an ASPEN simulation which yielded performance numbers in general agreement with the publication.

49. The term "cascaded" fuel cells is used here to describe a fuel cell system where the exhaust of a high-pressure fuel cell is utilized as an oxidant feed stream in a low-pressure fuel cell after passing through an expander.

Table 8-13 Stream Properties for the Natural Gas Fueled Pressurized SOFC

Strm No.	Description	Temp C	Press. atm	Mass Flow kg/hr	Mole Flow kgmol/hr	MW	Ar %	CH4 %	CO2 %	H20 %	N2 %	O2 %	Total %
1	Fuel feed	15	8.85	508	30.9	16.44		97.4	0.4		0.9		100.0
2	Pressurized Fuel	21	9.53	508	30.9	16.44		97.4	0.4		0.9		100.0
3	Heated HP Fuel	399	9.42	508	30.9	16.44		97.4	0.4		0.9		100.0
4	Cleaned HP Fuel	399	9.32	281	17.1	16.44		97.4	0.4		0.9		100.0
5	Heated LP Fuel	399	9.42	227	13.8	16.44		97.4	0.4		0.9		100.0
6	Cleaned LP Fuel	399	3.13	227	13.8	16.44		97.4	0.4		0.9		100.0
7	Air Feed	15	0.99	18,536	642.3	28.86	0.9		trace	1.0	77.2	20.8	100.0
8	Compressed Air	135	2.97	18,536	642.3	28.86	0.9		trace	1.0	77.2	20.8	100.0
9	Intercooled Air	27	2.69	18,351	635.9	28.86	0.9		trace	1.0	77.2	20.8	100.0
10	HP Air	160	8.80	18,351	635.9	28.86	0.9		trace	1.0	77.2	20.8	100.0
11	Heated Air	555	8.66	18,167	629.5	28.86	0.9		trace	1.0	77.2	20.8	100.0
12	HP FC Exhaust	860	8.39	18,448	646.5	28.53	0.9		2.7	6.2	75.2	15.0	100.0
13	HPT Exhaust	642	3.11	18,631	653.1	28.53	0.9		2.7	6.2	75.2	15.0	100.0
14	LP FC Exhaust	874	2.83	18,859	667.0	28.28	0.9		4.7	10.2	73.7	10.6	100.0
15	LPT Exhaust	649	1.01	18,859	667.0	28.28	0.9		4.7	10.2	73.7	10.6	100.0
16	Cycle Exhaust	258	1.00	19,044	673.4	28.28	0.9		4.6	10.1	73.7	10.7	100.0

Reference Source: (30).

The natural gas feed to the cycle (stream 1) is assumed to consist of 95 percent CH_4, 2.5 percent C_2H_6, 1 percent CO_2, and 1.5 percent N_2 by volume along with trace levels of sulfur odorants. The odorants must be reduced to 1 ppmv before entrance into the fuel cell to prevent performance and cell life deterioration. Because the desulfurization requires elevated temperatures, the fuel (streams 3 and 5) is fed through a heat exchanger that recovers heat from the fuel cell exhaust stream (stream 15). The hot desulfurized fuel stream (stream 4) enters the anodes of the high-pressure fuel cell at approximately 399 ºC (750 ºF) and 9.3 atmospheres. The fuel entering the low-pressure fuel cell (stream 6) is approximately 399 ºC (750 ºF) and 3.1 atmospheres. Ambient air (stream 7) is compressed to 3.0 atmospheres and 135ºC (275 ºF) (stream 8), subsequently intercooled to 27 ºC (81 ºF) (stream 9), compressed again to 8.8 atmospheres and 160 ºC (320 ºF) (stream 10), and heated to 555 ºC (1031 ºF) prior to entering the high-pressure fuel cell cathode (stream 11).

The hot desulfurized fuel and the compressed ambient air are electrochemically combined within the high-pressure fuel cell module with fuel and oxidant utilizations of 78 percent and 20.3 percent, respectively. The SOFC high-pressure module was assumed to operate at 0.63 volts per cell. The spent fuel and air effluents of the Siemens Westinghouse tubular geometry SOFC are combusted within the module to supply heat required for the endothermic reforming reaction within the pre-reformer. The majority of the reforming takes place within the tubular fuel cell itself. The heat for internal reforming is supplied by the exothermic fuel cell reaction. A gas recirculation loop provides water for the internal reforming and to prevent soot formation.

The combusted air and fuel stream (stream 12) from the high-pressure fuel cell are expanded (stream 13) in a turbine expander. The work of this turbine is used to drive the low- and high-pressure air compressors. The reduced pressure exhaust stream (stream 13) is utilized as the low-pressure fuel cell oxidant stream. Although vitiated, it still has 15 percent oxygen. The low-pressure TSOFC operates at 0.62 volts per cell, and fuel and air utilizations of 78 and 21.9 percent, respectively. The spent air and fuel effluents are combusted and sent (stream 14) to the low-pressure power turbine. The turbine generator produces approximately 1.4 MW AC. The low-pressure exhaust (stream 15) still has a temperature of 649 ºC (1200 ºF) and is utilized to

preheat the fuel and oxidant streams. The resulting cycle exhaust stream (stream 16) exits the plant stack at approximately 258 ºC (496 ºF).

Operating parameters are summarized in Table 8-14. Cycle performance is summarized in Table 8-15. The overall net electric LHV efficiency is 67 percent.

The high efficiency of this TSOFC/Heron combined cycle is a result of synergism that exists between the SOFC and the Heron turbine. The TSOFC is able to fully replace the gas turbine combustor. That is, the waste heat of the SOFC exhaust is able to completely eliminate the need for the gas turbine combustor at the design point. As seen in Table 8-16, the Heron combustor design temperature of roughly 860 ºC (1580 ºF) is well within the TSOFC operating temperature range. Conversely, the Heron cycle is able to act as an efficient bottoming cycle without requiring a waste heat boiler or steam turbine. In simple cycle mode, the Heron cycle has a respectable LHV net electric efficiency of 42.9 percent. Together, the TSOFC/Heron cycle operates at an efficient 67 percent. Another advantage of this cycle is the low NO_X emissions, because only the spent fuel is fired at the design point. The majority of the fuel reacts within the fuel cell. Overall NO_X levels of less than 4 ppmv are expected.

Table 8-14 Operating/Design Parameters for the NG Fueled Pressurized SOFC

Operating Parameters	HP FC	LP FC
Volts per Cell (V)	0.63*	0.62*
Current Density (mA/cm^2)	NA	NA
Cell Operating Temp. (ºC)	1000*	1000*
Cell Outlet Pressure (atm)	8.4*	2.9*
FC Fuel Utilization (percent)	78.0*	78.0*
FC Oxidant Utilization (percent)	20.3*	21.9*
DC to AC Inverter Effic. (percent)	96.0	
Generator Efficiency (percent)	96.0*	
Auxiliary Load (percent of gross)	1.0*	

Note: * assumed by Parsons to reasonably match the reference paper.

Table 8-15 Overall Performance Summary for the NG Fueled Pressurized SOFC

Performance Parameters	Value
LHV Thermal Input (MW)	6.68
Gross Fuel Cell Power (MW) Fuel Cell DC Power Inverter Loss Fuel Cell AC Power	 3.22 (0.13) 3.09
Gross AC Power (MW) Fuel Cell AC Power Turbine Expander Gross AC Power	 3.09 1.40 4.49
Auxiliary Power	0.04
Net Power	4.45
Electrical Efficiency (percent LHV)	66.6
Electrical Efficiency (percent HHV)	60.1
Heat Rate (Btu/kWh, LHV)	5,120

Table 8-16 Heron Gas Turbine Parameters

Performance Parameters	Value
Compressor Air Flow (kg/h)	18,540
HP Combustor Temperature (°C) LP Combustor Temperature (°C)	861 863
Compressor Pressure Ratio	8.8:1
Power Turbine Exhaust Temp. (°C)	620

The cycle discussed here is based on a Siemens Westinghouse publication for a 4.5 MWe plant. Recent information from Siemens Westinghouse, plans for commercialization of a scaled down 1 MWe version of this dual pressure TSOFC/Heron cycle. A 1 MW cycle was not available in the literature.

8.4.5 Natural Gas Fueled Multi-Stage Solid State Power Plant System

The fuel cell system presented below is based on an innovative solid state fuel cell system developed by U.S.DOE (19). Conventional fuel cell networks, in order to effectively use the supplied fuel, often employ fuel cell modules operating in series to achieve high fuel utilization[50] or combust the remaining fuel for possible thermal integration such as cogeneration steam or a steam bottoming cycle. Both of these conventional approaches utilize fuel cell modules at a single state-of-the-art operating temperature. In conventional fuel cell networks, heat exchangers are utilized between the fuel cell modules to remove heat so the subsequent fuel cell can operate at the desired temperature.

In the multi-stage fuel cell, the individual stages are designed to operate at different temperatures, so that heat exchangers are not required to cool the effluent gases between stages. Each stage is designed to accommodate the next higher temperature regime. In addition, the multi-stage fuel cell concept does not attempt to maximize the fuel utilization in each stage, but allows lower utilizations in comparison to the state-of-the-art design. The number of stages and the fuel utilization per stage in the multi-stage concept is a matter of design choice and optimization. An example of the fuel utilization for a five stage concept is presented in Table 8-17.

Table 8-17 Example Fuel Utilization in a Multi-Stage Fuel Cell Module

Stage	Fuel Balance for 100 Units of Fuel			Fuel Utilization	
	Fuel Feed	Fuel Out	Fuel Used	per Stage	Cumulative
1	100.0	81.0	19.0	19.0 %	19.0 %
2	81.0	62.0	19.0	23.5 %	38.0 %
3	62.0	43.0	19.0	30.6 %	57.0 %
4	43.0	24.0	19.0	44.2 %	76.0 %
5	24.0	6.0	18.0	75.0 %	94.0 %
Overall	100.0	6.0	94.0		94.0 %

A flow diagram for a natural gas fueled, 4 MW class, and solid state fuel cell power cycle is presented in Figure 8-30. A brief process description is given below, followed by a performance summary. Selected state point values are presented in Table 8-18.

[50]. Current state-of-the-art SOFCs have fuel utilizations of 75 to 85%. By utilizing a second fuel cell in series, the total utilization could be theoretically increased to 93 to 98%. Note: Two cascaded fuel cells operating with a fuel utilization of 85% will have an overall utilization of 98%. $1-(0.15)^2 = 1-0.02 = 0.98$ or 98%.

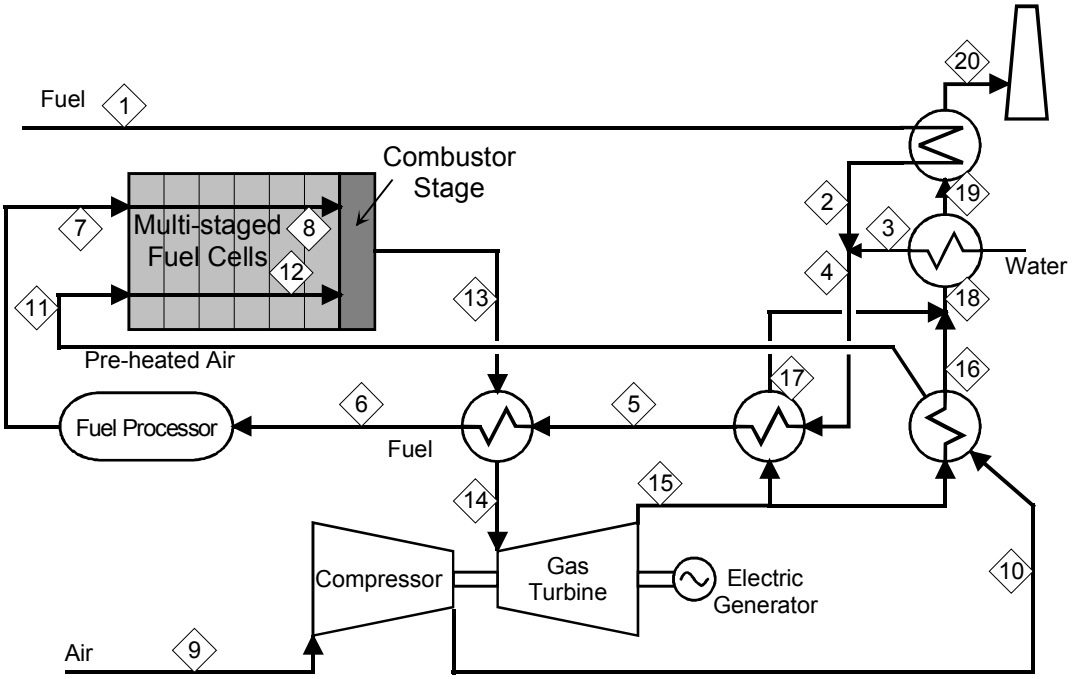

Figure 8-30 Schematic for a 4 MW Solid State Fuel Cell System

Table 8-18 Stream Properties for the Natural Gas Fueled Solid State Fuel Cell Power Plant System

Strm No.	Description	Temp. C	Press. atm	Mass Flow kg/hr	Mole Flow kgmol/hr	MW	CH4 %	C2H6 %	C3H8+ %	CO %	CO2 %	H2 %	H20 %	N2 %	O2 %	Total %
1	Fuel feed	25	3.74	373	21.64	17.23	93.9	3.2	1.1		1.0			0.8		100
2	Heated fuel	84	3.67	373	21.64	17.23	93.9	3.2	1.1		1.0			0.8		100
3	Humidification water	275	3.93	614	34.09	18.02							100.0			100
4	Humidified fuel	192	3.67	987	55.73	17.71	36.5	1.3	0.4		0.4		61.2	0.3		100
5	Heated fuel	725	3.60	987	55.73	17.71	36.5	1.3	0.4		0.4		61.2	0.3		100
6	Heated fuel	725	3.60	987	55.73	17.71	36.5	1.3	0.4		0.4		61.2	0.3		100
7	Processed fuel	494	3.53	987	63.70	15.50	29.1	0.0		0.6	6.0	##	41.6	0.3		100
8	Spent Fuel	999	3.46	2,319	98.40	23.57	1.1			0.3	21.7	0.6	76.1	0.2		100
9	Air feed	25	1.00	7,484	259.42	28.85								79.0	21.0	100
10	Compressed air	175	3.47	7,484	259.42	28.85								79.0	21.0	100
11	Heated air	725	3.40	7,484	259.42	28.85								79.0	21.0	100
12	Spent air	999	3.33	6,149	217.69	28.25								94.1	5.9	100
13	FC exhaust	1119	3.33	8,471	315.78	26.83					7.2		24.7	65.0	3.2	100
14	Cooled exhaust	1119	3.33	8,471	315.78	26.83					7.2		24.7	65.0	3.2	100
15	Expanded exhaust	856	1.04	8,471	315.78	26.83					7.2		24.7	65.0	3.2	100
16	Cooled exhaust	328	1.02	6,438	239.99	26.83					7.2		24.7	65.0	3.2	100
17	Cooled exhaust	333	1.02	2,033	75.79	26.83					7.2		24.7	65.0	3.2	100
18	Combined exhaust	329	1.02	8,471	315.78	26.83					7.2		24.7	65.0	3.2	100
19	Cooled exhaust	152	1.01	8,471	315.78	26.83					7.2		24.7	65.0	3.2	100
20	Cycle exhaust	147	1.00	8,471	315.78	26.83					7.2		24.7	65.0	3.2	100

Reference Source: (20).

The natural gas feed to the cycle (stream 1) is typical of pipeline quality natural gas within the U.S. containing both sulfur odorants and higher hydrocarbons (C_2H_6, C_3H_8, etc.). The odorants must be removed before entrance into the fuel cell to prevent performance and cell life

deterioration. Higher hydrocarbons are assumed to be pre-reformed to hydrogen and carbon monoxide in a mild reformer[51] to avoid "sooting" or carbon deposition within the fuel cell. Because both the desulfurization and reforming require elevated temperatures, the fuel is fed through a series of heat exchangers that recover heat from the fuel cell exhaust stream (streams 13 to 20). Humidification steam (stream 3) is added to the fuel to provide the required moisture for the reforming and water-gas shift reactions. The heated and humidified fuel is desulfurized in a sorbent bed and partially reformed in a mild reformer catalyst bed. The balance of the reforming will occur between the stages of the multi-stage fuel cell module. The hot desulfurized and partially reformed fuel stream (stream 7) enters the fuel cell anode at approximately 500 ºC (930 ºF).

Ambient air (stream 9) is compressed to 3.5 atmospheres and 175 ºC (347 ºF) (stream 10), and subsequently heated to 500 ºC (932 ºF) prior to entering the fuel cell cathode (stream 11).

The hot processed fuel and the compressed ambient air are electrochemically combined within the fuel cell module. The fuel hydrocarbons still remaining after the mild reformer are reformed within the fuel cell. The heat required for the endothermic steam reforming reactions is supplied by the exothermic fuel cell reactions. The overall reactions are exothermic, and the fuel and oxidant temperatures rise to 999 ºC (1830 ºF) (streams 8 and 12). The fuel cell is capable of utilizing both H_2 and CO as fuel and has an overall fuel utilization of 94 percent.

The spent fuel (stream 8) and oxidant (stream 12) are combusted upon exiting the multi-stage fuel cell module. The resulting exhaust stream (stream 13) has a temperature of 1119 ºC (2046 ºF) before being cooled in a fuel heater and expanded to 1.04 atmospheres and 856 ºC (1573 ºF) (stream 15). This nearly atmospheric exhaust stream passes through several additional heat exchangers before leaving the plant stack at 147 ºC (300 ºF).

Operating parameters are summarized in Table 8-19. Cycle performance is summarized in Table 8-20. The overall net electric LHV efficiency is 80.1 percent.

One advantage of this concept is the elimination of heat exchangers between fuel cell modules. This will minimize the cycle complexity, cost, and losses. Another advantage of the concept is the minimization of unreacted fuel leaving the fuel cell. By having discrete fuel cell stages, each operating with its own voltage and current density, fuel utilization can be pushed to very high levels without hurting the performance of the entire module. The voltage and performance degradation resulting from the low fuel concentrations (high utilization) is isolated to the latter fuel cell stage(s) whereas a single fuel cell module, the entire fuel cell performance is degraded. Experiencing a reduced voltage, power, and efficiency level in the latter stages of a multi-stage module is acceptable because it minimizes the heat released in the combustion stage, which is largely passed to the bottoming cycle, which typically has an efficiency of roughly 40 percent. That is, 60 percent of the heat liberated to the bottoming cycle is wasted. Thus, the minimization

[51]. A "mild reformer" is assumedto eliminate of the higher hydrocarbons prior to entering the fuel cell to prevent sooting. This reformer is called a "mild reformer" to indicate that the reforming reactions are not pushed to completion, for it is desired that the methane be reformed in the fuel cell for better temperature management. Some of the methane, however, will be reformed with the higher hydrocarbons in the mild reformer.

of heat passed to the bottom cycle is desirable, even at the "cost" of reduced efficiency in a fraction of the fuel cell module.

One obstacle for this concept is the uncertainty of fuel cell performance in a high utilization multi-stage concept. No testing has been performed to date utilizing a fuel cell in this manner. The exact loss of performance in the latter stages is not known. The reference document (21) for this multi-stage fuel cell concept did not attempt to specify the number of stages nor the fuel cell performance within each stage. Instead, an average fuel cell performance was assumed. This assumption may or may not represent of how a multi-stage fuel cell will perform. Additional development work of this novel and efficient concept is required.

Table 8-19 Operating/Design Parameters for the NG fueled Multi-Stage Fuel Cell System

Operating Parameters	Value
Volts per Cell (V)	0.800
Current Density (mA/cm^2)	unspecified
Number of Stages	to be determined
Cell Operating Temperature (^oC)	multiple temps (~650 to 850 ^oC)
Cell Outlet Pressure (atm)	3.3
Overall Fuel Utilization (percent)	94.0 percent
Overall Oxidant Utilization (percent)	81.5 percent
Steam to Carbon Ratio	1.5:1
DC to AC Inverter efficiency	97.0 percent
Generator efficiency	98.0 percent
Fuel Cell Heat Loss (percent of MW_{dc})	1.7 percent
Auxiliary Load	1.0 percent

Table 8-20 Overall Performance Summary for the NG fueled Multi-StageFuel Cell System

Performance Parameters	Value
LHV Thermal Input (MW)	4.950
Gross Fuel Cell Power (MW)	
Fuel Cell DC Power	3.579
Inverter Loss	(0.108)
Fuel Cell AC Power	3.471
Gross AC Power (MW)	
Fuel Cell AC Power	3.471
Net Compressor/Expander	0.534
Gross AC Power	4.005
Auxiliary Power	0.040
Net Power	3.965
Electrical Efficiency (percent LHV)	80.10 percent
Electrical Efficiency (percent HHV)	72.29 percent
Heat Rate (Btu/kWh, LHV)	4,260

8.4.6 Coal Fueled SOFC System

The coal fueled solid oxide fuel cell power system presented here is based on work performed for the Department of Energy's program (22) to develop high efficiency, low emission, fuel flexible (including coal) processes. This cycle is a coal-fueled version of the Siemens Westinghouse TSOFC cycle presented in Section 8.4.4 consists of a Destec gasifier, cascaded SOFCs at two pressure levels, an integrated reheat gas turbine, and a reheat steam turbine bottoming cycle. The high-pressure portion of the cycle is designed to operate at 15 atmospheres to capitalize on a reasonable gas turbine expansion ratio and an advanced, but not unrealistic, fuel cell pressure. An operating pressure of 30 atmospheres would yield better fuel cell and gas turbine performance, but has been conservatively limited to 15 atmospheres; this is lower than the typical Destec design pressure. Higher pressure operation is feasible and would have better performance. The coal analysis is presented in Table 8-22.

A flow diagram for the coal fueled 500 MW class cascaded TSOFC power cycle is presented in Figure 8-31. A brief process description is given below, followed by a performance summary. Selected state point values are presented in Table 8-23.

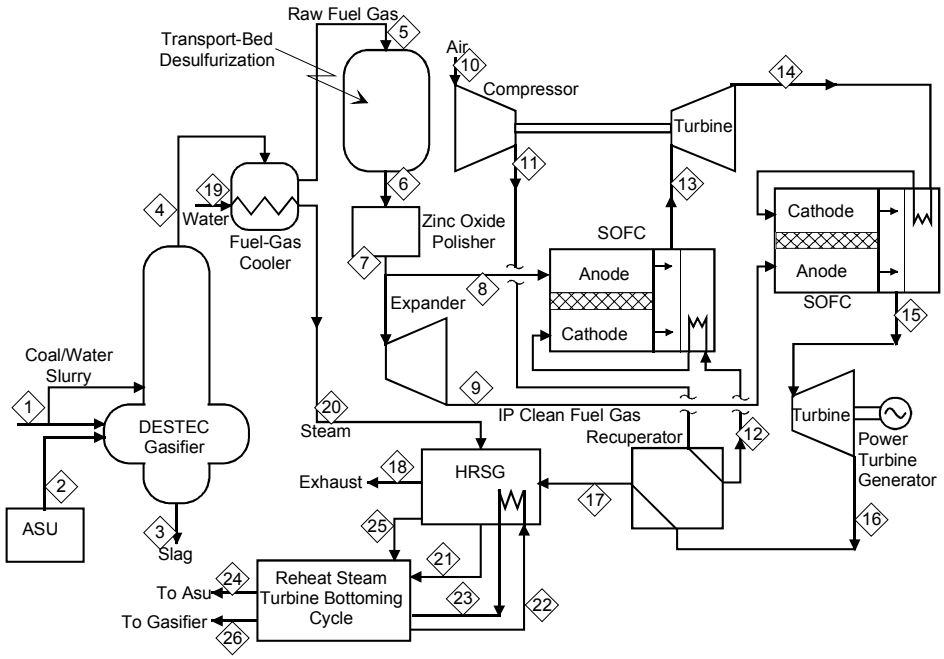

Figure 8-31 Schematic for a 500 MW Class Coal Fueled Pressurized SOFC

Table 8-21 Stream Properties for the 500 MW Class Coal Gas Fueled Cascaded SOFC

Strm No.	Description	Temp C	Press atm	Mass Flow t/h	Mole Flow kgmol/hr	MW	CH4 %	CO %	CO2 %	H2 %	H20 %	H2S %	N2+Ar %	NH3 %	O2 %	Total %
1	Coal Slurry Feed	18	23.8	151.2	-	NA										
2	ASU Oxygen	179	23.8	83.3	2,583	32.23							5.0		95.0	100.0
3	Slag Waste	93	19.1	11.6	-	NA										
4	Gasifier Effluent	1043	18.6	237.6	12,280	19.35	0.3	42.3	9.5	35.8	9.6	0.7	1.5	0.2		100.0
5	Raw Fuel Gas	593	17.6	237.6	12,280	19.35	0.3	42.3	9.5	35.8	9.6	0.7	1.5	0.2		100.0
6	Desulfurized Gas	593	16.6	236.2	12,280	19.23	0.3	42.3	9.6	35.8	10.3	trace	1.5	0.2		100.0
	Recycle to Gasifier	399	15.0	9.4	491	19.23	0.3	42.3	9.6	35.8	10.3	trace	1.5	0.2		100.0
7	Polished Gas	399	15.0	226.7	11,789	19.23	0.3	42.3	9.6	35.8	10.3	trace	1.5	0.2		100.0
8	HP Fuel Gas	399	15.0	108.8	5,659	19.23	0.3	42.3	9.6	35.8	10.3	trace	1.5	0.2		100.0
9	IP Fuel Gas	221	3.7	117.9	6,130	19.23	0.3	42.3	9.6	35.8	10.3	trace	1.5	0.2		100.0
10	Ambient Air	17	0.98	1,270.1	44,024	28.85			trace		1.1		78.1		20.8	100.0
11	Compressed Air	409	15.1	1,146.2	39,732	28.85			trace		1.1		78.1		20.8	100.0
12	Heated Air	579	15.0	1,146.2	39,732	28.85			trace		1.1		78.1		20.8	100.0
13	HP SOFC Exhaust	979	14.7	1,255.1	43,181	29.07			6.9		7.1	trace	72.1	trace	13.9	100.0
14	HPT Exhaust	645	3.6	1,296.3	44,609	29.06			6.6		6.9	trace	72.3	trace	14.1	100.0
15	IP SOFC Exhaust	982	3.3	1,414.2	48,346	29.25			12.7		12.3	trace	66.9	0.1	8.0	100.0
16	IPT Exhaust	691	1.01	1,477.7	50,547	29.23			12.2		11.8	trace	67.4	0.1	8.6	100.0
17	Cooled Exhaust	573	0.99	1,477.7	50,547	29.23			12.2		11.8	trace	67.4	0.1	8.6	100.0
18	Cycle Exhaust	126	0.98	1,477.7	50,540	29.24			12.2		11.8		67.5		8.6	100.0
19	Gas Cooler Water	306	107.4	244.6	13,580	18.02					100.0					100.0
20	Gas Cooler Steam	317	107.4	244.6	13,580	18.02					100.0					100.0
21	HP Steam	538	99.6	301.4	16,730	18.02					100.0					100.0
22	Cold Reheat	359	29.3	298.4	16,563	18.02					100.0					100.0
23	Hot Reheat	538	26.4	298.4	16,563	18.02					100.0					100.0
24	ASU Steam	538	26.4	3.9	218	18.02					100.0					100.0
25	LP Steam	310	6.1	15.6	865	18.02					100.0					100.0
26	Gasifier Steam	307	5.4	32.0	1,774	18.02					100.0					100.0

Reference Source: (30)

The Destec entrained bed gasifier is fed both coal water slurry (stream 1) and a 95 percent pure oxygen stream (stream 2) and operates with a cold gas conversion efficiency[52] of 84 percent. The gasifier fuel gas product (stream 4) is cooled in a radiant heater, which supplies heat to the bottoming cycle. The cooled fuel gas is cleaned (stream 6) in a hot gas desulfurizer at 593 ºC (1100 ºF) and a polisher (stream 7) at 399 ºC (750 ºF) to less than 1 ppmv of sulfur prior to entering the high-pressure fuel cell (stream 8). Part of the polished fuel is expanded to 3.7 atmospheres and 220 ºC (429 ºF) before being sent to the low-pressure fuel cell (stream 9).

Ambient air (stream 10) is compressed to 15.1 atmospheres and 409 ºC (275 ºF) (stream 11), and subsequently heated to 579 ºC (1075 ºF) prior to entering the high-pressure fuel cell cathode (stream 12).

The hot clean fuel gas and the compressed ambient air are electrochemically combined within the high-pressure fuel cell with fuel and oxidant utilizations of 90 percent and 24.5 percent, respectively. The SOFC module is set (sized) to operate at 0.69 volts per cell.[53] The spent fuel and air effluents of the SOFC are combusted within the module to supply heat for oxidant preheating. Unlike the natural gas case, the fuel does not require a pre-reformer with only 0.3 percent methane along with 36 percent hydrogen and 43 percent carbon monoxide. The carbon monoxide will be either water gas shifted to hydrogen or utilized directly within the fuel cell. A

[52]. Cold gas conversion efficiency is the ratio of the gasifier fuel gas total heating value [i.e., (heating value)(mass flow)] to that of the coal feed, [(heating value)(mass flow)].

[53]. Siemens Westinghouse provided TSOFC performance values for the HP and LP conditions, which Parsons incorporated into the systems analysis.

gas recirculation loop for the fuel cell has not been assumed, for water is not required for pre-reforming nor internal reforming.

The combusted air and fuel stream (stream 13) from the high-pressure fuel cell is expanded (stream 14) in a turbine expander. The work of this turbine is used to drive the low- and high-pressure air compressors. The reduced pressure exhaust stream (stream 14) is utilized as the low-pressure fuel cell oxidant stream. Although vitiated, it still has 14 percent oxygen. The low-pressure SOFC operates at 0.69 volts per cell and fuel and air utilizations of 90 and 34.7 percent, respectively (23). The spent air and fuel effluents are combusted and sent (stream 15) to the low-pressure power turbine. The turbine generator produces approximately 134 MWe. The low-pressure exhaust (stream 16) has a temperature of 691 ºC (1276 ºF) and is utilized to preheat the high-pressure oxidant. The resulting cooled exhaust stream (stream 17) still has a temperature of 573 ºC (1063 ºF) and is utilized to supply heat to a steam bottoming cycle.

Steam generated in the bottoming cycle is utilized in a reheat turbine to produce 118 MWe, as well as to supply the steam required by the air separation unit (ASU) and the gasifier coal slurry heater. The cycle exhaust exits the heat recovery steam generator at 126 ºC (259 ºF) and 0.98 atmospheres.

Operating parameters are summarized in Table 8-23. Cycle performance is summarized in Table 8-24. The overall cycle net HHV efficiency is 59 percent.

Table 8-22 Coal Analysis

Coal Parameters	Value
Source	Illinois No. 6
Ultimate Analysis, (wt percent, a.r.)	
Moisture	11.12
Carbon	63.75
Hydrogen	4.50
Nitrogen	1.25
Chlorine	0.29
Sulfur	2.51
Ash	9.70
Oxygen (by difference)	6.88
Total	100.00
HHV (Btu/lb)	11,666
LHV (Btu/lb)	11,129

Table 8-23 Operating/Design Parameters for the Coal Fueled Pressurized SOFC

Operating Parameters	HP FC	LP FC
Volts per Cell (V)	0.69	0.69
Current Density (mA/cm^2)	312	200
Cell Operating Temp. (^{o}F)	1794	1800
Cell Outlet Pressure (atm)	14.7	3.3
Overall Fuel Utilization (percent)	90	90
Overall Oxidant Utilization (percent)	18.7	20.4
DC to AC Inverter Efficiency	97.0 percent	
Generator Effic. - ST, GT	98.5 percent	
Generator Effic. - Expander	98.0 percent	
Auxiliary Load	7.2 percent	

Table 8-24 Overall Performance Summary for the Coal Fueled Pressurized SOFC

Performance Parameters	Value
LHV Thermal Input (MW)	875.8
Gross Fuel Cell Power (MW)	
Fuel Cell DC Power	310.9
Inverter Loss	(9.3)
Fuel Cell AC Power	301.6
Gross AC Power (MW)	
Fuel Cell AC Power	301.6
Combustion Turbine	133.7
Steam Turbine	118.1
Fuel Expander	9.6
Gross AC Power	562.9
Auxiliary Power	40.3
Net Power	522.6
Electrical Efficiency (percent HHV)	59.7
Electrical Efficiency (percent LHV)	62.6
Heat Rate (Btu/kWh, HHV)	5,720

This configuration has the potential to yield a very competitive cost of electricity. For example, for a fuel cell stack cost of $300 to $400/kW, it is estimated that the COE would range from 3.5 to 3.9 cents/kWh (Assuming 20 percent equity at 16.5 percent, 80 percent debt at 6.3 percent, and a levelized carrying charge of 0.12.)

8.4.7 Power Generation by Combined Fuel Cell and Gas Turbine System

In general, the oxidation of H_2, CO, CH_4, and higher hydrocarbons in fuel cells to produce power also produces reject heat. This heat arises from two sources:

- the entropy decrease, ΔS, resulting from the overall oxidation reaction -- accompanying the usual decrease in the number of mols of gas, from reactants to products; and
- the loss in work, or a conversion of "reversible" work from the oxidation process to heat, due to irreversible processes occurring in the operation of the cell.

Heat from these two sources must be rejected from the fuel cell in order to maintain its temperature at a desired level. The heat can be removed and recovered by transferring it across a bounding surface to a heat transfer fluid, but care must be taken to maintain the cell at its desired temperature in this and adjacent regions. Alternatively, heat can be removed in one of the reactant streams passing through the cell -- most practically the air, oxidant stream.

Also in the operation of a practical fuel cell, some unburned fuel must remain in the combustion products leaving the cell in order to maintain a significant generated voltage throughout the cell.

In order to obtain the highest possible efficiency in electrical generation, both the thermal energy in the heat and the unburned fuel rejected from the cell must be recovered and converted into additional electrical energy. This can be accomplished by means of a heat engine cycle making use of a gas turbine operating in a regenerative Brayton or combined Brayton-Rankine cycle or a steam turbine operating in a Rankine cycle. The relative merits of these three heat engine cycles depend on their overall efficiencies and on the practical aspects of integration, operation, and cost of the power generation plant as a whole.

8.4.8 Heat and Fuel Recovery Cycles

Simple representations of three fuel cell based heat and fuel recovery cycles are shown in Figures 8-32, 8-33, and 8-36.

Regenerative Brayton Cycle: The regenerative Brayton cycle, Figure 8-32, shows a gas turbine compressor for the air flow to the cell. The flow then passes through a countercurrent, recuperative heat exchanger to recover heat from the combustion product gases leaving the gas turbine. The air and the fuel streams then pass into the cathode and anode compartments of the fuel cell(s). The air and fuel streams leaving the cell(s) enter the combustor where they mix and the residual fuel burns. The combustion products enter the turbine, expand, and generate additional power. The turbine exhaust gases pass through the recuperative exchanger to the stack.

The most significant variables characterizing the cycle are the fuel cell operating temperature range and the temperature and pressure at the gas turbine expander inlet. These variables are directly related to certain operating variables: the air/fuel ratio entering the fuel cell, the fraction of the fuel leaving the cell unburned, and the temperature difference between the combustion products and air at the high temperature end of the recuperative heat exchanger. The operating variables must be selected and controlled to allow effective operation of the fuel cell, combustor, and gas turbine. There may well be an optimal quantity of unburned fuel leaving the fuel cell, depending on the acceptable fuel cell operating temperature range and turbine inlet temperature.

Further insight can be gained from the idealized T - S diagram for the cycle, Figure 8-32. The compression of the air and fuel streams is represented here as a single adiabatic reversible (constant S) process in which the temperature of the gases rises above ambient. The heating of

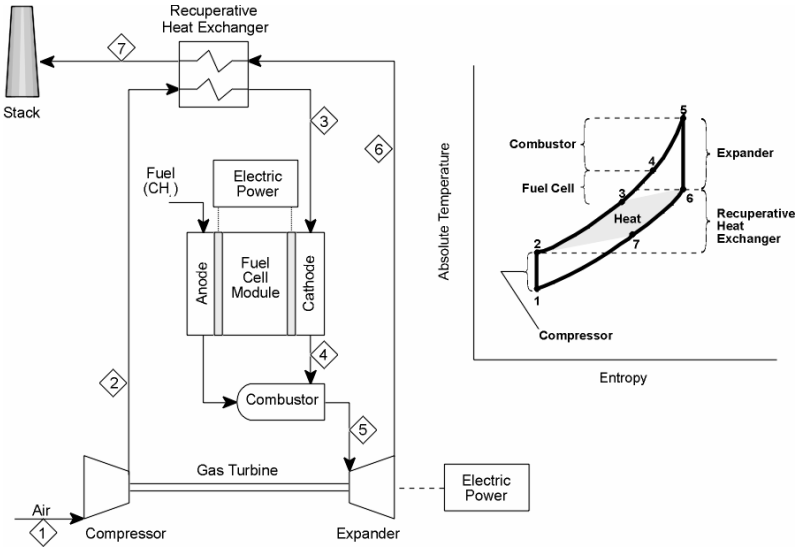

Figure 8-32 Regenerative Brayton Cycle Fuel Cell Power System

the air and also the fuel streams first in the recuperative exchanger, then in the fuel cell and finally in the combustor is assumed to occur along a single line of constant pressure. The subsequent expansion of the combustion gases in the turbine is also represented as an adiabatic reversible (constant S) process in which the temperature of the gases drops to a value close to that of the gases entering the fuel cell. The pressure ratio (PR) of the turbine (and of the compressor) is therefore established by the turbine nozzle inlet temperature (NIT) and the fuel cell operating temperature. In general, the pressure ratio of a regenerative Brayton cycle is low compared with that of a combined Brayton-Rankine cycle. A low pressure ratio allows a low outlet temperature of the exhaust gases from the recuperative exchanger as heat is transferred to the air leaving the compressor (and possibly also the fuel) and consequently results in low heat rejection and a high cycle efficiency.

The practical aspects of the cycle involve the efficiencies of the gas compressors, the turbine expander, and the fuel cell; the pressure losses as the gases flow through the system; and the temperature differences and the difference in heat capacities of the streams flowing through the recuperative heat exchanger. Other aspects of the fuel cell operation must be considered in greater detail for the design and evaluation of the power system. These include the possible need for fuel reforming external to the cell and the recycle of combustion product streams to provide the steam required to carry out the reforming process, to avoid carbon deposition, and to provide H_2 for effective cell operation.

Table 8-25 Performance Calculations for a Pressurized, High Temperature Fuel Cell (SOFC) with a Regenerative Brayton Bottoming Cycle; Approach Delta T=30 °F

COMPRESSOR EFF =	0.83			n = number of moles				
TURB EXPANDER EFF =	0.89			Cp = specific heat				
FUEL CELL EFF=	56.9			Hf = heat of formation at standard conditions				
CYCLE EFF=	82.1			So = entropy at standard conditions				
STREAM #	1	2	3	4	5	6	7	Cycle
p, PRESSURE, atm	1	1.48	1.48	1.48	1.48	1	1	
T, TEMPERATURE, K	298	337	1200	1311	1332	1216	352	
CH4, n	1	1	1	0.07	0	0	0	
CO, n								
H2, n								
CO2, n	0	0	0	0.93	1	1	1	
H2O, n	0	0	0	1.86	2	2	2	
O2, n	16.23	16.23	16.23	14.37	14.23	14.23	14.23	
N2, n	64.92	64.92	64.92	64.92	64.92	64.92	64.92	
SUM(n)	82.15	82.15	82.15	82.15	82.15	82.15	82.15	
SUM(nCp)	629.72	629.72	629.72	628.97	628.92	628.92	628.92	
SUM(nHf)	-17.9	-17.9	-17.9	-196.181	-209.6	-209.6	-209.6	
SUM(nSo)	3813.11	3813.11	3813.11	3811.99	3811.91	3811.91	3811.91	
GAMMA	1.350				1.351			
Q, HEAT, kcal/molCH4	0.0	543.5	0.0	-0.2	0.0	543.5		1086.8
W, WORK, kcal/molCH4	-24.4	0.0	109.1	0.0	72.7	0.0		157.4

The performance of a solid electrolyte fuel cell (SOFC) system (Hirschenhofer et al., 1994) operating with a regenerative Brayton bottoming cycle for heat and fuel recovery has been calculated. Table 8-25 illustrates the results. The work from the fuel cell burning CH_4 is assumed to be 60 percent the theoretical maximum; the corresponding fuel cell voltage is 0.63 volts. The efficiencies of the fuel and air compressors are 83 percent; and the expander of the turbine, 89 percent. It is assumed that the cell makes direct use of CH_4 fuel, or that oxidation and reforming are coincident; operation of the cell thus provides both the heat and the H_2O required for CH_4 reforming. Pressure losses in the fuel cell, combustor, recuperative exchanger, and the ducts of the system are ignored.

The results of the performance calculations are summarized in Table 8-26. The efficiency of the overall power system, work output divided by the lower heating value (LHV) of the CH_4 fuel, is increased from 57 percent for the fuel cell alone to 82 percent for the overall system with a 30 °F difference in the recuperative exchanger and to 76 percent for an 80 °F difference. This regenerative Brayton cycle heat rejection and heat-fuel recovery arrangement is perhaps the simplest approach to heat recovery. It makes minimal demands on fuel cell heat removal and gas turbine arrangements, has minimal number of system components, and makes the most of the inherent high efficiency of the fuel cell.

Table 8-26 Performance Computations for Various High Temperature Fuel Cell (SOFC) Heat Recovery Arrangements

General Conditions

SOFC, solid oxide fuel cell

Operating temperature, 1700-1900 F

Fuel cell output: 60% of theoretical maximum from CH4 fuel

Gas turbine compressor, expander efficiences: 83, 89%

Steam turbine efficiency: 90%

Notes

PR = pressure ratio of the gas turbine

NIT = nozzle inlet temperature of the turbine expander

Heat Recovery Arrangement	Work Output, %			Overall System Eff., %	Remarks
	Fuel Cell	Gas Turbine	Steam Turbine		
Regenerative Brayton Cycle	69.3	30.7	n/a	82.1	30 F Approach in Recuperative Exchanger Gas Turbine PR=1.48, NIT=1938 F
Regenerative Brayton Cycle	74.5	25.5		76.3	80 F Approach in Recuperative Exchanger Gas Turbine PR=1.35, NIT=1938 F
Combined Brayton-Rankine Cycl	75.3	10.3	14.3	75.6	Gas Turbine PR=12, NIT=2300 F Steam Turbine: 1600 psia, 1000 F, 1.5" Hg
Rankine Cycle	79.1		20.9	72.4	Steam Turbine: 1600 psia, 1000 F, 1.5" Hg

Combined Brayton-Rankine Cycle: The combined Brayton-Rankine cycle, Figure 8-33, again shows the gas turbine compressor for the air flow to the cell. This flow passes through a heat exchanger in direct contact with the cell; it removes the heat produced in cell operation and maintains cell operation at constant temperature. The air and fuel streams then pass into the cathode and anode compartments of the fuel cell. The separate streams leaving the cell enter the combustor and then the gas turbine. The turbine exhaust flows to the heat recovery steam generator and then to the stack. The steam produced drives the steam turbine. It is then condensed and pumped back to the steam generator.

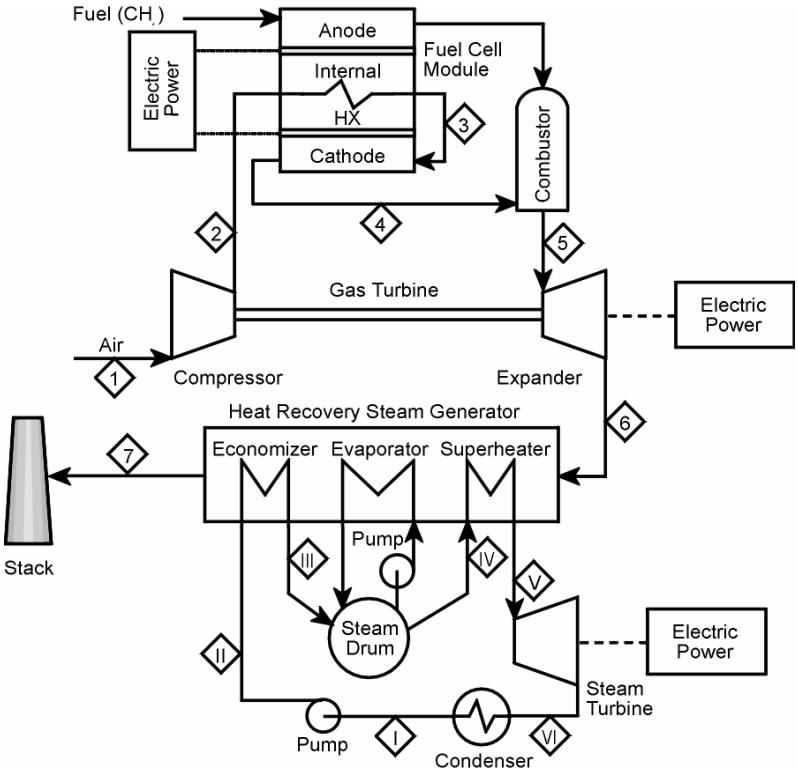

Figure 8-33 Combined Brayton-Rankine Cycle Fuel Cell Power Generation System

The air/fuel ratio entering the fuel cell and the fraction of the CH_4 fuel consumed in the cell are selected to achieve the desired fuel cell operating temperature range and gas turbine NIT and PR. These are selected to correspond with those of a conventional, large-scale, utility gas turbine.

Further insight can be gained from an idealized T- S diagram for the cycle, Figure 8-34, in which both the Brayton and the Rankine cycles are illustrated. Both the pressure and the temperature increase during fuel and air compression in this combined cycle will be significantly greater than in the regenerative Brayton cycle described above. The heating of the air and fuel, the operation of the fuel cell, and the burning of the residual fuel are assumed to occur at constant pressure. The expansion of the combustion product gases in the gas turbine again is represented as an adiabatic, reversible (constant S) process. Next, heat is removed from these gases at nearly constant pressure in the heat recovery steam generator; and they pass out through the stack.

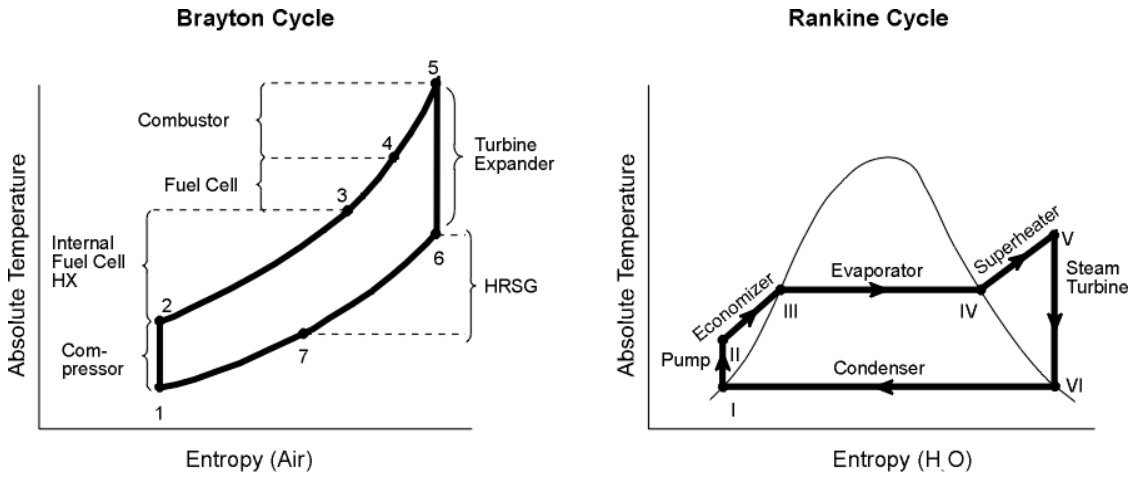

Figure 8-34 Combined Brayton-Rankine Cycle Thermodynamics

The Rankine cycle diagram placed adjacent the Brayton cycle in Figure 8-34 is indicated as a simple steam cycle with superheat, but no reheat and no multi-pressure steam generation. The thermodynamic advantage of the Rankine bottoming cycle is the lowered temperature of heat rejection, in the steam condenser, from the overall combined cycles.

The performance of a SOFC system with a Brayton-Rankine bottoming cycle for heat and fuel recovery has been calculated. Gas turbine compressor and expander efficiencies of 83 percent and 89 percent and a steam turbine efficiency of 90 percent have been assumed.

The significant operating conditions of the gas and steam turbines and the results of the computations are summarized in Table 8-26. The principal result is that the efficiency of the overall system, work output divided by the CH_4 LHV, is increased from 57 percent for the fuel cell alone to 75 percent for the overall system. This combined Brayton-Rankine cycle heat-fuel recovery arrangement is significantly more complex and less efficient than the simple regenerative Brayton cycle approach. It does, however, eliminate the requirement for a large, high temperature gas to gas heat exchanger.

The key link between the Brayton and the Rankine cycles is the heat recovery steam generator whose operation is illustrated by the temperature-heat (T-Q) plot in Figure 8-35. The temperatures of the gases and of the water, T, are plotted as a function of the heat, Q, transferred from the combustion product gases to the water-steam between their entrance and any point in the steam generator. The area between the temperature curves for the two flowing streams is an indication of the irreversibility, or loss in available work, resulting from the transfer of heat over a finite temperature difference. Reducing this area, moving the gas and steam curves closer, requires increased heat transfer surface area in the steam generator. Steam reheat and multi-pressure level heat recovery boilers are frequently proposed to minimize the loss in available work.

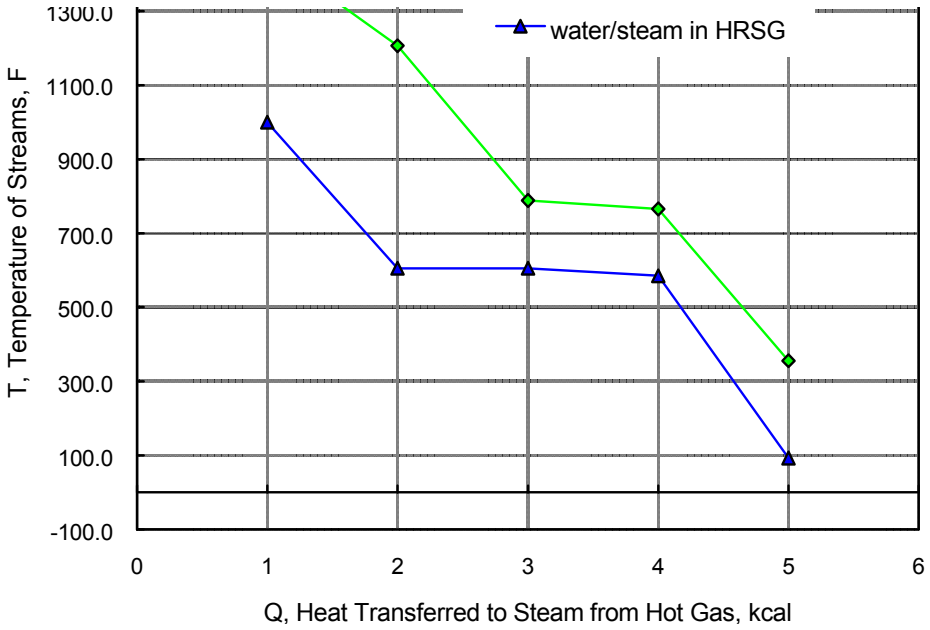

Figure 8-35 T-Q Plot for Heat Recovery Steam Generator (Brayton-Rankine)

Rankine Cycle: The fuel cell Rankine cycle arrangement in Figure 8-36 employs a heat recovery steam generator operating on the exhaust combustion product stream from the fuel cell and combustor at atmospheric pressure. This exhaust stream first provides the heat required to preheat and reform the CH_4 fuel, providing CO and H_2 at temperature to the fuel cell. Partially combusted fuel from the cell is recycled to provide the H_2O required for reforming the fuel. Depleted air from the cell exhaust is recycled to the air feed stream to raise its temperature to the desired value at the cell inlet. The operating conditions and the T - S diagram for the Rankine cycle are identical to those illustrated for the combined Brayton-Rankine cycle in Figure 8-34 and Table 8-26.

The results of the performance calculations for the fuel cell, Rankine cycle heat recovery system, summarized in Table 8-26, indicate that the efficiency of the overall system is increased from 57 percent for the fuel cell alone to 72 percent for the overall system. This Rankine cycle heat-fuel recovery arrangement is less complex but less efficient than the combined Brayton-Rankine cycle approach, and more complex and less efficient than the regenerative Brayton approach. It does, however, eliminate the requirement for a large, high temperature gas to gas heat exchanger. And in applications where cogeneration and the supply of heat are desired, it provides a source of steam.

The T - Q plot for the heat transfer processes involved in this fuel cell Rankine cycle arrangement is shown in Figure 8-37. Because heat is removed from the exhaust gases to heat and reform the CH_4 fuel feed, the temperature of the hot gas entering the heat recovery steam generator in this

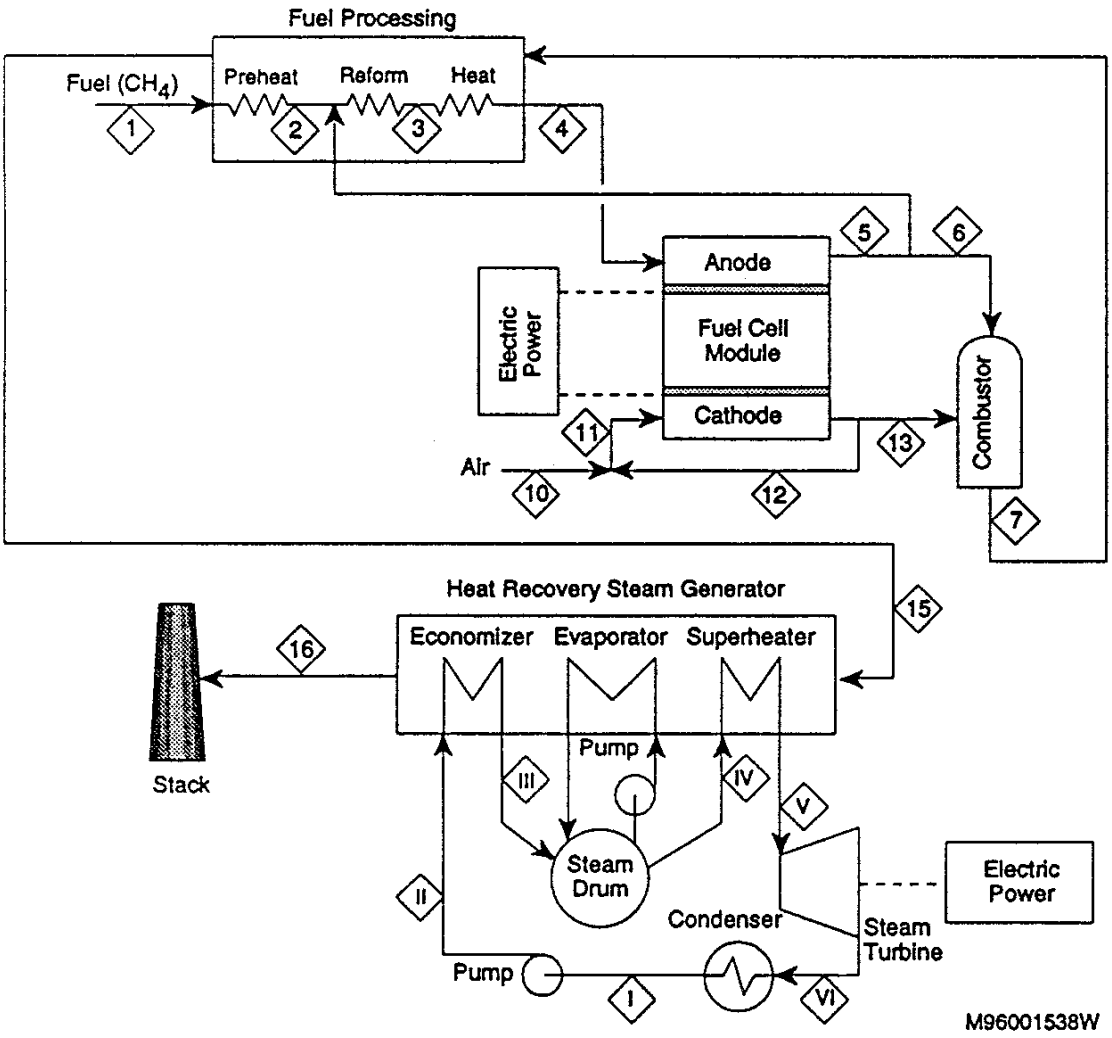

Figure 8-36 Fuel Cell Rankine Cycle Arrangement

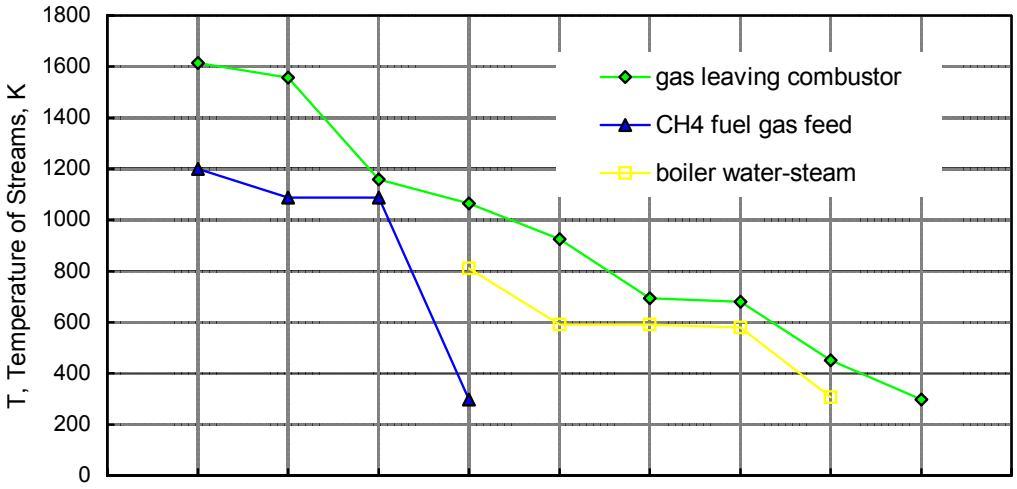

Figure 8-37 T-Q Plot of Heat Recovery from Hot Exhaust Gas

particular Rankine cycle fuel cell arrangement is significantly lower than in the previous combined Brayton-Rankine cycle arrangement. Increased surface area is, therefore, required in the heat recovery steam generator for this fuel cell Rankine cycle arrangement.

These three approaches to reject heat and exhaust fuel recovery with power generation apply primarily to the higher temperature, solid oxide (1800 ^{o}F) and molten carbonate (1200 ^{o}F), fuel cell systems operating on CH_4 fuel. The lower operating temperatures of the phosphoric acid (400 ^{o}F) and polymer electrolyte (175 ^{o}F) fuel cells severely limit the effectiveness of thermal cycle based power generation as a practical means of heat recovery.

All three of the heat recovery arrangements have calculated overall efficiencies greater that 70 percent as indicated in Table 8-26. None have been optimized in any sense -- in terms of efficiency, capital and operating costs, maintainability or availability. Each of the arrangements has its advantages and disadvantages. It appears, however, that the regenerative Brayton cycle has the advantage of greatest simplicity and highest potential overall efficiency over the combined Brayton-Rankine and Rankine cycle approaches.

The consideration of heat recovery and use in such fuel cell systems requires some consideration of heat generation and transfer within the cells of the system. Direct oxidation of CH_4 at the anode of the cell, if possible, would implement the overall process:

$$CH_4 + 2O_2 = CO_2 + 2H_2O\ (v)$$

This reaction, having equal number of mols of gas reactants and products, has a negligible change in entropy and thus a negligible heat effect if carried out reversibly at constant temperature. The maximum work available from a fuel cell under these circumstances would then be approximately the enthalpy change of the reaction, i.e., the heat of combustion of the

CH_4; the efficiency of the fuel cell power generation process could, therefore, approach 100 percent. However, work is lost and a corresponding quantity of heat is produced by irreversibilities both in fuel cell operation --

- the electrical resistance of the electrolyte to ion flow and of the electrodes, current collectors, and leads to electron flow;
- the kinetics of the processes involving reactants, ions, and electrons at the anode and cathode of the cell;
- the transport, or diffusion, of reactants within the anode and cathode chambers to the electrode;
- and also in overall system operation –
- the preheating of the air and fuel streams;
- the pretreating, or reforming, of the CH_4 fuel to provide more reactive H_2 and to prevent the deposition of carbon (C).

The heat resulting from these irreversibilities must then be removed in order to maintain the fuel cells at a desired operating temperature. Irreversibilities and the resulting quantity of heat produced can be reduced, in general, by increasing the active area of the fuel cells, heat exchangers, and fuel reformer; but increased equipment costs result.

In general, reforming of the CH_4 fuel with excess H_2O outside the cell has been practiced both in molten carbonate and solid oxide fuel cell systems in order to produce H_2, more reactive on a fuel cell anode, and to avoid the possible deposition of C. This reforming reaction

$$CH_4 + H_2O = CO + 3H_2$$

is associated with an increase in entropy and absorbs heat. Excess H_2O produces additional H_2 and reduces the CO content of the reformed gases, which may adversely affect anode reactions, by the shift reaction

$$H_2O + CO = H_2 + CO_2.$$

This reaction is thermally neutral. The heat absorbed in the CH_4 reforming reaction is released by the subsequent reaction of the H_2 product at the anode of the fuel cell. If, therefore, the reforming process can be carried out in close proximity to and in thermal contact with the anode process, the thermal neutrality of the overall CH_4 oxidation process can be approximated. And the heat removal and recovery process for the fuel cell system can deal merely with the heat produced by its operational irreversibilities.

Heat removal from fuel cells, and cell batteries, can be accomplished:

- directly through the flow of reactants to and products from them.
- indirectly through heat transfer surfaces in contact with the cell or included within a battery.

A specific fuel cell system is viewed here as having a fixed range of operating temperature between a maximum and minimum; heat must therefore be removed in such a manner to maintain the temperature within these limiting values. If heat is removed directly by reactant flows, then the quantity of flow must be adjusted so that inlet and outlet temperatures (as well as

the intermediate temperatures) of the cell and of the flow streams are within the permissible range. Practically, the air stream is adjusted to achieve this result, since the purpose of the fuel cell is to consume the fuel in the production of electrical energy. Increasing the fuel flow to remove heat from the cell increases the quantity of unburned fuel in the exhaust from the cell. If heat is removed from the fuel cell indirectly through adjacent or embedded surface, then the flow and temperature of the coolant stream can be selected somewhat independent of the cell operating temperature. But the distribution of heat transfer surface in the cell (or battery) and the rate of heat transfer across that surface must be carefully adjusted and controlled to maintain the temperature throughout the cell (or battery) within the prescribed temperature range.

The regenerative Brayton cycle, as presented, depends primarily on its fuel cell component for conversion of the fuel and thus for its overall efficiency. The gas turbine merely provides the means for recovery of the waste heat and residual fuel in the combustion product stream. The gas turbine operates, therefore, at a temperature only slightly elevated above that of the cell by the combustion of the residual fuel. The pressure ratio selected for the turbine in this regenerative cycle is determined by the ratio of the temperature of the gases leaving the auxiliary combustor to the temperature of the reactant gases entering the fuel cell. In general, for either molten carbonate or solid oxide cells, this selected pressure ratio will be less than two. The proposed method of cell cooling is air flow, which will be increased significantly, by a factor of 4-8 above that required for oxidation of the fuel. The feasibility of this cycle will depend on the availability of air compressor and turbine expander units with:

- the pressure ratio and temperature capability compatible with the fuel cell operation.
- a capacity appropriate to market applications.

The effectiveness of the regenerative Brayton cycle performance will depend on the efficiency of the fuel cell, compressor, and turbine units; the pressure loss of gases flowing through the system; the approach temperatures reached in the recuperative exchanger; and, most importantly, the cost of the overall system.

The combined Brayton-Rankine cycle depends on both the fuel cell and the gas turbine components for conversion of the fuel and thus for its overall efficiency. The extent of conversion of the fuel occurring in the fuel cell increases as the cell operating temperature and the range of coolant temperature rise increase. For this reason, the cycle as presented is based on indirect heat removal from the cell, heating the air stream temperature from the compressor outlet to the cell operating temperature. This provision maximizes the cell contribution to the energy output of the combined cycle. The PR and NIT of the turbine are those selected to match those of the current utility scale equipment -- a PR of 12 and an NIT of 2300 ^{o}F -- resulting in a combined cycle efficiency of perhaps 45 to 50 percent, not considering the electrical energy output of and the fuel input to the fuel cell. The fuel combustion occurring in the combustor and overall air/fuel ratio is then determined by the combination of the cell and the turbine inlet temperatures.

The fuel cell Rankine cycle arrangement has been selected so that all fuel preheating and reforming are carried out external to the cell and air preheating is accomplished by mixing with recycled depleted air. The air feed flow is adjusted so that no heat transfer is required in the cell

or from the recycled air. Consequently, the internal fuel cell structure is greatly simplified, and the requirement for a heat exchanger in the recycle air stream is eliminated.

Summary

Advantages, Disadvantages of Various Fuel Cell, Power Cycles

Regenerative Brayton

Advantages:

- simple cycle arrangement, minimum number of components.
- relatively low compressor and turbine pressure ratio, simple machines.
- relatively low fuel cell operating pressure, avoiding the problems caused by anode/cathode pressure differential and high pressure housing and piping.
- relatively low turbine inlet temperatures, perhaps 1950 ^{o}F for solid oxide and 1450 ^{o}F for molten carbonate fuel cell systems. Turbine rotor blade cooling may not be required.
- relatively simple heat removal arrangements in fuel cells, accomplished by excess air flow. No internal heat transfer surface required for heat removal.
- fuel conversion in cells maximized, taking full advantage of fuel cell efficiency.
- adaptability to small scale power generation systems.

Disadvantages:

- tailoring of compressor and turbine equipment to fuel cell temperature and cycle operating pressure required. (It is not clear to what extent available engine supercharging and industrial compressor and turbine equipment can be adapted to this application.)
- large gas to gas heat exchanger for high temperature heat recuperation required.
- efficiency and work output of the cycle sensitive to cell, compressor, and turbine efficiencies; pressure losses; and temperature differentials.

Combined Brayton-Rankine

Advantages:

- integrated plant and equipment available for adaptation to fuel cell heat recovery.
- high efficiency system for heat recovery.

Disadvantages:

- complex, multi component, large scale system for heat recovery.
- adaptation of existing gas turbine required to provide for air take off and return of hot depleted air and partially burned fuel.
- high pressure operation of the bulky fuel cell system required.
- precise balancing of anode and cathode pressures required to prevent rupture of fuel cell electrolyte.
- indirect heat removal required from fuel cells with compressed air, initially at low temperature, to enable significant conversion of the fuel flow in the cells.

Rankine

Advantages:

- ambient pressure operation within the fuel cell.
- heat recovery in a boiler, avoiding the high temperature gas to gas exchanger of a regenerative Brayton cycle.

- no gas turbine required, only fans for air and exhaust product gas flow.
- steam available for cogeneration applications requiring heat.

Disadvantages:

- inherently lower efficiency than regenerative Brayton and combined Brayton-Rankine cycles.
- requirement for cooling and feed water.
- greater complexity than regenerative Brayton cycle arrangement.

8.5 Fuel Cell Networks

8.5.1 Molten Carbonate Fuel Cell Networks: Principles, Analysis and Performance

The U.S. Department of Energy's National Energy Technology Laboratory (NETL) sponsors the research and development of engineered systems which utilize domestic fuel supplies while achieving high efficiency, economy and environmental performance. One of the most promising electric power generation systems currently being sponsored by NETL is the molten carbonate fuel cell (MCFC).

NETL looked at improving upon conventional MCFC system designs, in which multiple stacks are typically arranged in parallel with regard to the flow of reactant streams. As illustrated in Figure 8-38a, the initial oxidant and fuel feeds are divided into equal streams which flow in parallel through the fuel cell stacks.

In an improved design, called an MCFC network, reactant streams are ducted such that they are fed and recycled among multiple MCFC stacks in series. Figure 8-38b illustrates how the reactant streams in a fuel cell network flow in series from stack to stack. By networking fuel cell stacks, increased efficiency, improved thermal balance, and higher total reactant utilizations can be achieved. Networking also allows reactant streams to be conditioned at different stages of utilization. Between stacks, heat can be removed, streams can be mixed, and additional streams can be injected.

Stacks in series approach reversibility. MCFC stack networks produce more power than conventional configurations because they more closely approximate a reversible process. To illustrate this fact, consider Figure 8-39, which compares the maximum power that could be generated by three different MCFC systems having identical feed stream compositions[1].

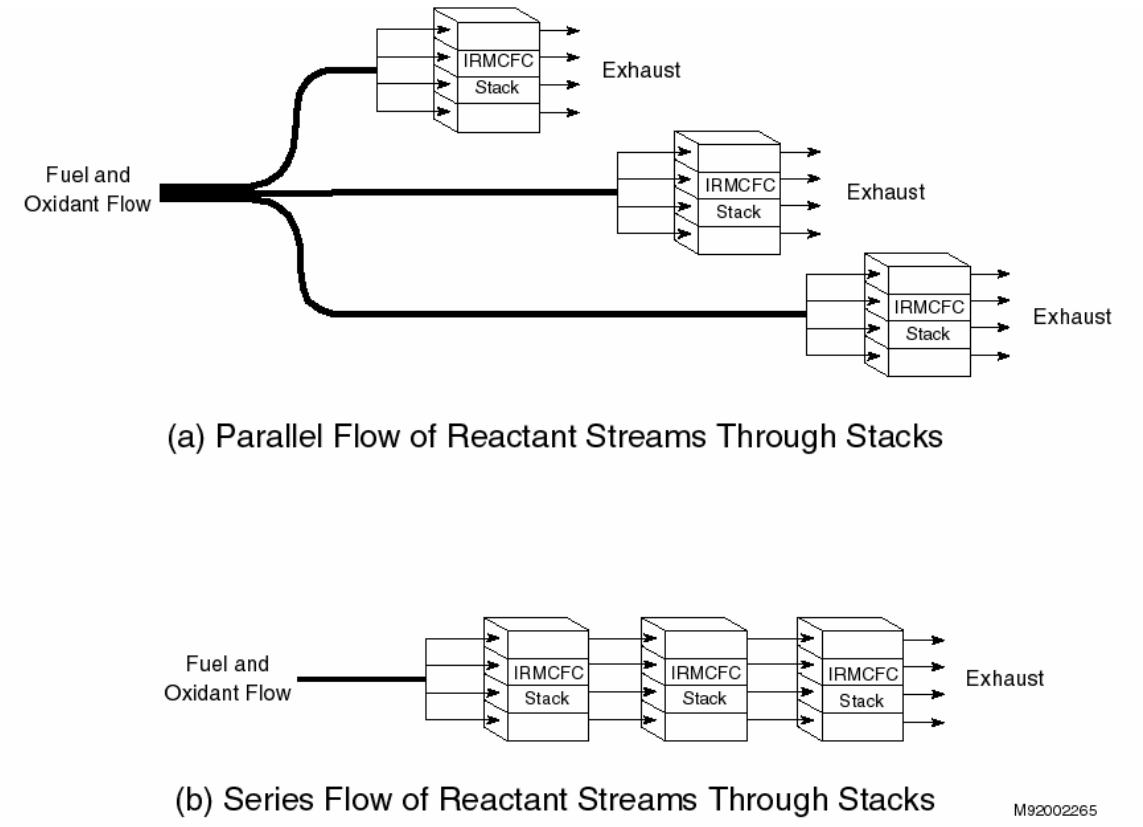

Figure 8-38 MCFC System Designs

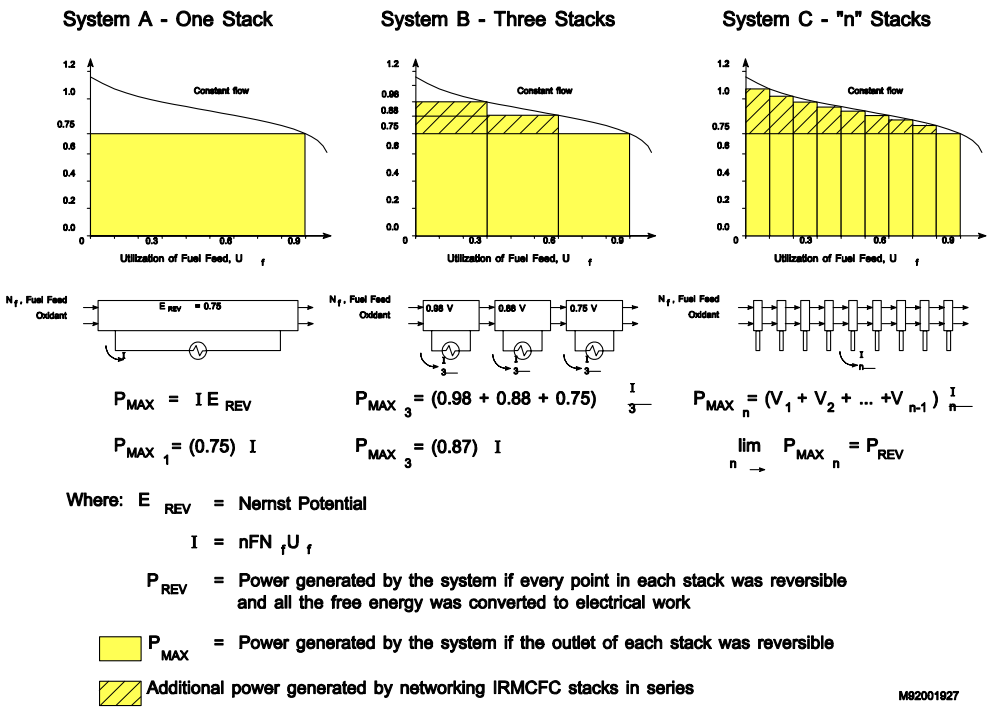

Figure 8-39 Stacks in Series Approach Reversibility

A graph of Nernst potential versus fuel utilization for the given feed stream compositions (60) was duplicated three times in Figure 8-39. The Nernst potential is the voltage which drives reversible electrode reactions. This reversible voltage, generated by the overall cell reaction, is a function of the local temperature, pressure, and reactant concentrations. As reactants are utilized, their concentrations change. Since Nernst potential is dependent upon the concentrations of reactants, it varies with the degree of utilization.

Fuel utilization is directly proportional to the charge transferred across the electrolyte. Therefore, the shaded areas of the graphs represent power -- the product of voltage and current. If reversibility is assumed at the outlet of each stack, no voltage losses are deducted from the Nernst potential. Therefore, each shaded area represents the maximum power, which each cell could generate.

System A in Figure 8-39 is composed of a single stack. Three stacks are arranged in series in system B. System C features many, or "n," stacks configured in series. In all three systems, the voltage of each stack corresponds to reactant concentrations at its outlet.

For comparison, each system is assumed to have the same total stack membrane area. That is, the area of each stack in system B is one third the area of the stack in system A. Similarly, the

area of each stack in system C is one "nth" the area of the single stack in system A. For simplicity, each stack is considered to contain only one cell.

Since each system achieves the same total fuel utilization (90 percent) across the same total area, each stack has the same average current density. Irreversible voltage loss is mainly a function of current density and stack temperature. Since these parameters are equivalent in each stack, it is assumed that the Nernst potential of each stack would be reduced by the same amount.

In system A, 90 percent of the fuel is utilized in a single stack, and all the current is generated at a single voltage. The power that this system can achieve is represented by the graph's shaded region.

In system B, three stacks in series each utilize 30 percent of the fuel. The current generated by each stack in system B is one third of the current generated in system A. Each stack in system B produces a different voltage. At the exit of the first stack, a high Nernst potential is generated because 70 percent of the fuel is still unburned. Likewise, at the exit of the second stack, 40 percent of the fuel remains unburned, generating another improved Nernst potential. Only ten percent of the fuel remains at the exit of the third stack, yielding the same Nernst potential that the single stack in system A produced. The three stack network can produce more power because two-thirds of the total charge is transferred at increased voltages. Comparing the shaded areas of the graphs illustrates the additional power that can be produced by arranging stacks in series.

In system C, many stacks are connected in series. Very small currents are generated at still higher voltages. As the number of stacks in series is increased, the maximum achievable power quickly approaches the power which a reversible system would generate, i.e. complete conversion of the available free energy. (A reversible system is reversible at every point in each stack, not just at the stack outlets.) The shaded area in the graph nearly fills the entire area under the curve - the reversible power.

Each system in Figure 8-38 converts an equivalent amount of free energy (90 percent fuel utilization) into heat and electrical work. The key difference, however, is that the systems with MCFC stacks networked in series transfer charge at higher voltages, thus converting more of the free energy directly into electrical work, and less into heat. As the number of stacks in series is increased, a reversible process is approached which would convert all the free energy into work and none into heat. Although heat that is produced from free energy can be reconverted into electrical work (e.g. via a steam turbine), an MCFC stack's direct conversion of free energy is intrinsically more efficient. Therefore, networking MCFC stacks in series results in more efficient power production even when waste heat is recovered.

Although each stack added to a series network would improve the system's efficiency, the incremental benefit obtained with each additional stack diminishes. A finite number of stacks could adequately, but not exactly, approach a reversible process. In a practical network, the number of stacks would be limited by economic, space, and design constraints.

In a similar study, Liebhafsky and Cairns (26) compared two arrangements of tubular, calcia-stabilized solid oxide fuel cells. In one arrangement, hydrogen and air were supplied to a single, 30-cm cell. In the other arrangement, the same cell was segmented into three, 10-cm cells which were ducted such that the same reactant streams flowed through them in series. Each arrangement had a total fuel utilization of 90 percent and each cell had the same average current density. Each cell in the series arrangement accomplished one-third of the total fuel utilization. Calculations showed that the series arrangement produced 5 percent more power than the single cell, and that further sectioning would produce greater improvements. It was concluded that the increase in irreversibility associated with changes in gas composition has nothing to do with electrode kinetics, but is rooted in the Nernst equation.

8.5.2 MCFC Network

When designing an MCFC power system, several requirements must be met. An MCFC system must properly condition both the fuel and oxidant gas streams. Methane must be reformed into the more reactive hydrogen and carbon monoxide. Carbon deposition, which can plug gas passages in the anode gas chamber, must be prevented. To supply the flow of carbonate ions, the air oxidant must be enriched with carbon dioxide. Both oxidant and fuel feed streams must be heated to their proper inlet temperatures. Each MCFC stack must be operated within an acceptable temperature range. Excess heat generated by the MCFC stacks must be recovered and efficiently utilized.

Figure 8-40 shows an MCFC network. The arrangement of stacks in series, as well as a unique recycle scheme, allows an MCFC network to meet all the requirements of an MCFC power system, while achieving high efficiency.

8.5.3 Recycle Scheme

In the network's recycle scheme, a portion of the spent fuel (Stream 5) and oxidant (Stream 4) is mixed and burned. The products of combustion (Stream 3) are then recycled through the cathode in order to provide the necessary carbon dioxide to the stacks. This eliminates the need for an external source of pure carbon dioxide. The cathode-cathode recycle (Stream 4) is large enough to cool the stacks, transferring excess energy to the heat recovery boilers. During the transfer of heat, enough energy is left in the oxidant recycle to heat the fresh air feed to the designated cathode inlet temperature. A second portion of the spent fuel (Stream 1) is recycled through the anode to provide enough steam to prevent carbon deposition and internally reform methane. This eliminates the need for steam to be supplied from another source. The anode-anode recycle also heats the fresh fuel feed to the designated anode inlet temperature.

8.5.4 Reactant Conditioning Between Stacks in Series

When MCFC stacks are networked in series, reactant streams can be conditioned between the stacks -- at different stages of utilization. The composition of reactant streams can be optimized between stacks by injecting a reactant stream (see Figure 8-40) or by mixing the existing reactant streams.

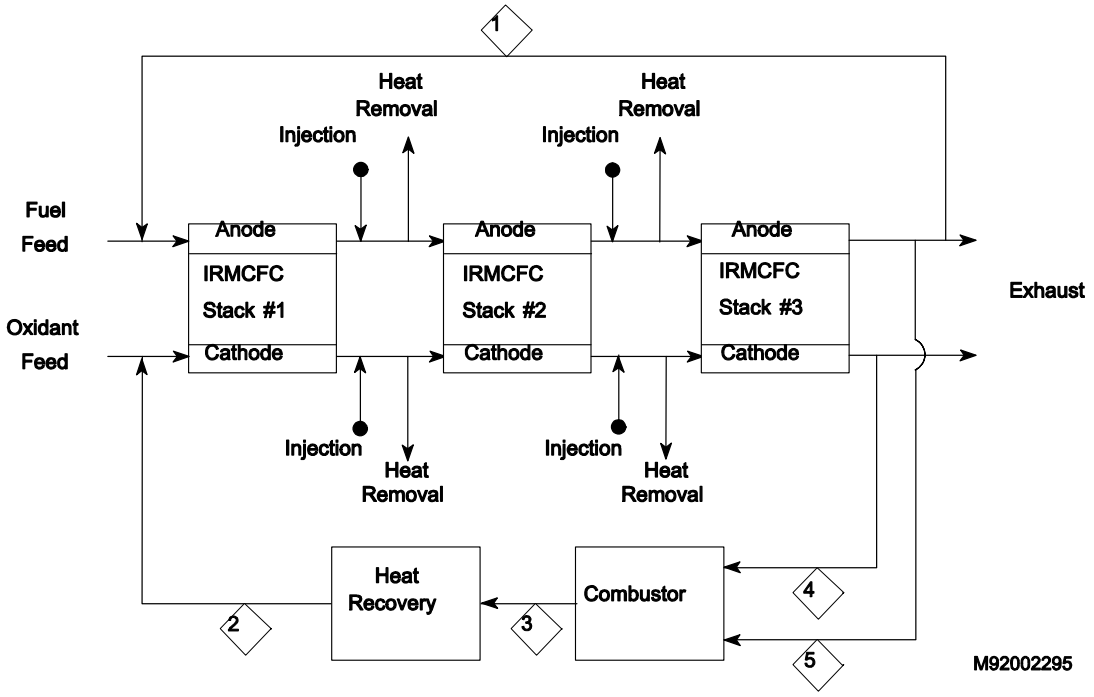

Figure 8-40 MCFC Network

Between stacks networked in series, heat can be removed from the reactant streams to assist in controlling stack temperatures. The heat in a network reactant stream can be transferred to a cooler process stream in a heat exchanger or hot and cold reactant streams can be mixed directly. The recovered heat may be utilized in a combined cycle or for cogeneration.

Methane can be injected into fuel streams between stacks networked in series. Since the reforming of methane into hydrogen is endothermic, its careful distribution among stacks in series is expected to improve the thermal balance of the system by allowing waste heat to be more evenly consumed throughout the total utilization of reactants. Improved thermal balance should allow stacks to be operated nearer their maximum temperature, reducing ohmic voltage losses. However, injecting portions of the fuel feed between stacks in series decreases the Nernst potential of every stack except the last one, since less fuel passes through each stack. (The amount of fuel which passes through the last stack does not change.) Optimizing the system requires an evaluation of the point at which the benefits of improved thermal balance outweigh the reduction in Nernst potential associated with such fuel redistribution.

8.5.5 Higher Total Reactant Utilization

The optimum total reactant utilization of stacks networked in series is higher than that of conventional, parallel stacks. Conventional designs avoid high utilization, because that would result in low voltages. In conventional configurations, the total utilization of reactants is accomplished in one stack. Therefore, when high utilizations are attempted, the low voltage which is generated adversely affects the total power production. In networks, however, the

utilization of reactants is accomplished incrementally, and the low voltage associated with high utilization is restricted to stacks which produce only a portion of the total power.

Manifolding problems can further limit the practical reactant utilization of conventional MCFC systems. Ideally, fuel and oxidant streams are distributed equally among individual cells in a stack. Today's manifolds, however, have not been able to achieve this, and cells are typically supplied with unequal reactant flows. This causes the composition of outlet reactant streams to be variable among the cells. At high utilizations, this variability leads to a significant reduction in stack voltage. Therefore, conventional systems avoid such high utilizations. However, when stacks are networked in series, reactant streams can be thoroughly mixed between cells. This reduces the variability in reactant composition and helps to minimize the stack voltage loss.

Another study (7) maximized the efficiency of conventional and series-connected fuel cell systems by optimizing cell voltage and current density. The study found that the optimum fuel utilization in the series-connected system was higher than that in the conventional system. Most importantly, the higher fuel utilization and lower current density of the series-connected system combined to give more efficient performance than the conventional system.

8.5.6 Disadvantages of MCFC Networks

For recycling to improve the performance of an MCFC network, it must provide benefits that outweigh its inherent disadvantages. If carbon dioxide is not separated from the anode-anode recycle, the concentration of carbon dioxide in the anode is increased. This reduces the Nernst potential. The Nernst potential is similarly reduced by the anode-cathode recycle if steam is not condensed out, since recycled steam dilutes reactant concentrations in the oxidant. In addition, part of the power generated by the network is consumed by the equipment necessary to circulate the recycle streams. Such circulation equipment, along with the additional ducting required by recycling, also increases the capital cost of the MCFC network.

Given the same initial feed streams, the flowrate of reactants through stacks networked in series is much larger than the flowrate of reactants through stacks in a conventional system. Conventional fuel cell systems divide the initial feed streams among many stacks arranged in parallel. However, the initial feed streams in an MCFC network are not divided, but fed directly into the first of a series of many stacks. Perhaps the greatest disadvantage of MCFC networks is that this increased flowrate creates larger pressure drops.

Another potential disadvantage of an MCFC network is the interdependence of the stacks in series. A problem with one stack could alter the performance of succeeding stacks. Furthermore, bypassing or isolating a problematic stack in a network could be a difficult control process. In the conventional parallel configuration, stack performance is not so interrelated.

8.5.7 Comparison of Performance

Two ASPEN (Advanced System for Process Engineering, public version) simulations compare the performance of conventional and networked fuel cell systems having identical recycle schemes and steam bottoming cycles. Each simulated system was composed of three MCFC stacks operating at the same temperature and pressure. The Nernst potential of each MCFC in both systems was reduced by 0.3 volts due to activation, concentration and ohmic voltage

polarizations. (This is a conservative estimate, representing a much higher outlet voltage polarization than would be expected.) Simple, single-pressure steam cycles produce secondary power.

When the total fuel utilization of each system was optimized for maximum efficiency, the efficiency of the fuel cell stacks networked in series was nearly 10 percent greater than that of the stacks arranged in parallel (44.9 percent vs. 35.4 percent, LHV). When the power generated by each system's steam bottoming cycle was considered in addition to its fuel cell power, the gap in efficiency narrowed to 5.5 percent. The efficiency of the total networked system is 56.8 percent, while that of the total conventional system was 51.3 percent.

The fuel cell network which was simulated was not fully optimized. Optimization of flow geometry, operating pressure, stack fuel utilization and current, reactant conditioning, and other parameters would be expected to yield further significant increases in total system efficiency.

8.5.8 Conclusions

Key to the concept of networking is the arrangement of multiple fuel cell stacks relative to the flow of reactant streams. Conventional fuel cells systems have been designed such that reactant streams flow in parallel through fuel cell stacks. In a fuel cell network, however, reactant streams are ducted such that they are fed and recycled through stacks in series.

Arranging fuel cell stacks in series offers several advantages over conventional fuel cell systems. Stacks networked in series more closely approach a reversible process, which increases the system efficiency. Higher total reactant utilizations can be achieved by stacks networked in series. Placing stacks in series also allows reactant streams to be conditioned at different stages of utilization. Between stacks, heat can be consumed or removed, (methane injection, heat exchange) which improves the thermal balance of the system. The composition of streams can be adjusted between stacks by mixing exhaust streams or by injecting reactant streams.

Computer simulations have demonstrated that a combined cycle system with MCFC stacks networked in series is significantly more efficient than an identical system with MCFC stacks configured in parallel.

8.6 Hybrids

This section presents hybrids for generating electricity or for providing power in automotive vehicles. Hybrid systems that incorporate gas turbines build upon the outstanding performance of the fuel cell by utilizing the exhausted fuel cell heat. Hybrid electric vehicles utilize fuel cells to provide electric power to augment or replace exiting power sources. These systems are highly efficient and deliver superior environmental performance. Presented below is a general discussion of hybrid technology as well as specific initiatives in the gas turbine/fuel cell and electric power hybrid vehicle areas.

8.6.1 Technology

Advanced power generation cycles that combine high-temperature fuel cells and gas turbines, reciprocating engines, or another fuel cell are the hybrid power plants of the future. These conceptual systems have the potential to achieve efficiencies greater than 70 percent and be

commercially ready by the year 2010 or sooner. The hybrid fuel cell/turbine (FC/T) power plant will combine a high-temperature, conventional molten carbonate fuel cell (MCFC) or a solid oxide fuel cell (SOFC) with a low-pressure-ratio gas turbine, air compressor, combustor, and in some cases, a metallic heat exchanger (27). The synergistic effects of the hybrid fuel cell/turbine technology will also provide the benefits of reduced greenhouse gas emissions. Nitrous (NO_X) emissions will be an order of magnitude below those of non-fuel cell power plants and carbon monoxide emissions will be less than 2 parts per million (ppm) (28). There will also be a substantial reduction in the amount of carbon dioxide produced compared to conventional power plants.

The hybrid system is key to the Department of Energy's program of achieving efficiencies greater than 75 percent (LHV) for natural gas. The higher efficiencies play a key role in reducing emissions. As a comparison, conventional coal-burning power plants are typically 35 percent efficient and natural gas fired plants are now 40 to 50 percent efficient. Figure 8-41 shows the estimated efficiency ranges of current and future power generation systems.

The combination of the fuel cell and turbine operates by using the rejected thermal energy and residual fuel from a fuel cell to drive the gas turbine. The fuel cell exhaust gases are mixed and burned, raising the turbine inlet temperature while replacing the conventional combustor of the gas turbine. Use of a recuperator, a metallic gas-to-gas heat exchanger, transfers heat from the gas turbine exhaust to the fuel and air used in the fuel cell. Figure 8-42 illustrates an example of a proposed fuel cell/turbine system.

There can be many different cycle configurations for the hybrid fuel cell/turbine plant. In the topping mode described above, the fuel cell serves as the combustor for the gas turbine while the gas turbine is the balance-of-plant for the fuel cell, with some generation. In the bottoming mode, the fuel cell uses the gas turbine exhaust as air supply while the gas turbine is the balance of plant. In indirect systems, high temperature heat exchangers are used (29).

The hybrid plants are projected to cost 25 percent below comparably sized fuel cells, (30) and be capable of producing electricity at costs of 10 to 20 percent below today's conventional plants (27). Operation of the plant is almost totally automatic. Therefore, it can be monitored and managed remotely with the possibility of controlling hundreds of the power plants from a single location (28).

Initial systems will be less than 20 MW, with typical system sizes of 1 to 10 MW. Future systems, in the megawatt class size, will boost efficiency even further by combining two solid oxide fuel cell modules with more advanced gas turbines and introducing sophisticated cooling and heating procedures. Another possibility of a hybrid power plant is to combine a solid oxide fuel cell with a polymer electrolyte (PEFC) fuel cell. The SOFC would produce both electric power and hydrogen. This hydrogen would then be utilized by the PEFC to generate more electric power (28).

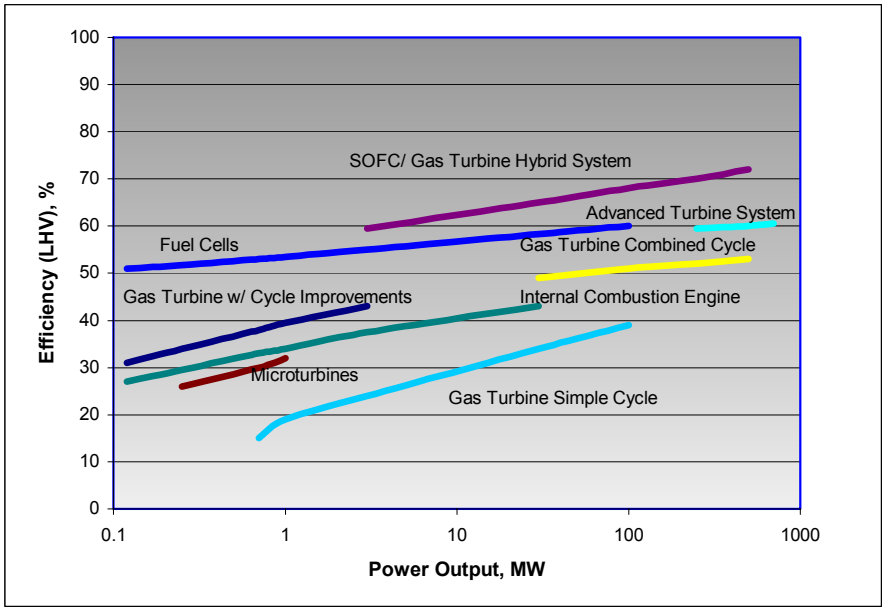

Figure 8-41 Estimated performance of Power Generation Systems

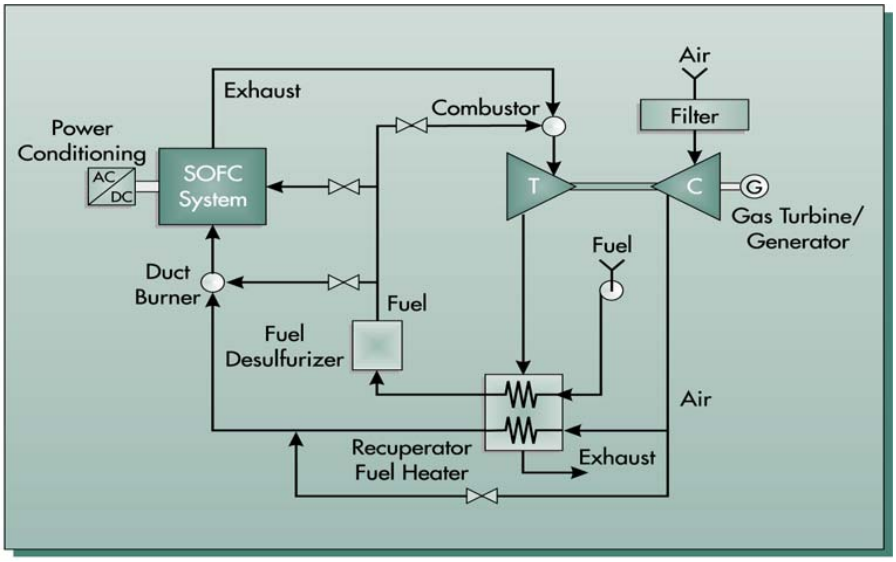

Figure 8-42 Diagram of a Proposed Siemens-Westinghouse Hybrid System
(Taken from DOE Project Fact Sheet – Fuel Cell/ ATS Hybrid Systems)

8.6.2 Projects

In 1997, a Program Research and Development Announcement (PRDA) was issued by the Department of Energy for conceptual feasibility studies of high-efficiency fossil power plants (HEFPPs). The terms of the conceptual power plant must be less than 20 MW in size, operate on natural gas and contain a high-temperature fuel cell. By late 1998, DOE awarded contracts to determine the feasibility of the highly efficient hybrid power plants.

FCE, of Danbury, CT, teamed with Allison Engine Company to evaluate a carbonate fuel cell combined with a gas turbine and a steam turbine generator. The system was operated at ambient pressure. The net power of the hybrid system was 20.6 MW and the NO_X levels were less than 1 ppm. The process showed a 65 percent efficiency with off-the-shelf turbomachinery and 72 percent efficiency with cycle specific machinery. The COE is predicted to be comparable to present day alternatives.

Siemens-Westinghouse Power Corporation, of Pittsburgh, PA, with a subcontract to Allison Engine Company, evaluated a pressurized solid oxide fuel cell coupled with conventional gas turbine technology without a steam plant. The system was operated at a pressure of 7 atm. The fuel cell generated 16 MW of power and the gas turbine generated 4 MW of power. The process showed 67 percent efficiency as developed. An efficiency of 70 percent is deemed achievable with improvement in component design. The COE is predicted to be comparable to present day alternatives. NO_X levels were less than 1 ppm.

McDermott Technology, Inc., of Alliance, OH, developed a conceptual design of a high efficiency power plant system that joins planar solid oxide fuel cell technology with micro-turbine technology in a combined cycle. The system was operated at atmospheric conditions. The power plant had a combined cycle output of 700 kW with the turbine supplying 70 kW. The results indicate 70 percent efficiency is possible and the COE is comparable to present day alternatives.

Siemens-Westinghouse Power Corporation, Pittsburgh, PA, and Solar Turbines developed a conceptual design of an economically and technically feasible 20-MW, 70- percent efficient natural gas-fueled power system that employs solid oxide fuel cells operating at elevated pressure in conjunction with an Advanced Turbine System gas turbine. The fuel cell, operated at 9 atm pressure, generated 11 MW of power. Two Solar Mercury 50 gas turbines were used to generate 9 MW of power. The results of the study indicated system efficiency near 60 percent. A low COE relative to conventional power generation is predicted.

In March of 1999, FCE, of Danbury, CT, with Allison Engine Company, Indianapolis, IN, and Capstone Turbine Corp., Woodland Hills, CA. was awarded a project to create a fuel cell/turbine system that meet or exceed DOE's efficiencies and emissions goals. The 3-year program will include four steps:

- Development of a high-utilization fuel cell,
- Development of key system components,
- Tests of the fuel cell/hybrid system to assess integration and system operation of an existing 250-kilowatt fuel cell stack with a commercially available micro-turbine, and
- Preparation of a conceptual design of a 40 MW ultra-high efficiency power plant.

A unique feature of the proposed system will allow the fuel cell and turbine modules to operate at independent pressures. The fuel cell will be operated at ambient pressure. This can increase the fuel cell stack life and save on piping and vessel costs. The turbine can then operate at its optimum pressure ratio.

Countries around the world are developing interest in the high-efficiency hybrid cycles. A 320 kW hybrid (SOFC and gas turbine) plant will enter service in Germany, operated by a consortium under the leadership of RWE Energie AG. This will be followed by the first 1 MW plant, which will be operated by Energie Baden-Wurttemberg AG (EnBW), Electricite de France (EDF), Gaz de France, and Austria's TIWAG (29).

Another project under development at the NETL is an advanced power plant system that combines a multistaged fuel cell with an extremely efficient turbine. Preliminary estimates show efficiencies greater than 80 percent (LHV). Studies showed that natural gas to electricity LHV efficiencies could break through an 80 percent barrier, while remaining cost competitive for a 4-MW solid oxide plant (tubular or planar). The Advanced Fuel Cell concept directly coincides with the long-term goals of the Fuel Cell Program. These include system costs of $400/kW and efficiencies of 70 to 80 percent or more (LHV to AC electricity), with fuel flexibility and a stack-life of 40,000 hours. They are intended for commercial application in 2015, maintaining ultra-low emissions.

8.6.3 World's First Hybrid Project

Siemens-Westinghouse Power Corporation of Pittsburgh, PA developed and fabricated the first advanced power plant to combine a solid oxide fuel cell and a gas turbine. The microturbine generator was manufactured by Northern Research and Engineering Corporation of Woburn, Mass. The factory acceptance test was completed in April 2000. Southern California Edison is operating the new hybrid plant at The National Fuel Cell Research Center at the University of California-Irvine. A year of testing in a commercial setting will be performed at this site. The system cycle is expected to generate electric power at 55 percent efficiency.

The pressurized system will generate 220 kilowatts of power and be operated at 3 atm of pressure. The fuel cell is made up of 1152 individual tubular ceramic cells and generates about 200 kilowatts of electricity. The microturbine generator will produce an additional 20 kilowatts of electricity at full power. No sulfur dioxide pollutants will be released into the air. Nitrogen oxide emissions are likely to be less than 1 ppm.

A 320-kilowatt hybrid system is also in the planning stages. An initial commercial offering of a one MW fuel cell-microturbine power plant in late 2002 will be the end results of this Department of Energy/Siemens Westinghouse partnership program (31).

8.6.4 Hybrid Electric Vehicles (HEV)

Hybrid Electric Vehicles (HEVs) typically combine the conventional internal combustion engine of the automobile with an energy storage device, such as a battery. However, there are many different arrangements for the HEV. The key components to an HEV are the energy storage system (batteries, ultracapacitors, and flywheels), the power unit (spark ignition engines,

compression ignition direct injection engines, gas turbines and fuel cells) and the vehicle propulsion system (electric motor). The benefits of HEVs, much like the hybrid power plants, are increased efficiency and lower emissions.

As of July 2004, DOE has completed 1 million miles of hybrid electric vehicle testing. The number of each type of hybrid electric vehicle tested, the total miles accumulated, and average fuel economy to date include:

- 4 Honda Civics, 284,000 miles and 38.0 mpg
- 6 Honda Insights, 347,000 miles and 46.0 mpg
- 6 Toyota Prius (model years 2002 and 2003) 380,000 miles and 41.1 mpg
- 2 Toyota Prius (model years 2004) 16,000 miles and 44.6 mpg

Fuel cell hybrid cars are not a new concept. In the early 1970s, K. Kordesch modified a 1961 Austin A-40 two-door, four-passenger sedan to an air-hydrogen fuel cell/battery hybrid car (32). This vehicle used a 6-kW alkaline fuel cell in conjunction with lead acid batteries, and operated on hydrogen carried in compressed gas cylinders mounted on the roof. The car operated on public roads for three years and about 21,000 km.

In 1994 and 1995, H-Power (Belleville, New Jersey) headed a team that built three PAFC/battery hybrid transit buses (33, 34). These 9 meter (30 foot), 25 seat (with space for two wheel chairs) buses used a 50 kW fuel cell and a 100 kW, 180 amp-hour nickel cadmium battery.

The major activity in transportation fuel cell development has focused on the PEFC. In 1993, Ballard Power Systems (Burnaby, British Columbia, Canada) demonstrated a 10 m (32 foot) light-duty transit bus with a 120 kW fuel cell system, followed by a 200 kW, 12 meter (40 foot) heavy-duty transit bus in 1995 (35). These buses use no traction batteries. They operate on compressed hydrogen as the on-board fuel. In 1997, Ballard provided 205 kW (275 HP) PEFC units for a small fleet of hydrogen-fueled, full-size transit buses for demonstrations in Chicago, Illinois, and Vancouver, British Columbia. Working in collaboration with Ballard, Daimler-Benz built a series of PEFC-powered vehicles, ranging from passenger cars to buses (36). The first such vehicles were hydrogen-fueled. A methanol-fueled PEFC A-class car unveiled by Daimler-Benz in 1997 has a 640 km (400 mile) range. A hydrogen-fueled (metal hydride for hydrogen storage), fuel cell/battery hybrid passenger car was built by Toyota in 1996, followed in 1997 by a methanol-fueled car built on the same RAV4 platform (37).

Ballard brought fuel cell technology into the public awareness a decade ago. Today, there are 50 companies in North America, Europe, and Japan developing fuel cells and related systems and components for cars, buses, and specialty vehicles, like golf carts and fork lifts. The Breakthrough Technologies Institute, Inc. entered a cooperative agreement with the U.S. Department of Energy to survey fuel cell vehicle developers, selected energy and component suppliers, and interested government agencies. This survey identified nearly 20 companies developing light-duty fuel cell vehicles and components. The survey also identified at least 12 companies or partnerships developing or demonstrating fuel cell buses. The results of the survey were published in February 2004 and the report can be viewed at http://www.fuelcells.org/info/charts/vehiclestudy.pdf.

Other major automobile manufacturers, including General Motors, Volkswagen, Volvo, Honda, DaimlerChrysler, Nissan, and Ford, also have announced plans to build prototype polymer electrolyte fuel cell vehicles operating on hydrogen, methanol, or gasoline (38). Honda's FCX, a fuel cell prototype sedan, includes both hydrogen- and methanol-based systems. The GM Precept will use a hydrogen hydride storage system to help it to attain a 108 miles per gallon gasoline equivalent (39). A list of auto manufactures with information on their prototype can be found at http://www.fuelcells.org/info/charts/carchart.pdf.

The Department of Energy's Transportation Fuel Cell program is a collaboration between government and industry that supports the Partnership for a New Generation of Vehicles. Domestic automakers, fuel cell developers, national labs, universities, component suppliers and the fuel industry have created a Fuel Cell Alliance. This alliance helps in collaborating government sponsored research and development within the auto industry. Some of the goals of the program include developing fuel cell stack systems that are greater than 57 percent efficient at 25 percent peak power, more than 100 times cleaner than EPA Tier 2 emissions, and capable of operating on hydrogen or hydrogen-rich fuel from gasoline, methanol, ethanol and natural gas. By 2004, the program hopes to have fuel cell power systems that are reliable, safe and cost competitive with internal combustion engines (40).

California has started a Fuel Cell Partnership with oil companies, automakers and fuel cell companies. They hope to have 50 fuel cell vehicles, both passenger cars and transit buses, on the road by 2003. The goals of the program include demonstrating vehicle performance, identifying fuel infrastructure issues and addressing commercialization challenges (41).

DOD is interested in new or novel advanced power and propulsion systems that will reduce fuel consumption, improve performance, extend vehicle range, reduce emissions, and reduce support costs. The Navy and Army are considering hybrids for ships, land vehicles, helicopters, and battlefield power requirements.

In 1997, the Office of Naval Research (ONR) initiated an advanced development program to demonstrate a ship service fuel cell (SSFC) power generation module. During Phase 1, competitive conceptual designs of 2.5 MW SSFC were prepared, along with critical component demonstrations. Phase 2 of the development program, scheduled for completion in 2002, will result in a nominal 500 kW fuel cell ship service generator demonstration module to be constructed and tested in a laboratory setting. The baseline concept is fueled by logistic fuel which is reformed in an adiabatic reformer designed and built by International Fuel Cells. Downstream of the reformer is a series of components that remove CO and H_2S before the gas is sent to the fuel cell. The spent fuel and air are mixed and burned to drive a turbocompressor and recover compression work.[54]

The Army has two programs that are looking at hybrids using fuel cells. In 1999, the Land Warrior Operational Combat System was approved. The goal is to develop a portable hybrid fuel cell system that weighs less than one kilogram and meets the power demand of the Land Warrior Power requirements. The second program is the Future Combat System. This program

[54] R.M. Privette, et al., "2.5 MW PEFC System for Navy Ship Service Power," paper presented at the 1999 Review Conference on Fuel Cell Technology, Chicago, Illinois, August 3-5, 1999.

plans to develop technologies and systems for a lightweight, overwhelming lethal, strategically deployable, self-sustaining combat systems.[55]

8.7 Fuel Cell Auxiliary Power Systems

In addition to high-profile fuel cell applications such as automotive propulsion and distributed power generation, the use of fuel cells as auxiliary power units (APUs) for vehicles has received considerable attention (see Figure 8-43). APU applications may be an attractive market because it offers a true mass-market opportunity that does not require the challenging performance and low cost required for propulsion systems for vehicles. In this section, a discussion of the technical performance requirements for such fuel cell APUs, as well as the current status of the technology and the implications for fuel cell system configuration and cost is given.

Participants	Application	Size range	Fuel /Fuel Cell type	Nature of Activity
BMW, International Fuel Cells1	passenger car, BMW 7-series	5kW net	Hydrogen, Atmospheric PEM	Demonstration
Ballard, Daimler-Chrysler2	Class 8 Freightliner heavy-duty Century Class S/T truck cab	1.4 kW net for 8000 BTU/h A/C unit	Hydrogen, PEM	Demonstration
BMW, Delphi, Global Thermoelectric3	passenger car	1 to 5kW net	Gasoline, SOFC	Technology development program

Figure 8-43 Overview of Fuel Cell Activities Aimed at APU Applications

Auxiliary power units are devices that can provide all or part of the non-propulsion power for vehicles. Such units are already in widespread use in a range of vehicle types and for a variety of applications, in which they provide a number of potential benefits (see Figure 8-44). Although each of these applications could provide attractive future markets for fuel cells, this section will focus on application to on-road vehicles (specifically trucks).

Vehicles Types	Loads Serviced	Potential Benefits
• Heavy-duty & utility trucks • Airplanes • Trains • Yachts & Ships • Recreational vehicles • Automobiles & light trucks (not commercial yet)	• Space conditioning • Refrigeration • Lighting and other cabin amenities • Communication and information equipment • Entertainment (TV, radio)	• Can operate when main engine unavailable • Reduce emissions and noise while parked • Extend life of main engine • Improve power generation efficiency when parked

Figure 8-44 Overview of APU Applications

[55] J.C. Stephens, K. Gardner, and R. Jacobs, "US Army CECOM Fuel Cell Program," presented at the World Association for Case Method Research and Application, Lucerne, Switzerland, January 5-7, 2000.

In 1997, the Office of Naval Research initiated an advanced development program to demonstrate a ship service fuel cell power generation module. The ship service generator supplies the electrical power requirements of the ship. This program will provide the basis for a new fuel cell-based design that will be an attractive option for the future Navy surface ships. This program will provide the Navy with a ship service that is more efficient and incorporates a distributive power system that will remain operating even if the engine is destroyed.

Fuel cells can serve as a generator, battery charger, battery replacements and heat supply. They can adapt to most environments, even locations in Arctic and Antarctic regions. One effort, being run in collaboration with the Army Research Office, has demonstrated a prototype fuel cell designed to replace in many applications a popular military standard battery. The target application is the Army's BA-5590 primary (i.e., use-once-and-dispose) lithium battery. The Army purchases approximately 350,000 of these batteries every year at a cost of approximately $100 per battery, including almost $30 per battery for disposal. Fuel cells, on the other hand, are not thrown away after each use but can be reused hundreds of times. Mission weight savings of factors of 10 or more are projected. The prototype fuel cell, which has the same size and delivers the same power as a battery, has been tested in all orientations and under simulated adverse weather conditions, and was enthusiastically received by Army senior management.

8.7.1 System Performance Requirements

A key reason for interest in fuel cell APU applications is that there may be a good fit between APU requirements and fuel cell system characteristics. Fuel cells could be efficient and quiet, and APUs do have the load following requirements and physical size and weight constraints associated with propulsion applications. However, in order to understand the system requirements for fuel cell APUs, it is critical to understand the required functionality (refer to Figure 8-44) as well as competing technologies. To provide the functionality of interest, and to be competitive with internal combustion engine (ICE) driven APUs, fuel cell APUs must meet various requirements; an overview is provided in Figure 8-45.

Key Parameter	*Typical Requirements*	*Expected fuel cell performance*
Power output	12 to 42 V DC is acceptable for most applications, 110 / 220 V AC may be desirable for powering power tools etc.	DC power output simplifies the power conditioning and control for fuel cells
System Capacity	1 to 5 kW for light duty vehicles and truck cabins up to 15 kW for truck refrigeration	Fits expected range for PEFCs and probably also advanced SOFCs
System Efficiency	More than 15 to 25 percent based on LHV	Efficiency target should be achievable, even in smallest capacity range
Operating life and reliability	Greater than about 5,000 hours stack life, with regular service intervals less than once every 1,000 hours	Insufficient data available to assess whether this is a challenge or not

Figure 8-45 Overview of typical system requirements

Fuel cell APUs will likely have to operate on gasoline, and for trucks preferably on diesel fuel, in order to match the infrastructure available, and preferably to be able to share on-board storage tanks with the main engine. The small amount of fuel involved in fueling APUs would likely not justify the establishment of a specialized infrastructure (e.g. a hydrogen infrastructure) for APUs alone. Similarly, fuel cell APUs should be water self-sufficient, as the need to carry water for the APU would be a major inconvenience to the operator, and would require additional space and associated equipment.

In addition to the requirement for stationary operation mentioned in Figure 8-45, fuel cell APUs must be able to provide power rapidly after start-up, and must be able to follow loads. While the use of batteries to accomplish this is almost a given, a system start-up time of about ten minutes or less will likely be required to arrive at a reasonable overall package.

Finally, fuel cell APUs are clean. These attributes may well be the key competitive advantage that fuel cell APUs have over conventional APUs, and hence their performance must more than match that of internal combustion engines APUs.

8.7.2 Technology Status

Active technology development efforts in both PEFC and planar SOFC technology, driven primarily by the interest in distributed generation and automotive propulsion markets, have achieved significant progress in the development of these technologies. For distributed power applications refined and even early commercial prototypes are being constructed. However, in the case of planar SOFC a distinction must be made between different types of SOFC technologies. Neither the tubular nor the electrolyte supported SOFC technology is suitable for APU applications due to their very high operating temperature, large size and weight. Only the electrode supported planar SOFC technology may be applicable to APU applications. Since it has only been developed over the past nine years, as opposed to several decades for PEFC and other SOFC technologies, it is not developed as far, although it appears to be catching up quickly (See Figure 8-46).

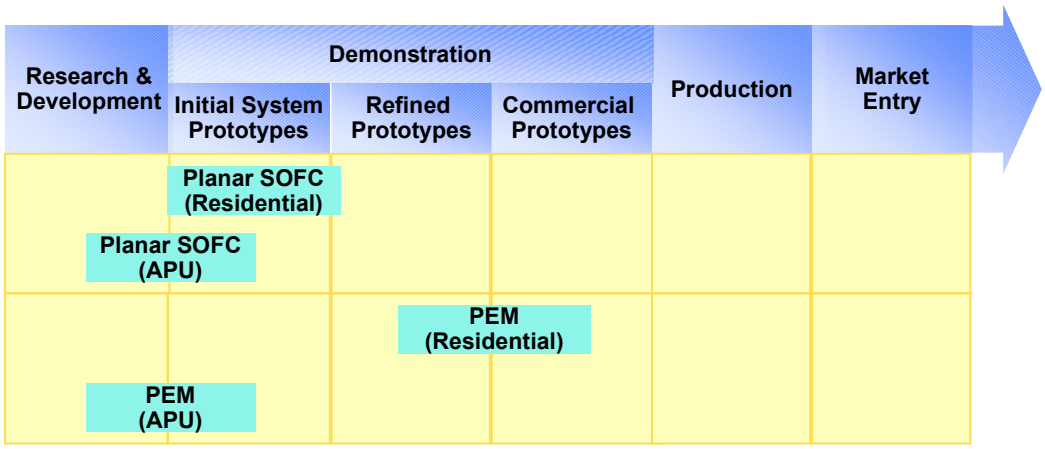

Figure 8-46 Stage of development for fuel cells for APU applications

Fuel cell APU applications could benefit significantly from the development of distributed generation systems, especially from residential scale systems, because of the similarity in scale and duty cycle. However, distributed generation systems are designed mostly for operation on natural gas, and do not face as stringent weight and volume requirements as APU applications. As a result, fuel cell APUs are in the early initial system prototype stage.

Several developers, including Nuvera, Honeywell, and Plug Power are active in the development for residential PEFC power systems. Most of the PEFC system technology can be adapted for APU application, except that a fuel processor capable of handling transportation fuels is required. However, most of the players in the residential PEFC field are also engaged in the development of PEFC systems for automotive propulsion applications, which are targeting the ability to utilize transportation fuels for PEFC systems.

Relatively few developers of SOFC technology have paid attention to non-stationary markets. All are focused on small to medium sized distributed generation and on-site generation markets. Only Global Thermoelectric (Calgary, Canada) has been active in the application of its technology to APUs. A recently conducted a detailed conceptual design and cost estimate of a 5-kWnet SOFC-based truck APU conclude that, provided continued improvement in several technology areas, planar SOFCs could ultimately become a realistic option for this mass-market application.

8.7.3 System Configuration and Technology Issues

Based on the system requirements discussed above, fuel cell APUs will consist of a fuel processor, a stack system and the balance of plant. Figure 8-47 lists the components required in SOFC and PEFC based systems. The components needed in a PEFC system for APU applications are similar to that needed in residential power. The main issue for components for PEM-based systems is the minimization or elimination of the use of external supplied water. For both PEFC and SOFC systems, start-up batteries (either existing or dedicated units) will be needed since external electric power is not available.

Detailed cost and design studies for both PEFC and SOFC systems at sizes ranging from 5kW to 1 MW were made that point to the fundamental differences between PEFC and SOFC technology that impact the system design and by implication the cost structure. These differences will be discussed in the following paragraphs.

The main components in a SOFC APU are the fuel cell stack, the fuel processor, and the thermal management system. In addition there are several balance of plant components, which are listed in Figure 8-47. The relatively simple reformer design is possible because the SOFC stack operates at high temperatures (around 800 °C) and is capable of utilizing both carbon monoxide and certain hydrocarbons as fuel. Since both the anode and cathode exhaust at temperatures of 600 to 850 °C, high temperature recuperators are required to maintain system efficiency. These recuperators are of expensive materials (high temperature reducing and oxidizing atmosphere), making it an expensive component in the system. However, if hydrocarbons are converted inside the stack, this leads to a less exothermic overall reaction so that the stack cooling requirements are reduced.

Further system simplification would occur if a sulfur-free fuel was used or if the fuel cell were sulfur tolerant, in that case, the fuel can be provided directly from the reformer to the fuel cell. In order to minimize system volume, (and minimize the associated system weight and start-up time) integration of the system components is a key design issue. By recycling the entire anode tailgas to provide steam, a water management system can be avoided, though a hot gas recirculation system is required.

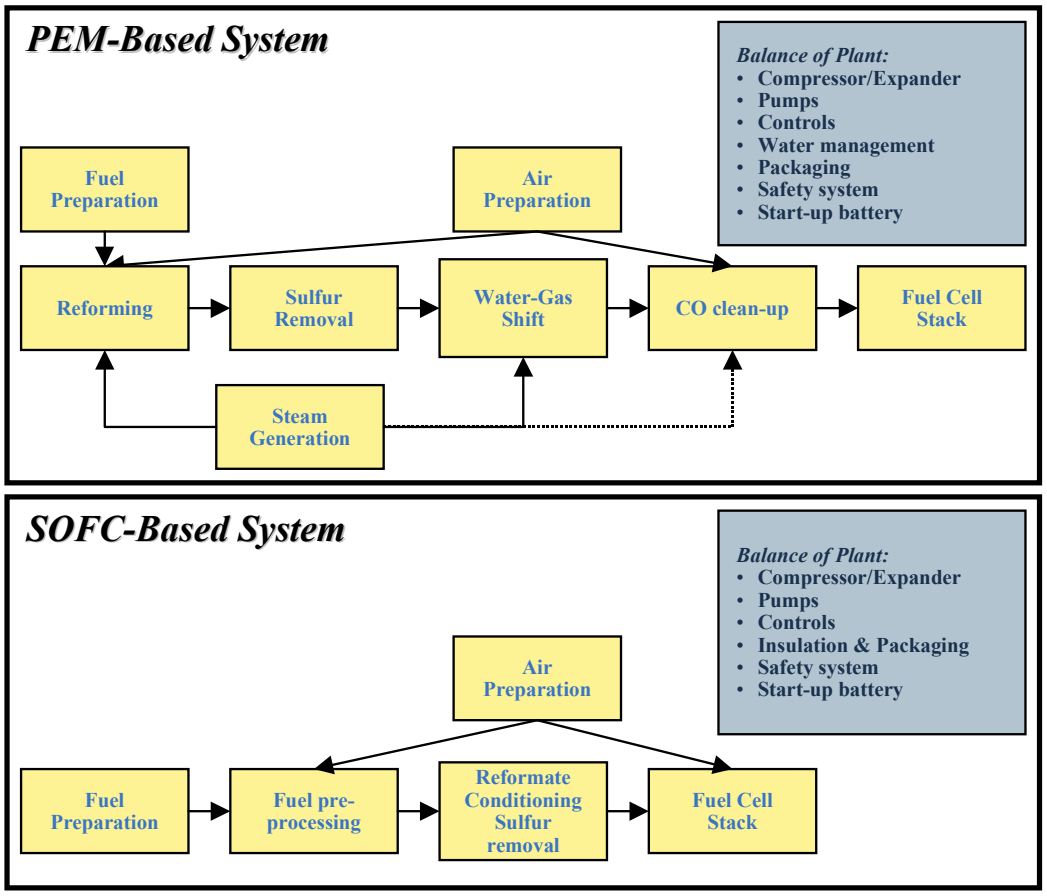

Figure 8-47 Overview of subsystems and components for SOFC and PEFC systems

Figure 8-48 shows a simplified layout for an SOFC-based APU. The air for reformer operation and cathode requirements is compressed in a single compressor and then split between the unit operations. The external water supply shown in Figure 8-48 will most likely not be needed; the anode recycle stream provides water. Unreacted anode tail gas is recuperated in a tail gas burner. Additional energy is available in a SOFC system from enthalpy recovery from tail gas effluent streams that are typically 400 to 600 °C. Current thinking is that reformers for transportation fuel based SOFC APUs will be of the exothermic type (i.e. partial oxidation or autothermal reforming), as no viable steam reformers are available for such fuels.

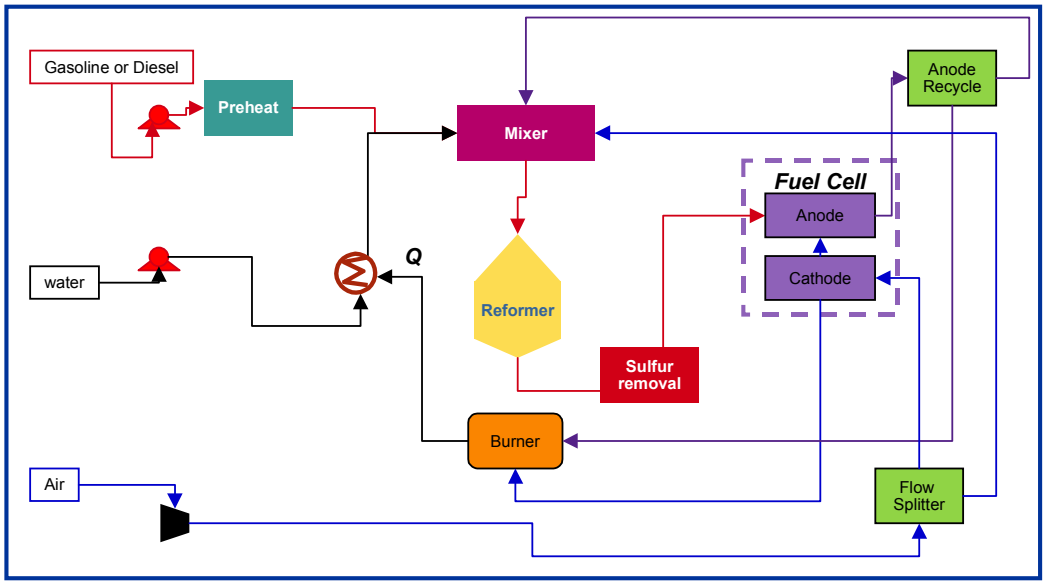

Figure 8-48 Simplified System process flow diagram of pre-reformer/SOFC system

Due to the operating requirements of PEFC stack technology, shift reactors and a carbon monoxide removal step are required to produce reformate of sufficient quality. Similarly, the stack operating temperature and its humidity requirements require a water management system as well as radiators for heat rejection. Some developers are developing pressurized systems to the benefit from higher reactant partial pressures on both anode and cathode. Fuel processing for PEFC APU systems is identical to that needed in residential power or propulsion applications. The additional issue for PEFC is the minimization of steam needed for the fuel processor system. Since an APU is a mobile and/or remote unit, the need for external sources of water should be minimized. The reformate stream is further diluted by additional steam, if that water is not removed prior to the fuel cell stack.

Another design integration issue in PEFC systems is water management for hydrating the electrolyte and providing the necessary steam for reforming and water-gas shift operations. Additional steam may be required for the CO clean-up device. Some reformate-based PEFC systems are run under pressure to increase the partial pressure of reactants for the PEFC anode and cathode, increasing efficiency. Pressure operation also aids in heat integration for the internal generation of steam at pressures greater than atmospheric (i.e. steam generated at temperatures greater than 100 °C). PEFC system integration involves the integration of a reformer (either exothermic or endothermic overall, ~850 to 1000 °C), shift reactors (exothermic, 150-500 °C), CO-cleanup (primarily exothermic, 50 to 200 °C), and the fuel cell stack (exothermic, 80 °C). Each reaction zone operates at a significantly different temperature thus providing a challenge for system integration and heat rejection. To alleviate some of these drawbacks, and further reduce the cost of the PEFC systems, developers are now investigating the possibility of using higher temperature membranes (e.g. operating slightly above 100 °C).

This would increase the carbon monoxide tolerance, potentially simplifying the fuel processor design, and simplify the heat rejection.

The power requirements for auxiliary power applications require smaller fuel cell stack duties. The heat losses for a SOFC stack operating at a smaller power duty are a larger proportion of the gross rating that in a stationary power application. Insulation required for specified system skin temperatures requirements could conceivably result in large proportion of the total system volume. Integration of the high temperature components is important in order to reduce the system volume and insulation requirements. SOFC APU systems will require inexpensive high performance insulation materials to decrease both system volume and cost.

8.7.4 System Cost Considerations

As for any new class of product, total cost of ownership and operation of fuel cells will be a critical factor in their commercialization, along with the offered functionality and performance. This total cost of ownership typically has several components for power systems such as fuel cells. These components include fuel cost, other operating costs such as maintenance cost, and the first cost of the equipment. This first cost has a significant impact on fuel cells' competitiveness.

The main component of a fuel cell's first cost is the manufacturing cost, which is strongly related to the physical configuration and embodiment of the system, as well as to the manufacturing methods used. System configuration and design in turn are directly related to the desired system functionality and performance, while the manufacturing methods used are strongly linked to the anticipated production volume.

Arthur D. Little has carried out cost structure studies for a variety of fuel cell technologies for a wide range of applications, including SOFC tubular, planar and PEFC technologies. Because phenomena at many levels of abstraction have a significant impact on performance and cost, they have developed a multi-level system performance and cost modeling approach (see Figure 8-49). At the most elementary level, it includes fundamental chemical reaction/reactor models for the fuel processor and fuel cell as one-dimensional systems.

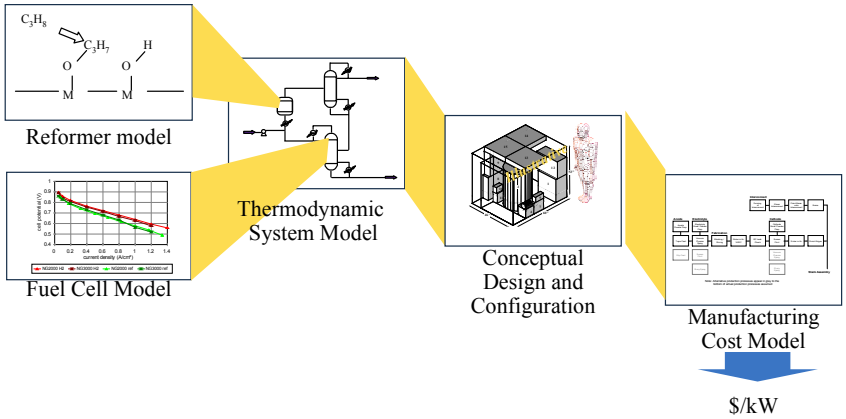

Figure 8-49 Multilevel system modeling approach.

Each of the detailed sub-models feed into the thermodynamic system model, and provides sizing information directly to the conceptual design and configuration. The thermodynamic system model provides a technical hub for the multi-level approach. It provides inputs on the required flow rates and heat duties in the system. Sizing information, together with information from the thermodynamic model then flows to the conceptual design.

8.7.5 SOFC System Cost Structure

The main difference in SOFC stack cost structure as compared to PEFC cost relates to the simpler system configuration of the SOFC-based system. This is mainly due to the fact that SOFC stacks do not contain the type of high-cost precious metals that PEFCs contain. This is off-set in part by the relatively complex manufacturing process required for the manufacture of the SOFC electrode electrolyte plates and by the somewhat lower power density in SOFC systems. Low temperature operation (enabled with electrode supported planar configuration) enables the use of low cost metallic interconnects which can be manufactured with conventional metal forming operations.

The balance of plant contains all the direct stack support systems, reformer, compressors, pumps, and the recuperating heat exchangers. Its cost is low by comparison to the PEFC because of the simplicity of the reformer. However, the cost of the recuperating heat exchangers partially offsets that.

To provide some perspective on the viability of SOFCs in APU applications from a cost perspective, NETL sponsored an estimate of the cost structure of small-scale (5 kW), simple-cycle SOFC anode-supported system, operated on gasoline. The estimated manufacturing cost for such systems (see Figure 8-50) could well be close to that estimated for comparable PEFC systems, while providing somewhat higher system efficiency.

While the stack, insulation and stack balance in this simple-cycle system is a key component; the balance of plant is also an important factor. The stack cost again mainly depends on the achievable power density. Small systems like these will likely not be operated under high pressure. While this simplifies the design and reduces cost for compressors and expanders (which are not readily available at low cost for this size range in any case) it might also negatively affect the power density achievable.

One of the key challenges with small-scale SOFC systems is to overcome heat losses. The higher the heat losses are, the more recuperation is required to maintain the fuel cell within an acceptable operating temperature range and hence to ensure good performance.

The large fraction of cost related to balance of plant issues is mainly due to the very small scale of this system, which results in a significant reverse economy of scale. While design work is still ongoing, it is anticipated that the cost structure of this system will change rapidly to reduce the cost of balance of plant further, and further improve the competitiveness of these systems.

SOFC System Cost Structure:

Manufacturing Costs: $350-550/kW

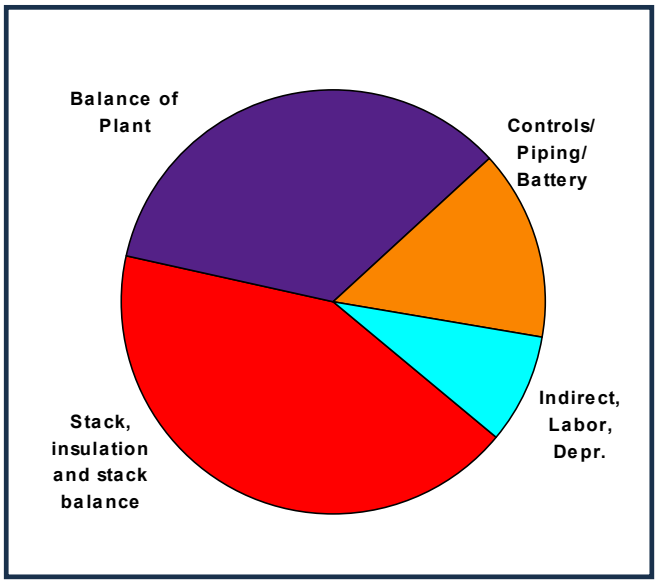

Figure 8-50 Projected cost structure of a 5kWnet APU SOFC system. Gasoline fueled POX reformer, Fuel cell operating at 300mW/cm^2, 0.7 V, 90 percent fuel utilization, 500,000 units per year production volume.

8.7.6 Outlook and Conclusions

In conclusion, both PEFC and SOFC have the potential to meet the allowable cost targets, provided successful demonstrations prove the technology. It is critical however, that for the current technologies to be commercially successful, especially in small-capacity markets, high production volumes will have to be reached. APU applications might provide such markets. It is similarly critical that the technologies be demonstrated to perform and achieve the projected performance targets, and demonstrate long life. These are the challenges ahead for the fuel cell industry in the APU market segment.

8.8 References

1. James M. Douglas, *Conceptual Design of Chemical Processes*, McGraw-Hill, Inc., New York, NY, 1988.
2. Max S. Peters, and Klaus D. Timmerhaus, *Plant Design and Economics for Chemical Engineers*, 3rd Edition, McGraw-Hill, Inc., New York, NY, 1980.
3. Warren L. McCabe, Julian C. Smith, Peter Harriot, *Unit Operations of Chemical Engineering*, 4th Edition, 1985.
4. M.C. Williams, and T.J. George, "Research Issues in Molten Carbonate Fuel Cells: Pressurization," *presented at the 1992 IECEC*, Vol. 3, pp. 263-267.
5. "Overview of 11 MW Fuel Cell Power Plant," non-published information from Tokyo Electric Power Company, September 1989.
6. T. Koshimizu, et al., "Development of 5000 kW and 1000 kW PAFC Plants," *presented at the JASME-ASME Joint Conference (ICOPE-93)*, Tokyo, September 1993.

7. R. Shreve and J. Brink, *Chemical Process Industries*, fourth edition, McGraw-Hill, 1977.
8. T. Okado, et al., "Study of Temperature Control in Indirect Internal Reforming MCFC Stack," presented at 25th IECEC, pp. 207-212, 1990.
9. N.Q. Minh, "High-Temperature Fuel Cells, Part 2: The Solid Oxide Cell," Chemtech, Vol. 21, February 1991.
10. V. Minkov, et al., "Topping Cycle Fuel Cells Effective Combined with Turbines," Power Engineering, July 1988, pp. 35-39. "Design and Economics of Large Fuel Cell Power Plants," presented at 1986 Fuel Cell Seminar, Tucson, AZ, p 255.
11. F.G. Baily, "Steam Turbines for Advanced Combined Cycles," *presented at the 35th GE Turbine State-of-the-Art Technology Seminar*, 1991.
12. M.S. Peters, and K.D. Timmerhaus, *Plant Design and Economics for Chemical Engineers*, Third Edition, McGraw-Hill, 1980.
13. M. Farooque, "Development of Internal Reforming Carbonate Fuel Cell Stack Technology," Performed under Contract No. DE-AC21-87MC23274, DOE/MC/23374-2941, October 1990.
14. M. Farooque, et al., "Comparative Assessment of Coal-Fueled Carbonate Fuel Cell and Competing Technologies," *presented at the 25th IECEC*, Vol. 3, pp.193-200, 1990.
15. Dawn M. Bernardi, "Water-Balance Calculations for Solid-Polymer-Electrolyte Fuel Cells," Journal of Electrochemical Society, Vol. 137, No. 11, November 1990.
16. David P. Wilkinson, (Ballard Power Systems) and David Thompsett (Johnson Matthey Technology Centre), "Materials and Approaches for CO and CO_2 Tolerance for Polymer Electrolyte Membrane Fuel Cells," *presented at the 1997 Proceedings of the Second International Symposium on New Materials for Fuel Cells and Modern Battery Systems*, Montreal, Quebec, Canada, July 6-10, 1997.
17. David P. Wilkinson, and Alfred E. Steck, "General Progress in the Research of Solic Polymer Fuel Cell Technology at Ballard," *presented at the 1997 Proceedings of the Second International Symposium on New Materials for Fuel Cells and Modern Battery Systems*, Montreal, Quebec Canada, July 6-10, 1997.
18. Thomas L. Buchanan, John H. Hirschenhofer, David B. Stauffer, and Jay S. White, "Carbon Dioxide Capture in Fuel Cell Power Systems," September 1994, G/C Report 2981.
19. "Overview of 11 MW Fuel Cell Power Plant," Non-published information from Tokyo Electric Power Company, September 1989.
20. F. P. Bevc, W. L. Lundberg and D. M. Bachovchin, "Solid Oxide Fuel Cell Combined Cycles," ASME Paper 96-GT-447, *presented at International Gas Turbine and Aeroengine Congress & Exhibition*, Birmingham, UK, June 1996.
21. R. Hendricks, "Heron Turbine Prototype Test Results," 20th International Congress on Combustion Engines, International Council on Combustion Engines (CIMAC), London, 1993.
22. T.J. George, K.D Lyons, and R. James III, "Multistaged Oxide Fuel Cell Power Plant Concept," May 1998.
23. Fax Transmittal from J. Hirschenhofer of Parsons Energy & Chemicals Group to Tom George of USDOE/FETC, dated August 26, 1998, Re: Aspen Analysis Results of the Multistaged SOFC Concept.
24. Parsons Energy & Chemical, work for the U.S. DOE, Spring 1998.
25. Appleby, A.J.; Foulkes F.R. *Fuel Cell Handbook*; Van Nostrand Reinhold: New York, 1989.

26. " Fuel-Flexible Fuel Processor," J. Cuzens, J. Mauzey, and R. Woods, Hydrogen Burner Technology, Pg. 234 Fuel Cell Seminar Abstracts, Courtesy Associates, Inc., November 1998.
27. Theory and Application; Paper presented at the 1992 AIChE Annual Meeting: Miami Beach, FL, 1-6 November, 1992.
28. "Developing Power Systems for the 21st Century – Fuel Cell/ATS Hybrid Systems," U.S. Dept. of Energy, National Energy Technology Center & Office of Industrial Technologies, Project facts for Advanced Clean/ Efficient Power Systems, PS031.1099.
29. U. Eberl, "Fuel Cells and Gas Turbines: A Marriage of Efficiency," Research and Innovation, January 2000.
30. R. Gemmen, et al, "Technical Development Issues and Dynamic Modeling of Gas Turbine and Fuel Cell Hybrid Systems," *Proceedings of the 1999 Review Conference on Fuel Cell Technology*, August 1999.
31. "Fuel Cells- Opening New Frontiers in Power Generation," U.S. Department of Energy, Office of Fossil Energy, National Energy Technology Center, November 1999.
32. DOE Techline Press Release, "Department of Energy Announces World's First "Hybrid" Fuel Cell-Turbine," April 2000.
33. "Auto Show Attendees get a Glimpse of Future Concept Cars," Alternative Fuel News, Vol.4 No.1, US Department of Energy, Office of Energy Efficiency and Renewable Energy.
34. K.V. Kordesh, "City Car with H2-Air Fuel Cell and Lead Battery," *6th Intersociety Energy Conversion Engineering Conference*, SAE Paper No. 719015, 1971.
35. A. Kaufman, "Phosphoric Acid Fuel Cell Bus Development," *Proceedings of the Annual Automotive Technology Development Contractors' Coordination Meeting*, Dearborn, MI, October 1994, SAE Proceedings Volume P-289, pp. 289-293, 1995.
36. R.R. Wimmer, "Fuel Cell Transit Bus Testing & Development at Georgetown University," *Proceedings of the Thirty Second Intersociety Energy Conversion Engineering Conference*, July 1997, Honolulu, HI, pp. 825-830.
37. N.C. Otto, P.F. Howard, "Transportation Engine Commercialization at Ballard Power Systems," Program *and Abstracts 1996 Fuel Cell Seminar*, November 1996, Orlando, FL, pp.559-562.
38. F. Panik, "Fuel Cells for Vehicle Applications in Cars – Bringing the Future Closer," J. Power Sources, 71, pp.36-38, 1998.
39. S. Kawatsu, "Advanced PEFC Development for Fuel Cell Powered Vehicles," J. Power Sources, 71, pp. 150-155, 1998.
40. *Fuel Cell Technology: Powering the Future*, Electric Line, November/December 1996.
41. J. Milliken, "The DOE Transportation Fuel Cell Program: Recent Accomplishments and Future Plans," U.S. Dept. of Energy, Office of Transportation Technologies. "Questions and Answers – California Fuel Cell Partnership," www.drivingthefuture.org.

9. SAMPLE CALCULATIONS

This section presents sample problems to aid the reader in understanding the calculations behind a fuel cell power system. The sample calculations are arranged topically with unit operations in Section 9.1, system issues in Section 9.2, supporting calculations in Section 9.3, and cost calculations in Section 9.4. A list of conversion factors common to fuel cell systems analysis is presented in Section 9.5, and a sample automotive design calculation is presented in Section 9.6.

9.1 Unit Operations

The following examples are presented for individual unit operations found within a fuel cell system. Unit operations are the individual building blocks within a complex chemical process. By analyzing example problems for each unit operation, one can learn about the underlying scientific principles and engineering calculation methods that are applied to various processes. This approach will provide the reader with a better understanding of fuel cell power system building blocks as well as the interactions between unit operations. For example, the desired power output from the fuel cell unit will determine the fuel flow requirement from the fuel processor. This section starts by examining the fuel cell unit operation, and continues on to the fuel processor and power conditioner.

9.1.1 Fuel Cell Calculations

Example 9-1 Fuel Flow Rate for 1 Ampere of Current (Conversion Factor Derivation)
What hydrogen flow rate is required to generate 1.0 ampere of current in a fuel cell? (This exercise will generate a very useful conversion factor for subsequent calculations.)

Solution:
For every molecule of hydrogen (H_2) that reacts within a fuel cell, two electrons are liberated at the fuel cell anode. This is most easily seen in the PAFC and PEFC because of the simplicity of the anode (fuel) reaction, although the rule of two electrons per diatomic hydrogen molecule (H_2) holds true for all fuel cell types. The solution requires knowledge of the definition of an ampere (A) and an equivalence of electrons.[56]

$H_2 \rightarrow 2H^+ + 2e^-$

The moles of hydrogen liberated to generate one amp can be calculated directly:

[56] One equivalence of electrons is 1 g mol of electrons or 6.022×10^{23} electrons (Avagadro's number). This quantity of electrons has the charge of 96,487 coulombs (C) (Faraday's constant). Thus, the charge of a single electron is 1.602×10^{-19} C. One (1) ampere of current is defined as 1 C/sec.

$$\dot{n}_{H_2} = (1.0\ \text{A})\left(\frac{1\ \text{coulomb/sec}}{1\ \text{A}}\right)\left(\frac{1\ \text{equivalence of } e^-}{96{,}487\ \text{coulombs}}\right)\left(\frac{1\ \text{g mol } H_2}{2\ \text{equiv. of } e^-}\right)\left(\frac{3600\ \text{sec}}{1\ \text{hr}}\right) = 0.018655\ \frac{\text{g mol}}{\text{hr - A}}\ H_2$$

$$\dot{m}_{H_2} = \left(0.018655\ \frac{\text{g mol}}{\text{hr - A}}\ H_2\right)\left(\frac{2.0158\ \text{g}}{1\ \text{g mol } H_2}\right)\left(\frac{1\ \text{kg}}{1000\ \text{g}}\right) = 37.605\text{x}10^{-6}\ \frac{\text{kg } H_2}{\text{hr - A}}\ \text{or}\ 0.037605\ \frac{\text{kg } H_2}{\text{hr - kA}}$$

The result of this calculation, 0.037605 kg H_2 per hour per kA (0.08291 lb H_2 per hour per kA), is a convenient factor that is often used to determine how much fuel must be provided to supply a desired fuel cell power output, as illustrated in the next example.

Example 9-2 Required Fuel Flow Rate for 1 MW Fuel Cell

A 1.0 MW_{DC} fuel cell stack is operated with a cell voltage of 700 mV on pure hydrogen with a fuel utilization, U_f of 80 percent. (a) How much hydrogen will be consumed in lb/hr? (b) What is the required fuel flow rate? (c) What is the required air flow rate for a 25 percent oxidant utilization, U_{ox}?

Solution:

(a) The solution of this problem will be simplified by assuming that the individual fuel cells are arranged in parallel. That is, the fuel cell stack voltage is the same as each individual cell voltage, and the fuel cell stack current is equal to the current of an individual cell times the number of cells.

Recalling that power (P) is the product of voltage (V) and current (I),

$P = I \times V$

Therefore, the current through the fuel cell stack can be calculated as

$$I = \frac{P}{V} = \left(\frac{1.0\ \text{MW}}{0.7\ \text{V}}\right)\left(\frac{10^6\ \text{W}}{1\ \text{MW}}\right)\left(\frac{1\ \text{VA}}{1\ \text{W}}\right)\left(\frac{1\ \text{kA}}{1000\ \text{A}}\right) = 1429\ \text{kA}$$

The quantity of hydrogen consumed within the fuel cell stack is

$$\dot{m}_{H_2,\text{consumed}} = (1429\ \text{kA})\left(\frac{0.08291\ \text{lb } H_2}{\text{hr - kA}}\right) = 118.4\ \frac{\text{lb } H_2}{\text{hr}}$$

Note that without the simplifying assumption that the fuel cells were arranged in parallel, the same hydrogen mass flow could have been calculated with a few extra steps. For example, if the fuel cell stack was composed of 500 cells in series, then the stack voltage would have been 350 volts [(500 cells)(0.7 V/cell)], and the stack current would have been 2.858 kA/cell [1429 kA / 500 cells]. Because this stack current passes through 500 cells arranged in series, the hydrogen consumption is calculated as

$$m_{H_2,\text{consumed}} = \left(2.858\,\frac{\text{kA}}{\text{cell}}\right)\left(\frac{0.08291\,\text{lb}\,H_2}{\text{hr - kA}}\right)(500\,\text{cells}) = 118.4\,\frac{\text{lb}\,H_2}{\text{hr}}$$

Thus, the reader may find it more expedient and less error prone to envision parallel arrangement when calculating the mass flow requirement of hydrogen.

(b) The utilization of fuel in a fuel cell is defined as

$$U_f = \frac{H_{2,\text{consumed}}}{H_{2,\text{in}}}$$

Therefore the fuel flow rate required to generate 1 MW_{DC} can be calculated as

$$H_{2,\text{in}} = \frac{H_{2,\text{consumed}}}{U_f} = \frac{118.4\,\frac{\text{lb}\,H_2}{\text{hr}}}{80\,\%} = 148.0\,\frac{\text{lb}\,H_2}{\text{hr}}$$

(c) To determine the air requirement, first observe that the stoichiometric[57] ratio of hydrogen to oxygen is 2 to 1 for H_2O. Thus, the moles of oxygen required for the fuel cell reaction are determined by

$$n_{O_2,\text{consumed}} = \left(118.4\,\frac{\text{lb}\,H_2}{\text{hr}}\right)\left(\frac{1\,\text{lb mol}\,H_2}{2.0158\,\text{lb}\,H_2}\right)\left(\frac{1\,\text{lb mol}\,O_2}{2\,\text{lb mol}\,H_2}\right) = 29.38\,\frac{\text{lb mol}\,O_2}{\text{hr}}$$

If 25 percent utilization is required, then the air feed must contain four times the oxygen that is consumed

$$n_{O_2,\text{supplied}} = \left(29.38\,\frac{\text{lb mol}\,O_2\ \text{consumed}}{\text{hr}}\right)\left(\frac{1\,\text{lb mol}\,O_2\ \text{supplied}}{0.25\,\text{lb mol}\,O_2\ \text{consumed}}\right) = 117.5\,\frac{\text{lb mol}\,O_2}{\text{hr}}$$

Because dry air contains 21 percent O_2 by volume, or by mole percent, the required mass flow rate of dry air is

$$m_{\text{air, supplied}} = \left(117.5\,\frac{\text{lb mol}\,O_2\ \text{supplied}}{\text{hr}}\right)\left(\frac{1\,\text{lb mol air}}{0.21\,\text{lb mol}\,O_2}\right)\left(\frac{28.85\,\text{lb dry air}}{1\,\text{lb mol of air}}\right) = 16{,}142\,\frac{\text{lb dry air}}{\text{hr}}$$

Example 9-3 PAFC Effluent Composition

A PAFC, operating on reformed natural gas (900 lb/hr) and air, has a fuel and oxidant utilization of 86 percent and 70 percent, respectively. With the fuel and oxidant composition and molecular weights listed below, how much hydrogen will be consumed in lb mol/hr? (b) How much oxygen is consumed in lb mol/hr? (c) What is the required air flow rate in lb mol/hr and lb/hr?

---

[57] The stoichiometric ratio is the ratio of atoms in a given molecule.

(d) How much water is generated? (e) What is the composition of the effluent (spent) fuel and air streams in mol percent?

Fuel Data	mol percent
CH_4	4.0
CO	0.4
CO_2	17.6
H_2	75.0
H_2O	3.0
Total	100.0
MW	10.55

Air Data	mol percent, dry	mol percent, wet
H_2O	0.00	1.00
N_2	79.00	78.21
O_2	21.00	20.79
Total	100.00	100.00
MW	28.85	28.74

Solution:

(a) To determine the lb mol/hr of hydrogen, first determine the molar fuel flow

$$n_{\text{fuel, supplied}} = \left(900\frac{\text{lb fuel}}{\text{hr}}\right)\left(\frac{1\text{ lb mol fuel}}{10.55\text{ lb fuel}}\right) = 85.29\frac{\text{lb mol fuel}}{\text{hr}}$$

Thus,

$$n_{H_2\text{ consumed}} = \left(85.29\frac{\text{lb mol fuel}}{\text{hr}}\right)\left(\frac{75\text{ lb mol }H_2}{100\text{ lb mol fuel}}\right)\left(\frac{86\text{ lb mol }H_2\text{ consumed}}{100\text{ lb mol }H_2\text{ supplied}}\right) = 55.01\frac{\text{lb mol }H_2}{\text{hr}}$$

(b) To determine how much oxygen is consumed, it is useful to note the overall fuel cell reaction

$$H_{2\,(g)} + \tfrac{1}{2}\,O_{2\,(g)} \rightarrow H_2O_{\,(g)}$$

Therefore,

$$n_{O_2\text{, consumed}} = \left(55.01\frac{\text{lb mol }H_2}{\text{hr}}\right)\left(\frac{\tfrac{1}{2}\text{ lb mol }O_2}{1\text{ lb mol }H_2}\right) = 27.51\frac{\text{lb mol }O_2}{\text{hr}}$$

(c) The required air flow will be determined on a wet air basis, thus

$$n_{\text{air, required}} = \left(27.51\frac{\text{lb mol }O_2}{\text{hr}}\right)\left(\frac{100\text{ lb mol }O_2\text{ supplied}}{70\text{ lb mol }O_2\text{ consumed}}\right)\left(\frac{100\text{ lb mol wet air}}{20.79\text{ lb mol }O_2}\right) = 189.01\frac{\text{lb mol wet air}}{\text{hr}}$$

$$m_{\text{air, required}} = \left(189.01\frac{\text{lb mol wet air}}{\text{hr}}\right)\left(\frac{28.74\text{ lb wet air}}{1\text{ lb mol wet air}}\right) = 5{,}433\frac{\text{lb wet air}}{\text{hr}}$$

(d) Per the overall fuel cell reaction above, the water generated is equal to the moles of hydrogen consumed

$$n_{H_2O\ generated} = n_{H_2\ consumed} = 55.01 \frac{lb\ mol\ H_2}{hr}$$

(e) The composition of the effluent is developed in the table below, by working from the left to right. The composition is determined by converting the composition to moles, accounting for the fuel cell reaction, and converting back to the desired units, mol percent. (Note: mol percent is essentially equivalent to volume percent for low pressure gases.)

Spent Fuel Effluent Calculation

	mol percent	lb mol/hr			mol percent
Gas	**FC inlet**	**FC inlet**	**FC reaction**	**FC outlet**	**FC outlet**
CH_4	4.0	3.41		3.41	11.27
CO	0.4	0.34		0.34	1.13
CO_2	17.6	15.01		15.01	49.58
H_2	75.0	63.97	-55.01	8.96	29.58
H_2O	3.0	2.56		2.56	8.45
Total	**100.0**	**85.29**	**-55.01**	**30.28**	**100.00**

In the PAFC, only the moles of hydrogen change on the anode (fuel) side of the fuel cell. The other fuel gas constituents simply pass through to the anode exit. These inert gases act to dilute the hydrogen, and as such will lower the cell voltage. Thus, it is always desirable to minimize these diluents as much as possible. For example, to reform natural gas, significant quantities of steam are typically added to maximize the reforming reactions. The wet reformer effluent would commonly have a water composition of 30 to 50 percent. The reformate gas utilized in this example has been "dried" to only 3 percent moisture via condensation in a contact cooler.

The spent oxidant composition is calculated in a similar manner. Note that in both the PAFC and PEFC, the water is generated on the cathode (air) side. This can be seen from the cathode reaction listed below and the following table listing the fuel cell reaction quantities.

$$\tfrac{1}{2}O_2 + 2H^+ + 2e^- \rightarrow H_2O$$

Spent Air Effluent Calculation

	mol percent	lb mol/hr			mol percent
Gas	**FC inlet**	**FC inlet**	**FC reaction**	**FC outlet**	**FC outlet**
H_2O	1.00	1.89	55.01	56.90	26.28
N_2	78.21	147.82		147.82	68.27
O_2	20.79	39.30	-27.51	11.79	5.44
Total	**100.00**	**189.01**	**27.51**	**216.51**	**100.00**

Example 9-4 MCFC Effluent Composition - Ignoring the Water Gas Shift Reaction
An MCFC operating on 1,000 lb/hr of fuel gas and a 70 percent air/30 percent CO_2 oxidant has a fuel and oxidant utilization of 75 percent and 50 percent respectively. With the fuel and oxidant composition and molecular weights listed below, (a) How much hydrogen will be consumed in lb mol/hr? (b) How much oxygen is consumed in lb mol/hr? (c) What are the required air and oxidant flow rates in lb mol/hr? (d) How much CO_2 is transferred from the cathode to the anode? (e) What is the composition of the effluent (spent) fuel and oxidant streams in mol percent (ignoring the water gas shift reaction)?

Fuel Data	Mol percent
CH_4	0.0
CO	0.0
CO_2	20.0
H_2	80.0
H_2O	0.0
Total	100.0
MW	10.42

Oxidant Data	Air	Air + CO_2
	mol percent, wet	Mol percent, wet
CO_2	0.00	30.00
H_2O	1.00	0.70
N_2	78.21	54.75
O_2	20.79	14.55
Total	100.00	100.00
MW	28.74	33.32

Solution:
(a) To determine the lb mol/hr of hydrogen, first determine the molar fuel flow

$$n_{\text{fuel, supplied}} = \left(1000 \frac{\text{lb fuel}}{\text{hr}}\right)\left(\frac{1 \text{ lb mol fuel}}{10.42 \text{ lb fuel}}\right) = 96.02 \frac{\text{lb mol fuel}}{\text{hr}}$$

Thus,

$$n_{H_2 \text{ consumed}} = \left(96.02 \frac{\text{lb mol fuel}}{\text{hr}}\right)\left(\frac{80 \text{ lb mol } H_2}{100 \text{ lb mol fuel}}\right)\left(\frac{75 \text{ lb mol } H_2 \text{ consumed}}{100 \text{ lb mol } H_2 \text{ supplied}}\right) = 57.61 \frac{\text{lb mol } H_2}{\text{hr}}$$

(b) To determine how much oxygen is consumed, it is useful to note the overall fuel cell reaction

$$H_{2\,(g)} + \tfrac{1}{2}\, O_{2\,(g)} \rightarrow H_2O_{\,(g)}$$

Therefore,

$$n_{O_2, \text{consumed}} = \left(57.61 \frac{\text{lb mol } H_2}{\text{hr}}\right)\left(\frac{\tfrac{1}{2} \text{ lb mol } O_2}{1 \text{ lb mol } H_2}\right) = 28.81 \frac{\text{lb mol } O_2}{\text{hr}}$$

(c) The required air flow will be determined on a wet air basis:

$$n_{\text{air, required}} = \left(28.81 \frac{\text{lb mol O}_2}{\text{hr}}\right)\left(\frac{100 \text{ lb mol O}_2 \text{ supplied}}{50 \text{ lb mol O}_2 \text{ consumed}}\right)\left(\frac{100 \text{ lb mol wet air}}{20.79 \text{ lb mol O}_2}\right) = 277.11 \frac{\text{lb mol wet air}}{\text{hr}}$$

The oxidant flow rate will be calculated knowing that air is 70 percent of the total oxidant flow:

$$n_{\text{oxidant, required}} = \left(277.11 \frac{\text{lb mol wet air}}{\text{hr}}\right)\left(\frac{100 \text{ lb mol oxidant}}{70 \text{ lb mol wet air}}\right) = 395.86 \frac{\text{lb mol oxidant}}{\text{hr}}$$

(d) Per the overall fuel cell reaction presented below, the quantity of CO_2 transferred from the cathode to the anode side of the fuel cell equals the moles of hydrogen consumed:

$$H_{2,\text{ anode}} + \tfrac{1}{2} O_{2,\text{ cathode}} + CO_{2,\text{ cathode}} \rightarrow H_2O_{,\text{ anode}} + CO_{2,\text{ anode}}$$

Therefore,

$$n_{CO_2 \text{ transferred}} = n_{H_2 \text{ consumed}} = 57.61 \frac{\text{lb mol}}{\text{hr}}$$

(e) The composition of the fuel effluent is developed in the table below, by working from left to right. The composition is determined by converting the composition to moles, accounting for the fuel cell reaction, and converting back to the desired units, mol percent.

Spent Fuel Effluent Calculation

	mol percent	lb mol/hr			Mol percent
Gas	**FC inlet**	**FC inlet**	**FC reaction**	**FC outlet**	**FC outlet**
CH_4	0.0	0.00		0.00	0.00
CO	0.0	0.00		0.00	0.00
CO_2	20.0	19.20	57.61	76.82	50.00
H_2	80.0	76.82	-57.61	19.20	12.50
H_2O	0.0	0.00	57.61	57.61	37.50
Total	**100.0**	**96.02**	**-57.61**	**153.63**	**100.00**

The oxidant effluent composition is calculated in a similar manner. Note that in the MCFC, both oxygen and carbon dioxide are consumed on the cathode (air) side. This can be seen from the cathode reaction listed below and the following table listing the fuel cell reaction quantities.

$$½O_2 + CO_2 + 2e^- \rightarrow CO_3^{=}$$ (MCFC cathode reaction)

Spent Oxidant Effluent Calculation

	mol percent	lb mol/hr			Mol percent
Gas	**FC inlet**	**FC inlet**	**FC reaction**	**FC outlet**	**FC outlet**
CO_2	30.00	83.13	-57.61	25.52	13.38
H_2O	0.70	1.94		1.94	1.02
N_2	54.70	151.71		151.71	79.56
O_2	14.6	40.33	-28.81	11.52	6.04
Total	**100.00**	**277.11**	**-86.42**	**190.69**	**100.00**

Example 9-5 MCFC Effluent Composition - Accounting for the Water Gas Shift Reaction
For the above example, determine the composition of the effluent (spent) fuel stream in mol percent including the effect of the water gas shift reaction. Assume an effluent temperature of 1200 ºF and that the water gas shift reaction proceeds to equilibrium.

Solution:
For convenience, the water gas shift reaction is presented below:

$$CO + H_2O \Leftrightarrow CO_2 + H_2$$

The double headed arrow is used to indicate that the reaction is in equilibrium. That is, the reaction does not proceed completely to the left or to the right. Instead, the reaction proceeds to an equilibrium point, where both "products" and "reactants" remain. The equilibrium composition depends on the initial composition and final temperature and pressure. Fortunately, the equilibrium concentrations can be determined by a temperature dependent equilibrium constant, K, and the following equation:

$$K = \frac{[CO_2][H_2]}{[CO][H_2O]}$$

The quantities in brackets represent the thermodynamic activities of the reacting species. Because the reaction is equimolar, the quantities in brackets are also equal to the mole fractions of the respective components. At 1200 ºF, the equilibrium constant is 1.967[58]. A check of the compositions from the preceding example shows that those concentration levels are not in equilibrium.

$$\frac{[CO_2][H_2]}{[CO][H_2O]} = \frac{[0.50][0.125]}{[0.0][0.375]} = \infty \neq 1.967$$

[58] Equilibrium constants can be calculated from fundamental chemical data such as Gibbs free energy, or can be determined from temperature dependent tables or charts for common reactions. One such table has been published by Girdler Catalysts (1). The following algorithm fits this temperature dependent data to within 5% for 800 to 1800 ºF, or within 1% for 1000 to 1450 ºF: $Kp = e^{(4,276/T - 3.961)}$. Kp(1200 ºF or 922K) equals 1.967.

Because the numerator contains the products of the reaction and the denominator contains the reactants, it is clear that the reaction must proceed more towards the reactants. By introducing a variable, x, to represent the extent of the reaction to proceed to the right and rewriting the equilibrium equation as:

$$K = \frac{[CO_2][H_2]}{[CO][H_2O]} = \frac{[0.50 + x][0.125 + x]}{[0.0 - x][0.375 - x]} = 1.967$$

This can be solved algebraically as follows:

$$K = \frac{[CO_2 + x][H_2 + x]}{[CO - x][H_2O - x]}$$

can be written as

$$K[CO - x][H_2O - x] = [CO_2 + x][H_2 + x]$$

which can be expanded as

$$K\left\{x^2 - ([CO] + [H_2O])x + [CO][H_2O]\right\} = x^2 + ([CO_2] + [H_2])x + [CO_2][H_2]$$

which can be combined to

$$\underbrace{(1 - K)}_{a}x^2 + \underbrace{\left\{[CO_2] + [H_2] + K([CO] + [H_2O])\right\}}_{b}x + \underbrace{\left\{[CO_2][H_2] - [CO][H_2O]K\right\}}_{c} = 0$$

This is in the standard quadratic form of

$$ax^2 + bx + c = 0$$

which can be solved by the quadratic formula

$$x = \frac{-b \pm \sqrt{b^2 - 4ac}}{2a}$$

Substituting the appropriate values for K and the concentrations yields two roots of -0.0445 and 1.454. The larger root is physically impossible; it "wants to" react more CO and H_2O than are initially present. The remaining root of -0.0445 is used to compute the equilibrium gas composition, which is shown in the following table.

Spent Fuel Effluent Calculation

	mol percent	Lb mol/hr, assuming 100 lb mol/hr basis			Mol percent
Gas	FC outlet w/o shift.	FC outlet w/o shift	effect of shift rxn	FC outlet in shift equil.	FC outlet in shift equil.
CO	0.00	0.00	4.45	4.45	4.45
CO_2	50.00	50.00	-4.45	45.55	45.55
H_2	12.50	12.50	-4.45	8.05	8.05
H_2O	37.50	37.50	4.45	41.95	41.95
Total	**100.0**	**100.00**	**0.00**	**100.00**	**100.00**

Example 9-6 SOFC Effluent Composition - Accounting for Shift and Reforming Reactions
An SOFC operates at 1800 °F on 100 percent methane (CH_4) and a fuel utilization of 85 percent. What is the composition of the effluent (spent) fuel in mol percent? Assume that the methane is completely reformed within the fuel cell, and the moisture required for reforming is supplied by internal recirculation.

Solution:
There are many different ways to approach this problem, some of which may seem rather complex because of the simultaneous reactions (fuel cell, reforming, and water gas shift reactions) and the recycle stream supplying moisture required for the reforming reaction. The solution to this problem can be simplified by focusing on the fuel cell exit condition.

First, write the relevant reactions:

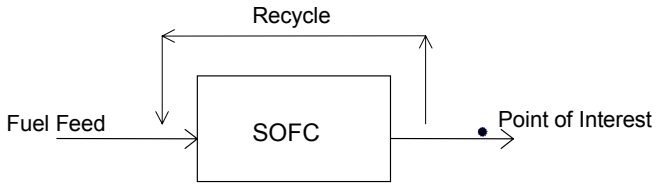

$CH_4 + 2H_2O \rightarrow 4H_2 + CO_2$ (Steam Reforming Reaction)

$H_{2,\,anode} + \frac{1}{2}O_{2,\,cathode} \rightarrow H_2O_{,\,anode}$ (Fuel Cell Reaction)

$CO + H_2O \Leftrightarrow CO_2 + H_2$ (Water Gas Shift Reaction)

Next combine the reforming reaction and the fuel cell reaction into an overall reaction for that portion of the fuel that is consumed (i.e., 85 percent). The combined reaction is developed by adding the steam reforming reaction to 4 times the fuel cell reaction. The factor of four allows the hydrogen molecules to drop out of the resulting equation because it is fully utilized.

$$CH_{4,\,anode} + 2H_2O_{,\,anode} \rightarrow 4H_{2,\,anode} + CO_{2,\,anode}$$ (Steam Reforming Reaction)

$$4H_{2,\,anode} + 2O_{2,\,cathode} \rightarrow 4H_2O_{,\,anode}$$ (Fuel Cell Reaction)

$$CH_{4,\,anode} + 2O_{2,\,cathode} \rightarrow 2H_2O_{,\,anode} + CO_{2,\,anode}$$ (Combined Reforming and FC Reactions)

For ease of calculation, assume a 100 lb/hr basis for the methane.

$$n_{\text{fuel, supplied}} = \left(100\,\frac{\text{lb CH}_4}{\text{hr}}\right)\left(\frac{1\,\text{lb mol CH}_4}{16.043\,\text{lb CH}_4}\right) = 6.23\,\frac{\text{lb mol CH}_4}{\text{hr}}$$

Thus, 85 percent, or 5.30 lb mol CH_4 /hr, will be reformed and consumed by the fuel cell. The remainder will be reformed but not consumed by the fuel cell reaction. These changes are summarized in the following table:

Spent Fuel Effluent Calculation

	mol percent	lb mol/hr				mol percent
Gas	**FC inlet**	**FC inlet**	**Ref / FC rxn**	**Reforming**	**FC outlet**	**FC outlet**
CH_4	100.0	6.23	-5.30	-0.93	0.00	0.00
CO	0.0	0.00	0.00	0.00	0.00	0.00
CO_2	0.0	0.00	5.30	0.93	6.23	33.33
H_2	0.0	0.00	0.00	3.74	3.74	20.00
H_2O	0.0	0.00	10.60	-1.87	8.73	46.67
Total	**100.0**	**6.23**	**10.60**	**1.87**	**18.70**	**100.00**

This intermediate solution reflects only two out of three reactions. Now apply the water gas shift reaction to determine the true exit composition. Use the quadratic equation listed in Example 9-5 to determine how far the reaction will proceed, where x is the extent of the reaction in the forward direction as written:

$$CO + H_2O \xleftrightarrow{x} CO_2 + H_2$$

$$x = \frac{-b \pm \sqrt{b^2 - 4ac}}{2a}$$

The equilibrium constant, K, at 1800 °F (1255 °K) is

$$K = e^{(4276/1255 - 3.961)} = 0.574$$

$$a = (1 - K) = (1 - 0.574) = 0.426$$

$$b = \{[CO_2] + [H_2] + K([CO] + [H_2O])\} = 0.3333 + 0.2000 + 0.574 * (0.00 + 0.4667) = 0.8012$$

$$c = \{[CO_2]\,[H_2] - [CO]\,[H_2O]K\} = (0.3333)(0.20) - (0.00)(0.4667)(0.574) = 0.0666$$

$$x = \frac{-b \pm \sqrt{b^2 - 4ac}}{2a} = \frac{-0.8012 \pm \sqrt{(0.8012)^2 - 4(0.426)(0.0666)}}{2(0.426)} = -0.0873 \text{ and } -1.794$$

The only root that is physically possible is x = -0.0873. The following table summarizes the effect of accounting for the water gas shift equilibrium:

Spent Fuel Effluent Calculation

	mol percent	Lb mol/hr, assuming 100 lb mol/hr basis			Mol percent
Gas	**FC outlet w/o shift.**	**FC outlet w/o shift**	**Effect of shift rxn**	**FC outlet in shift equil.**	**FC outlet in shift equil.**
CO	0.00	0.00	-(-8.73)	8.73	8.73
CO_2	33.33	33.33	-8.73	24.61	24.61
H_2	20.00	20.00	-8.73	11.27	11.27
H_2O	46.67	46.67	-(-8.73)	55.39	55.39
Total	**100.00**	**100.00**	**0.00**	**100.00**	**100.00**

Example 9-7 Generic Fuel Cell - Determine the Required Cell Area and Number of Stacks
Given a desired output of 2.0 MW_{DC} and the desired operating point of 600 mV and 400 mA/cm^2, (a) How much fuel cell area is needed? (b) Assuming a cell area of 1.00 m^2 per cell and 280 cells per stack, how many stacks are needed for this 2.0 MW unit?

Solution:

(a) Recalling that power is the product of voltage and current, first determine the total current for the fuel cell as

$$I = \frac{P}{V} = \left(\frac{2.0 \text{ MW}}{0.600 \text{ V}}\right)\left(\frac{10^6 \text{ W}}{1 \text{ MW}}\right)\left(\frac{1 \text{ VA}}{1 \text{ W}}\right)\left(\frac{1 \text{ kA}}{1000 \text{ A}}\right) = 3{,}333 \text{ kA}$$

Because each individual cell will operate at 400 mA/cm^2, determine the total area as

$$\text{Area} = \frac{I}{\text{Current Density}} = \left(\frac{3{,}333 \text{ kA}}{400 \text{ mA / cm}^2}\right)\left(\frac{1000 \text{ mA}}{1 \text{ A}}\right)\left(\frac{1000 \text{ A}}{1 \text{ kA}}\right) = 8{,}333{,}333 \text{ cm}^2$$

b) The number of required cells and stacks are calculated simply as

$$\text{No. of Cells} = \frac{\left(8{,}333{,}333 \text{ cm}^2\right)}{\left(1 \text{ m}^2 \text{ per cell}\right)}\left(\frac{1 \text{ m}^2}{10{,}000 \text{ cm}^2}\right) = 833 \text{ cells}$$

$$\text{No. of Stacks} = \frac{(833 \text{ cells})}{(280 \text{ cells per stack})} = 2.98 \text{ stacks} \cong 3 \text{ stacks}$$

9.1.2 Fuel Processing Calculations

Example 9-8 Methane Reforming - Determine the Reformate Composition

Given a steam reformer operating at 1400 ºF, 3 atmospheres, pure methane feed stock, and a steam to carbon ratio of 2 (2 lb mol H_2O to 1 lb mol CH_4), (a) List the relevant reactions; (b) Determine the concentration assuming the effluent exits the reactor in equilibrium at 1400 ºF; (c) Determine the heats of reaction for the reformer's reactions; (d) Determine the reformer's heat requirement assuming the feed stocks are preheated to 1400 ºF; (e) Considering LeChâtelier's Principle, indicate whether the reforming reaction will be enhanced or hindered by an elevated operating temperature; (f) Considering LeChâtelier's Principle, indicate whether increased pressure will tend to promote or prevent the reforming reaction.

Solution:

(a) The relevant reactions for the steam reformer are presented below:

$CH_4 + H_2O \Leftrightarrow 3H_2 + CO$ (Steam Reforming Reaction)

$CO + H_2O \Leftrightarrow CO_2 + H_2$ (Water Gas Shift Reaction)

A third reaction is presented below; this reaction is simply a combination of the other two. Of the three reactions, any two can be used as an independent set of reactions for analysis, and can be chosen for the user's convenience.

$CH_4 + 2H_2O \Leftrightarrow 4H_2 + CO_2$ (Composite Steam Reforming Reaction)

(b) The determination of the equilibrium concentrations is a rather involved problem, requiring significant background in chemical thermodynamics, and will not be solved here. One aspect that makes this problem more difficult than Example 9-6, which accounted for the steam reforming reaction within the fuel cell, is that the reforming reaction cannot be assumed to proceed to completion as in the former example. In Example 9-6, hydrogen was consumed within the fuel cell, thus driving the reforming reaction to completion. Without being able to assume the reforming reaction goes to completion, two independent equilibrium reactions must be solved simultaneously. The solution to this problem is most easily accomplished with chemical process simulation programs using a technique known as the minimization of Gibbs free energy. To solve this problem by hand is an arduous, time-consuming task.

The ASPEN™ computer solution to this problem is provided below:

	Inlet Composition (lb mols/hr)	Effluent Composition (lb mols/hr)	Effluent Composition (mol fraction)
CH_4	100	11.7441	2.47
CO	0	64.7756	13.59
CO_2	0	23.4801	4.93
H_2	0	288.2478	60.49
H_2O	200	88.2639	18.52
Total	300	476.5115	100.00

(c) This problem is rather time-consuming to solve without a computer program, and will therefore be left to the ambitious reader to solve[59] from thermodynamic fundamentals. As an alternative, the reader may have access to tables that list heat of reaction information for important reactions. The following temperature-dependent heats of reaction were found for the water gas shift and reforming reactions in the Girdler tables (1).

$CH_4 + H_2O \Leftrightarrow 3H_2 + CO$ $\quad\quad$ $\Delta H_r(1800\ ^oF) = 97{,}741$ Btu/lb mol

$CO + H_2O \Leftrightarrow CO_2 + H_2$ $\quad\quad$ $\Delta H_r(1800\ ^oF) = -13{,}892$ Btu/lb mol

Note: a positive heat of reaction is endothermic (heat must be added to maintain a constant temperature), while a negative heat of reaction is exothermic (heat is given off).

(d) With knowledge of the equilibrium concentration and the heats of reaction, the heat requirement for the reformer can be approximated. Knowing that for each lb mol of CH_4 feed, 88.3 percent [(100-11.7)/100= 88.3 percent] of the CH_4 was reformed, and 26.6 percent [23.5/88.3= 26.6 percent] of the formed carbon monoxide shifts to carbon dioxide, then the overall heat generation for each lb mol of methane feed can be developed from

$$(1\ \text{lbmol}\ CH_4)\left(\frac{88.3\%\ CH_4\ \text{reacted}}{100\%\ CH_4\ \text{feed}}\right)\left(97{,}741\ \frac{\text{Btu}}{\text{lbmol reformed}\ CH_4}\right) = 86{,}300\ \frac{\text{Btu}}{\text{lbmol}\ CH_4\ \text{feed}}$$

$$(1\ \text{lbmol}\ CH_4)\left(\frac{88.3\%\ CH_4\ \text{rxtd.}}{100\%\ CH_4\ \text{feed}}\right)\left(\frac{1\ \text{lbmol CO}}{\text{lbmol}\ CH_4\ \text{rxtd}}\right)\left(\frac{26.6\%\ \text{CO shifts}}{\text{lbmol CO feed}}\right)\left(\frac{-13{,}982\ \text{Btu}}{\text{lbmol CO rxn}}\right) = -3{,}300\ \frac{\text{Btu}}{\text{lbmol}\ CH_4\ \text{feed}}$$

Summing these results, the heat requirement for the reformer is about 83,000 Btu/lb mol of CH_4 fed to the reformer. Because this value is positive, the overall reaction is endothermic and heat must be supplied. This approximate value neglects the change in sensible heat in taking the reactants from 1400 °F to the reference temperature of 1800 °F, and then the products from the reference temperature (1800 °F) back to 1400 °F.

(e) LeChâtelier's Principle simply states that "*if a stress is applied to a system at equilibrium, then the system readjusts, if possible, to reduce the stress*". In this reforming example, LeChâtelier's Principle dictates whether higher or lower temperatures will promote the reforming reaction just by knowing that the reaction is endothermic. To facilitate the application of the principle, write the endothermic reforming reaction (which is the dominant heat of reaction) with a heat term on the left side of the equation.

$CH_4 + H_2O + \text{Heat} \Leftrightarrow 3H_2 + CO$

[59] The reader can refer to Reference 2, Example 4-8 for the solution of a related problem.

Consider that raising the temperature of the system is the applied stress; the stress will be relieved when the reaction proceeds forward. Therefore, the reforming reaction is thermodynamically favored by high temperatures.

(f) To solve this application of LeChâtelier's Principle, write the reforming reaction in terms of the number of gaseous molecules on the left and right sides.

$CH_{4(g)} + H_2O_{(g)} \Leftrightarrow 3H_{2(g)} + CO_{(g)}$

$2Molecules_{(g)} \Leftrightarrow 4Molecules_{(g)}$

Now imagine the reformer at equilibrium, and increase the pressure (the applied stress), then the reaction will try to proceed in a direction that will reduce the pressure (stress). Because a reduction in the number of molecules will reduce the stress, elevated pressure will tend to inhibit the reforming reaction. (Note: reformers often operate at moderate pressures, for operation at pressure will reduce the equipment size and cost. To compensate for this elevated pressure, the designer may be required to raise the temperature.)

Example 9-9 Methane Reforming - Carbon Deposition
Given the problem above, (a) List three potential coking (carbon deposition, or sooting) reactions, and (b) Considering LeChâtelier's Principle, indicate whether excess steam will tend to promote or inhibit the coking reactions.

Solution:
(a) Three of the most common/important carbon deposition equations are presented below.

$CH_4 \Leftrightarrow C + 2H_2$ (Methane Coking)

$2CO \Leftrightarrow C + CO_2$ (Boudouard Coking)

$CO + H_2 \Leftrightarrow C + H_2O$ (CO Reduction)

(b) Considering LeChâtelier's Principle, the addition of steam will clearly inhibit the formation of soot from the CO Reduction reaction. The introduction of excess steam will encourage the reaction to proceed towards the reactants, i.e., away from the products, of which water is one. Since water does not participate in the other two reactions, excess steam does not have a direct effect on either the Methane coking or the Boudouard coking reactions except that the presence of steam will dilute the reactant and product concentrations. Because neither reaction is equimolar with respect to gaseous species, the effect will be ambivalent; the Methane coking reaction will be driven forward while the Boudouard coking reaction will reverse. In addition, the reverse reaction of CO-reduction stimulated by excess steam will increase the presence of CO, driving the Boudouard coking reaction forward. Overall, the addition of steam is useful at preventing soot from ruining the expensive catalysts used in reformers and fuel cell systems. Too much steam, however, simply adds an unnecessary operating cost.

Determination of the minimum steam to carbon ratio that will inhibit carbon deposition is of interest to the fuel cell system designer. The interested reader is referred to references (4), (5), and (6).

The quantity of steam that would preclude the formation of soot based upon thermodynamic equilibrium could be calculated based on minimization of Gibbs free energy. However, it may not be necessary to add as much steam as is implied by this method. Although soot formation may be thermodynamically favored under certain conditions, the kinetics of the reaction can be so slow that sooting would not be a problem. Thus, the determination of sooting on a kinetic basis rather than equilibrium basis is of significant interest. The interested reader is referred to reference (6). When temperature drops to about 750 ºC, kinetic limitations preclude sooting (7). However, above this point, the composition and temperature together determine whether sooting is kinetically precluded. Typically, steam reformers have operated with steam to carbon ratios of 2 to 3, depending on the operating conditions in order to provide an adequate safety margin. An example calculation presented in reference (6) reveals that conditions requiring a steam to carbon ratio of 1.6 on a thermodynamic basis can actually support a steam to carbon ratio of 1.2 on a kinetic basis.

9.1.3 Power Conditioners

Example 9-10 Conversion between DC and AC Power

Given a desired output of 1.0 MW_{AC}, and an inverter efficiency of 96.5 percent, what DC output level is required from the fuel cell stack?

Solution:

(a) The required DC power output level is found simply as the quotient of AC power and the inverter efficiency as demonstrated below.

$$MW_{DC} = (1.0\ MW_{AC})\left(\frac{1\ MW_{DC}}{96.5\%\ MW_{AC}}\right) = 1.036\ MW_{DC}$$

9.1.4 Others

Numerous other unit operations and subsystems can be found in fuel cell processes. These operations and subsystems are well documented in many references (2,8,9,10). For convenience, the unit operations that are commonly found within fuel cell power system are listed below:

- heat exchangers
- pumps
- compressors
- expanders
- intercoolers
- direct contact coolers
- gasification
- gas clean up

9.2 System Issues

This section covers performance issues such as higher heating value (HHV), lower heating value (LHV), cogeneration efficiency, heat rate, and cogeneration steam duty calculations.

9.2.1 Efficiency Calculations

Example 9-11 LHV, HHV Efficiency and Heat Rate Calculations

Given a 2.0 MW_{AC} fuel cell operating on 700 lb/hr of methane, what is (a) the HHV[60] thermal input of the methane gas, (b) the LHV thermal input, (c) the HHV electric efficiency, (d) the LHV electric efficiency, and (e) the HHV heat rate? Assume the higher and lower heating value of methane as 23,881 and 21,526 Btu/lb respectively.

Solution:

(a) The HHV thermal input of the methane gas is

$$\text{HHV Thermal Input} = \left(700\ \text{lb/hr}\ \ CH_4\right)\left(\frac{23{,}881\ \text{Btu, HHV}}{1\ \text{lb}\ CH_4}\right)\left(\frac{1\ \text{MMBtu}}{10^6\ \text{Btu}}\right) = 16.716\ \text{MMBtu/hr}$$

or

$$\text{HHV Thermal Input} = \left(16.716\ \text{MMBtu/hr}\right)\left(\frac{1\ \text{MW}}{3.412\ \text{MMBtu}}\right) = 4.899\ MW_t$$

(b) The LHV thermal input of the methane gas is

$$\text{LHV Thermal Input} = \left(700\ \text{lb/hr}\ \ CH_4\right)\left(\frac{21{,}526\ \text{Btu, LHV}}{1\ \text{lb}\ CH_4}\right)\left(\frac{1\ \text{MMBtu}}{10^6\ \text{Btu}}\right) = 15.068\ \text{MMBtu/hr}$$

or

$$\text{LHV Thermal Input} = \left(15.068\ \text{MMBtu/hr}\right)\left(\frac{1\ \text{MW}}{3.412\ \text{MMBtu}}\right) = 4.416\ MW_t$$

(c) The HHV electrical efficiency is

$$\text{Electrical Efficiency (HHV)} = \left(\frac{\text{Output}}{\text{Input, HHV}}\right) = \left(\frac{2.0\ MW_{AC}}{4.899\ \text{MWt, HHV}}\right) = 40.8\%\ \text{HHV}$$

(d) The LHV electrical efficiency is

$$\text{Electrical Efficiency (LHV)} = \left(\frac{\text{Output}}{\text{Input, LHV}}\right) = \left(\frac{2.0\ MW_{AC}}{4.416\ \text{MWt, LHV}}\right) = 45.3\%\ \text{LHV}$$

Note: Because a fuel's LHV is less than or equal to its HHV value, the LHV efficiency will always be greater than or equal to the HHV efficiency.

(e) Heat rate is the amount of heat (Btu/hr) required to produce a kW of electricity. Alternatively it can be thought of as an inverse efficiency. Because 1 kW is equivalent to 3,412 Btu/hr, a heat rate of 3,412 Btu/kWh represents an efficiency of 100 percent. Note

---

[60] Heating values are expressed as higher or lower heating values (HHV or LHV). Both higher and lower heating values represent the amount of heat released during combustion. The difference between the HHV and LHV is simply whether the product water is in the liquid phase (HHV), or the gaseous phase (LHV).

that as the efficiency goes up, the heat rate goes down. The HHV heat rate for this example can be calculated easily from either the HHV efficiency or the thermal input. Both methods are demonstrated below:

$$\text{Heat Rate (HHV)} = \left(\frac{3412\ \text{Btu/kWh}}{\text{Efficiency, HHV}}\right) = \left(\frac{3412\ \text{Btu/kWh}}{40.8\%}\right) = 8{,}360\ \frac{\text{Btu}}{\text{kWh}}\ \text{(HHV)}$$

or

$$\text{Heat Rate (HHV)} = \left(\frac{\text{Input, HHV}}{\text{Output}}\right) = \left(\frac{16{,}716{,}000\ \text{Btu/hr}}{2{,}000\ \text{kW}}\right) = 8{,}360\ \frac{\text{Btu}}{\text{kWh}}\ \text{(HHV)}$$

Note: The LHV to HHV ratio of 90 percent for methane (21,526/23,881 = 90 percent) is typical for natural gas, while this ratio is roughly 94 percent for fuel oils. Common coals typically have a LHV to HHV ratio of 92 to 96 percent depending upon the hydrogen and moisture content[61]. Typically, gas turbine based cycles are presented on an LHV basis. Conventional power plants, such as coal-, oil-, and gas-fired steam generator/steam turbine cycles are presented on an HHV basis within the U.S. and on an LHV basis throughout the rest of the world.

Example 9-12 Efficiency of a Cogeneration Fuel Cell System
Given the system described in Example 9-11, what is the combined heat and power efficiency assuming that cycle produces 2 tons/hr of 150 psia/400 ºF steam? Assume a feedwater temperature of 60 ºF.

Solution:
Before calculating the cogeneration efficiency, first determine the heat duty associated with steam production. This requires knowledge of the steam and feed water enthalpies, which can be found in the ASME Steam Tables (11) as indicated below:

	Temperature (ºF)	Pressure (psia)	Enthalpy (Btu/lb)
Steam	400	150	1219.1
Feedwater	60	180	28.6

The steam heat duty is calculated as

$$\text{Heat Duty} = (\text{mass flow})(\text{Change in enthalpy}) = (4000\ \text{lb/hr})(1219.1 - 28.6\ \text{Btu/lb})\left(\frac{1\ \text{MMBtu}}{10^6\ \text{Btu}}\right) = 4.762\ \text{MMBtu/hr}$$

Alternatively, this heat duty can be expressed as 1.396 MWt, [4.762 / 3.412 = 1.396 MW]. Thus, the combined heat and power efficiency is calculated as

[61] The difference between the LHV and HHV heating values can be estimated by (1055 Btu/lb)*w, where w is the lbs moisture after combustion per lb of fuel. Thus, w can be determined from the fuel's hydrogen and moisture content by w= moisture + 18/2 * hydrogen. [e.g., for a fuel with 10% moisture and 4% hydrogen, the LHV to HHV difference is 485 Btu/lb, [i.e., 1055*(0.10 + 0.04*9)=485.]

$$\text{Combined Heat \& Electrical Efficiency (HHV)} = \left(\frac{\text{Output}}{\text{Input, HHV}}\right) = \left(\frac{2.00\ \text{MW}_{AC} + 1.396\ \text{MWt}}{4.899\ \text{MWt, HHV}}\right) = 69.3\%\ \text{HHV}$$

9.2.2 Thermodynamic Considerations

Example 9-13 Production of Cogeneration Steam in a Heat Recovery Boiler (HRB)

Given 10,000 lb/hr of 700 ºF cycle exhaust gas passing through a heat recovery boiler (HRB) (a) How much 150 psia, 400 ºF steam can be produced? (b) How much heat is transferred from the gas in the HRB? (c) What is the exhaust temperature of the gas leaving the HRB? and (d) Sketch the T-Q (temperature-heat) diagram for the HRB. Assume a gas side mean heat capacity of 0.25 Btu/lb-ºF, an evaporator pinch temperature of 30 ºF, a feedwater temperature of 60 ºF, and an evaporator drum pressure of 180 psia to allow for pressure losses.

Solution:

(a) Develop a solution strategy by examining a typical HRB T-Q diagram presented below. From this diagram, observe that the pinch point (the minimum temperature differential between the gas and saturated steam) limits the steam production. To produce more steam, the lower steam line would be stretched to the right until it "bumped" into the hot gas line. At the point of contact, both the hot gas and saturated steam would be at the same temperature. This is thermodynamically impossible, because heat will only "flow" from a higher temperature to a lower one. In practice, the temperature approach at the pinch point is kept large enough (15 to 40 ºF) to prevent an unusually large and expensive evaporator. Because the pinch limits the steam production, the sensible heat available in the exhaust gas from 700 °F to the pinch point will determine how much steam can be produced.

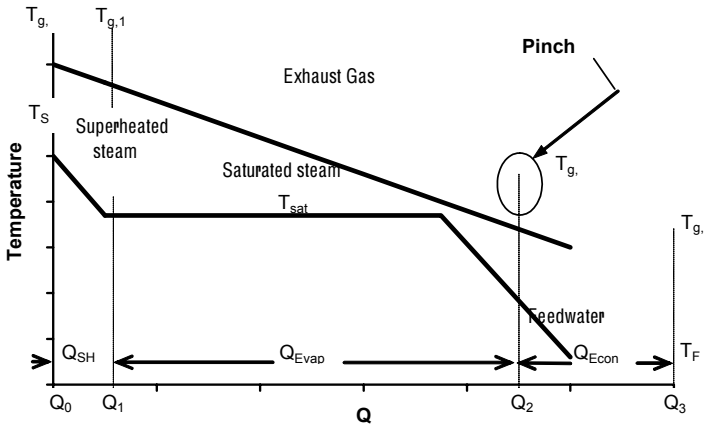

The governing equations for the heat available in the gas down to the pinch point ($T_{g,0}$ to $T_{g,2}$), and the corresponding heat absorbed by the superheated and saturated steam are presented below.

$$Q^{gas}_{SH + Evap} = (m_{gas})(C_p)(T_{g,0} - T_{g,2})$$

$$Q^{steam}_{SH + Evap} = (m_{steam})(h_{superheated} - h_f)$$

$$Q^{gas}_{SH + Evap} = Q^{steam}_{SH + Evap}$$

Calculate $Q^{gas}_{SH + Evap}$ based on the steam saturation temperature from the steam tables. By using the ASME steam tables (11), determine the saturation temperature and enthalpies of interest:

$h_{superheated}$ (150 psia, 400 ºF) = 1219.1 Btu/lb

h_f (180 psia, saturated water) = 346.2 Btu/lb

T_{sat} (180 psia, saturated steam/water) = 373.1 ºF

$T_{g,2} = T_{sat} + 30 = 403.1$ °F

Now solve for $Q^{gas}_{SH + Evap}$

$$Q^{gas}_{SH + Evap} = \left(10{,}000\,\frac{lb}{hr}\right)\left(0.25\,\frac{Btu}{lb^{o}F}\right)\left(700 - 403.1\ ^{o}F\right) = 742{,}000\,\frac{Btu}{hr}$$

Substitute this heat value into the steam side equation to solve directly for the steam mass flow rate:

$$m_{steam} = \frac{Q^{steam}_{SH + Evap}}{(h_{superheated} - h_f)} = \frac{742{,}000\ \frac{Btu}{hr}}{\left(1219.1 - 346.2\ \frac{Btu}{lb}\right)} = 850\ \frac{lb}{hr}$$

(b) Knowing the water/steam mass flow rate, the HRB heat duty can be calculated using the following equations:

$h_{feedwater}$ (60 ºF) = 28.6 Btu/lb

$$Q^{steam}_{Total} = (m_{steam})(h_{superheated} - h_{feedwater}) = \left(850\ \frac{lb}{hr}\right)\left(1219.1 - 28.6\,\frac{Btu}{lb}\right) = 1{,}012{,}000\,\frac{Btu}{hr}$$

(c) The gas temperature leaving the HRB ($T_{g,3}$) is now easily calculated, because the total heat transferred to the steam is equivalent to that lost by the gas stream:

$$Q^{gas}_{Total} = (m_{gas})(C_p)(T_{g,0} - T_{g,3})$$

Thus,

$$1{,}012{,}000\,\frac{Btu}{hr} = \left(10{,}000\,\frac{lb\ gas}{hr}\right)\left(0.25\,\frac{Btu}{lb^{o}F}\right)\left(700\ ^{o}F - T_{g,3}\right)$$

Solving, $T_{g,3} = 295$ ºF.

(d) Because a constant mean Cp was assumed for the exhaust gas over the temperature range of interest, simply draw a straight line from 700 ºF to 295 ºF, with the 295 ºF corresponding to a transferred quantity of heat of 1.01 MMBtu/hr. On the steam side, separately determine the heat absorbed by the superheater, the evaporator, and the economizer. These heats are determined by the following equations:

$$Q_{SH}^{steam} = (m_{steam})(h_{superheated} - h_g)$$

$$Q_{Evap}^{steam} = (m_{steam})(h_g - h_f)$$

$$Q_{Econ}^{water} = (m_{water})(h_f - h_{feedwater})$$

Substitute the known flow and enthalpy data and solve for these three quantities:

h_g (180 psia, saturated steam) = 1196.9 Btu/lb

$$Q_{SH}^{steam} = (850\,\tfrac{lb}{hr})(1219.1 - 1196.9\,\tfrac{Btu}{lb}) = (850\,\tfrac{lb}{hr})(22.2\,\tfrac{Btu}{lb}) = 18{,}900\,\frac{Btu}{hr}$$

$$Q_{Evap}^{steam} = (850\,\tfrac{lb}{hr})(1196.9 - 346.2\,\tfrac{Btu}{lb}) = (850\,\tfrac{lb}{hr})(850.7\,\tfrac{Btu}{lb}) = 723{,}100\,\frac{Btu}{hr}$$

$$Q_{Econ}^{water} = (850\,\tfrac{lb}{hr})(346.2 - 28.6\,\tfrac{Btu}{lb}) = (850\,\tfrac{lb}{hr})(317.6\,\tfrac{Btu}{lb}) = 270{,}000\,\frac{Btu}{hr}$$

Use these values to calculate cumulative heat duties:

$$Q_1 = Q_{SH}^{steam} = 18{,}900\,\frac{Btu}{hr} = 0.019\,\frac{MMBtu}{hr} \text{ at } 373.1\ ^{o}F$$

$$Q_2 = Q_1 + Q_{Evap}^{steam} = 18{,}900 + 723{,}100\,\frac{Btu}{hr} = 742{,}000\,\frac{Btu}{hr} = 0.742\,\frac{MMBtu}{hr} \text{ at } 373.1\ ^{o}F$$

$$Q_3 = Q_2 + Q_{Econ}^{water} = 742{,}000 + 270{,}000\,\frac{Btu}{hr} = 1{,}012{,}000\,\frac{Btu}{hr} = 1.012\,\frac{MMBtu}{hr} \text{ at } 60\ ^{o}F$$

Plotting these points on the chart below yields the following T-Q diagram.

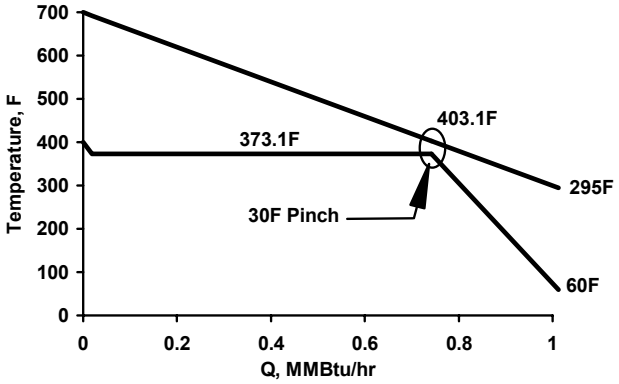

9.3 Supporting Calculations

Example 9-14 Molecular Weight, Density and Heating Value Calculations
Given the fuel gas composition presented below, what is (a) the molecular weight, (b) the higher heating value in Btu/ft^3? (c) the density of the gas in lb/ft^3 at 1 atm and 60 ºF? (d) the higher heating value in Btu/lb, and (e) the lower heating value in Btu/ft^3?

Fuel Constituent	mol percent
CH_4	4.0
CO	0.4
CO_2	17.6
H_2	75.0
H_2O	3.0
Total	100.0

Solution:
(a) Before determining the molecular weight of the fuel gas mixture, develop the molecular weights of each of the gas constituents in the following table:

Fuel Constituent	MW Derivation	MW
CH_4	(12.01) + 4*(1.008) = 16.04	16.04
CO	(12.01) + 1*(16.00) = 28.01	28.01
CO_2	(12.01) + 2*(16.00) = 44.01	44.01
H_2	2*(1.008) = 2.016	2.016
H_2O	2*(1.008) +1*(16.00) = 18.02	18.02

The molecular weight for the gas mixture is calculated below for a 100 lb mol basis:

Fuel Constituent	mol percent	100 lb mol basis			1 lb mol
		lb mols	MW (lb/lb mol)	Weight (lb)	MW (lb/lb mol)
CH_4	4.0	4.0	16.04	64.16	
CO	0.4	0.4	28.01	11.20	
CO_2	17.6	17.6	44.01	774.58	
H_2	75.0	75.0	2.016	151.20	
H_2O	3.0	3.0	18.02	55.06	
Total	100.0	100.0		1056.2	10.56

b) The higher heating value of the fuel gas can be reasonably predicted from the composition. The following table presents the higher heating value for common fuel gas constituents:

Table 9-1 HHV Contribution of Common Gas Constituents

Gas	Higher Heating Value	
	Btu/lb	Btu/ft^3
H_2	60,991	325
CO	4,323	321
CH_4	23,896	1014
C_2H_6	22,282	1789
C_3H_8	22,282	2573
C_4H_{10}	21,441	3392
H_2O, CO_2, N_2, O_2	0	0

Reference (12)
HHV (Btu/ft^3) at 1 atm and 60 ºF.

Using these HHV contributions, the gas composition, and the ideal gas law, calculate the overall HHV on a basis of 100 ft^3 in the following table:

Fuel Constituents	mol percent	100 ft^3 Basis			1 ft^3 Basis
		Volume (ft^3)	HHV (Btu/ft^3)	Heat Input (Btu)	HHV (Btu/ft^3)
CH_4	4.0	4.0	1014	4056	
CO	0.4	0.4	321	128	
CO_2	17.6	17.6	0	0	
H_2	75.0	75.0	325	24,375	
H_2O	3.0	3.0	0	0	
Total	100.0	100.0		28,559	285.6

Thus, the higher heating value for the specified fuel gas is 285.6 Btu/ft^3.

(c) The density of any ideal gas can be calculated by modifying the ideal gas law, presented below:

$$PV = nRT$$

Because density is simply the mass of a substance divided by its volume, multiply both sides of the ideal gas equation by the molecular weight, MW, of the gas mixture. Recall that the moles of a substance, n, times its molecular weight equals its mass.

$$PV(MW) = n(MW)RT$$

$$PV(MW) = (mass)RT$$

Rearrange this equation to derive an ideal gas law equation that will calculate the density of any ideal gas given the temperature, pressure and MW:

$$\text{density} = \frac{\text{mass}}{\text{volume}} = \frac{P(MW)}{RT}$$

The selection of the ideal gas constant, R, in convenient units such as (atm-ft^3)/(lb mol-R) will simplify the density calculation in units of lbs per ft^3

$$\text{density} = \frac{P(MW)}{RT} = \frac{(1\,\text{atm})(10.56\,\frac{\text{lb}}{\text{lbmol}})}{(0.7302\,\frac{\text{atm-ft}^3}{\text{lbmol-R}})(60+460\,\text{R})} = 0.02781\,\frac{\text{lb}}{\text{ft}^3}\,(\text{at } 1\,\text{atm}, 60\ ^{\circ}\text{F})$$

(d) The HHV in Btu/lb can be calculated from the HHV in Btu/ft^3 and the density:

$$\text{HHV} = \left(285.6\,\frac{\text{Btu}}{\text{ft}^3}\right)\left(\frac{1\,\text{ft}^3}{0.02781\,\text{lb}}\right) = 10{,}270\,\frac{\text{Btu}}{\text{lb}}$$

(e) The LHV can be calculated by recalling that the fundamental difference between HHV and LHV is the state of the product water. That is, HHV is based on a liquid water product, while LHV is based on a gaseous water product. Because energy is consumed to evaporate liquid water into gaseous water, LHV values are always less than or equal to HHV values. To convert liquid water to water vapor at 1 atm and 60 ºF requires approximately 1050 Btu/lb, or 50 Btu/ft^3 of water vapor. For a given gas mixture, the quantitative difference between the HHV and LHV is, obviously, a function of how much water is produced by the given fuel. So the first step in converting HHV to LHV is the determination of the amount of water produced by the fuel. This is done in the table below. The LHV to HHV adjustment is calculated by multiplying the water volume times the change in enthalpy going from liquid to vapor (50 Btu/ft^3):

Fuel Constituent	mol percent	Basis: 1.0 ft^3 of Fuel Gas			
		Fuel Gas Volume (ft^3)	Stoichiometric Factor[62] for Gas to H_2O	Water Volume (ft^3)	LHV to HHV Adjustment (Btu/ft^3)
CH_4	4.0	0.04	2.0	0.08	4.0
CO	0.4	0.004	0.0	0.00	0.0
CO_2	17.6	0.176	0.0	0.00	0.0
H_2	75.0	0.75	1.0	0.75	37.5
H_2O	3.0	0.03	0.0	0.00	0.0
Total	100.0	1.00		0.83	41.5.

Thus, the LHV can be estimated from the HHV of 285.6 Btu/ft^3 as 246.1 Btu/ft^3 (285.6 - 41.5= 244.1 Btu/ft^3).

9.4 Cost Calculations

This section presents information on developing the Cost of Electricity (COE), as well as information for the development of capital costs.

9.4.1 Cost of Electricity

Three major components are considered in the computation of the COE for a fuel cell power plant: 1) capital cost, 2) fuel cost and 3) operation and maintenance costs. The cost of electricity ($/MWh) can be calculated using these parameters as follows:

$$COE = \frac{0.125CC}{H} + \frac{3.412\,FC}{\varepsilon_s} + \frac{O\&M}{H}$$

where 0.125 is a typical capital recovery rate (excluding taxes and insurance), CC is the capital cost ($/kW), FC is the fuel cost ($/$10^6$ Btu), 3.412 is the theoretical heat rate for 100 percent efficiency (3412 Btu/kWh) divided by 1000 for units consistency, ε_s is the fractional efficiency, H is the annual operating hours divided by 1000, and O&M is the operating and maintenance cost ($/kW-yr total, including fixed and variable costs).

Example 9-15 Cost of Electricity

Given a capital cost of $1000/kW, a fuel cost of $2 per MMBtu, a net plant efficiency of 40 percent (LHV), 6000 operating hours, and a total O&M cost of $20/kW-yr, what is the estimated cost of electricity?

Solution:

$$COE = \frac{(0.125)(1000)}{6} + \frac{(3.412)\,(2)}{0.40} + \frac{(20)}{6}$$

[62] The stoichiometric factor is the number of water molecules produced per fuel molecule in complete combustion. For example, for CH_4, which combusts to 2 H_2O, the stoichiometric factor is two.

$$COE = 20.8 + 17.1 + 3.3 = \$41.2 / MWh, \text{ or } 4.1 \text{ cents} / kWh$$

9.4.2 Capital Cost Development

There is a need for an easily understood, flexible, and reasonably accurate methodology for rapidly estimating the cost of conceptual fuel cell power plants.

One method proposed for estimating the cost of fuel cell power plants is to calculate distributive (bulk) costs as a function of the equipment cost using established factors based on conventional generating technologies. When applied to compensate for the differences associated with a fuel cell plant, this approach can yield reasonable results. Based on the international prominence of the Association for the Advancement of Cost Engineering (AACE), this approach is useful for conceptualizing the costs for fuel cell/turbine power plant systems.

Typical factors in common use are listed in Table 9-2. These factors apply to processes operating at temperatures in excess of 400 ^{o}F at pressures of under 150 psig, and are taken from the AACE Recommended Practice No. 16R-90, *Conducting Technical and Economic Evaluations in the Process and Utility Industries*.

Table 9-2 Distributive Estimating Factors

Area	Material	Labor
Foundations	0.06	1.33
Structural Steel	0.05	0.50
Buildings	0.03	1.00
Insulation	0.02	1.50
Instruments	0.07	0.75
Electrical	0.06	0.40
Piping	0.40	0.50
Painting	0.005	3.00
Misc.	0.04	0.80

The suggested material factors are applied to direct equipment costs, whereas the labor factors apply to the corresponding material item. Because the distributive factors are based on large scale field-built plants, an alternative factory fabrication adjustment can be made to reflect a modular construction approach requiring less field fabrication, as would likely be the case with smaller plant configurations. This approach is illustrated in reference (16).

The approach discussed above does not preclude the use of alternate methodologies. One such alternate methodology, currently in the early stages of development, is based on the premise that fuel cell plant costs could be more accurately estimated using factors developed specifically for fuel cell applications, rather than factors based on conventional generating technologies. An overview of this approach along with a “first cut” at developing new fuel cell specific factors is presented in reference (18). Fuel cell-specific factors developed to date are based on limited data and should be considered highly preliminary. Continued refinement will be required as additional fuel cell plant costing information becomes available.

9.5 Common Conversion Factors

To Convert From	To	Multiply by	To Convert From	To	Multiply by
A (amperes)	Faradays/sec	1.0363E-05	Joule (J)	V-coulomb	1
A/ft^2	mA/cm^2	1.0764			
atm	kg/cm^2	1.0332			
atm	lb/in^2	14.696			
atm	bar	1.01325	kg	lb	2.2046
atm	Pa	101,325	kg/cm^2	lb/in^2	14.223
Avagadro's number	particles/g mol	6.022E+23			
bar	atm	0.98692	Kcal	Btu	3.9686
bar	lb/in^2	14.504	kPa	lb/in^2	0.14504
bar	kg/cm^2	1.0197	kW	Btu/hr	3412.1
bar	Nm^2	100,000	kW	kcal/sec	0.23885
bar	Pa	100,000	kW	hp	1.3410
Btu	cal	251.98	lb	grams	453.59
Btu	ft-lb	778.17	lb	kg	0.45359
Btu	J (Joules)	1055.1			
Btu	kWh	2.9307E-04			
Btu/hr	W	0.29307	lb/in^2	kg/cm^2	0.070307
Btu/lb-°F	cal/g-°C	1.0000	lb/in^2	Pa	6894.7
°C	°F	°C*(9/5)+32	l (liter)	m^3	1.0000E-03
°C	°K	°C+273.16	m (meter)	ft	3.2808
cal	J	4.1868	m (meter)	in	39.370
cm	ft	0.032808	m^2	ft^2	10.764
cm	in	0.39370	m^3	ft^3	35.315
°F	°C	(°F-32)*(5/9)	m^3	gal	264.17
Faradays	C (coulombs)	96,487	mA/cm^2	A/ft^2	0.92903
Faradays/sec	A	96,487	MMBtu/hr	MW	0.29307
ft	m	0.30480	MW	MMBtu/h	3.4121
ft	cm	30.480	Pa	lb/in^2	1.4504E-04
ft^2	cm^2	929.03	R (gas constant)	atm-ft^3/lbmol-R	0.73024
ft^2	m^2	0.092903	R (gas constant)	Btu/lb mol-R	1.9859
ft^3	liters	28.317	R (gas constant)	cal/g mol-K	1.9857
ft^3	m^3	0.028317	R (gas constant)	ft-lbf/lb mol-R	1545.3
ft^3	gal	7.4805	R (gas constant)	J/g mol-K	8.3144126
gal	liters	3.7854	R (gas constant)	l-atm/g mol-K	0.082057
grams (g)	lb	2.2046E-03	tonne	kg	1000.0
hp	ft-lb/sec	550.00	tonne	lb	2204.6
horsepower (hp)	kW	0.74570	Watts	Btu/hr	3.4121
hp	W	745.70	Watts	hp	1.3410E-03

9.6 Automotive Design Calculations

The total power, P, needed from a vehicle's power system must be sufficient for vehicle acceleration, aerodynamic drag losses, rolling resistance, changes in elevation, and auxiliary power for vehicle accessories (19, 20). These power terms are, respectively:

$$P = (mav + 0.5\varrho C_D A_F v^3 + mgC_R v + mgv \cdot \sin(\alpha)) / \varepsilon + P_{aux}$$

Where P = total power (W)
m = vehicle mass (kg)
a = vehicle acceleration (m/sec^2)
v = vehicle velocity (m/sec)
ϱ = air density (kg/m^3)
C_D = aerodynamic drag coefficient
A_F = vehicle area normal to direction of travel (m^2)
g = gravitation constant (9.8 m/sec^2)
C_R = coefficient of rolling resistance
α = inclined angle of road (radians)
ε= efficiency of motor, controller, and gearing
P_{aux} = auxiliary power for lights, radio, wipers, air conditioner, cigarette lighter, etc. (W)

The power system may consist of the fuel cell plus peak power storage device(s). Criteria established by the Partnership for a New Generation of Vehicles (PNGV) specify that:

- The fuel cell system (without peak power device) must provide enough power to sustain a speed of 55 mph (24.58 m/sec) on a 6.5 percent grade, and
- The output of the fuel cell system plus peak power device must allow acceleration for high speed passing of 3 mph/sec (1.34 m/sec^2) on a level road at 65 mph (29.05 m/sec)

These values are computed for a conventional mid-size passenger vehicle using the following assumptions:

m = 1360 kg (vehicle weight) + 272 kg (weight of passengers plus cargo)
ϱ = 1.29 kg/m^3 (at standard temperature and pressure)
C_D = 0.3
A_F = 2.0 m^2
g = 9.8 m/sec^2
C_R = 0.0085
ε = 0.77
P_{aux} = 400 W (= 400 kg-m^2/sec^3)

Substituting these values into the equation above, the minimum power needed by the fuel cell alone to sustain 24.58 m/sec on a 6.5 percent grade (0.0649 radians) is

$$P_S = ((0.5)(1.29)(0.3)(2.0)(24.58)^3 + (1632)(9.8)(0.0085)(24.58) + (1632)(9.8)(24.58)\sin(0.0649))/0.77 + 400$$

$P_S = 45{,}339$ kg-m^2/sec^3 = 4.53 kW

The minimum power needed by the power system to accelerate on a level road at 1.34 m/sec^2 at 29.05 m/sec is

$P_A = ((1632)(1.34)(29.05) + (0.5)(1.29)(0.3)(2.0)(29.05)^3 + (1632)(9.8)(0.0085)(29.05))/0.77 + 400$

$P_A = 100{,}355$ kg-m^2/sec^3 = 10.03 kW

9.7 References

1. "Physical and Thermodynamic Properties of Elements and Compounds," Girdler Catalysts, Chemetron Corporation, Catalysts Division.
2. J. M. Smith, H. C. Van Ness, Introduction to Chemical Engineering Thermodynamics, Third Edition, McGraw-Hill, 1975.
3. Chemistry: Principles and Applications, M. J. Sienko, R. A. Plane, McGraw-Hill, New York, NY, 1979.
4. D. B. Stauffer, J. S. White, J. H. Hirschenhofer, "An ASPEN/SP MCFC Performance User Block," DOE Contract DE-AC21-89-MC25177, Task 7, July 1991.
5. D. B. Stauffer, R. R. Engleman Jr., J. S. White, J. H. Hirschenhofer, "An ASPEN/SP SOFC Performance User Block," DOE Contract DE-AC21-88-FE-61684, Task 14, September 1993.
6. E. S. Wagner, G. F. Froment, "Steam Reforming Analyzed," Hydrocarbon Processing, July 1992, pp. 69 -77.
7. Fuel Cell Systems, Edited by L. J. M. Blomen, M. N. Mugerwa, Plenum Press, New York, NY, 1993.
8. W. L. McCabe, J. C. Smith, P. Harriot, Unit Operations of Chemical Engineering, 4th Edition, 1985.
9. Chemical Engineers' Handbook, Edited by R. H. Perry, D. Green, 6th Edition, McGraw-Hill, 1984.
10. M. S. Peters, K. D. Timmerhaus, Plant Design and Economics for Chemical Engineers, 3rd Edition, McGraw-Hill, Inc., New York, NY, 1980.
11. C. A. Meyers, R. B. McClintok, G. J. Silvestri, R. C. Spencer, Jr., 1967 ASME Steam Tables, New York, 1967.
12. Combustion, Fossil Power: A Reference Book on Fuel Burning and Steam Generation, 4th Edition, edited by J. G. Singer, P.E., Combustion Engineering, 1991.
13. B. J. McBride, "Coefficients for Calculating Thermodynamic and Transport Properties of Individual Species," NASA Technical Memorandum 4513, October 1993.
14. B. J. McBride, "Thermodynamic Data for Fifty Reference Elements," NASA Technical Paper 3287, January 1993.
15. H. M. Spencer, *Ind. Eng. Chem.*, 40:2152 (1948), as presented in Introduction to Chemical Engineering Thermodynamics, Third Edition, J. M. Smith and H. C. Van Ness, McGraw-Hill, 1975.

16. T. J. George, R. James III, K. D. Lyons, "Multi-Staged Fuel Cell Power Plant (Targeting 80% Lower Heating Value Efficiency)," *Power Generation International 1998 Conference*, December 9-11, 1998, Orange County Convention Center, Orlando, Florida.
17. Recommended Practice No. 16R-90, *Conducting Technical and Economic Evaluations in the Process and Utility Industries*.
18. L. L. Pinkerton, "Express Method for Estimating the Cost of Fuel Cell Plants," *1998 Fuel Cell Seminar*, November 16-19, 1998, Palm Springs Convention Center, Palm Springs, California.
19. J. M. Ogden, M. M. Steinbugler, and T. G. Kreutz. 1999. "A Comparison of Hydrogen, Methanol, and Gasoline as Fuels for Fuel Cell Vehicles: Implications for Vehicle Design and Infrastructure Development." Journal of Power Sources, 79 (1999) 143-168.
20. K. H. Hauer, D. J. Friedmann, R. M. Moore, S. Ramaswamy, A. Eggert, and P. Badranarayanan, March 6-9, 2000. "Dynamic Response of an Indirect-Methanol Fuel Cell Vehicle." Fuel Cell Power for Transportation 2000. Society of Automotive Engineers World Congress, Detroit, Michigan.

10. APPENDIX

10.1 Equilibrium Constants

Figure 10-1 presents the temperature dependence of the equilibrium constants for the water gas shift reaction,

$$CO_2 + H_2 = CO + H_2O \qquad (10\text{-}1)$$

the carbon deposition (Boudouard reaction) reaction,

$$2CO \rightarrow C + CO_2 \qquad (10\text{-}2)$$

the methane decomposition reaction,

$$CH_4 \rightarrow C + 2H_2 \qquad (10\text{-}3)$$

and the methane formation reaction,

$$CO + 3H_2 \rightarrow CH_4 + H_2O \qquad (10\text{-}4)$$

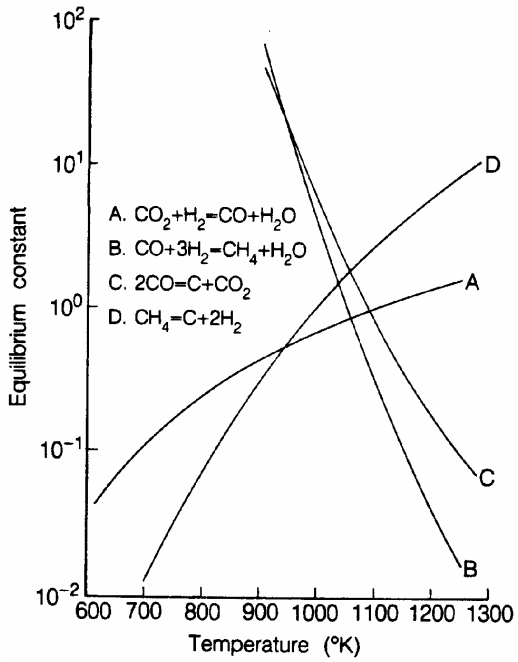

Figure 10-1 Equilibrium Constants (Partial Pressures in MPa) for (a) Water Gas Shift, (b) Methane Formation, (c) Carbon Deposition (Boudouard Reaction), and (d) Methane Decomposition (J.R. Rostrup-Nielsen, in Catalysis Science and Technology, Edited by J.R. Anderson and M. Boudart, Springer-Verlag, Berlin GDR, p.1, 1984.)

10.2 Contaminants from Coal Gasification

A list of contaminant levels that result from various coal gasification processes is presented in Table 10-1. The contaminant levels obtained after a first stage of hot gas cleanup with zinc ferrite also are listed.

Table10-1 Typical Contaminant Levels Obtained from Selected Coal Gasification Processes

Parameters	Coal Gasification Process		
	LURGI Fixed Bed	**METC (raw gas) Fixed Bed**	**Cleaned Gas**
Max. Product Temp. (EC)	750	1300	<800
Gasification	O_2 blown	Air blown	Regenerative
Pressure (psi)	435	220	150
Product Gas (EC)	600	650	<700
Methane (vol percent)	11	3.5	3.5
Coal type	Sub-bitum. Navajo	Sub-bitum. New Mexico	(Humidified Output)
Particulates (g/l)	0.016	0.058	0.01 est.
Sulfur (ppm) (Total H_2S, COS, CS_2, mercaptans)	2,000	5,300	<10
NH_3 (vol percent)	0.4	0.44	0.25
Trace metals (ppm)			
As	2	NS[a]	NS
Pb	0.8	2	1.7
Hg	0.4	NS	NS
Zn	0.4	NS	140
Halogens (ppm)	200	700	500
Hydrocarbons (vol percent)			
C_2H_6	1	NS	NS
C_2H_4	1	0.3	NS
C_2H_2	1	NS	NS
Oil tar	0.09	NS	NS

a - Not specified

Source: A. Pigeaud, Progress Report prepared by Energy Research Corporation for U.S. Department of Energy, Morgantown, WV, Contract No. DC-AC21-84MC21154, June 1987.

10.3 Selected Major Fuel Cell References, 1993 to Present

Books on Fuel Cells:

1. A.J. Appleby, F.R. Foulkes, *Fuel Cell Handbook*, Van Norstand Reinhold, New York, N.Y., 1989. Republished by Krieger Publishing Company, Melborne, FL, 1993.

2. L.J. Blomen, M.N. Mugerwa, editors, *Fuel Cell Systems*, ISBN 0-306-44158-6, Kluwer Academic Publishers, 1994.

3. M. Corbett, Opportunities in Advanced Fuel Cell Technologies – Volume One – Stationary Power Generation 1998-2008, Kline & Company, Inc., Fairfeild, NJ, 1998.

4. EscoVale Consultancy Services, *Fuel Cells: The Source Book.*

5. S. Gottesfeld, T.A. Zawodzinski, "Polymer Electrolyte Fuel Cells," *Advances in Electrochemical Science and Engineering*, *Volume 5,* edited by R.C. Alkire, et al., Wiley-VCH, 1998.

6. G. Hoogers, *Fuel Cell Technology Handbook,* CRC Press, ISBN: 0849308771 August, 2002.

7. T. Koppel, *Powering the Future: The Ballard Fuel Cell and the Race to Change the World*, John Wiley & Sons, ISBN: 047-1646296, 2001.

8. K. Kordesch, G. Simander, *Fuel Cells and Their Applications*, VCH Publishers, New York, N.Y., ISBN: 3-527-28579-2, 1996.

9. J. Larminie, A. Dicks, *Fuel Cell Systems Explained,* John Wiley and Sons, ISBN: 0-471-49026-1, 2000.

CD's on Fuel Cells:

1. Fuel Cell Handbook, 6th Edition - November 2002. The latest technical specifications and description of fuel cell types. Prepared by EG&G Technical Services and Science Applications International Corporation for the National Energy Technology Laboratory.

2. Distributed Generation Primer – May 2002. This CD provides the background for decision makers to evaluate the options, market conditions, drivers and issues related to successful use of distribution generation. Prepared by Science Applications International Corporation and EG&G Technical Services for the National Energy Technology Laboratory.

3. Hybrid Fuel Cell Technology Overview - May 2001. Prepared by Energy and Environmental Solutions for the National Energy Technology Laboratory.

Periodicals and Newsletters:

1. Advanced Fuel Cell Technology – monthly. Published by Seven Mountains Scientific, Inc. Boalsburg, PA 16827. Online subscription available at http://www.7ms.com/fct/index.html

2. Alternative Fuel News – quarterly. Published by U.S. Department of Energy's Alternative Fuel Data Center and the Clean Cities Program. Available online at http://www.eere.energy.gov/cleancities/ccn/archive/archive.html#afn

3. Clean Fuels and Electric Vehicles Report – Published 4 times per year. Published by Energy Futures, Inc. Boulder, CO 80306. Online subscription available at www.energy-futures.com/

4. Electrifying Times – 3 issues per year. Published by Bruce Meland, Bend, Oregon 97701. Table of contents and past issue archives available online at www.electrifyingtimes.com/

5. Fuel Cell Catalyst – quarterly. Published by U.S. Fuel Cell Council and National Fuel Cell Research Center and sponsored by National Energy Technology Laboratory. To subscribe http://lb.bcentral.com/ex/manage/subscriberprefs.aspx?customerid=9927

6. Fuel Cell Connection – monthly e-mail. Published by U.S. Fuel Cell Council and National Fuel Cell Research Center and sponsored by National Energy Technology Laboratory. To subscribe http://lb.bcentral.com/ex/manage/subscriberprefs.aspx?customerid=9927

7. Fuel Cell Industry Report – monthly. Published by Scientific American Newsletter, New York, NY 10003. To subscribe http://www.sanewsletters.com/fcir/FCIRinfo.asp

8. Fuel Cell Magazine – a supplement in March, June, September 2002 issues of Battery Power Products and Technology. Will be standalone bimonthly magazine in October 2002. To subscribe http://www.fuelcell-magazine.com

9. Fuel Cell Quarterly – quarterly. Published by Fuel Cells 2000, Washington DC 20006. To subscribe: http://www.fuelcells.org/info/pub_fcq.html

10. Fuel Cell Technology News – monthly. Published by Business Communications Company, Inc. Norwalk, CT 06855.

11. Fuel Cell World – quarterly (in German). Published by World Fuel Cell Council, Frankfurt am Main, Germany.

12. Fuel Cells Bulletin – monthly. Published by Elsevier Advanced Technology, Kidlington, Oxford OX5 1AS, United Kingdom. For ordering information: http://www.sciencedirect.com/science?_ob=JournalURL&_cdi=6202&_auth=y&_acct=C000058399&_version=1&_urlVersion=0&_userid=2638189&md5=cf981e59da40bc59c7a73e84e672c33e

13. Fuel Cells: From Fundamentals to Systems – Journal. Published by Wiley – VCH. Online ordering information: http://www.interscience.wiley.com/jpages/1615-6846/

14. Hybrid Vehicles – bimonthly. Published by Energy Futures, Inc. Boulder, CO 80306. Online subscription available at www.energy-futures.com/

15. Hydrogen and Fuel Cell Letter – monthly. Published by Peter Hoffman, Rhinecliff, NY 12574. Headlines and ordering information available online at www.hfcletter.com/

16. The Hydrogen – Gazette – Newsletter published by HyWeb and the German Hydrogen Association. Available online at www.hydrogen.org

17. Hydrogen Mirror / Wasserstoff-Spiegel – bimonthly. Published by Deutscher-Wasserstoff-Verband (German Hydrogen Association). To subscribe http://www.dwv-info.de/e/

18. International Journal of Hydrogen Energy – monthly. Published by Elsevier Advanced Technology, Kidlington, Oxford OX5 1AS, United Kingdom. For ordering information: http://www.sciencedirect.com/science?_ob=JournalURL&_cdi=5729&_auth=y&_acct=C000058399&_version=1&_urlVersion=0&_userid=2638189&md5=d022b0d976d72b556eb2f49a97c97601

19. Journal of Power Sources - monthly. Published by Elsevier Advanced Technology, Kidlington, Oxford OX5 1AS, United Kingdom. For ordering information: http://www.sciencedirect.com/science?_ob=JournalURL&_cdi=5269&_auth=y&_acct=C000058399&_version=1&_urlVersion=0&_userid=2638189&md5=32db478e73fce31e72368c9928505ff4

20. Platinum Metals Review – quarterly. Published by Johnson Matthey PLC, London, United Kingdom. Available online at http://www.platinum.matthey.com/publications/pmr.php

21. SCNG News – monthly. Published by the U.S. Department of Energy's Strategic Center for Natural Gas. Available online at http://www.netl.doe.gov/scng/news/news_toc.html

Proceedings and Abstracts from Major U.S. Fuel Cell Conferences:

1. *Fuel Cell Seminar, Programs and Abstracts*, Fuel Cell Seminars, sponsored by Fuel Cell Seminar Organizing Committee. For information visit web site at: http://www.fuelcellseminar.com/index.asp

   November /December 1994 – San Diego, California.
   November 1996 – Orlando, Florida.
   November 1998 – Palm Springs, California.
   November 2000 – Portland, Oregon.
   November 2002 – Palm Springs, California.
   November 2003 – Miami, Florida.
   November 2004 – San Antonio, Texas

2. *Proceedings of the Annual Fuel Cells Review Meeting*. Meetings held annually at the U.S. DOE Morgantown Energy Technology Center (now the National Energy Technology Laboratory), Morgantown, WV, until 1998, then at U.S. locations:

   DOE/METC-94/1010, August 1994
   DOE/METC-95/1020, August 1995
   DOE/METC CD-ROM, August 1996
   DOE/FETC–98/1054 CD-ROM, August 1997
   Joint DOE/EPRI/GRI Workshop on Fuel Cell Technology, May 1998, San Francisco, CA
   Joint DOE/EPRI/GRI Workshop on Fuel Cell Technology, August 1999, Chicago, IL

3. *EPRI/GRI Fuel Cell Workshop on Technology Research and Proceedings*, Cosponsored by EPRI and GRI, Proceedings by EPRI, Palo Alto, CA, March 1994.

   March 1994, Atlanta, Georgia
   April 1995, Irvine, California.
   April 1996, Temple, Arizona
   In 1997, the EPRI/GRI Workshop joined with the DOE Annual Fuel Cells Contractors Meeting. See Item 2 for information in 1997 and beyond.

4. J.R. Selman, et al., ed. *Carbonate Fuel Cell Technology IV*, Proceedings Vol. 97-4, Montreal, Canada, The Electrochemical Society, Inc., Pennington, NJ, 1997.

5. K. Hemmes, et al*., Proceedings of the Fifth International Symposium on Molten Carbonate Fuel Cell Technology*, Honolulu, Hawaii, The Electrochemical Society, Inc., Pennington, NJ, October 1997.

6. S.C. Singhal, et al., *Proceedings at the Fourth International Symposium on Solid Oxide Fuel Cells*, Proceedings Vol. 95-1, Yokohama, Japan, The Electrochemical Society, Inc., Pennington, NJ, 1995.

7. S.C. Singhal, et al., *Proceedings of the Fifth International Symposium on Solid Oxide Fuel Cells*, Proceedings Vol. 97-40, Aachen, Germany, The Electrochemical Society, Inc., Pennington, NJ, 1997.

8. S.C. Singhal, et al., *Proceedings of the Sixth International Symposium on Solid Oxide Fuel Cells*, Proceedings Vol. 99-19, Honolulu, Hawaii, The Electrochemical Society, Inc., Pennington, NJ, 1999.

9. A.R. Landgrebe, S. Gottesfeld*, First International Symposium on Proton Conducting Membrane Fuel Cells*, Chicago, IL, Proceedings Vol. 95-23, The Electrochemical Society, Inc., Pennington, NJ, 1995.

10. S. Gotts, et al., *Second International Symposium on Proton Conducting Membrane Fuel Cells*, Boston, MA, The Electrochemical Society, Inc., Pennington, NJ, 1998.

11. *Proceedings of the Workshop on Very High Efficiency Fuel Cell/Gas Turbine Power Cycles*, edited by M.C. Williams, C.M. Zeh, U.S. DOE Federal Energy Technology Center, Morgantown, WV, October 1995.

12. *Proceedings of the National Hydrogen Association Meetings*, National Hydrogen Association, usually in Alexandria, VA, annually in spring.

13. *Proceedings of the Intersociety Energy Conversion Engineering Conference*. Sponsorship of meeting rotates among six technical societies. Meetings are held annually (usually in August) in different cities of the United States:

    29th - Part 2, Sponsor - American Institute of Aeronautics and Astronautics, Monterey, CA, August 1994.
    30th - Volume 3, Sponsor - American Society of Mechanical Engineers, Orlando, Fl, August 1995.
    31st - Volume 2, Sponsor - Institute of Electrical and Electronics Engineers, Washington, D.C., August 1996.
    32nd - Sponsor - American Institute of Chemical Engineers, Honolulu, Hawaii, July/August 1997.
    33rd - CD-ROM, Sponsor - American Nuclear Society, Colorado Springs, Colo., August 1998.
    34th - CD-ROM, Sponsor – Society of Automotive Engineers, Vancouver, BC, August 1999.
    35th – Sponsor - American Institute of Aeronautics and Astronautics, Las Vegas, NV, July 2000.
    36th – Sponser - American Society of Mechanical Engineers, Savannah, Georgia, July 2001.

14. *Proceedings of the 58th American Power Conference*, Volume 58-1, Sponsored by Illinois Institute of Technology, Chicago, IL, 1996.

15. *Proceedings of U.S. Russian Workshop on Fuel Cell Technologies*, Sandia National Laboratories, Albuquerque, N.M., September 1995.

16. *Lake Tahoe Fuel Cell Conference Proceedings*, Desert Research Institute, Energy & Environmental Engineering Center, P.O. Box 60220, Reno, NV 69506-0220, July 1998.

17. *Next Generation Fuel Cells Workshop: Workshop Proceedings* – National Energy Technology Laboratory (formerly Federal Energy Technology Center), Morgantown, WV, December 1998.

18. *Proceedings of the NETL Workshop on Fuel Cell Modeling*, National Energy Technology Center, Morgantown, WV, April 2000.

19. *Proceedings of the Second Annual Small Fuel Cells & Batteries Conference*, New Orleans, LA, The Knowledge Foundation, Brookline, MA, April 2000.

20. *Proceedings of the U.S. DOE Natural Gas/Renewable Energy Hybrids Workshops.* Morgantown, WV. Proceedings can be found online at http://www.netl.doe.gov/publications/proceedings/01/hybrids/hybrid01.html

21. *Proceedings of the Second DOE/UN International Conference and Workshop on Hybrid Power Systems.* April 16-17, 2002. Proceedings can be found online at http://www.netl.doe.gov/publications/proceedings/02/Hybrid/hybrid02.html

22. *Proceedings of the Solid State Energy Conversion Alliance Workshops,* SECA is coordinated by the National Energy Technology Center and Pacific Northwest National Laboratory. Proceedings can be found online at: http://www.netl.doe.gov/scng/seca/past-events.html

First Workshop	Baltimore, Maryland	June 2000
Second Workshop	Arlington, Virginia	March 2001
Third Workshop	Washington, DC	March 2002
Fourth Workshop	Seattle, Washington	April 2003

23. *Proceedings of the Fuel Cell Summits on Codes and Standards*, Originated in the Department of Energy's Office of Building Equipment, State and Community Programs, but has now transferred to the Departments Office of Power Technologies. Results of the Summits can be found online at: http://www.pnl.gov/fuelcells/summits/

Summit I	April 1997
Summit II	May 1998
Summit III	April 1999
Summit IV	May 2000
Summit V	May 2001
Summit VI	May 2002
Summit VII	May 2003
Summit VIII	June 2004

Other Important Information on Fuel Cells:

1. U.S. DOE, *Fuel Cell Program Plans*, published each Fiscal Year by U.S. Department of Energy, Assistant Secretary of Fossil Energy:

   1994 - DOE/FE-0311P
   1995 - DOE/FE-0335
   1996 - DOE/FE-0350

2. NEDO, *Research and Development on Fuel Cell Power Generation Technology*, published yearly by the New Energy and Industrial Technology Development Organization, Tokyo, Japan.

3. *Fuel Cell RD&D in Japan*, Published annually by the Fuel Cell Development Information Center c/o The Institute of Applied Energy, Tokyo, Japan, usually in August.

4. *Proceedings of the Grove Anniversary Fuel Cell Symposium*, London, UK, September 1995, Journal of Power Sources, Elsevier Sequoia Science, The Netherlands, January 1995.

5. *Proceedings of the Grove Anniversary Fuel Cell Symposium*, London, UK, September 1997, Journal of Power Sources, Elsevier Sequoia Science, The Netherlands, March 1998.

6. *Proceedings of the 6th Grove Anniversary Fuel Cell Symposium*, London, UK, September 1999, Journal of Power Sources, Elsevier Sequoia Science, The Netherlands, March 2000.

7. *Proceedings of the 7th Grove Anniversary Fuel Cell Symposium*, London, UK, September 2001, Journal of Power Sources, Elsevier Sequoia Science, The Netherlands. For information see http://www.grovefuelcell.com/

8. U. Bossel, editor, *Proceedings of the European Solid Oxide Fuel Cell Forums*, European Fuel Cell Group and IEA Advanced Fuel Cell Programme, 1994, 1996, 1998.

9. Various Technical Reports Posted on the Strategic Center for Natural Gas Fuel Cell Reference Shelf. Available online at http://www.netl.doe.gov/scng/enduse/fc_refshlf.html

10.4 List of Symbols

Abbreviations:

®	registered
AACE	Association for the Advancement of Cost Engineering
A.R.	as received
ABS	acrylonytril-butadiene-styrene
AES	air electrode supported
AFC	alkaline fuel cell
AFV	alternative fuel vehicle
ANL	Argonne National Laboratory
APU	auxiliary power unit
ASF	amps/ft^2
ASME	American Society of Mechanical Engineers
ASR	area specific resistance
ASU	air separation unit
CC	capital cost
CEC	California Energy Commission
CFD	computational fluid dynamics
CHP	combined heat and power
COE	cost of electricity
CVD	chemical vapor deposition
DIR	direct internal reforming

DOE	Department of Energy
EMF	electromotive force
EV	electric vehicle
EVD	electrochemical vapor deposition
FC	fuel cost
FCE	Fuel Cell Energy
FEP	fluoro-ethylene-propylene
FETC	Federal Energy Technology Center
GDL	gas diffusion layer
H	annual plant operating hours
HEV	hybrid electric vehicle
HHV	higher heating value
HR	heat rate
HRB	heat recovery boiler
IIR	indirect internal reforming
IEC	International Electrotechnical Commission
IEEE	Institute of Electrical and Electronics Engineers
INEEL	Idaho National Engineering and Environmental Laboratory
iR	ohmic loss
ITSOFC	intermediate temperature solid oxide fuel cell
J-M	Johnson Mathey Technology Center
LHV	lower heating value
MCFC	molten carbonate fuel cell
MEA	membrane/electrode assembly
NETL	National Energy Technology Laboratory
NFPA	National Fire Protection Association
NREL	National Renewable Energy Laboratory
O&M	operating and maintenance costs
ODS	oxide dispersion strengthened anode
OS/IES	on-site/integrated energy systems
PAFC	phosphoric acid fuel cell
PC	phthalocyanines
PEFC	polymer electrolyte fuel cell
PEM	proton exchange membrane
PMSS	pyrolysis of metallic soap slurry
PNNL	Pacific Northwest National Laboratory
PR	pressure ratio
Pt	platinum
PTFE	polytetrafluoroethylene
RDF	refuse derived fuel
SAE	Society of Automotive Engineers
SCF	standard cubic feet
SMR	steam methane reforming
SOFC	solid oxide fuel cell
TAA	tetraazaannulenes
TBA	tetrabutyl ammonium

tcf	trillion cubic feet
TFMSA	trifluoromethane sulfonic acid
THT	tetrahydrothiophene (thiophane)
TMPP	tetramethoxyphenylporphyrins
TPB	triple phase boundary
TPP	tetraphenylporphyrins
TSOFC	tubular solid oxide fuel cell
TZP	tetragonal phase
™	trade mark
UL	Underwriters' Laboratories, Inc.
U.S.	United States of America
WSF	watts/ft^2
YSZ	yttria stabilized zirconia
ZEV	zero-emission vehicle

Letter Symbols:

ΔE	potential difference
ΔG	Gibbs free energy
ΔH_c	heat available from combustion of fuel gas
ΔH_r	enthalpy of reaction
ΔS_r	entropy of reaction
ΔV	voltage difference
<D>	equilibrium pore size
a	$(-2.3RT/\alpha n\mathit{F})$ log i_o
a	acceleration
A	area
a	coefficient
AC	alternating current
b	$2.3RT/\alpha n\mathit{F}$
b	coefficient
b	Tafel slope
Btu	British Thermal Unit
c	coefficient
C_B	bulk concentration
C_D	drag coefficient
C_p	heat capacity
C_R	coefficient of rolling resistance
C_S	surface concentration
D	diffusion coefficient
D	pore diameter
dBA	average decibles
DC	direct current
e^-	electron
E	equilibrium (reversible) potential
E°	standard potential

E_a	activation energy
$\boldsymbol{F}$	Faraday's constant
f	fugacity
f	gas flow rate
g	gravitational constant
G	Gribbs free energy
H	enthalpy
hrs	hours
I	current
i	current density
i_L	limiting current density
i_o	exchange current density
J	current density
K	equilibrium constant
k(T)	constant, function of temperature
kW	kilowatt
lb	pound
m	mass
m	mass flow rate
MM	million
mol	mole
MW	molecular weight
MW	megawatt (1000 kW)
MWhr	megawatt-hour
n	mole flow rate
n	number of electrons participating in a reaction
n_{max}	maximum stoichiometric value
p	power
P	pressure
P_i	partial pressure
ppm	parts per million
P_T	total pressure
Q	heat duty
R	cell resistance
R	universal gas constant
S	entropy
t	electrolyte thickness
T	temperature
U	utilization
V	cell voltage
v	rate at which reactant species are consumed
v	velocity
V	volume
V_c	voltage of single cell
vol	volume
W_{el}	maximum electrical work

wt	weight
X	mole fraction
yr	year

Greek Letter Symbols:

α	road angle of incline
α	electron transfer coefficient
β	hydrogen utilization
ε	motor efficiency
γ	interfacial surface tension
γ	oxidant utilization
δ	diffusion layer thickness
η	thermal efficiency
η_{act}	activation polarization
η_{conc}	concentration polarization
η_{ohm}	ohmic polarization
θ	electrolyte contact angle
θ_{CO}	CO coverage
k	air density

Subscripts:

a	anode
c	cathode
e	electrolyte
f	fuel
i	species
in	cell inlet
out	cell outlet
ox	oxygen or oxidant
p	pressure
t	temperature

10.5 Fuel Cell Related Codes and Standards

10.5.1 Introduction

The rapid development and application of fuel cells throughout the world has created the need for fuel cell technology related codes and standards. Several organizations and committees are currently working on the development of codes and standards related to fuel cells.

According to the National Fire Protection Agency (NFPA) Regulations Governing Committee Projects, codes and standards are defined as follows:

Code: A standard that is an extensive compilation of provisions covering broad subject matter or that is suitable for adoption into law independently of other codes and standards.

***Standard*:** A document, the main text of which contains only mandatory provisions using the word "shall" to indicate requirements and which is in a form generally suitable for mandatory reference by another standard or code or for adoption into law. Non-mandatory provisions shall be located in an appendix, footnote, or fine-printnote and are not to be considered a part of the requirements of a standard.

This section provides a brief overview of the existing and developing codes and standards related to fuel cell technologies. The discussion focuses on participating organizations, specific codes and standards, and more generally applied codes and standards (e.g., the Uniform Building Code) that apply to system installation.

10.5.2 Organizations

Below is a listing and brief description of organizations involved in the development of codes and standards pertaining to fuel cell technology.

American National Standards Institute (ANSI): ANSI has served in its capacity as administrator and coordinator of the United States private sector voluntary standardization system for 80 years. The Institute is a private, non-profit membership organization supported by a diverse constituency of private and public sector organizations. ANSI Z21.83 has been published and provides a means of testing and certifying the safety of stationary fuel cell power plants having a capacity of less than 1 MW.

American Society of Mechanical Engineers (ASME): ASME is an international engineering society that conducts one of the world's largest technical publishing operations. ASME International is a non-profit educational and technical organization serving a worldwide membership. Its mission is to promote and enhance the technical competency and professional well-being of engineers through programs and activities in mechanical engineering. To this end, ASME has developed the Boiler and Pressure Vessel Code, which is referenced as part of the AGA certification. Additionally, ASME issued a fuel cell standard, ASME PTC 50, Performance Test Code on Fuel Cell Power Systems Performance.

Institute of Electrical and Electronics Engineers (IEEE): The mission of IEEE is to advance global prosperity by promoting the engineering process of creating, developing, integrating, sharing, and applying knowledge about electrical and information technologies. IEEE Standards Coordinating Committee 21 (SCC21) oversees the development of standards in the area of fuel cells, photovoltaics, distributed generation, and energy storage. SCC21 coordinates efforts in these fields among the various IEEE societies and other appropriate organizations to ensure that all standards are consistent and properly reflect the views of all applicable disciplines. Working Group 1547 - Standard for Distributed Resources Interconnected with Electric Power Systems - establishes criteria and requirements for interconnection by distributed resources with electric power systems. The purpose is to provide a uniform standard for interconnection of distributed resources with electric power systems and requirements relevant to the performance, operation, testing, safety considerations, and maintenance of the interconnection.

International Code Council (ICC): The International Code Council was established in 1994 as a non-profit organization dedicated to developing a single set of comprehensive and coordinated national model construction codes without regional limitations.

International Electrotechnical Commission (IEC): The IEC is the world organization that prepares and publishes international standards for all electrical, electronic, and related technologies. The membership consists of more than 50 participating countries, including all of the world's major trading nations and a growing number of industrialized countries. The IEC's mission is to promote, through its members, international cooperation on all questions of electrotechnical standardization and related matters, such as the assessment of conformity to standards, in the fields of electricity, electronics, and related technologies. The IEC charter embraces all electrotechnologies including electronics, magnetics and electromagnetics, electroacoustics, telecommunication, and energy production and distribution, as well as associated general disciplines such as terminology and symbols, measurement and performance, dependability, design and development, safety, and the environment.

The National Fire Protection Association (NFPA): NFPA is non-profit organization that publishes the National Electrical Code®, the Life Safety Code®, the Fire Prevention Code™, the National Fuel Gas Code®, and the National Fire Alarm Code®. The mission of NFPA is to reduce the worldwide burden of fire and other hazards on the quality of life by providing and advocating scientifically based consensus codes and standards, research, training, and education. NFPA 853, "Standard for the Installation of Stationary Fuel Cell Power Plants" covers the design, construction, and installation of stationary fuel cells of at least 50 kW output.

Society of Automotive Engineers (SAE): SAE is a resource for technical information and expertise used in designing, building, maintaining, and operating self-propelled vehicles for use on land, sea, air, or in space. Composed of nearly 80,000 engineers, business executives, educators, and students from more than 97 countries, the network of members share information and exchange ideas for advancing the engineering of mobility systems. Technical committees write more new aerospace and automotive engineering standards than any other standards-writing organization in the world. In late 1999, a Fuel Cell Standards Forum was created to establish standards and test procedures for fuel cell powered vehicles. It will address the safety, performance, reliability, and recyclability of fuel cell systems in vehicles with an emphasis on efficiency and environmental impact.

Underwriters Laboratories Inc. (UL): UL is an independent, not-for-profit product safety testing and certification organization. UL has tested products for public safety for more than a century with more than 14 billion UL Marks applied to products worldwide. UL has developed a standard for inverters that can be applied to fuel cells.

10.5.3 Codes & Standards

A summary of existing and pending fuel cell related codes and standards is presented in Table 10-2. More detailed descriptions are provided subsequently based on their specific area of application.

Table 10-2 Summary of Related Codes and Standards

CODE/STANDARD	ORGANIZATION	SUMMARY
1. PTC 50	ASME	***Performance Test Code*** - Provides test procedures, methods, and definitions for the performance characterization of fuel cell power systems.
2. IEEE SCC 21	IEEE	***Standards coordinating committee*** - Fuel cells, photovoltaics, dispersed generation and energy storage
3. IEEE P1547	IEEE	***DG Interconnection Standard*** - Establishes criteria and requirements for interconnecting distributed resources with electric power systems
4. ANSI Z21.83-1998	ANSI	***Product Standard*** - Provides detailed test and examination criteria for fuel cell power plants that use natural and liquefied petroleum gases.
5. NFPA 853	NFPA	***Installation Standard*** - Applies to installation of stationary fuel cell power plants.
6. NEC/NFPA 70 Article 690,691 & 705	NFPA	690 – Solar Photovoltaic Systems 691 – Fuel Cells 705 – Interconnected Power Production Sources
7. IEEE SCC 36	IEEE	***Standards Coordinating Committee*** - Pertains to utility communications
8. UL 1741	UL	***Electric Inverters*** - Standard for testing, listing and safety certification for inverters
9. SAE Standards Forum	SAE	***Vehicle Standards*** - In the early stages of developing standards for safety, performance, reliability, and recyclability. Also establish testing procedures.
10. IEC TC 105	IEC	***Technical Committee 105*** – Seeking to expand the scope of ANSI Z21.83 for international basis and additional fuel cell technologies.
11. IMC 2000/ 924	ICC	***Installation Standard*** – Must be in compliance with ANSI Z21.83.

10.5.4 Codes and Standards for Fuel Cell Manufacturers

ANSI Z21.83: American National Standard - Fuel Cell Power Plants provides a means of testing and certifying the safety of stationary fuel cell power plants with a nominal electric capacity not exceeding 1.0 MW. This standard is intended for applications other than residential when installed outdoors and operated on a gaseous hydrocarbon as the reactant. The current version of

the standard is based on two specific fuel cell technologies and is being revised to take into consideration the characteristics of additional fuel cell power plant technologies. Many state and local regulatory authorities have adopted this standard.

ASME PTC 50: ASME Performance Test Code 50 - Fuel Cell Power Systems provides test procedures, methods, and definitions for the performance characterization of fuel cell power systems. The code specifies the methods and procedures for conducting and reporting fuel cell system ratings. Specific methods of testing, instrumentation, techniques, calculations and reporting are presented.

IEC TC 105: The International Electrotechnical Committee has established a Technical Committee charged with the preparation of an international standards regarding fuel cell technologies for all fuel cell applications including stationary power plants, transportation propulsion systems, transportation auxiliary power units, and portable power generation systems. The standards will have four parts: Terminology and Definitions, Stationary Fuel Cell Systems, Fuel Cell Systems in Transportation, and Portable Fuel Cell Systems. The committee was established in 2000 and plans to have the standards approved and published in 2004.

IEEE SCC21/P1547: The Institute of Electrical and Electronic Engineers has established a Standards Coordinating Committee (SCC 21) chartered with the development of a standard for the interconnection of distributed resources. This standard focuses on electrical interface standards for the application of distributed generation technologies described as fuel cells, photovoltaics, dispersed generation, and energy storage. The resulting standard will be IEEE P1547, which will establish criteria and requirements for the interconnection of distributed resources with electric power systems.

IEEE SCC 36: This committee reviews, recommends, and solicits the development of standards relevant to the gas, water, and electric utility industries on a worldwide basis with respect to utility communication architecture. This SCC coordinates standards-development activities with other relevant IEEE groups and sponsors standards-development activities that are appropriate to the needs of the utility industry.

IMC 2000/ 924.1**:** The International Code Council develops the International Mechanical Code. Section 924.1 of the IMC 2000 requires stationary fuel cell power plants not exceeding 1,000 kW to be tested and listed to ANSI Standard Z21.83.

ISO TC 197**:** The International Organization for Standardization has developed a committee to develop international safety standards for the production, storage, transport, measurement, and use of hydrogen.

UL 1741: Underwriters Laboratory 1741 is a standard for the testing, listing, and safety certification for electric inverters. This standard is for static inverters and charge controllers for use in photovoltaic power systems, but may be used for fuel cells.

10.5.5 Codes and Standards for the Installation of Fuel Cells

NFPA 853: National Fire Protection Association 853 - Standard for Fuel Cell Power Plants provides a standard for the design, construction, and installation of stationary packaged, self contained, and field constructed fuel cell power plants with a capacity greater than 50 kW.

NFPA 70: National Fire Protection Association 70 is also known as the National Electric Code (NEC). Revisions and addenda to the code have been developed that specifically address fuel cells. Article 690 - Solar Photovoltaic Systems has been targeted for revision to include fuel cells and alternate energy sources systems. This proposal is not expected to be approved since the technological and operational differences between fuel cells and photovoltaic systems are considerable. A new article, Article 692 deals with rules covering fuel cell systems for buildings or residential dwellings. This standard addresses the electrical interface between the fuel cell system and a building's electrical distribution panel. NFPA Article 705 - Interconnected Electrical Power Production Sources has also been revised to address fuel cell power sources.

10.5.6 Codes and Standards for Fuel Cell Vehicles

SAE established a Fuel Cells Standard Forum that is chartered with the establishment of standards and test procedures for fuel cell powered vehicles. The committee was established in 1999. The standards will cover the safety, performance, reliability, and recyclability of fuel cell systems in vehicles with emphasis on efficiency and environmental impact. The standards will also establish test procedures for uniformity in test results for the vehicle/systems/components performance, and define interface requirements of the systems to the vehicle. Working Groups have been formed in the areas of safety, performance, emissions, recyclability, interface, and terminology. The working groups have created the following documents:

J2572 – Draft - Recommended Practice for Measuring the Exhaust Emissions, Energy Consumption and Range of Fuel Cell Powered Electric Vehicles Using Compressed Gaseous Hydrogen.
J2574 – Published March 2002 - Fuel Cell Electric Vehicle Terminology.
J2578 – Published December 2002 – Recommended Practices for General Fuel Cell Vehicle Safety.
J2579 – Draft – Recommended Practices for Hazardous Fluid Systems in Fuel Cell Vehicles.
J2594 – Published September 2003 – Recommended Practice to Design for Recycling Proton Exchange Membrane (PEM) Fuel Cell Systems.
J2600 – Published October 2002 – Compressed Hydrogen Surface Vehicle Refueling Connection Devices.
J2601 – Draft – Compressed Hydrogen Vehicle Fueling Communication Devices.
J2615 – Draft – Performance Test Procedure of Fuel Cell Systems for Automotive Applications.
J2616 – Draft – Performance Test Procedure for the Fuel Processor Subsystem of Automotive Fuel Cell System.
J2617 – Draft – Performance Test Procedure of PEFC Stack Subsystem for Automotive Applications.

10.5.7 Application Permits

The installation of stationary fuel cells requires adherence to a variety of building codes. In April 2001, The National Evaluation Service published a "Protocol for Evaluation of Stationary

Fuel Cell Power Plants." This is used by NES to facilitate the process of evaluating stationary fuel cell power plant technology for compliance to all codes. A few of the major codes are summarized below.

International Mechanical Code 2000: Published by the International Code Council. At the present time, it is the only code to provide specific guidance on stationary fuel cell power plants.

Uniform Building Code: The Uniform Building Code (UBC) is the most widely-adopted model building code in the world, and is a proven document meeting the needs of government units charged with enforcement of building regulation. Published triennially, the UBC provides complete regulations covering all major aspects of building design and construction relating to fire and life safety and structural safety. The requirements reflect the latest technological advances in the building and fire and life-safety industry.

Uniform Mechanical Code: Provides a complete set of requirements for the design, construction, installation, and maintenance of heating, ventilating, cooling and refrigeration systems, incinerators, and other heat-producing appliances.

Uniform Plumbing Code: Published by the International Association of Plumbing and Mechanical Officials (IAPMO), the Uniform Plumbing Code covers all aspects of plumbing, including requirements for plumbing materials and IAPMO installation standards.

National Electric Code: The National Electrical Code (NFPA 70) provides "practical safeguarding of persons and property from hazards arising from the use of electricity." More specifically, the National Electric Code covers the installation of electric conductors and equipment in public and private buildings or other structures (including mobile homes, recreational vehicles, and floating buildings), industrial substations, and other premises (such as yards, carnivals, and parking lots). The National Electric Code also covers installations of optical fiber cable. Wiring, general electrical equipment, the use of electricity in specific occupancies (from aircraft hangars to health care facilities), and equipment (ranging from elevators to hot tubs) are covered, as well as special conditions (emergency and stand-by power, or conditions requiring more than 600 volts, for example) and communication systems.

National Fire Code: The National Fire Code consists of approximately 300 codes and standards as published by the National Fire Protection Association (NFPA). These codes address the practices to reduce the burden of fire on the quality of life by advocating scientifically based consensus codes and standards, research and education for fire and related safety issues. The most widely applied codes are:

(1.) NFPA 70 – National Electric Code
(2.) NFPA 101 – Life Safety Code
(3.) NFPA 30 – Flammable and Combustible Liquids Code
(4.) NFPA 13 – Standard for the Installation and Maintenance of Automatic Fire Sprinkler Systems

10.5.8 References

1. M. Glass, *Fuel Cell Codes and Standards Summit III Summary*, April 5-7, 1999, Pacific Northwest National Laboratory.
2. ASME, *Object & Scope for the Proposed Code on Fuel Cell Power Systems*, August 2000, http://www.asme.org.
3. IEEE, *Distributed Resources and Electrical Power Systems Interconnection Working Group - Meeting Minutes*, June 7-8, 2000, http://grouper.ieee.org.
4. SAE, *SAE Initiates Activities in Area of Fuel Cells*, August 1999, http://www.sae.org.
5. UL, *Standard for Safety for Static Inverters and Charge Controllers for Use in Photovoltaic Power Systems*, 2000, http//:ulstandardsinfonet.ul.com.
6. National Evaluation Service, *National Evaluation Protocol for Stationary Fuel Cell Power Plant*, June 5, 2000, http://www.nateval.org.
7. International Electrotechnical Commission, IEC TC 105 Strategic Policy Statement, March 2000, CA/1719A/R, http://www.iec.ch.
8. R. Bielen, *Telephone Contact*, August 9, 2000, NFPA.
9. S. Kazubski, *Telephone Contact*, August 14, 2000, CSA International.
10. D. Conover, *Telephone Contact*, August 9, 2000, National Evaluation Service.

10.6 Fuel Cell Field Site Data

This section of the handbook contains field site information. Most of the worldwide summaries were extracted from an IEA paper[63] and updated with information taken from "Fuel Cell Technology News"[64]. Information on the U.S. Department of Defense (DoD) Fuel Cell Demonstration was taken from the following web site: www.dodfuelcell.com. Finally, updating the information for Fuel Cell Energy, IFC, and Siemens Westinghouse was taken from "Fuel Cell Technology News". The IFC PAFC summary includes a number of projects reported by DoD. In the DoD demonstration program, a total of 30 PAFC units were installed at DoD sites across the United States. These were model B and C PC-25 units.

10.6.1 Worldwide Sites

Worldwide information reported in this handbook is for stationary application of fuel cells in different countries. Data on PEFC, PAFC, AFC, MCFC, and SOFC has been collected. The main worldwide projects are summarized below:

PEFC

Canada: Canada has focused primarily on PEFC research and development over the last decade. To commercialize its PEFC technology, Ballard Power Systems has developed a major international network of strategic partners, including DaimlerChrysler, Ford Motor Company, GPU international (US), Alstom SA (a UK company based in France), and Ebara Corporation (Japan). Ballard 250 kWe stationary prototypes are developed by Ballard Generation Systems. The first prototype operating is in Vancouver, Canada. Ballard delivered a second 250-kilowatt PEFC power system to Cinergy Technology. This is the first field trial unit built by Ballard. The

[63] K. Kono, "Implementing Agreement "Advanced Fuel Cells," Annex IX Fuel Cells for Stationary Applications, Subtask 2," draft IEA paper, April 1999.

[64] Fuel Cell Technology News, January 2002, published by Business Communications Company, Inc.

unit runs on natural gas, and was commissioned in 1999 at the Naval Surface Warfare Center in Crane, Indiana. A third unit in Berlin, Germany at Bewag Treptow Heating Plant started operating the second half of 1999. In 2001, Ballard completed 10-kW and 60-kW engineering prototype stationary fuel cell generators.

Japan: In 2002, Japan nearly doubled its fuel cell R&D budget to $220 million from $119 million. It created a new large-scale Polymer Electrolyte Fuel Cell Development Program to develop PEFC fuel cells for both transport and stationary applications, leaving molten carbonate fuel cell and solid oxide fuel cell R&D under the New Sunshine Program.

Ministry of International Trade and Industry (MITI, now METI) has been sponsoring five companies to develop PEFC technologies since 1992. Sanyo, Toshiba, and Mitsubishi Electric have been developing 2-kW, 10-kW, and 30-kW stacks, respectively. Asahi Chemical Industry and Asahi Glass are developing fuel cell components, including polymer membranes and separators, according to METI documents. In 2002, Japan nearly quadrupled its budget for PEFCs to $156 million and created a 10-year Polymer Electrolyte Fuel Cell Development program, which aims to develop PEFCs for both stationary and transport applications. Japan will equally focus on both stationary and transportation applications.

United States: Plug Power has installed over 300 residential systems for unattended operation. Plug Power delivered more than 106 5-kW grid-parallel systems through October 31, 2001, against its milestone of 125 to 150 units for the year. Deliveries included 44 units to the New York State Research & Development Authority and 57 systems to the Long Island Power Authority.

PAFC

Europe: The Energetic Utility of Milan, the National Agency for Energy, New Technology and Environment (ENEA), and Ansaido Ricerche designed, built, and tested a 1.3 MWe PAFC system in Milan. The powerplant had an actual capacity of 930 kW and an energy efficiency of 38 percent (LHV). It has operated for over 5,000 hours.

Japan: Fuji Electric developed a 100 kWe on-site system. To date, they have tested a 50 kW power plant using an innovative cell design that improves electrolyte management. They tested this stack (154 cells) for about 2,000 hours. They have tested 65, 50 kWe units for a total cumulative operating tome of over 1 million hours. They have tested 3, 500 kWe units for a total of 43,437 hours. Their latest design, FP100E, has been shown to have a net AC efficiency of 40.2 percent (LHV).

Mitsubishi Electric developed a 200 kWe class on-site powerplant. As of 2002, 11 units were operated in the field with applications ranging from an electric utility to a brewery factory. Four of the units operated for more than 2,000 hours.

AFC

United Kingdom: ZeTek Power, an UK based company with plants in the US and Europe, is developing alkaline fuel cells. They are putting AFCs in fleet vehicles and boats in Europe.

AFCs are getting greater than 50 percent efficiency over most of the power curve (5 to 95 percent). Capital cost for the AFC stack is $300/kWe, and approximately $700 for the system.

MCFC

Japan: Japan has been providing support to three companies to develop MCFC technology. Ishikawajima-Harima Heavy Industries and Hitachi developed 250-kW stacks and built a 1-MW MCFC pilot plant with an external reformer at Kawagoe, Mie Prefecture, consisting of four 250-kW stacks. The test operation started in July 1999 and ended in January 2000 after 5,000 hours of test operations. Since 2000, Japan has focused on commercialization and is supporting development of a pressurized 300-kW MCFC cogeneration system, followed by a 750-kW system to be completed in March 2004. Japan hopes to see commercialization start immediately thereafter, according to METI officials. Japan's budget was $17 million on MCFC R&D in 2002.

Europe: Italy and Spain have been working on research and development of MCFC systems as a collaborative project called MOLCARE program. The project has a budget of 10 billion pesetas (35 percent by Spain and 65 percent by Italy). They have partnered with industry to develop and conduct a 1,000-hour test on a 100 kWe unit.

The European Direct Fuel Cell Consortium carries out the largest European program for the commercialization of MCFC. They are developing an innovative direct fuel cell process which is internally reformed and operates on humidified hydrocarbon fuels. They have successfully tested a 292 cell, 155 kW stack (60 percent of maximum power).

United States: FuelCell Energy is developing an externally manifolded internally reformed MCFC. FuelCell Energy has reached the 50 MW manufacturing capacity and plans to have 400 MW capacity by 2004. They have also constructed a 400 kWe test facility. They have successfully completed the manufacture and test of 16 stack (4 modules), 2 MWe test in Santa Clara, California, for 4,000 hours. Details on Fuel Cell Energy field site are found in Table 10-3.

SOFC

Japan: The Kansai Electric Company has tested a four-cell stack and accumulated 10,529 hours of operation at high current densities and completed 101 thermal cycles. Tokyo Gas started research and development of a planar SOFC in 1993. They conducted a 1.7 kW module test with stable performance.

Australia: Ceramic Fuel Cells Limited demonstrated a 5 kWe laboratory prototype fuel cell in 1997. Their system has thin sheet steel components as interconnects in a planar fuel cell design. They are scaling up to a 25 kWe pre-commercial stack module.

Canada: Ontario Hydro has tested a single Siemens-Westinghouse cell for 1725 hours. Over 1425 of the hours were at elevated pressure of 5 atm.

Europe: The ELSAM/EDB project for a 100 kWe Siemens-Westinghouse SOFC field unit has operated from January 1998. The unit was to operate until January 2000 with a total of 17,500 test hours according to the plan.

Spain: A consortium called SEGE is developing an intermediate temperature planar fuel cell.

United States: Siemens Westinghouse projects on SOFC include a 250 kWe tubular prototype at the Irvine University campus (California), that is operated by Southern California Edison Company. It is pressurized to 3.5 bar and gives 200 kWe; a coupled microturbine gives an additional 50 kWe. The have operated a tubular SOFC at pressures up to 15 atm. Worldwide fuel cell installations and general information as of 2004 for installations are reported by Fuel Cells 2000 at http://www.fuelcells.org/ info/charts/FCInstallationChart.pdf.

10.6.2 DoD Field Sites

DoD's Climate Change Fuel Cell program included purchasing and installing 30 ONSI PC25 200 kWe PAFC at DoD installations in addition to providing rebates of $1,000/kW (up to 1/3 of the installed cost). Many factors determine the availability and efficiency of individual units; maintenance programs and application are two factors. The summary table, Table 10-3, provides information on operating hours, efficiency, and availability. The following website provides additional information on DoD field sites: www.dodfuelcell.com.

10.6.3 IFC Field Units

IFC provided DOE with information on their 59 fuel cell unit operating in North America. This information is provided in Table 10-4. Several of these units operate on DoD field sites and are reported in Table 10-3.

10.6.4 FuelCell Energy

FuelCell Energy provided DOE with information on their fuel cell field units. This information is provided in Table 10-5.

10.6.5 Siemens Westinghouse

Siemens Westinghouse provided DOE with information on their fuel cell field units. This information is provided in Table 10-6.

Table 10-3 DoD Field Site

Through January 31, 2002

SITE NAME	SERVICE	START DATE	OPER. HOURS	MWHRS OUTPUT	AVG kWe	ELEC. EFF.	AVAIL.
MODEL B UNITS							
Naval Station Newport	Navy	1/23/95	42,375	6,387.537	150.7	30.2%	76.1%
U.S. Army Soldier Systems Center	Army	1/27/95	38,608	6,379.235	165.2	31.2%	61.2%
US Military Academy	Army	11/17/95	28,393	4,872.371	171.6	31.5%	63.0%
934th Airlift Wing	Air Force	2/1/95	26,777	4,653.232	173.8	29.7%	48.2%
Picatinny Arsenal	Army	10/11/95	32,053	5,316.291	165.9	30.9%	62.4%
Naval Hospital MCB Camp Pendleton	Marines	10/6/95	26,859	4,507.218	167.8	33.9%	55.1%
Naval Hospital MCAGCC Twentynine Palms	Marines	6/20/95	21,652	3,522.419	162.7	32.3%	44.6%
Nellis AFB	Air Force	9/23/95	19,996	3,383.481	169.2	32.5%	38.7%
Watervliet Arsenal	Army	10/29/97	28,875	4,117.735	142.6	31.4%	77.3%
Fort Eustis	Army	9/12/95	27,705	4,256.532	157.2	31.9%	50.7%
Kirtland AFB	Air Force	7/20/95	16,713	2,502.970	149.8	31.0%	32.5%
Naval Oceanographic Office	Navy	10/7/97	19,641	3,574.854	182.0	34.6%	51.4%
Pine Bluff Arsenal	Army	10/21/97	9,343	1,747.040	187.0	34.9%	39.6%
CBC Port Hueneme	Navy	9/18/97	18,001	3,332.808	185.1	34.3%	46.3%
B's TOTAL/AVG:			356,991	58,553.723	164.3	32.2%	53.4%
MODEL C UNITS*							
911th Airlift Wing	Air Force	12/18/96	35,234	6,037.038	171.3	31.6%	79.8%
Naval Hospital NAS Jacksonville	Navy	3/18/97	33,284	6,193.403	186.1	31.6%	78.4%
NAS Fallon	Navy	3/30/97	31,054	4,880.720	157.2	30.8%	80.1%
Subase New London	Navy	9/30/97	32,848	5,884.840	179.2	31.8%	84.8%
Fort Richardson	Army	12/17/96	30,593	5,617.251	183.6	31.5%	68.1%
Little Rock AFB	Air Force	8/17/97	23,104	4,336.428	187.7	31.7%	68.2%
Westover AFB	Air Force	9/19/97	32,844	6,316.483	192.3	30.7%	86.3%
Barksdale AFB	Air Force	7/24/97	28,554	5,289.629	185.2	31.1%	72.0%
Fort Huachuca	Army	7/28/97	31,776	5,744.980	180.8	32.4%	80.3%
Laughlin AFB	Air Force	9/16/97	29,558	5,584.936	188.9	32.4%	77.0%
US Naval Academy	Navy	9/22/97	37,928	4,736.374	124.9	27.9%	80.9%
Edwards AFB	Air Force	7/5/97	23,866	4,603.664	192.9	32.6%	59.9%
Fort Bliss	Army	10/10/97	23,973	3,936.077	164.2	32.0%	63.6%
Davis-Monthan AFB	Air Force	10/14/97	26,462	4,513.985	170.6	32.1%	71.5%
NDCEE	Other	8/14/97	17,167	2,083.041	121.3	30.5%	58.1%
C's TOTAL/AVG:			438,245	75,758.849	172.9	31.4%	73.9%
B+C TOTAL/AVG:			795,236	134,312.570	169.0	31.8%	64.0%

Disclaimer

Electrical efficiency calculations include fuel cell idle time (such as when the fuel cell is awaiting the return to operation of the utility grid, etc.). If values were adjusted for idle time, fuel cell electrical efficiencies would be higher. ONSI fuel cells passed DoD Fuel Cell Program electrical efficiency criteria during unit acceptance tests (range = 33.5 to 37.2 percent, Higher Heating Value).

Availability values are not adjusted for times when the fuel cell was down for extended periods unrelated to typical fuel cell operation (delays in maintenance personnel response, site operating conditions, etc.). Adjusting for these times would result in higher availability values.

Table 10-4 IFC Field Units

PC25 C Fuel
Cell Power Plant
(Run hours, etc.
as of 8/4/00)

North America

	Status	Country/State	Site	Start Date	Load hrs	MW-hrs	
1	Active	SOUTH WINDSOR, CT	PROTOTYPE FOR R&D	N/A	N/A	N/A	0
2	Active	DEL RIO, TX	HOSPITAL	9/6/97	20,143	3,743.4	37181
3	Active	LITTLE ROCK, AR	HOSPITAL	10/6/97	21,408	3,872.6	36024
4	Active	SHREVEPORT, LA	HOSPITAL	7/18/97	19,577	3,786.3	35954
5	Active	GROTON, CT	CENTRAL BOILER PLANT	9/27/97	23,175	4,044.2	24942
6	Active	ANNAPOLIS, MD	DORMITORY	9/20/97	20,274	2,945.9	11593
7	Active	STATEN ISLAND, NY	CHEMICAL PLANT	8/22/96	27,412	4,940.3	28415
8	Active	ANCHORAGE, AK	YMCA	11/18/96	21,589	3,572.0	25504
9	Active	JACKSONVILLE, FL	HOSPITAL	3/17/97	24,396	4,580.2	24704
10	Active	EL PASO, TX	LAUNDRY	10/7/97	16,775	2,870.1	26707
11	Active	STATEN ISLAND, NY	CHEMICAL PLANT	8/27/96	29,333	5,342.8	25001
12	Active	PITTSBURGH, PA	CENTRAL BOILER PLANT	12/16/96	28,105	4,988.9	25171
13	Active	SYRACUSE, NY	SCHOOL	1/22/97	27,222	2,802.1	34626
14	Active	CAPE COD, MA	COLLEGE	3/31/99	10,995	2,016.5	32982
15	Active	OMAHA, NE	BANK	3/25/99	11,084	1,569.1	32825
16	Active	YONKERS, NY	ANAEROBIC DIGESTER GAS	4/8/97	18,321	2,349.2	29169
17	Active	OMAHA, NE	BANK	3/24/99	11,030	1,565.1	32496
18	Active	ANCHORAGE, AK	ARMORY BUILDING	12/24/96	9,046	1,739.4	29658
19	Active	ANCHORAGE, AK	ARMORY BUILDING	12/11/96	22,321	4,061.2	18430
20	Active	DEER ISLAND, MA	ANAEROBIC DIGESTER GAS	9/4/97	2,760	395.7	34506
21	Being Installed	ANN ARBOR, MI	RESEARCH LAB		0	0.0	31842
22	Active	FALLON, NV	GALLEY BUILDING	2/28/97	25,781	4,211.7	30955
23	Active	OMAHA, NE	BANK	3/24/99	10,648	1,521.4	32128
24	Active	SPOKANE, WA	HOTEL	6/11/97	22,680	4,370.4	11799
25	Active	CHICOPEE, MA	CENTRAL BOILER	9/15/97	22,230	4,393.4	30078

			PLANT				
26	Active	TUCSON, AZ	CENTRAL BOILER PLANT	10/18/97	20,577	3,644.0	11941
27	Active	ROSAMOND, CA	CENTRAL BOILER PLANT	6/19/97	19,325	3,367.7	29133
28	Active	SIERRA VISTA, AZ	BARRACKS	7/28/97	20,812	3,893.1	11961
29	Will be restarted Fall '00	JOHNSTOWN, PA	OFFICE/RESEARCH LAB	7/28/97	9,637	1,180.7	26736
30	Active	HARTFORD, CT	OFFICE BUILDING	6/18/97	26,023	4,800.7	29284
31	Active	WINDSOR LOCKS, CT	DATA CENTER	12/19/97	19,634	2,135.2	19838
32	Active	MERIDAN, CT	OFFICE BUILDING	9/21/97	20,987	3,991.5	31961
33	Being Installed	ALCORN STATE, MS	UNIVERSITY		0	0.0	29302
34	Active	BRAINTREE, MA	LANDFILL	9/10/99	5,211	906.2	25556
35	Being Installed	BRONX, NY	HOSPITAL		0	0.0	26786
36	Active	SOUTH WINDSOR, CT	INDUSTRIAL SPACE HEATING	3/9/98	19,689	3,771.9	26612
37	Active	PORTLAND, OR	WASTE WATER TREATMENT PLANT	5/21/99	7,259	1,051.5	28749
38	Active	OMAHA, NE	BANK	3/25/99	11,068	1,570.6	29117
39	Owner sold property; being relocated	HARVEY, LA	COMMERCIAL FACILITY	3/13/99	6,823	1,185.1	0
40	Active	HOUSTON, TX	MANUFACTURING	5/12/98	17,871	1,847.8	30063
41	Not Yet Installed	NY, USA	TBD		0	0.0	0
42	Active	GULFPORT, MI	DINING FACILITY	5/13/99	7,775	1,504.3	11956
43	Not Yet Installed	NJ, USA	COLLEGE		0	0.0	23561
44	Active	NEW YORK, NY	SKYSCRAPER OFFICE BUILDING	12/15/99	5,220	920.5	18165
45	Active	NEW YORK, NY	SKYSCRAPER OFFICE BUILDING	12/16/99	5,553	1,039.2	25284
46	Active	RAMAPO, NJ	COLLEGE	3/29/00	2,448	429.1	24466
47	Active	NEW YORK, NY	POLICE STATION	4/17/99	11,108	231.1	24929
48	Active	MESA, AZ	MUNICIPAL BUILDING	4/29/00	2,192	410.2	26467
49	Active	ANCHORAGE, AK	POST OFFICE DISTRIBUTION CENTER	6/28/00	3,396	475.2	13848

50	Active	ANCHORAGE, AK	POST OFFICE DISTRIBUTION CENTER	6/28/00	3,329	518.0	27416
51	Active	ANCHORAGE, AK	POST OFFICE DISTRIBUTION CENTER	6/28/00	3,939	612.0	0
52	Active	ANCHORAGE, AK	POST OFFICE DISTRIBUTION CENTER	6/28/00	4,123	614.1	0
53	Active	ANCHORAGE, AK	POST OFFICE DISTRIBUTION CENTER	6/28/00	3,563	531.4	0
54	Active	CALABASAS, CA	ANAEROBIC DIGESTER GAS	12/15/99	6,613	953.9	23010
55	Active	CALABASAS, CA	ANAEROBIC DIGESTER GAS	12/15/99	8,322	1,216.0	9431
56	Active	JOHNSTOWN, PA	RESEARCH LAB	1/6/00	3,655	497.9	18813
57	Active	SOUTH KINGSTOWN, RI	HOSPITAL	10/18/99	6,532	1,032.4	26779
58	Active	SYRACUSE, NY	HIGH SCHOOL	2/4/00	4,427	803.0	25143
59	Active	BELLAIR, TX	INDUSTRIAL BUILDING	5/24/00	1,867	364.7	22582

Table 10-5 FuelCell Energy Field Sites (mid-year 2000)

Fuel Cell Type	Location	Status	Start Date	Operating Hours	MWhrs Output	Size, kw Design	Actual*	Eff. Percent	Avail. Percent
Direct Fuel Cell	Santa Clara, CA	Completed	3/1996	5,800	2,570	1,800	1,930	44	99**
Direct Fuel Cell	Danbury, CT	Completed	2/1999	11,800	1,906	250	263	45	93
Direct Fuel Cell	Bielefeld, Germany	Continuing	11/1999	4,300+	500+	250	225	45	90
* Maximum attained									
** BOP availability									

Table 10-6 Siemens Westinghouse SOFC Field Units (mid-year 2002)

Year	Customer	Size, kWe	Fuel	Cell Type	Cell Length (cm)	Operating Hours	Cell Number	MWH (DC)
1986	TVA	0.4	H2+CO	TK-PST	30.0	1,760	24	0.5
1987	Osaka Gas	3.0	H2+CO	TK-PST	36.0	3,012	144	6
1987	Osaka Gas	3.0	H2+CO	TK-PST	36.0	3,683	144	7
1987	Tokyo Gas	3.0	H2+CO	TK-PST	36.0	4,882	144	10
1992	JGU-1	20.0	PNG	TK-PST	50.0	817	576	11
1992	Utilities–A	20.0	PNG	TK-PST	50.0	2,601	576	36
1992	Utilities-B1	20.0	PNG	TK-PST	50.0	1,579	576	26
1993	Utilities-B2	20.0	PNG	TK-PST	50.0	7,064	576	108
1994	SCE-1	20.0	PNG	TK-PST	50.0	6,015	576	99
1995	SCE-2	27.0	PNG/DF-JP-8	AES	50.0	5,582	576	118
1995	JGU-2	25.0	PNG	AES	50.0	13,194	576	282
1998	SCE-2/NFCRC	27.0	PNG	AES	50.0	3,394+	576	73+
1997	EDB/ELSAM-1	125.0	PNG	AES	150.0	4,035	1152	471
1999	EDB/ELSAM-2	125.0	PNG	AES	150.0	12,577	1152	1,153+
2000	SCE	180.0	PNG	AES	150.0	770+	1152	25+
2001	RWE	125.0	PNG		150.0	3,700+	1152	

PNG = Pipeline Natural Gas
TK-PST = Thick Wall Porous Support Tube
TN-PST = Thin Wall Porous Support Tube
AES = Air Electrode Support
+ = Testing Continues

10.7 Hydrogen

10.7.1 Introduction

The use of hydrogen in the United States energy infrastructure has been considered for decades. For economic reasons, the hydrogen economy has not developed; for environmental reasons, the potential of hydrogen becoming a major commodity exists. In 1990, the United States Congress passed the Matsunaga Hydrogen Research and Development Act. The Act required the Department of Energy to develop critical hardware for hydrogen technology. The Act also established the Hydrogen Technical Advisory Panel, which is composed of experts from industry and academia, to advise the Secretary of Energy on the status and recommended direction of hydrogen energy development. In 1996, Congress passed the Hydrogen Future Act; the Act authorized the spending of $164.5 million between 1996 and 2001 on the research, development, and demonstration of hydrogen production, storage, transport, and use. In February 2003, President Bush announced the *FutureGen* initiative to build the world's first integrated sequestration and hydrogen production research power plant with zero-emissions. When operational, the prototype will be the cleanest fossil fuel-fired power plant in the world.

The demand for hydrogen grew 23 percent per year between 1994 and 1999 and is projected to continue to grow by 14 percent per year through 2004. Oil refining accounts for 67 percent of the hydrogen usage in the United States. The manufacture of petrochemicals accounts for 26 percent, and the final 7 percent is used in the reduction of metals, electronics, glass, rocket fuel, food processing, laboratory use, and power generation. Many believe that the demand for hydrogen will continue to grow for the following reasons:

- As domestic reserves of oil decline and heavier imported crude oil is refined, increased amounts of hydrogen will be required
- As higher sulfur crude oils are refined, additional hydrogen for desulfurization to meet existing and more stringent future regulations will be required
- The number of hydrogen-powered vehicles will increase
- Electricity produced by hydrogen-fueled technology will increase
- The increased use of hydrogen will reduce the dependency on imported oil

The interest in hydrogen as pollution-free energy has sparked legislation. The following is some of the Federal and state legislation:

- The "Hydrogen Future Act of 1996" focuses Federal hydrogen research on the basic scientific fundamentals needed "to provide the foundation for private sector investment and development of new and better energy sources."
- California's "zero-emission" standard for passenger cars requires that 2 percent of new cars in the state be non-polluting.
- As part of California's Clean Transportation Fuels Initiative, the California Energy Commission (CEC) will assist in establishing publicly accessible clean-fuel refueling facilities to serve clean-fuel fleets and vehicles in California. Eligible projects include all non-petroleum fuels such as natural gas, alcohol, and hydrogen (for fuel cell applications).
- In April 2000, the Arizona Legislature passed SB 1504 - an important piece of legislation for the alternative fuels movement and most particularly the hydrogen program. The Hydrogen Grant Program allows up to $500,000 for hydrogen programs that benefit the public.

- The State of Georgia offers an income tax credit of $5,000 for the purchase or lease of a zero emission vehicle (ZEV). ZEVs include battery-only electric vehicles (EVs) and hydrogen fuel cells.
- New York's Alternative-Fuel (Clean-Fuel) Vehicle Tax Incentive Program offers tax credits and a tax exemption for people who purchase alternative fuel vehicles (AFVs). Purchasers of compressed natural gas, liquefied petroleum gas, methanol, ethanol, and hydrogen-powered vehicles, as well as hybrid electric vehicles (HEVs), are eligible for a tax credit worth 60 percent of the incremental cost.
- In 1992, the state of Pennsylvania established a program to reduce Pennsylvania's dependence on imported oil and improve air quality through the use of alternative fuels. Eligible alternative motor fuels and fuel systems are compressed natural gas, liquefied natural gas, liquid propane gas, ethanol, methanol, hydrogen, hythane, electricity, coal-derived liquid fuels, fuels derived from biological materials, and fuels determined by the Secretary of the U.S. Department of Energy as meeting the requirements of Section 301 of the Energy Policy Act of 1992. After July 1, 2001, qualified projects will receive funding for 20 percent of eligible project costs.
- Effective January 1, 1996, Virginia's sales and use taxes were reduced by 1.5 percent for any motor vehicle that has been manufactured, converted, or retrofitted to operate on compressed natural gas, liquefied natural gas, liquefied petroleum gas, hydrogen, or electricity.
- The University of Wisconsin-Milwaukee Center for Alternative Fuels offers a Congestion Mitigation Air Quality Alternative Fuels Grant Program for the incremental cost of purchasing AFVs. Wisconsin municipalities, in an 11 county area (including Milwaukee, Waukesha, Racine, Kenosha, Walworth, Washington, Ozaukee, Sheboygan, Manitowoc, Kewaunee, and Door counties), are eligible to participate in the grant program. Eligible vehicles include dedicated, bi-fuel, or flexible fuel vehicles. Eligible fuels include ethanol, methanol, hydrogen, compressed natural gas, liquefied natural gas, propane, biodiesel, and electricity. Grant awards are allocated through a competitive grant application process. The maximum grant award per passenger vehicle is $6,500 and $12,000 per truck, van, or bus with a total of $50,000 per municipality.

The opportunities for R&D to advance hydrogen production, utilization, and storage hold great potential. "Much of the recent ferment over hydrogen and fuel cells has taken place in the auto industry. DaimlerChrysler has committed $1 billion over 10 years to fuel cell development, and is working with Ford and Ballard Power Systems to put transit fuel cell buses on the road in Europe. General Motors aims to be the first car company to sell one million fuel cell vehicles, beginning mass production in 2010, and has announced major investments in two companies specializing in hydrogen storage and delivery. Toyota sent shock waves through the industry by announcing it would start selling its fuel cell car in Japan. The energy industry is also getting serious about hydrogen. Both Shell and BP have established core hydrogen divisions within their companies. ExxonMobil is teaming up with GM and Toyota to develop fuel cells. Texaco has become a major investor in hydrogen storage technology (4)." For additional information on industry announcements, see The Hydrogen and Fuel Cell Letter.

10.7.2 Hydrogen Production

A number of hydrogen manufacturing plants are sited (see Table 10-7) across the United States. Any carbonaceous material can be used to make hydrogen from steam reforming, but they are

more likely to contain contaminants than natural gas, and would require cleanup before use. The main reason natural gas is used is that the supply of natural gas is abundant and the price continues to remain low. If the prices or availability of natural gas becomes prohibitive, water is another abundant source of hydrogen. Several forms of energy can be used to make hydrogen:

- **Thermal:** Thermal decomposition of water into hydrogen and oxygen occurs at temperatures around 2,500 ^{o}C. The process isn't attractive because few materials can withstand that temperature. In the plasma arc process, water is heated to 5,000 ^{o}C by an electric field resulting in the cracking products H, H_2, O, O_2, OH, HO_2, and H_2O. A fraction of 50 percent by volume of H and H_2 is possible. The plasma gases are quenched with a cryogenic liquid to prevent the gases from recombining. This process consumes a lot of energy and is very expensive to operate.
- **Thermochemical:** Today, hydrogen is produced mainly from natural gas by steam methane reforming. Steam methane reforming (SMR) is not only the most common, but is also the least expensive method of producing hydrogen; almost 48 percent of the world's hydrogen is produced from SMR (1). Refineries produced and used 2,500 billion scf in 1998.
- **Electrochemical:** Water electrolysis passes a direct current between two electrodes in water. The water is made more conductive by adding an electrolyte such as potassium hydroxide. Hydrogen gathers around the negative electrode (cathode) and oxygen gathers around the positive electrode (anode). The gases are collected separately.
- **Photoelectrochemical:** Sunlight (photons) provides the source of energy for this process. Photons interact with dissolved chemicals to produce activated species, which in turn deactivate by releasing hydrogen from water. This is solar-powered electrolysis.
- **Photobiologial:** Sunlight provides the source of energy for this process. Living organisms, such as green algae, make enzymes. The pigment of algae absorbs solar energy, and the enzyme in the cell acts as a catalyst to split the water molecules.

Table 10-7 Hydrogen Producers[3]

Producer	Capacity*
Merchant Cryogenic Liquid	
Air Products and Chemicals, New Orleans, LA	26,800
Air Products and Chemicals, Pace, FL	11,500
Air Products and Chemicals, Sacramento, CA	2,300
Air Products and Chemicals, Sarnia, Ont.	11,500
BOC, Magog, Quebec	5,900
HydrogenAL, Becancour, Quebec	4,600
Praxair, East Chicago, IN	11,500
Praxair, McIntosh, AL	11,500
Praxair, Niagara Falls, NY	15,000
Praxair, Ontario, CA	8,500
Total Merchant Cryogenic Liquid	109,100
Merchant Compressed Gas	
Air Liquide (11 locations)	67,960
Air Products and Chemicals (20 locations)	740,440
BOC (6 locations)	14,650
Brown Industries (3 locations)	460
General Hydrogen, Natrium, WV	200

Producer	Capacity*
Holox, Augusta, GA	400
Industrial Gas Products, Sauget, IL	1,500
Javelina, Corpus Christi, TX	35,000
Jupiter Chemicals, Westlake, LA	35,000
Lagus, Decatur, AL	9,000
Equistar, Channelview, TX	80,000
MG Industries (3 locations)	1,300
Praxair (22 locations)	425,960
Prime Gas, Delaware City, DE	200
Rohm and Haas, Deer Park, TX	n.a.
T&P Syngas Supply, Texas City, TX	32,400
Total Merchant Compressed Gas	1,444,470
Total Merchant Product	1,553,570

* Thousands standard cubic feet (SCF) per day merchant hydrogen from steam reforming of light hydrocarbons or recovered as by-product from chloralkali plants or chemical synthesis operations.

Hydrogen Utilization
Hydrogen can be used to power vehicles, run turbines or fuel cells to produce electricity, and generate heat and electricity for buildings. Hydrogen is used as a chemical in the petrochemical, electronics, and food industries. The zero-emission potential of using hydrogen as a fuel has sparked interest in the utility and transportation sectors.

10.7.3 DOE's Hydrogen Research

Concerns about air pollution, global warming, and long-term fuel availability have focused international attention on the development of alternative fuels. Hydrogen will be an important part of future energy systems addressing these concerns. Whether processed in a fuel cell or burned in a combustion process, hydrogen represents an exceptionally clean energy source. Development is underway on processes that economically produce hydrogen from methane, coal, water, and other abundant sources.

DOE's hydrogen research draws upon core competence in several engineering and technology areas, including systems engineering, safety and risk assessment, chemical and mechanical engineering, manufacturing and materials, sensors and controls, plasma processing, fuel cell technology, biotechnology engineering, and alternative fuel vehicle fueling infrastructure development. Hydrogen programs are managed at the National Energy Technology Laboratory, the Idaho National Engineering and Environmental Laboratory (INEEL), and the National Renewable Energy Laboratory (NREL). Promising technologies related to production, infrastructure, and utilization of hydrogen are:

- Production of hydrogen from coal (NETL)
- Thermal-plasma/quench process for converting methane to hydrogen, with solid carbon produced as a by-product (INEEL)
- Biotechnology processes for production of hydrogen from carbon-containing waste and renewable resources (INEEL)

- Photoconversion production uses either biological organisms (bacteria or algae) or semiconductors to absorb sunlight, split water, and produce hydrogen (NREL)
- Thermochemical production uses heat to produce hydrogen from biomass and solid waste (NREL)
- Low-pressure storage of hydrogen in the use of metal ion intercalated graphite fibers as a medium (INEEL)
- Fleet and fueling systems engineering analysis of hydrogen-powered buses and supporting fueling stations (INEEL)
- Safety and risk assessment of hydrogen as transportation fuel (INEEL)
- Demonstration of hydrogen-powered vehicles and related transportation system infrastructure, including hydrogen production, storage, and fueling
- Demonstration of hydrogen-fueled, small-scale power generation for local (distributed) electricity production
- Since hydrogen can neither be seen nor smelled, as an added safety precaution for hydrogen-fueled vehicles, hydrogen sensors are being developed. To detect hydrogen, a very thin sensor that reacts to hydrogen by changing colors is applied to the end of a fiber optic cable. The sensors can be placed throughout the vehicle to relay information on leak detection to a central control panel (NREL)

As research and development progresses, collaboration with private sector partners to conduct demonstration testing of hydrogen-fueled vehicles, and demonstration testing of prototype hydrogen-fueled distributed electric power stations will be done. A list of worldwide hydrogen fuel stations can be viewed at http://www.fuelcells.org/info/charts/h2fuelingstations.pdf.

10.7.4 Hydrogen Storage

The four most common methods for storing hydrogen are:

- **Compressed gas in pressure vessels:** New materials have allowed pressure vessels and storage tanks to be constructed that can store hydrogen at extremely high pressures.
- **Hydrogen absorbing materials:**
  1. Metals (pure and alloyed) can combine with hydrogen to make a metal hydride. The hydride releases hydrogen when heated. Hydrogen stored in hydrides under pressure has a very high energy density.
  2. Hydrogen molecules that have been absorbed on charcoal can approach the storage density of liquid hydrogen.
  3. Small glass spheres (microspheres), carbon nanotubes, and fullerenes can hold hydrogen if it is induced at high pressure and temperature. The hydrogen is held captive in the solid matrix when the temperature lowers. Hydrogen can be released by heating the solid.
- **Liquid storage:** Hydrogen can be converted into a liquid by reducing the temperature to –253 ^{o}C. This can save cost in transportation, but requires additional energy and cost to keep the hydrogen at the low temperature. Refrigerating hydrogen in liquid form uses the equivalent of 25 to 30 percent of its energy content. A concern of storing liquid hydrogen is minimizing loss of liquid hydrogen by evaporation.
- **Underground storage in depleted oil and natural gas reservoirs, aquifers, and salt cavities:** For underground storage of hydrogen, a large cavern of porous rock with an

impermeable caprock above it would be needed to contain the gas. As much as 50 percent of the hydrogen pumped into the formation would remain in the formation.

10.7.5 Barriers

A number of key barriers must be addressed by federal, state, and local governments along with industry and academia (2). These barriers are listed below:

- The primary constraint on remote fuel cells generating electricity from hydrogen is economical. Power is inexpensive in the United States. For a fuel cell to compete with other generation sources, its price must be reduced dramatically. Remote power applications offer the best opportunities for fuel cells to compete economically. Generally speaking, the cost of hydrogen should be under $10/MMBtu to be competitive with other energy sources. Fuel cells at customer sites with a use for the waste heat must be acquired and installed at a cost under $2,000/kW.
- Research and development is required to improve the performance and reduce the cost of renewables, storage, and fuel cell technologies. Technologies are needed that can produce hydrogen for the same price as gasoline. Storage technologies must be developed to allow cheap, safe hydrogen storage. Finally, fuel cell technology must advance to improve efficiency.
- Safety is a prime consideration for stationary fuel cells. As fuel cells come closer to the customer, codes must be written and building inspectors educated to allow the introduction of fuel cell power systems. Standards are being developed for on-board hydrogen, but these efforts must be expanded to include standards in building codes and for on-site hydrogen production, storage, and use at industrial sites. Codes and standards activities along these lines are underway.
- Difficulty in obtaining insurance is of prime concern for siting hydrogen projects. Efforts must be undertaken for the government to provide a layer of insurance coverage. In addition, insurance companies must be educated as to the proper handling of hydrogen and the associated risks. This would allow for property, liability, and efficacy insurance to be offered at reasonable rates.
- Public outreach is necessary for the development of hydrogen technologies. The public perception is that hydrogen is dangerous. EPA lists hydrogen as a hazardous chemical. The public requires positive experiences in using hydrogen at work or in transportation to overcome negative perceptions. Children can be educated at school with a curriculum that includes studying hydrogen as a renewable, non-polluting energy source.

10.8 The Office of Energy Efficiency and Renewable Energy Work in Fuel Cells

The Office of Energy Efficiency and Renewable Energy (EERE), whose mission is to develop and deploy efficient and clean energy technologies, is part of the United States Department of Energy. EERE partners with the private sector, state and local governments, DOE national laboratories, and universities to conduct its program activities. To help accomplish its mission, EERE is aided by the Golden Field Office and six regional offices, each of which serves a specific geographic region of the United States and its territories.

In early 2002, the Office of Energy Efficiency and Renewable Energy organized into eleven Program Offices. These offices include:

1. Solar
2. Wind and Hydropower
3. Geothermal
4. Distributed Energy, Electricity, Infrastructure, and Reliability
5. Biomass
6. Industrial Technologies
7. FreedomCAR & Vehicle Technologies
8. Hydrogen, Fuel Cells and Infrastructure Technologies
9. Building Technologies
10. Weatherization and Intergovernmental Grants
11. Federal Energy Management Programs

EERE's fuel cell research is focused on low temperature fuel cells for transportation applications and distributed energy systems. A short summary of the activities conducted in the focus areas follows:

- **Transportation Systems**: Conduct R&D and analysis activities that address key barriers, including cost and reliability, to fuel cell systems for transportation applications. Activities support the development of individual component technology critical to systems integration, as well as systems-level modeling activities that guide R&D activities, benchmark systems progress, and explore alternate systems configurations on a cost-effective basis.
- **Distributed Energy Systems**: Develop high-efficiency polymer electrolyte fuel cell power systems as an alternative power source to grid-based electricity for buildings and other stationary applications. Activities focus on overcoming the barriers to stationary fuel cell systems, including cost, durability, heat utilization, startup time, and managing power transients and load-following requirements.
- **Fuel Processing**: Develop onboard fuel processors as an alternative to the direct hydrogen approach for transportation and stationary applications.
- **Stack Components**: In collaboration with partners, research and develop technologies to overcome the most critical technical hurdles for polymer electrolyte fuel cell stack components for both stationary and transportation applications. Critical technical hurdles include cost, durability, efficiency, and overall performance of components such as the proton exchange membranes, oxygen reduction electrodes, advanced catalysts, bipolar plates, etc.
- **Technology Validation**: Validate component R&D in a systems-context under real-world operating conditions to quantify the performance and reliability, document any problem areas, and provide valuable information to researchers to help refine and direct future R&D activities related to fuel cell vehicles.

DOE's Office of Energy Efficiency and Renewable Energy (EERE) develops fuel cell technologies with an emphasis on the polymer electrolyte fuel cell for both stationary and transportation applications. In general, PEFC technology, a low temperature fuel cell system, has attractive performance characteristics for smaller-scale systems, while the high temperature systems developed under the Fossil Energy program are most attractive in larger sized systems. The FreedomCAR partnership between DOE and USCAR (a pre-competitive research

organization consisting of General Motors, Ford, and DaimlerChrysler) is the vehicle through which PEFC fuel cells are being developed for use in automotive applications. EERE also has the responsibility for developing PEFC fuel cells for portable and distributed generation applications as well as the technologies required for the hydrogen energy infrastructure that is important in the long-term for large-scale use of PEFC fuel cells.

EERE addresses a recommendation in the National Energy Policy to integrate hydrogen and fuel cell activities by creating the Hydrogen, Fuel Cells & Infrastructure Technologies Program. The program recognizes the direct linkage between a robust cost-effective hydrogen infrastructure and the effective utilization of fuel cell technologies. This program consists of three teams: Hydrogen Production, Hydrogen Storage, and Fuel Cells. Similarly, the FreedomCAR Partnership now includes a Hydrogen Storage and Refueling Interface Technical Team, a Fuel Cell Technical Team, and a new team formed to address hydrogen production and infrastructure issues. The teams consist of automotive and energy industry professionals along with DOE personnel to ensure adequate industry input in the planning and evaluation of program activities.

10.9 Rare Earth Minerals

10.9.1 Introduction

In an effort to reduce fuel cell manufacturing cost, low-priced rare earth minerals are being considered. Rare earth minerals such as lanthanum are used in making cathodes for the solid oxide fuel cell. Lower purity minerals, such as lanthanide manganite, are being tested to determine whether these materials will perform without serious degradation of fuel cell performance.

The rare earth minerals are composed of scandium, yttrium, and the lanthanides. The lanthanides comprise a group of 15 elements that include: lanthanum, cerium, praseodymium, neodymium, promethium, samarium, europium, gadolinium, terbium, dysprosium, holmium, erbium, thulium, ytterbium, and lutetium. Cerium is the most abundant element in the rare earth group at 60 ppm, followed by yttrium at 33 ppm, lanthanum at 30 ppm, and neodymium at 28 ppm. Thulium and lutetium are the least abundant at 0.5 ppm.

Molycorp, a wholly owned subsidiary of Unocal Corp., was the only company to mine rare earth minerals in the United States in 2002. The rare-earth separation plant operations stopped in 2003. Molycorp mined bastnasite, a rare earth fluorocarbonate mineral, as a primary product at Mountain Pass, California. The value of domestic ore production was estimated at $31 million in 2002; the estimated value of refined rare earth minerals was more than $1 billion. The end uses for rare earth products in 2000 were as follows: automotive catalytic, 22 percent; glass polishing and ceramics, 39 percent; permanent magnets, 16 percent; petroleum refining catalysts, 12 percent; metallurgical additives and alloys, 9 percent; rare earth phosphors for lighting, televisions, computer monitors, radar, and x-ray intensifying film, 1 percent, and miscellaneous, 1 percent.

Rare earth minerals are relatively abundant in the Earth's crust, but discovered minable concentrations are less common than for most other ores. U.S. and world resources are contained primarily in bastnasite and monazite. Bastnasite deposits in China and the United

States constitute the largest percentage of the world's rare earth economic reserves, while monazite deposits in Australia, Brazil, China, India, Malaysia, South Africa, Sri Lanka, Thailand, and the United States constitute the second largest segment. Xenotime, rare earth bearing clays, loparite, phosphorites, apatite, eudialyte, secondary monazite, cheralite, and spent uranium solutions make up most of the remaining resources. Undiscovered resources are thought to be very large relative to expected demand. Table 10-8 provides world mine production and reserves.[65]

Table 10-8 World Mine Production and Reserves

Country	Mine Production, 2003	Reserves
United States	--	13,000,000
Australia	--	5,200,000
Brazil	--	110,000
Canada	--	940,000
China	90,000	27,000,000
Commonwealth of Independent States	2,000	19,000,000
India	2,700	1,100,000
Malaysia	450	30,000
South Africa	--	390,000
Sri Lanka	120	12,000
Other Countries	--	21,000,000
World Total (rounded)	95,000	88,000,000

Rare earth prices are quite competitive, causing product prices to be quoted on a daily basis. Table 10-9 shows Rhodia, Inc. quoted prices[66] during 2002.

Table 10-9 Rhodia Rare Earth Oxide Prices in 2002

Product (oxide)	Percentage purity	Standard package quantity (kilograms)	Price (dollars per kilogram)
Cerium	96.00	25	19.20
Cerium	99.50	900	31.50
Dysprosium	99.00	3	120.00
Erbium	96.00	2	155.00
Europium	99.99	1	990.00[1]
Gadolinium	99.99	3	130.00
Holmium	99.90	10	440.00[2]
Lanthanum	99.99	25	23.00
Lutetium	99.99	2	3,500.00
Neodymium	95.00	20	28.50

[65] U.S. Geological Survey, Mineral Commodity Summaries, January 2004.
[66] U.S. Geological Survey, Mineral Yearbook, 2002 edition.

Praseodymium	96.00	20	36.80
Samarium	99.90	25	360.00
Samarium	99.99	25	435.00
Scandium	99.99	1	6,000.00
Terbium	99.99	5	535.00
Thulium	99.90	5	2,300.00
Ytterbium	99.00	10	340.00
Yttrium	99.99	50	88.00

[1] Price for quantity greater than 40 kilograms is $900.00 per kilogram
[2] Price for quantity less than 10 kilograms is $485.00 per kilogram

10.9.2 Outlook

The demand for rare earth minerals is expected to increase as demand for products such as automobiles, computers, electronics, and portable equipment grow. Rare-earth markets are expected to require greater amounts of higher purity mixed and separated products to meet the demand. Growth in autocatalysts has been strong in response to legislation on lower emission levels, and between 1997 and 2000 the demand for rare earth magnets grew at 21 percent per year in spite of the uncertainties created by the financial crisis in Asia. Over the past 5 to 6 years China has increased its dominance of the world market, supplying an estimated 95 percent of world demand in 2003.

World reserves are believed to be sufficient to meet forecast world demand well into the 21st century. Several world class rare earth deposits in Australia and China have yet to be developed because world demand is currently met by existing production. The long-term outlook is for an increasing competitive and diverse group of rare earth suppliers. As research and technology continue to advance the knowledge of rare earth minerals and their interactions with other elements, the economic base of the rare earth industry is expected to continue to grow. New applications are expected to be discovered and developed.

10.10 References

1. K. Kono, "Implementing Agreement 'IEA Advanced Fuel Cells,' Annual Report 2001." February 2002.
2. Fuel Cell Technology News, January 2002, published by Business Communications Company, Inc.
3. "Hydrogen Rising in Energy Policy Debate: Global race for "tomorrow's petroleum" heats up," Worldwatch News Release, August 2, 2001.
4. C Padro and V. Putsche, "Survey of the Economics of Hydrogen Technologies," NREL/TP-570-27079, September 1999.
5. National Renewable Energy Laboratory web site: http://www.nrel.gov/hydrogen
6. Idaho National Engineering and Environmental Laboratory web site: http://www.inel.gov/energy/fossil/hydrogen
7. National Hydrogen Association Near-term Hydrogen Implementation Plan 1999-2005; http://www.hydrogenus.com/implementationplan.asp
8. U.S. Geological Survey, Mineral Commodity Summaries, January 2002.
9. U.S. Geological Survey, Mineral Yearbook, 1999 edition.
10. Source: www.roskill.co.uk/rey.html

11. INDEX